Analysis of
Random Pulse-Width Modulation Techniques
for Power Electronic Converters

by

Michael M. Bech

Preface

This thesis is submitted to the Faculty of Engineering and Science at Aalborg University in partial fulfilment of the requirements for the Ph.D. degree in Electrical Engineering. The research has been conducted at the Department of Electrical Energy Conversion which is part of the Institute of Energy Technology (IET), Aalborg University.

Aalborg, August 2000

Michael M. Bech

Abstract

The research documented in this thesis addresses random pulse-width modulation (PWM) and its applications in hard-switched power electronic converters. This emerging PWM technology has gained considerable interest in academia during the last decade, although industrial applications are still few in number.

The key property that differentiates random PWM from classic PWM, which generates time-periodic switching functions, is that random PWM produces switching functions that have a non-deterministic (random) component. For a well-designed random PWM technique it is, nonetheless, still possible to get an accurate synthesis of the commanded reference waveform, i.e. random PWM behaves exactly as its deterministic counterpart with respect to generating a switching function that allows the reference signal to be extracted by, typically, low-pass filtering.

As a consequence of the non-repetitive switching functions, the frequency-domain spectra for randomized modulators are very different from the spectra caused by a deterministic modulation strategy. Essentially, the spectrum for classic PWM consists of discrete frequency components clustered around multiples of the PWM carrier frequency, whereas random PWM — as least partially — transfers the power carried by the harmonics into the continuous density spectrum.

This spectral spreading property is the key to understand the current interest in random PWM. In particular, it has been demonstrated by experiments in the literature that the otherwise annoying tonal acoustic noise emitted from ac motors and other magnetic components in converter-based systems operating with a carrier frequency in the audible range may be alleviated substantially from a psycho-acoustic point of view in an inexpensive manner by using random PWM instead of deterministic PWM. Other investigations have shown that random PWM may also be used to obtain compliance with standards for electro-magnetic compatibility with less filtering/shielding efforts, because the spectral peaks are reduced compared to deterministic PWM operation.

Deterministic modulators are well understood, but many details relating to random PWM have not yet been properly analyzed from a theoretical point of view. This research attempts to narrow this gap by providing thorough analyses of different random PWM schemes that are considered possible candidates for industrial applications. The main emphasis is put on the standard three-phase voltage-source converter which is widely used for ac drives, active mains rectifiers, uninterruptible power supplies, etc., although much of the work is of general validity in power electronics.

Prior to giving a detailed analysis of specific random PWM strategies, the basic principles for random PWM are discussed. It is shown how randomized modulators may be categorized and how new modulators may be constructed by concatenation of random PWM schemes belonging to different categories. From a practical point of view, however, only a few of the resultant random PWM techniques are of any immediate relevance. Therefore, the main focus is put on simple strategies that rely on dithering of either the PWM carrier frequency, the pulse positions, or possibly the pulse widths.

A substantial part of the thesis concentrates on spectral analysis of random PWM waveforms, i.e. on the problem of calculating analytically the frequency versus power distribution for signals, such as the output voltage from a random pulse-width modulated converter. Like for deterministic modulators, frequency-domain information forms an important supplement to the time-domain information; the spectrum may, for instance, be used to get a better understanding of how a randomized modulator interacts with the system which the modulator belongs to.

A powerful framework for spectral analysis that encompasses all random PWM schemes of interest is developed. To complete a spectral analysis of a particular random PWM signal, the statistical properties that govern the randomization must be known in advantage. Also, the spectral theory takes periodic variations in the duty ratios properly into account, i.e. the analysis is applicable to e.g. sinusoidal, space-vector, and discontinuous modulators besides constant duty ratio operation (dc/dc converters).

A high priority has been given to verify the correctness of the theoretical investigations. For this purpose, all random PWM schemes investigated theoretically have been implemented in a laboratory set-up in order to record real voltage spectra. Based on extensive measurements on both a three-phase dc/ac converter and on a dc/dc converter, it is concluded that the derived spectral analysis agrees almost exactly with the experimental results for all examined random PWM strategies.

Although great ingenuity may be put into inventing random PWM schemes that correctly track the reference voltage within each PWM period, it should not be forgotten that a modulator should always be consistent with the operating principles of the system which it is intended for. To illustrate, an investigation of the current waveforms within one carrier period has been completed for various random PWM schemes for three-phase applications. It is shown that the change of the average current depends on the randomization unless certain criteria related to the symmetry of the switching functions are fulfilled. Such a correlation is undesirable since it adds distortion to the fundamental current component, but also, it turns out that the usual sampling methods to detect the per carrier period average currents in a three-phase system fail. To remedy, a new current sampling method has been developed.

The last topic treated relates to high-performance applications of random PWM, such as ac drives using field-oriented control (FOC) and active mains rectifiers which both rely on feed-back control. The problems of designing and implementing such systems using random PWM are largely unexplored in the literature despite the appealing properties of such a combined approach: good dynamic properties and a possibility to reduce the acoustic annoyance.

Among other issues two key problems have been identified: first, error-free acquisition of current feedbacks requires careful attention when random PWM is used. Second, the synchronization of the controller to the PWM unit may require a control system which is capable of operating with a randomly changing sampling frequency. A methodology has been developed that allows continuous-time transfer functions to be emulated in non-uniformly sampled discrete-time control systems without requiring much computational overhead compared to a fixed sampling frequency implementation.

Laboratory tests on an FOC induction motor drive confirm that it is indeed possible to get the same dynamic performance with random PWM as with classic PWM and, simultaneously, the tonal acoustic noise is greatly alleviated.

Dansk resumé

Denne afhandling er dokumentation for et forskningsprojekt omhandlende stokastisk pulsbredde modulation (PWM[1]) og dens anvendelser i direkte kommuterede effektelektroniske konvertere. I det seneste årti har dette modulationsprincip tiltrukket betydelig interesse fra akademiske institutioner, men de industrielle anvendelser er fåtallige.

Den væsentligste egenskab som adskiller stokastisk PWM fra almindelig PWM, der altid genererer tids-periodiske koblingsfunktioner, er, at stokastisk PWM giver en koblingsfunktion, der har en ikke-deterministisk komposant. For en korrekt designet stokastisk modulator er det imidlertid stadigvæk muligt at lave en eksakt syntese af referencesignalet, dvs. stokastisk PWM opfører sig præcist som en almindelig modulator mht. at generere en koblingsfunktion, der tillader demodulation af referencesignalet ved lavpas filtrering eller lignende.

Som en konsekvens af de ikke-periodiske koblingsfunktioner er frekvensdomæne spektret for en stokastisk modulator meget forskelligt fra det spektrum som en deterministisk modulator forårsager. Spektret for almindelige modulatorer består typisk af en række diskrete frekvenskomposanter grupperet i klynger omkring heltals multipla af PWM bærefrekvensen, hvorimod stokastisk PWM flytter — i det mindste delvist — effekten båret af de harmoniske komposanter til det kontinuerte densitetsspektrum.

Denne spredning i frekvensdomænet er nøglen til at forstå interessen for stokastisk PWM. Med primær fokus på ac motorer er det påvist i faglitteraturen, at de støjgener, der ofte forefindes ved brug af konvertere som arbejder med en bærefrekvens inden for det hørbare område, kan afhjælpes betydeligt — ud fra en psyko-akustisk betragtning — på en tilmed prismæssig billig måde ved at bruge stokastisk PWM i stedet for almindelig PWM. Andre undersøgelser har vist, at stokastisk PWM kan anvendes til at opnå overholdelse af standarder inden for det elektro-magnetiske område med mindre filtre/afskærmninger, fordi amplituden af de spektrale komposanter reduceres i forhold til deterministisk PWM.

Grundige analyser af deterministiske modulatorer findes allerede i litteraturen, men mange tilsvarende forhold omkring stokastisk PWM er ikke klarlagt endnu. Denne afhandling forsøger at indsnævre dette misforhold ved at give en grundig analyse af en række stokastiske modulationsteknikker, som anses for at være kandidater for praktiske anvendelser. Hovedvægten er lagt på den trefasede spændingsstive konverter, der typisk anvendes til ac motorstyringer, aktive ensrettere, nødstrømsanlæg mm.

Før en detaljeret analyse af specifikke teknikker påbegyndes, diskuteres de grundlæggende principper for stokastisk modulation. Det vises herunder hvordan stokastiske modulatorer kan opdeles i kategorier og hvordan nye modulatorer kan konstrueres ved at sammensætte forskellige grundprincipper. Set fra et praktisk synspunkt er det dog kun et fåtal af de mulige teknikker, der spås nogen umiddelbar anvendelighed. Hovedvægten lægges derfor på nogle simple teknikker der baserer sig på stokastiske ændringer af enten PWM bærefrekvensen, pulsplaceringen eller pulsbredden.

---

[1]Fra engelsk: *Pulse-width modulation.*

En væsentlig del af afhandlingen fokuserer på spektralanalyse af stokastiske PWM signaler, dvs. på hvordan beregnes analytisk effektfordelingen i frekvensdomænet for f.eks. udgangsspændingen i en konverter styret efter stokastiske principper. Som for deterministiske modulatorer er frekvensanalysen et vigtigt supplement til et signals tidsdomæneegenskaber; spektret kan b.la. bruges til at få en bedre forståelse af samspillet mellem en stokastisk modulator og det resterende system.

Der er udviklet et slagkraftigt analyseværktøj af general gyldighed der tillader spektralanalyse af alle stokastiske modulatorer af interesse i nærværende afhandling. For at kunne beregne spektret for et stokastisk PWM signal skal de statistiske sandsynlighedsfunktioner, der beskriver de stokastiske egenskaber, være kendte på forhånd. Derudover tager den udviklede teori hensyn til eventuelle periodiske variationer i referencesignalet, dvs. analysen er anvendelig for f.eks. sinus, rumvektor og diskontinuert PWM modulation foruden dc/dc konvertere, hvori referencen er konstant.

Verifikation af gyldigheden af de teoretiske overvejelser har haft høj prioritet, og derfor er alle de analyserede stokastiske PWM teknikker også blevet implementeret i en laboratorieopstilling for at kunne måle faktiske spektra. Ud fra en række målinger på både en trefaset dc/ac konverter og en dc/dc konverter kan det konkluderes, at de beregnede spektra er næsten identiske med de eksperimentelle resultater for alle undersøgte stokastiske PWM teknikker.

Selvom der kan udvises stor opfindsomhed for at udvikle stokastiske PWM teknikker, som alle følger referencen korrekt i hver PWM periode, bør det ikke glemmes, at en modulator altid skal være forenelig med funktionsprincipperne for det system den indgår i. For at illustrere dette er der b.la. gennemført en analyse af strømmens forløb inden for en periode af bæresignalet for forskellige stokastiske PWM teknikker for trefasede applikationer. Det er vist, at ændringen af strømmens middelværdi afhænger af den stokatiske modulator, hvis visse kriterier, der relaterer sig til symmetrien af koblingsfunktionerne, ikke opfyldes. En sådan korrelation er uønskelig, da dette giver forvrængning af strømmens grundtonekomposant, og derudover viser det sig også, at de almindelige teknikker baseret på måling af strømmens øjebliksværdi (sampling) til bestemmelse af strømmens middelværdi inden for een PWM periode er utilstrækkelige. For at afhjælpe dette problem er der udviklet en ny samplingsstrategi.

Det sidste emne, der behandles, omhandler høj-performance applikationer af stokastisk PWM, herunder ac motorstyringer og aktive ensrettere, der afhænger af lukketsløjfe kontrol. Problemerne med at designe og implementere sådanne systemer i forbindelse med stokastisk PWM er stort set uudforsket i litteraturen til trods for de indbydende egenskaber som et sådan system kan have: gode dynamiske egenskaber og mulighed for at mindske den akustiske støj.

I den forbindelse er følgende to problemer centrale: det skal tilses, at strømmålingerne er korrekte, da disse indgår i tilbagekoblingen; derudover kan kravet om at kontrolsystemet og PWM enheden skal arbejde i synkronisme betyde, at kontrolsystemet skal være i stand til at arbejde med en variabel samplingsfrekvens. Hertil er der udviklet en metode der muliggør emulation af vilkårlige kontinuert-tids overføringsfunktioner i et diskret-tids kontrolsystem hvori samplingsfrekvensen ikke behøver at være konstant.

Laboratorieforsøg med en felt-vektor styring af en induktionsmotor bekræfter, at det er muligt at opnå samme dynamiske performance med stokastisk PWM som med almindelig PWM, men den generende akustiske støj fra motoren mindskes betydeligt.

Contents

Part IV   Conclusion

Part V   Appendices

List of abbreviations

CSC	Current-source converter
DFT	Discrete Fourier transformation
DIMC	Diagonal internal model control
DPWM	Discontinuous PWM
DSA	Dynamic signal analyzer
DSP	Digital signal processor
DTC	Direct torque control
EMI	Electro-magnetic interference
FCF	Fixed carrier frequency
FCF-RPWM	Fixed carrier frequency random PWM
FOC	Field-oriented control
HPWM	Hybrid pulse-width modulation
IMC	Internal model control
pdf	Probability density function
PSD	Power spectral density
PWM	Pulse-width modulation
PWR	Power
RCD	Random center displacement
RCF	Random carrier frequency
RLL	Random lead-lag
RNG	Random number generator
RPP	Random pulse position
RPP-DPWM	Random pulse-position modulation for discontinuous PWM
RSS	Random sequence selection
RZV	Random zero-vector distribution
SIN	Sinusoidal modulation
SVM	Space-vector modulation
THI	Third harmonic injection
VSC	Voltage-source converter
WSS	Wide-sense stationary (random process)

Part I

Preliminaries

Chapter 1

Introduction

The research documented in this thesis relates to pulse-width modulation (PWM) techniques used in hard-switched power electronic converters. More precisely, focus is put on a special class of modulators that incorporates a degree of uncertainty for reasons to be described shortly. Such modulators are generally designated as random PWM techniques in the literature to emphasize their non-deterministic properties.

Further information regarding the background and the motivation for the current research on random PWM techniques is provided below. Also, the scope of the thesis is defined. An outline of the thesis concludes the chapter.

1.1 Background

Spurred by technological progresses, static power electronic converters based on semi-conductor devices are used in a vast number of applications today. Spanning from low-power converters for milli-watt applications to high-voltage dc transmission systems that transmit power in the hundreds of mega-watts range, other typical applications include switch-mode power supplies, electronic ballasts, adjustable-speed drives, welding machines, uninterruptible power supplies, electric vehicles, and traction drives in locomotives.

Without pursuing a general classification of apparatus using power electronics, it may safely be stated that a large class of converters of great practical importance is based on switching technology. In such switching converters, the power devices are controlled in an on-off manner, and — as stated in [1] — this switching mode of operation is dictated by efficiency and power loss requirements. Although soft-switching converters are gaining some foothold in special applications, the majority of all switching converters are still of the hard-switched type, where the controllable devices must toggle rapidly between conducting and blocking state to keep switching power losses at tolerable levels. In such hard-switched converters the average energy flow is regulated by proper timing of the gate signals controlling the active semiconductor devices. As reviewed in [2], conceptually different methods exist to maintain correct average quantities, but the prevailing methods rely on pulse-width modulation, which yields a good performance over a wide power and frequency range.

In recognition of the widespread industrial use of pulse-width modulated hard-switched converters, which must be expected to continue in the foreseeable future, this thesis analyzes an emerging class of PWM techniques, which may alleviate some

of the problems that still remain a challenge to combat when classic PWM is used. These so-called random PWM techniques have attracted considerable interest in the last decade, because they are said to have a beneficial impact on some secondary issues in hard-switched converters.

To further encircle the motivation for studying random PWM, it may initially be noted that PWM techniques generate a time-periodic switching function[1], which maps into the frequency domain as a spectrum consisting of discrete frequency components [3]. PWM methods having these characteristics are denoted as deterministic modulators in this thesis. Apart from the frequency components coming from the reference signal, all other components (harmonics) are generally unwanted as they may cause current and voltage distortion, extra power losses and thermal stress, electro-magnetic interference (EMI), torque ripple in rotating machines, mechanical vibrations, and radiation of acoustic noise; see [4] for a discussion of especially EMI-related secondary issues.

The traditional method to alleviate such problems is to insert filters that trap e.g. the current harmonics to places where they are less harmful. For example, some kind of high-frequency filtering is almost obligatory to ensure that the level of conducted EMI emission from a hard-switched converter does not exceed limits set up by legislative bodies. In a similar manner, output filters may be used to reduce the impact of harmonics in adjustable-speed drives, although this option is often waived due to the costs and space requirements associated with such filters.

Now, random PWM has been suggested as an alternative to deterministic PWM for two distinct reasons which both aim at reducing the impact of harmonics in systems based on pulse-width modulated hard-switched converters:

Reduction of subjective acoustic noise
> It has been demonstrated that random PWM may reduce the subjective noise emitted from whistling magnetics in the audible frequency range. Investigations have focused on noise from converter-fed ac machines [5–7], but noise from dc machines [8] and ac reactors in line-side converters [9] has also been studied.

Alleviation of electro-magnetic noise
> Compliance with standards defining limits for emission of conducted and radiated EMI may be obtainable with less filtering and shielding efforts, if deterministic PWM is replaced by random PWM [10–13].

Hence, the reasons for the current interest in random PWM among power electronic engineers are the prospects of alleviating such diverse problems as perception of tonal acoustic noise from electro-magnetics and, on the other hand, EMI. To this end, an important feature of random PWM is that those issues are addressed in a way that does not involve analogue power-levels filters, which tend to be bulky and costly; only modifications to the control circuitry are needed in order to randomize an existing deterministic modulator.

The randomization can be accomplished in many different ways as explained in later chapters, but to facilitate the presentation, the general characteristics of random PWM may be summarized as:

---

[1]As elaborated in Chapter 2, a switching function is a time-continuous binary function that carries information of the instantaneous state of a controllable semiconductor device in a switching converter.

Time-domain properties

In contrast to deterministic modulators, a randomized pulse-width modulator generates switching functions which are non-repetitive in the time domain, even during steady-state operation. Despite of the randomization, precise synthesis of the reference signal may still be maintained.

Spectral properties

The power carried by the discrete frequency components associated with deterministic PWM during steady-state operation is (partially) transferred into the continuous density spectrum. This means that a spectrum originally consisting of narrow-band harmonics is mapped into a spectrum whose power is more evenly distributed over the frequency range.

Due to the redistribution of the spectral power over a wider frequency range, it may be understood that random PWM affects secondary issues in PWM-based converter systems including acoustic noise and EMI. The precise impact depends heavily on the modulator and on the system in question.

1.2   Random PWM in power electronics

Random PWM techniques for power electronic converters and applications have attracted considerable interest for more than one decade. This has resulted in almost 150 scientific papers and reports mainly from academia. All publications known to the author are listed in Appendix B starting on page 301. An in-depth review of this prior work will become quite voluminous and, therefore, only the main landmarks and achievements are outlined and commented.

Alternatively, a more technical review of the work up to 1993 may be found in [14]; an updated review is presented in [15].

1.2.1   Pioneering investigations

As acknowledged in [16], the use of random modulation in power electronics can be tracked back to work of Clarke around 1970: the paper [17] contains a rudimentary description of how a random noise signal is added to the reference voltage of the modulator in order to resolve acoustic annoyance problems in a thyristor-based dc/dc converter. The pertinent details of this particular randomization method are given in the US patent [18] filed in 1969. Twenty seven years later, a Finnish patent application was filed: the 1986 invention [19] aims at reducing the acoustic noise from inverter-fed electric motors by means of a modulator that incorporates random variations in the frequency of the triangular carrier used to modulate the reference waveform.

In chronological order, the next publication known to the author focusing on random PWM is the 1987 paper [20] by Trzynadlowski, Legowski, and Kirlin. Note, however, that earlier scientific papers or — in particular — patents may very well exist. Nevertheless, there seems to be a consensus in the literature that [20] was the main incentive to the (renewed) interest in random PWM during the nineteen nineties. This paper demonstrated that by combining a deterministic modulator for three-phase converters
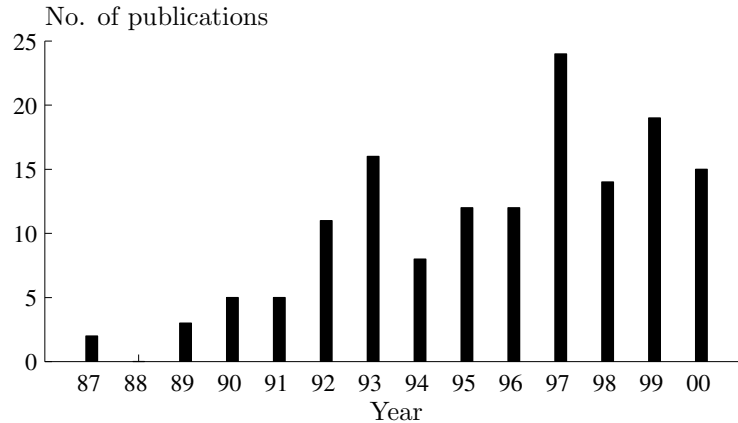
No. of publications

Figure 1.1 Number of publications per year in the period 1987 – August 2000 dealing with random PWM in power electronic converters and their applications. A bibliography for all publications may be found in Appendix B.

with a random number generator, it is possible to reduce the spectral peaks normally associated with pulse-width modulation. The particular random PWM method used in [20] has serious defects, such as excessive switching power losses and inaccurate tracking of the (deterministic) reference waveforms, but, still, the work in [20] should be acknowledged for its originality.

Following [20], the publications investigating random PWM accelerated as visualized in Fig. 1.1 above, which shows the number of references per year dealing with the topic. The majority of the work stem from academia in the form of scientific papers, but a few US and Japanese patents filed by industry have also been found, [21–24]; this list of patents is probably incomplete — finding all relevant patents is a time-consuming process that requires access to better databases than those available to the author.

Apart from these references mentioned above, a few other distinguished publications should be acknowledged for their analysis of random PWM: In 1989, Tanaka et al. [10] proposed and analyzed a random carrier frequency dc/dc converter in order to mitigate EMI peaks caused by the otherwise time-period turn-on and turn-off of power devices. At the same 1989 conference, Habetler and Divan [5] suggested a technique very similar to that of [10], but for a completely different application: [5] demonstrated that acoustic noise generated by an induction machine fed from a three-phase converter can be blurred by changing the PWM carrier frequency randomly around some center value. Although similar in scope and method to the earlier patents [19, 21], it was clearly demonstrated in [5] that pure tones emitted from electric machines due to PWM operation can be eliminated by random PWM.

1.2.2 Abatement of acoustic and electro-magnetic noise

A graphical representation of the research efforts spent on random PWM is given in Fig. 1.2, which presents a classification ordered by the main topic treated in each reference. The diagram reveals, for example, that only a few publications have investigated the impact of random PWM on EMI in dc/ac converters, whereas the study of acoustic noise effects has been a popular research topic for both dc/dc and dc/ac applications.

It should be emphasized that the hierarchy in Fig. 1.2 is a crude classification as
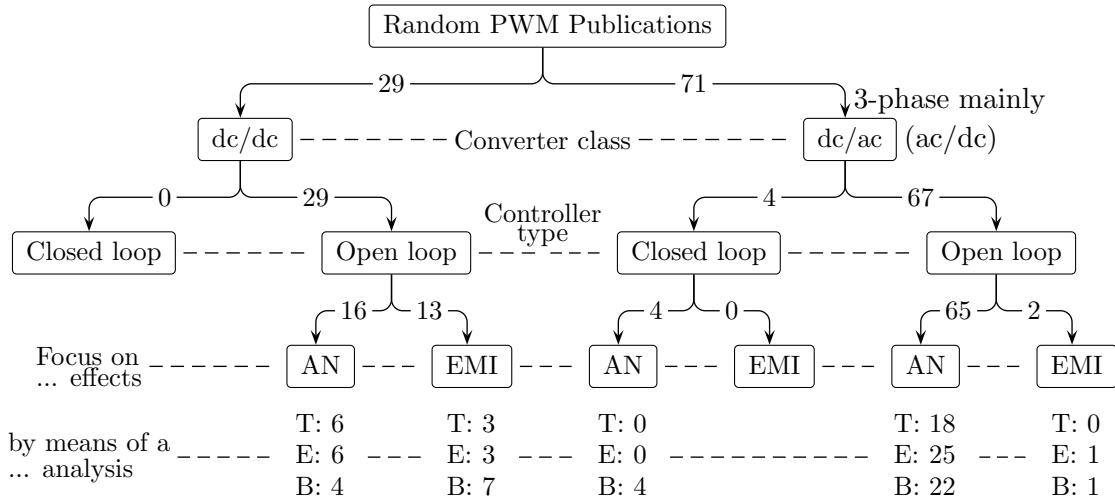
Figure 1.2 Percentage distribution of publications on random PWM organized by the main topic. The papers are divided in two categories: AN (audible noise) or EMI. As indicated in the last row, each reference has further been classified as mainly theoretically (T), experimentally (E), or both (B) theoretically and experimentally oriented.

some references investigate more than one topic. The diagram is, however, useful for the purpose of identifying the focal research areas discussed in more details below.

Audible noise from electro-magnetic components

The main sources of acoustic noise in power electronic systems are magnetic components like smoothing inductors, transformers, and electric machines due to the risk of getting mechanical vibrations excited by Lorentz forces or by deformations caused by magnetostriction [2, 25]. In particular, an annoying whistling noise consisting of almost pure tones may be emitted from such components when they carry switched currents having harmonics in the 0.5–10 kHz range. Constraints related to efficiency, thermal management, and EMI imply that many hard-switched converters in the 1–1000 kW range operate with carrier frequencies that coincide with this range, where, unfortunately, human beings have a high audible sensitivity. Hence, the fundamental idea of using random PWM is to utilize that most people find broad-band noise less annoying than narrow-band noise, probably because wide-band noise blends with background noise. Extensive investigations reported in [26] and summarized in [27] show that this masking effect is most effective during long-term exposures (several hours).

On this background, note from Fig. 1.2 that 85 % of all publications focus on issues related to acoustic noise reduction, which clearly outweighs the investigations dealing with EMI. Also, it may be observed from Fig. 1.2 that 71 % of the references focus on applications that involve dc to ac conversion or vice versa.

Although it does not follow directly from Fig. 1.2, a closer examination reveals that almost all references dealing with acoustic noise focus on external loads connected to hard-switched converters. In particular, acoustic noise from three-phase induction machines fed by a standard voltage-source converter (VSC) has been thoroughly examined. A few applications for dc and switched-reluctance machines do also exist. Also, random PWM has been used to combat acoustic noise in other types of equipment, notably

line-side reactors [9] and high-intensity discharge lamps fed by electronic ballasts [28] (which is a non-magnetic component). Finally, an — perhaps exorbitant — application of random modulation is due to [29]: here, it is suggested that random variations are imposed on the dc reference voltage for high-voltage dc transmission systems handling hundreds of mega watts at hundreds of kilo volts in order to reduce acoustic noise from dc-link smoothing inductors.

Reduction of electro-magnetic interference

According to Fig. 1.2 on the page before, this topic has been treated in 15 % of all publications on random modulation. Here, the objective is to alleviate EMI problems caused by high voltage and current gradients in hard-switched converters by replacing deterministic PWM with random PWM.

The investigations in [30] focus on mains-conducted EMI in the 150 kHz–30 MHz frequency range. It is experimentally demonstrated that compliance with standards for conducted EMI can be met with a smaller EMI filter when random PWM is used. Here, advantage is taken of the fact that compliance with regulations for electro-magnetic compatibility is easier to obtain when the bandwidth of the emitted noise is greater than the (standardized) bandwidth of the receiver. Random modulation certainly smears out the narrow-band power associated with harmonics, even though the total emitted power remains unaffected.

As mentioned in [11–13] this approach to reduce EMI peaks may appear questionable, because it is merely a trick to circumvent regulations. Nevertheless, it is possible to affect both common and differential mode conducted interference simultaneously using spectral spreading techniques at the source; this is in contrast to the normal filtering and shielding approach [12].

Ref. [11] claims that random PWM may be beneficial from a purely functional point of view, since smearing out the radio-frequency power could reduce unwanted interaction between different subsystems within a converter. Indeed, this sounds interesting, but [11] does not give any experimental evidence of this claim, nor has it been pursued in other publications known to the author.

Open-loop versus closed-loop control principles

Attention should be paid to the overall control principles used in the literature. Fig. 1.2 shows that the bulk of the investigations assumes an open-loop control. In the references dealing with dc/ac converters for induction machines, switching functions with random properties are typically generated by enforcing a constant volts per hertz ratio and then measurements of voltage and, sometimes, acoustic noise spectra are given.

Open-loop control is sufficient in applications with minimal performance requirements, but in many applications of power electronics feed-back control is mandatory. For example, closed-loop current control is often employed in switch-mode power supplies, in dc and ac drives, and in active mains rectifiers in order to fulfil specifications for static and dynamic performance. Surprisingly, the use of random PWM is almost unexplored in conjunction with such closed-loop systems. The best contribution in this field is due to Jacobina et al. [31], who designed and implemented a current controller for an induction motor based on random carrier frequency modulation.

1.2.3 Theoretical issues

In parallel with the investigations of random PWM focusing on experiments, a series of theoretical analyses has been reported as well. In particular, the problem of predicting the frequency-domain distribution of the power carried by signals generated by randomized modulators has been studied. As elaborated below, such spectral analyses of random PWM waveforms have been dominated by two independent research groups.

In [32, 33], Kirlin et al. contributed with spectral analysis of voltages generated by standard three-phase dc/ac inverters controlled by two different random PWM techniques. Based on the obtained analytical expressions, initial investigations of the inverse problem have also been addressed (see e.g. [34]): which settings for the random part of the modulator will yield a certain spectral distribution? This difficult problem is sometimes referred to as the spectral shaping problem.

The theoretical investigations of dc/dc and dc/ac converters by Stanković published in the 1993 thesis [11] form a major contribution to spectral analysis of random PWM. Although some of the random PWM schemes analyzed in [11] are of little practical interest, the theoretical framework set up herein has proved to be very powerful. Ref. [11] does also include work on the spectral shaping problem. An excellent summary of [11] is given in the 1995 paper [35].

Common for both groups of authors is that stochastic models coming from statistical communication theory are used, which — from the viewpoint of a power electronic engineer — may appear somewhat alien due to the extent of the mathematics involved in the analysis. (The work of Stanković is based on the seminal 1960 book [36] by Middleton, whereas Kirlin et al. generalize work of [37].) Stochastic signal processing techniques are, nevertheless, mandatory for proper spectral analysis due to the inherently non-deterministic nature of switching functions having partial random properties.

1.3 Problem statement

Despite the intensity of the research efforts spent on random pulse-width modulation, it should be noted that more than thirty years after its inception [18], industrial applications of random PWM are still few in number. In fact, the author is aware of only three[2] companies that officially state that they use some kind of random pulse-width modulation: these are Italian REEL, Polish ENEL, and PDL Electronics in New Zealand, which all manufacture frequency converters with options relying on random modulation to suppress whistling noise from induction machines. Certainly, other industrial products are likely to exist — especially, where random PWM is used for EMI suppression.

Random PWM has not yet gained a firm foothold in industry, but, nevertheless, it is believed that this approach is a simple, but yet sufficient, method to alleviate the annoying acoustic noise in many applications, where electro-magnetic components carry switched currents having large spectral components in the audible range. This has been demonstrated in reports originating from academia, in some of the patents cited in section 1.2.1, and by the manufacturers listed above.

---

[2]Judging from their technical catalogues, Mitsubishi Electric does also use random modulation in some of their frequency converters — this is, however, not specified in an unambiguous manner.

As a curiosity, the perhaps strongest exposition in public of a non-deterministic control method is due to ABB and their frequency converters for ac machines based on direct torque control (DTC). Here, by means of hysteresis controllers for flux and torque, non-repetitive switching patterns are generated in a way completely different from those control philosophies based on PWM. Nevertheless, the spectral characteristics for DTC are very similar to those obtainable with random PWM; this duality in the frequency-domain has been pointed out clearly in [38] by a series of experiments.

1.3.1   Motivation

To summarize, the main motivation for the research on random PWM leading to this thesis is the documented reduction of acoustic annoyance from converters and interconnected equipment, such as electric motors and line-side filters. Despite continuing improvements of power devices with respect to switching speed and on-state conduction losses, the acoustic noise problem must be expected to remain a major concern in power electronics using hard-switching technology. Except for special applications, it is not believed that ultra-sonic switching frequencies will become the mainstream solution in the near future to acoustic noise problems for throughput power levels exceeding a few kilo-watts.

Having stated this, it should also be stated that the applications of random PWM to ease compliance with EMI standard are not the main motivating factor for the present research. Certainly, advantage of spectral spreading by random modulation can be taken, if compliance with regulations using the least possible filtering effort is all that matters; such issues are not pursued any further in this thesis.

1.3.2   Scope of the thesis

Having presented the background for the use of random PWM in power electronics, the two problems addressed in this thesis are outlined below.

Problem #1

For reasons given below, the first focal area is spectral analysis of a series of random PWM techniques, which are believed to be candidates for practical applications. Hence, the first problem is

> *to derive and to experimentally verify analytical expressions for the power spectra[3] for the terminal voltages produced by different converters using random PWM with known settings taking the following into account:*
>
> - *The investigated methods must be applicable to two-level full-bridge dc/dc or three-phase voltage source converters.*
>
> - *Focus should be put on simple random PWM methods that do not differ significantly from established deterministic PWM techniques.*
>
> - *The analyzed methods should be compatible with the spectral shaping problem described below.*

---

[3]Refer to Chapter 3 for a formal definition of the power spectrum of a signal.

Due to the complexity of the mathematics involved in the spectral analyses, a high priority is given to experimental verifications of the derived theoretical results. Surprisingly, concise comparisons of theory with measurements are hardly ever reported in the literature; it is believed that earlier attempts to verify spectral theories are insufficient, because — at best — only rudimentary comparisons of calculated spectra with either laboratory results or with computer simulations are provided.

Note also that to ease the practical implementation, focus is put on simple random PWM techniques that may be derived straightforwardly from well-known deterministic modulation principles. Other constraints related to the practical applicability of random PWM are also investigated including compliance with current sampling techniques in three-phase systems.

Apart from being a most challenging intellectual exercise, it may be asked at this point which advantages a theoretical spectral analysis of signals arising in randomly modulated converters offer. Here, the following points should be kept in mind:

- In signal analysis, precise information of the frequency-domain distribution of the power carried by a signal is of equal importance as is time-domain information. A major reason is that most physical systems only respond in a limited range of frequencies to an external excitation. Taking advantage of this band-pass behavior, greatly simplifies the study [39].

- For non-periodic waveforms, like those voltages generated by random PWM, the power spectrum is a much more stationary (noise-free) and stable picture of a signal than its time-domain representation. Due to this smoothing property, the power spectrum gives direct information of average effects, which may be useful for e.g. response analysis and diagnostics [39].

- Better understanding of how a random pulse-width modulator affects the system, which it is part of, could also justify a spectral analysis. In particular, if the studied system is linear/linearized, frequency-domain analysis is an indispensable tool in engineering for e.g. design of filters (EMI, line-side filters, etc.). Frequency-dependent mechanisms, like acoustic noise or power losses, could also be investigated.

- Having information of the precise spectrum allows an objective comparison and evaluation of the frequency-domain properties of random PWM techniques. For example, performance indices, like the total power in some specified frequency band or the ability to reduce spectral peaks, may be compared.

- Knowledge of how to calculate analytically the power spectrum given the settings of a randomized modulator may also be used to analyze the inverse problem: which settings are needed to shape the power spectrum in a certain way? Note that there is absolutely no guarantee that a given spectral distribution can be generated by an intelligent parameterization of the modulator.

To elaborate the potentials of spectral shaping, consider a scenario where the possibilities of alleviating acoustic noise from a converter-fed electric machine by means of random PWM are to be explored: First, analytical expressions for the spectrum of

the excitation (the applied voltage) are formulated. Combining this with knowledge of the transfer function between the driving voltage and the emitted acoustic noise, the next step towards noise reduction is to select the settings of the randomized modulator in such a way that some performance index is minimized. For example, the objective could be to minimize the risk of exciting an electro-mechanical resonance by minimizing the power in some (narrow or wide) band around a known resonance frequency in the system.

This thesis addresses the problem of analytically calculating the voltage spectrum given the settings of different random PWM schemes, but the spectral shaping problem is not addressed in details. However, care is exercised during the selection of random PWM techniques subjected to detailed spectral analysis, i.e. all investigated techniques may easily be incorporated into constrained numerical optimization routines (analytical optimization is infeasible due to the complexity of the expressions resulting from the spectrum analysis).

Problem #2

Encouraged by the reported improvements on the acoustic annoyance from motor drives based on open-loop random PWM, the second topic for this study is an analysis of random PWM in conjunction with power converters operating in closed-loop mode. The problems pertinent to such use of random PWM are almost unexplored, as mentioned on page 8, despite the appealing characteristics of such a unified system: less acoustic annoyance combined with accurate control. Formally, the objective is

> *to analyze the problems relating to design and to implementation of closed-loop digital structures (controllers, filters, etc.) for random pulse-width modulated power electronic converters taking the following into account:*
>
> - *Preferably, the same performance in terms of stationary and dynamic responses should be achieved in a random PWM-based system compared to a non-randomized system.*
>
> - *A suitable procedure for design of digital systems operating at a randomly varying sampling rate should be derived.*
>
> - *Attention should be paid to limit the computational burden required for real-time evaluation of (new) algorithms.*

In other words, the objective of this part of the study is to investigate the feasibility of using random PWM together with commonly used feed-back control techniques. Many of the obtained results are of general validity, but to limit the extent of the work, focus is put on the three-phase VSC, which is the work-horse in many industrial products in the kilo-watt range and upwards.

Without going into details, the investigated system consists of a direct rotor-flux oriented vector controller for an induction motor drive. It turns out that such a control system incorporates functional units (current controllers, flux estimator, speed controller, etc.), which requires careful attention, if performance deterioration shall be avoided when random PWM is used.

1.3.3   Limitations

It should be emphasized that this thesis focuses almost exclusively on aspects closely related to random pulse-width modulators themselves. On the other hand, system-level consequences and comparisons of random PWM techniques are not investigated to any significant extent: For example, only a very few measurements of acoustic noise spectra are included in the thesis despite the fact that the prospect of reducing acoustic noise is one of the few phenomena that may justify the use of random PWM.

Such system-level comparisons based mainly on measurements of acoustic noise spectra are reported in [40–42], which all are co-written by the author of this thesis.

1.4   Thesis outline

The research documented in this thesis is organized into four main parts besides two appendices. A brief outline of the individual chapters follows below.

Part I   Preliminaries

1. Introduction
This chapter.

2. Principles of random pulse-width modulation
The principles of pulse-width modulation are briefly reviewed, including definitions of switching functions and duty ratios. Space vectors and their application to three-phase systems and converters are covered. The principles for random modulation are then explained and different approaches to get random PWM are discussed. At the end, the random PWM techniques selected for further investigations are presented.

Part II   Analysis of random PWM schemes

3. Spectral analysis of random pulse trains
Starting from well-known Fourier series expansion of periodic signals, the proper definition for the power spectrum for a random signal is presented. Issues relating to estimation of spectra based on measurements are discussed, and it is shown that correct comparisons of measured and analytically calculated spectra require careful attention. Next, a general mathematical framework for spectral analysis of randomly modulated pulse trains is derived. This result is intensively used in Chapters 4, 5, and 6.

4. Analysis of random PWM schemes for full-bridge dc/dc converters
The general theory developed in Chapter 3 is used to derive analytical expressions for the spectrum of the terminal voltage in a full-bridge dc/dc converter. Two different random PWM techniques are studied. Laboratory results show that the developed theory predicts the measured spectral estimates with a very high degree of accuracy.

5. Spectral analysis of random carrier frequency dc/ac PWM schemes
A discussion of advantages and disadvantages of different types of probability density functions is given (these functions describe the probabilistic properties of a random PWM scheme). Using the results of Chapter 3, formulas for the power spectrum of the

terminal voltage in a three-phase dc/ac converter modulated with a randomly varying carrier frequency are derived. Comparisons with measurements show that the theory is fully capable of predicting the actual spectrum irrespective of the modulation method (sinusoidal, space-vector modulation, etc.).

6. Analysis of fixed carrier frequency random dc/ac PWM schemes
Different approaches to randomize a three-phase converter running at a fixed carrier frequency are discussed and a number of constraints related to the practical applicability of a given randomization method is formulated. The impact on the current ripple and on the fundamental current component is analyzed. Spectral analyses of three fixed-frequency random PWM techniques for dc/ac applications are carried out based on results from Chapter 3. Good agreements with measurements are demonstrated.

Part III   Random PWM in closed-loop applications

7. Aspects of random PWM in closed-loop applications
Problems of using closed-loop digital controllers synchronized to the pulse-width modulator are investigated for the case of practical importance where a randomly changing carrier is used. A procedure for design and implementation is suggested that allows a controller to operate at a non-uniform sampling rate without any loss of performance or any significant computational overhead.

8. Field-oriented control using random PWM — a case study
To illustrate the usefulness of the theory set forth in Chapter 7, a complete rotor-field oriented vector controller is designed and implemented in a laboratory set-up. The converter is modulated with a randomly changing carrier frequency. Experimental results show that the obtainable performance is identical to the performance using fixed frequency PWM for both the fast-acting current controller and for the slower speed controller. However, the emitted acoustic noise is less annoying when random PWM is used due to the spread spectrum characteristics.

Part IV   Conclusion

9. Conclusion
This chapter summarizes the main conclusions drawn in the individual chapters. Also, contributions believed to be novel are highlighted. A list of topics suggested for future research is also given.

Part V   Appendices

A. Laboratory facilities
Laboratory experiments are used throughout the thesis to support the theoretical investigations. This appendix describes the used power converters and their loads, the control system, and the instrumentation used for recordings of measurements.

B. References on random PWM
All publications known to the author dealing with random PWM in power electronics are listed here. This bibliography has been used to generate the diagrams in Fig. 1.1 and 1.2 shown on page 6 and 7, respectively.

Bibliography

[1] J. D. van Wyk, "Power Electronic Control for Drives," in *Power Electronics and Variable Frequency Drives. Technology and Applications*, B. K. Bose, Ed., New York, 1997, pp. 80–137, IEEE Press.

[2] J. Holtz, "Pulse Width Modulation for Electronic Power Conversion," in *Power Electronics and Variable Frequency Drives. Technology and Applications*, B. K. Bose, Ed., New York, 1997, pp. 138–208, IEEE Press.

[3] F. Jenni and D. Wüerst, *Steuerverfahren für Selbstgeführte Stromrichter*, B. G. Teubner, Stuttgart, 1995.

[4] R. J. Kerkman, "Twenty Years of PWM AC drives: When Secondary Issues become Primary Concerns," *Proc. of the 22nd IEEE International Conference on Industrial Electronics, Control, and Instrumentation*, vol. 1, pp. LVII–LXIII, 1996.

[5] T. G. Habetler and D. M. Divan, "Acoustic Noise Reduction in Sinusoidal PWM Drives Using a Randomly Modulated Carrier," *Proc. of the 20th IEEE Power Electronics Specialists Conference*, vol. 2, pp. 665–671, 1989.

[6] J. K. Pedersen, F. Blaabjerg, and P. S. Frederiksen, "Reduction of Acoustical Noise Emission in AC-Machines by Intelligent Distributed Random Modulation," *Proc. of 5th European Conference on Power Electronics and Applications*, vol. 4, pp. 369–375, 1993.

[7] G. A. Covic and J. T. Boys, "Noise Quieting with Random PWM AC Drives," *IEE Proc. Electric Power Applications*, vol. 145, no. 1, pp. 1–10, Jan. 1998.

[8] P. G. Handley, M. Johnson, and J. T. Boys, "Elimination of Tonal Acoustic Noise in Chopper-Controlled DC Drives," *Applied Acoustics*, vol. 32, pp. 107–119, 1991.

[9] J. Holtz and L. Springob, "Reduced Harmonics PWM Controlled Line-Side Converter for Electric Drives," *Conference Record of the 25th IEEE Industry Applications Society Annual Meeting*, vol. 2, pp. 959–964, 1990.

[10] T. Tanaka, T. Ninomiya, and K. Harada, "Random-Switching Control in DC-to-DC Converters," *Proc. of the 20th IEEE Power Electronics Specialists Conference*, vol. 1, pp. 500–507, 1989.

[11] A. M. Stanković, *Random Pulse Modulation with Applications to Power Electronic Converters*, Ph.D. thesis, Massachusetts Institute of Technology, Feb. 1993.

[12] D. C. Hamill, J. H. B. Deane, and P. J. Aston, "Some Applications of Chaos in Power Converters," *Proc. of the IEE Colloquium on Update on New Power Electronic Techniques*, pp. 5/1–5/5, May 1997.

[13] M. Kuisma, P. Silventoinen, T. Järveläinen and T. Vesterinen, "Effects of Nonperiodic and Chaotic Switching on the Conducted EMI Emissions of Switch Mode Power Supplies," *Proc. of the IEEE Nordic Workshop on Power and Industrial Electronics*, pp. 185–190, 2000.

[14] A. M. Trzynadlowski, F. Blaabjerg, J. K. Pedersen, R. L. Kirlin, and S. Legowski, "Random Pulse Width Modulation Techniques for Converter Fed Drive Systems — A Review," *Conference Record of the 28th IEEE Industry Applications Society Annual Meeting*, vol. 2, pp. 1136–1143, 1993.

[15] M. M. Bech, J. K. Pedersen, and F. Blaabjerg, "Random Modulation Techniques in Power Conversion — an Update," *Proc. of the International Power Electronics and Motion Control Conference*, vol. 3, pp. 357–365, 1996.

[16] W. McMurray, "Power Electronics in the 1990s," *Proc. of the 16th IEEE International Conference on Industrial Electronics, Control, and Instrumentation*, vol. 1, pp. 839–843, 1990.

[17] P. W. Clarke, "Self-Commutated Thyristor DC-to-DC Converter," *IEEE Trans. on Magnetics*, vol. 6, no. 1, pp. 10–15, Mar. 1970.

[18] P. W. Clarke, Bell Telephone Laboratories, "Switching Regulator with Random Noise Generator," US Patent No. 3.579.091, Filed May 18, 1969.

[19] Kone Osakeyhtiö, "Förfarande och anordning för minskning av bullerolägenheterna vid en med chopperprincip matad elmotor (*Method and Apparatus for Reduction of Noise from Chopper-Fed Electrical Machines*)," Finnish Patent Application No. 861.891, Filed May 6, 1986.

[20] A. M. Trzynadlowski, S. Legowski, and R. L. Kirlin, "Random Pulse Width Modulation Technique for Voltage-controlled Power Inverters," *Conference Record of the 22nd IEEE Industry Applications Society Annual Meeting*, vol. 1, pp. 863–868, 1987.

[21] Y. Kawashima and K. Tokuoka, Toyo Electric, "PWM Inverter," Japanese Patent No. 1.136.572, Filed Nov. 20, 1987.

[22] T. Koga and H. Hayashi, Toyo Electric, "Modulation System for PWM Inverter," Japanese Patent No. 6.014.557, Filed June 23, 1992.

[23] H. Hosei and K. Tanaka, Nippon Steel Corp., "Switching Regulator," US Patent No. 5.640.315, Filed March 17, 1995.

[24] L. Garces and V. T. N'Guyen Phuoc, Schneider Electric SA, "Inverter Control Device," US Patent No. 5.552.980, Filed March 1, 1995.

[25] L. Låftman, *The Contribution to Noise from Magnetostriction and PWM Inverter in an Induction Machine*, Ph.D. thesis, Department of Industrial Electrical Engineering and Automation, Lund University, Sweden, Aug. 1995.

[26] L. Sjöberg and H. Weibull, *Buller från frekvensomriktar-matade asynkronmaskiner (Acoustic Noise from Frequency Converter-Fed Induction Machines)*, Report TEIE-7074, Department of Industrial Electrical Engineering and Automation, Lund University, Sweden, 1993.

[27] I. Ekdahl, L. Sjöberg, H. Weibull, and J. Valis, "Annoyance from Inverter-Fed Induction Motors," *Proc. of Internoise — People versus Noise*, Leuven, Belgium, 1993.

[28] L. Laskai, P. Enjeti, and I. J. Pitel, "White-Noise Modulation of High-Frequency High-Intensity Discharge Lamp Ballasts," *Conference Record of the 29th IEEE Industry Applications Society Annual Meeting*, vol. 3, pp. 1953–1961, 1994.

[29] M. Alaküla, L. Sjöberg, and P. Johansson, "Random Modulation of Line Commutated Power Converters," *Proc. of 7th European Conference on Power Electronics and Applications*, vol. 1, pp. 278–280, 1997.

[30] D. Stone and B. Chambers, "The Effect of Carrier Frequency Modulation of PWM Waveforms on Conducted EMC Problems in Switched Mode Power Supplies," *EPE Journal*, vol. 5, no. 3/4, pp. 32–37, Jan. 1996.

[31] C. B. Jacobina, A. M. N. Lima, E. R. C. da Silva, and R. L. de A. Ribeiro, "Current Control for a Random PWM Voltage Source Inverter," *Proc. of the 28th IEEE Power Electronics Specialists Conference*, vol. 2, pp. 1440–1446, 1997.

[32] A. M. Trzynadlowski, R. L. Kirlin, and S. Legowski, "Space Vector PWM Technique with Minimum Switching Losses and a Variable Pulse Rate," *Proc. of the 19th IEEE International Conference on Industrial Electronics, Control, and Instrumentation*, vol. 2, pp. 689–694, 1993.

[33] R. L. Kirlin, S. Kwok, S. Legowski, and A. M. Trzynadlowski, "Power Spectra of a PWM Inverter with Randomized Pulse Position," *IEEE Trans. on Power Electronics*, vol. 9, no. 5, pp. 463–472, Sept. 1994.

[34] R. L. Kirlin, S. Legowski, and A. M. Trzynadlowski, "An Optimal Approach to Random Pulse Width Modulation in Power Inverters," *Proc. of the 26th IEEE Power Electronics Specialists Conference*, vol. 1, pp. 313–318, 1995.

[35] A. M. Stanković, G. C. Verghese, and D. J. Perreault, "Analysis and Synthesis of Randomized Modulation Schemes for Power Converters," *IEEE Trans. on Power Electronics*, vol. 10, no. 6, pp. 680–693, Nov. 1995.

[36] D. Middleton, *An Introduction to Statistical Communication Theory*, McGraw-Hill Book Company, New York–Toronto–London, 1960.

[37] J. J. Stiffler, *Theory of Synchronous Communication*, Prentice-Hall, Englewood Cliffs, New Jersey, 1971.

[38] L. Xu, Z. Q. Zhu, D. Stone, and D. Howe, "Acoustic Noise Radiated by Space Vector PWM, Random PWM and Direct Torque Controlled Induction Motor Drives," *Proc. of the International Conference on Electric Machines*, vol. 3, pp. 1746–1751, 1998.

[39] R. B. Randall, *Frequency Analysis*, Brüel & Kjær, Nærum, Denmark, third edition, 1987, ISBN 87-87355-07-8.

[40] M. M. Bech, F. Blaabjerg, and A. M. Trzynadlowski, "Experimental Evaluation of Modern Random PWM Techniques for Induction Motor Drives," *Conference Record of the 1997 IEEE International Electric Machines and Drives Conference*, pp. TB3–10.1–TB3–10.3, May 1997.

[41] M. M. Bech, F. Blaabjerg, J. K. Pedersen, and A. M. Trzynadlowski, "Comparative Investigation of Random PWM Techniques with Variable Switching Frequency and Pulse Position for Inverter-Fed Induction Motors," *Proc. of 7th European Conference on Power Electronics and Applications*, vol. 1, pp. 343–349, 1997.

[42] M. M. Bech, F. Blaabjerg, and J. K. Pedersen, "Random Modulation Techniques with Fixed Switching Frequency for Three-Phase Power Converters," *Proc. of the 30th IEEE Power Electronics Specialists Conference*, vol. 1, pp. 544–551, June 1999.

Chapter 2

Principles of random pulse-width modulation

2.1 Introduction

As evident from the discussions in Chapter 1, random pulse-width modulation (PWM) may be regarded as a superset of deterministic PWM. The primary objective of this chapter is to show how random PWM techniques may be derived from their deterministic counterparts and to outline different ways to inject random properties into a modulator. As demonstrated at the end of this chapter, there is hardly no end to the ingenuity that can be put into this randomization, but in this thesis focus is put on methods which are believed to be at least candidates for practical applications.

Furthermore, the focal area is limited to random PWM in conjunction with voltage-source converters (VSC), although (random) PWM is, at least in principle, consistent with current-source converters (CSC) as well. Two standard VSC topologies are investigated in details in the thesis: the full-bridge dc/dc converter and the three-phase dc/ac converter. Both these converters consist of a parallel connection of identical building blocks, namely half-bridge converters. To facilitate the discussion of random PWM and its use for those converters, a second objective of this chapter is to briefly review the principles for voltage synthesis[1] of three-phase VSC's, which is a superior topology for many applications. Another reason for this review is to assure that the upcoming spectral analysis in Part II of various random PWM schemes is compatible with commonly used strategies for voltage control of converters.

Chapter outline

In the first section, preliminaries regarding switching functions and modulated signals are given. Next, the principles of voltage control are reviewed focusing on three-phase converters and space-vector theory. Afterwards, the fundamental principles of random PWM are introduced, and several ways to randomize a modulator are discussed. Finally, the random PWM techniques selected for further investigation are presented.

---

[1]Despite that the bulk of the work focuses on the voltage-controlled VSC, a current-regulated VSC is included in the system studied in Part III. In fact, the trend is that this approach to get current-source characteristics by means of a VSC switching with high frequencies is replacing the classic CSC, even in high-power applications which have traditionally relied on current-stiff topologies [1].

2.2   Preliminaries

Much of the theory presented in this thesis relies on fundamental concepts of pulse-width modulation. These include the use of switching functions to characterize the instantaneous value of the output of a pulse-width modulation process. Also, the relationship between switching functions and duty ratios is commented below. The principles presented in this section are well-known to power electronic engineers, but many interesting generalizations of the established theories may be found in thesis [2].

2.2.1   The switching function

PWM may be regarded as a process in which a signal is supplied in pulses of possibly varying widths and positions. In practice, the modulation is performed by controlling one or more power transistors in an on-off manner in order to achieve small switching losses and high efficiency. As an example, the single-switch step-down topology shown in Fig. 2.1 may be considered.

Assuming ideal conditions the power transistors may be regarded as switches having only two defined states: on and off. This makes it possible to assign a binary variable q to a switch, and this binary description of the time-dependency of the position of the switch is usually called the switching function or the existence function [2, 3]. Switching functions are used throughout this thesis, and using Fig. 2.1 again, the following definition applies

$$q(t) = \begin{cases} 1, & \text{if the switch is ``on,''} \\ 0, & \text{if the switch is ``off.''} \end{cases} \tag{2.1}$$

Hence, q is defined for all time instants, but q can only attain the two discrete values. It should also be noted that for the converter in Fig. 2.1 the voltage u across the load is not uniquely determined by the value of q: when $q = 1$, the output u is clamped to U_{dc}, but during the free-wheeling state ($q = 0$), the value of u may be either 0 or e depending on whether the current conduction mode is continuous or discontinuous.

In many applications of VSC's, the converter topology is built up of identical legs (half-bridges) consisting of two transistors and two anti-parallel diodes as shown in
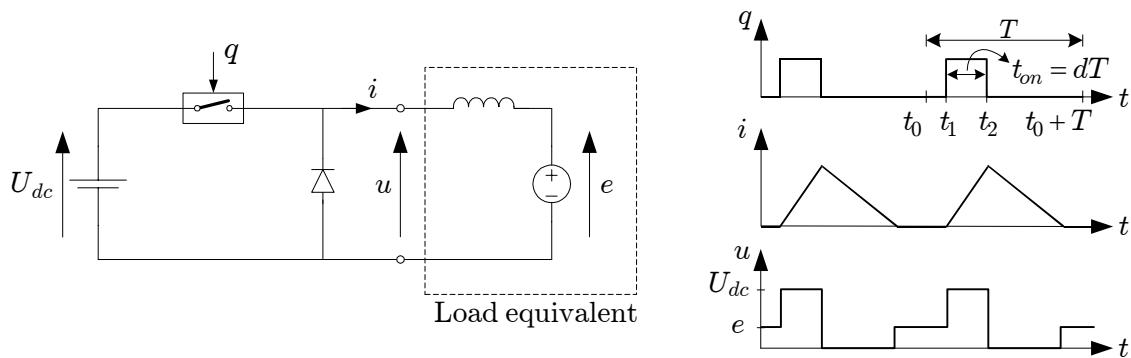
Figure 2.1 Step-down converter controlled by a switching function q. Also shown are waveforms for the output current and voltage.
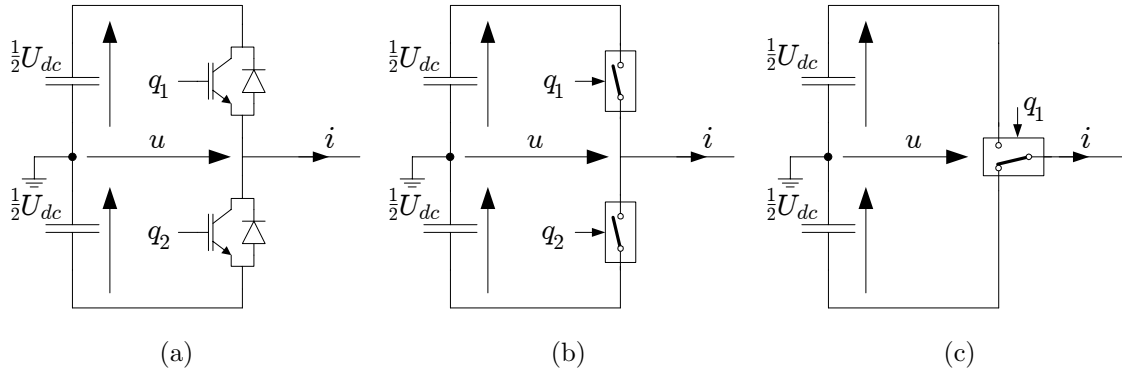
Figure 2.2 Classic converter leg (half-bridge): (a) hardware configuration, (b) two-switch model, and (c) model based on a single two-pole change-over switch.

Fig. 2.2. Each of the two switches (a transistor and its free-wheeling diode) may now be assigned their own switching function: q_1 and q_2, respectively. The only restriction imposed on q_1 and q_2 follows immediately from the voltage axiom [2]: "don't short-circuit a voltage source," i.e. q_1 and q_2 should never equal 1 simultaneously.

However, this individual control of the two transistors is never used in practice, because by imposing the constraint $q_2 = \overline{q_1}$ (logic negation), a desirable property arises: the output voltage u is then independent[2] of the direction of the load current i. In this case the equivalent two-pole change-over switch in Fig. 2.2(c) may be used to model the physical circuit in Fig. 2.2(a). The output voltage is given as $u = (q_1 - \frac{1}{2})U_{dc}$.

The fact that the output voltage may be controlled independently of the load current eases the design of the modulators. Yet another advantage of the restriction $q_2 = \overline{q_1}$ is that the calculation of the spectrum for the output voltage may be done without paying attention to the load current. (As it will be demonstrated in Part II, it is, however, not possible to say that these calculations are trivial even if $q_2 = \overline{q_1}$.)

2.2.2 The duty ratio

The switching function defined above describes the instantaneous state of a switch. Using the terminology of [4], the switching function describes the system on a microscopic time scale. The phenomena associated with this time scale are important issues, especially during design of hardware, but also for the analysis of random PWM.

As shown in Fig. 2.1, the microscopic time scale is useful to visualize the well-known duty ratio concept. Within a prescribed time interval T, the pulse may be defined by the turn-on and turn-off instants, t_1 and t_2, respectively. The width of the pulse is given by $t_{on} = (t_2 - t_1) \triangleq dT$ which defines the duty ratio d.

Formally, the mapping from a switching function q to its corresponding duty ratio d is given by the average from $t = t_0$ to $t = t_0 + T$:

$$d = \frac{1}{T} \int_{t_0}^{t_0+T} q(t)\ dt, \tag{2.2}$$

---

[2]Again, real-world concerns like finite switching times and the insertion of blanking time are ignored. For example, when both transistors are in the blocking state, the polarity of the midpoint voltage is determined by the sign of the current.

i.e. d may be determined uniquely from the waveform q. On the other hand, it should be noted that the course of q within the same interval $[t_0; t_0 + T]$ cannot uniquely be determined for a given value of d. As will be demonstrated in section 2.4, advantage of this trivial ambiguity may be taken in order to randomize the switching patterns.

Referring to [4] again, d relates to a macroscopic time scale in order to emphasize the loss of detailed information about the exact course of q. For the purpose of designing control laws, it is normally sufficient to model the converter on this macroscopic time scale, which carries information of the average quantities only.

Now, the ideal average voltage $\bar{u}$ produced by the half-bridge shown in Fig. 2.2 may be found simply as $\bar{u} = (d - \frac{1}{2})U_{dc}$. In dc/dc converters, the value of $\bar{u}$ and therefore also d is constant in steady state, whereas in dc/ac converters d must have periodical variations in order to synthesize an alternating output voltage. Precise control of d must be assured in randomized converters as well.

2.3   Voltage control of converters by PWM

The issue of converting a voltage from one type into another by means of a converter (which needs not to be static) has a long and rich history going back to the dawn of the century, see [5] for a review of the historical development. It seems that the major breakthrough for the use of PWM together with static converters took place in 1964 in Switzerland, thanks to Schönung and Stemmler [6]. This comprehensive paper presents an adjustable-speed drive comprising a pulse-width modulated hard-switched converter based on thyristors with added turn-off circuits. Although technological advances in micro electronics and power electronic devices have lead to many improvements since 1964, these fundamental ideas for power conversion are still in use. Also in 1964, the book [7] by Bedford appeared.

The principle itself of conveying information by PWM was pioneered by researchers belonging to the communication theory society many years before [6] was published. The esteemed 1953 monograph [8] — acknowledged by the classic paper [9], among others — refers to a US patent filed in 1928 besides numerous publications in the nineteen forties dealing with details of pulse-width modulation.

A detailed review of the current state-of-the-art of PWM in power electronics falls beyond the scope of this chapter; [10] may be consulted for a recent review. In the first subsection below focus is rather put on space vectors and their use for voltage synthesis of three-phase VSC's. One of the characteristics that differentiates the PWM techniques is the used reference waveform; this subject is treated in subsection 2.3.2 in order to assure that the subsequent analysis of random PWM schemes complies with commonly used modulation waveforms.

2.3.1   Space vectors and switching vectors

Complex-valued space vectors were invented by Kovács and Rácz in 1959 [11] to aid the analysis of machine dynamics. The theory stems from the spatial distribution of the windings in sinusoidal-wound three-phase ac machines, but the technique is also applicable to non-distributed three-phase circuits including filters, converters, etc.

Formally, space vectors are defined by

$$\boldsymbol{y}^s = \tfrac{2}{3}\left(y_a + \boldsymbol{a}y_b + \boldsymbol{a}^2 y_c\right), \quad \boldsymbol{a} \triangleq e^{j\frac{2\pi}{3}}, \tag{2.3}$$

where y_a, y_b, and y_c constitute a set of three-phase time-varying variables, e.g. voltages, currents, or flux linkages, and $\boldsymbol{y}^s$ is the equivalent complex-valued representation of that set. Other values than $\tfrac{2}{3}$ for the scaling factor are also used: [12] uses no scaling at all whereas the factor $(\tfrac{2}{3})^{0.5}$ is commonly used in power systems engineering.

Essentially, the mapping (2.3) transforms a three-phase system into an equivalent orthogonal two-phase system, whose real and imaginary axes are normally denoted by α and β, respectively. All space vectors expressed in $\alpha\beta$-coordinates are appended an s superscript as in $\boldsymbol{y}^s$ to indicate that the vector is referred to a stationary reference frame. The complex-valued space vector $\boldsymbol{y}^s$ may be resolved into its real y_α and imaginary y_β components, i.e. $\boldsymbol{y}^s = y_\alpha + jy_\beta$.

Also, the following transformations between phase quantities and their associated space vector may be obtained from (2.3):

$$\begin{bmatrix} y_\alpha \\ y_\beta \end{bmatrix} = \begin{bmatrix} \mathcal{R}(\boldsymbol{y}^s) \\ \mathcal{I}(\boldsymbol{y}^s) \end{bmatrix} = \tfrac{2}{3} \begin{bmatrix} 1 & -\tfrac{1}{2} & -\tfrac{1}{2} \\ 0 & \tfrac{\sqrt{3}}{2} & -\tfrac{\sqrt{3}}{2} \end{bmatrix} \begin{bmatrix} y_a \\ y_b \\ y_c \end{bmatrix} \tag{2.4}$$

$$\begin{bmatrix} y_a \\ y_b \\ y_c \end{bmatrix} = \begin{bmatrix} \mathcal{R}(\boldsymbol{y}^s) \\ \mathcal{R}(\boldsymbol{a}^2\boldsymbol{y}^s) \\ \mathcal{R}(\boldsymbol{a}\boldsymbol{y}^s) \end{bmatrix} = \begin{bmatrix} 1 & 0 \\ -\tfrac{1}{2} & \tfrac{\sqrt{3}}{2} \\ -\tfrac{1}{2} & -\tfrac{\sqrt{3}}{2} \end{bmatrix} \begin{bmatrix} y_\alpha \\ y_\beta \end{bmatrix}, \tag{2.5}$$

where $\mathcal{R}(\cdot)$ and $\mathcal{I}(\cdot)$ are the real and imaginary parts of the argument, respectively.

The universality of the transformation (2.3) implies that it is valid not only under steady-state, symmetrical, sinusoidal conditions, but also for arbitrary waveforms as long as the instantaneous sum equals zero. In fact, for three-phase systems without a neutral connection, zero-sequence currents cannot flow, and in that case the use of the three-to-two phase transformation may still be justified, even if the sum of the voltages is non-zero [12] — this is the case for the output voltage of a three-phase VSC. In cases with finite zero-sequence impedance, an equation for the zero-sequence component must be included as well. Further details of the definitions and properties of space vectors may be found in e.g. [11–13].

Switching vectors for three-phase converters

In the three-phase converter in Fig. 2.3(a), each of the three half-bridges may be controlled independently and, therefore, the converter is capable of operating in eight different states. Using the standard binary notation [10, 14], it should be noted that the two zero-voltage space vectors $\boldsymbol{v}_{000}$ and $\boldsymbol{v}_{111}$ short-circuit the load terminals leaving only six different vectors for the active control of the load, see Fig. 2.3(b). Using (2.3), it may be shown by transformation of the set of voltages $\{u_{ag}, u_{bg}, u_{cg}\}$ for the possible combinations of the switching functions $\{q_a, q_b, q_c\}$ that the six active vectors expressed in the $\alpha\beta$-coordinate system are

$$\boldsymbol{v}_n = \tfrac{2}{3}U_{dc}\, e^{j\theta_n}, \quad \theta_n = \tfrac{\pi}{3}(n-1) \quad \text{for} \quad 1 \le n \le 6. \tag{2.6}$$

(a)

(b)

(c)
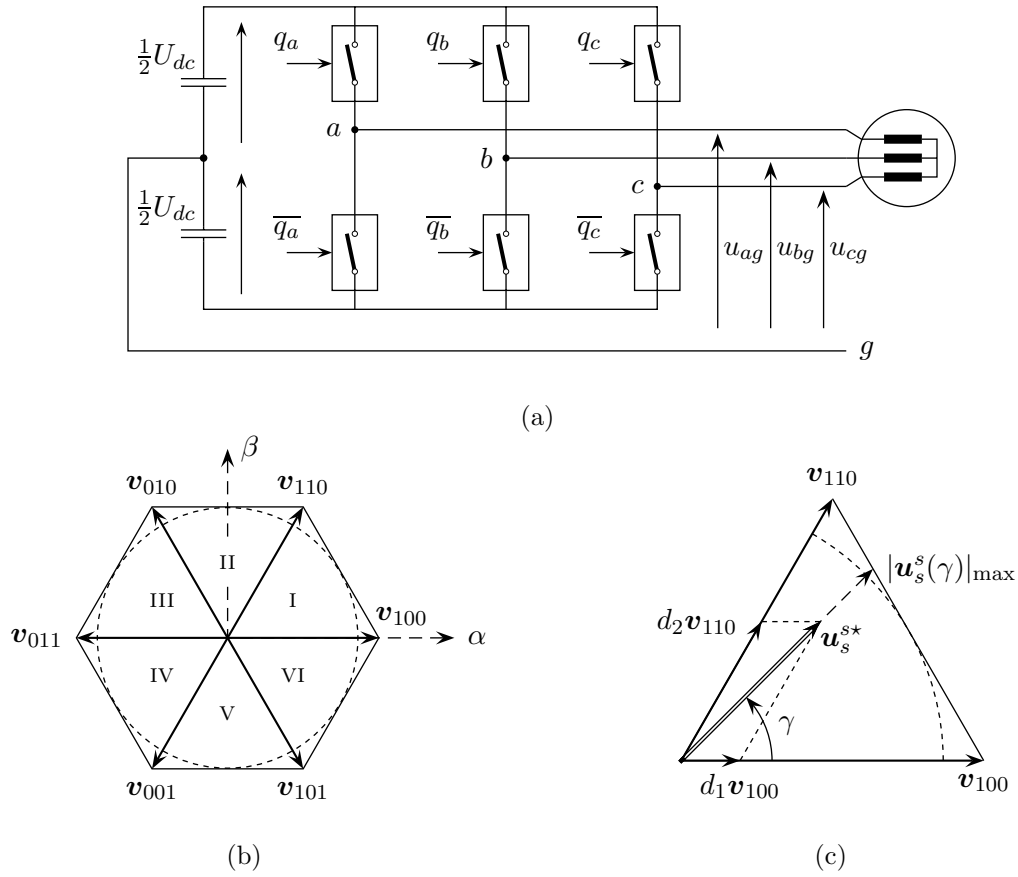
Figure 2.3 Three-phase voltage-source converter: (a) circuit diagram, (b) possible voltage space vectors in $\alpha\beta$ coordinates, and (c) decomposition of a voltage vector into two adjacent switching vectors by space-vector modulation.

The amplitude of the active switching vectors equals $|\boldsymbol{v}_n| = \frac{2}{3}U_{dc}$ and they are spaced $\pi/3$ radians apart.

Space-vector modulation (SVM)

Following the 1982 publications [15–17], an arbitrary voltage space vector $\boldsymbol{u}_s^{s\star} = |\boldsymbol{u}_s^{s\star}|e^{j\gamma}$ belonging to the interior of the hexagon in Fig. 2.3(b) may be decomposed into two adjacent active vector components. For the sake of simplicity, it is assumed that the reference falls within the first sector where $\boldsymbol{u}_s^{s\star} = d_1\boldsymbol{v}_{100} + d_2\boldsymbol{v}_{110}$ as shown in Fig. 2.3(c). The duty ratios d_1 and d_2 may be found by vector algebra and a few trigonometric identities as:

$$d_1 = \sqrt{3}\frac{|\boldsymbol{u}_s^{s\star}|}{U_{dc}}\sin(\tfrac{\pi}{3} - \gamma), \tag{2.7}$$

$$d_2 = \sqrt{3}\frac{|\boldsymbol{u}_s^{s\star}|}{U_{dc}}\sin\gamma. \tag{2.8}$$

The corresponding widths of the application of the active vectors are $t_1 = d_1 T$ and $t_2 = d_2 T$, respectively, where T is the duration of the whole modulation interval.
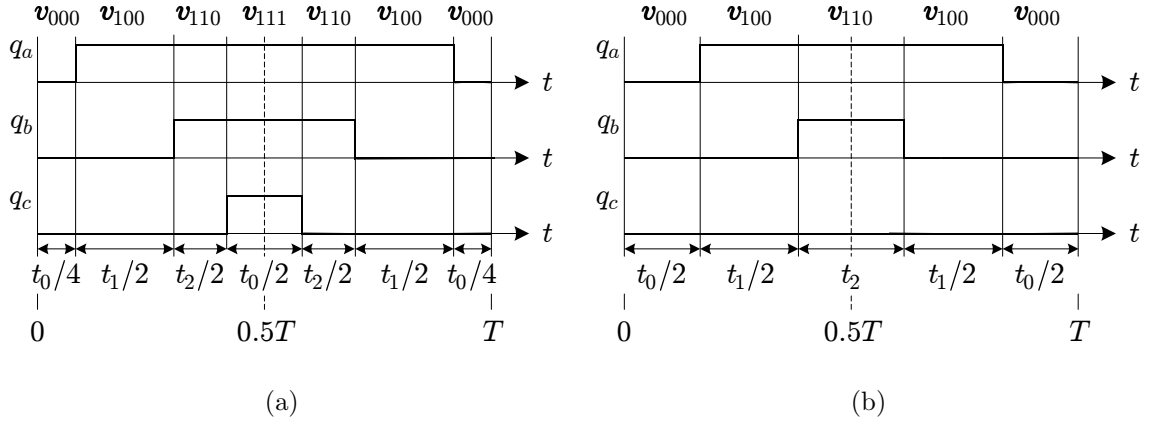
Figure 2.4 Example of switching functions produced by (a) standard SVM and (b) modified SVM. In both cases, the same average voltage vector is generated.

During the remaining time $t_0 = (1 - d_1 - d_2)T$, zero vectors should be applied. In the classic SVM scheme, t_0 is divided into four parts of equal duration, i.e. in sector I the switching sequence becomes

$$\begin{aligned}
&\boldsymbol{v}_{000}\langle t_0/4 \rangle \rightarrow \boldsymbol{v}_{100}\langle t_1/2 \rangle \rightarrow \boldsymbol{v}_{110}\langle t_2/2 \rangle \rightarrow \boldsymbol{v}_{111}\langle t_0/4 \rangle \rightarrow \\
&\boldsymbol{v}_{111}\langle t_0/4 \rangle \rightarrow \boldsymbol{v}_{110}\langle t_2/2 \rangle \rightarrow \boldsymbol{v}_{100}\langle t_1/2 \rangle \rightarrow \boldsymbol{v}_{000}\langle t_0/4 \rangle.
\end{aligned} \tag{2.9}$$

The $\langle \cdot \rangle$ symbol is used to indicate the duration of the associated vector [10]. The sequence (2.9) maps into the switching functions in Fig. 2.4(a). Note that all legs are switched twice in each period T and that the switching functions are symmetric around $\frac{1}{2}T$.

Another variant of SVM, which only gives four commutations per PWM period, may also be used [18]:

$$\begin{aligned}
&\boldsymbol{v}_{000}\langle t_0/2 \rangle \rightarrow \boldsymbol{v}_{100}\langle t_1/2 \rangle \rightarrow \boldsymbol{v}_{110}\langle t_2/2 \rangle \rightarrow \\
&\qquad \boldsymbol{v}_{110}\langle t_2/2 \rangle \rightarrow \boldsymbol{v}_{100}\langle t_1/2 \rangle \rightarrow \boldsymbol{v}_{000}\langle t_0/2 \rangle.
\end{aligned} \tag{2.10}$$

Here, one of the legs is not switched because the available zero-vector time t_0 is assigned to one zero vector only. This sequence is shown in Fig. 2.4(b).

Voltage limitations in three-phase converters

The maximum voltage capability $|\boldsymbol{u}_s^s(\gamma)|_{\max}$ of a VSC depends on the reference angle γ as indicated in Fig. 2.3(c). The peak value may be found by using (2.7) and (2.8) under the constraint that $d_1 + d_2 = 1$. Hence,

$$1 = \sqrt{3}\,\frac{|\boldsymbol{u}_s^s(\gamma)|_{\max}}{U_{dc}}\left(\sin(\tfrac{\pi}{3} - \gamma) + \sin\gamma\right) \tag{2.11}$$

$$\Leftrightarrow |\boldsymbol{u}_s^s(\gamma)|_{\max} = \frac{U_{dc}}{\sqrt{3}\cos(\tfrac{\pi}{6} - \gamma)}, \quad 0 \le \gamma \le \tfrac{\pi}{3}. \tag{2.12}$$

By sweeping through the $\gamma = [0; \frac{1}{3}\pi]$ interval, it may be shown that the matching $|\boldsymbol{u}_s^s(\gamma)|_{\max}$ values constitute the line connecting the tips of $\boldsymbol{v}_{100}$ and $\boldsymbol{v}_{110}$, see Fig. 2.3(c).

For continuous operation without overmodulation, the maximum voltage capability for the SVM technique is $U_{dc}/\sqrt{3}$, which is the value obtained by (2.12) for $\gamma = \pi/6$. If the amplitude of the reference voltage vector is below this value, the converter can maintain the proper volt-second balance on the macroscopic time scale. Otherwise, the volt-second balance is lost on the macroscopic scale, but using special overmodulation techniques it is, however, possible to preserve the balance on a per fundamental output period basis on the expense of low-order harmonics [19, 20].

2.3.2 Unification of carrier-based and space-vector PWM

There is no doubt that SVM has been very popular ever since its introduction in the eighties, but judging from the trends of the trade, the original per-phase modulators are gaining an increased interest again. Forecasting the upcoming analysis of different random PWM techniques, it will be advantageous to be able to encompass these conceptually different kinds of modulators into a common framework. This task may be accomplished by the modulator structure shown in Fig. 2.5, which may be found directly in [21, 22] and in [23] specifically for an analog SVM implementation.

Description of generalized modulator

The input to the modulator is the balanced set $\{u_a^\star, u_b^\star, u_c^\star\}$ representing the instantaneous values for the reference voltages to be modulated by the converter[3]:

$$
\begin{bmatrix} u_a^\star \\ u_b^\star \\ u_c^\star \end{bmatrix} = U_1^\star \begin{bmatrix} \sin(\gamma) \\ \sin(\gamma - \frac{2\pi}{3}) \\ \sin(\gamma - \frac{4\pi}{3}) \end{bmatrix},
\tag{2.13}
$$

i.e. $\{u_a^\star, u_b^\star, u_c^\star\}$ is uniquely determined by the peak value $U_1^\star$ and the reference angle γ for phase a. Depending on the wanted characteristics, a zero-sequence voltage u_0 may be added to all phases, i.e. the modified references become $u_a^{\star\star} = u_a^\star + u_0$, etc. Specific choices of u_0 are commented below. By comparing the modified reference waveforms to a triangular carrier waveform, the switching functions for all three legs are generated by the comparators. The depicted signal flow diagram may be implemented in analog or digital hardware; in the digital implementation the reference waveforms are sampled once or, possibly, twice per carrier period, see Fig. 2.5(b).

The peak values of the carrier waveform are $\pm\frac{1}{2}U_{dc}$, i.e. during normal operation the duty ratios become

$$
d_x = \frac{1}{2}\left(1 + \frac{u_x^{\star\star}}{\frac{1}{2}U_{dc}}\right), \quad \text{for } x \in \{a, b, c\}.
\tag{2.14}
$$

Note[4] that this equation requires that the modified reference signals adhere to $|u_x^{\star\star}| \leq \frac{1}{2}U_{dc}$. The selection of u_0 has a high influence on when this condition is violated, and

---

[3]If the reference voltages are packed into an equivalent space vector $\boldsymbol{u}_s^{s\star}$, the needed per-phase voltages may easily be found by (2.5).

[4]Overmodulation is not considered in any details in this thesis, although much of the work can be extended to this range of operation. Equation (2.14) is one of the exceptions.
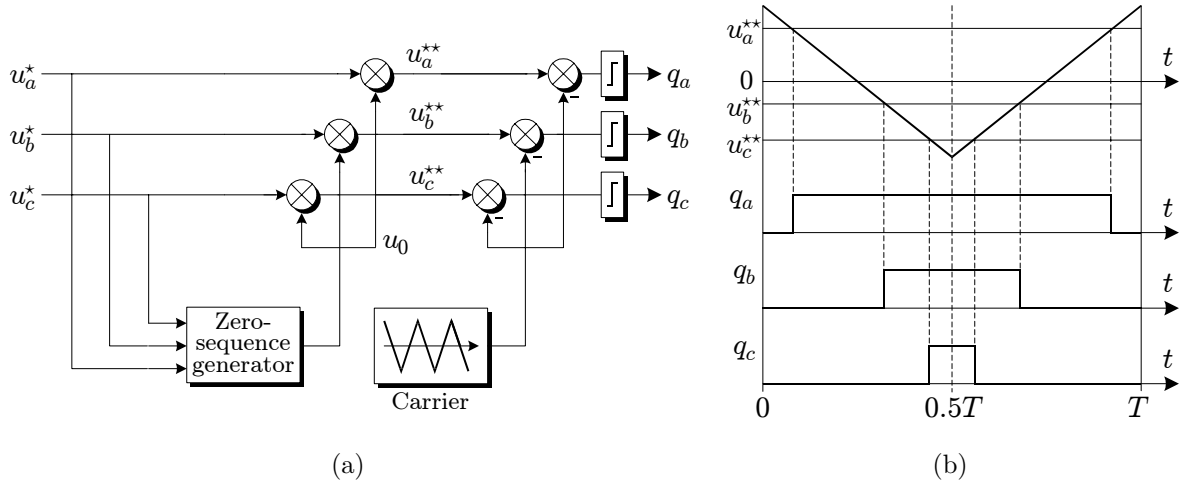
Figure 2.5 Generalized pulse-width modulator based on injection of a zero-sequence voltage. (a) Block diagram and (b) generation of switching functions on the microscopic time scale (the reference waveforms are sampled once per carrier period).

in order to compare different techniques, the modulation index (or depth) m is often used. m represents the normalized amplitude of the fundamental component of the modulated voltage. In the multitude of publications on PWM, different normalizations for m may be found, but the prevailing definition seems to be

$$m = \frac{U_1}{U_{1,\,\text{six-step}}}, \tag{2.15}$$

where $U_{1,\,\text{six-step}} = \frac{2}{\pi}U_{dc}$ is the peak value of the fundamental phase-to-neutral voltage in six-step operation [10]; U_1 is the peak value of the fundamental component of the produced output voltage. This definition is adopted by [10, 24], and many others. Another popular definition requires that U_1 is divided by $\frac{1}{2}U_{dc}$. Using the definition (2.15), $m = 1$ can be attained only in six-step operation, whereas for the $\frac{1}{2}U_{dc}$ normalization, the modulation index is $\frac{4}{\pi} \approx 1.273$ in six-step mode.

For the ideal modulator $U_1 = \max(u_a^\star) = U_1^\star$, but when the modulator saturates (i.e. when $|u_x^{\star\star}| > \frac{1}{2}U_{dc}$), the equality between the reference peak value $U_1^\star$ and actually produced value U_1 is lost. For the sinusoidal modulator used originally in [6], the maximum modulation index is $m_{\max} = \pi/4 = 0.785$. For the SVM techniques described in the previous subsection, the maximum value becomes $m_{\max} = \sqrt{3}\pi/6 = 0.907$, which is the theoretically largest modulation index for continuous operation, i.e. without entering the pulse-dropping region.

Common zero-sequence voltage injection methods

Research has uncovered that the selection of the zero-sequence voltage u_0 has a large impact on the switching losses, on the current distortion, and on the maximum obtainable modulation index [4, 22]. Many publications have dealt with the selection of u_0, but according to [24] only a handful of useful methods exists. The four examples shown in Fig. 2.6 are commented below.

The pioneering 1975 work by Buja and Indri [25] suggested to select $u_0 = \frac{1}{6}U_1^\star \sin(3\gamma)$ to increase the maximum output voltage. Using such a third harmonic injection (THI),

the maximum modulation index becomes $\sqrt{3}\pi/6 = 0.907$ before pulse-dropping begins. Sample waveforms are shown in Fig. 2.6(b).

It has been demonstrated by [23, 24, 26, 27] that for the SVM technique the value of u_0 should be selected according to this procedure: among the three references $u_a^\star, u_b^\star$, and $u_c^\star$ the signal with the smallest absolute value is found. Next, u_0 is set to this value divided by 2. For example, if $|u_b^\star| < |u_c^\star| < |u_a^\star|$ then $u_0 = \frac{1}{2}u_b^\star$. In this way, the almost triangular waveform for u_0 shown in Fig. 2.6(c) may be obtained. This establishes a link between classic SVM and carrier-based modulators.

It should be noted, however, that already in 1974, King realized in [28][5] that the addition of a zero-sequence voltage can be used to get a higher voltage utilization ratio compared to sinusoidal modulation. Also, [28] suggested a very simple analogue rectifier circuit to extract a u_0 waveform from the reference voltages. In fact, the resulting u_0 waveform in [28] is identical to the u_0 waveform generated by SVM; King should be acknowledged for this achievement which has apparently been completely overlooked by the power electronics community.

The examples mentioned so far are generally classified as continuous PWM techniques, whereas the last example shown in Fig. 2.6(d) belongs to a class of discontinuous modulation methods. These methods are characterized by the fact that only two of the three legs are modulated in each carrier period, i.e. no switchings occur in the remaining leg. The method used in Fig. 2.6(d) prevents switchings in the leg with the largest absolute value of the references, i.e. if $|u_a^\star| < |u_c^\star| < |u_b^\star|$, then $u_0 = \frac{1}{2}\text{sign}(u_b^\star)U_{dc} - u_b^\star$ [24, 29]. Note the similarities between discontinuous PWM and the modified SVM in Fig. 2.4(b).

For a fixed value of T, discontinuous PWM methods are, in theory, able to reduce the switching losses to 50 percent of the losses during continuous PWM operation and simultaneously, the maximum modulation index can be maintained at $\sqrt{3}\pi/6 = 0.907$ as for SVM. Alternatively, for the same losses, it is possible to get a lower harmonic current distortion by using DPWM compared to SVM. Details may be found in e.g. [4, 20, 22, 24].

Advantages of the generalized modulator

One of the salient features of the generalized modulator is that transitions between different modes of operation can be accomplished by simply changing the injected voltage u_0; the modulator structure itself remains the same. Such properties are clearly advantageous, because in industrial applications different modulators may be used in different operating regions. For example, the performance (in terms of current distortion versus switching losses) of the SVM is superior to the discontinuous modulators only for modulation indices below approximately 0.6 [20]. Above this value, some of the DPWM techniques analyzed in [4, 22, 24] offer substantially less current distortion for the same switching losses.

Apart from a seamless transition between different modes, the modulator structure in Fig. 2.5 also offers an elegant solution with respect to implementation in, for example, a digital signal processor (DSP). In fact, as stated in [24], a carrier-based generalized modulator using simple magnitude comparison tests to determine u_0 is much

---

[5]The author became aware of this remarkable paper thanks to [22].
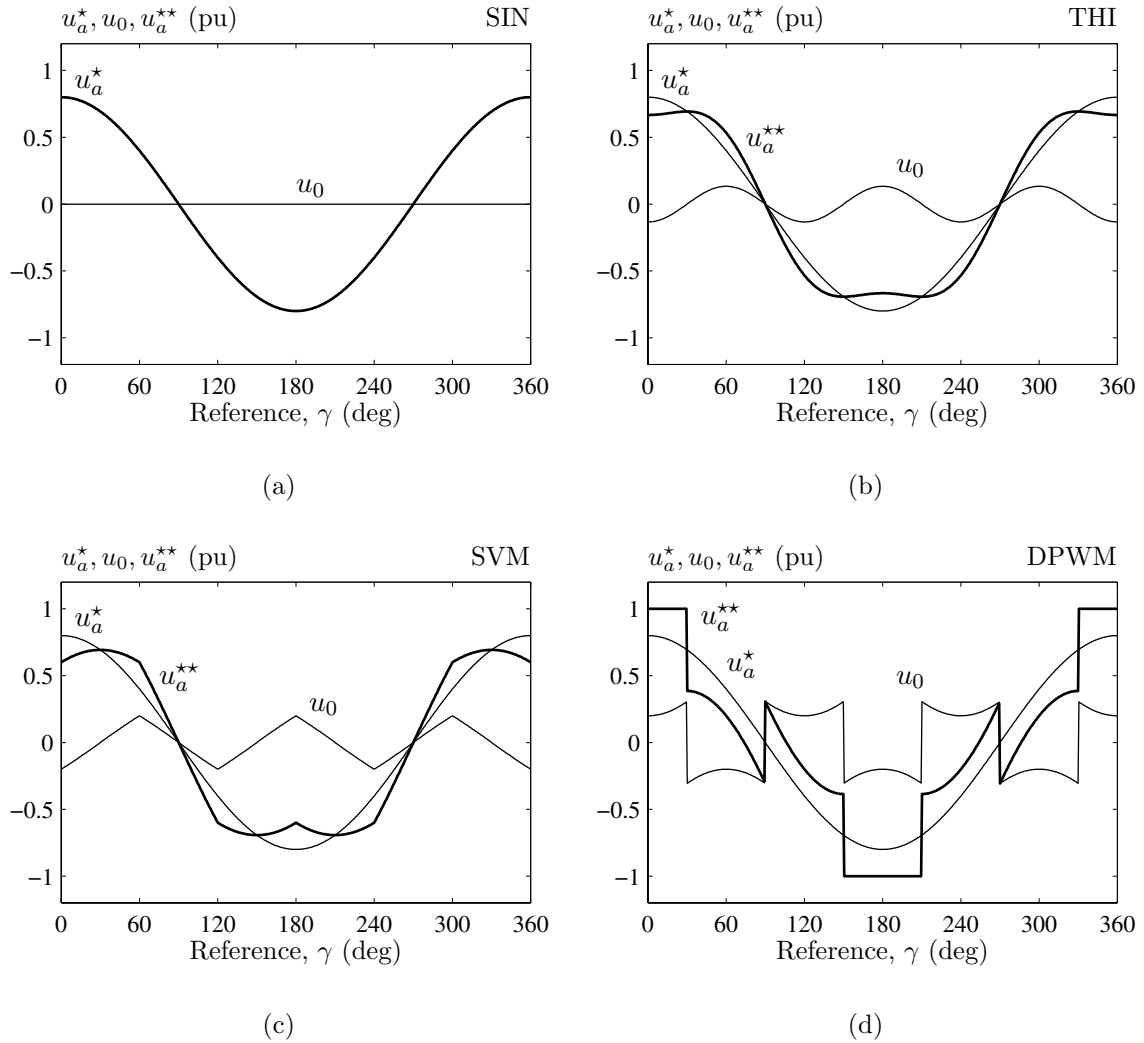
Figure 2.6 Examples of modulation waveforms based on injection of a zero-sequence voltage. The reference waveforms are normalized by $\frac{1}{2}U_{dc}$. (a) Purely sinusoidal (SIN) modulation, (b) one-sixth third harmonic injection (THI), (c) space-vector modulation (SVM), and (d) discontinuous modulation (DPWM).

easier to implement than the traditional digital approach to SVM. The latter requires many sequential operations: (a) identification of the sector which the reference voltage belongs to, (b) calculation of the active vector duty ratios d_1 and d_2 besides the zero-vector time t_0, (c) determination of the phase duty ratios, and (d) determination of the sequence in which the phases must be switched.

On the other hand, for the generalized modulator, the task is simple because the phase duty ratios follow directly from (2.14) once the value of u_0 is added to the reference voltages. Using the SVM technique as a benchmark, the calculation of u_0 is also simple because u_0 can be determined (as mentioned above) by a comparison of the magnitudes of the original references without using any trigonometric functions at all. For completeness, it should be mentioned that the input to the modulator may very well be given as a space-vector $\boldsymbol{u}_s^{s\star}$, either in polar or in rectangular form, and not as three phase voltages. However, even in this case the linear algebraic transformations

given by (2.5) into the equivalent phase voltages do not add much overhead.

The generalized modulator has been used in the experiments and the simulations reported in this thesis, because this approach makes it simple to toggle between different modulation techniques, such as SIN, SVM, and DPWM.

As it turns out in Part II, another advantage is that the phase duty ratios d_a, d_b, and d_c are calculated directly by the generalized modulator, because the spectral analysis requires knowledge of phase duty ratios themselves rather than knowledge of the duty ratios for the active vectors.

2.4   Overview of random pulse-width modulation

The general principles of random modulation are considered in this section. The presentation is made without mathematics in order to focus on the principles of random PWM rather than on a detailed analysis.

The outline is as follows: first, the basic ideas of random PWM are explained and then, a number of more sophisticated randomization principles are discussed in order to demonstrate alternative ways to inject uncertainty into a modulator. Next, a discussion is given of problems that may be encountered in some converter topologies if a classic deterministic modulator is replaced with a randomized modulator. Finally, the random PWM schemes selected for further analysis in this thesis are presented.

2.4.1   Fundamentals of random modulation

The starting point is the definition (2.2) on page 21 of the duty ratio d. To streamline the notation, it is assumed that observation interval at hand begins at time zero, i.e.

$$d = \frac{1}{T} \int_0^T q(t) \, dt. \tag{2.16}$$

It should be recalled that the duty ratio relates to the macroscopic time scale (a per carrier-period average), but the state of the switching function q must be defined for all time instants, i.e. on the microscopic time scale.

Now, the overall objective of a modulator is to map a reference value for d into a switching function $q(t)$ for $t = [0; T]$ in such a way that (2.16) is fulfilled. Clearly, this mapping is not one-to-one: for a certain value of d, no unique q can be determined. To circumvent this ambiguity, constraints are added in classic modulators in order to get a unique correlation between d and q: typically, the value of the T is fixed and, furthermore, a certain pulse position is specified as well (leading-edge, lagging-edge, or center-aligned). Imposing such constraints, a unique course for q in (2.16) may be determined for a specific value of d. Fig. 2.7(a) shows an example using center-aligned pulses.

The fundamental idea behind random PWM is to relax the standard constraints of fixed carrier period and, say, center-aligned pulse positions in order to leave room for the randomization: it follows directly from (2.16) that within a carrier interval T the switching function q may be altered in the following ways without distorting the value of d:
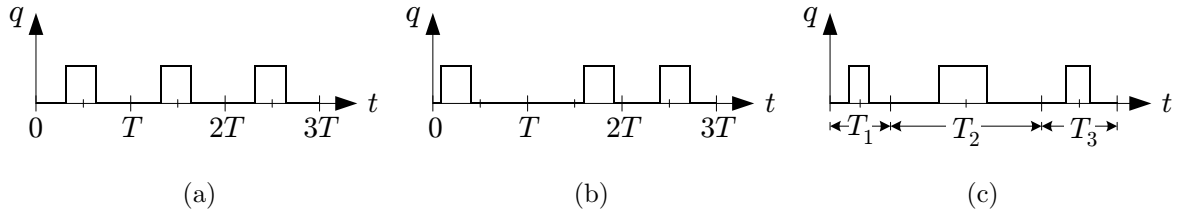
Figure 2.7 Fundamental principles of random pulse-width modulation. Illustration of (a) deterministic, (b) random pulse position, and (c) random carrier frequency modulation. The duty ratio is the same in all examples.

Random pulse position (RPP) modulation [30, 31]

The position of the on-state pulse of width dT is randomized within each interval of constant duration T. The displacement should be selected so that the edges of the pulse do not extend into the adjacent PWM intervals to prevent overlap and to assure that the switching function is implementable in real-time systems.

Random carrier frequency (RCF) modulation [32–35]

The duration of the carrier frequency, or, equivalently, the carrier period T is randomized while the duty ratio d is kept constant, i.e. the width of the pulse is changed in proportion to the instantaneous value of T. Also, the pulse position is fixed, e.g. the leading pulse edge is aligned with the beginning of each T.

The two complementary ways to randomize a modulator are illustrated in Fig. 2.7(b) and Fig. 2.7(c), respectively. It is important to note that both methods guarantee that the average of the q waveform equals d in each carrier period, i.e. the volt-second balance is maintained on the macroscopic scale.

Aspects of implementation of random modulation

To facilitate the discussion, the principles for implementation of random PWM techniques are briefly described below. It is impossible to give detailed guidelines, because the implementation depends strongly on the hardware used for the pulse-width modulator. However, irrespective of the hardware, it is evident that apart from the normal input signals to the modulator, a randomized modulator must rely on at least one additional input in order to quantify the randomization. This extra input is a variable x, and, in addition, x should be a random variable in the sense known from the theory of stochastic processes.

To fix the ideas, the block diagram shown in Fig. 2.8 for the RCF technique introduces some of the key elements. The modulator should convert the duty ratio d and the carrier period T into a switching function q, which governs the state of the converter. Clearly, the details of how the modulator interfaces with the converter are hardware specific; the hardware used may very well contain specialized peripheral circuits like dedicated PWM timers, which can be programmed through a set of registers, but many other solutions do also exist. The hardware used in all the experiments shown in this thesis is described in more details in Appendix A.

Once the duty ratio d in Fig. 2.8 has been calculated by a modulator (Fig. 2.5, for example) the next step for the RCF technique is to determine the value T for carrier period. To fulfil this task, two functions are needed:
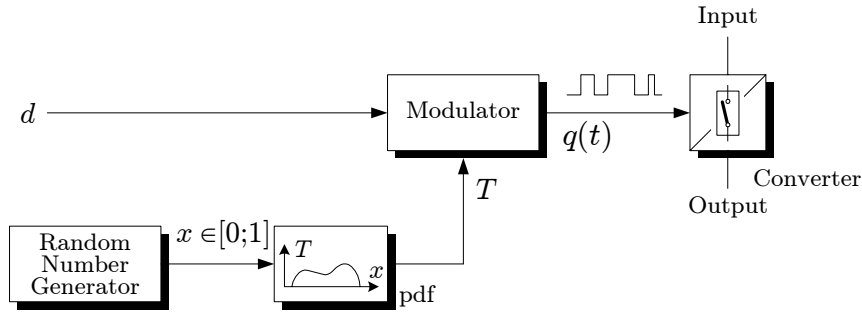
Figure 2.8 Example of an overall implementation of an RCF-based pulse-width modulator.

1. **A random number generator (RNG)**
   In each new carrier period, the RNG calculates a value for the random variable x, which is used below. Normally, an RNG generate uniform deviates in the $x \in [0;1]$ range, i.e. all values between zero and one occur with the same probability. More information may be found in Appendix A.

2. **A probability density function (pdf)**
   The value x is now used to get the value for the carrier period in the particular PWM period at hand. The precise mapping from x to T is determined by a pdf as indicated in Fig. 2.8. More details on this step may be found in Chapter 5.

The block diagram in Fig. 2.8 only serves as an example of the implementation of an RCF modulator. Over the years, many different implementations have been suggested (both software- and hardware-based). Some of these techniques are collected in [36], but it is important to recall that they share the property that a noise source is needed to generate a random variable, which then is processed in some way to get T.

2.4.2   Overview of candidate randomization methods

Apart from the two fundamental techniques, RPP and RCF, many other possibilities exist as well. Some of the principles discussed below have been presented in the literature; other principles offspring as generalizations of those known methods. No attempts are made to cite all references used in the investigation; references are only made to the primary sources. More exhaustive lists of references may be found in the review papers [36–38] besides the bibliography in Appendix B.

Unity-gain versus random-gain methods

The RPP and RCF methods may be regarded as belonging to a class of unity-gain methods, because they guarantee that the actual average of $q(t)$ equals the reference value for d in each cycle of the carrier. The random-gain methods are different: this class relies on dithering principles that introduce a random component into the gain of the modulator, i.e. an exact volt-second balance is not assured. In fact the first application of random modulation in power electronics is a random-gain modulator: [39, 40] adds a noise signal with a long-term zero-mean value to the reference voltage.

   Another example of a random-gain method includes the first published randomization technique for a three-phase VSC. In [41] the controller outputs a new voltage
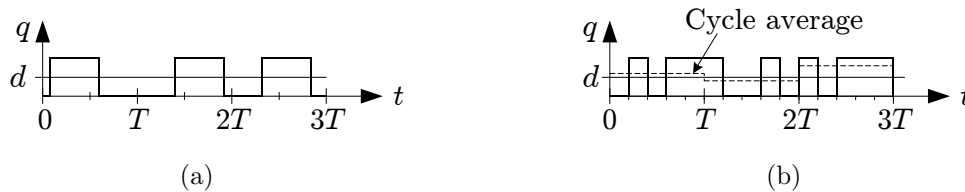
Figure 2.9 Example of (a) a unity-gain (RPP) and (b) a random-gain modulation method where each sampling period of width T is divided into $N = 5$ sub intervals.

reference each T seconds. This interval is divided into N sub-intervals of equal duration $T_N = T/N$, and within each T_N, the outcome of a random number generator is used to select the value of the switching function such that the average value of q measured across the whole interval T approximates the reference duty ratio. This is illustrated in Fig. 2.9(b) for $N = 5$. Strictly speaking, this method is not pulse-width modulation in the classic sense, but rather an example of a discrete-time[6] modulator.

In general, the random-gain methods suffer from three defects: (a) there is a non-zero error between the reference and the synthesized voltage, (b) a very high sampling to fundamental frequency ratio (in the order of 480 kHz to 50 Hz according to [41]) is required to get a satisfactory performance, but still the capability of tracking the reference duty ratio is poor in the low modulation index range, and (c) dedicated hardware circuits are needed to realized these high sampling rates.

Apart from [41], a closely related random-gain method intended for dc/ac conversion has been studied by [44] and in a dozen companion papers from the same group of researchers. Even though it is claimed that the sampling frequency can be reduced to 30 kHz, the fundamental problems still remain. Slightly different random-gain methods applicable for single-switch dc/dc converters have been investigated in [33, 45], but again the randomization is added at the expense of a unity gain.

In summary, it is hard to justify the use of random-gain methods in non-academic applications.

Single versus multiple random variable methods

It has implicitly been assumed so far that either only one switching function is available for randomization or that the same random variable x is used to dither all switching functions in a converter with multiple switches (and switching functions). For example, in the RPP technique originating from [30], the same random pulse position (leading- or lagging-edge modulation — abbreviated RLL) is used for all three legs of a three-phase converter in a certain carrier period as shown in Fig. 2.10(a). In order to emphasize that this particular RPP technique uses the same random variable to dither all phases in a three-phase converter, it may be said that the technique belongs to the class of single random variable methods.

Other examples of random PWM techniques belonging to this class may be found in e.g. [34, 46–48], which all treat variants of the RCF technique. Also, [49] and to a lower extent [21], both use a single random variable to dither the magnitude of the

---

[6]Discrete-time modulators are useful for the control of resonance converters [42] by means of sigma-delta modulation. Other variants of discrete-time modulation may also be used for a standard hard-switched VSC [43] in conjunction with a simple scalar controller.
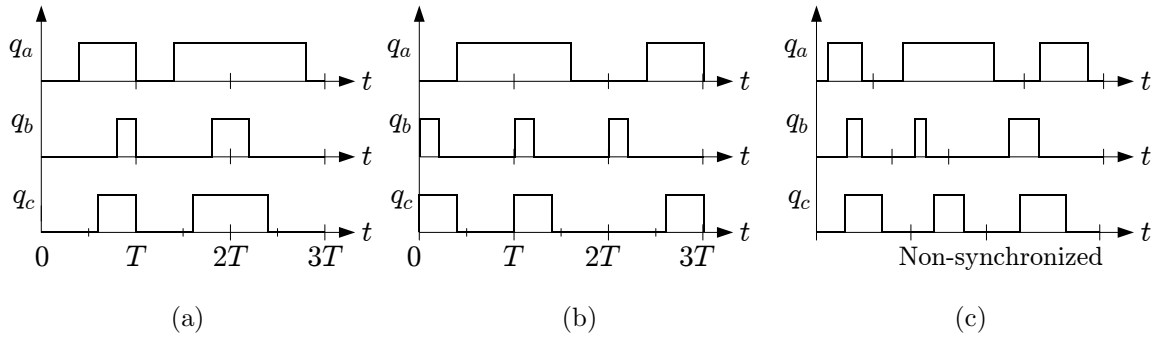
Figure 2.10 In multi-leg systems the randomization may be (a) the same on all legs using the same random variable (RLL example shown). (b) and (c) show examples of the RLL and the RCF techniques where different random variables (pulse position and carrier widths, respectively) are used to control each leg individually.

zero-sequence voltage u_0 (recall Fig. 2.5) injected into a modulator for a three-phase voltage-source converter.

Unlike the single random variable methods discussed so far, the multiple random variable methods do not rely on a single random variable, but rather on several random variables limited in number by the number of switching functions needed to control a certain converter. Using the RLL technique as an example again, it is possible to extend the original idea of [30] to use different pulse alignments in each leg, see Fig. 2.10(b). Here, three random variables are generated in each period T in order to modulate each leg individually. To the knowledge of the author, this simple modification has never been investigated, despite that the RLL technique has been investigated in many other publications [31, 45, 50, 51] apart from [30].

It is possible to extend the RCF technique in a similar manner: by using different values for the carrier frequency for each leg in a converter, another multiple random variable method arises, see Fig. 2.10(c). Unfortunately, this kind of asynchronous operation among the legs does not comply well with real-time digital implementations in micro-controllers and the like, but, in principle, it is straightforward to do this kind of randomization in analog hardware, where carrier signals with different slopes could be used in each phase. For instance, analog implementations of RCF modulation have been reported in [32–34].

For completeness, it should be mentioned that using different methods for each leg is also a possibility, which has never been pursued in the literature. For example, leg a could be controlled by some RPP method and the two other phases could be controlled by the RCF technique. Other combinations could also be used.

To the knowledge of the author, the family of multiple-variable methods introduced above has never been studied nor reported in the literature. Certainly, they add complexity to the implementation compared to the single-variable methods, but at least the modified RLL technique (or other methods based on RPP) could be implemented without much computational overhead. Whether these kinds of methods are better in terms of acoustic annoyance suppression than the other methods remains an unanswered question, but in theory the proper macroscopic voltage balance can be assured.

Time-invariant versus time-varying randomization methods

A common feature for the methods considered until now is the fact that the same kind of randomization is applied in all carrier periods: in the RPP technique, a new pulse placement is chosen in each interval, but the underlying randomization mechanism remains the same. These kinds of methods may be characterized as being a part of a time-invariant family of methods. Again, it is not necessary to impose this time-invariance constraint upon the modulator. Heavily based on the ideas of [45], the following kind of time-varying methods may be devised:

Random choice of random modulation

In each carrier period one out of two predetermined randomization methods is selected according to some probability law. Then, another independent random variable determines the appropriate parameter associated with the selected method. Ref. [45] applies this idea for the RPP and the RCF techniques, but obviously the number of methods can be larger than two and other methods can also be used.

Cascaded random modulation

Here, two or more random modulation methods are applied simultaneously, based on one or two random variables. For example [45] analyses a scheme for single-switch dc/dc converters, where the RPP and the RCF techniques are both applied: within a randomly selected carrier period T, the pulse position is chosen at random, too.

Alternate random modulation

The idea is to alternate between two or more PWM schemes in a fixed sequence. As least one of the PWM techniques in the set should be a random PWM method, but otherwise the use of deterministic methods is not prohibited. For instance, one could alternate between the RPP and RCF techniques or even simpler: between a non-deterministic PWM method and, say, RCF modulation.

Again, these methods can be designed so that a proper volt-second balance is maintained, but apart from the preliminary spectral investigations of [45], not much is known about such methods compared to the time-invariant methods.

2.4.3   Compliance of random PWM with converter topologies

Having described a lot of different ways to randomize a modulator, it should not be forgotten that a modulator must always be consistent with the operating principles of the power converter which it is supposed to control. To put it differently, a certain random PWM technique may be an acceptable alternative control philosophy for some converters, but that does not unconditionally imply that the same technique is compatible with other topologies.

As an example of this lack of universality, the VSC shown in Fig. 2.3(a) and the single-switch flyback converter may be compared. The VSC complies with both the RPP and RCF strategies, because — as explained in section 2.2.1 — the output voltage is directly controlled by the value of the switching function.

For the flyback converter, the situation is more complicated due to the tight interaction between the modulator and the internal operation of the converter. Usually, the switch is turned on at the beginning of each carrier period to get enough time to build up the flux and to transfer the hereby stored energy to the secondary side of the transformer before the beginning of the next carrier period. Therefore, the use of RPP modulation is very problematic in a flyback converter: it is difficult to assure that the flux in the transformer core is reset to its initial value before the next turn-on pulse is applied to the switch, if the leading edge of the on-pulse is delayed from the start of the carrier period. In a similar manner, randomization of the carrier frequency, while keeping the duty ratio constant, is problematic.

The difference between the use of random PWM in a VSC and a flyback converter may also be illustrated by considering the switch peak currents in the two converters. In the VSC, the peak currents are mainly determined by the load and to a much lower extent by the ripple currents caused by the switchings. Therefore, the RCF technique does not necessarily require re-selection of power devices provided that reasonable (random) variations of the carrier frequency are used. For the flyback (and many other dc/dc converters), the switch peak current relates linearly to the value of the carrier period, provided that the transformer does not saturate. Therefore, the design and the selection of all circuit elements strongly depend on the chosen statistics for T which makes it mandatory to design the hardware and the modulator as a whole.

A good description of such design problems is included in the patent [52], which focuses on a single-switch forward converter modulated with a random carrier frequency. As explained in this patent, the major problems of using RCF instead of a fixed carrier frequency modulator include (a) magnetics (transformer and output choke) must be oversized to avoid saturation and overheating, (b) the peak currents in all components increase, and (c) a larger output filter is needed to meet ripple voltage specifications.

In total it may be stated that random modulation is well-suited for converter topologies where the pulse-width modulator can be designed more or less independently of the power circuit. However, it should also be emphasized that the use of random PWM requires careful considerations if there is a strong interaction between the modulator and the intrinsic operating principles of the power circuit.

2.4.4   Random modulation methods selected for further study

The consensus of the discussions above is that the converter topology must be known in advance before it makes any sense to investigate specific random PWM methods. In agreement with the statements in Chapter 1, focus is put on the two well-known topologies shown in Fig. 2.11. In contrary to e.g. flyback and forward converters, these two converters comply well with the principles of random PWM which makes it possible to investigate a variety of different random PWM schemes on the same topology.

It is evident that quite a large number of random modulators can be constructed by combining the outlined principles in different ways. However, it is also clear that most of them are of little practical importance, if any at all. For example, it is hard to find good reasons to study the RCF technique using different carrier frequencies in each leg of a three-phase converter cascaded with an RPP technique, unless this particular combination has some unforeseen advantages. It may be argued that the potentials of
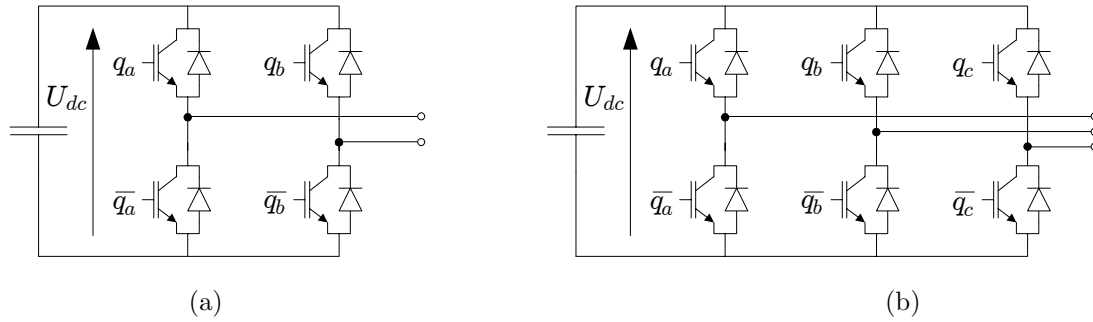
Figure 2.11 The two converter topologies of primary interest is this thesis: (a) full-bridge dc/dc converter and (b) full-bridge dc/ac voltage-source converter.

this particular technique are unknown until it has been investigated, but on the other hand, much work still remains to be done for the less complicated techniques.

The criteria used for selection are that candidate modulators should be both (a) structurally simple in order to ease the practical implementation and (b) preserve the volt-second balance in each carrier period. These requirements rule out most of the exotic methods, and using the terminologies of subsection 2.4.2, focus is therefore put on the following unity-gain, single-random variable, time-invariant groups of modulators:

Fixed carrier frequency random PWM (FCF-RPWM)
> Essentially, this group of methods consists of the random pulse position modulators (RPP), but for the three-phase VSC other simple techniques may also be devised, see further in Chapter 6. Apart from adhering to the two requirements set up above, FCF-RPWM methods comply well with existing closed-loop control concepts, because the carrier is constant; this makes these techniques attractive.

Random carrier frequency PWM (RCF-PWM)
> Random variation of the carrier frequency is also a simple strategy and, furthermore, RCF modulation is probably the most effective method for acoustic annoyance reduction. The major disadvantage of the RCF principle relates to closed-loop control, if the sampling instants of the controller are synchronized to the randomized modulator.

Both these techniques have been studied in the literature, but still a number of important characteristics are not yet completely characterized or described in an exhaustive manner. Hence, in the remaining parts of the thesis, these modulators are analyzed with respect to the output voltage spectrum, the current waveforms, and their compliance with current sampling techniques. Also, aspects relating to closed-loop control systems incorporating random PWM modulators are investigated.

2.5   Summary

Based on definitions of switching functions, duty ratios and space vectors, principles for voltage control of three-phase voltage-source converters have been reviewed. In particular, a flexible structure based on carrier-frequency modulation and zero-sequence

voltage injection has proved useful for three-phase VSC's. This framework is used as a starting point for the analyses in the remaining parts of the thesis.

Next, the basic principles of random modulation were introduced and it was shown how random modulation schemes can be categorized and combined in different ways in order to construct new and sophisticated modulators. From a practical point of view, however, only a few of the techniques are of any immediate relevance. It was also briefly discussed that even the most simple techniques are not universality applicable, i.e. care should always be exercised to assure that the internal operating principles of a converter comply with the intended randomization strategy.

Finally, two classes of random PWM techniques, which are believed to be candidate for practical applications, were selected for further analysis. Random PWM techniques belonging to the first class all operate with a constant carrier frequency, i.e. in this case the randomization relies (mainly) on random pulse-position modulation. The second class of modulators randomizes the carrier frequency, but not the pulse position.

Bibliography

[1] M. P. Kaźmierkowski and L. Malesani, "Guest Editorial. Special Section on PWM Converter Current Control," *IEEE Trans. on Industrial Electronics*, vol. 45, no. 5, pp. 689–690, Oct. 1998.

[2] J. Kyyrä, *Switching Vector Theory — Unification of Switching and Space-Vector Theory in Polyphase Converter Applications*, Electrical Engineering Series No. 83. Acta Polytechnica Scandinavica, Helsinki, Finland, 1995.

[3] L. Gyugyi and B. R. Pelly, *Static Power Frequency Changers: Theory, Performance and Application*, John Wiley & Sons, New York, 1976.

[4] J. W. Kolar, H. Ertl, and F. C. Zach, "Minimizing the Current Harmonics RMS Value of Three-Phase PWM Converter Systems by Optimal and Suboptimal Transition between Continuous and Discontinuous Modulation," *Proc. of the 22nd IEEE Power Electronics Specialists Conference*, vol. 1, pp. 372–381, 1991.

[5] J. D. van Wyk, "Power Electronic Control for Drives," in *Power Electronics and Variable Frequency Drives. Technology and Applications*, B. K. Bose, Ed., New York, 1997, pp. 80–137, IEEE Press.

[6] A. Schönung and H. Stemmler, "Geregelter Drehstrom-Umkehrantrieb mit gesteuertem Umrichter nach dem Unterschwingungsverfahren," *Brown Boveri Mitteilungen*, vol. 51, no. 8/9, pp. 555–577, Aug./Sept. 1964.

[7] B. D. Bedford and R. G. Hoft, *Principles of Inverter Circuits*, John Wiley & Sons, New York, 1964.

[8] H. S. Black, *Modulation Theory*, D. Van Nostrand Company, Princeton, New Jersey, 1953.

[9] S. R. Bowes and B. M. Bird, "Novel Approach to the Analysis and Synthesis of Modulation Processes in Power Convertors," *Proc. IEE*, vol. 122, no. 5, pp. 507–513, May 1975.

[10] J. Holtz, "Pulse Width Modulation for Electronic Power Conversion," in *Power Electronics and Variable Frequency Drives. Technology and Applications*, B. K. Bose, Ed., New York, 1997, pp. 138–208, IEEE Press.

[11] P. K. Kovács, *Transient Phenomena in Electrical Machines*, Studies in Electrical and Electronic Engineering Vol. 9. Elsevier Scientific Publishers, Amsterdam, 1984, (English translation and expansion of P. K. Kovács and I. Rácz, *Transiente Vorgänge in Wechselstrommaschinen,* Akadémiai Kiadó, Budapest, Hungary, 1959).

[12] W. Leonhard, *Control of Electrical Drives*, Springer-Verlag, Berlin–Heidelberg–New York, second edition, 1996.

[13] M. P. Kaźmierkowski and H. Tunia, *Automatic Control of Converter-Fed Drives*, Studies in Electrical and Electronic Engineering 45. Elsevier, Amsterdam–London–New York–Tokyo, 1994.

[14] V. G. Török, "Near-Optimum On-line Modulation of PWM Inverters," *IFAC Control in Power Electronics and Electrical Drives Conference*, pp. 247–254, 1983.

[15] G. Pfaff, A. Weschta, and A. Wick, "Design and Experimental Results of a Brushless AC Servo-Drive," *Conference Record of the 17th IEEE Industry Applications Society Annual Meeting*, pp. 692–697, 1982.

[16] A. Busse and J. Holtz, "Multiloop Control of a Unity Power Factor Fast Switching AC to DC Converter," *Proc. of the 13th IEEE Power Electronics Specialists Conference*, pp. 171–179, 1982.

[17] M. Gekeler, "Digitales Steuergerät für dreiphasige Pulswechselrichter," *Elektronik*, vol. 18, pp. 103–107, Sept. 1982.

[18] S. Ogasawara, H. Akagi, and A. Nabae, "A Novel PWM Scheme of Voltage Source Inverters Based on Space Vector Theory," *Proc. of 3rd European Conference on Power Electronics and Applications*, vol. 3, pp. 1197–1202, 1989.

[19] J. Holtz, W. Lotzkat, and A. M. Khambadkone, "On Continuous Control of PWM Inverters in the Overmodulation Range Including the Six-Step Mode," *IEEE Trans. on Power Electronics*, vol. 8, no. 4, pp. 546–553, Oct. 1993.

[20] A. M. Hava, *Carrier Based PWM-VSI Drives in the Overmodulation Region*, Ph.D. thesis, University of Wisconsin–Madison, 1998.

[21] V. Blasko, "Analysis of a Hybrid PWM Based on Modified Space-Vector and Triangle-Comparison Methods," *IEEE Trans. on Industry Applications*, vol. 33, no. 3, pp. 756–764, May/June 1997.

[22] A. M. Hava, R. J. Kerkman, and T. A. Lipo, "A High Performance Generalized Discontinuous PWM Algorithm," *Proc. of the 12th IEEE Applied Power Electronics Conference and Exposition*, vol. 2, pp. 886–894, 1997.

[23] D. G. Holmes, "The Significance of Zero Space Vector Placement for Carrier Based PWM Schemes," *Conference Record of the 30th IEEE Industry Applications Society Annual Meeting*, vol. 3, pp. 2451–2458, 1995.

[24] A. M. Hava, R. J. Kerkman, and T. A. Lipo, "Simple Analytical and Graphical Methods for Carrier-Based PWM-VS Drives," *IEEE Trans. on Power Electronics*, vol. 14, no. 1, pp. 49–61, Jan. 1999.

[25] G. Buja and G. Indri, "Improvement of Pulse Width Modulation Techniques," *Archiv für Elektrotechnik*, vol. 57, pp. 281–289, 1975.

[26] J. T. Boys and P. G. Handley, "Harmonic Analysis of Space Vector Modulated PWM Waveforms," *IEE Proceedings Part B*, vol. 137, no. 4, pp. 197–204, July 1990.

[27] S. R. Bowes and Y.-S. Lai, "Relationship Between Space-Vector Modulation and Regular-Sampled PWM," *IEEE Trans. on Industrial Electronics*, vol. 44, no. 5, pp. 670–679, Oct. 1997.

[28] K. G. King, "A Three-Phase Transistor Class-B Inverter with Sine-Wave Output and High Efficiency," *International Conference on Power Electronics — Power Semiconductors and their Applications*, pp. 204–209, 1974, IEE Conf. Publication No. 123.

[29] M. Depenbrock, "Pulse Width Control of a 3-Phase Inverter with Non-Sinusoidal Phase Voltages," *Record of the 1977 IEEE Industry Applications Society International Semiconductor Power Conference*, pp. 399–403, 1977.

[30] S. Legowski, J. Bei, and A. M. Trzynadlowski, "Analysis and Implementation of a Grey-Noise PWM Technique Based on Voltage Space Vectors," *Proc. of the 7th IEEE Applied Power Electronics Conference and Exposition*, pp. 586–593, 1992.

[31] R. L. Kirlin, S. Kwok, S. Legowski, and A. M. Trzynadlowski, "Power Spectra of a PWM Inverter with Randomized Pulse Position," *IEEE Trans. on Power Electronics*, vol. 9, no. 5, pp. 463–472, Sept. 1994.

[32] Kone Osakeyhtiö, "Förfarande och anordning för minskning av bullerolägenheterna vid en med chopperprincip matad elmotor (*Method and Apparatus for Reduction of Noise from Chopper-Fed Electrical Machines*)," Finnish Patent Application No. 861.891, Filed May 6, 1986.

[33] T. Tanaka, T. Ninomiya, and K. Harada, "Random-Switching Control in DC-to-DC Converters," *Proc. of the 20th IEEE Power Electronics Specialists Conference*, vol. 1, pp. 500–507, 1989.

[34] P. G. Handley, M. Johnson, and J. T. Boys, "Elimination of Tonal Acoustic Noise in Chopper-Controlled DC Drives," *Applied Acoustics*, vol. 32, pp. 107–119, 1991.

[35] T. G. Habetler and D. M. Divan, "Acoustic Noise Reduction in Sinusoidal PWM Drives Using a Randomly Modulated Carrier," *Proc. of the 20th IEEE Power Electronics Specialists Conference*, vol. 2, pp. 665–671, 1989.

[36] M. M. Bech, J. K. Pedersen, and F. Blaabjerg, "Random Modulation Techniques in Power Conversion — an Update," *Proc. of the International Power Electronics and Motion Control Conference*, vol. 3, pp. 357–365, 1996.

[37] A. M. Trzynadlowski, F. Blaabjerg, J. K. Pedersen, R. L. Kirlin, and S. Legowski, "Random Pulse Width Modulation Techniques for Converter Fed Drive Systems — A Review," *Conference Record of the 28th IEEE Industry Applications Society Annual Meeting*, vol. 2, pp. 1136–1143, 1993.

[38] A. M. Trzynadlowski, F. Blaabjerg, J. K. Pedersen, R. L. Kirlin, and S. Legowski, "Random Pulse Width Modulation Techniques for Converter Fed Drive Systems — A Review," *IEEE Trans. on Industry Applications*, vol. 30, no. 5, pp. 1166–1175, Sep./Oct. 1994.

[39] P. W. Clarke, Bell Telephone Laboratories, "Switching Regulator with Random Noise Generator," US Patent No. 3.579.091, Filed May 18, 1969.

[40] P. W. Clarke, "Self-Commutated Thyristor DC-to-DC Converter," *IEEE Trans. on Magnetics*, vol. 6, no. 1, pp. 10–15, Mar. 1970.

[41] A. M. Trzynadlowski, S. Legowski, and R. L. Kirlin, "Random Pulse Width Modulation Technique for Voltage-controlled Power Inverters," *Conference Record of the 22nd IEEE Industry Applications Society Annual Meeting*, vol. 1, pp. 863–868, 1987.

[42] A. Mertens and H.-C. Skudelny, "Calculations on the Spectral Performance of Discrete Pulse Modulation Strategies," *Proc. of the 22nd IEEE Power Electronics Specialists Conference*, vol. 1, pp. 357–365, 1991.

[43] A. M. Trzynadlowski, M. M. Bech, F. Blaabjerg, and J. K. Pedersen, "An Integral Space-Vector PWM Technique for DSP-Controlled Voltage-Source Inverters," *IEEE Trans. on Industry Applications*, vol. 35, no. 5, pp. 1091–1097, Sept./Oct. 1998.

[44] S. Y. R. Hui, S. Sathiakumar, and K. K. Sung, "Novel Random PWM Schemes with Weighted Switching Decision," *Proc. of the 6th International Conference on Power Electronics and Variable Speed Drives*, pp. 348–353, 1996, IEE Conf. Publication No. 429.

[45] A. M. Stanković, *Random Pulse Modulation with Applications to Power Electronic Converters*, Ph.D. thesis, Massachusetts Institute of Technology, Feb. 1993.

[46] T. G. Habetler and D. M. Divan, "Acoustic Noise Reduction in Sinusoidal PWM Drives Using a Randomly Modulated Carrier," *IEEE Trans. on Power Electronics*, vol. 6, no. 3, pp. 356–363, July 1991.

[47] J. K. Pedersen and F. Blaabjerg, "Implementation and Test of a Digital Quasi-Random Modulated SFAVM PWM in a High Performance Drive System," *Proc. of the 18th IEEE International Conference on Industrial Electronics, Control, and Instrumentation*, vol. 1, pp. 265–270, 1992.

[48] A. M. Trzynadlowski, R. L. Kirlin, and S. Legowski, "Space Vector PWM Technique with Minimum Switching Losses and a Variable Pulse Rate," *Proc. of the 19th IEEE International Conference on Industrial Electronics, Control, and Instrumentation*, vol. 2, pp. 689–694, 1993.

[49] Y. S. Lai, H. C. Huang, Y. S. Kuan, and C. M. Young, "A New Random Inverter Control Technique for Motor Drives," *Proc. of the 13th IEEE Applied Power Electronics Conference and Exposition*, vol. 1, pp. 101–107, Feb. 1998.

[50] A. M. Stanković, G. C. Verghese, and D. J. Perreault, "Analysis and Synthesis of Randomized Modulation Schemes for Power Converters," *IEEE Trans. on Power Electronics*, vol. 10, no. 6, pp. 680–693, Nov. 1995.

[51] R. L. Kirlin and A. M. Trzynadlowski, "Spectral Design of Randomized Pulse Width Modulation in DC to AC Converters," *Proc. of the 7th IEEE Signal Processing Workshop on Statistical Signal and Array Processing*, pp. 387–391, June 1994.

[52] H. Hosei and K. Tanaka, Nippon Steel Corp., "Switching Regulator," US Patent No. 5.640.315, Filed March 17, 1995.

Part II

Analysis of random PWM schemes

Chapter 3

Spectral analysis of random pulse trains

3.1 Introduction

Motivated by the fact that the frequency-domain properties of switching functions generated by random pulse-width modulation are completely different from those spectra generated by deterministic PWM techniques, the main objective of this chapter is to present a general spectral analysis for randomly modulated waveforms.

The presented spectral analysis is not tailored towards a specific random PWM scheme, but rather a general theory encompassing all schemes of interest has been developed. Details on how to apply the theory to specific random PWM schemes are given in Chapters 4, 5, and 6.

Seen from an engineering point of view this thesis may appear to be somewhat theoretically focused due to the amount of mathematics involved in the spectral analyses. However, to support the theoretical investigations, a high priority has been assigned to experimental verifications of all developed analytical expressions for the frequency-domain properties of random PWM schemes: based on measurements, it is possible to compare the theory to real-world facts, which — again from an engineering point of view — is a much more scientifically sound working methodology than sticking to computer simulations only. (This does not imply that computer simulations have not been used — many ideas were tested on a preliminary basis by running MATLAB or SABER[1] simulations before laboratory implementations and tests.)

It turns out, however, that due to the special spectral characteristics of random PWM signals, the task of comparing theoretical results to measurements is not a trivial task due to a number of pitfalls relating to digital signal processing. Hence, a second objective of the chapter is to explain these problems and to present a methodology that ensures a proper comparison of theoretical predictions to laboratory measurements.

---

[1]SABER is an advanced all-purpose simulator from ANALOGY based on a powerful model description language named MAST. Among many other features, SABER includes a good time-domain numerical solver and SABER gives the opportunity to link MAST models with object files generated from a C-source file. This feature is very useful for off-line debugging in SABER of DSP source code, because the used development software for the DSP supports the C programming language. In this way, the code developed and debugged in SABER can be re-used in the DSP system with only minor modifications. See also Appendix A.

Chapter outline

The organization of this chapter is as follows: first general aspects of spectral analysis are reviewed, including the proper theoretical framework to be used for the randomly modulated signals of interest. Next, issues relating to the practical estimation of spectral characteristics are discussed and sample measurements are shown to demonstrate the fundamental problems and pitfalls.

Then, starting from a review of related work found in the scientific literature, a detailed derivation of a set of formulas for the spectrum of a randomly modulated pulse trains is then presented. A summary concludes this chapter.

3.2 Spectral analysis of random signals

The mathematical framework, on which the frequency-domain description of random PWM pulse trains is based, is the theory of power spectral density analysis known from stochastic processes. In order to familiarize the reader with these generalizations of the well-known Fourier series theory, a number of extensions of the Fourier series expansion may be applied in order to arrive at the definition of the power spectrum.

For an in-depth treatment of these topics, the reader is urged to study the classic reference on random signals, namely [1] by Davenport and Root. Many other well-written books do also exist, e.g. [2–5]. Also, the thesis [6] on random modulation discusses quite similar topics. In a mathematical sense, the present presentation is less stringent than the work of [6], i.e. a more heuristic approach is adopted in order to focus on engineering aspects.

3.2.1 Fourier series expansion of periodic signals

As mentioned several times already, power electronic converters controlled in a deterministic manner generate periodic output voltage and current waveforms in steady state. Such waveforms may be characterized by their Fourier series components by which a signal $x(t)$ with period T_1 is resolved[2] into individual frequency components with different amplitudes and phase angles such that

$$x(t) = \sum_{n=-\infty}^{\infty} a_n e^{j2\pi n f_1 t} \quad f_1 = \frac{1}{T_1}, \tag{3.1}$$

where the n'th complex-valued Fourier coefficient a_n is

$$a_n = \frac{1}{T_1} \int_0^{T_1} x(t) e^{-j2\pi n f_1 t} \, dt. \tag{3.2}$$

For the time-periodic functions treated here, the set of Fourier coefficients constitutes an amplitude spectrum $A(f)$ given by

$$A(f) = \sum_{n=-\infty}^{\infty} |a_n| \, \delta(f - n f_1), \tag{3.3}$$

---

[2]See [1] for a mathematical discussion of the convergence conditions which $x(t)$ must fulfil to legitimate this series expansion.

where $\delta(\cdot)$ is the Dirac impulse function of the argument. This shows that the amplitude spectrum consists of impulsive components only, which implies that $A(f)$ is a discontinuous function of frequency. Another point of importance is the physical units associated with $x(t)$ and its spectrum of amplitudes, $A(f)$: if $x(t)$ is a voltage measured in volts, then the impulse parts of $A(f)$ do also have units of volts.

3.2.2 Power spectral density for periodic signals

The next step concerns the introduction of the power spectral density (PSD) for periodic signals. Formally, the PSD of a periodic signal $x(t)$ is defined by

$$S(f) = \sum_{n=-\infty}^{\infty} |a_n|^2\, \delta(f - nf_1), \tag{3.4}$$

which is closely related to Parseval's theorem [1]. This theorem states that the time average of the energy in a signal (i.e. its power) equals the sum of powers related to each frequency component. The use of the phrase "power" may be justified by the fact that $S(f)$ expresses the frequency distribution of the real power dissipated in a 1 Ω resistor when a voltage $x(t)$ is applied to it; in this case the impulsive parts of $S(f)$ have units of volts squared, i.e. volt^2.

To recapitulate, (3.4) defining the PSD gives the distribution in frequency of the power of a periodic signal, but the PSD does not retain the phase information of the Fourier coefficients.

3.2.3 Time autocorrelation function for periodic signals

To pave the way for the treatment of random pulse trains, the important ideas of time autocorrelation function $\mathcal{R}(\tau)$ and its relationship to the power spectral density $S(f)$ are introduced. Formally, the following identities apply

$$S(f) = \int_{-\infty}^{\infty} \mathcal{R}(\tau) e^{-j2\pi f\tau}\, d\tau \tag{3.5}$$

for the forward transformation; the inverse transformation is defined by

$$\mathcal{R}(\tau) = \int_{-\infty}^{\infty} S(f) e^{j2\pi f\tau}\, df. \tag{3.6}$$

$S(f)$ and $\mathcal{R}(\tau)$ are said to form a Fourier transform pair.

For convenience, the Fourier transformation of a signal $x(t)$ is often written as $\mathcal{F}(x(t))$ or simply $X(f)$ in accordance with the formal definition

$$X(f) = \mathcal{F}(x(t)) = \int_{-\infty}^{\infty} x(t) e^{-j2\pi ft}\, dt. \tag{3.7}$$

Details of the existence of the transformation may be found in [1].

Returning to the definition of the PSD, it is clear that (3.5) does not resemble the definition introduced in (3.4). It may, however, be shown that for periodic signals (3.4)
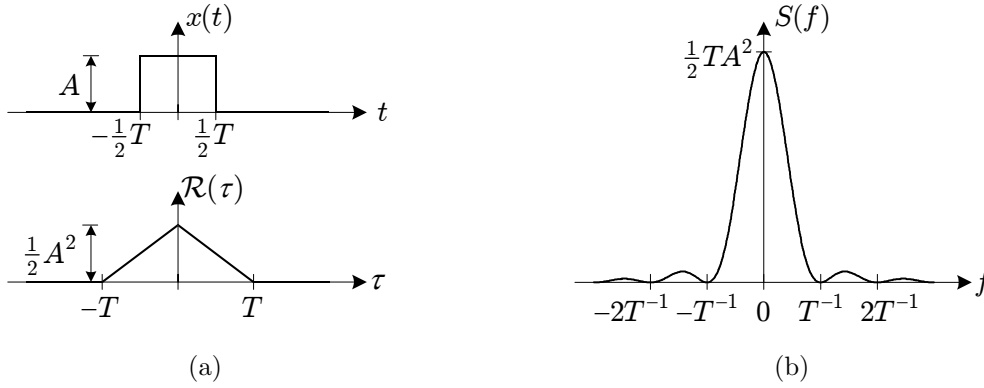
Figure 3.1 (a) Non-periodic signal and its autocorrelation function and (b) power spectral density for the same signal.

is a special case of (3.5). The proof relies on the definition of the time autocorrelation function for an arbitrary signal $x(t)$ (which needs not be periodic):

$$\mathcal{R}(\tau) = \lim_{T_0 \to \infty} \frac{1}{2T_0} \int_{-T_0}^{T_0} x(t)\, x(t - \tau)\, d\tau, \tag{3.8}$$

which is a function of the time lag, τ. For a periodic function with the Fourier series expansion (3.1), it may be shown that the time autocorrelation function is

$$\mathcal{R}(\tau) = \sum_{n=-\infty}^{\infty} |a_n|^2\, e^{-j2\pi n f_1 \tau}. \tag{3.9}$$

By inserting this result into the definition (3.5) of the power spectral density, it may readily be verified that (3.4) is a special case of (3.5).

3.2.4   Power spectral density for non-periodic signals

The examples treated so far have all considered periodic signals, but the definition (3.5) of the PSD may also be applied for functions that do not repeat themselves after T seconds. As an example, the pulse shown in Fig. 3.1(a) and defined by

$$x(t) = \begin{cases} A, & \text{for } |t| < \frac{1}{2}T, \\ 0, & \text{otherwise,} \end{cases} \tag{3.10}$$

may be considered. By inserting $x(t)$ into (3.8), the following expression for the time autocorrelation results:

$$\mathcal{R}(\tau) = \begin{cases} \frac{1}{2}A^2 \left(1 - \frac{|\tau|}{T}\right), & \text{for } |\tau| < T, \\ 0, & \text{otherwise.} \end{cases} \tag{3.11}$$

The result is shown in Fig. 3.1 together with the power spectral density obtained by Fourier transformation of $\mathcal{R}(\tau)$ according to (3.5), i.e.

$$S(f) = \frac{1}{2}A^2 \int_{-T}^{T} \left(1 - \frac{|\tau|}{T}\right) e^{-2\pi f \tau}\, d\tau = \frac{1}{2}TA^2\, \frac{\sin^2(\pi f T)}{(\pi f T)^2}. \tag{3.12}$$

It is important to note the units involved. Again, if $x(t)$ is a voltage waveform, then it follows from (3.12) that $S(f)$, the power spectral density, has units of volt^2·sec or, equivalently, volt^2/Hz. This spectral unit justifies the use of "density," because $S(f)$ expresses the power as a continuous function of frequency. For periodic functions, the impulses in $S(f)$ correspond to infinite density making the PSD a discontinuous function of frequency. Hence, for periodic signals the meaning of "density" should be understood as a limiting property rather than a literal property as for non-periodic signals.

It turns out that many of the signals of interest in this thesis have a spectrum with both an impulsive and a density part, i.e. a non-empty set of frequencies exists in which the pure density parts (volt^2/Hz) vanish due to time-periodic components in the signal at hand.

3.2.5 Power spectral density for random signals

At this point, it should be recalled that the whole purpose of random modulation is to suppress the otherwise periodic components in the PWM switching functions, except for the fundamental component. Based on the brief review of spectral analysis given above, it must be expected that the spectra of randomly modulated pulse trains mainly consists of density parts, and to a much lower extent of harmonics. However, it is not straightforward to apply the formulas (3.5) and (3.8) to find the time autocorrelation function and the PSD, respectively, because the signal $x(t)$ cannot be described in a deterministic manner when random PWM is involved. Now, $x(t)$ is partially dependent on the outcome of random experiment (the random number generator introduced in section 2.4), which can be described on a probabilistic level only.

For random waveforms (including those of interest here) the proper mathematical framework originates from the theory of stochastic processes. Specifically, for so-called wide-sense stationary (WSS) random processes, the definition of the PSD is almost identical to the previous definition (3.5), apart from one important detail explained below [1]:

$$S(f) = \int_{-\infty}^{\infty} R(\tau)e^{-j2\pi f\tau}\,d\tau. \tag{3.13}$$

The difference is the autocorrelation function, which now is labeled $R(\tau)$ instead of $\mathcal{R}(\tau)$ in order to emphasize that $R(\tau)$ is an average taken over the whole ensemble of realizations. Accordingly, the statistical autocorrelation function for a WSS process is defined as

$$R(\tau) = \lim_{T_0 \to \infty} \frac{1}{2T_0} \int_{-T_0}^{T_0} E\big\{x(t)\,x(t-\tau)\big\}\,dt, \tag{3.14}$$

where $E\{\cdot\}$ is the statistical expectation[3] of the argument. Note that for a deterministic signal, where the ensemble only consists of a single realization, (3.14) collapses to (3.8) making the two definitions consistent.

---

[3]Again, reference should be made to a textbook such as [1–5] for details on statistical concepts like WSS processes, ensembles, statistical expectation, autocorrelation functions, etc.

Detailed information on how to calculate the autocorrelation function and the PSD for a variety of signals of interest in power converters controlled by random PWM methods follows in section 3.4, and in later chapters.

3.3   Measurement of power spectral density

As stated in the introduction to this chapter, experimental verifications of the developed spectral theory form an important part of the work. The used laboratory facilities are described in Appendix A, but for the current discussion, it is sufficient to know that a dynamic signal analyzer (DSA) is used to measure the PSD for e.g. the output voltage in a three-phase converter. Unfortunately, the digital signal processing carried out by the DSA is imperfect implying that only an estimate of the true PSD can be obtained. The limitation on the accuracy by which a PSD can be measured is not caused by the use of a poor-performing instrument[4], but rather the accuracy is bounded by fundamental theorems in digital signal processing theory.

The problem gets more pronounced for PSD measurements of random PWM waveforms both having a pure density part (volt^2/Hz) and a harmonic (volt^2) part. Random PWM schemes that give rise to such mixed spectra are often encountered in the literature (e.g. [6, 7]), but so far very little attention has been paid to the fundamental difficulties in comparing calculated and measured PSD, and, hence, only rudimentary agreements between theoretical predictions and measurements can be observed in many scientific publications. The only exception is [8] which takes the characteristics of a spectrum analyzer into account in order to compare theory with measurements.

In the opinion of the author, this lack of a proper verifications combined with a critical evaluation of the results is a serious flaw which has led to hasty conclusions. For example, using measurements and rudimentary simulations [9] claims to have invented a random PWM strategy that provides "optimal spectrum performance" — a conclusion which impossibly can be drawn from the perfunctory presentation in [9].

A plausible cause for the lack of attention paid to the verification problem may be the fact that in most power electronic systems, the continuous part of the PSD is often considered to form an unwanted distortion that mainly complicates the measurement of periodic signal components. With a few exceptions, such as [10] which includes correctly scaled measurements of the current spectra produced by a hysteresis current controller, the existence of mixed spectra is rarely acknowledged or commented.

Thus, the purposes of this section are to outline the causes to possible disagreements between measured and calculated spectra and to present a procedure that solves the difficulties. Examples of measurements demonstrating the problems are also provided.

3.3.1   Numerical estimation of the power spectral density

Numerous numerical methods exist for estimating the PSD of a WSS random process. Nevertheless, the prevailing non-parametric method still seems to be a scheme developed by Welch back in 1967 [11]. Despite more recent developments of other non-parametric estimators, such as multi-taper and eigenvector methods, the classic Welch

---

[4]Actually, the DSA used in all measurements is a sophisticated instrument from a reputable vendor of high-quality instruments. See Appendix A for more information.
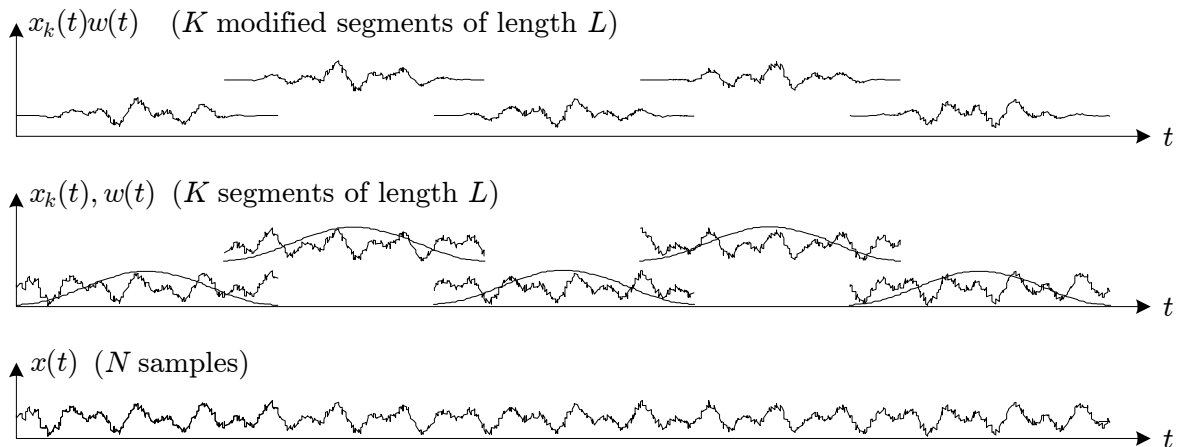
Figure 3.2 Principles of the Welch PSD estimator: (lower trace) original time record, (middle trace) division into K overlapping segments besides the window function, and (top trace) the modified time-domain segments used to calculated the periodograms.

method is the work horse of general-purpose signal analyzers, including the DSA used here. These, and other modern PSD estimators, are also available in the MATLAB Signal Processing Toolbox [12].

The idea of Welch's so-called averaged periodogram method originating from [11] is to estimate the PSD directly without an intermediate estimate of the autocorrelation function as dictated by the definition in (3.13). This direct approach is based on the Wiener-Khintchine theorem, which states that for a wide-sense stationary process $x(t)$, the PSD may be determined by

$$S(f) = \lim_{T_0 \to \infty} E\left\{ \frac{1}{2T_0} |X_{2T_0}(f)|^2 \right\}, \tag{3.15}$$

where $X_{2T_0}(f)$ is the Fourier transformation of the truncated version of $x(t)$ in the interval $-T_0 < t < T_0$. It may be proved that (3.15) is consistent with the earlier definition (3.13) using the autocorrelation function [4].

Welch's modified periodogram

In measurements, it is impossible to apply (3.15) directly because of two facts: (a) only a finite time record $T_0 < \infty$ is available and (b) only one realization of the ensemble is accessible, i.e. the expectation operation becomes impossible.

Despite these two problems, Welch showed how a good estimate $\hat{S}(f)$ of the true spectrum $S(f)$ can be obtained from a finite measurement record. First, a batch of N equidistant samples of the signal is taken. Next, the record is divided into K segments $x_k(t)$ each of length L. These K segments may overlap each other as illustrated in Fig. 3.2. Then all segments are multiplied by a chosen window function $w(t)$, and all the modified time segments are Fourier transformed individually. In this way, a set of K so-called modified periodograms $\tilde{P}_k(f)$ for $k = 1, 2, \cdots, K$ may be obtained. Finally, the estimate of the spectrum is calculated as $\hat{S}(f) = \frac{1}{K} \sum \tilde{P}_k(f)$. Note that in a sense the averaging of the periodograms plays the role of the statistical expectation in (3.15). A detailed treatment of Welch's method and other closely related methods may be found in [13] and in many other textbooks on digital signal processing.

3.3.2 Limitations of digital signal processing techniques

The discussion so far of spectral estimation has assumed that the periodograms $\tilde{P}_k(f)$ can be calculated accurately. However, as the calculation must be based on sampled data only, the continuous Fourier transform defined in (3.7) cannot be applied and, hence, the discrete Fourier transform (DFT) must be used instead. Despite the huge advantages of using digital signal processing techniques (including the DFT), the use of digital techniques is tightly connected to phenomena that easily can distort measurements of e.g. spectra. Hence, if proper precautions are not taken during the interpretation of the obtained results, wrong conclusions may easily be drawn.

Detailed discussions of these topics may be found in e.g. [13], and also an engineering treatment of the limitations of the DFT is given in [14]. In these references, it is elucidated how the phenomena listed below influence the accuracy of the estimated spectrum:

Picket fence
   The number of analysis frequencies (or "lines") is limited to about 0.4 times the record length N. The separation of two adjacent lines is determined as $\Delta f = f_s/N$, where f_s is the sampling frequency of the analog-to-digital converter in the DSA. If a periodic component in the signal does not coincide with an analysis line, both an amplitude and a frequency error occur.

Windowing
   Due to a finite record length, the signal is effectively multiplied by a finite window in the time-domain. This is equivalent to a convolution in the frequency domain, which gives rise to spectral leakage, i.e. power from one frequency line leaks into the adjacent lines. The effects of windowing are especially troublesome if the signal has a discrete as well as a continuous part or if the analysis bandwidth is large compared to the distance between individual signal components.

Aliasing
   Any frequency component in the signal to be sampled that exceeds half the sampling rate will cause aliased components below the Nyquist frequency. Using a commercial DSA aliasing is of little concern due to built-in analogue low-pass filters that guarantee sufficient attenuation of those frequencies that can cause aliasing. It must be stressed, however, that in computer simulations one has to be acutely aware of aliasing, if the input to the DFT-routine is taken from samples of a non-bandwidth limited signal, such as an ideal two-state switching function.

A much more in-depth discussion of these topics may be found in the classic paper [15] by Harris, which gives an excellent presentation of how to use windows in conjunction with the DFT.

Filter and DFT analogy

It is shown below how the computation of the estimated PSD in a DSA may be executed. To facilitate this presentation, an analogy between filter analysis and the DFT is used as a starting point, see [16] for further details.
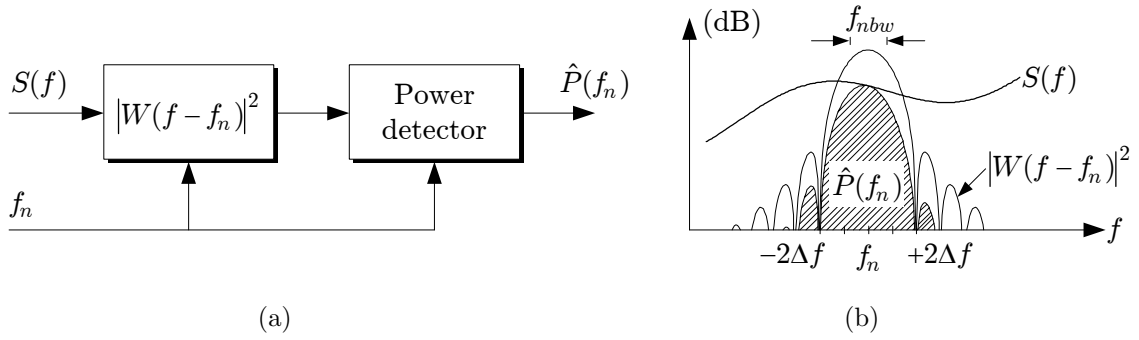
Figure 3.3 Estimation of the total power in the vicinity of the frequency line f_n. (a) functional overview and (b) illustration of the total power transmitted through the window (a Hanning window is used).

The output from the DFT at a certain frequency $f_n = n\Delta f$, where $n = 0, 2, \cdots, \frac{N}{2}$ and $\Delta f = f_s/N$ is the separation between two adjacent analysis lines, may be visualized as shown in Fig. 3.3. The true $S(f)$ is filtered by the transformed window function squared, $|W(f)|^2$, shifted to have center at the f_n line, and the detector measures the total power transmitted through the filter, $\hat{P}(f_n)$. For an arbitrary frequency f_n, Fig. 3.3(b) illustrates this principle. It is important to note that the total power around f_n is estimated, and not the power spectral density exactly at $f = f_n$. Also, the value of $\hat{P}(f_n)$ depends strongly on the applied window function. A simple measure of $W(f)$ is the -3 dB bandwidth, which gives an estimate of the obtainable resolution.

In mathematical terms the outlined process to find the total power $\hat{P}(f_n)$ transmitted through the filter (or window) centered at f_n may be determined by means of the convolution integral:

$$\hat{P}(f_n) = S(f_n) \star |W(f_n)|^2 = \int_{-\infty}^{\infty} S(f) \, |W(f - f_n)|^2 \, df. \tag{3.16}$$

In order to estimate the power density $\hat{S}(f_n)$ based on the total power estimated by (3.16), it is necessary to normalize $\hat{S}(f_n)$ by the effective noise bandwidth f_{nbw} of the window [16]. The effective noise bandwidth is defined as the width of an ideal filter that would transmit the same power from a white-noise source, i.e. a source that emits the same power at all frequencies. Hence,

$$\hat{S}(f_n) = \frac{1}{f_{nbw}} \hat{P}(f_n). \tag{3.17}$$

For a rectangular window f_{nbw} equals Δf, and for the classic Hanning window, $f_{nbw} = 1.5\Delta f$. In this way the power $\hat{P}(f_n)$ measured in volt^2 is converted into an equivalent density $\hat{S}(f_n)$ having units of volt^2/Hz. Furthermore, under idealized conditions $\hat{S}(f_n)$ is independent of f_{nbw}.

The dilemma of spectral units

For the random part of a signal, which causes a continuous density spectrum, the normalization in (3.17) by the noise bandwidth gives the correct density in volt^2/Hz as dictated by the theory. To emphasize that the spectrum is a continuous function of

frequency, the subscript c may be used as in $S_c(f)$. In a similar manner, $S_h(f)$ is used for the harmonic part of the spectrum which is caused by all time-periodic components in the underlying signal. The components in $S_h(f)$ exist at localized frequencies only, and, as shown in section 3.2.2, the proper spectral unit for harmonics is volt^2.

For convenience, a signal having both continuous and discrete parts may be regarded as the summation $S(f) \simeq S_c(f) + S_h(f)$. Although physically incorrect due to the different units involved in the summation, this informal representation may still be useful to illustrate the dilemma of spectral units: should proper density or proper power be measured? The core of the dilemma is that it is impossible to estimate both $S_c(f)$ and $S_h(f)$ simultaneously: if the normalization in (3.17) is used, a good estimate of $S_c(f)$ is usually obtained, but near those frequency components related to $S_h(f)$, the value of $\hat{S}(f_n)$ has got nothing to do with the true value (in volt^2) of $S_h(f)$.

To measure the correct value of the power carried by a discrete frequency component, the following procedure should be used: the scaling of the detected total power $\hat{P}(f)$ transmitted through the window centered at f_n should be chosen so that the highest frequency line[5] is equal to the power carried by the periodic component in the signal [16]. This type of scaling can be obtained by requiring that $W(0) = 1$, i.e. the Fourier transformation of the applied window function should be unity at $f = 0$ Hz. Using the $W(0) = 1$ scaling implies that the correct volt^2 value is obtained for all harmonic components provided that the individual lines in $S_h(f)$ are sufficiently spaced. When this kind of scaling is used the density part of the spectrum will, however, not be scaled properly.

The two different normalizations are abbreviated as PSD and PWR, respectively. The PSD is the density type of scaling giving the correct volt^2/Hz value for the continuous part $S_c(f)$ of the spectrum. The PWR notation is used to indicate the proper power (volt^2) scaling useful for the harmonic spectrum, $S_h(f)$.

Summary

To recapitulate the main conclusions concerning the problem of estimating the spectral properties of signals, the following points should be kept in mind:

1. Concerning the continuous part $S_c(f)$, the output from the power detector shown in Fig. 3.2 at some line f_n collects the total power of $S(f)$ in the neighbourhood of f_n, including the power related to any harmonic (discrete) components in $S_h(f)$. If $S_c(f)$ is constant in a local sense around f_n and $S_h(f)$ vanishes, then the estimated density $\hat{S}(f_n) = \frac{1}{f_{nbw}}\hat{P}(f_n)$ is accurate. Otherwise, errors are introduced.

2. If $S(f)$ has a continuous part (volt^2/Hz) and also a harmonic part (volt^2), the power related to the harmonics may be completely masked, if the power carried by the continuous part of $S(f)$ in the $|f - f_n| < f_{nbw}$ range is comparable to the strength of the harmonic(s) in the neighbourhood of f_n.

---

[5]Here, it should be recalled that even if the signal to be estimated only consists of a single sinusoidal, the estimated spectrum will have several frequency lines due to the spectral leakage effect. Therefore, the scaling should be selected so that the highest line coincides with the power of the underlying sinusoidal.

3. If the noise bandwidth f_{nbw} of the power transmission characteristic of the window given by $|W(f)|^2$ is comparable with the local deviations of $S(f)$ around some frequency f_n, the result is a severe distortion of the estimated $\hat{S}(f_n)$. For example, for the Hanning window $f_{nbw} = 1.5\Delta f$ [14], i.e. if $S(f)$ changes significantly for frequency perturbation of $1.5\Delta f$, the envelope curve of the estimate of $S(f)$ may be incorrect.

Keeping these points in mind, it is perceived that direct comparison of the analytically calculated spectrum, $S(f)$, with the measured (or estimated by processing of simulation results) spectrum is, in fact, not always feasible. In particular, the fundamental problem of proper selection of units and scale is an issue of great practical concern when the spectrum to be estimated is a mixture of density and harmonics.

3.3.3   Examples of spectral measurements

To exemplify the difficulties, a number of measurements have been conducted using the same DSA which is used in all subsequent experiments. The input signal to the DSA is a switching function generated by one of the random PWM schemes discussed in Chapter 5 having both a continuous density part besides discrete harmonics clustered around 12 kHz and 24 kHz; the side lobes are spaced 40 Hz apart from each other, which is the same as the fundamental frequency used in the modulator. The same time-domain signal was analyzed using different DSA settings. In all measurements, a Hanning window is applied while the following settings were varied:

The spacing Δf between two adjacent analysis frequencies
As explained, the value Δf heavily influences the noise bandwidth of the analyzer making it possible to examine the effect of f_{nbw} on the measurements of both pure density and harmonics. $\Delta f = \{1, 8, 32, 64\}$ Hz was used.

The spectral unit
The effects of using either volt^2/Hz scaling (PSD) or volt^2 scaling (PWR) are demonstrated. As explained above, the chosen scaling determines whether correct density or correct harmonics can be measured.

The recorded results shown in Fig. 3.4 cover the dc to 25 kHz frequency range whereas the results in Fig. 3.5 show details of the measurements around 12 kHz. All plots are given in dB[6], where the reference is 1 volt^2/Hz for PSD scaling and 1 volt^2 for PWR scaling. At a first glance, the plots in Fig. 3.4 look similar to each other, but a closer look reveals a number of differences to be commented below. Furthermore, from the six plots, it is not straightforward to spot the plot which is the most accurate estimate of the true spectrum.

The first thing to notice is that for the PSD scaling (left column in Fig. 3.4), the major part of the spectrum has the same magnitude irrespective of the resolution Δf.

---

[6]Referring to the comments on page 50, another common "trick" in many publications on random PWM is to use a linear scale for the presentation of measured spectra, see [9, 17–19], among others. A linear scaling is, however, useless for evaluation of random PWM spectra due to widely different orders of magnitudes involved.

(a)

(b)

(c)

(d)

(e)

(f)
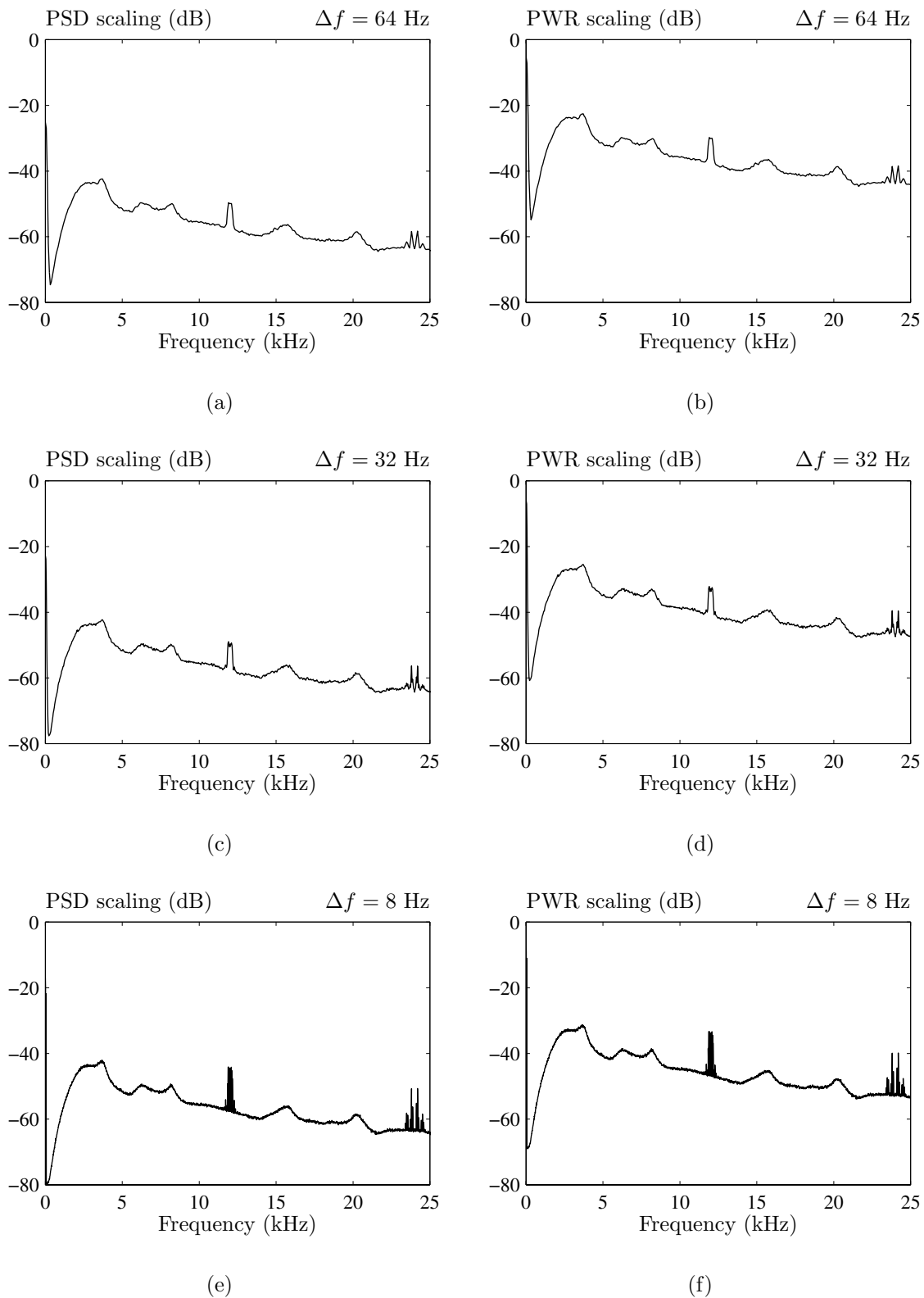
Figure 3.4 Base-band (0–25 kHz) estimations of the spectra for the same signal measured using different settings of the DSA. The resolution Δf is varied as shown in the plots. (Left column) PSD scaling (correct density) and (right column) PWR scaling (correct power).
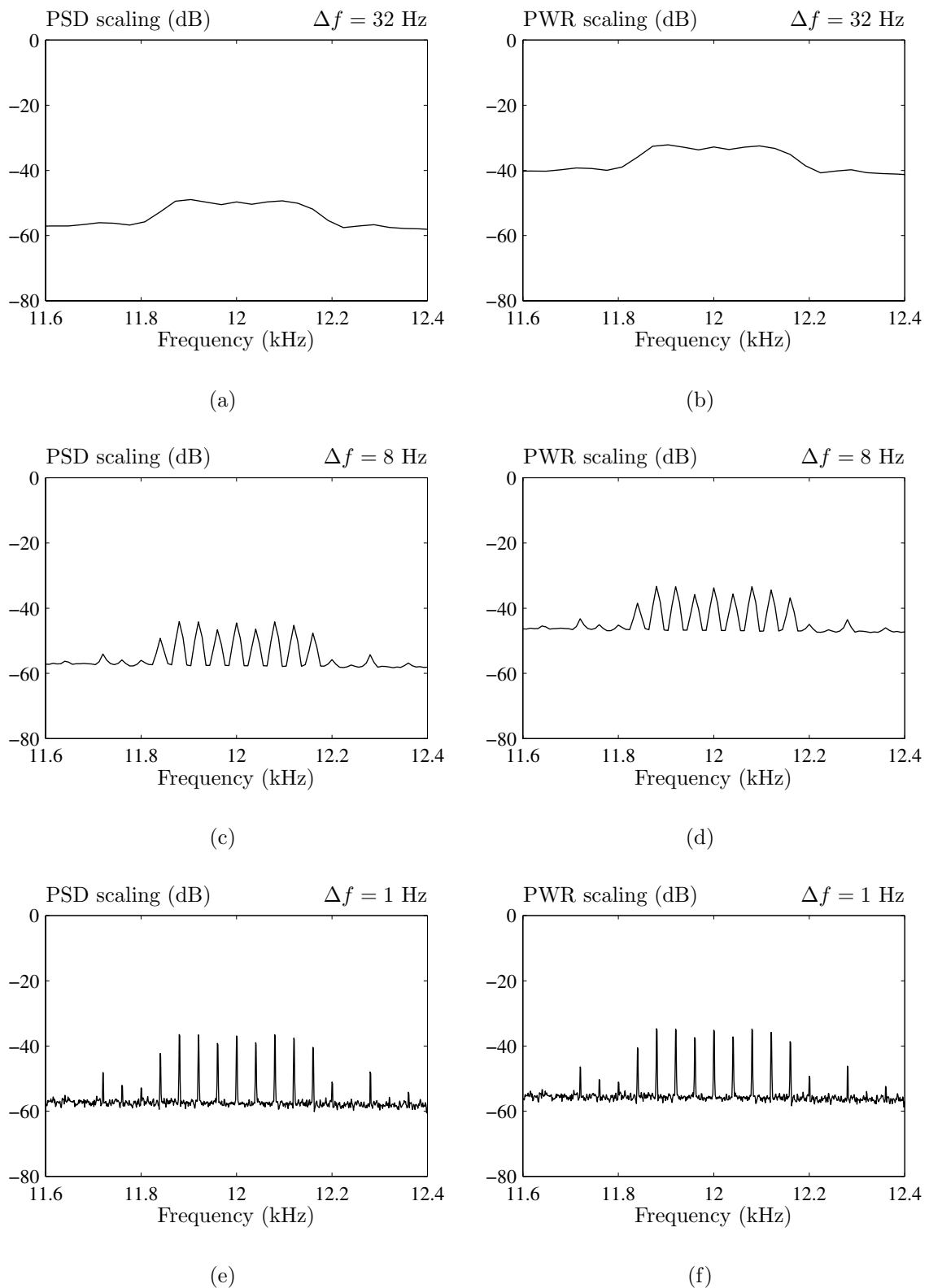
Figure 3.5 Zoom of the measurement results around 12 kHz for the same signal as in Fig. 3.4. The resolution Δf is varied as shown in the plots. (Left column) PSD scaling (correct density) and (right column) PWR scaling (correct power).

This indicates that the true spectrum has a significant density part. However, around 12 kHz and 24 kHz, the amplitudes of the readings depend strongly on the Δf value, when PSD scaling is used. Also, the envelope curve around those frequencies changes dramatically from Fig. 3.4(a) to Fig. 3.4(e). These facts suggest that the true spectrum has harmonic components clustered around 12 kHz and 24 kHz, but if only a single measurement (e.g. Fig. 3.4(a)) of the spectrum were made, it would be difficult to imagine that the true spectrum has harmonics around 12 kHz and not just a local peak of density. Another subtle pitfall relates to the correct interpretation of the measurements shown in Fig. 3.4(e). Here, the harmonics peak up and it would be very tempting to determine their strength by the displayed values (see Fig. 3.5(c) for a zoom around 12 kHz). However, this is a faulty conclusion to draw; the power of harmonics cannot be determined directly from a spectrum scaled in density units.

Using the PWR scaling, the plots in the right column in Fig. 3.4 show that the peaks around 12 kHz and 24 kHz remain almost constant as the resolution Δf is varied, but the remaining part of the spectrum translates vertically for a change in Δf. This suggests that the signal has periodic components buried in an otherwise random signal. However, the density cannot be determined directly using PWR units.

Returning to the question: which plot is the most accurate estimate of the true spectrum, the short answer is that none of the plots are accurate in the whole examined frequency range. The more exhaustive and physically meaningful answer is to combine the results of a PSD measurement with the results of a PWR measurement. To put it differently, any of the results shown for PSD scaling (the left column) are accurate estimates of the density part of the true spectrum, except near those discrete frequencies that can be determined from the PWR results. For those frequencies, the (normalized) power carried by each component must be determined from the right column in Fig. 3.4.

Fig. 3.5 on page 57 shows details of the measured spectra around 12 kHz. When the resolution $\Delta f = 32$ Hz is used, the harmonics are completely masked as shown in Fig. 3.5(a) and (b). This is due to both picket fence and leakage. Otherwise, the plots confirm the comments given above; the density part can only be measured correctly using the PSD scaling and for the harmonics, it is mandatory to used PWR scaling and a small value for Δf. Note also that even if a narrow frequency resolution is used, the results in Fig. 3.5(e) and (f) for $\Delta f = 1$ Hz clearly show that smooth and detailed curves are no guarantee for accuracy; results obtained by digital techniques must always be interpreted carefully in order to separate density and harmonics.

3.3.4 Methodology to ensure a fair comparison

Since many of the spectra of importance in random PWM have mixed spectral characteristics, it is impossible to estimate both density and harmonics simultaneously. This makes a comparison between theory and measurements somewhat cumbersome: in order to investigate the correctness of a certain spectral analysis, the calculations have to be compared to both a PSD-scaled measurement and to a PWR-scaled measurement. Furthermore, the frequencies having the harmonics must be known explicitly aforehand or they must be determined by comparing different measurements using different resolutions. Indeed, this procedure could be followed, but it would make the verification more time-consuming and less elegant than the alternative suggested below.

Methodology

Based on the filter analogy discussed in section 3.3.2, the suggested procedure to ensure a fair comparison of analytical and estimated PSD's is as follows:

1. By using the analytical expressions which should be verified, evaluate the continuous part, $S_c(f)$, and the harmonic part, $S_h(f)$, of the predicted spectrum in the frequency range of interest.

2. Calculate the convolutions (3.16) at the frequency lines $n\Delta f$ that the DSA uses internally; normalize this result by means of (3.17) to get the equivalent density spectrum denoted as $\tilde{S}(f)$.

3. Measure the spectral estimate by the DSA using PSD scaling and the same settings for the window and for the frequency resolution as used in step 2.

4. Compare the results of step 2 directly to the measurements obtained in step 3.

The first step should, of course, always be completed, but by adding the second step, a much more refined comparison becomes possible, because now "errors" similar to those of the DSA are injected into the analytical calculations. In this way otherwise conceptually incomparable quantities become comparable; the only additional task is the convolution integral discussed in greater details below.

Evaluation of the convolution integral

Some care should be exercised regarding the evaluation of the convolution integral (3.16) when the harmonic part $S_h(f)$ is non-zero at a set of known frequencies $\{f_h\}$. In this case, the discrete power spectrum $S_h(f)$ may be written as

$$S_h(f) = \sum_h s_h^2 \, \delta(f - f_h), \tag{3.18}$$

where s_h^2 is the power associated with a particular frequency f_h. By means of (3.16), the total power detected by the DSA at some frequency line f_n then becomes

$$
\begin{aligned}
P(f_n) &= \int_{-\infty}^{\infty} \Big(S_c(f) + S_h(f) \Big) \, |W(f - f_n)|^2 \, df \\
&= \int_{-\infty}^{\infty} \Big(S_c(f) + \sum_h s_h^2 \, \delta(f - f_h) \Big) \, |W(f - f_n)|^2 \, df.
\end{aligned}
\tag{3.19}
$$

Now, it should be recalled that for an arbitrary function $g(f)$, integration with a delta function effectively samples the integral at the singularity: $\int_{-\infty}^{+\infty} g(f)\delta(f-f')\,df = g(f')$. Hence, (3.19) reduces to

$$P(f_n) = \sum_h s_h^2 \, |W(f_h - f_n)|^2 + \int_{-\infty}^{\infty} S_c(f) \, |W(f - f_n)|^2 \, df. \tag{3.20}$$

The total power calculated in this way may now be divided by the noise bandwidth in order to get a calculated density equivalent to the density estimated by the DSA.

The procedure implies knowledge of the DSA window function and the spacing be-
tween adjacent analysis lines, but this information is always available: on DSA's the
window function is user-selectable, and the line spacing is normally shown on-screen
as well. This information makes it possible to evaluate (3.20) using a simple numerical
approximation routine.

   The justification of the outlined methodology will become clear from the results
reported in later chapters. Also, this procedure was used in [20], reappearing in a
slightly edited version in [21].

3.4   Derivation of a general formula for the power spectrum in random PWM

In this section, key equations for the power spectral density of randomly modulated
pulse trains are derived. The analysis is generalized in the sense that no particular
random PWM scheme is considered, but rather a broad class of important schemes
may be treated as special cases of the analysis in this section.

   Before the details of the derivations are given, the scope of the analysis is stated in
more precise terms based on the requirements set up in Chapter 2. Also, a review of
the relevant literature dealing with similar theoretical topics is provided.

3.4.1   Preliminaries

The upcoming spectral theory should as a minimum encompass the different random-
ization classes selected in Chapter 2 for further study. This includes random carrier
frequency (RCF) PWM and, on the other hand, fixed carrier frequency random PWM
(FCF-RPWM) techniques. The latter class may initially be regarded as variants of
random pulse-position (RPP) modulation, although other approaches belonging to this
class are treated in Chapter 6 also. Furthermore, the theory must comply with both
three-phase dc/ac converters and full-bridge dc/dc converters, which, in turn, may be
treated as a special case of dc/ac schemes.

   A key property of modulators for dc/ac converters is that the duty ratio d changes
value from one carrier period to the next in order to track an oscillating reference
waveform. This waveform consists of a fundamental component and, as discussed in
Chapter 2, harmonic components may also be present. For all random PWM strategies
considered in details in this thesis, d varies periodically in a deterministic manner to
assure full control of the fundamental voltage component. On this background, the
scope of the remaining part of this chapter may be formulated as:

> Given the time variations of the duty ratio d, derive a general analytical
> formula for the power spectral density for the corresponding pulse train
> that may be randomized both with respect to pulse position and duration
> of the carrier period, provided all probability density functions are known.

The mentioned pulse train may initially be interpreted as the switching function for
one leg of a three-phase converter, e.g. the q_a variable shown in Fig. 3.6. However,
the developed spectral theory has also proved to be useful for analysis of the PSD for

(a)   (b)
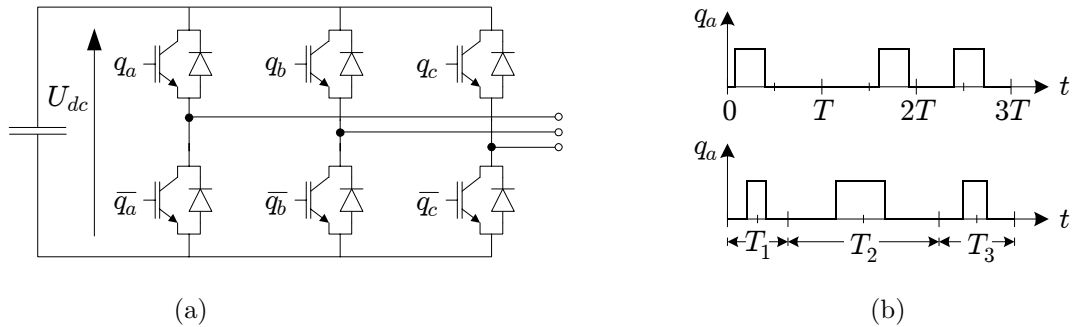
Figure 3.6 Three-phase VSC controlled by switching functions q_a, q_b, and q_c. (a) Circuit diagram and (b) examples of switching function q_a for random pulse-position and random carrier frequency modulation.

the line-to-line voltage and the phase-to-neutral voltage of a symmetrical load. This suggests that the term "pulse train" may have a broader interpretation than simply an array of rectangular pulses. More details may be found in Chapters 4–6.

The probability density functions mentioned above relate to the probability by which a certain randomization parameter is selected. Again, details are postponed until Chapter 5, but as a simple example, the random lead-lag technique mentioned in Chapter 2 may be considered: if leading and lagging pulse positions shall occur the same number of times, then the probability density functions for leading- and lagging-edge modulation should be $p(\text{lead}) = p(\text{lag}) = 0.5$, respectively. A mathematical treatment of the definitions and theorems related to such functions may be found in any textbook on probability theory, for example [1–5].

3.4.2 Related previous work

Many publications have examined variants of the RCF and the RPP techniques experimentally, but, as reviewed below, the literature dealing with theoretical analysis of frequency-domain properties is limited, especially for the dc/ac case, where the variations in the duty ratios must be taken into account.

Random carrier frequency PWM

One of the first publications on the subject is [22] by Boys, where an approximate analysis was outlined. The reported results show that the method gives satisfactory results if the carrier frequency ratio fulfills $f_{\max}/f_{\min} < 1.2$. In practice this ratio must be larger in order to get a sufficient spreading of the spectral power. Realistic $f_{\max}/f_{\min}$ ratios imply, unfortunately, that some of the assumptions taken in [22] are heavily violated, which leads to a large deviation between calculated and measured voltage spectra in cases of practical importance.

Another early source of information on random PWM in power electronics is [6] by Stanković. In this thesis, a principle for the analysis of the PSD for dc/ac converters with random carrier frequency PWM is outlined. Unfortunately, only a rudimentary treatment of the RCF method is presented making it difficult to evaluate the general applicability of the method, and the obtainable accuracy in particular. Also, no supporting measurements are included. Having stated that, it must also be emphasized

that the theoretical work of [6] has had a great impact on much of the spectral theory developed and presented in this thesis, including this chapter. There is no doubt that the investigations in [6] and the companion papers [23–27] have led to a well-established framework for the analysis of random PWM schemes.

The work of [28, 29] by Kirlin et al. is commented next. In these references, an approximate analysis of the power spectral density of the switching functions is provided based on an expansion of composite trigonometric functions by means of Bessel functions. The method may be promising, but unfortunately, the analysis is tailored towards purely sinusoidal modulators, making treatment of zero-sequence injection techniques very hard, if possible at all. Also, no decisive experimental work is included.

The analysis in [28, 29] has been revised in [30]. Here, it has been demonstrated that an exact analysis of the continuous density part generated by dc/ac RCF modulation is extremely complicated — even in case of a purely sinusoidal variation of the duty ratios. The difficulties originate from the fact that consecutive duty ratios are highly correlated in dc/ac converters.

Random pulse-position PWM

The literature dealing with spectral analysis of random pulse-position schemes for dc/ac conversion is very sparse. The publications may conveniently be categorized in two groups sorted by the authors who, furthermore, coincide with the researchers who have investigated RCF modulation.

The publications [6, 24, 26] originating from Stanković et al. partially deals with theoretical aspects of the RPP scheme for dc/ac converters. An analytic formula for the PSD is derived by extending earlier research in communication theory conducted by Middleton [31]. The theory is verified by an example being of academic interest only; no examples for cases of practical relevance are reported. The principles presented in [6] to calculate the spectral characteristics have, however, been applied successfully in Chapter 6, which validates much of the work of [6].

The other main source of information on RPP modulation is the work of Kirlin et al. reported in [7, 32, 33]. Here, an alternative spectral analysis is presented based on generalizations of a theorem in [34], which describes the spectral properties of binary signals. The theory is partially verified by laboratory measurements for the lead-lag random pulse position, but as shown in Chapter 6 this particular variant of RPP modulation is, unfortunately, inferior to other RPP schemes.

Discussion

When the work in the cited publications is compared to the work reported in this thesis, overlaps are, of course, found. However, in the opinion of the author, many details that need careful attention have not yet been investigated in an exhaustive manner without sacrificing either the generality of the theory at hand or the experimental validation of theoretical expressions.

The remaining part of this chapter seeks to establish a general theoretical framework that includes all random PWM schemes of interest. Detailed examples of how to apply this general spectral theory follow in later chapters, including verifications of all analytic results by laboratory measurements.
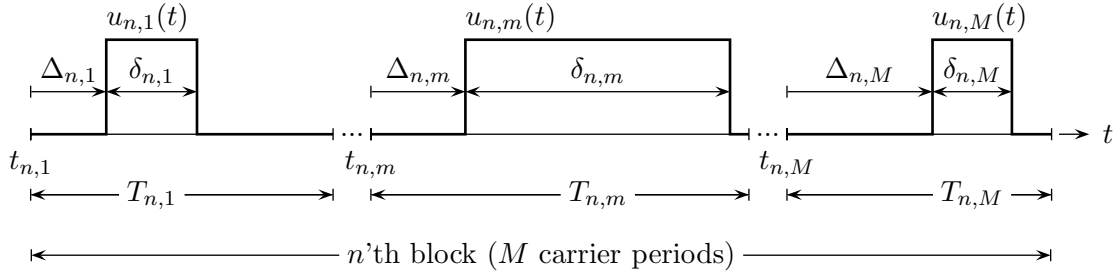
Figure 3.7 Parameterization of a pulse train consisting of an infinity of identical blocks which each are subdivided into M sampling intervals.

3.4.3   Outline of the spectral analysis methodology

The method used below for spectral analysis of random PWM schemes is based on work of [6], which, in turn, adopts a method originating from [31]. The derivation relies on the following three main steps:

1. The studied pulse train is parameterized. The pulse train is a continuous function of time, and in its simplest form it is identical to the switching function used to control a switch in e.g. a three-phase converter.

2. The autocorrelation function for one member of the ensemble of possible pulse trains is set up based on the parametric description obtained in step 1.

3. The expectation of the autocorrelation function is found. Then by using the fact that this function and the power spectral density function form a Fourier transformation pair, a general expression for the latter is formulated.

By comparing this procedure with the earlier definition (3.13) of the PSD on page 49, it may be seen that the derivations are very similar to the formal definition.

3.4.4   Parametric representation of the pulse train

The sequence of pulses that is analyzed is shown in Fig. 3.7. First, a truncated ensemble member $u_N^{(j)}(t)$ is created by concatenation of $(2N+1)$ blocks, where each block consists of M cycles of the carrier. As shown in Fig. 3.7, the start of the m'th carrier period in the n'th block is labeled $t_{n,m}$. The pulse position within the (n, m)'th interval is determined by the delay $\Delta_{n,m}$ with respect to $t_{n,m}$. The pulse width is denoted $\delta_{n,m}$.

Using these definitions, the truncated waveform may be expressed as the double summation

$$u_N^{(j)}(t) = \sum_{n=-N}^{N} \sum_{m=1}^{M} u(t - (t_{n,m} + \Delta_{n,m}); \delta_{n,m}), \qquad (3.21)$$

where the sampling pulse[7] $u(t - t'; \delta_{n,m})$ shown in Fig. 3.7 is zero outside the interval $0 \le t - t' \le \delta_{n,m}$.

---

[7]Here, it should be emphasized that the theory does not require the sampling pulse to be rectangular, although this particular waveform is used for the illustration in Fig. 3.7.

In some of the subsequent derivations, the pulse width $\delta_{n,m}$ and the delay $\Delta_{n,m}$ are rewritten in terms of the related duty ratio, i.e.

$$\delta_{n,m} = d_{n,m} T_{n,m} \tag{3.22}$$

for the pulse width; the delay of the pulse within the carrier cycle $T_{n,m}$ becomes

$$\Delta_{n,m} = \alpha_{n,m} T_{n,m}. \tag{3.23}$$

As an example of the normalized delay, $\alpha_{n,m} = \frac{1}{2}(1 - d_{n,m})$ should be used, if center-alignment of the pulses within the carrier period $T_{n,m}$ is required.

It should also be noted that for RCF the duty ratio $d_{n,m}$ is a random variable, because it is a function of the sampling time, which strongly depends on $t_{n,m}$. However, to simplify the derivations, it is assumed that all duty ratios are known a priori, i.e. to each carrier period $T_{n,m}$ an average duty ratio $d_{n,m}$ is assigned. These average duty ratios are precalculated on an equidistant time grid sampled at $\overline{T}$ seconds apart, where $\overline{T} = E\{T\}$ is the average duration of the (possibly random) carrier period. Further comments on this approach may be found in section 5.4 starting on page 122.

3.4.5 The autocorrelation function

Using the expression for the pulse train (3.21), the autocorrelation function $R^{(j)}(\tau)$ is found by (3.14) on some j'th member of the ensemble as the number of blocks N goes to infinity[8]:

$$
\begin{aligned}
R^{(j)}(\tau) &= \lim_{T_0 \to \infty} \frac{1}{2T_0} \int_{-T_0}^{+T_0} u_N^{(j)}(t) u_N^{(j)}(t - \tau) \, dt \\
&= \lim_{N \to \infty} \frac{1}{(2N+1)M\overline{T}} \int_{-\infty}^{+\infty} \sum_{n=-N}^{N} \sum_{m=1}^{M} u(t - (t_{n,m} + \Delta_{n,m}); \delta_{n,m}) \\
&\qquad\qquad\qquad \times \sum_{\tilde{n}=-N}^{N} \sum_{\tilde{m}=1}^{M} u(t - (t_{\tilde{n},\tilde{m}} + \Delta_{\tilde{n},\tilde{m}} + \tau); \delta_{\tilde{n},\tilde{m}}) \, dt.
\end{aligned}
\tag{3.24}
$$

The sampling pulses occurring in (3.24) may be expressed in terms of their inverse Fourier transformations

$$u(t - (t_{n,m} + \Delta_{n,m}); \delta_{n,m}) = \int_{-\infty}^{+\infty} U(f_1; \delta_{n,m}) e^{-j\omega_1(t_{n,m} + \Delta_{n,m})} e^{j\omega_1 t} \, df_1, \tag{3.25}$$

$$u(t - (t_{\tilde{n},\tilde{m}} + \Delta_{\tilde{n},\tilde{m}} + \tau); \delta_{\tilde{n},\tilde{m}}) = \int_{-\infty}^{+\infty} U(f_2; \delta_{\tilde{n},\tilde{m}}) e^{-j\omega_2(t_{\tilde{n},\tilde{m}} + \Delta_{\tilde{n},\tilde{m}} + \tau)} e^{j\omega_2 t} \, df_2, \tag{3.26}$$

where f_1 and f_2 are dummy integration variables over the frequency axis, $\omega_1 = 2\pi f_1$, and $\omega_2 = 2\pi f_2$. Also, the $U(\cdot)$ terms are the Fourier transformations of the sampling pulse shown in Fig. 3.7.

---

[8]To reduce the length of the following equations, the expectation operator appearing in (3.14) is not inserted until section 3.4.6.

Inserting (3.25) and (3.26) into (3.24), and changing the order of the summations, the autocorrelation function becomes

$$
R^{(j)}(\tau) = \sum_{m=1}^{M} \sum_{\tilde{m}=1}^{M} \left[\lim_{N\to\infty} \frac{1}{(2N+1)M\overline{\overline{T}}} \right.
$$

$$
\int_{-\infty}^{+\infty} \sum_{n=-N}^{N} \sum_{\tilde{n}=-N}^{N} \iint_{-\infty}^{+\infty} U(f_1; \delta_{n,m}) e^{-j\omega_1(t_{n,m}+\Delta_{n,m})} e^{j\omega_1 t}
$$

$$
\left. U(f_2; \delta_{\tilde{n},\tilde{m}}) e^{-j\omega_2(t_{\tilde{n},\tilde{m}}+\Delta_{\tilde{n},\tilde{m}}+\tau)} e^{j\omega_2 t} \, df_2 \, df_1 \, dt \right]. \quad (3.27)
$$

The partial autocorrelation function

Now, $R^{(j)}(\tau)$ may be interpreted as the double summation of the partial autocorrelation functions $R^{(j)}_{m,\tilde{m}}(\tau)$ defined by the expression in the square brackets in (3.27), i.e.

$$
R^{(j)}(\tau) = \sum_{m=1}^{M} \sum_{\tilde{m}=1}^{M} R^{(j)}_{m,\tilde{m}}(\tau), \quad (3.28)
$$

where the individual terms are given by

$$
R^{(j)}_{m,\tilde{m}}(\tau) = \lim_{N\to\infty} \frac{1}{(2N+1)M\overline{\overline{T}}}
$$

$$
\int_{-\infty}^{+\infty} \sum_{n=-N}^{N} \sum_{\tilde{n}=-N}^{N} \iint_{-\infty}^{+\infty} U(f_1; \delta_{n,m}) e^{-j\omega_1(t_{n,m}+\Delta_{n,m})} e^{j\omega_1 t}
$$

$$
U(f_2; \delta_{\tilde{n},\tilde{m}}) e^{-j\omega_2(t_{\tilde{n},\tilde{m}}+\Delta_{\tilde{n},\tilde{m}}+\tau)} e^{j\omega_2 t} \, df_2 \, df_1 \, dt. \quad (3.29)
$$

Changing the order of the integrations in (3.29) yields

$$
R^{(j)}_{m,\tilde{m}}(\tau) = \lim_{N\to\infty} \frac{1}{(2N+1)M\overline{\overline{T}}}
$$

$$
\sum_{n=-N}^{N} \sum_{\tilde{n}=-N}^{N} \iiint_{-\infty}^{+\infty} \left[U(f_1; \delta_{n,m}) e^{-j\omega_1(t_{n,m}+\Delta_{n,m})} \right.
$$

$$
\left. U(f_2; \delta_{\tilde{n},\tilde{m}}) e^{-j\omega_2(t_{\tilde{n},\tilde{m}}+\Delta_{\tilde{n},\tilde{m}}+\tau)} \right] e^{j(\omega_1+\omega_2)t} \, dt \, df_2 \, df_1. \quad (3.30)
$$

It is possible to reduce the triple integral to a double integral by noting that the term in brackets $[\cdot]$ is independent of t. Then, (3.30) may be simplified by using the rule [31]

$$
\int_{-\infty}^{+\infty} e^{j(\omega_1+\omega_2)t} \, dt = \delta(f_1 + f_2). \quad (3.31)
$$

This is called the Poisson identity, which relates the Dirac delta function to an improper integral of the exponential function from minus to plus infinity. Using (3.31) to simplify

(3.30) yields the following expression for the latter:

$$R_{m,\tilde{m}}(\tau) = \lim_{N\to\infty} \frac{1}{(2N+1)M\overline{T}}$$
$$\sum_{n=-N}^{N} \sum_{\tilde{n}=-N}^{N} \iint_{-\infty}^{+\infty} U(f_1; \delta_{n,m}) e^{-j\omega_1(t_{n,m}+\Delta_{n,m})}$$
$$U(f_2; \delta_{\tilde{n},\tilde{m}}) e^{-j\omega_2(t_{\tilde{n},\tilde{m}}+\Delta_{\tilde{n},\tilde{m}}+\tau)} \delta(f_1+f_2)\, df_2\, df_1. \quad (3.32)$$

The sampling property of the δ-function is now used. Since [31]

$$\int_{-\infty}^{+\infty} g(f)\delta(f-f')\, df = g(f'), \quad (3.33)$$

the double integration in (3.32) may be replaced by a single integration over the frequency f_1 because $f_2 = -f_1$ according to (3.33). This gives in total that

$$R_{m,\tilde{m}}^{(j)}(\tau) = \lim_{N\to\infty} \frac{1}{(2N+1)M\overline{T}} \sum_{n=-N}^{N} \sum_{\tilde{n}=-N}^{N}$$
$$\int_{-\infty}^{+\infty} U(f_1; \delta_{n,m}) U^\star(f_1; \delta_{\tilde{n},\tilde{m}}) e^{-j\omega_1(t_{n,m}-t_{\tilde{n},\tilde{m}})} e^{-j\omega_1(\Delta_{n,m}-\Delta_{\tilde{n},\tilde{m}})} e^{j\omega_1\tau}\, df_1, \quad (3.34)$$

where the fact that for real-valued functions like $u(t)$, the Fourier transformed version has the property that $U(-f_1) = U^\star(f_1)$, where the star * denotes the complex-conjugate operator.

The summation is now modified by substituting a dummy variable ℓ defined by $\ell = \tilde{n} - n \Leftrightarrow \tilde{n} = n + \ell$ into (3.34). Also, since there is only one integration over the frequency axis left, f_1 may safely be replaced simply by f. Hence,

$$R_{m,\tilde{m}}^{(j)}(\tau) = \lim_{N\to\infty} \frac{1}{(2N+1)M\overline{T}} \int_{-\infty}^{+\infty} \sum_{n=-N}^{N} \sum_{\ell=-N-n}^{N-n}$$
$$U(f; \delta_{n,m}) U^\star(f; \delta_{n+\ell,\tilde{m}}) e^{-j\omega(t_{n,m}-t_{n+\ell,\tilde{m}})} e^{-j\omega(\Delta_{n,m}-\Delta_{n+\ell,\tilde{m}})} e^{j\omega\tau}\, df. \quad (3.35)$$

Two auxiliary binary variables $y_{n,m}$ and $y_{n+\ell,\tilde{m}}$ defined by

$$y_{n,m} = \begin{cases} 1, & \text{if } |n| < N, \\ 0, & \text{otherwise,} \end{cases} \qquad y_{n+\ell,\tilde{m}} = \begin{cases} 1, & \text{if } |n+\ell| < N, \\ 0, & \text{otherwise,} \end{cases} \quad (3.36)$$

are now introduced in order to expand the limits of the ℓ summation in (3.35) to $\pm\infty$:

$$R_{m,\tilde{m}}^{(j)}(\tau) = \lim_{N\to\infty} \frac{1}{(2N+1)M\overline{T}} \int_{-\infty}^{+\infty} \sum_{\ell=-\infty}^{\infty} \sum_{n=-N}^{N}$$
$$y_{n,m} y_{n+\ell,\tilde{m}} U(f; \delta_{n,m}) U^\star(f; \delta_{n+\ell,\tilde{m}}) e^{-j\omega(t_{n,m}-t_{n+\ell,\tilde{m}})} e^{-j\omega(\Delta_{n,m}-\Delta_{n+\ell,\tilde{m}})} e^{j\omega\tau}\, df. \quad (3.37)$$

3.4.6 The expectation of the autocorrelation function

To get the ensemble average $R_{m,\tilde{m}}(\tau) = E\{R^{(j)}_{m,\tilde{m}}(\tau)\}$ of the partial autocorrelation function, the E-operator appearing in (3.14) is now inserted into (3.37). Hence,

$$R^{(j)}_{m,\tilde{m}}(\tau) = \lim_{N \to \infty} \frac{1}{(2N+1)M\overline{\overline{T}}} \int_{-\infty}^{+\infty} E\bigg\{ \sum_{\ell=-\infty}^{\infty} \sum_{n=-N}^{N} y_{n,m} y_{n+\ell,\tilde{m}}$$

$$U(f;\delta_{n,m})U^{\star}(f;\delta_{n+\ell,\tilde{m}})e^{-j\omega(t_{n,m}-t_{n+\ell,\tilde{m}})}e^{-j\omega(\Delta_{n,m}-\Delta_{n+\ell,\tilde{m}})}\bigg\}e^{j\omega\tau}\,df. \quad (3.38)$$

Since the statistical properties of the dithering parameters are assumed to form stationary random processes (i.e. they do not very over time), the expectation $E\{\cdot\}$ in (3.38) is a function of the delay ℓ only. This implies that the summation over n may be replaced by a multiplication by the number of terms in the summation, i.e. $2N+1$. Also for $N \to \infty$, the auxiliary variables $y_{n,m}$ and $y_{n+\ell,\tilde{m}}$ may be omitted. In total, these observations lead to the final expression for the autocorrelation

$$R_{m,\tilde{m}}(\tau) = \frac{1}{M\overline{\overline{T}}} \int_{-\infty}^{+\infty} E\bigg\{ \sum_{\ell=-\infty}^{\infty} U(f;\delta_{0,m})U^{\star}(f;\delta_{\ell,\tilde{m}})$$

$$e^{-j\omega(t_{0,m}-t_{\ell,\tilde{m}})}e^{-j\omega(\Delta_{0,m}-\Delta_{\ell,\tilde{m}})}\bigg\}e^{j\omega\tau}\,df. \quad (3.39)$$

3.4.7 General expression for the power spectral density

The autocorrelation function $R_{m,\tilde{m}}(\tau)$ and the power spectral density $S_{m,\tilde{m}}(f)$ forms by definition (3.13) on page 49 a Fourier transformation pair. It follows then from (3.39) that the partial PSD is

$$S_{m,\tilde{m}}(f) = \frac{1}{M\overline{\overline{T}}} E\bigg\{ \sum_{\ell=-\infty}^{\infty} U(f;\delta_{0,m})U^{\star}(f;\delta_{\ell,\tilde{m}})e^{j\omega(t_{\ell,\tilde{m}}-t_{0,m})}e^{j\omega(\Delta_{\ell,\tilde{m}}-\Delta_{0,m})}\bigg\} \quad (3.40)$$

By virtue of (3.28), the total PSD for the pulse train becomes

$$S(f) = \sum_{m=1}^{M} \sum_{\tilde{m}=1}^{M} S_{m,\tilde{m}}(f), \quad (3.41)$$

where the individual terms are found by (3.40).

In total, (3.41) together with (3.40) constitute a set of general formulas for the power spectral density of a block-stationary pulse train with randomized duration of the carrier periods (or, alternatively, frequency). Also, the pulse position and the pulse width may be random variables, and they may be either dependent or independent of the current carrier period.

These results are used as a starting point for the derivations of analytical expressions for the spectral characteristics of different random PWM techniques.

3.5   Summary

In this chapter focus has been put on theoretical and experimental aspects closely related to frequency-domain analysis of randomly modulated pulse trains. In this connection, the key topic of power spectral density, which may be regarded as a generalization of Fourier series expansion of periodic signals, was briefly explained in order to fix concepts of fundamental importance in this thesis. Textbooks cited in section 3.2 should be consulted for an exhaustive treatment of these mathematical topics.

To evaluate the validity of the spectral analyses of various random PWM techniques set forth in the following chapters, comparisons with laboratory measurements play a vital role. It turns out, however, that due to the mixed spectral characteristics (the spectrum may have both a density and a discrete part) of randomly modulated pulse trains, such comparisons require careful attention due to limitations of DSA's. The problems were highlighted by sample laboratory measurements by estimating the spectrum for the same signal using different settings of the DSA. It was shown that misinterpretation may easily result, if the operating principles of the DSA are not taken into account. Also, the impossibility of simultaneously measuring the density part and the harmonic part of such a mixed spectrum was demonstrated.

The reasons for those pitfalls and limitations were explained using a minimum of mathematics. Instead, an analogy between analog filters and the DFT (discrete Fourier transformation) was used, because the DFT forms the core of many DSA functions, including the numerical methods used in such instruments for PSD estimation.

To compare spectra calculated by analytical expressions with spectra estimated by a DSA, a simple methodology was then devised that ensures a fair comparison. The idea is to imitate the "errors" that the DSA is known to perform, i.e. the calculated spectrum is filtered (or, more precisely, convoluted) with the characteristics of the DSA before the actual comparison to measurements is made.

The second topic treated in this chapter was a general spectral analysis of pulse trains existing in random PWM converters. In this connection, a review was first given of earlier research results. As elaborated in section 3.4.2 valuable theoretical contributions do exist in the literature, although the results available do not encompass all random PWM techniques of current interest.

Therefore, by extending work of Middelton [31], which has successfully been used by Stanković [6] for closely related problems, a set of general formulas was derived for the power spectral density of randomly modulated pulse trains. Using these results as a starting point, it is possible to derive expressions for the spectral characteristics of a variety of random PWM schemes, where variables like the carrier frequency, the pulse width, and the pulse position within each carrier period are subjected to random variations. Furthermore, the duty ratio may vary periodically in order to track a sinusoidal reference, etc.

The work reported in this chapter is clearly based on existing stochastic and digital signal processing theory, which from an engineering point of view unfortunately may be difficult to comprehend due to the amount of the mathematics involved in those disciplines. Therefore — from a strictly mathematical point of view — the originality of the contributions is probably limited. On the other hand, it is still believed that valuable contributions have been made with respect to proper analysis of random PWM

in power electronic applications, including:

- A treatment focusing on engineering aspects rather than on mathematical details of how to use (or misuse) dynamic signal analyzers for spectral analysis.

- Presentation of a simple methodology that ensures a fair and physical correct comparison of calculated and measured spectra that have mixed characteristics.

- Derivation of a general framework for spectral analysis that encompasses a large class of nondeterministic signals of interest in random PWM applications.

As documented in later chapters, these results have proved very useful for spectral analysis of random PWM techniques, and for experimental verification of the derived analytical expressions.

Bibliography

[1] W. B. Davenport, Jr. and W. L. Root, *An Introduction to the Theory of Random Signals and Noise*, IEEE Press Selected Reprint Series (reprint of the original 1958 edition), New York, 1987.

[2] A. Papoulis, *Probability, Random Variables, and Stochastic Processes*, Electrical & Electronic Engineering Series. McGraw-Hill, third edition, 1991.

[3] P. Z. Peebles, *Probability, Random Variables, and Random Signal Principles*, McGraw-Hill Series in Electrical Electronic Engineering. McGraw-Hill Book Company, second edition, 1987.

[4] G. R. Cooper and C. D. McGillem, *Probabilistic Methods of Signal and Systems Analysis*, Harcourt Brace Jovanovich College Publishers, Orlando, Florida, second edition, 1986.

[5] K. S. Shanmugan and A. M. Breipohl, *Random Signals. Detection, Estimation and Data Analysis*, John Wiley & Sons, New York, 1988.

[6] A. M. Stanković, *Random Pulse Modulation with Applications to Power Electronic Converters*, Ph.D. thesis, Massachusetts Institute of Technology, Feb. 1993.

[7] R. L. Kirlin, S. Kwok, S. Legowski, and A. M. Trzynadlowski, "Power Spectra of a PWM Inverter with Randomized Pulse Position," *IEEE Trans. on Power Electronics*, vol. 9, no. 5, pp. 463–472, Sept. 1994.

[8] T. Tanaka, H. Kameda, and T. Ninomiya, "Noise Analysis of DC-to-DC Converter with Random Switching Control," *Proc. of the IEEE International Telecommunications Energy Conference*, pp. 283–290, Nov. 1991.

[9] T.-J. Liang, J.-F. Chen, and J.-L. Shyu, "Novel Multi-Random PWM Technique for Inverter Design," *Proc. of the IEEE 1999 International Conference on Power Electronics and Drive Systems*, vol. 2, pp. 942–946, 1999.

[10] J. Holtz, "Pulse Width Modulation for Electronic Power Conversion," in *Power Electronics and Variable Frequency Drives. Technology and Applications*, B. K. Bose, Ed., New York, 1997, pp. 138–208, IEEE Press.

[11] P. D. Welch, "The Use of Fast Fourier Transform for the Estimation of Power Spectra: A Method based on Time Averaging over Short, Modified Periodograms," *IEEE Trans. on Audio Electroacoustics*, vol. AU-15, pp. 70–73, June 1967.

[12] The MathWorks, *Signal Processing Toolbox User's Guide, Version 4*, The Math-Works Inc., Dec. 1996.

[13] J. G. Proakis and D. G. Manolakis, *Digital Signal Processing. Principles, Algorithms, and Applications*, Prentice Hall, Upper Saddle River, New Jersey, third edition, 1996.

[14] R. B. Randall, *Frequency Analysis*, Brüel & Kjær, Nærum, Denmark, third edition, 1987, ISBN 87-87355-07-8.

[15] F. J. Harris, "On the Use of Windows for Harmonic Analysis with Discrete Fourier Transform," *Proceedings IEEE*, vol. 66, pp. 51–83, 1978.

[16] S. Gade and H. Herlufsen, "Use of Weighting Functions in DFT/FFT Analysis (Part I & II)," *Brüel & Kjær Technical Review*, no. 3 and 4, 1987, ISSN 007–26211987.

[17] Y. S. Lai, H. C. Huang, Y. S. Kuan, and C. M. Young, "A New Random Inverter Control Technique for Motor Drives," *Proc. of the 13th IEEE Applied Power Electronics Conference and Exposition*, vol. 1, pp. 101–107, Feb. 1998.

[18] V. G. Agelidis and D. Vincenti, "Optimum Non-Deterministic Pulse-Width Modulation for Three-Phase Inverters," *Proc. of the 19th IEEE International Conference on Industrial Electronics, Control, and Instrumentation*, vol. 2, pp. 1234–1239, 1993.

[19] S. Y. R. Hui, S. Sathiakumar, and K. K. Sung, "Novel Random PWM Schemes with Weighted Switching Decision," *Proc. of the 6th International Conference on Power Electronics and Variable Speed Drives*, pp. 348–353, 1996, IEE Conf. Publication No. 429.

[20] M. M. Bech, F. Blaabjerg, J. K. Pedersen, and A. M. Trzynadlowski, "A Methodology for True Comparison of Analytical and Measured Frequency Domain Spectra in Random PWM Converters," *Proc. of the 29th IEEE Power Electronics Specialists Conference*, vol. 1, pp. 36–43, May 1998.

[21] M. M. Bech, J. K. Pedersen, F. Blaabjerg, and A. M. Trzynadlowski, "A Methodology for True Comparison of Analytical and Measured Frequency Domain Spectra in Random PWM Converters," *IEEE Trans. on Power Electronics*, vol. 14, no. 3, pp. 578–586, May 1999.

[22] J. T. Boys, "Theoretical Spectra for Narrow-Band Random PWM Waveforms," *IEE Proc. Part B*, vol. 140, no. 6, pp. 393–400, Nov. 1993.

[23] A. M. Stanković, G. C. Verghese, and R. O. Hinds, "Monte-Carlo Verification of Power Spectrum Formulas for Random Modulation Schemes," *Proc. of the 3rd IEEE Workshop on Computers in Power Electronics*, pp. 187–194, Aug. 1992.

[24] A. M. Stanković, G. C. Verghese, and D. J. Perreault, "Analysis and Synthesis of Random Modulation Schemes for Power Converters," *Proc. of the 24th IEEE Power Electronics Specialists Conference*, pp. 1068–1074, 1993.

[25] A. M. Stanković, G. C. Verghese, and D. J. Perreault, "Randomized Modulation Schemes for Power Converters Governed by Markov Chains," *Proc. of the 4th IEEE Conference on Control Applications*, pp. 372–377, 1995.

[26] A. M. Stanković, G. C. Verghese, and D. J. Perreault, "Analysis and Synthesis of Randomized Modulation Schemes for Power Converters," *IEEE Trans. on Power Electronics*, vol. 10, no. 6, pp. 680–693, Nov. 1995.

[27] A. M. Stanković, G. C. Verghese, and D. J. Perreault, "Randomized Modulation of Power Converters via Markov Chains," *IEEE Trans. on Control Systems Technology*, vol. 5, no. 1, pp. 61–73, Jan. 1997.

[28] R. L. Kirlin, A. M. Trzynadlowski, M. M. Bech, F. Blaabjerg, and J. K. Pedersen, "Analysis of Spectral Effects of Random PWM Strategies for Voltage Source Inverters," *Proc. of 7th European Conference on Power Electronics and Applications*, vol. 1, pp. 146–151, 1997.

[29] R. L. Kirlin and A. M. Trzynadlowski, "A Unified Approach to Analysis and Design of Random Pulsewidth Modulation in Voltage Source Inverters," *IEEE Trans. on Circuits and Systems — I: Fundamental Theory and Applications*, vol. 44, no. 8, pp. 763–766, Aug. 1997.

[30] R. L. Kirlin, "Continuous Spectrum for Random Segment Width PWM DC-AC Conversion," private correspondence, Jan. 1998.

[31] D. Middleton, *An Introduction to Statistical Communication Theory*, McGraw-Hill Book Company, New York–Toronto–London, 1960.

[32] S. Legowski, J. Bei, and A. M. Trzynadlowski, "Analysis and Implementation of a Grey-Noise PWM Technique Based on Voltage Space Vectors," *Proc. of the 7th IEEE Applied Power Electronics Conference and Exposition*, pp. 586–593, 1992.

[33] R. L. Kirlin, S. Legowski, A. M. Trzynadlowski, Y. Cui, and S. Kwok, "Power Spectra of a Three-Phase Inverter with Random Pulse Width Modulation Modes," *Proc. of the 3rd IEEE Workshop on Computers in Power Electronics*, pp. 265–267, Aug. 1992.

[34] J. J. Stiffler, *Theory of Synchronous Communication*, Prentice-Hall, Englewood Cliffs, New Jersey, 1971.

Chapter 4

Analysis of random PWM schemes for full-bridge dc/dc converters

4.1 Introduction

Random PWM schemes suited for voltage control of full-bridge dc/dc converters are studied in this chapter. Focus is put on spectral analysis of the output voltage during operation with two of the random PWM modulators discussed in Chapter 2. In particular, the random carrier frequency (RCF) technique and a simple variant of random pulse-position (RPP) modulation are investigated.

The main objectives of this chapter are to derive analytic expressions for the voltage spectrum and to verify the correctness of the derivations by comparing calculated and measured spectra. Also, a somewhat more implicit objective is a partial verification of the generalized spectral analysis presented in Chapter 3. Finally, the usefulness of the methodology sketched in section 3.3.4 to ensure a fair comparison of calculated and estimated spectra is demonstrated by a series of examples.

The work in this chapter is by no means attempted to be self-contained — much of it strongly relates to ideas and results presented in the previous chapter. Also, results enclosed in the following chapters dealing with random PWM in three-phase dc/ac applications may be adapted to full-bridge dc/dc converters. For example, a discussion of current-quality issues is omitted in this chapter, because the main conclusions drawn on this topic in Chapter 6 apply equally well to randomly pulse-width modulated full-bridge dc/dc converters. Another important topic, which is treated in a more exhaustive manner in Chapter 5, but still of importance here, relates to spectral analysis of the voltage between two output terminals in a multi-legged converter.

Chapter outline

The principal content is divided into three sections. The first section presents preliminary information relating to the spectral analysis of randomly modulated full-bridge dc/dc converters besides derivations of formulas for the spectra caused by either random carrier frequency modulation or random pulse-position modulation. The next two sections provide detailed examples of spectral analysis of both the RCF and the RPP techniques, including detailed comparisons to laboratory measurements.

(a)   (b)   (c)
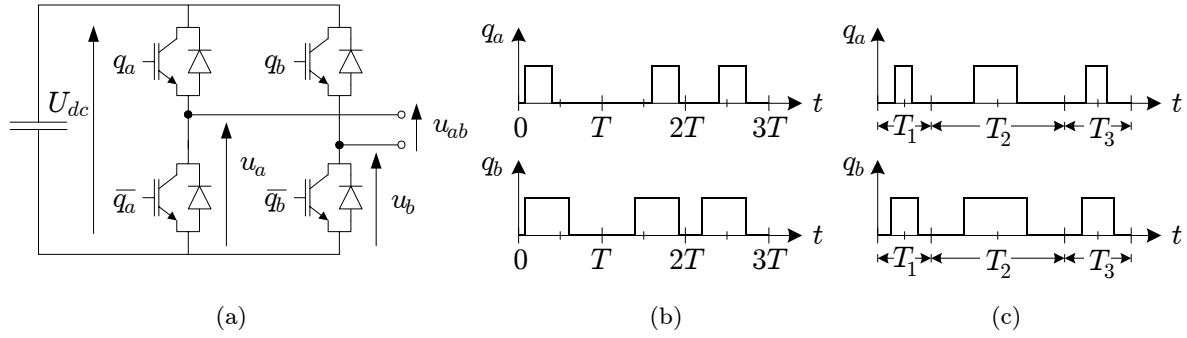
Figure 4.1 Full-bridge dc/dc converter controlled by two switching functions q_a and q_b. (a) Circuit diagram; typical switching functions for (b) random pulse-position and (c) random carrier frequency modulation.

4.2   Preliminaries

Besides information regarding the used notation, this section does also include a more detailed outline of the scope of the chapter. A brief review of past investigations treating similar topics is also provided.

4.2.1   Scope of current work

The power spectral density of the output voltage from a full-bridge dc/dc converter controlled by various random PWM schemes is the main topic for the study in this chapter. Fig. 4.1 defines the used nomenclature for the full-bridge converter topology, and it follows immediately that the output voltage is $u_{ab} = U_{dc}(q_a - q_b)$ at any time instant. Apart from an essentially constant factor (U_{dc}), the stochastic quantity of interest (u_{ab}) is the difference of two other random variables: the switching functions q_a and q_b used to control each of the two legs in the converter.

This situation is very similar to the line-to-line voltage generated by a three-phase voltage source converter: the quantities of interest are not the switching functions themselves, but rather the difference of two switching functions. The consequences of this detail have not yet been fully investigated. For example, the investigations in [1, 2] and also in [3] relating to three-phase converters assume that the switching functions for the legs are mutually displaced in time by one third of the fundamental period T_1, i.e. it is assumed that $q_b(t) = q_a(t - \frac{1}{3}T_1)$, etc. In practice, this assumption is always violated, because in a specified carrier period, all switching functions are dithered by the outcome of the same random experiment[1]; the fundamental components of the switching functions are displaced in time, but generalizing this property to include the random part as well can never be justified. The consequences of ignoring this fact are demonstrated in section 5.5 starting on page 137.

Irrespective of whether a dc/dc converter or a three-phase dc/ac converter is studied, the proper procedure is to take the mutual dependence of the control of the legs into account. For the full-bridge dc/dc converter, this interdependence is manifested by the fact that the same random carrier frequency would be used to control both legs for

---

[1]Refer to section 2.4 starting on page 30 for a classification of random PWM schemes.

the RCF technique, see Fig. 4.1(c). Likewise for the random pulse-position PWM, the same random variable governs the delay as illustrated in Fig. 4.1(b). Now, starting from $u_{ab} = U_{dc}(q_a - q_b)$, it may straightforwardly be shown by using fundamental properties of jointly dependent stochastic signals (see [4, 5], for example) that for a converter with two legs controlled by two switching functions q_a and q_b, the power spectral density (PSD) denoted by $S_{ab}(f)$ of the difference $(q_a - q_b)$ is

$$S_{ab}(f) = S_a(f) + S_b(f) - C_{ab}(f) - C_{ba}(f), \tag{4.1}$$

where $S_a(f)$ and $S_b(f)$ are the spectra of q_a and q_b, respectively. Also, $C_{ab}(f)$ and $C_{ba}(f)$ are the cross power spectral densities defined as the Fourier transformation of the matching cross correlation functions. For example, $C_{ab}(f)$ may be determined from its cross correlation function $R_{ab}(\tau)$ defined by

$$R_{ab}(\tau) = \lim_{T_0 \to \infty} \frac{1}{2T_0} \int_{-T_0}^{+T_0} E\{q_a(t)q_b(t - \tau)\} \, dt, \tag{4.2}$$

which closely resembles the auto correlation function previously defined by (3.14) on page 49. For the random PWM techniques studied here, $S_a(f)$ and $S_b(f)$ in (4.1) can be found relatively easily, but expressions for the cross terms $C_{ab}(f)$ $(= C_{ba}^{\star}(f))$ for two correlated random variables are harder to find.

At this point it should be emphasized that the quantity of primary interest in dc/dc converter applications is the terminal voltage u_{ab} shown in Fig. 4.1(a), and not the voltages u_a and u_b, simply because the load is fed by the u_{ab} voltage. Stated in other words, it is impossible to cut corners and study q_a and q_b only, if the terminal characteristics are of primary concern. On the other hand, the spectrum of the internal voltages u_a and u_b could also be the main objective for the study, for example in relation to predictions of leakage currents caused by fast charging (discharging) of stray capacitances between e.g. a power transistor and its grounded heat sink.

Keeping these points in mind, the first objective of this chapter is to give examples of how the spectra $S_a(f)$ and $S_b(f)$ in (4.1) for the switching functions q_a and q_b, respectively, can be found analytically for two random PWM schemes for full-bridge dc/dc converters. Also, according to (4.1), knowledge of $S_a(f)$ and $S_b(f)$ is insufficient information to determine the spectrum of the output voltage as the cross spectra are also needed. Hence, a second objective is to find $S_{ab}(f)$ for both RPP and RCF modulation, but instead of attempting to find the cross terms in (4.1), an alternative method has been developed rendering explicit knowledge of the cross spectra superfluous.

As a final comment, the case where q_a and q_b are controlled in a statistically independent manner may be considered. Under this condition, the two cross terms in (4.1) vanish, which simplifies the analysis considerably. Random PWM schemes that may allow such independence were classified in section 2.4.2 as "multiple random variable methods," but it was also pointed out in Chapter 2 that a practical use of such asynchronous techniques is hard to imagine. Although it cannot justify the practical use, an (academic) advantage of such schemes is the mathematically simpler spectral analysis thanks to the vanishing cross spectral densities.

4.2.2   Related previous work

No publications dealing directly with random modulation in conjunction with full-bridge dc/dc converters have been traced in the literature listed in Appendix B. Investigations of transformer-less single-switch dc/dc converters may be found [6–10], but the major source of information on spectral analysis of random PWM for such converters offspring from the thesis [3] by Stanković, which is summarized in [11]. Other papers like [12–16] do also provide informative analyses.

Ref. [3] examines different modulators and presents several theoretical results, but only a few supporting measurements accompany the analyses. Still, in some aspects the work presented below resembles earlier work of Stanković, although the analyses in this chapter focus to a much higher degree on details of great practical importance. For example, [3] does not include analysis of schemes with center-aligned pulses, but rather very academic schemes, like random choice of random modulation (refer to section 2.4 in Chapter 2), are studied to some extent in [3].

In summary, some overlap between the subsequent theoretical analyses and earlier reports is inevitable, but still many details and verification issues included below have not been reported elsewhere to the knowledge of the author.

4.3   Spectral analysis of random PWM schemes

Compared to modulators for dc/ac conversion, modulators for dc/dc converters are less complicated to analyze due to the mere fact that the reference duty ratios remain constant, at least in the schemes studied here[2]. As shown below, this also simplifies the spectral analysis of random PWM schemes for dc/dc converters compared to the general case treated in Chapter 3. Also, expressions for the PSD caused by the random carrier frequency and the random pulse-position schemes are derived in this section. Specific examples of how to use these equations are given in subsequent sections.

4.3.1   General power spectral density formula

The starting point for all spectral analysis in this chapter is the main result of Chapter 3, where general expressions for the spectrum of randomly modulated pulse trains were derived. The key equations (3.40) and (3.41) on page 67, which are valid for modulators that include deterministic variations in the duty ratios, may be simplified in the current case, because it is adequate to use a block-length M equal to one in (3.41) for dc/dc random PWM schemes. Hence, the expression

$$S(f) = \frac{1}{T} E\left\{ \sum_{\ell=-\infty}^{\infty} U(f;\delta_0)U^{\star}(f;\delta_\ell)e^{j\omega(t_\ell-t_0)}e^{j\omega(\Delta_\ell-\Delta_0)} \right\} \qquad (4.3)$$

follows immediately. Here, $U^{\star}(f;\delta_\ell)$ is the complex-conjugated of the Fourier transformation of the sampling pulse $u_\ell(t)$ shown in Fig. 4.2 parameterized by the pulse

---

[2]As argued in section 2.4, the modulators that assure proper volt-seconds balance are preferable to randomization schemes that rely on dithering of several consecutive carrier periods. Only schemes that guarantee constant duty ratio operation are considered here.
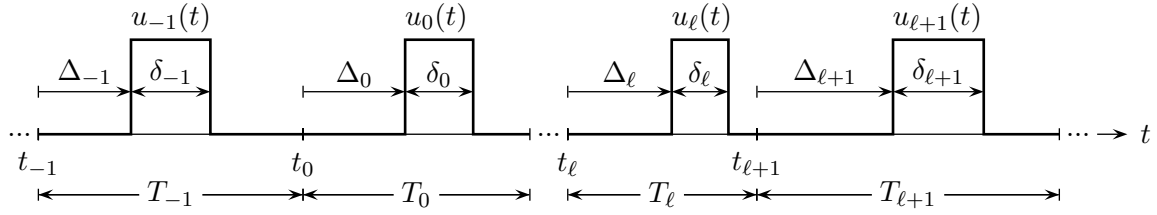
Figure 4.2 Parametric representation of pulse trains for dc/dc random PWM schemes operating at constant duty ratio. $\ell > 0$ is assumed in this diagram.

width δ_ℓ; t_ℓ marks the starting point of the ℓ'th carrier period, and finally Δ_ℓ is the delay of the pulse within the ℓ'th carrier period with respect to t_ℓ. In (4.3), the pulse-position Δ_ℓ and the pulse width δ_ℓ may be random variables, and they may be either dependent or independent of the random carrier period $T_\ell \triangleq t_{\ell+1} - t_\ell$. An expression very similar to (4.3) may be found in [11] also.

To facilitate the subsequent derivations, the RPP and RCF modulators may be characterized using the terminology of (4.3). Hence,

Random pulse position

Successive pulse positions are randomized within the limits of the constant carrier period $T \triangleq T_\ell$, i.e. the delay in the ℓ'th interval must fulfill $0 \leq \Delta_\ell \leq (1-d)T$, where d is the duty ratio. Also, the pulse width $\delta_\ell = dT$ is constant.

Random carrier frequency

The duration of the instantaneous carrier period T_ℓ (or, equivalently: the carrier frequency) is selected at random. The pulses are center-aligned within each interval, which implies that the delay $\Delta_\ell = \frac{1}{2}(1-d)T_\ell$ and the pulse width $\delta_\ell = dT_\ell$ both are random variables heavily correlated with T_ℓ.

A detailed analysis of these two schemes, which retain volt-second balance on the macroscopic time scale by completely different principles, follows below.

4.3.2 Random pulse-position modulation

For random PWM techniques like RPP operating at a constant carrier frequency, the $t_\ell - t_0$ term in (4.3) is simply $t_\ell - t_0 = \ell T$, because all instances of T_ℓ are identical. Under this constraint, (4.3) reduces to

$$S(f) = \frac{1}{T} \sum_{\ell=-\infty}^{\infty} E\{U(f;\delta_0)U^\star(f;\delta_\ell)e^{j\omega(\Delta_\ell - \Delta_0)}\}e^{j\omega T\ell}. \tag{4.4}$$

The expectation of products may be rewritten as a product of expectations, because it is assumed that all delays Δ_ℓ are randomized in a statistically independent manner. It should be noted, however, that the $\ell = 0$ case requires special attention, i.e. (4.4) may

be re-factored as

$$S(f) = \frac{1}{T} \sum_{\ell=-\infty}^{\infty} E\{U(f;\delta_0)e^{-j\omega\Delta_0}\} E\{U^\star(f;\delta_\ell)e^{j\omega\Delta_\ell}\} e^{j\omega T\ell}$$

$$+ \frac{1}{T}\Big(\underbrace{E\{U(f;\delta_0)U^\star(f;\delta_0)\}}_{\text{Correct } \ell=0 \text{ term}} - \underbrace{E\{U(f;\delta_0)e^{-j\omega\Delta_0}\}E\{U^\star(f;\delta_0)e^{j\omega\Delta_0}\}}_{\text{Wrong } \ell=0 \text{ term in summation}} \Big), \quad (4.5)$$

where the expressions on the last line correct the errors caused by the $\ell = 0$ term in the summation on the first line of (4.5). Once more, advantage of the stationary modulation used in dc/dc conversion is taken: since the Fourier transformation $U(f;\delta_\ell)$ of the sampling pulse is independent of ℓ, these factors can be moved outside the expectation operators. Also, the indices on the δ_ℓ and Δ_ℓ terms become unnecessary. In total, by combining complex-conjugated terms, the spectrum becomes

$$S(f) = \frac{1}{T}|U(f;\delta)|^2 |E\{e^{-j\omega\Delta}\}|^2 \sum_{\ell=-\infty}^{\infty} e^{j\omega T\ell}$$

$$+ \frac{1}{T}|U(f;\delta)|^2 \Big(1 - |E\{e^{-j\omega\Delta}\}|^2\Big). \tag{4.6}$$

The next step is now to evaluate the sum of exponentials. Here, the following identity is needed, which relates a sum of complex exponentials to a sum of impulse functions [17]

$$\sum_{\ell=-\infty}^{\infty} e^{j\omega T\ell} = \frac{1}{T} \sum_{n=-\infty}^{\infty} \delta\Big(f - \frac{n}{T}\Big), \quad \omega = 2\pi f. \tag{4.7}$$

Using this relationship, (4.6) may be put into its final form

$$S(f) = \frac{1}{T}|U(f;\delta)|^2 \bigg[1 - |E\{e^{-j\omega\Delta}\}|^2 + \frac{1}{T}|E\{e^{-j\omega\Delta}\}|^2 \sum_{n=-\infty}^{\infty} \delta\Big(f - \frac{n}{T}\Big) \bigg], \tag{4.8}$$

which shows that the spectrum produced by a random PWM technique operating at a constant switching carrier $1/T$ has both a density part and a harmonic part. Equation (4.8) requires that all sampling pulses are identical and also, the randomization of the delay Δ must be determined by independent trials in such a way that no overlap is generated between consecutive intervals in order to assure that the system is causal.

4.3.3   Random carrier frequency modulation

To evaluate (4.3), the expectation of the infinite sum across ℓ must be found. In RCF, the width of the carrier period $T_\ell = t_{\ell+1} - t_\ell$ is selected at random according to a known probability density function and the delay Δ_ℓ within each interval must be set so that a center-alignment occurs. This implies that $\Delta_\ell = \frac{1}{2}(1-d)T_\ell$, where d is the duty ratio. In order to shorten the notation, another parameter $\alpha \triangleq \frac{1}{2}(1-d)$ is introduced, which allows us to write $\Delta_\ell = \alpha T_\ell$.

To proceed the analysis, the differences $(t_\ell - t_0)$ and $(\Delta_\ell - \Delta_0)$ in (4.3) must be found as well. Based on Fig. 4.2 besides the auxiliary parameters introduced above, these differences become

$$\Delta_\ell - \Delta_0 = \alpha(T_\ell - T_0), \quad \text{for all } \ell, \tag{4.9}$$

and

$$t_\ell - t_0 = \begin{cases} -\sum\limits_{n=\ell}^{-1} T_n, & \text{for } \ell \leq -1, \\ 0, & \text{for } \ell = 0, \\ \sum\limits_{n=0}^{\ell-1} T_n, & \text{for } \ell \geq 1. \end{cases} \tag{4.10}$$

Inserting these differences into the general formula for the spectrum (4.3) by expanding the summation over ℓ yields

$$\begin{aligned}
\overline{T}S(f) = E\Big\{ \quad & \cdots \; + U(f;\delta_0)\,U^\star(f;\delta_{-3})\,e^{-j\omega(T_{-1}+T_{-2}+T_{-3})}e^{j\omega\alpha(T_{-3}-T_0)} \\
& + U(f;\delta_0)\,U^\star(f;\delta_{-2})\,e^{-j\omega(T_{-1}+T_{-2})}e^{j\omega\alpha(T_{-2}-T_0)} \\
& + U(f;\delta_0)\,U^\star(f;\delta_{-1})\,e^{-j\omega T_{-1}}e^{j\omega\alpha(T_{-1}-T_0)} \\
& + U(f;\delta_0)\,U^\star(f;\delta_0) \\
& + U(f;\delta_0)\,U^\star(f;\delta_1)\,e^{j\omega T_0}e^{j\omega\alpha(T_1-T_0)} \\
& + U(f;\delta_0)\,U^\star(f;\delta_2)\,e^{j\omega(T_0+T_1)}e^{j\omega\alpha(T_2-T_0)} \\
& + U(f;\delta_0)\,U^\star(f;\delta_3)\,e^{j\omega(T_0+T_1+T_2)}e^{j\omega\alpha(T_3-T_0)} \; + \; \cdots \Big\},
\end{aligned} \tag{4.11}$$

where the expressions have been typed out for $-3 \leq \ell \leq 3$ only.

Now the fact that there is no correlation between sequential carrier frequencies is used, i.e. all values of T_ℓ are independent (see Chapter 5 also). The expectation of products in (4.11) may then be rewritten as a product of expectations leading to

$$\overline{T}S(f) =$$

$$E\big\{U(f;\delta_0)\,e^{-j\omega\alpha T_0}\big\}\Big[\cdots + E\big\{U^\star(f;\delta_{-3})\,e^{-j\omega(1-\alpha)T_{-3}}\big\}E\big\{e^{-j\omega T_{-1}}\big\}E\big\{e^{-j\omega T_{-2}}\big\}$$

$$+ E\big\{U^\star(f;\delta_{-2})\,e^{-j\omega(1-\alpha)T_{-2}}\big\}E\big\{e^{-j\omega T_{-1}}\big\}$$

$$+ E\big\{U^\star(f;\delta_{-1})\,e^{-j\omega(1-\alpha)T_{-1}}\big\}\;\Big]$$

$$+ E\big\{U(f;\delta_0)\,U^\star(f;\delta_0)\big\}$$

$$+ E\big\{U(f;\delta_0)\,e^{j\omega(1-\alpha)T_0}\big\}\Big[\quad E\big\{U^\star(f;\delta_1)\,e^{j\omega\alpha T_1}\big\}$$

$$+ E\big\{U^\star(f;\delta_2)\,e^{j\omega\alpha T_2}\big\}E\big\{e^{j\omega T_1}\big\}$$

$$+ E\big\{U^\star(f;\delta_3)\,e^{j\omega\alpha T_3}\big\}E\big\{e^{j\omega T_2}\big\}E\big\{e^{j\omega T_1}\big\} + \cdots \Big].$$

$$\tag{4.12}$$

To simplify this expression further, note that all individual values for T_ℓ have the same statistical properties even though they are independent random variables. Hence, we have

$$E\{e^{j\omega T}\} \triangleq E\{e^{j\omega T_\ell}\} \quad \text{for all } \ell. \tag{4.13}$$

For similar reasons, the following terms in (4.12) are identical in a statistical sense:

$$
\begin{aligned}
E\{U^\star(f;\delta)\, e^{-j\omega(1-\alpha)T}\} &\triangleq E\{U^\star(f;\delta_{-1})\, e^{-j\omega(1-\alpha)T_{-1}}\} \\
&= E\{U^\star(f;\delta_{-2})\, e^{-j\omega(1-\alpha)T_{-2}}\} \\
&= \cdots.
\end{aligned} \tag{4.14}
$$

and

$$
\begin{aligned}
E\{U^\star(f;\delta)\, e^{j\omega\alpha T}\} &\triangleq E\{U^\star(f;\delta_1)\, e^{j\omega\alpha T_1}\} \\
&= E\{U^\star(f;\delta_2)\, e^{j\omega\alpha T_2}\} \\
&= \cdots.
\end{aligned} \tag{4.15}
$$

Note that the indices on all δ_ℓ and T_ℓ terms have been omitted on the left hand side of (4.14) and (4.15). Inserting these results into (4.12) leaves the following expression for the sum of expectations

$$
\begin{aligned}
\overline{T} S(f) &= E\{U(f;\delta)\, e^{-j\omega\alpha T}\} E\{U^\star(f;\delta)\, e^{-j\omega(1-\alpha)T}\} \sum_{\ell=0}^\infty E\{e^{-j\omega T}\}^\ell \\
&\quad + E\{\,|U(f;\delta)|^2\,\} \\
&\quad + E\{U(f;\delta)\, e^{j\omega(1-\alpha)T}\} E\{U^\star(f;\delta)\, e^{j\omega\alpha T}\} \sum_{\ell=0}^\infty E\{e^{j\omega T}\}^\ell
\end{aligned} \tag{4.16}
$$

The infinite power series is convergent if $\left|E\{e^{j\omega T}\}\right| < 1$, and in this case

$$\sum_{\ell=0}^\infty E\{e^{j\omega T}\}^\ell = \frac{1}{1 - E\{e^{j\omega T}\}}. \tag{4.17}$$

Also, it should be noted that the expressions on the first and the third line in (4.16) are the complex conjugates of each other. Hence, the formula for the power spectrum generated by the RCF method becomes

$$
S(f) = \frac{1}{\overline{T}} \Bigg[E\{\,|U(f;\delta)|^2\,\} \\
+ 2\mathcal{R}\left(\frac{E\{U(f;\delta)\, e^{j\omega(1-\alpha)T}\} E\{U^\star(f;\delta)\, e^{j\omega\alpha T}\}}{1 - E\{e^{j\omega T}\}} \right) \Bigg], \tag{4.18}
$$

where $\mathcal{R}(\cdot)$ is the real part of the complex-valued argument. This is a key equation for spectral analysis of dc/dc converters operating with fixed duty ratios, center-aligned pulses, and a random carrier frequency.

4.4 Spectral analysis of switching functions

Examples are given in this section of how the key expressions (4.8) and (4.18) derived so far can be applied to predict the spectral properties of switching functions generated by the random pulse-position and the random carrier frequency methods. Based on assignment of probability density functions for the random variables (pulse positions or duration of carrier frequencies), it is shown how closed-form expressions for the spectra may be obtained.

To support the theoretical investigations, all calculations are compared to laboratory measurements obtained under similar conditions.

4.4.1 Random pulse-position modulation

To emphasize that the analysis in this section relates to the individual switching functions (and not their difference) controlling the legs of a full-bridge converter, index a or b may be added for clarity reasons to the variables in the previously derived expression (4.8) for the spectrum. Then, the spectrum $S_a(f)$ for the switching function q_a becomes

$$S_a(f) = \frac{1}{T}\left|U_a(f;\delta_a)\right|^2\left[\,1 - \left|E\{e^{-j\omega\Delta_a}\}\right|^2 + \frac{1}{T}\left|E\{e^{-j\omega\Delta_a}\}\right|^2 \sum_{n=-\infty}^{\infty} \delta\!\left(f - \frac{n}{T}\right)\right].$$

(4.19)

A similar result holds for $S_b(f)$ by substitution of indices. All terms needed to evaluate the (4.19) are derived below.

The sampling pulse

The sampling pulse $u_a(t)$ is a rectangular pulse defined in the time-domain by

$$u_a(t) = \begin{cases} 1, & \text{for } 0 \le t \le \delta_a, \\ 0, & \text{otherwise,} \end{cases}$$

(4.20)

where $\delta_a = d_a T$ is the constant pulse width given by the product of the duty ratio d_a and the reciprocal of the carrier frequency, i.e. T. Using this definition, the Fourier transformation $U_a(f;\delta_a)$ of the sampling pulse becomes

$$U_a(f;\delta_a) = \int_{-\infty}^{\infty} u_a(t)e^{-j\omega t}\,dt = \int_{0}^{\delta_a} 1 e^{-j\omega t}\,dt = \frac{j}{\omega}\left(e^{-j\omega\delta_a} - 1\right),$$

(4.21)

where $\omega = 2\pi f$. Hence, the magnitude squared of $U_a(f;\delta_a)$ evaluates to

$$\left|U_a(f;\delta_a)\right|^2 = \frac{\sin^2(\pi f \delta_a)}{(\pi f)^2}.$$

(4.22)

The pulse position (delay)

As already mentioned on page 77, the delay must fall within the $0 \le \Delta_a \le \Delta_{a,\max}$ interval, where $\Delta_{a,\max} = (1 - d_a)T$, but otherwise the selection of Δ_a is unconstrained.

A simple case where only two discrete pulse positions are allowed has been very popular in the literature, and in this case the delay is

$$\Delta_a = \begin{cases} 0, & \text{for leading pulses,} \\ \Delta_{a,\max}, & \text{for lagging pulses.} \end{cases} \tag{4.23}$$

This approach is normally designated as lead-lag modulation [1]. To calculate the expectation terms in (4.19), a probability density function $p(\Delta_a)$ must be assigned to Δ_a and the standard choice is to require that leading and lagging pulses occur with the same probabilities. Hence,

$$p(\Delta_a) = \frac{1}{2}\Big(\delta(\Delta_a - 0) + \delta(\Delta_a - \Delta_{a,\max})\Big). \tag{4.24}$$

It should be noted that $p(\Delta_a)$ obeys the fundamental laws of probability density functions [4]: first of all, $p(\Delta_a) \geq 0$ for all values of Δ_a and also, $\int_{-\infty}^{+\infty} p(\Delta_a)\, d\Delta_a = 1$. The expectation may now be found as

$$E\{e^{-j\omega\Delta_a}\} = \int_{-\infty}^{\infty} p(\Delta_a) e^{-j\omega\Delta_a}\, d\Delta_a = \frac{1}{2}\int_{-\infty}^{\infty} \Big(\delta(\Delta_a - 0) + \delta(\Delta_a - \Delta_{a,\max})\Big) e^{-j\omega\Delta_a}\, d\Delta_a$$

$$= \frac{1}{2}\Big(1 + e^{-j\omega\Delta_{a,\max}}\Big) \tag{4.25}$$

and the magnitude squared becomes

$$\left|E\{e^{-j\omega\Delta_a}\}\right|^2 = \left|\frac{1}{2}\Big(1 + e^{-j\omega\Delta_{a,\max}}\Big)\right|^2 = \frac{1}{2}\Big(1 + \cos(\omega\Delta_{a,\max})\Big). \tag{4.26}$$

By inserting (4.22) and (4.26) into the main expression (4.19), the spectrum $S_a(f)$ of the randomly lead-lag modulated switching function q_a may finally be determined. An algorithm is given in Fig. 4.3 using MATLAB syntax. In section 4.4.3 numerical examples are provided.

As a final comment, it may be observed that other distributions of the delay than the lead-lag type used here are analyzed using similar procedures.

4.4.2   Random carrier frequency modulation

Like for the random pulse-position example presented above, the derived expression (4.18) is rewritten by adding an index a at the appropriate places. The spectrum $S_a(f)$ then becomes

$$S_a(f) = \frac{1}{T}\Bigg[E\big\{\,|U(f;\delta_a)|^2\,\big\} $$

$$+ 2\mathcal{R}\Bigg(\frac{E\big\{U(f;\delta_a)\, e^{j\omega(1-\alpha_a)T}\big\} E\big\{U^\star(f;\delta_a)\, e^{j\omega\alpha_a T}\big\}}{1 - E\big\{e^{j\omega T}\big\}}\Bigg)\Bigg]. \tag{4.27}$$

```
% Calculation of the spectrum for a switching function using
% random lead-lag modulation

D = 0.8;      % Duty ratio
T = 1/5000;   % 1/(carrier frequency)

Del_max = abs(1-D)*T;
f_carr  = 1/T;
f_d     = [1:8]*f_carr; % Frequencies for the discrete spectrum
f_c     = [0:40000];    % Frequencies for the density  spectrum

U_sq_c  = ((sin(pi*f_c*D*T))./(pi*f_c)).^2;  % (4.22) at f_c
U_sq_d  = ((sin(pi*f_d*D*T))./(pi*f_d)).^2;  % (4.22) at f_d
E_sq_c  = 0.5*(1+cos(2*pi*f_c*Del_max));     % (4.26) at f_c
E_sq_d  = 0.5*(1+cos(2*pi*f_d*Del_max));     % (4.26) at f_d

S_density  = 1/T   * U_sq_c .* (1 - E_sq_c); % Density  spectrum by (4.19)
S_discrete = 1/T^2 * U_sq_d .* E_sq_d;        % Discrete spectrum by (4.19)
```

Figure 4.3 MATLAB source file for calculation of the spectra for switching function q_a using RLL modulation. Equations (4.19), (4.22), and (4.26) are used.

Probability density function for the carrier period

All expectations in (4.27) must be taken over the range of T and to facilitate the calculations, it is assumed that the carrier period is uniformly distributed (other distributions are proposed in Chapter 5). Normally, constraints on performance and switching losses determine the upper T_2 and the lower T_1 values for the carrier periods. Hence,

$$p(T) = \begin{cases} (T_2 - T_1)^{-1} \triangleq \Delta T^{-1} & T_1 \leq T \leq T_2, \\ 0, & \text{otherwise,} \end{cases} \tag{4.28}$$

is a feasible probability density function for T, which meets the requirements for such functions stated below (4.24). The average of T immediately follows as

$$\overline{T} = E\{T\} = \int_{T_1}^{T_2} p(T)T \, dT = \frac{1}{2}(T_2 + T_1). \tag{4.29}$$

The denominator in (4.27) contains the $E\{e^{j\omega T}\}$ term, which evaluates to

$$E\{e^{j\omega T}\} = \int_{-\infty}^{\infty} p(T)e^{j\omega T} \, dT$$

$$= \frac{1}{\Delta T} \int_{T_1}^{T_2} e^{j\omega T} \, dT = \frac{j}{\omega \Delta T}\left(e^{j\omega T_1} - e^{j\omega T_2}\right). \tag{4.30}$$

The sampling pulse

Again, the sampling pulse $u_a(t)$ is defined in the time-domain by the pulse width $\delta_a = d_a T$ as

$$u_a(t) = \begin{cases} 1, & \text{for } 0 \le t \le \delta_a, \\ 0, & \text{otherwise,} \end{cases} \tag{4.31}$$

which maps into the frequency domain according to

$$U_a(f; \delta_a) = \int_{-\infty}^{\infty} u_a(t) e^{-j\omega t}\, dt = \int_0^{\delta_a} 1 e^{-j\omega t}\, dt = \frac{j}{\omega}\left(e^{-j\omega\delta_a} - 1\right), \tag{4.32}$$

and

$$|U_a(f; \delta_a)|^2 = \frac{\sin^2(\pi f \delta_a)}{(\pi f)^2}. \tag{4.33}$$

Now, because δ_a is a function of the random variable T, the $E\{\,|U(f;\delta_a)|^2\,\}$ term in (4.27) requires averaging across T, i.e.

$$\begin{aligned} E\{\,|U_a(f; \delta_a)|^2\,\} &= \int_{-\infty}^{\infty} p(T)\,|U(f;\delta_a)|^2\, dT \\ &= \frac{1}{\Delta T} \int_{T_1}^{T_2} \frac{\sin^2(\pi f d_a T)}{(\pi f)^2}\, dT. \end{aligned} \tag{4.34}$$

Solving this definite integral involving the sine function squared yields

$$E\{\,|U_a(f; \delta_a)|^2\,\} = \frac{1}{(\pi f)^2}\left[\frac{1}{2} - \frac{\sin\left(\pi f d_a (T_2 + T_1)\right)\cos\left(\pi f d_a (T_2 - T_1)\right)}{2\pi f \Delta T}\right]. \tag{4.35}$$

The remaining two expectations in (4.27) are found in a similar manner, and for the sake of brevity, the results are given directly:

$$\begin{aligned} &E\{U_a(f; \delta_a)\, e^{j\omega(1-\alpha_a)T}\} \\ &\quad = \frac{1}{\omega^2 \Delta T}\left[\frac{e^{j\omega(1-\alpha_a-d_a)T_2} - e^{j\omega(1-\alpha_a-d_a)T_1}}{1 - \alpha_a - d_a} - \frac{e^{j\omega(1-\alpha_a)T_2} - e^{j\omega(1-\alpha_a)T_1}}{1 - \alpha_a}\right] \end{aligned} \tag{4.36}$$

$$\begin{aligned} &E\{U_a^{\star}(f; \delta_a)\, e^{j\omega\alpha_a T}\} \\ &\quad = \frac{1}{\omega^2 \Delta T}\left[\frac{e^{j\omega(d_a+\alpha_a)T_1} - e^{j\omega(d_a+\alpha_a)T_2}}{d_a + \alpha_a} - \frac{e^{j\omega\alpha_a T_1} - e^{j\omega\alpha_a T_2}}{\alpha_a}\right]. \end{aligned} \tag{4.37}$$

Using these expressions for the individual terms in (4.27), the density spectrum for RCF scheme is obtained. Fig. 4.4 shows a MATLAB source file, which implements the necessary algebra.

```
% Calculation of the spectrum for a switching function using
% random carrier frequency modulation

D   = 0.8;              % Duty ratio
T_2 = 1/4000;           % 1/(minimum carrier frequency)
T_1 = 1/6000;           % 1/(maximum carrier frequency)

f_c = [1:40000];        % Frequencies for the density spectrum
w_c = 2*pi*f_c;

T_avg = (T_2+T_1)/2; % Average T for uniform p(T)
del_T = T_2 - T_1;
alpha = (1-D)/2;        % Centered pulse position

% (4.34):
E_exp = j*( exp(j*w_c*T_1) - exp(j*w_c*T_2) ) ./ (w_c*del_T);

% (4.35):
E_sq = (0.5-1./(w_c*D*del_T) .* cos(pi*f_c*D*(T_2+T_1)) .* ...
                               sin(pi*f_c*D*del_T))    .* (pi*f_c).^(-2);
% (4.36):
E_U1 = 1./(w_c.^2*del_T).* ( ...
   (exp(j*w_c*(1-alpha-D)*T_2) - exp(j*w_c*(1-alpha-D)*T_1))/(1-alpha-D) ...
  -(exp(j*w_c*(1-alpha)*  T_2) - exp(j*w_c*(1-alpha)  *T_1))/(1-alpha) );

% (4.37):
E_U2 = 1./(w_c.^2*del_T).* ( ...
  (exp(j*w_c*(D+alpha)*T_1) - exp(j*w_c*(D+alpha)*T_2))/(D+alpha) ...
 -(exp(j*w_c*   alpha *T_1) - exp(j*w_c*   alpha *T_2))/alpha   );

S_density   = 1/T_avg * (E_sq + 2*real(E_U1.*E_U2./(1-E_exp))); % (4.27)
```

Figure 4.4 MATLAB source file for calculation of the spectra for switching function q_a using RCF modulation. Eq. (4.27) is used together with (4.34)–(4.37).

4.4.3 Comparison of calculated and measured spectra

The spectral theories presented so far for the RPP and the RCF techniques are now compared to laboratory measurements on the set-up shown in Fig. 4.5. Details on the power converter, the control unit, the load, and the measuring system can be found in Appendix A.

Settings of the modulators and the dynamic signal analyzer (DSA)

The settings of modulators used in the tests are listed in Table 4.1(a) on the following page. All results are reported for the two different operating points labeled case A and case B in this table.
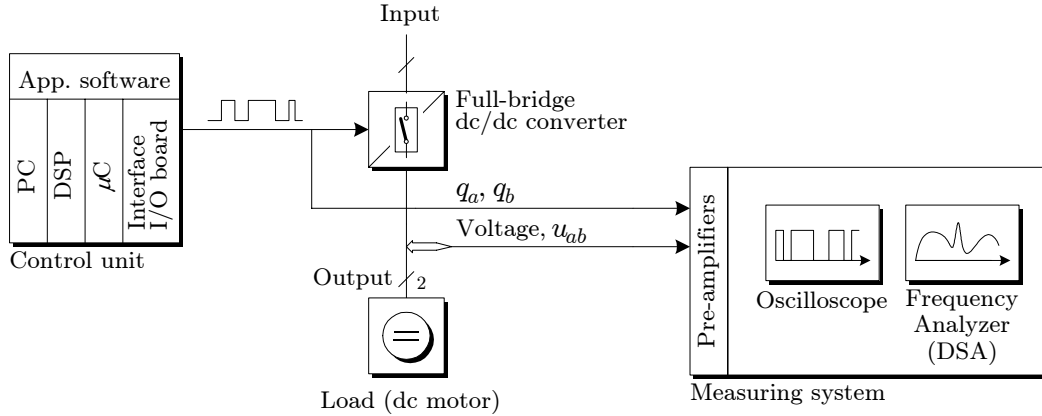
Figure 4.5 Set-up used to test random PWM schemes for dc/dc converters. See Appendix A for more information.

	Case A			Case B		
	d_a	d_b	T (μs)	d_a	d_b	T (μs)
RPP[1]	0.8	0.3	200	0.9	0.05	400
RCF [2]	0.8	0.3	167–250[3]	0.9	0.05	333–500[3]

(a)

Resolution	Sampling freq.	Window type	Record length
32 Hz	131.072 kHz	Hanning	4096

(b)

Table 4.1 (a) Settings of the examined random modulators: [1] lead-lag modulation is used, [2] all pulses are centered, and [3] uniformly distributed within this range. (b) Settings of the dynamic signal analyzer used in all tests.

To visualize the operation of the modulators, sample time-domain waveforms for the switching functions q_a, q_b, and their difference $q_a - q_b$ are shown in Fig. 4.6 measured at 5 V logic level for the case A settings of the modulator. Furthermore, all measurement results reported below are obtained by feeding the switching functions q_a and q_b to the signal analyzer. In this way, all secondary effects, including blanking time, voltage drops, and finite switching times, do not influence the measurements, i.e. the major source of error is the resolution of the PWM timers (50 ns). Refer to section 4.5 for measurements obtained at the output terminals of the converter.

Notation

As explained in Chapter 3, measurement of spectra having both a density and a harmonic part is problematic in the sense that it is impossible to measure these spectra separately. Hence, instead of comparing analytically obtained results for the RPP

top: q_a mid: q_b bot: $q_a - q_b$ (V)   RPP

top: q_a mid: q_b bot: $q_a - q_b$ (V)   RCF

(a)

(b)
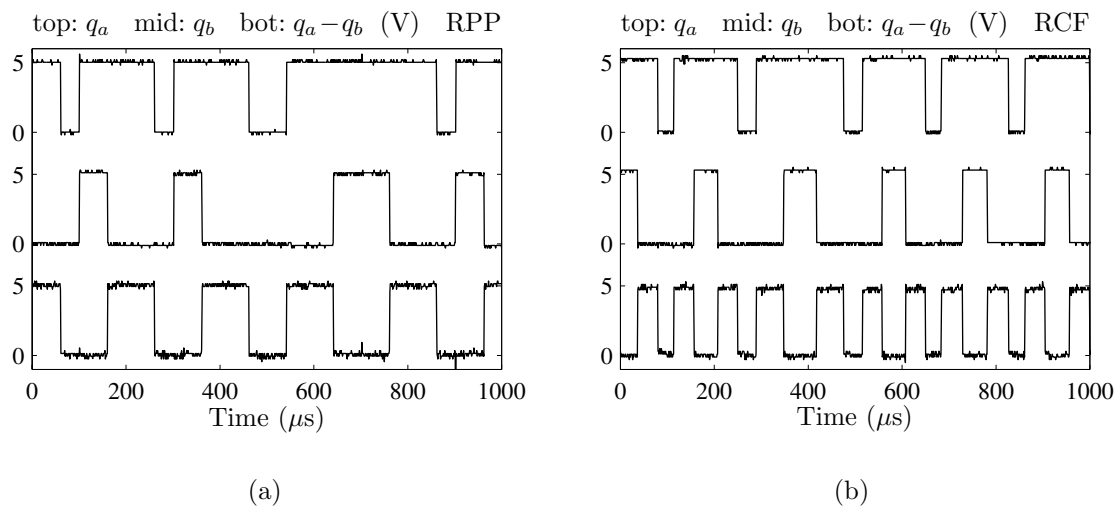
Figure 4.6 Typical time-domain waveforms for the generated switching functions for case A in Table 4.1. q_a, q_b and their difference $q_a - q_b$ are shown. (a) The RPP (the lead-lag variant) technique and (b) the RCF technique.

scheme to both a density and a power scaled estimate, the procedure outlined in section 3.3.4 to convert a mixed spectrum into an equivalent density spectrum is used below. To separate different spectra, the notation for signals related to leg a is as follows (substitute $a \rightarrow b$ for leg b):

$S_a(f)$ The theoretically expected spectrum for switching function q_a. In the RPP case $S_a(f)$ has both a density part and a harmonic part, whereas RCF only has a density part (except for the power (in volt^2) carried by the dc component).

$\tilde{S}_a(f)$ The equivalent density spectrum obtained by mimicking the operating principles of the DSA, i.e. the power carried by all harmonic components is lumped into the density part of the spectrum.

$\hat{S}_a(f)$ The measured density spectrum of the switching function. The spectra are scaled in power density units (volt^2/Hz), i.e. the PSD unit introduced in section 3.3.2 is used.

According to the instructions on page 58ff, the mapping from $S_a(f)$ into $\tilde{S}_a(f)$ requires information of the settings of the DSA. All measurements are based on the parameters shown in Table 4.1(b). Furthermore, $\hat{S}_a(f)$ is estimated by averaging 500 periodograms having a 25 % overlap.

All results are given in (dB), where 0 dB $\sim$ 1 volt^2/Hz for all density parts and 0 dB $\sim$ 1 volt^2 for the harmonics in $S_a(f)$ and $S_b(f)$.

Results

The plots in Figs. 4.7–4.10 on pages 88–91 show the calculated results and the spectra obtained in the laboratory under similar conditions.
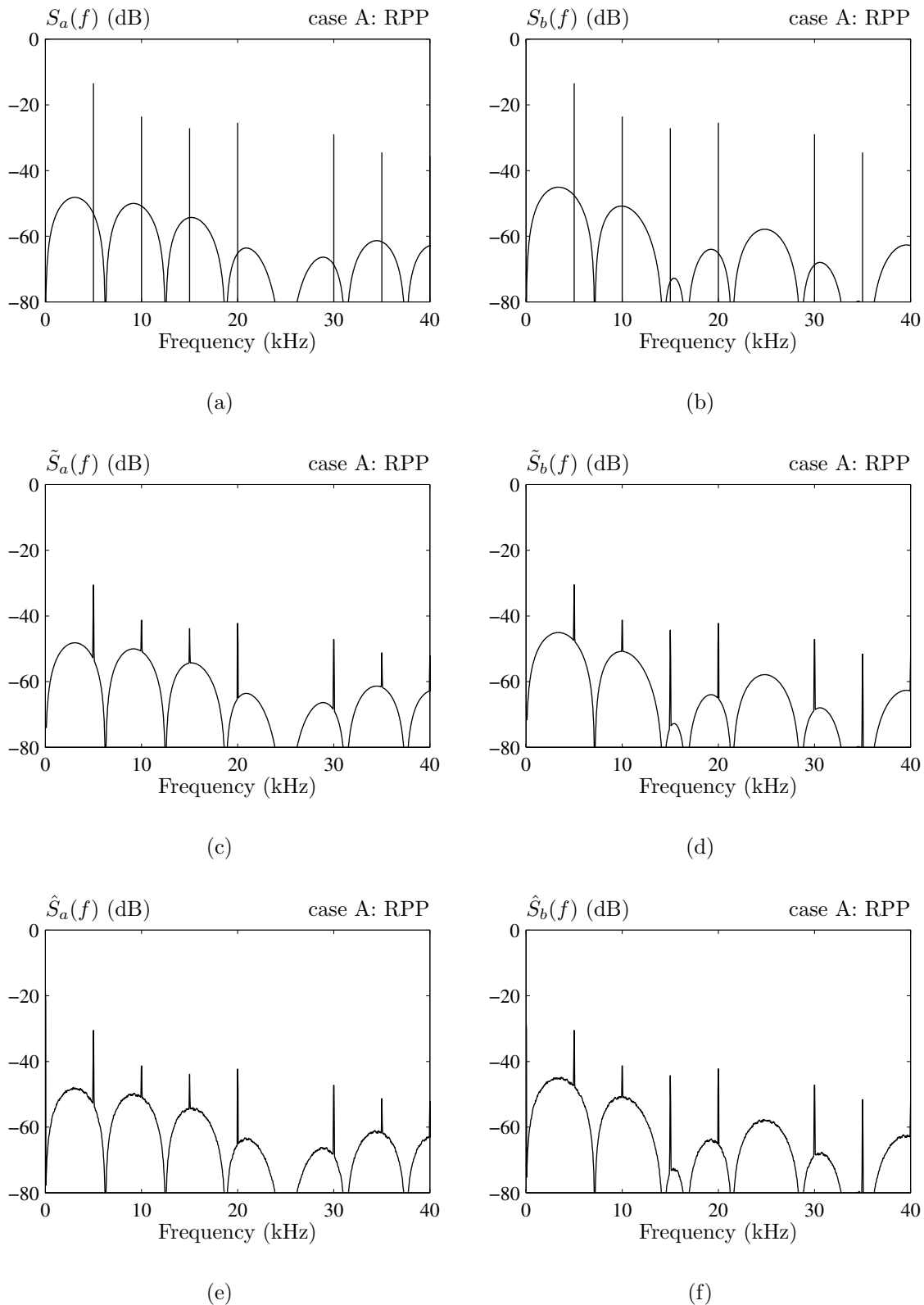
Figure 4.7 Spectra of switching functions q_a and q_b for RPP (lead-lag) modulation using case A settings in Table 4.1(a). (a, b) Calculated density and harmonic spectra, (c, d) calculated density spectra including power due to harmonics, and (e, f) measured estimates of density spectra.
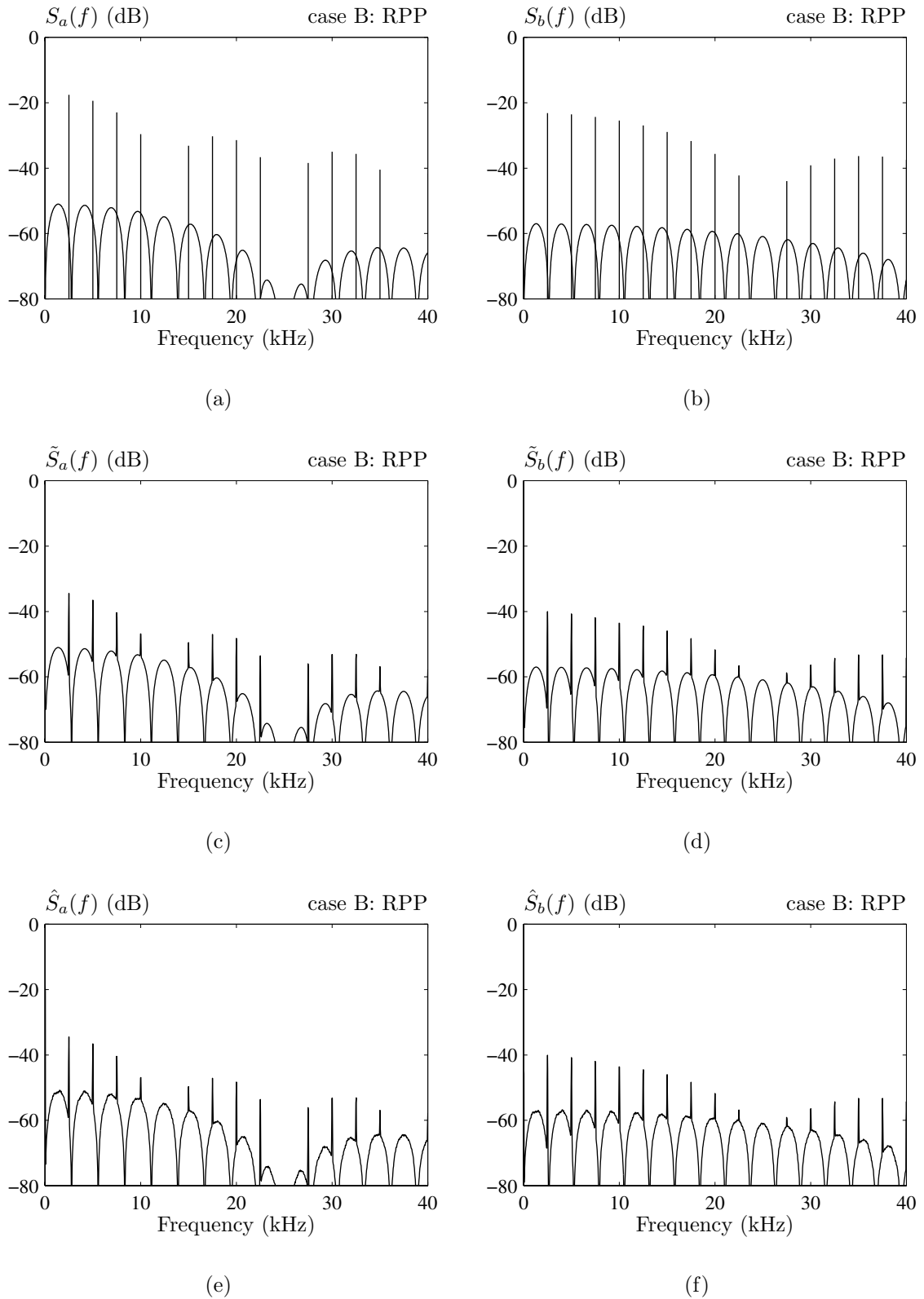
Figure 4.8 Spectra of switching functions q_a and q_b for RPP (lead-lag) modulation using case B settings in Table 4.1(a). (a, b) Calculated density and harmonic spectra, (c, d) calculated density spectra including power due to harmonics, and (e, f) measured estimates of density spectra.

(a)

(b)

(c)

(d)

(e)

(f)
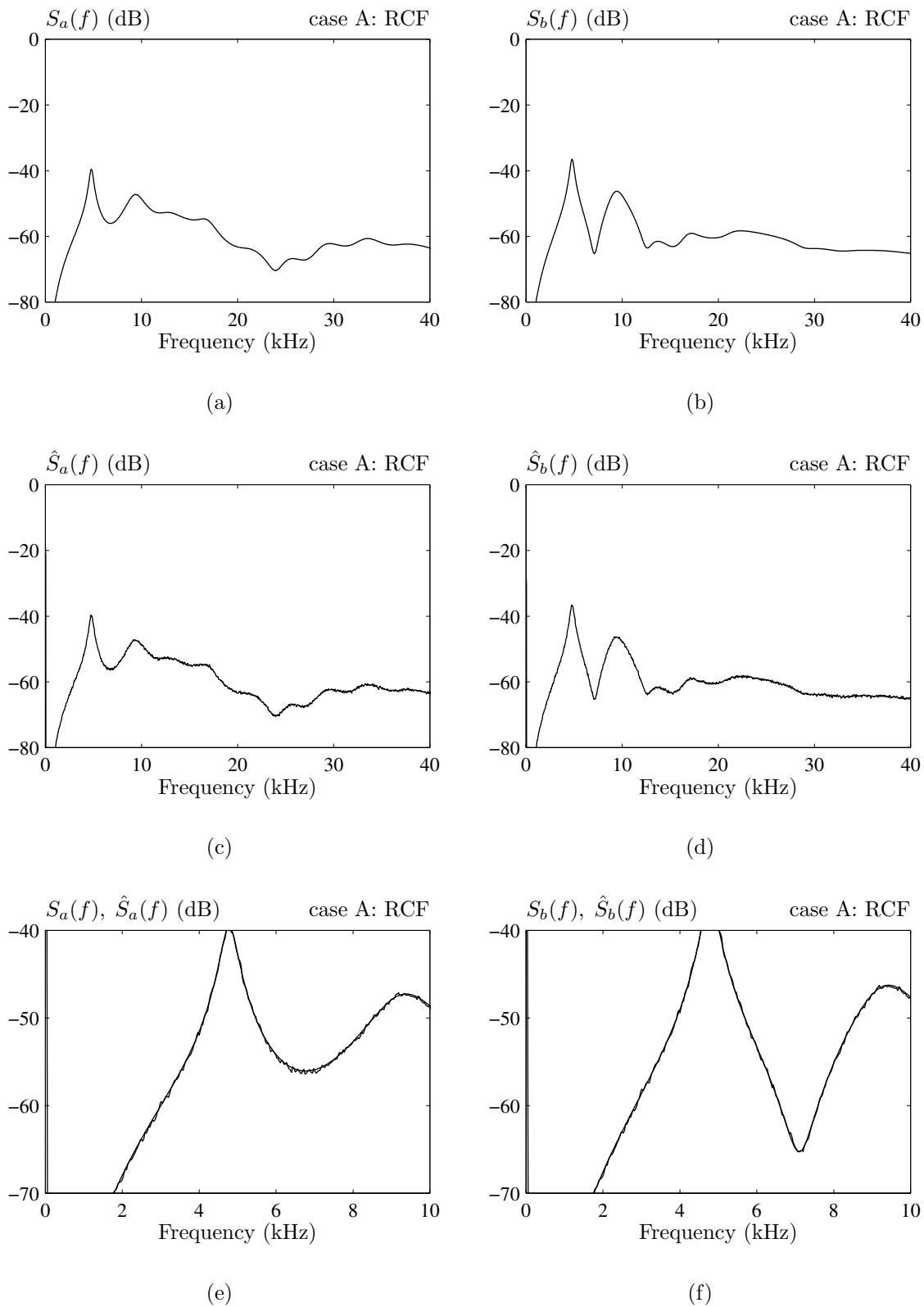
Figure 4.9 Spectra of switching functions q_a and q_b for RCF modulation using case A settings in Table 4.1(a). (a, b) Calculated densities, (c, d) measured estimates of the density spectra, and (e, f) details of calculated and measured density spectra in the $[0; 10]$ kHz range.
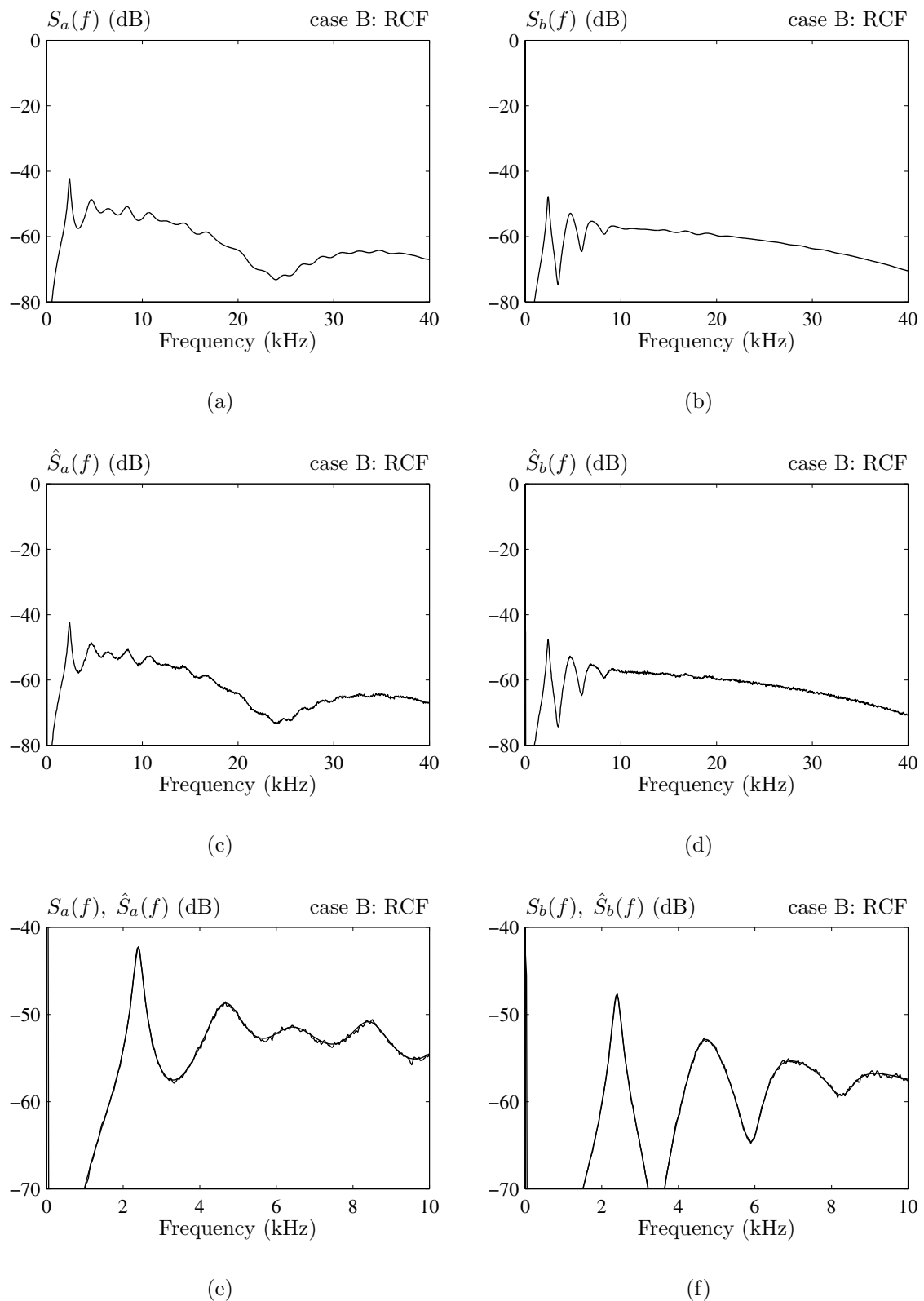
Figure 4.10 Spectra of switching functions q_a and q_b for RCF modulation using case B settings in Table 4.1(a). (a, b) Calculated densities, (c, d) measured estimates of the density spectra, and (e, f) details of calculated and measured density spectra in the $[0; 10]$ kHz range.

Note the mixed spectra $S_a(f)$ and $S_b(f)$ for the RPP scheme shown in Figs. 4.7(a, b) and 4.8(a, b), the density and the harmonic parts are converted to (dB) using different normalizations, because they have different physical units.

By comparing Figs. 4.7(b) and 4.7(f), it may be seen that the calculated density part of the spectrum exactly matches the measured density. Also, it is meaningless to expect the strength of the harmonics in Fig. 4.7(b) to match the peaks in Fig. 4.7(f) because of the different spectral units involved. However, when the characteristic of the DSA is included in the calculations, the theoretically expected result shown in Fig. 4.7(d) is hardly discernible from the estimate based on measurements in Fig. 4.7(f). Similar comments can be given for all other plots in Fig. 4.7 and Fig. 4.8.

Regarding RCF modulation, the comparison is more straightforward because no harmonics exist except for the dc component. Hence, it makes sense to compare the theory directly to the PSD-scaled measurements, because the noise bandwidth f_{nbw} of the analyzer is sufficiently small: $f_{nbw} = 1.5\Delta f = 48$ Hz for the used Hanning window and resolution $\Delta f = 32$ Hz. Figs. 4.9 and 4.10 show the obtained results. It may be seen that in all cases, $S_a(f)$ is almost identical to the estimate $\hat{S}_a(f)$ for all frequencies due to the absence of harmonics. Even in the zoomed views shown in Figs. 4.9(e, f) and 4.10(e, f), it is difficult to separate the analytically calculated spectra from the measurements.

In total, a very good agreement between the theory and the laboratory measurements can be observed. This fully verifies the correctness of the spectral analysis developed for the switching functions. Furthermore, the power of the procedure outlined in section 3.3.4 for comparisons of calculated and estimated spectra having mixed characteristics is clearly demonstrated by the examples for the RPP scheme.

4.5   Spectral analysis of the output voltage

Having completed the spectral analysis of the individual switching functions, attention is now turned to the characteristics of the output voltage produced by full-bridge dc/dc converters. As elaborated further below, the starting point for the analysis is the discussion of cross spectra densities given in section 4.2.1. It is demonstrated how the spectrum for the output voltage may be calculated without knowing the cross spectral densities. This procedure is applied to the RPP and the RCF schemes. Finally, the obtained theoretical results are verified by laboratory measurements.

4.5.1   Preliminaries

Referring to (4.1) on page 75, it is evident that a proper analysis of the spectrum $S_{ab}(f)$ for $u_{ab} = U_{dc}(q_a - q_b)$ requires knowledge of the cross spectral densities $C_{ab}(f) = C_{ba}^\star(f)$. These spectra can be analyzed in a manner similar to the auto spectrum investigated in details in Chapter 3. A general analysis encompassing dc/ac modulators becomes complicated, but for random modulators for dc/dc converters, the derivations are manageable. Taking the RPP scheme as an example, it can be shown, using the same methods as in Chapter 3 and in section 4.3.2 in the current chapter, that the
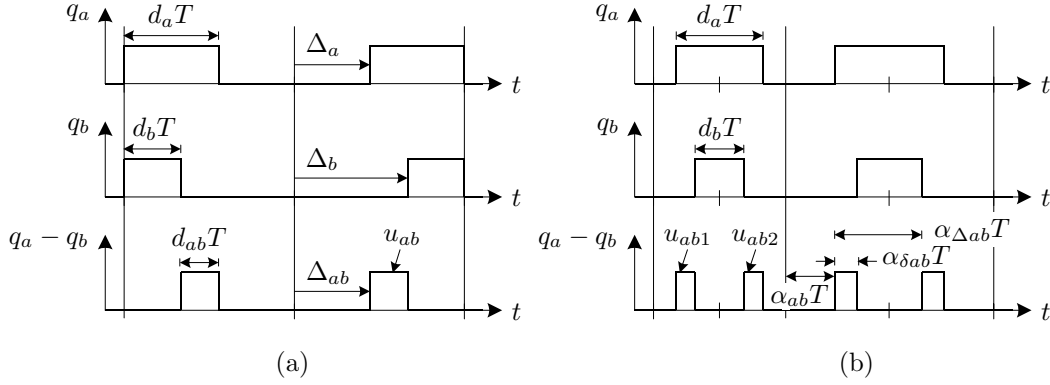
Figure 4.11 Definition of parameters that describe the time-domain waveforms q_a, q_b, and $q_a - q_b$. (a) Lead-lag RPP modulation and (b) RCF modulation.

formula for $C_{ab}(f)$ becomes

$$C_{ab}(f) = \frac{1}{T}U_a(f;\delta_a)U_b^\star(f;\delta_b)\left[E\{e^{-j\omega(\Delta_a-\Delta_b)}\} - E\{e^{-j\omega\Delta_a}\}E^\star\{e^{-j\omega\Delta_b}\}\right.$$

$$\left. + \frac{1}{T}E\{e^{-j\omega\Delta_a}\}E^\star\{e^{-j\omega\Delta_b}\}\sum_{n=-\infty}^{\infty}\delta\left(f - \frac{n}{T}\right)\right], \quad (4.38)$$

where $U_a(f;\delta_a)$ and $U_b(f;\delta_b)$ are the Fourier transformations of the sampling pulses of widths $\delta_a = d_aT$ and $\delta_b = d_bT$, respectively. Also, Δ_a and Δ_b are the delays with respect to the start of the carrier period as illustrated in Fig. 4.11(a).

The expectations in (4.38) involving only one of the delays Δ_a or Δ_b are straightforwardly found, but the $E\{e^{-j\omega(\Delta_a-\Delta_b)}\}$ term is more tricky. Formally, we have

$$E\{e^{-j\omega(\Delta_a-\Delta_b)}\} = \int_{-\infty}^{+\infty} p(\Delta_a - \Delta_b)e^{-j\omega(\Delta_a-\Delta_b)} \, d(\Delta_a - \Delta_b) \quad (4.39)$$

and for the sake of simplicity, the lead-lag type of modulation may be assumed. When the same pulse position is used for both legs, $(\Delta_a - \Delta_b)$ can attain only two values, i.e.

$$\Delta_a - \Delta_b = \begin{cases} 0, & \text{for leading pulses,} \\ (d_b - d_a)T, & \text{for lagging pulses,} \end{cases} \quad (4.40)$$

which may be verified from Fig. 4.11(a). Then, if leading and lagging positions occur with equal probability, the expectation (4.39) may be determined as

$$E\{e^{-j\omega(\Delta_a-\Delta_b)}\} = \frac{1}{2}\left(1 + e^{-j\omega(d_b-d_a)T}\right). \quad (4.41)$$

All terms in (4.38) are known now, and an evaluation of the total cross spectrum becomes possible, i.e. the spectrum $S_{ab}(f)$ for $u_{ab}(t)$ can also be calculated.

Although this direct approach is feasible for the random lead-lag modulation, the following general disadvantages are evident from this case study:

1. Expressions similar to (4.38) for the cross spectra are needed. The derivations leading to (4.38) spans about three pages, i.e. generalizations to random dc/ac modulators must be expected to be involved and lengthy.

2. Even in the case where a formula for the cross spectrum is known, evaluation still requires knowledge of terms not needed for the auto spectrum. The term $E\{e^{-j\omega(\Delta_a-\Delta_b)}\}$ in (4.38) is such an example.

Hence, instead of pursuing the route of cross spectra for other kinds of random modulation, another method has been developed to obtain the spectrum of differences like $q_a - q_b$, which governs the characteristics of the terminal voltage u_{ab}. The merits of this novel method are much more pronounced for the dc/ac random modulators examined in Chapter 5 and Chapter 6, but the examples for dc/dc schemes still demonstrate the power of this direct approach.

4.5.2   Random lead-lag pulse-position modulation

If Fig. 4.11(a) is considered, it is seen that for the lead-lag case, all output pulses $q_a - q_b$ have the same shape, i.e. the same width and height. Actually, this rectangular pulse shape is similar to the shape of the pulses that constitute the switching functions, although their positions and widths are different. Therefore, the fundamental idea behind all subsequent derivations is to study the $q_{ab} \triangleq q_a - q_b$ waveform directly instead of regarding q_{ab} as a difference of the two underlying functions q_a and q_b, which are correlated.

It is perfectly legitimate to use the pulse labeled u_{ab} in Fig. 4.11(a) as the sampling pulse, and in this case (4.8) on page 78 may be formulated as

$$S_{ab}(f) = \frac{1}{T}\left|U_{ab}(f;\delta_{ab})\right|^2\left[1 - \left|E\{e^{-j\omega\Delta_{ab}}\}\right|^2 + \frac{1}{T}\left|E\{e^{-j\omega\Delta_{ab}}\}\right|^2 \sum_{n=-\infty}^{\infty}\delta\left(f-\frac{n}{T}\right)\right].$$

(4.42)

in order to stress that the spectrum of a pulse train consisting of sampling pulses u_{ab} is sought.

Evaluation of terms

The sampling pulse u_{ab}, which is a part of the $q_a - q_b$ waveform in Fig. 4.11(a), is defined by[3]

$$u_{ab}(t) = \begin{cases} 1, & \text{for } \Delta_{ab} \leq t \leq \Delta_{ab} + d_{ab}T, \\ 0, & \text{otherwise.} \end{cases}$$

(4.43)

The width $d_{ab}T$ is constant, but the delay Δ_{ab} is a random variable. Since only two positions with respect to the start of the current carrier period are possible, Δ_{ab} becomes

$$\Delta_{ab} = \begin{cases} d_bT, & \text{for leading pulses,} \\ (1-d_a)T, & \text{for lagging pulses.} \end{cases}$$

(4.44)

To simplify the analysis, the time origin is shifted by d_bT. Hence, for leading and lagging edge modulation $\Delta_{ab} = 0$ or $\Delta_{ab} = |1 - d_a - d_b|T$, respectively (the absolute

---

[3]In the following derivations it is assumed that $d_a > d_b$ — this does not limit the validity of the derivations in any way.

value is required if $d_a + d_b > 1$). Assigning equal probabilities to lead and lag, the probability density function for the delay then becomes

$$p(\Delta_{ab}) = \frac{1}{2}\Big(\delta(\Delta_{ab} - 0) + \delta(\Delta_{ab} - \Delta_{ab,\mathrm{max}})\Big), \qquad (4.45)$$

where $\Delta_{ab,\mathrm{max}} = |1 - d_a - d_b|\,T$. The expectation of Δ_{ab} then follows as

$$E\{e^{-j\omega\Delta_{ab}}\} = \int_{-\infty}^{\infty} p(\Delta_{ab})e^{-j\omega\Delta_{ab}}\,d\Delta_{ab} = \frac{1}{2}\Big(1 + e^{-j\omega\Delta_{ab,\mathrm{max}}}\Big), \qquad (4.46)$$

due to the sampling property of the density function. The needed magnitude squared of the expectation becomes

$$\big|E\{e^{-j\omega\Delta_{ab}}\}\big|^2 = \left|\frac{1}{2}\Big(1 + e^{-j\omega\Delta_{ab,\mathrm{max}}}\Big)\right|^2 = \frac{1}{2}\Big(1 + \cos(\omega\Delta_{ab,\mathrm{max}})\Big). \qquad (4.47)$$

Also, the sampling pulse (4.43) should be translated by $d_b T$ seconds, i.e. $u_{ab}(t) = 1$ for $0 \le t \le (d_a - d_b)T$, and 0 otherwise (assuming $d_a > d_b$). The Fourier transformation of the sampling pulse is then

$$U_{ab}(f;\delta_{ab}) = \int_{-\infty}^{\infty} u_{ab}(t)e^{-j\omega t}\,dt = \int_{0}^{d_{ab}T} 1e^{-j\omega t}\,dt = \frac{j}{\omega}\Big(e^{-j\omega d_{ab}T} - 1\Big), \qquad (4.48)$$

where $d_{ab} \triangleq d_a - d_b$ as indicated in Fig. 4.11(a). Hence,

$$|U_{ab}(f;\delta_{ab})|^2 = \frac{\sin^2(\pi f d_{ab}T)}{(\pi f)^2}. \qquad (4.49)$$

These derivations show that only minor modifications of the derivations for the switching functions are needed in order to calculate the spectrum for $q_a - q_b$. Also, with a few changes only, the procedure sketched in Fig. 4.3 (page 83) may be reused to get numerical values for the spectrum.

4.5.3 Random carrier frequency modulation

Next, formulas for the RCF technique with centered pulse position and constant duty ratio are presented. As for the RPP method, the idea is to study the waveform for the output directly and formally, the spectrum for u_{ab} becomes

$$S_{ab}(f) = \frac{1}{T}\bigg[E\{\,|U_{ab}(f;\delta_{ab})|^2\,\}$$
$$+ 2\mathcal{R}\bigg(\frac{E\{U_{ab}(f;\delta_{ab})\,e^{j\omega(1-\alpha_{ab})T}\}\,E\{U_{ab}^{\star}(f;\delta_{ab})\,e^{j\omega\alpha_{ab}T}\}}{1 - E\{e^{j\omega T}\}}\bigg)\bigg], \quad (4.50)$$

in analogy with (4.27) for the switching function q_a.

Evaluation of terms

To find the spectrum $S_{ab}(f)$, the sampling pulse $u_{ab}(t)$ must be known. For this type of control, where the pulses are centered in each leg, two pulses u_{ab1} and u_{ab2} occur in each carrier period as shown in Fig. 4.11(b). Using this notation, the effective sampling pulse u_{ab} for the output may be expressed as

$$u_{ab}(t) = u_{ab1}(t) + u_{ab2}(t) = u_{ab1}(t) + u_{ab1}(t - \alpha_{\Delta ab}T), \qquad (4.51)$$

where $\alpha_{\Delta ab} \triangleq \frac{1}{2}(d_a + d_b)$ is the normalized time by which u_{ab2} lags u_{ab1}. Also[4],

$$u_{ab1}(t) = \begin{cases} 1, & 0 \le t \le \alpha_{\delta ab}T, \\ 0, & \text{otherwise.} \end{cases} \qquad (4.52)$$

Here, $\alpha_{\delta ab} \triangleq \frac{1}{2}(d_a - d_b)$ is the width of u_{ab1} divided by T.

The remaining task is to calculate analytically the statistical expectations of various Fourier transformations in (4.50) in order to find the spectrum of the output voltage. All expectations must be taken over the range of T and for convenience the same uniform distribution as in section 4.4.2 is used. Hence, according to (4.29) and (4.30), $\overline{T} = \frac{1}{2}(T_1 + T_2)$ and $E\{e^{j\omega T}\} = j(e^{j\omega T_1} - e^{j\omega T_2})/(\Delta T \omega)$, where $\Delta T = T_2 - T_1$ is the difference between the maximum T_2 and minimum T_1 carrier periods.

By using (4.52), the Fourier transformation of the sampling pulse (4.51) becomes

$$U_{ab}(f; \delta_{ab}) = \int_{-\infty}^{\infty} u_{ab}(t)e^{-j\omega t}\, dt = \int_{-\infty}^{\infty} \big(u_{ab1}(t) + u_{ab1}(t - \alpha_{\Delta ab}T)\big)e^{-j\omega t}\, dt$$

$$= \big(1 + e^{-j\omega\alpha_{\Delta ab}T}\big)\int_{0}^{\alpha_{\delta ab}T} 1 e^{-j\omega t}\, dt = \frac{j}{\omega}\big(1 + e^{-j\omega\alpha_{\Delta ab}T}\big)\big(e^{-j\omega\alpha_{\delta ab}T} - 1\big). \qquad (4.53)$$

Taking the absolute value squared of (4.53) and averaging with respect to the probability density $p(T)$, it may be shown that

$$E\big\{|U_{ab}(f;\delta_{ab})|^2\big\} = \frac{2}{\Delta T \omega^2}\Bigg(2\Delta T + 2\frac{\sin(\omega\alpha_{\Delta ab}T_2) - \sin(\omega\alpha_{\Delta ab}T_1)}{\omega\alpha_{\Delta ab}}$$

$$- 2\frac{\sin(\omega\alpha_{\delta ab}T_2) - \sin(\omega\alpha_{\delta ab}T_1)}{\omega\alpha_{\delta ab}}$$

$$- \frac{\sin(\omega(\alpha_{\Delta ab} - \alpha_{\delta ab})T_2) - \sin(\omega(\alpha_{\Delta ab} - \alpha_{\delta ab})T_1)}{\omega(\alpha_{\Delta ab} - \alpha_{\delta ab})}$$

$$- \frac{\sin(\omega(\alpha_{\Delta ab} + \alpha_{\delta ab})T_2) - \sin(\omega(\alpha_{\Delta ab} + \alpha_{\delta ab})T_1)}{\omega(\alpha_{\Delta ab} + \alpha_{\delta ab})}\Bigg).$$

$$(4.54)$$

---

[4]Again $d_a > d_b$ may safely be assumed.

Likewise, straightforward derivations lead to

$$E\big\{U_{ab}(f;\delta_{ab})e^{j\omega(1-\alpha_{ab})T}\big\} = \frac{1}{\Delta T\omega^2}\bigg(\frac{e^{-j\omega(\alpha_{ab}+\alpha_{\delta ab}-1)T_1} - e^{-j\omega(\alpha_{ab}+\alpha_{\delta ab}-1)T_2}}{\alpha_{ab}+\alpha_{\delta ab}-1}$$

$$-\frac{e^{-j\omega(\alpha_{ab}-1)T_1} - e^{-j\omega(\alpha_{ab}-1)T_2}}{\alpha_{ab}-1}$$

$$+\frac{e^{-j\omega(\alpha_{\Delta ab}+\alpha_{ab}+\alpha_{\delta ab}-1)T_1} - e^{-j\omega(\alpha_{\Delta ab}+\alpha_{ab}+\alpha_{\delta ab}-1)T_2}}{\alpha_{\Delta ab}+\alpha_{ab}+\alpha_{\delta ab}-1}$$

$$-\frac{e^{-j\omega(\alpha_{\Delta ab}+\alpha_{ab}-1)T_1} - e^{-j\omega(\alpha_{\Delta ab}+\alpha_{ab}-1)T_2}}{\alpha_{\Delta ab}+\alpha_{ab}-1}\bigg)$$

$$(4.55)$$

and

$$E\big\{U_{ab}^\star(f;\delta_{ab})e^{j\omega\alpha_{ab}T}\big\} = \frac{1}{\Delta T\omega^2}\bigg(\frac{e^{j\omega\alpha_{ab}T_2} - e^{j\omega\alpha_{ab}T_1}}{\alpha_{ab}}$$

$$+\frac{e^{j\omega(\alpha_{\Delta ab}+\alpha_{ab})T_2} - e^{j\omega(\alpha_{\Delta ab}+\alpha_{ab})T_1}}{\alpha_{\Delta ab}+\alpha_{ab}}$$

$$-\frac{e^{j\omega(\alpha_{\delta ab}+\alpha_{ab})T_2} - e^{j\omega(\alpha_{\delta ab}+\alpha_{ab})T_1}}{\alpha_{\delta ab}+\alpha_{ab}}$$

$$-\frac{e^{j\omega(\alpha_{\Delta ab}+\alpha_{\delta ab}+\alpha_{ab})T_2} - e^{j\omega(\alpha_{\Delta ab}+\alpha_{\delta ab}+\alpha_{ab})T_1}}{\alpha_{\Delta ab}+\alpha_{\delta ab}+\alpha_{ab}}\bigg).$$

$$(4.56)$$

The spectrum for u_{ab} may now be calculated by inserting the partial results (4.54)–(4.56) into the key expression (4.50). The MATLAB code shown previously in Fig. 4.4 on page 85 may be modified to output the spectrum for u_{ab} by inserting those expressions.

At this point it may be noted that even for a uniform distribution of T, the needed expectations become lengthy expressions. This indicates that other distributions, like the Gaussian (normal) distribution, are likely to produce substantially more complicated expressions due to the definite integrals like (4.34).

Another problem of practical concern relates to that many continuous distributions (including, but not limited to, the Gaussian distribution) do not directly comply with real-world constraints for the upper and the lower values for the carrier frequency. This indicates that a discrete distribution of the carrier frequency is more attractive from a practical point of view, and as elaborated in Chapter 5, discrete distributions have many other nice advantages in conjunctions with random PWM. One advantage relates to the problem of evaluating expectations similar to those in (4.34).

4.5.4 Comparison of calculated and measured spectra

In order to validate the correctness of the developed theory for the spectrum of the terminal voltage, measurements are compared to the analytically expected spectra for both the RPP and the RCF schemes. The effect of blanking time is also examined.

Experimental set-up

The experimental set-up shown in Fig. 4.5 on page 86 is used again. Also, the settings of the modulator and the signal analyzer are the same as previously used (see Table 4.1 on page 86).

Unlike the comparison in section 4.4.3, measurements are also provided for the real terminal voltage when the converter is loaded by a dc motor, which in turn is loaded by a dc generator. The power supplied to the load is approximately 250 W using case A settings and 500 W in case B. The active power drawn from the converter causes a dc-link voltage ripple ΔU_{dc}, which amounts to $\Delta U_{dc}/U_{dc} \approx 5/200$ (V/V) and $\Delta U_{dc}/U_{dc} \approx 10/200$ (V/V) in cases A and B, respectively. A blanking time on $t_d = 2.2$ μs is used.

Notation

To separate spectra of slightly different origin, the used notation is as follows:

$S_{ab}(f)$ The theoretically expected spectrum, which in the RPP case has both a density part and a harmonic part.

$\tilde{S}_{ab}(f)$ The equivalent density spectrum, where the calculated power components (harmonics) are merged into the calculated continuous density part according to the guidelines given earlier.

$\hat{S}_{ab}(f)$ The measured density spectrum (PSD scaling) based on a logic-level difference $q_a - q_b$ of the switching functions generated by the modulator. $q_a - q_b$ was generated from the TTL-referred digital voltages q_a and q_b by means of a simple operational amplifier circuit.

$\hat{S}_{ab}^{p}(f)$ The measured density spectrum (PSD scaling) on power level, i.e. the terminal voltage is fed to the measuring unit. The high-voltage differential probe P5205 (see Appendix A) was used.

Under ideal conditions, the spectra $\hat{S}_{ab}(f)$ and $\hat{S}_{ab}^{p}(f)$ are equal, but as demonstrated below, the non-ideal behaviour of the power converter causes slight disagreements. Also, for the RCF scheme, which does not generate any harmonics, $S_{ab}(f)$ and $\tilde{S}_{ab}(f)$ are equal, because the noise bandwidth of the DSA is sufficiently small to capture all variations in the density spectra.

All results are given in (dB), where 0 dB $\sim$ 1 volt^2/Hz for all density parts and 0 dB $\sim$ 1 volt^2 for the harmonics in $S_{ab}(f)$.

Results

The obtained results are shown in Fig. 4.12 and Fig. 4.13. The measurements $\hat{S}_{ab}(f)$ based on logic-level signals (Fig. 4.12(c, d) and Fig. 4.13(c, d)) show a very good agreement between theory $\tilde{S}_{ab}(f)$ and the measured spectra $\hat{S}_{ab}(f)$. The two curves shown in each of these plots are hardly discernible.

The last row in Fig. 4.12 and Fig. 4.13, respectively, compares the theory to measurements obtained directly from the output power terminals of the converter. As
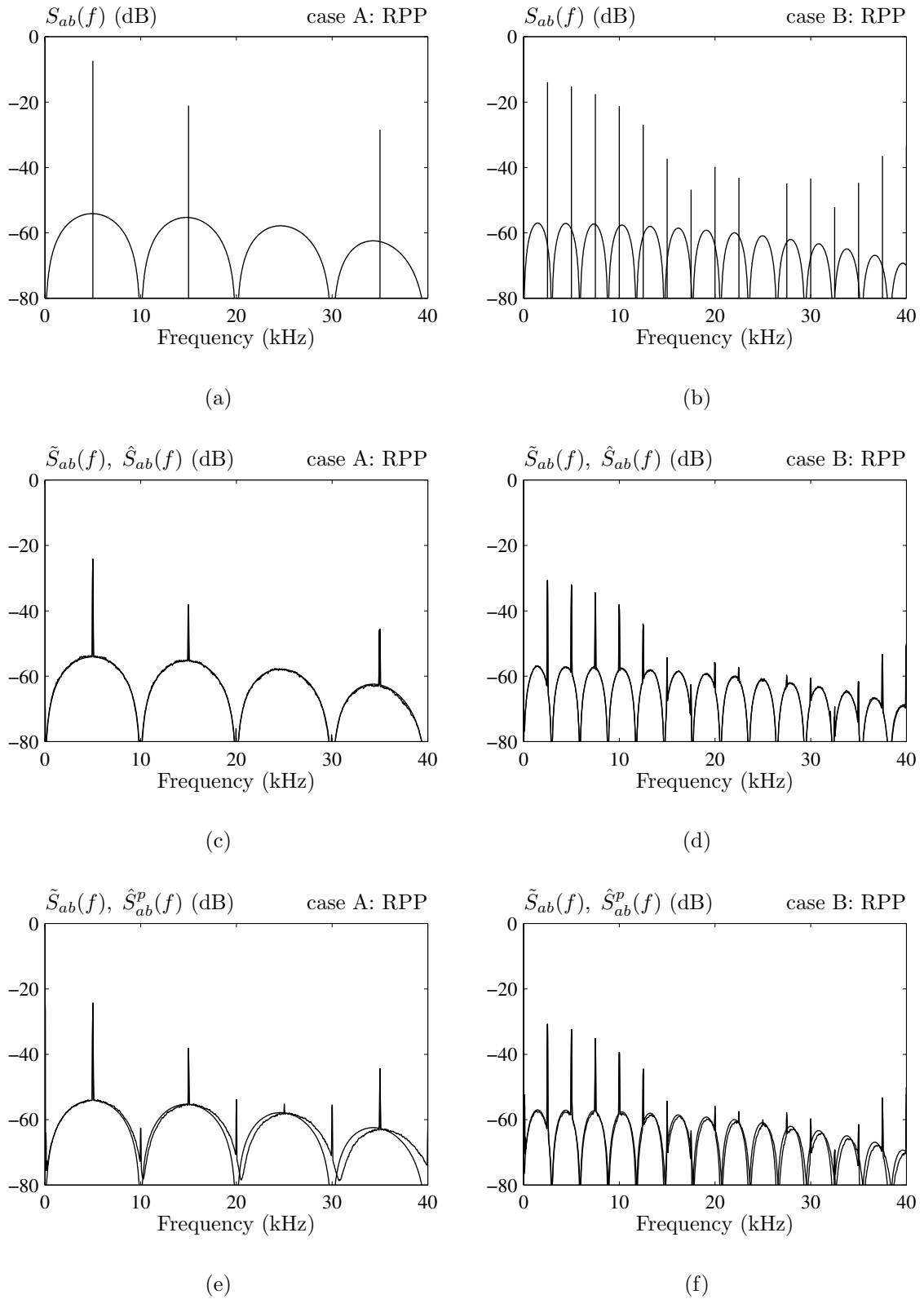
Figure 4.12 Spectra for the output voltage u_{ab} for RPP (lead-lag) modulation. (a, b) Calculated density and harmonic spectra, (c, d) calculated density spectra including power due to harmonics and measured spectrum (logic level), and (e, f) calculated density spectra including power due to harmonics and measured spectrum (power level).

(a)

(b)

(c)

(d)

(e)

(f)
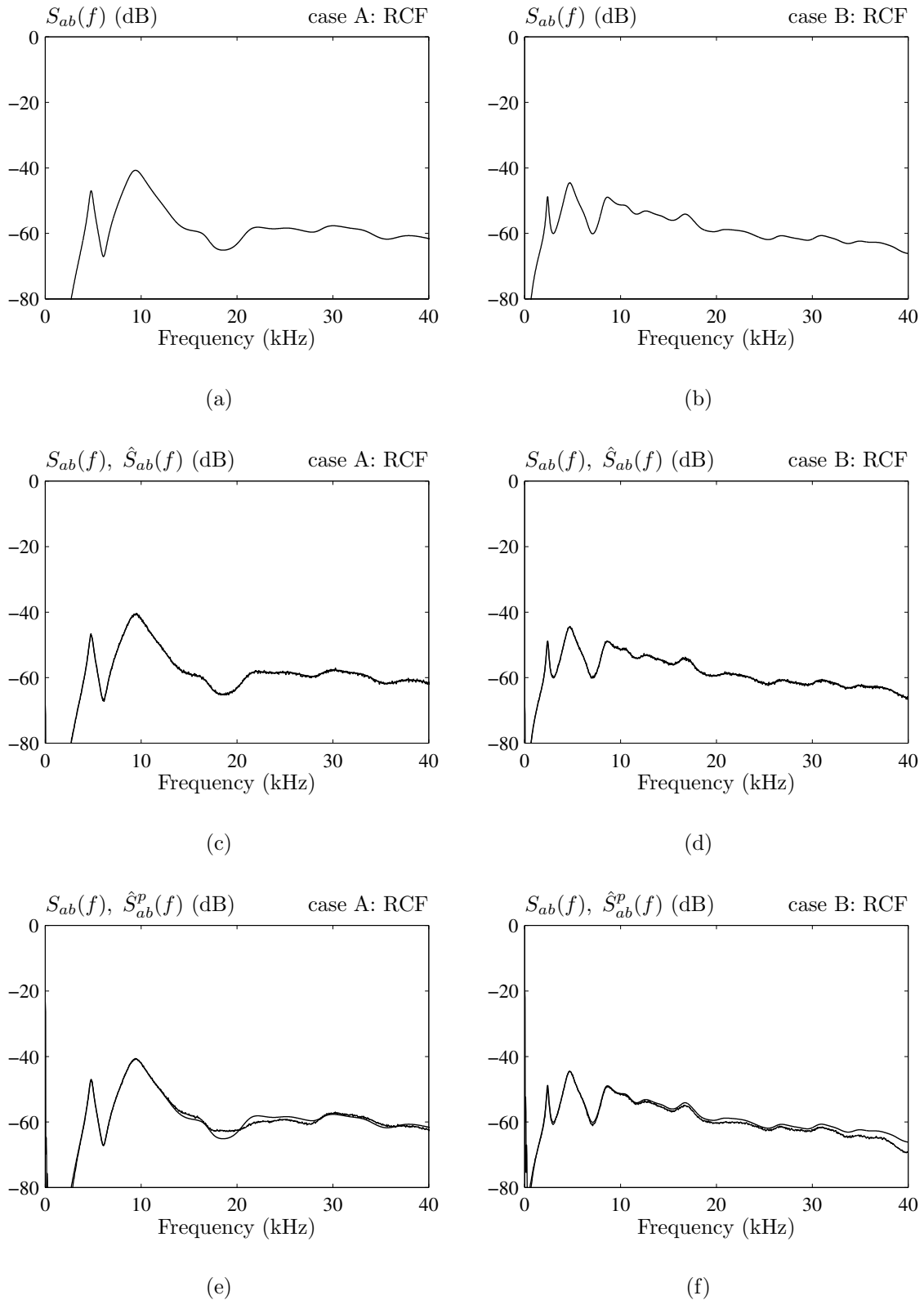
Figure 4.13 Spectra for the output voltage u_{ab} for RCF (lead-lag) modulation. (a, b) Calculated density spectra, (c, d) calculated density spectra and measured spectrum (logic level), and (e, f) calculated density spectra and measured spectrum (power level).
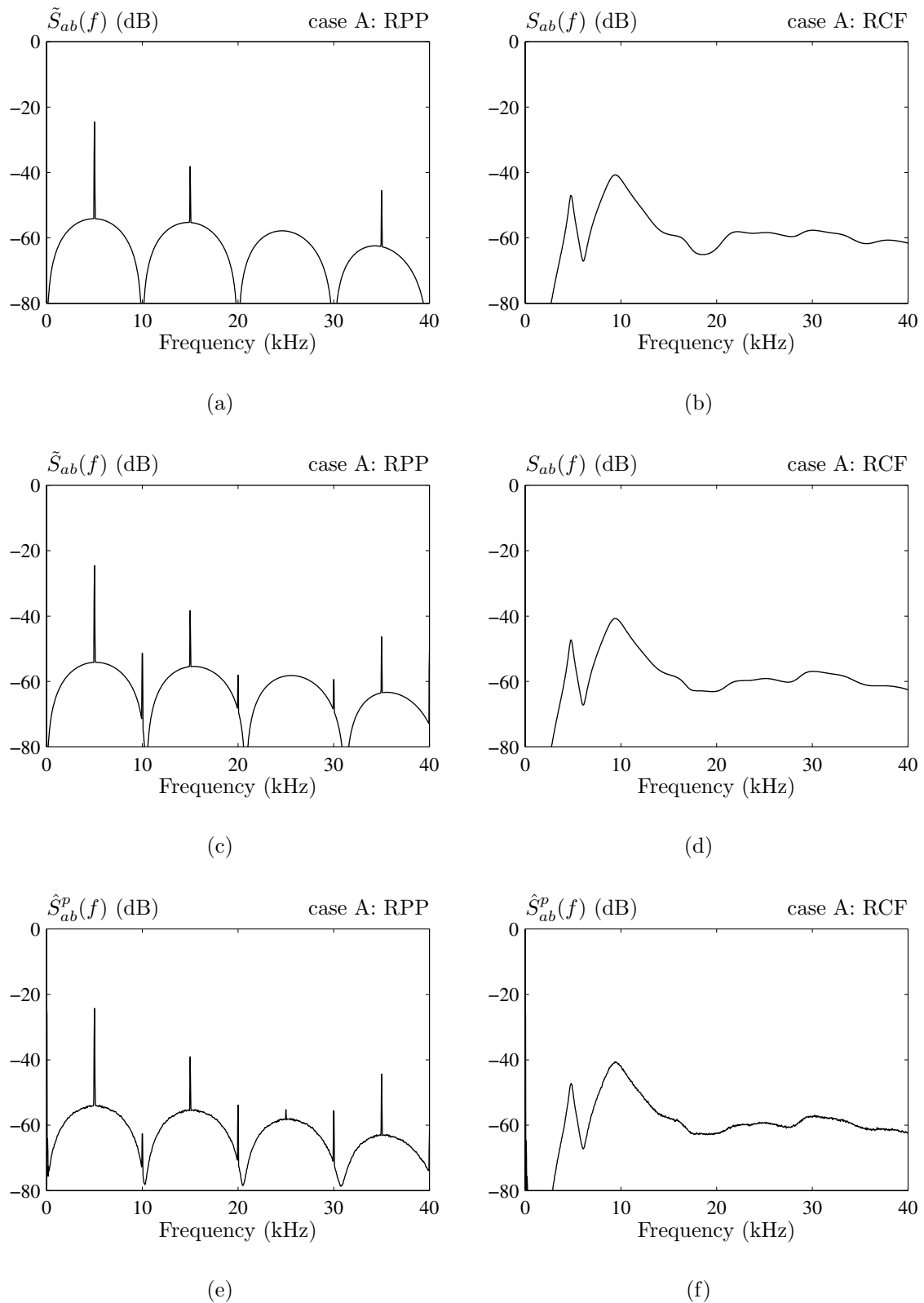
Figure 4.14 Spectra for the output voltage u_{ab} showing the effects of blanking time. Results for RPP and RCF (case A only). (a, b) Calculated density (for reference duty ratios), (c, d) calculated density (for modified duty ratios), and (e, f) measured density (at output terminals of converter).

opposed to the logic-level measurements, the spectra obtained here are not exempted from the effects of dc-link voltage ripple, blanking time, and voltage drop across the power devices. Although the agreement is still acceptable, better results may be obtained as elaborated below by including the effects of the blanking time in the analysis. No attempts are made to take the voltage drops and finite switching times into account.

The insertion of a blanking time between the turn-off of one transistor and the turn-on of its complementary device causes the effective duty ratio to be slightly different from the reference duty ratio. Sometimes, compensation for this error is included in the modulator [18], but for simplicity, this was not done here. Instead, the effects of a blanking time t_d is incorporated into the calculations.

For the RCF technique, the duty ratios used to calculate the spectrum are modified according to $d'_a = d_a - t_d/\overline{T}$ and $d'_b = d_b + t_d/\overline{T}$, where the different signs of the correcting terms reflect that the load current flows in opposite directions in leg a and b. Also, $\overline{T}$ is the average value of the carrier period. Numerically, $t_d/\overline{T} = 2.2/200 = 0.0110$ for the case A settings, which may be compared in magnitude to the duty ratios $d_a = 0.8$ and $d_b = 0.3$.

The treatment of the RPP scheme is essentially the same, but here the possibility of two pulses merging back to back has to be included, because in this case the number of commutations is reduced. Hence, when leading and lagging pulses occur with the same probabilities, the effective duty ratios are $d'_a = d_a - \frac{3}{4}t_d/T$ and $d'_b = d_b + \frac{3}{4}t_d/T$, where T is the (constant) carrier period duration. For $T = 200$ μs and $t_d = 2.2$ μs, this yields a deviation of 0.0083 from the reference duty ratio.

Introducing these modified duty ratios, the theoretically expected spectra were recalculated; the results are shown in Fig. 4.14 on page 101 for the case A settings. For the RCF technique, the modifications significantly narrow the gap between $\tilde{S}_{ab}(f)$ and $\hat{S}_{ab}^p(f)$ around 20 kHz; this may be seen from Fig. 4.14(b, d, and f). For the RPP scheme, similar improvements regarding the density part may be observed in Fig. 4.14(a, c, and e). The overall improvement is, however, not quite as good as in the RCF case, mainly because mismatches at the minor harmonics located at 10, 20, 30, and 40 kHz persist.

4.6   Summary

Detailed information on how to perform spectral analysis of random PWM schemes suitable for full-bridge dc/dc converters has been presented in this chapter. Based on the general analysis in the previous chapter, closed-form expressions for the spectra of pulse trains generated by both random carrier frequency modulation and random pulse-position modulation were derived. An important characteristic for both these schemes is that the proper volt-second balance is maintained on a per carrier period basis.

Examples have been included of how these formulas may be used to calculate the spectra analytically, provided probability density functions are known for the duration of carrier period and the pulse position. It was also shown how these expressions may be evaluated numerically by means of MATLAB algorithms.

The analysis also includes a method to calculate the spectrum of the output voltage in a full-bridge converter. This voltage is proportional to the difference of the switching

functions used to control the two legs. As elaborated in the text, the suggested method does not require knowledge of the cross spectra; this simplifies significantly the analysis of composite signals such as the output voltage.

Comparing the work in this chapter to past work reported in the literature, the main new contributions are believed to include:

- All theoretical results, which relate to spectral analysis of the RCF scheme taking the important detail of center-alignment of the pulses in each carrier period into account, are believed to be completely novel. Expressions similar to those reported in this chapter for the RLL technique may be found in e.g. [3], but only for the switching functions themselves.

- The procedure used for spectral analysis of the difference of (statistically dependent) switching functions are considered novel. The results obtainable with this procedure are exact in a mathematical sense without requiring knowledge of any cross spectra, which generally are considered more difficult to calculate than auto spectra.

- All closed-form analytic expressions for the spectra of the difference $q_{ab} \triangleq q_a - q_b$, which determines the output voltage in a full-bridge converter, are considered new, except for an earlier publication by the author [19], reappearing with only minor modifications in [20].

Also, it must be stressed that all theoretical results have been verified by laboratory measurements using the methodology described in section 3.3.4. Such a thorough validation of spectral analyses has hardly ever been reported in the literature despite the large number of publications dealing with random PWM.

In conclusion, it may be stated that the presented framework for spectral analysis of signals relating to random PWM has been proved to be very powerful; an excellent agreement between theory and measurements has been observed for both RPP and RCF modulation. The validity of the used principles is, however, not limited to those two strategies; extensions to other variants of random PWM are certainly possible as well.

Bibliography

[1] R. L. Kirlin, S. Kwok, S. Legowski, and A. M. Trzynadlowski, "Power Spectra of a PWM Inverter with Randomized Pulse Position," *IEEE Trans. on Power Electronics*, vol. 9, no. 5, pp. 463–472, Sept. 1994.

[2] R. L. Kirlin and A. M. Trzynadlowski, "A Unified Approach to Analysis and Design of Random Pulsewidth Modulation in Voltage Source Inverters," *IEEE Trans. on Circuits and Systems — I: Fundamental Theory and Applications*, vol. 44, no. 8, pp. 763–766, Aug. 1997.

[3] A. M. Stanković, *Random Pulse Modulation with Applications to Power Electronic Converters*, Ph.D. thesis, Massachusetts Institute of Technology, Feb. 1993.

 [4] W. B. Davenport, Jr. and W. L. Root, *An Introduction to the Theory of Random Signals and Noise*, IEEE Press Selected Reprint Series (reprint of the original 1958 edition), New York, 1987.

 [5] A. Papoulis, *Probability, Random Variables, and Stochastic Processes*, Electrical & Electronic Engineering Series. McGraw-Hill, third edition, 1991.

 [6] A. Wang and S. R. Sanders, "Random and Programmed Pulse-Width Modulation Techniques for DC-DC Converter," *IEEE International Symposium on Systems Engineering*, pp. 589–592, 1990.

 [7] F. Mihalič, T. Bezjak, and M. Milanovič, "Random Modulated Boost Converter with Improved Harmonic Spectrum," *Proc. of the IEEE International Symposium on Industrial Electronics*, vol. 2, pp. 268–273, 1997.

 [8] F. Mihalič, T. Bezjak, and M. Milanovič, "Improved Harmonics Spectrum and Reduced EMI in Boost Converter by Using the Random Modulation," *Proc. of 7th European Conference on Power Electronics and Applications*, vol. 2, pp. 366–371, 1997.

 [9] S. Y. R. Hui, Y. Shrivastava, S. Sathiakumar, K. K. Tse, and S. H. Chung, "A Comparison of Nondeterministic and Deterministic Switching Methods for dc-dc Power Supplies," *IEEE Trans. on Power Electronics*, vol. 13, no. 6, pp. 1046–1055, Nov. 1998.

[10] K. K. Tse, S.-H. Chung, S. Y. R. Hui, and H. C. So, "A Comparative Investigation on the Use of Random Modulation Schemes for DC/DC Converters," *IEEE Trans. on Industrial Electronics*, vol. 47, no. 2, pp. 253–263, Apr. 2000.

[11] A. M. Stanković, G. C. Verghese, and D. J. Perreault, "Analysis and Synthesis of Randomized Modulation Schemes for Power Converters," *IEEE Trans. on Power Electronics*, vol. 10, no. 6, pp. 680–693, Nov. 1995.

[12] T. Tanaka, T. Ninomiya, and K. Harada, "Random-Switching Control in DC-to-DC Converters," *Proc. of the 20th IEEE Power Electronics Specialists Conference*, vol. 1, pp. 500–507, 1989.

[13] P. G. Handley, M. Johnson, and J. T. Boys, "Elimination of Tonal Acoustic Noise in Chopper-Controlled DC Drives," *Applied Acoustics*, vol. 32, pp. 107–119, 1991.

[14] T. Tanaka, H. Kameda, and T. Ninomiya, "Noise Analysis of DC-to-DC Converter with Random Switching Control," *Proc. of the IEEE International Telecommunications Energy Conference*, pp. 283–290, Nov. 1991.

[15] T. Tanaka and T. Ninomiya, "Random-Switching Control for DC-to-DC Converter: Analysis of Noise Spectrum," *Proc. of the 23rd IEEE Power Electronics Specialists Conference*, vol. 1, pp. 579–586, 1992.

[16] J. T. Boys, "Theoretical Spectra for Narrow-Band Random PWM Waveforms," *IEE Proc. Part B*, vol. 140, no. 6, pp. 393–400, Nov. 1993.

[17] D. Middleton, *An Introduction to Statistical Communication Theory*, McGraw-Hill Book Company, New York–Toronto–London, 1960.

[18] F. Blaabjerg, J. K. Pedersen, and P. Thoegersen, "Improved Modulation Techniques for PWM-VSI Drives," *IEEE Trans. on Industrial Electronics*, vol. 44, no. 1, pp. 87–95, Feb. 1997.

[19] M. M. Bech, F. Blaabjerg, J. K. Pedersen, and A. M. Trzynadlowski, "A Methodology for True Comparison of Analytical and Measured Frequency Domain Spectra in Random PWM Converters," *Proc. of the 29th IEEE Power Electronics Specialists Conference*, vol. 1, pp. 36–43, May 1998.

[20] M. M. Bech, J. K. Pedersen, F. Blaabjerg, and A. M. Trzynadlowski, "A Methodology for True Comparison of Analytical and Measured Frequency Domain Spectra in Random PWM Converters," *IEEE Trans. on Power Electronics*, vol. 14, no. 3, pp. 578–586, May 1999.

Chapter 5

Spectral analysis of random carrier frequency dc/ac PWM schemes

5.1 Introduction

Modulators operating with a randomly changing carrier frequency are investigated in this chapter in conjunction with three-phase voltage-source converters (VSC). Initially, it may be noted that power electronic engineers often think in terms of the carrier frequency during analysis of modulators, which leads to the acronym RCF-PWM (random carrier frequency pulse-width modulation), but to facilitate much of the math involved in the subsequent spectral analysis, the inverse quantity — the carrier period — is used extensively also. In the literature many other formulations may be found[1].

The main objective of this chapter is to show how the framework developed in Chapter 3 can be used to perform spectral analysis of an RCF modulated three-phase VSC for arbitrary modulation principles including e.g. space-vector modulation or discontinuous PWM (see further in Chapter 2). As mentioned in Chapter 4 dealing with full-bridge dc/dc converters, attention must be paid to precisely which voltage, the analysis is tailored towards. Unlike for deterministic modulators, it is, in general, impossible to extract the spectral characteristics of the line-to-line voltage from the spectra of the switching functions when RCF or other random PWM schemes are used. Therefore, a second objective is to discuss in greater details the procedure used already in Chapter 4 for spectral analysis of composite waveforms, such as the line-to-line voltage in a three-phase converter.

Finally, it may be noted that the current chapter almost focuses exclusively on spectral analysis of RCF. However, more information relating to the RCF family of techniques may also be found in Chapter 6 where current-quality issues of importance to RCF-PWM are addressed. Also, an analysis of the possibilities of using RCF in closed-loop applications may be found in Part III.

---

[1]A multitude of notations exists for the principle of dithering the instantaneous carrier frequency: Ref. [1] introduced "random-switching control," [2] talks of "spread-spectrum switching," [3] uses a "randomly modulated carrier PWM," [4, 5] analyze a "randomized aperiodic modulator," [6] suggests a "variable pulse rate" modulator, [7] designs a "random slope PWM inverter" while others including [8] classify the principle at hand as "random switching frequency PWM."

Chapter outline

Before the spectral analysis is commenced, efforts have been made to assure that the studied variants of the RCF scheme comply with a number of issues of practical importance. Such issues are discussed in the first section below. In the next section, a general formula for the spectrum of the RCF scheme is derived and afterwards, examples of how to perform the spectral analysis are provided. The examples are grouped into three sections dealing with the switching function, the line-to-line voltage, and the phase-to-neutral voltage, respectively. Due to the theoretical nature of the analyses, comparative laboratory measurements are included adhering to the guidelines put forth in Chapter 3. A summary concludes the chapter.

5.2   Aspects of probability density functions

For the RCF technique, the parameter of paramount importance for the frequency contents of the modulated signal is, of course, the variations of the carrier frequency. Equivalently, the variations of the carrier period T may be studied and in this section, overall strategies for the selection of T are discussed, because it turns out that the way in which T is determined is very important for the further spectral analysis and for the implementation of RCF-based modulators. Specifically, the concept of probability density function is used as a basis for the discussion.

5.2.1   Assignment of a probability density function for T

In principle, the choice of T is completely arbitrary, but in practice constraints are imposed, which limits the permissible values to some range $T_1 \leq T \leq T_2$. In general, the bounds T_1 and T_2 depend on the allowable switching losses, the blanking time, the driver circuitry, the acceptable current ripple, the desired closed-loop control bandwidth, etc.

Memory-less versus Markov-chain based approaches

The technical constraints limit the range of usable carrier frequencies, but they do not dictate how the next T is selected provided it belongs to the allowable range. The selection of the next carrier period T may be made in two conceptually different ways:

The next value of T depends on past values of T
> The next T depends on the state of an underlying Markov chain. In [4, 9, 10] it is stated that this approach yields less local current ripple (in an accumulating sense). The reason is that it is possible to design a Markov chain in such a way that the probability of applying many "long" carrier periods in a row is significantly diminished.

The next values of T is independent of all past values of T
> T is determined by the outcome of a memory-less random experiment. This approach is by far the most common principle used in the literature. The implementation of methods based on statistically independent trials is simpler than those using Markov chains, which requires more sophisticated programming with bookkeeping of past and present values for T.
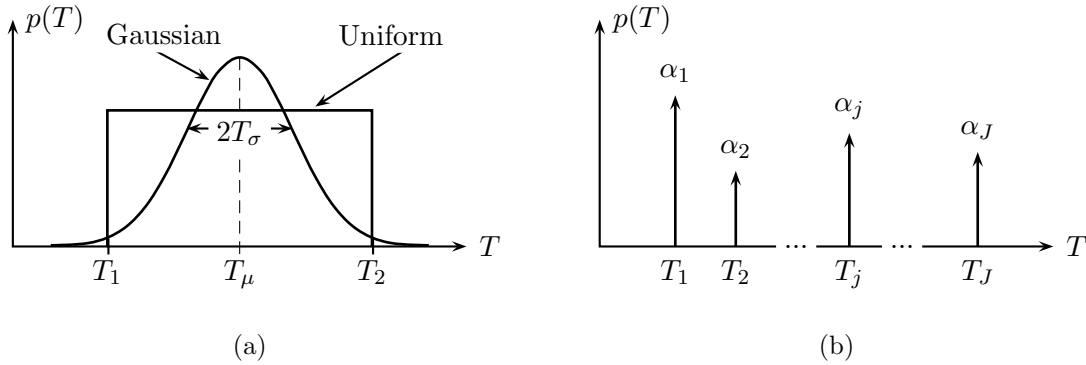
Figure 5.1 Examples of (a) continuous and (b) discrete probability density functions $p(T)$ for the carrier period T.

In this thesis, only the class of memory-less methods is studied for several reasons: they are simple to implement and judging from the work in [10], the spectral analysis of random PWM schemes based on Markov chains are very complicated, even for the relatively simple examples studied in [10], which, unfortunately, are of no immediate practical relevance. Also, even though the memory-less methods do not give the same controllability of the time-domain ripple waveforms as do Markov-based techniques, this fact is not considered decisive.

Continuous versus discrete probability density function (pdf)

Another concept that needs attention regarding the random selection of carrier frequencies/periods is the pdf that determines the statistical properties. In order to make a particular pdf for T, denoted as $p(T)$, physically meaningful, constraints must be imposed, viz.

$$p(T) \geq 0 \quad \text{for all } T,$$
$$\int_{-\infty}^{+\infty} p(T) \, dT = 1. \tag{5.1}$$

Clearly, these requirements can be met in an infinity of different ways, but in order to facilitate the discussion, two main classes of density functions are commented further below:

Continuous probability density function
   For a continuous density function, all values of T in some range $T_1 \leq T \leq T_2$ typically appear with a non-zero probability. For example the uniform distribution and the Gaussian[2] (normal) distributions depicted in Fig. 5.1(a) have been used in experimental investigations of the RCF technique in [11–13], among many others.

---

[2]Theoretically, all values of T, including those outside the $T \in [T_1; T_2]$ range, occur with non-zero probability, but for practical purposes all out-of-range values must be removed. Strictly speaking then, the effective pdf is only approximately Gaussian.

Discrete (impulsive) probability density function

A discrete pdf implies that only a finite number of values for T occurs as illustrated in Fig. 5.1(b). Using the nomenclature, $p(T)$ may conveniently be represented by a sum of delta impulses, i.e.

$$p(T) = \sum_{j=1}^{J} p_j \, \delta(T - T_j), \qquad (5.2)$$

where J is the number of different carrier periods in the pool and p_j is the weight assigned to the j'th carrier period T_j. The weights p_j must all be non-negative and also $\sum p_j = 1$ in order to comply with (5.1).

It should be mentioned that it is possible to construct a pdf for T which has both a continuous and a discrete part. However, such mixed density functions are not pursued.

5.2.2   Evaluation of continuous and discrete density functions

The implications of the continuous and the discrete type of pdf for random PWM are commented in some details below. To facilitate the presentation, the discussion has been divided into the following four overall areas:

- Implementation of a random carrier period generator

- Smoothness of the output voltage spectrum

- Complexity of spectral analysis

- Compliance with the spectral shaping problem

For reference, the discussion is concluded with a table of comparison, see Table 5.1 on page 115.

Implementation of a random carrier period generator

Irrespective of the chosen pdf for T, some kind of random number generator (RNG) that outputs random numbers is required. Only software-based RNG's are considered although hardware-based RNG's have occasionally occurred in the literature on random PWM [7, 14–17].

For a continuous pdf, the starting point is an RNG that generates uniform deviates x in the $x \in [0; 1]$ range. In the ideal case, the number of different values that x may attain in this range is infinite, but due to the finite period of practical RNG's the number of different x values is finite. Typically, as shown in [18], the period length is greater than 10^8 for RNG's of just modest complexity (a few lines of C code), which corresponds to a repetition period of more than five hours, if the average carrier frequency is 5 kHz. Hence, the periodicity is not an issue of importance, provided that just a modest computational power is available[3]. References to the particular routine used for all results reported in this thesis may be found in Appendix A.

---

[3]Some of the early implementations in micro controllers of random PWM used an off-line generated look-up table having in the order of a few thousands entries only [2, 3, 19, 20]. Such a short sequence deteriorates the performance — [21] gives more detailed information.

If the pdf for T is uniform (constant over some range $[T_1; T_2]$), the next random T may be found straightforwardly by $T = T_1 + (T_2 - T_1)x$, once a new value for x is known. If the desired pdf is non-uniform, transform methods are normally used to generate e.g. a Gaussian distribution from a uniform distribution. Details may be found in [18], but in general non-uniform distributions require extra computations compared to the uniform case.

Regarding the discrete pdf, only a few different values for T's are needed and therefore, an RNG that outputs only J different integers with prescribed probabilities p_j is sufficient. Direct methods that generate random bits are discussed in [22], but for the sake of simplicity these schemes are disregarded in the current discussion. Hence, it is assumed that a uniformly distributed random number x is available, and then the random choice of T from the finite set $\{T_j\}$ may be found by means of a series of comparisons, i.e.

$$
T = \begin{cases}
T_1, & \text{if } 0 \leq x < p_1, \\
T_2, & \text{if } p_1 \leq x < p_1 + p_2, \\
\vdots \\
T_J, & \text{if } p_1 + p_2 + \cdots + p_{J-1} \leq x < 1.
\end{cases} \tag{5.3}
$$

This simple procedure requires at most $J - 1$ comparisons when the value of x is known. For small values of J this is an acceptable solution. For larger pool sizes, an elegant method based on a single table look-up operation described in [22] should be considered, because this approach is very fast to execute in real-time. Here, the main task is to initialize the look-up table.

Smoothness of the output voltage spectrum

Without anticipating the forthcoming spectral analysis, it may be stated that for a continuous $p(T)$ experiments have shown that the produced output voltage spectrum is a purely continuous function of frequency, except for the discrete component at the fundamental frequency. No other harmonics exist, i.e. all the power normally carried by the harmonics clustered around multiples of the carrier frequency is transferred to the continuous density spectrum. This characteristic may be observed for the uniform distribution of T used for the dc/dc converter studied in Chapter 4. Also, results in [23] besides many other references support this statement.

For the discrete distributions, however, the smoothness of the voltage spectrum is not guaranteed, i.e. harmonics may peak up at discrete frequencies despite of the randomization. Therefore, care must be exercised when the pool of carrier frequencies (periods) is selected, because non-fundamental harmonics may be generated, if the frequencies in the pool fulfill requirements stated by [24] and published in [25]. A more elaborative discussion is given in section 5.4.3. Fortunately, when the pool of frequencies is properly selected, the generated voltage spectrum has a continuous density part only as observed by [21] apart from the harmonic at the fundamental frequency. Note that a discrete $p(T)$ does not in general unconditionally imply that the spectrum has discrete components, too.

Complexity of spectral analysis

Whether a continuous or a discrete pdf is used, explicit knowledge of the particular $p(T)$ is crucial in order to perform the spectral analysis. This has been demonstrated in Chapter 4 by the examples relating to dc/dc converters. These examples also show that even in the most simple case where $p(T)$ is constant in some range (uniform pdf), the calculations become somewhat involved due to the many definite integrals needed to evaluate various expectations over T. The mathematics becomes much worse for the dc/ac schemes studied in the current chapter, even for a uniform[4] $p(T)$.

If a calculation of the spectrum for other continuous distributions of the carrier period is wanted, new and tedious algebraic manipulations are necessary for each pdf of interest. In fact, there is no guarantee that a solution can be found; at best, the derivations are involved — at worst, no closed-form solution exists.

The analysis of dc/dc schemes in Chapter 4 has shown that for the random lead-lag modulation, the derivations leading to expressions for the spectrum are relatively simple due to the discrete pdf for the delay. This is equivalent to the discrete pdf for the carrier period of interest here. Therefore, evaluation of expectations across T simplifies significantly compared to the cases with a continuous pdf, due to the sampling property of the underlying delta-functions in (5.2). Special care must, however, be taken to determine the existence of harmonics and their strength, if they exist [24, 25].

Compliance with the spectral shaping problem

Apart from gaining a better understanding of the behavior of random PWM techniques, another reason for calculating the spectra given the pdf for the randomized variables is that this knowledge opens the opportunity to "custom design" the output spectrum — at least to some extent. As mentioned in Chapter 1, a procedure to select the (optimal) modulator parameters would be of high interest in practical applications of random PWM, because otherwise it is hard to prove whether or not the full potentials of non-deterministic modulation have been explored.

Initial research in this area has been reported in [4, 5] targeted towards meeting predefined frequency-domain specifications in the best possible way without violating physical constraints like disallowing negative duty ratios, etc. One of the examples in these references relates to minimizing the weighted sum of the power carried by a certain set of harmonics generated by a random pulse-position scheme. In another example, the total power in some specified frequency range is minimized for the same dc/dc random scheme. In both cases, numerical optimization methods are used to determine the parameters for the modulator, i.e. the numerical values of the parameters describing the probability density function.

Using the same terminology as in optimization theory[5], formulas for the spectrum given the pdf are essential in order to evaluate the objective function, which, for ex-

---

[4]The spectral analysis of RCF-PWM for dc/ac converters reported in later sections of this chapter does not include any examples of a uniform pdf for T. Such analyses, which agree perfectly with measurements, have, nevertheless, been completed, but for sake of brevity, the derivations and the results for uniform pdf are omitted in the thesis.

[5]Among many others, the excellent book [26] by Gill et al. may be consulted for a well-written introduction to the theory (and practice) of mathematical optimization by numerical methods.
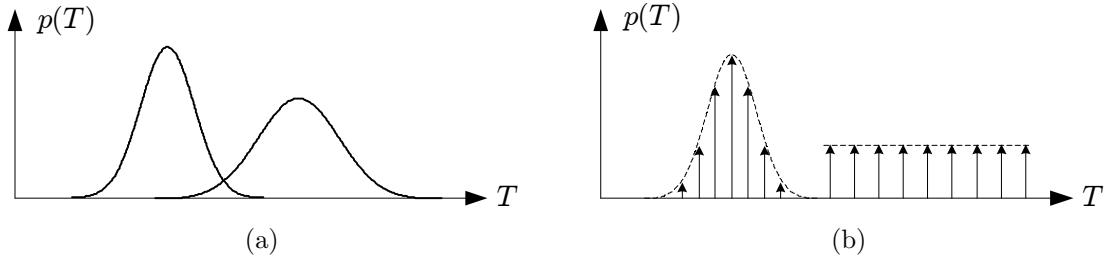
Figure 5.2 Illustration of possible (envelope) curves for (a) a continuous and (b) a discrete pdf for two different sets of parameters.

ample, could be the total power in some frequency band. Also, the design variables are the parameters in the pdf, e.g. the T_1 and T_2 values for the uniform distribution of carrier periods. Constraints like upper and lower bounds for T_1 and T_2 must also be taken into account during the search for the optimal values of the design variables, which minimize the objective function within the region spanned by the constraints.

Although the work reported in this thesis allows the evaluation of objective functions for a large class of random PWM schemes applicable for widely-used converters, such as the three-phase VSC, the synthesis part of the shaping problem is not addressed in details. However, in order to facilitate the extension of the current work to investigate the spectral shaping problem, care must be exercised already at this stage regarding the selection of the type of pdf (continuous or discrete) to focus on in later sections of the chapter.

To elaborate, it may be recalled from Fig. 5.1(a) that a continuous pdf is typically described by a few parameters. For example, the uniform pdf needs only two parameters: lower T_1 and upper T_2 bounds, respectively; for the Gaussian distribution the average T_μ and standard deviation T_σ must be specified. From an optimization point of view, this low number of design variables is attractive, because low-order problems are relatively easy to handle compared to high-order problems.

Unfortunately, a serious defect outweighs this advantage: a new set of parameters does not change the "shape" of the distribution, but it merely changes e.g. the upper and lower limit for T; the underlying (uniform) distribution remains. Fig. 5.2(a) illustrates this fact using the Gaussian pdf as an example. It is therefore impossible to find the true optimal pdf that minimizes some objective function due to the fact that only one class of distributions can be searched at the time (and each class of pdf requires its own tedious spectral analysis as pointed out earlier). To put it differently, only the optimal distribution within this particular family can be found, but there is no guarantee that the minimum found is the global minimum, if all possible continuous distributions are considered as candidates for the solution of a particular optimization problem. Clearly, this is a serious flaw of continuous probability density functions.

For the discrete type of pdf given by (5.2) on page 110, compliance with the spectral shaping problem is obtained immediately as explained below. First, in this case a pool of carrier periods $\{T_1, T_2, \cdots, T_J\}$ is selected beforehand. Then, the corresponding p_j-weights in (5.2) may be interpreted as the parameters (or design variables) to be determined by the optimization algorithm in such a way that the objective function is minimized. The key point is now that even for modest values of J, good approximations to arbitrary continuous pdf's may be obtained by simply changing the p_j weights. For

example, if all $p_j = 1/J$, an approximation to a continuous uniform pdf arises; the Gaussian distribution may be emulated by choosing $\{p_j\}$ in a bell-shaped fashion. Fig. 5.2(b) shows how the discrete pdf may be used to approximate totally different continuous distributions by simply changing the set of weights.

It is seen that this approach to spectral shaping is much more appealing than the continuous pdf case described on the page before, because the optimizer may search the entire space of candidate pdf at once without any need for hand derivations of complicated expressions for different continuous distributions.

Comparison of continuous and discrete pdf for T

To summarize the key points, Table 5.1 gives an overview of how well the continuous pdf and the discrete pdf perform in the different categories of interest.

The smooth voltage spectrum produced by the RCF technique with a continuous $p(T)$ is undoubtedly a very desirable property from an acoustic point of view, since the frequency contents of the acoustic noise emitted from a load strongly depends[6] on the spectrum for the voltage supplied to the load. Regarding the smoothness of the spectrum, the discrete family of pdf's can be made sufficiently good by adhering to design rules given later. Therefore, the ($\div$) score in Table 5.1 is only included in order to indicate that precaution must be exercised during the selection of the pool of carrier frequencies.

In the other disciplines the discrete pdf seems preferable to the continuous pdf: it is easier to implement, although this is not a major concern when modern processors are used, but rather the major advantages relate to the spectral analysis and to the compliance with the prospective spectral shaping problem. The last row in Table 5.1 relating to how well the two kinds of density functions comply with closed-loop applications has not been discussed yet, but, nevertheless, the discrete pdf scores better than the continuous pdf. This topic is treated in details in Part III starting on page 223, where it is demonstrated how commonly used feed-back digital control techniques may be unified with random carrier frequency PWM.

Based on this discussion, only the discrete type of pdf for T is selected for further analysis in this chapter. Also, the method based on Markov chains is not considered any further in this thesis despite the appealing characteristics reported earlier by Stanković in [4, 9, 10].

To partly remedy the fact that no evidence has been provided so far for the claimed similarity in performance between a discrete and a continuous $p(T)$, experimental results reported by [21] may be considered. In this reference, it is shown that a voltage spectrum almost identical to the spectrum produced by a continuous pdf may be obtained using only a very small pool size J of selectable carrier frequencies, typically in the order of $J = 5$. According to [21] there is only a little noticeable difference in the emitted acoustic noise from an induction motor using the reduced set of five carrier frequencies compared to a continuous pool of frequencies. However, the difference becomes noticeable if less than five frequencies are used.

---

[6]The relationship from input voltage to emitted noise from e.g. an ac motor forms a complicated transfer function involving interconnected electro-magnetic and mechanical subsystems. This implies that the emitted acoustic noise is a highly nonlinear function of the supplied voltage.

	Continuous pdf	Discrete pdf
Implementation	0	+
Smoothness of spectrum	+	+ ($\div$)
Amenable to theoretical analysis	$\div$	0
Spectral shaping	$\div$	+
Closed-loop compliance	$\div$	0

Table 5.1 Evaluation of continuous and discrete probability density functions for the carrier period. The used ratings are: ($\div$): poor/difficult, (0): fair/manageable, and (+): good.

For completeness, it should also be noted that a small pool of different carrier frequencies was used in experimental investigations already in 1993 by [27], but solely in order to reduce storage and microprocessor requirements; compliance with the issues summarized in Table 5.1 was not considered. Also, initial theoretical results dealing with the shaping problem based on a discrete pdf for T may be found in [28–30], and recently in [31] also.

Final comments on the choice of pdf

Although the discussion of the merit and demerits of the two kinds of pdf offspring from the RCF technique, many of the conclusions apply equally well to the random PWM techniques studied in the next chapter which all operate with a fixed carrier frequency, but random pulse positions (or widths). For such schemes, the spectral analysis is simpler for a discrete distribution than for a continuous distribution; the same holds for the spectral shaping problem.

5.3 Spectral analysis of dc/ac random carrier frequency PWM

The spectral analysis of the RCF technique is based on the main results obtained in Chapter 3. In this chapter, a review of related previous work may also be found in section 3.4.2 making a repetition superfluously here. Therefore, the objective of this section is solely to apply the results of Chapter 3 to derive a set of formulas for the spectrum generated by RCF-PWM schemes suitable for dc/ac converters. In particular, no constraints are imposed on the kind of modulation method, i.e. the analysis is valid for purely sinusoidal modulation, but also for space-vector PWM, discontinuous PWM, etc., which all have been briefly described in Chapter 2.

This section is organized into three parts. First, the basis for the derivations is specified and next, details of the mathematical derivations are provided. The section is concluded with a summary of the main results which are extensively used in the remaining part of this chapter.
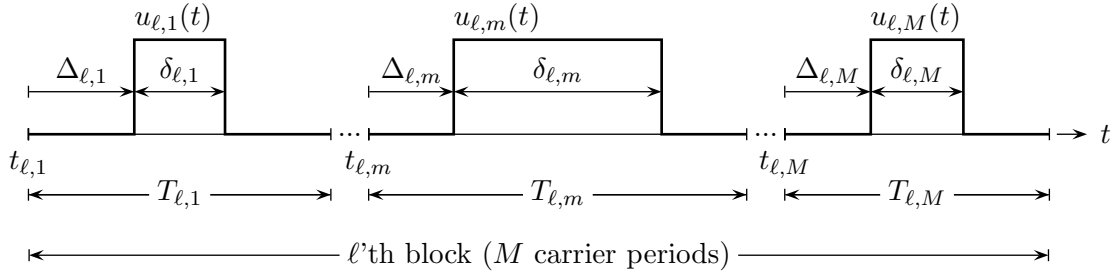
Figure 5.3 Switching function for the RCF technique employing variable duty ratios. The illustration assumes that the on-state pulse is center-aligned in each carrier period. (However, the theory is also valid for non-centered and non-rectangular pulses.)

5.3.1   Parametric representation of switching functions

The randomization technique to be studied has the following properties:

1. The on-state pulses are center-aligned within each carrier period. This is the standard choice in all regular-sampled symmetric PWM, which samples the reference once per carrier period T.

2. The instantaneous value of T is determined by the outcome of independent random experiments, i.e. there is no correlation between adjacent carrier periods.

Formally, the switching function may be represented by the train of pulses shown in Fig. 5.3. It may be noted that both the delay $\Delta_{\ell,\tilde{m}}$ and the pulse width $\delta_{\ell,\tilde{m}}$ are random variables because of the relations stated in (3.22) and (3.23), repeated here for reference:

$$\delta_{\ell,m} = d_{\ell,m} T_{\ell,m} \tag{5.4}$$

$$\Delta_{\ell,m} = \alpha_{\ell,m} T_{\ell,m}. \tag{5.5}$$

These variables depend on the sampling instant $t_{\ell,m}$, which is a function of all past values of the carrier period $T_{\ell,m}$. This makes the analysis complicated when it comes to evaluation of the statistical expectation $E\{\cdot\}$ needed to calculate the total power spectrum $S(f)$ by the formulas summarized in section 3.4.7 on page 67:

$$S(f) = \sum_{m=1}^{M} \sum_{\tilde{m}=1}^{M} S_{m,\tilde{m}}(f), \tag{5.6}$$

where $S_{m,\tilde{m}}(f)$ is given by

$$S_{m,\tilde{m}}(f) = \frac{1}{M\overline{T}} E\left\{ \sum_{\ell=-\infty}^{\infty} U(f;\delta_{0,m}) U^{\star}(f;\delta_{\ell,\tilde{m}}) e^{j\omega(t_{\ell,\tilde{m}}-t_{0,m})} e^{j\omega(\Delta_{\ell,\tilde{m}}-\Delta_{0,m})} \right\} \tag{5.7}$$

The evaluation of the partial contributions $S_{m,\tilde{m}}(f)$ to the total spectrum is based on expansion of (5.7).

5.3.2 Evaluation of partial contribution to the total spectrum

To evaluate (5.7), the expectation of the infinite sum across ℓ must be found. Below, details of the derivations are given for the three sub-cases (a) $m = \tilde{m}$, (b) $m < \tilde{m}$, and (c) $m > \tilde{m}$.

The diagonal terms: m = $\tilde{\mathbf{m}}$

In practical applications, the duration of the carrier period $T_{\ell,m}$ is selected at random, but (5.7) is expressed in terms of epochs like $t_{\ell,\tilde{m}}$ and $t_{0,m}$. Referring to Fig. 5.3 on the facing page, the time difference term $(t_{\ell,\tilde{m}} - t_{0,m})$ may be found as

$$t_{\ell,\tilde{m}} - t_{0,m}$$

$$= \begin{cases} \dots \\ -(T_{-2,m} + \dots + T_{-2,M} + T_{-1,1} + \dots + T_{-1,M} \\ \qquad\qquad\qquad +T_{0,1} + \dots + T_{0,m-1}), & \ell = -2, \quad 2M \text{ terms}, \\ -(T_{-1,m} + \dots + T_{-1,M} + T_{0,1} + \dots + T_{0,m-1}), & \ell = -1, \quad M \text{ terms}, \\ 0, & \ell = 0, \quad 0 \text{ terms}, \\ T_{0,m} + \dots + T_{0,M} + T_{1,1} + \dots + T_{1,m-1}, & \ell = 1, \quad M \text{ terms}, \\ T_{0,m} + \dots + T_{0,M} + T_{1,1} + \dots + T_{1,M} + T_{2,1} + \dots + T_{2,m-1}, & \ell = 2, \quad 2M \text{ terms}. \\ \dots \end{cases}$$

$$(5.8)$$

Using (5.5), the difference $(\Delta_{\ell,\tilde{m}} - \Delta_{0,m})$ between the pulse positions becomes

$$\Delta_{\ell,\tilde{m}} - \Delta_{0,m} = \alpha_{\ell,\tilde{m}} T_{\ell,\tilde{m}} - \alpha_{0,m} T_{0,m}. \tag{5.9}$$

The sum of expectations in (5.7) may now be expanded by inserting (5.8) and (5.9):

$$E\{\cdot\} = \quad \cdots$$

$$+ E\Big\{ U(f;\delta_{0,m}) U^\star(f;\delta_{-2,\tilde{m}}) e^{-j\omega \overbrace{(T_{-2,m} + \cdots + T_{0,m-1})}^{2M\,\text{terms}}} e^{j\omega(\alpha_{-2,\tilde{m}} T_{-2,\tilde{m}} - \alpha_{0,m} T_{0,m})} \Big\}$$

$$+ E\Big\{ U(f;\delta_{0,m}) U^\star(f;\delta_{-1,\tilde{m}}) e^{-j\omega \overbrace{(T_{-1,m} + \cdots + T_{0,m-1})}^{M\,\text{terms}}} e^{j\omega(\alpha_{-1,\tilde{m}} T_{-1,\tilde{m}} - \alpha_{0,m} T_{0,m})} \Big\}$$

$$+ E\Big\{ U(f;\delta_{0,m}) U^\star(f;\delta_{0,\tilde{m}}) \Big\}$$

$$+ E\Big\{ U(f;\delta_{0,m}) U^\star(f;\delta_{1,\tilde{m}}) e^{j\omega \overbrace{(T_{0,m} + \cdots + T_{1,m-1})}^{M\,\text{terms}}} e^{j\omega(\alpha_{1,\tilde{m}} T_{1,\tilde{m}} - \alpha_{0,m} T_{0,m})} \Big\}$$

$$+ E\Big\{ U(f;\delta_{0,m}) U^\star(f;\delta_{2,\tilde{m}}) e^{j\omega \overbrace{(T_{0,m} + \cdots + T_{2,m-1})}^{2M\,\text{terms}}} e^{j\omega(\alpha_{2,\tilde{m}} T_{2,\tilde{m}} - \alpha_{2,m} T_{0,m})} \Big\} + \cdots .$$

$$(5.10)$$

The expectation of the products may now be rewritten as a product of expectations, because there is no correlation between successive values of the carrier period. Hence,

$$
E\{\cdot\} =
$$

$$
E\Big\{U(f;\delta_{0,m})e^{-j\omega\alpha_{0,m}T_{0,m}}\Big\}
$$

$$
\Big[\cdots + E\Big\{U^\star(f;\delta_{-2,\tilde{m}})e^{-j\omega(1-\alpha_{-2,\tilde{m}})T_{-2,m}}\Big\}\overbrace{E\{e^{-j\omega T_{-2,m+1}}\}\cdots E\{e^{-j\omega T_{0,m-1}}\}}^{2M-1 \text{ terms } (\ell=-2)}
$$

$$
+ E\Big\{U^\star(f;\delta_{-1,\tilde{m}})e^{-j\omega(1-\alpha_{-1,\tilde{m}})T_{-1,m}}\Big\}\overbrace{E\{e^{-j\omega T_{-1,m+1}}\}\cdots E\{e^{-j\omega T_{0,m-1}}\}}^{M-1 \text{ terms } (\ell=-1)}\Big]
$$

$$
+ E\Big\{U(f;\delta_{0,m})U^\star(f;\delta_{0,\tilde{m}})\Big\}
$$

$$
+ E\Big\{U(f;\delta_{0,m})e^{j\omega(1-\alpha_{0,m})T_{0,m}}\Big\}
$$

$$
\Big[\ E\Big\{U^\star(f;\delta_{1,\tilde{m}})e^{j\omega\alpha_{1,\tilde{m}}T_{1,m}}\Big\}\overbrace{E\{e^{j\omega T_{0,m+1}}\}\cdots E\{e^{j\omega T_{1,m-1}}\}}^{M-1 \text{ terms } (\ell=1)}
$$

$$
+ E\Big\{U^\star(f;\delta_{2,\tilde{m}})e^{j\omega\alpha_{2,\tilde{m}}T_{2,m}}\Big\}\overbrace{E\{e^{j\omega T_{0,m+1}}\}\cdots E\{e^{j\omega T_{2,m-1}}\}}^{2M-1 \text{ terms } (\ell=2)}\ +\ \cdots\Big].
$$

$$
(5.11)
$$

The pulse widths (the δ's) and the pulse-position parameters (the α's) are independent of the block number, i.e. these parameters depend only on the position m (or $\tilde{m}$) within the block. Also, it is known that all carrier periods are identically, independently distributed, although the particular probability density function is unknown. Under these circumstances, (5.11) may be simplified to

$$
E\{\cdot\} = E\big\{|U(f;\delta_m)|^2\big\}
$$

$$
+ E\Big\{U(f;\delta_m)e^{-j\omega\alpha_m T}\Big\}E\Big\{U^\star(f;\delta_{\tilde{m}})e^{-j\omega(1-\alpha_{\tilde{m}})T}\Big\}\sum_{\ell=1}^{\infty}E\{e^{-j\omega T}\}^{M\ell-1}
$$

$$
+ E\Big\{U(f;\delta_m)e^{j\omega(1-\alpha_m)T}\Big\}E\Big\{U^\star(f;\delta_{\tilde{m}})e^{j\omega\alpha_{\tilde{m}}T}\Big\}\sum_{\ell=1}^{\infty}E\{e^{j\omega T}\}^{M\ell-1}
$$

$$
(5.12)
$$

where the fact that $m = \tilde{m}$ has been used to simplify the term corresponding to $\ell = 0$. The second summation in the preceding equation forms a convergent power series if $|E\{e^{j\omega T}\}| < 1$, and in this case it may be shown that

$$
\sum_{\ell=1}^{\infty}E\{e^{j\omega T}\}^{M\ell-1} = \frac{E\{e^{j\omega T}\}^{M-1}}{1 - E\{e^{j\omega T}\}^{M}}\ .
$$

$$
(5.13)
$$

Also, it may be noted that the expressions on the second and on the third line of (5.12) are each other's complex conjugates. Using this fact and the series (5.13), the final

result for the contribution to total spectrum for the $m = \tilde{m}$ case becomes

$$
\begin{aligned}
S_{m,\tilde{m}}(f) = \frac{1}{M\overline{T}} \Bigg[& E\big\{|U(f;\delta_m)|^2\big\} \\
& + 2\,\mathcal{R}\bigg(E\big\{U(f;\delta_m)e^{j\omega(1-\alpha_m)T}\big\} E\big\{U^\star(f;\delta_{\tilde{m}})e^{j\omega\alpha_{\tilde{m}}T}\big\} \frac{E\big\{e^{j\omega T}\big\}^{M-1}}{1 - E\big\{e^{j\omega T}\big\}^M} \bigg) \Bigg].
\end{aligned}
\tag{5.14}
$$

The off-diagonal terms: m < m̃

The expansion of (5.7) is basically the same as for the $m = \tilde{m}$ case, but the time difference term $(t_{\ell,\tilde{m}} - t_{0,m})$ requires special attention. Referring again to Fig. 5.3 on page 116, this term expands into

$$
t_{\ell,\tilde{m}} - t_{0,m}
$$
$$
= \begin{cases}
\cdots & \\
-(T_{-2,\tilde{m}} + \cdots + T_{-2,M} & \\
\quad + T_{-1,1} + \cdots + T_{-1,M} + T_{0,1} + \cdots + T_{0,m-1}), & \ell = -2, \ 2M - (\tilde{m}-m) \text{ terms}, \\
-(T_{-1,\tilde{m}} + \cdots + T_{-1,M} + T_{0,1} + \cdots + T_{0,m-1}), & \ell = -1, \ M - (\tilde{m}-m) \text{ terms}, \\
T_{0,m} + \cdots + T_{0,\tilde{m}-1}, & \ell = 0, \quad\quad (\tilde{m}-m) \text{ terms}, \\
T_{0,m} + \cdots + T_{0,M} + T_{1,1} + \cdots + T_{1,\tilde{m}-1}, & \ell = 1, \quad M + (\tilde{m}-m) \text{ terms}, \\
T_{0,m} + \cdots + T_{0,M} + T_{1,1} + \cdots + T_{1,M} & \\
\quad + T_{2,1} + \cdots + T_{2,\tilde{m}-1}, & \ell = 2, \quad 2M + (\tilde{m}-m) \text{ terms}. \\
\cdots &
\end{cases}
\tag{5.15}
$$

As before, the difference $(\Delta_{\ell,\tilde{m}} - \Delta_{0,m})$ is given by (5.9), which may be used together with (5.15) to get the following expression for the sum of expectations in (5.7):

$$
E\{\cdot\} = \ \cdots
$$
$$
+ E\Big\{ U(f;\delta_{0,m})U^\star(f;\delta_{-2,\tilde{m}}) e^{-j\omega \overbrace{(T_{-2,\tilde{m}} + \cdots + T_{0,m-1})}^{2M-(\tilde{m}-m)\ \text{terms}}} e^{j\omega(\alpha_{-2,\tilde{m}}T_{-2,\tilde{m}} - \alpha_{0,m}T_{0,m})} \Big\}
$$
$$
+ E\Big\{ U(f;\delta_{0,m})U^\star(f;\delta_{-1,\tilde{m}}) e^{-j\omega \overbrace{(T_{-1,\tilde{m}} + \cdots + T_{0,m-1})}^{M-(\tilde{m}-m)\ \text{terms}}} e^{j\omega(\alpha_{-1,\tilde{m}}T_{-1,\tilde{m}} - \alpha_{0,m}T_{0,m})} \Big\}
$$
$$
+ E\Big\{ U(f;\delta_{0,m})U^\star(f;\delta_{0,\tilde{m}}) e^{j\omega \overbrace{(T_{0,m} + \cdots + T_{0,\tilde{m}-1})}^{(\tilde{m}-m)\ \text{terms}}} e^{j\omega(\alpha_{0,\tilde{m}}T_{0,\tilde{m}} - \alpha_{0,m}T_{0,m})} \Big\}
$$
$$
+ E\Big\{ U(f;\delta_{0,m})U^\star(f;\delta_{1,\tilde{m}}) e^{j\omega \overbrace{(T_{0,m} + \cdots + T_{1,\tilde{m}-1})}^{M+(\tilde{m}-m)\ \text{terms}}} e^{j\omega(\alpha_{1,\tilde{m}}T_{1,\tilde{m}} - \alpha_{0,m}T_{0,m})} \Big\}
$$
$$
+ E\Big\{ U(f;\delta_{0,m})U^\star(f;\delta_{2,\tilde{m}}) e^{j\omega \overbrace{(T_{0,m} + \cdots + T_{2,\tilde{m}-1})}^{2M+(\tilde{m}-m)\ \text{terms}}} e^{j\omega(\alpha_{2,\tilde{m}}T_{2,\tilde{m}} - \alpha_{0,m}T_{0,m})} \Big\} + \cdots.
\tag{5.16}
$$

The expectation of the products may now be rewritten as a product of expectations, because the T's are independent:

$$E\{\cdot\} = E\left\{U(f;\delta_{0,m})e^{-j\omega\alpha_{0,m}T_{0,m}}\right\}$$

$$\left[\cdots + E\left\{U^\star(f;\delta_{-2,\tilde{m}})e^{-j\omega(1-\alpha_{-2,\tilde{m}})T_{-2,m}}\right\} \overbrace{E\left\{e^{-j\omega T_{-2,\tilde{m}+1}}\right\}\cdots E\left\{e^{-j\omega T_{0,m-1}}\right\}}^{2M-(\tilde{m}-m)-1 \text{ terms } (\ell=-2)}\right.$$

$$\left. + E\left\{U^\star(f;\delta_{-1,\tilde{m}})e^{-j\omega(1-\alpha_{-1,\tilde{m}})T_{-1,m}}\right\} \overbrace{E\left\{e^{-j\omega T_{-1,\tilde{m}+1}}\right\}\cdots E\left\{e^{-j\omega T_{0,m-1}}\right\}}^{M-(\tilde{m}-m)-1 \text{ terms } (\ell=-1)}\right]$$

$$+ E\left\{U(f;\delta_{0,m})e^{j\omega(1-\alpha_{0,m})T_{0,m}}\right\}$$

$$\left[\quad E\left\{U^\star(f;\delta_{0,\tilde{m}})e^{j\omega\alpha_{0,\tilde{m}}T_{0,\tilde{m}}}\right\} \overbrace{E\left\{e^{j\omega T_{0,m+1}}\right\}\cdots E\left\{e^{j\omega T_{0,\tilde{m}-1}}\right\}}^{(\tilde{m}-m)-1 \text{ terms } (\ell=0)}\right.$$

$$+ E\left\{U^\star(f;\delta_{1,\tilde{m}})e^{j\omega\alpha_{1,\tilde{m}}T_{1,\tilde{m}}}\right\} \overbrace{E\left\{e^{j\omega T_{0,m+1}}\right\}\cdots E\left\{e^{j\omega T_{1,\tilde{m}-1}}\right\}}^{M+(\tilde{m}-m)-1 \text{ terms } (\ell=1)}$$

$$\left. + E\left\{U^\star(f;\delta_{2,\tilde{m}})e^{j\omega\alpha_{2,\tilde{m}}T_{2,m}}\right\} \overbrace{E\left\{e^{j\omega T_{0,m+1}}\right\}\cdots E\left\{e^{j\omega T_{2,\tilde{m}-1}}\right\}}^{2M+(\tilde{m}-m)-1 \text{ terms } (\ell=2)} + \cdots\right].$$

$$(5.17)$$

Further simplification leads to

$$E\{\cdot\} = E\left\{U(f;\delta_m)e^{-j\omega\alpha_m T}\right\}E\left\{U^\star(f;\delta_{\tilde{m}})e^{-j\omega(1-\alpha_{\tilde{m}})T}\right\}\sum_{\ell=1}^{\infty}E\left\{e^{-j\omega T}\right\}^{M\ell-(\tilde{m}-m)-1}$$

$$+ E\left\{U(f;\delta_m)e^{j\omega(1-\alpha_m)T}\right\}E\left\{U^\star(f;\delta_{\tilde{m}})e^{j\omega\alpha_{\tilde{m}}T}\right\}\sum_{\ell=0}^{\infty}E\left\{e^{j\omega T}\right\}^{M\ell+(\tilde{m}-m)-1}$$

$$(5.18)$$

where the subscript indicating the block number has been dropped.

As for the $m = \tilde{m}$ case, the sums are converging if $|E\{\cdot\}| < 1$, and in these cases it may be shown that the two sums in (5.18) equal

$$\sum_{\ell=1}^{\infty}E\left\{e^{-j\omega T}\right\}^{M\ell-(\tilde{m}-m)-1} = \frac{E\left\{e^{-j\omega T}\right\}^{M-(\tilde{m}-m)-1}}{1 - E\left\{e^{-j\omega T}\right\}^M} \qquad (5.19)$$

and

$$\sum_{\ell=0}^{\infty}E\left\{e^{j\omega T}\right\}^{M\ell+(\tilde{m}-m)-1} = \frac{E\left\{e^{j\omega T}\right\}^{(\tilde{m}-m)-1}}{1 - E\left\{e^{j\omega T}\right\}^M}. \qquad (5.20)$$

Using the power series (5.19) and (5.20), the final result for the contribution to total

spectrum for the $m < \tilde{m}$ case becomes

$$
S_{m,\tilde{m}}(f) = \frac{1}{M\overline{T}} \left[E\Big\{ U(f;\delta_m)e^{-j\omega\alpha_m T} \Big\} E\Big\{ U^\star(f;\delta_{\tilde{m}})e^{-j\omega(1-\alpha_{\tilde{m}})T} \Big\} \frac{E\big\{ e^{-j\omega T} \big\}^{M-(\tilde{m}-m)-1}}{1 - E\big\{ e^{-j\omega T} \big\}^M} \right.
$$

$$
\left. + E\Big\{ U(f;\delta_m)e^{j\omega(1-\alpha_m)T} \Big\} E\Big\{ U^\star(f;\delta_{\tilde{m}})e^{j\omega\alpha_{\tilde{m}}T} \Big\} \frac{E\big\{ e^{j\omega T} \big\}^{(\tilde{m}-m)-1}}{1 - E\big\{ e^{j\omega T} \big\}^M} \right].
$$

$$(5.21)$$

The off-diagonal terms: m > m̃

The only difference from the $m < \tilde{m}$ case is the expansion of the $(t_{\ell,\tilde{m}} - t_{0,m})$ term for $\ell = 0$. Now $t_{0,\tilde{m}} - t_{0,m} = -(T_{0,\tilde{m}} + \cdots T_{0,m-1})$, which includes $-(\tilde{m} - m)$ number of terms. The consequence for the derivation of the sum of expectations is that the summation limits for the two occurrences of the ℓ variable in (5.18) are interchanged, i.e. the first sum is $\sum_{\ell=0}^{\infty} E\{\cdot\}$ and the second sum is $\sum_{\ell=1}^{\infty} E\{\cdot\}$. Hence, the result becomes

$$
S_{m,\tilde{m}}(f) = \frac{1}{M\overline{T}} \left[\quad E\Big\{ U(f;\delta_m)e^{-j\omega\alpha_m T} \Big\} E\Big\{ U^\star(f;\delta_{\tilde{m}})e^{-j\omega(1-\alpha_{\tilde{m}})T} \Big\} \frac{E\big\{ e^{-j\omega T} \big\}^{(\tilde{m}-m)-1}}{1 - E\big\{ e^{-j\omega T} \big\}^M} \right.
$$

$$
\left. + E\Big\{ U(f;\delta_m)e^{j\omega(1-\alpha_m)T} \Big\} E\Big\{ U^\star(f;\delta_{\tilde{m}})e^{j\omega\alpha_{\tilde{m}}T} \Big\} \frac{E\big\{ e^{j\omega T} \big\}^{(M-\tilde{m}-m)-1}}{1 - E\big\{ e^{j\omega T} \big\}^M} \right].
$$

$$(5.22)$$

5.3.3 Summary of formula for the spectrum using RCF-PWM

To recapitulate the results obtained so far, the derived equations for the spectrum $S(f)$ for the random carrier frequency (period) technique is summarized. Hence,

$$
S(f) = \sum_{m=1}^{M} \sum_{\tilde{m}=1}^{M} S_{m,\tilde{m}}(f) = \sum \begin{bmatrix} S_{1,1}(f) & S_{1,2}(f) & \cdots & \cdots & S_{1,M}(f) \\ S_{2,1}(f) & S_{2,2}(f) & \cdots & \cdots & S_{2,M}(f) \\ \vdots & \vdots & \ddots & & \\ \vdots & \vdots & & \ddots & \\ S_{M,1}(f) & S_{M,2}(f) & & & S_{M,M}(f) \end{bmatrix}, \quad (5.23)
$$

where the individual entries are calculated by one of the following three equations depending on the values of m and $\tilde{m}$.

The diagonal terms (m = m̃)

$$
S_{m,\tilde{m}}(f) = \frac{1}{M\overline{T}}\Bigg[E\big\{|U(f;\delta_m)|^2\big\}
$$

$$
+ 2\,\mathcal{R}\Bigg(E\big\{U(f;\delta_m)e^{j\omega(1-\alpha_m)T}\big\} E\big\{U^\star(f;\delta_{\tilde{m}})e^{j\omega\alpha_{\tilde{m}}T}\big\}\frac{E\big\{e^{j\omega T}\big\}^{M-1}}{1-E\big\{e^{j\omega T}\big\}^M}\Bigg)\Bigg]. \quad (5.24)
$$

The off-diagonal terms (m < m̃)

$$
S_{m,\tilde{m}}(f) = \frac{1}{M\overline{T}}\Bigg[E\big\{U(f;\delta_m)e^{-j\omega\alpha_m T}\big\} E\big\{U^\star(f;\delta_{\tilde{m}})e^{-j\omega(1-\alpha_{\tilde{m}})T}\big\}\frac{E\big\{e^{-j\omega T}\big\}^{M-(\tilde{m}-m)-1}}{1-E\big\{e^{-j\omega T}\big\}^M}
$$

$$
+ E\big\{U(f;\delta_m)e^{j\omega(1-\alpha_m)T}\big\} E\big\{U^\star(f;\delta_{\tilde{m}})e^{j\omega\alpha_{\tilde{m}}T}\big\}\frac{E\big\{e^{j\omega T}\big\}^{(\tilde{m}-m)-1}}{1-E\big\{e^{j\omega T}\big\}^M}\Bigg].
$$

$$
(5.25)
$$

The off-diagonal terms (m > m̃)

$$
S_{m,\tilde{m}}(f) = \frac{1}{M\overline{T}}\Bigg[E\big\{U(f;\delta_m)e^{-j\omega\alpha_m T}\big\} E\big\{U^\star(f;\delta_{\tilde{m}})e^{-j\omega(1-\alpha_{\tilde{m}})T}\big\}\frac{E\big\{e^{-j\omega T}\big\}^{(\tilde{m}-m)-1}}{1-E\big\{e^{-j\omega T}\big\}^M}
$$

$$
+ E\big\{U(f;\delta_m)e^{j\omega(1-\alpha_m)T}\big\} E\big\{U^\star(f;\delta_{\tilde{m}})e^{j\omega\alpha_{\tilde{m}}T}\big\}\frac{E\big\{e^{j\omega T}\big\}^{(M-\tilde{m}-m)-1}}{1-E\big\{e^{j\omega T}\big\}^M}\Bigg].
$$

$$
(5.26)
$$

Hence, for a certain frequency f, evaluation of M^2 partial contributions is needed in order to get the total density spectrum $S(f)$ at this particular frequency.

5.4 Spectral analysis of switching functions

In the present and in the next two sections, examples are given of how the developed set of formulas may be used to get numerical values for the spectra of different voltages when RCF-PWM is to control modulate a three-phase converter. Formulas are derived for the following three voltages of interest in a voltage-source converter as shown in Fig. 5.4:

1. the output-to-negative-rail voltage (switching function for one leg),

2. the line-to-line output voltage (section 5.5 starting on page 137), and

3. the phase-to-neutral voltage for symmetric loads (section 5.6 starting on page 147).
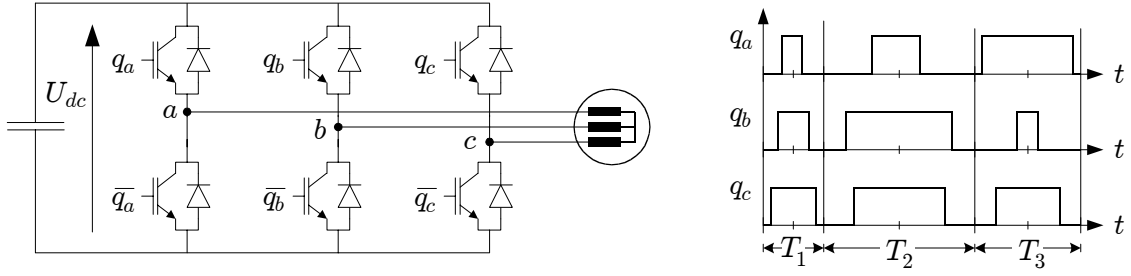
Figure 5.4 Three-phase voltage-source converter and examples of switching functions for random carrier frequency (period) modulation using center-aligned pulses in each carrier period.

To support the validity of the theoretical calculations, all spectra analyses are compared to measurements on the experimental set-up described in greater details in Appendix A. In accordance with the conclusions of section 5.2.2, a discrete type of probability density function (pdf) is used for the randomization of the carrier periods. Also, to illustrate the generality of the spectral theory, different zero-sequence injection methods are used for the verifications.

5.4.1   Spectrum for the switching function

The procedure to calculate the power spectral density (PSD) is a stepwise evaluation of (5.23) by finding all the expectations in the supporting equations (5.24)–(5.26). All expectations must be taken with respect to the carrier period T, i.e.

$$E\{g(T)\} = \int_{-\infty}^{+\infty} p(T)g(T)\,dT, \tag{5.27}$$

where $g(T)$ is an arbitrary function of T.

   For the particular case studied here, the probability density function $p(T)$ for the carrier period shown in Fig. 5.1(b) on page 109 is formulated as

$$p(T) = \sum_{j=1}^{J} p_j\,\delta(T - T_j), \tag{5.28}$$

where J is the pool size and p_j is the weight assigned to the j'th interval T_j. The δ-functions in (5.28) simplify the integration in (5.27) to

$$E\{g(T)\} = \sum_{j=1}^{J} p_j g(T_j), \tag{5.29}$$

which implies that integration is replaced with a much simpler operation, namely summation. This property was already used in Chapter 4 for the evaluation of the lead-lag random pulse-position modulation.
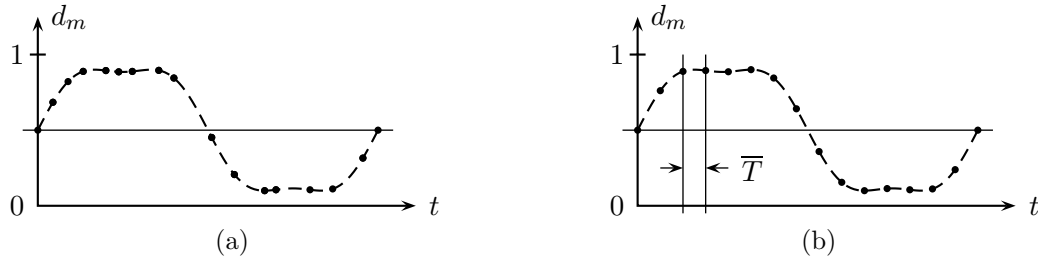
Figure 5.5 Examples of (a) actual random carrier period sampling and (b) equidistant sampling to get M values for the average duty ratio within one period of the fundamental output voltage.

Assignment of average duty ratios

At this point, the concept of average duty ratios introduced in Chapter 3 must be kept in mind, because the derivations in section 5.3 rely on this also: in order to make the analysis feasible, it is assumed that the modulation function governing the deterministic operation of the (randomized) modulator is sampled on an equidistant time grid as illustrated in Fig. 5.5.

The average time distance $\overline{T}$ between the samples is determined as

$$\overline{T} = E\{T\} = \sum_{j=1}^{J} p_j T_j, \tag{5.30}$$

and, furthermore, the number of carrier periods is set as $M = \lfloor 1/(f_1 \overline{T}) \rfloor$, where f_1 is the fundamental frequency of the modulated voltage. (The rounding $\lfloor \cdot \rfloor$ operation is needed since there is no guarantee that $1/(f_1 \overline{T})$ is an integer.)

The average duty ratio d_m in the m'th period is found by equidistant sampling of the reference waveforms produced by the modulator. Several commonly used modulators have been discussed in Chapter 2, and a major advantage of the developed spectral theory is that no constraints are imposed on how the duty ratios are produced; the theory is applicable to arbitrary modulators, and not to only purely sinusoidal modulation like the theory in [32]. In this way, an array of duty ratios d_m is obtained, and by setting $\alpha_m = \frac{1}{2}(1 - d_m)$, the pulses become center-aligned within each carrier period.

5.4.2 Equations for partial spectra

In this case the sampling pulse $u(t; \delta_m)$ is defined as

$$u(t; \delta_m) = \begin{cases} 1, & 0 \le t \le d_m T, \\ 0, & \text{otherwise.} \end{cases} \tag{5.31}$$

and the Fourier transformation $U(f; \delta_m)$ becomes

$$U(f; \delta_m) = \mathcal{F}(u(t; \delta_m)) = \int_0^{d_m T} e^{-j\omega t}\, dt = \frac{1}{j\omega}\left(1 - e^{-j\omega d_m T}\right), \qquad \omega = 2\pi f. \tag{5.32}$$

The diagonal terms (m = m̃)

Below follows a list of the expectations needed to find the diagonal terms in (5.24): Using (5.32) together with (5.29), it may be shown by straightforward algebra that

$$E\big\{|U(f;\delta_m)|^2\big\} = \sum_{j=1}^{J} p_j \frac{\sin^2\left(\pi f d_m T_j\right)}{(\pi f)^2}, \tag{5.33}$$

$$E\Big\{U(f;\delta_m)e^{j\omega(1-\alpha_m)T}\Big\} = \sum_{j=1}^{J} p_j \frac{1}{j\omega}\left(1 - e^{-j\omega d_m T_j}\right) e^{j\omega(1-\alpha_m)T_j}, \tag{5.34}$$

$$E\Big\{U^\star(f;\delta_{\tilde{m}})e^{j\omega\alpha_{\tilde{m}}T}\Big\} = \sum_{j=1}^{J} p_j \frac{1}{j\omega}\left(e^{j\omega d_{\tilde{m}} T_j} - 1\right) e^{j\omega\alpha_{\tilde{m}}T_j}, \tag{5.35}$$

$$E\big\{e^{j\omega T}\big\} = \sum_{j=1}^{J} p_j\, e^{j\omega T_j}. \tag{5.36}$$

The off-diagonal terms (m ≠ m̃)

The partial spectra for the $m \neq \tilde{m}$ case is found by using (5.34)–(5.36) besides the two equations below:

$$E\Big\{U(f;\delta_m)e^{-j\omega\alpha_m T}\Big\} = \sum_{j=1}^{J} p_j \frac{1}{j\omega}\left(1 - e^{-j\omega d_m T_j}\right) e^{-j\omega\alpha_m T_j} \tag{5.37}$$

$$E\Big\{U^\star(f;\delta_{\tilde{m}})e^{-j\omega(1-\alpha_{\tilde{m}})T}\Big\} = \sum_{j=1}^{J} p_j \frac{1}{j\omega}\left(e^{j\omega d_{\tilde{m}} T_j} - 1\right) e^{-j\omega(1-\alpha_{\tilde{m}})T_j}. \tag{5.38}$$

These equations are then inserted into (5.25) and (5.26) for $m < \tilde{m}$ and $m > \tilde{m}$, respectively, which allows numerical results to be obtained by assigning values to the parameters in the derived expressions.

5.4.3 Modulator settings and laboratory set-up

All results are compared to laboratory measurements by using the set-up shown in Fig. 5.6 to acquire measurements of spectra. The set-up is described in more details in Appendix A, but in brief, a standard frequency converter rated at 4 kVA is used as a power amplifier. The converter consists of a diode-bridge front-end feeding power into a dc-link capacitor through a smoothing inductor; the inversion stage is a standard three-phase VSC of the kind shown in Fig. 5.4 using six-pack IGBT power module. The converter is loaded by a 1.5 kW 2-pole induction motor running at light load.

Modulator settings

The evaluation of the spectral analysis theory is based on the settings listed in Table 5.2. It may be noted that three well-known deterministic modulation techniques are subjected to randomization. In all cases, a simple V/Hz controller that ensures
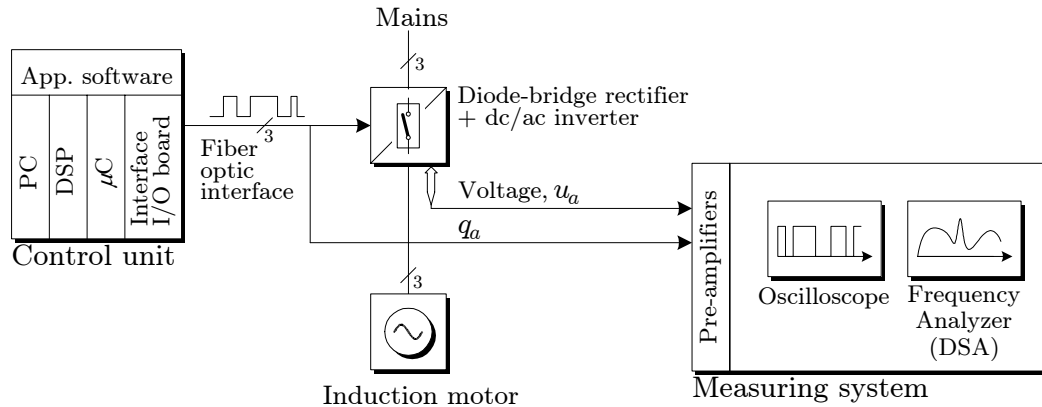
Figure 5.6 Set-up used to test RCF-PWM schemes for three-phase converters. Appendix A contains more information on the set-up and on the used instrumentation.

rated magnetizing current in steady state is used. The voltage controller is not operating entirely in open-loop: the dc-link voltage is fed back and also, a simple blanking time compensation based on [33] is implemented using phase current feedback.

Using the pool of discrete frequencies f_j listed in Table 5.2, the probability density function for T is set as $p(T) = \sum_{j=1}^{J} p_j \, \delta(T - 1/f_j)$, where $p_j = 1/J$ for all j. This is as crude approximations to a uniform distribution in the $[2; 4]$ kHz range.

Example of current waveforms

To demonstrate the time-domain characteristics of the system, sample waveforms of the phase currents are provided in Fig. 5.7 (page 128. All plots are valid for a 5 Hz fundamental frequency, and for reasons of comparison, the results obtained for $J = 5$ are compared to results obtained for fixed carrier frequency of 3 kHz. Regarding the operation on the macroscopic time scale, the randomized modulator produces results very similar to the deterministic modulator, because no discernible difference exists between the fundamental component of the current.

Notation

The spectrum for the switching function q_a is measured on both 5 V logic level and at power level (output terminal to negative dc-link rail) as indicated in Fig. 5.6. Like in Chapter 4, the following notation is used to separate different spectra:

$S_a(f)$ The theoretically expected spectrum for the switching function q_a. $S_a(f)$ has only a density part, i.e. no harmonic component can be predicted by the theory.

$\hat{S}_a(f)$ The measured density spectrum of the switching function. The spectra are scaled in PSD units, see further in section 3.3.2.

$\hat{S}_a^p(f)$ The density spectrum (PSD scaling) measured by feeding the differential voltage between phase a and the negative dc-rail to the DSA.

Note that no equivalent density spectrum is used in this chapter, because of (a) the theory does not predict the existence of any harmonic components and (b) the resolution bandwidth of the DSA is sufficiently small. 0 dB corresponds to 1 volt^2/Hz.

Type of modulator	Fundamental frequency	Carrier frequencies (kHz)
SIN: sinusoidal	Low: $f_1 = 5$ Hz	$J = 5$: $f_j = \{2, 2.5, 3, 3.5, 4.0\}$
SVM: space-vector	High: $f_1 = 40$ Hz	$J = 3$: $f_j = \{2, 3, 4\}$
DPWM: discontinuous[1]		

Table 5.2 Used settings of modulators for examining the spectral theory for random carrier frequency modulation. [1]The Depenbrock clamping scheme, see further in Chapter 2.

5.4.4 Comparison of calculated and measured spectra

Examples using pool size of five carrier frequencies

The results are shown in Figs. 5.8–5.10 (pages 129–131) for the different modulators and fundamental frequencies. A somewhat surprising observation is that the difference between $\hat{S}_a(f)$ and $\hat{S}_a^p(f)$ is very small — at least for the density part of the spectrum. In other words, the net effect of converter non-linearities on the spectrum is less pronounced than for the dc/dc converter studied in Chapter 4. The main reason is that the voltage error caused by blanking time etc. is divided among all phases, which prevents accumulation of errors on one leg only as for the dc/dc converter. Also, the figures show that SIN and SVM cause similar looking continuous spectra whereas the DPWM modulator deviates from the others, especially for the low fundamental frequency.

Regarding the comparison of calculated and measured continuous power spectral densities, the plots reveal excellent agreements for all examined modulators and operating points — in particular for frequencies greater than some threshold (0.2–1.0 kHz depending on the modulator and fundamental frequency). In the low-frequency range, harmonic (volt^2) components related to the modulation waveform appear at multiples of the fundamental frequency, but in its current form, the theory is incapable of calculating these components. A further discussion of this topic follows in section 5.4.5.

Examples using pool size of three carrier frequencies

On pages 132–134, Figs. 5.11–5.13 show calculated and measured spectra for the case that only uses three different carrier frequencies. It is evident that the spectra are considerably less smooth than for $J = 5$; several local minima and maxima exist.

Again, the overall agreement is very good, which supports the developed theory. However, it must be noted that the measured spectra are no longer purely continuous. The plots show harmonics around 12 kHz and 24 kHz (this is best seen for the $f_1 = 40$ Hz examples). To provide more information, Fig. 5.14(a, b, c) on page 135 shows details around 12 kHz for the SVM modulator (SIN and DPWM have similar characteristics). Here, a resolution of $\Delta f = 2$ Hz is used for both measured and calculated spectra. It appears from Fig. 5.14(a) that the calculated spectrum $S_a(f)$ includes the harmonics, but this interpretation is unfortunately wrong. What appears to be harmonics around 12 kHz is in fact part of the continuous spectrum, i.e. the peaks in Fig. 5.14(a) are just local peaks of density rather than harmonics. The analysis fails to predict the harmonics and also the calculated peaks of density are incorrect.
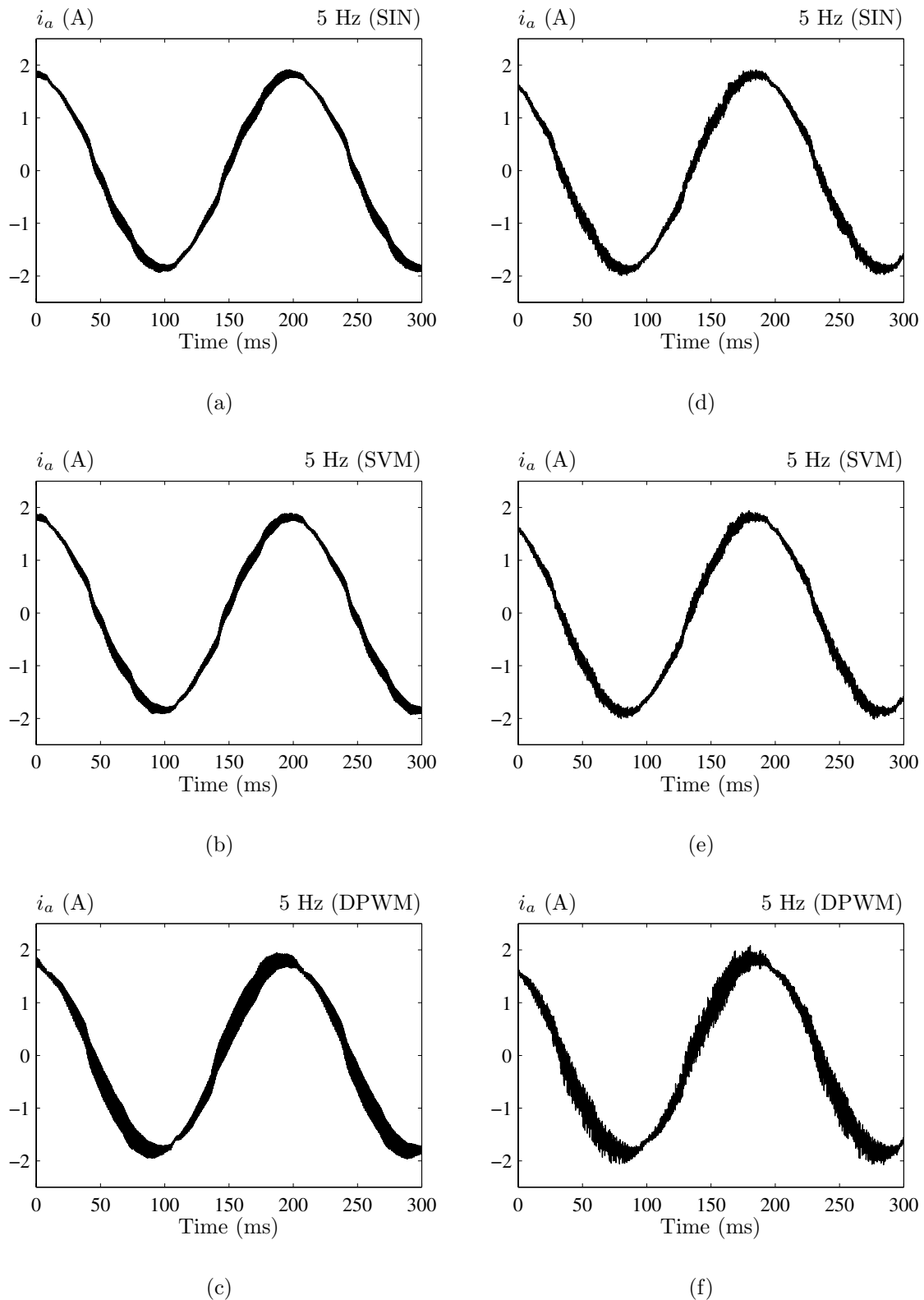
Figure 5.7 Phase current measurements for 5 Hz fundamental frequency using sinusoidal, space-vector, and discontinuous modulation. Blanking time compensation was enabled. (left column): Fixed 3 kHz and (right column): RCF modulation using the settings for $J = 5$.
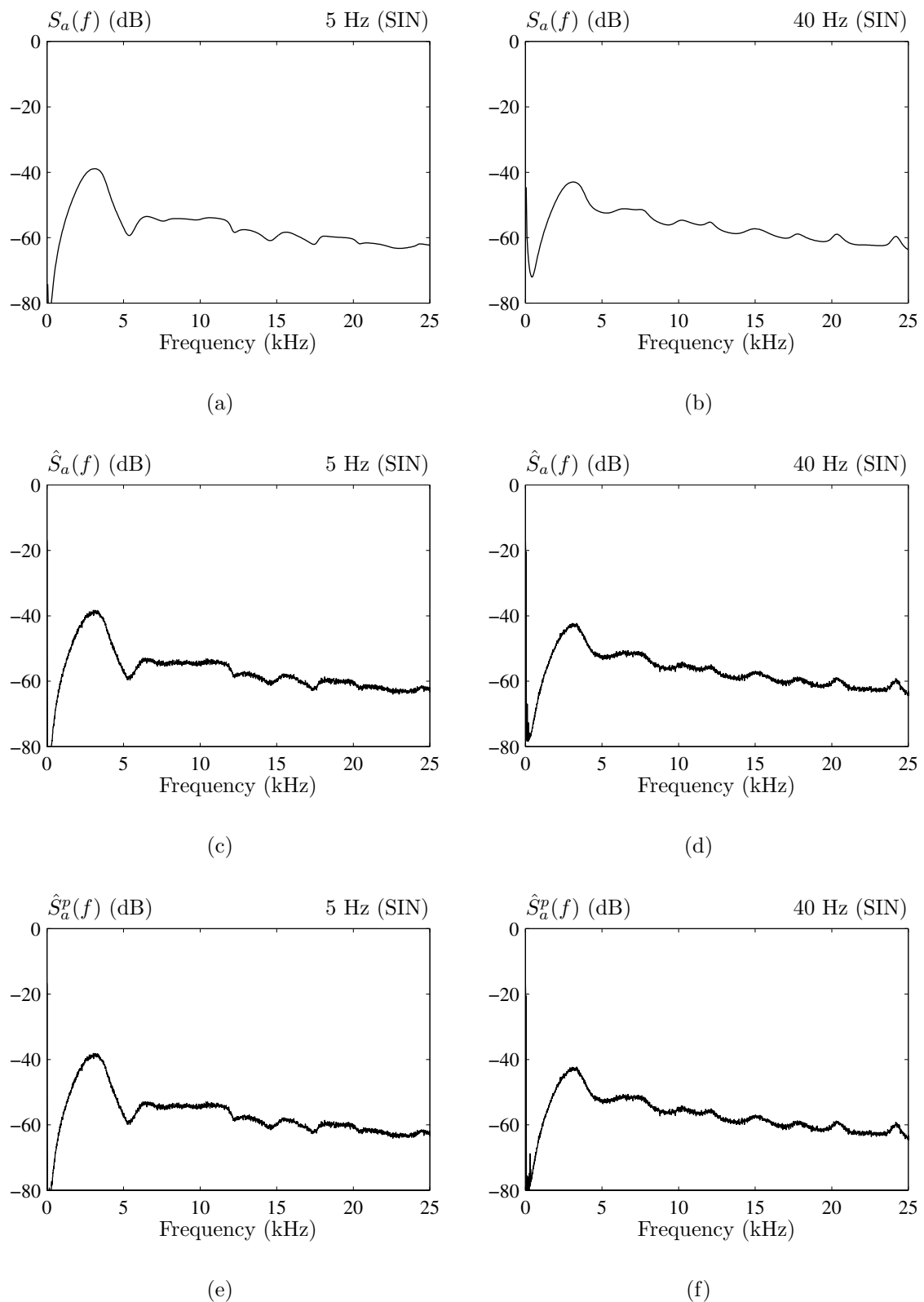
Figure 5.8 Spectra for the switching function using sinusoidal modulation, pool size $J = 5$, and fundamental frequency 5 Hz (left column) and 40 Hz (right column). (a, b) Calculated density spectra, (c, d) measured spectrum (logic level), and (e, f) measured spectrum (power level).

(a)   (b)

(c)   (d)

(e)   (f)
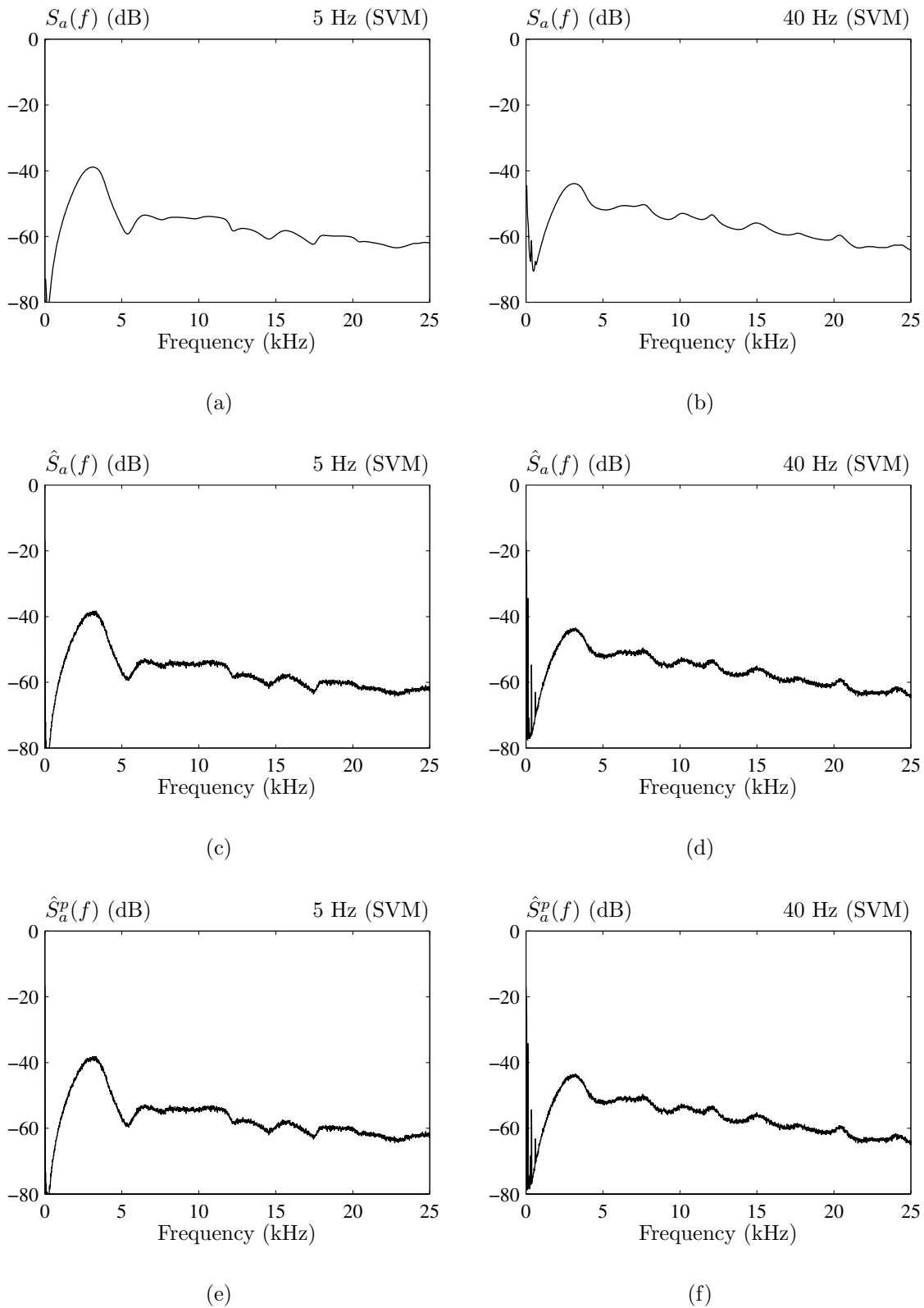
Figure 5.9 Spectra for the switching function using space-vector modulation, pool size $J = 5$, and fundamental frequency 5 Hz (left column) and 40 Hz (right column). (a, b) Calculated density spectra, (c, d) measured spectrum (logic level), and (e, f) measured spectrum (power level).
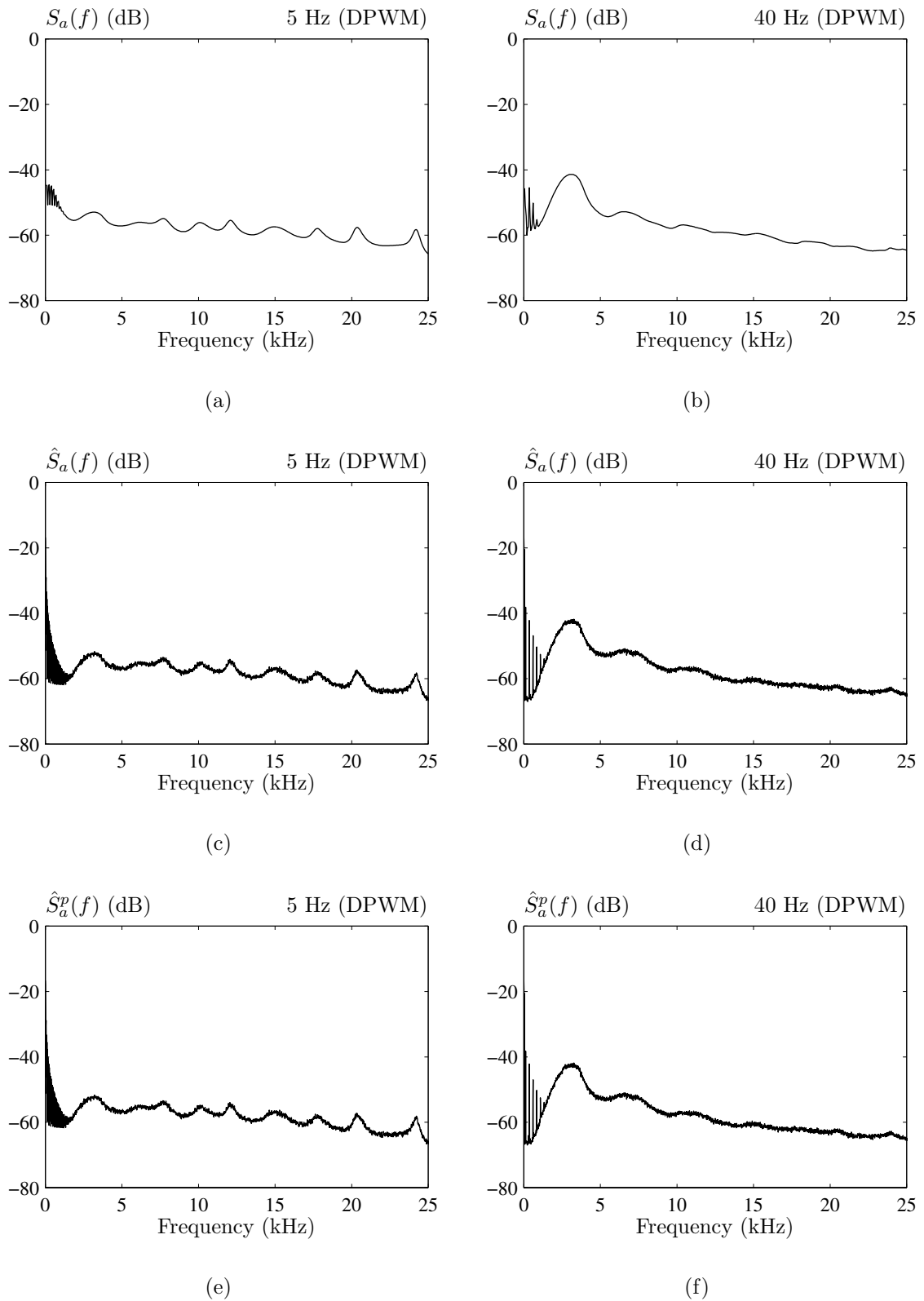
Figure 5.10 Spectra for the switching function using discontinuous modulation, pool size $J = 5$, and fundamental frequency 5 Hz (left column) and 40 Hz (right column). (a, b) Calculated density spectra, (c, d) measured spectrum (logic level), and (e, f) measured spectrum (power level).
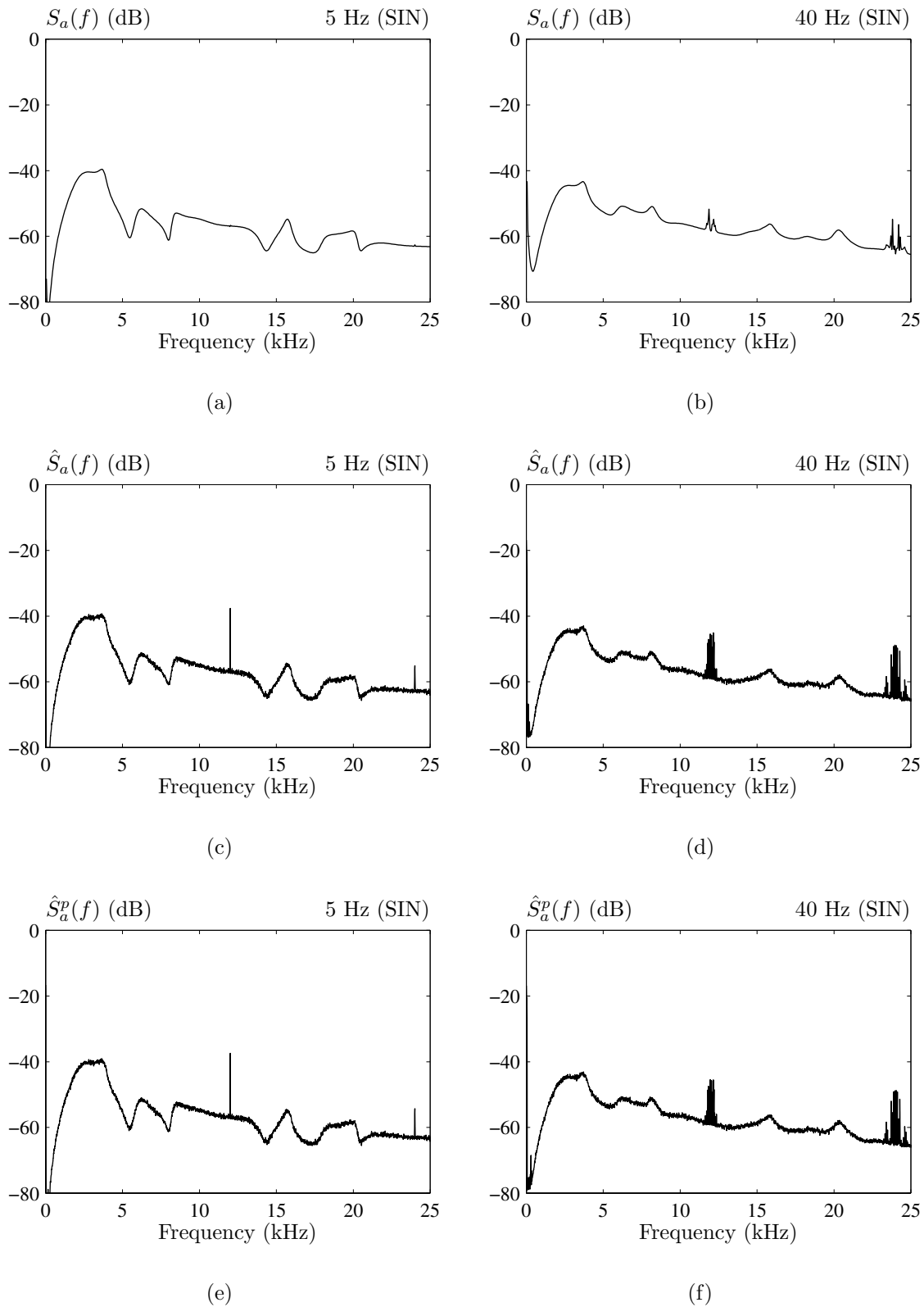
Figure 5.11 Spectra for the switching function using sinusoidal modulation, pool size $J = 3$, and fundamental frequency 5 Hz (left column) and 40 Hz (right column). (a, b) Calculated density spectra, (c, d) measured spectrum (logic level), and (e, f) measured spectrum (power level).
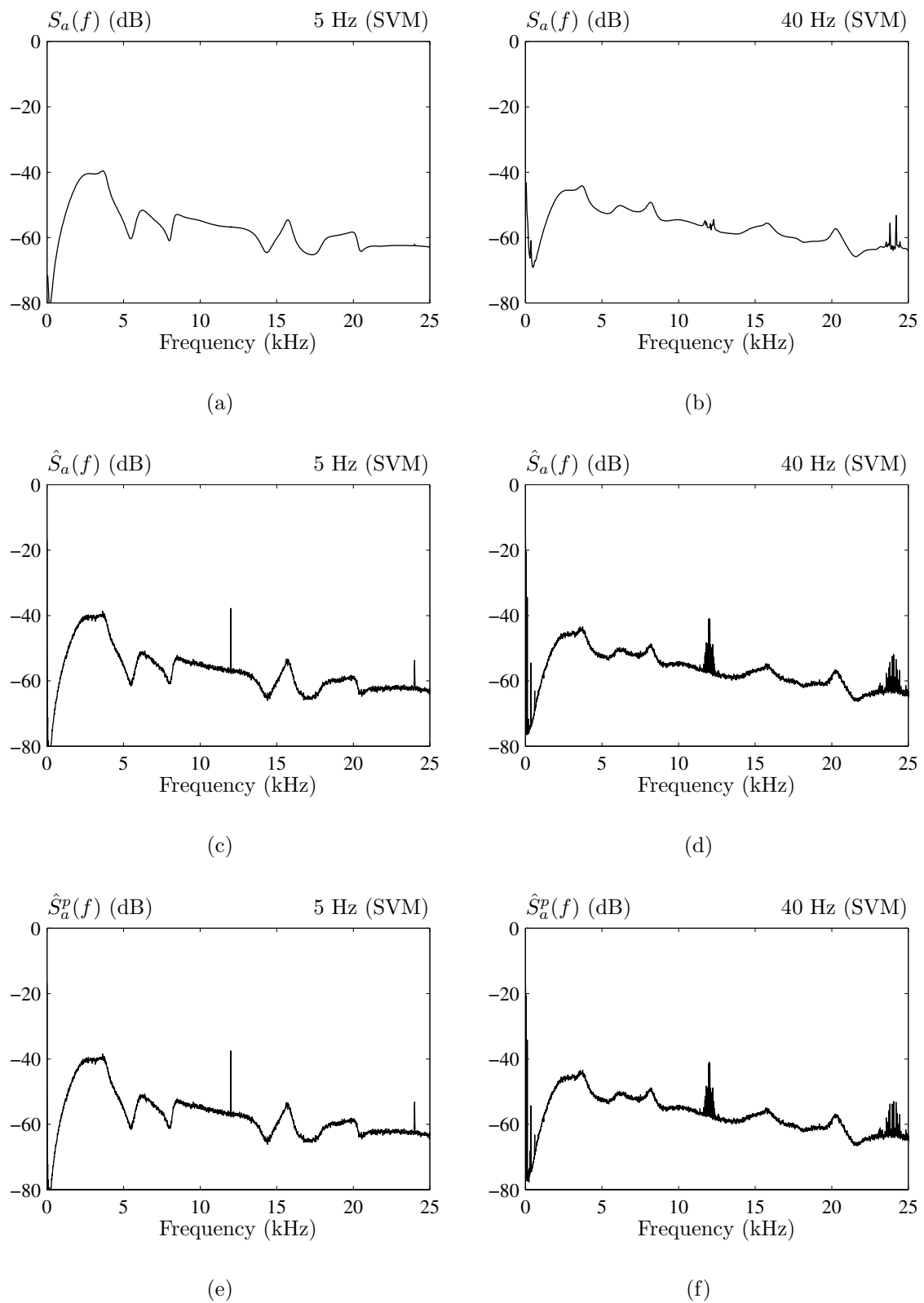
Figure 5.12 Spectra for the switching function using space-vector modulation, pool size $J = 3$, and fundamental frequency 5 Hz (left column) and 40 Hz (right column). (a, b) Calculated density spectra, (c, d) measured spectrum (logic level), and (e, f) measured spectrum (power level).
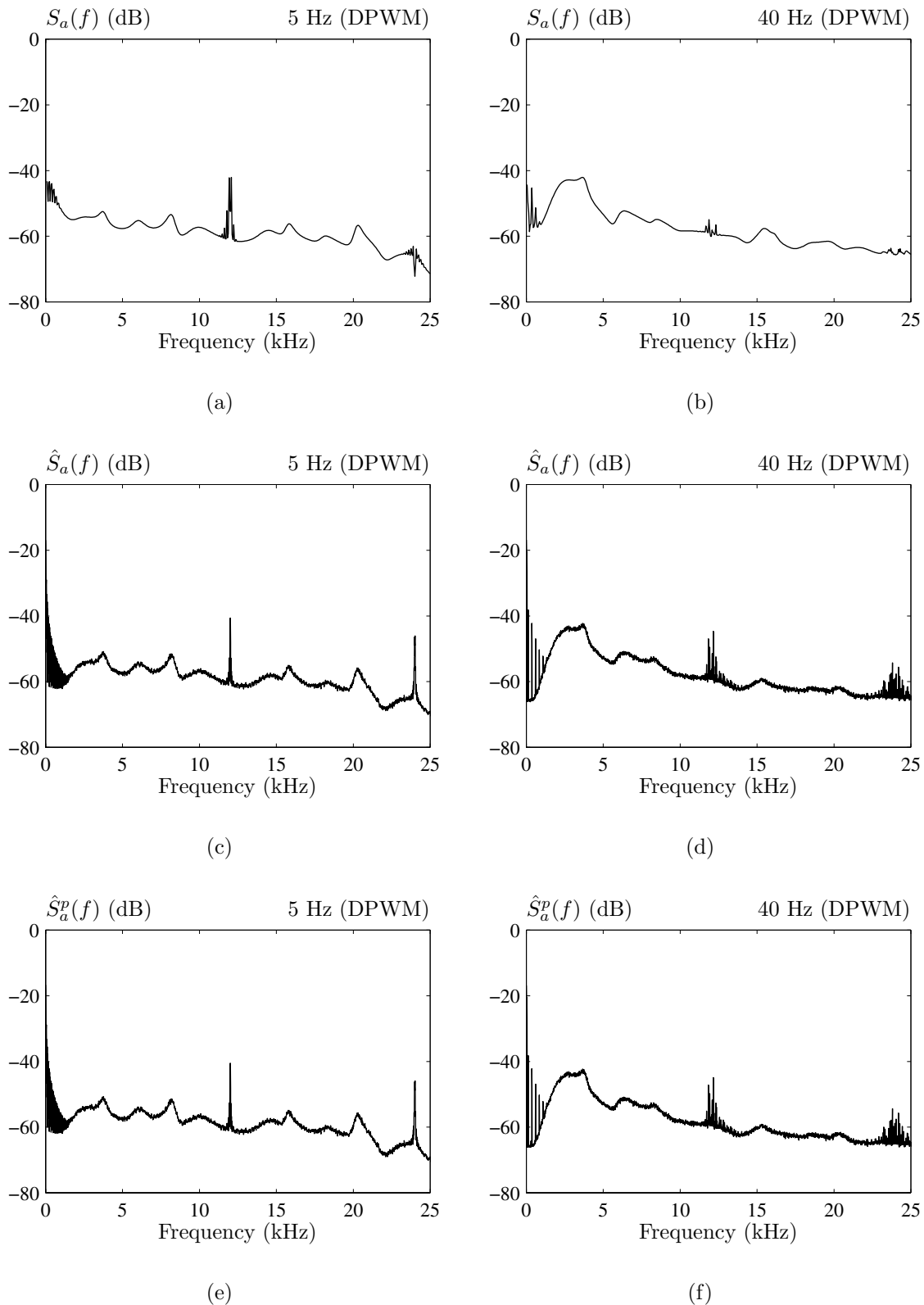
Figure 5.13 Spectra for the switching function using discontinuous modulation, pool size $J = 3$, and fundamental frequency 5 Hz (left column) and 40 Hz (right column). (a, b) Calculated density spectra, (c, d) measured spectrum (logic level), and (e, f) measured spectrum (power level).
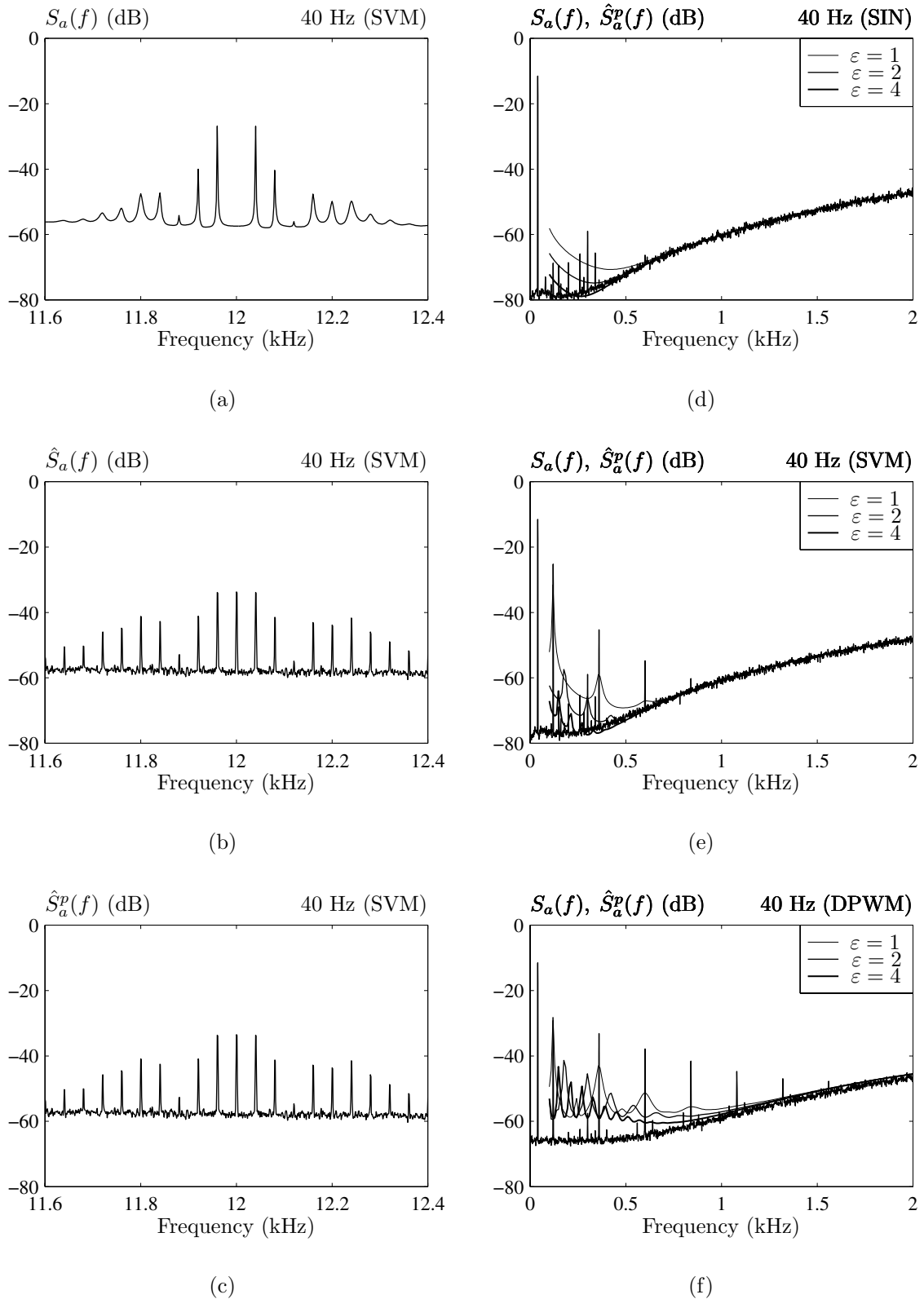
Figure 5.14 Details for the switching function using pool size $J = 3$ and a 40 Hz fundamental. (Left column) zoom around 12 kHz: (a) calculated, (b) estimated at logic level, and (c) estimated at power level. (Right column) below 2 kHz showing the effect of over-sampling rates for (d) sinusoidal, (e) space-vector, and (f) discontinuous PWM.

5.4.5   Discussion of results

From the examples shown in Figs. 5.8–5.14 the following conclusions regarding the developed spectral theory for dc/ac RCF-PWM may be drawn:

- The analysis accurately predicts the continuous density part of the real spectrum irrespective of the modulation method (sinusoidal, space-vector, discontinuous PWM, etc.) and operating conditions (fundamental frequency and modulation index). (The accuracy in the low-frequency range is elaborated below.)

- Measurements show that harmonics may appear in the actual spectrum, but not necessarily always (disregarding the fundamental component and related low-order harmonics caused by added zero-sequence components).

- If the true spectrum contains discrete frequency components, the predicted results for the continuous part of the spectrum around those frequencies become less accurate. This may also be stated as if the true harmonics are leaked into the predicted continuous part of the spectrum, though.

Additional comments are given below.

The low-frequency range

Regarding the low-frequency range, Fig. 5.14(d, e, and f) shows details for the $J = 3$ case using $f_1 = 40$ Hz. The harmonics caused by the zero-sequence components added in the SVM and DPWM modulators may be identified. The amplitude of these harmonics cannot be calculated using the developed theory, but of more concern is that the calculated density spectrum starts to deviate considerably from $\hat{S}_a^p(f)$ for low frequencies. The error becomes large for $f < 0.5$ kHz (SIN), $f < 0.6$ kHz (SVM), and $f < 1.0$ kHz (DPWM).

The cause of the error is that the spectral analysis is based on an assumption which is actually violated heavily by the RCF scheme: The reference waveform for the duty ratios are sampled at equidistant time instants in order to get the needed precalculated duty ratio. Hence, the duty ratios are considered to be known, constant parameters, but in reality they are random variables in the dc/ac RCF family of randomization schemes. An in-depth discussion of the mathematical details pertinent to this problem may be found in [25, 34].

A partial fix to this discrepancy may be obtained by a somewhat heuristic approach. Instead of setting the number of carrier periods M per fundamental cycle as $M = \lfloor 1/(f_1 \overline{T}) \rfloor$ as initially done on page 124, an over-sampling factor is introduced, i.e. $M' = \varepsilon M$. Hereby, the number of samples of the duty ratio reference waveform is increased by a factor of ε. Setting $\varepsilon = \{1, 2, 4\}$ gives the results reported in Fig. 5.14(d, e, and f). It may be seen that $\varepsilon > 1$ extends the frequency range downwards in which the predicted density equals the actual density. However, the problems due to harmonics do still exist making this over-sampling approach less effective for the DPWM method (which is rich on low-order harmonics) than for the SVM and SIN modulators.

High-frequency harmonics

In its current form, the theory is incapable of predicting whether harmonic components exist or not. It may be noted, however, that the $J = 5$ case does not produce harmonics whereas the $J = 3$ case does, but the correlation between the pool size J, the set of carriers $\{f_j\}$, and the harmonics is unknown. Fortunately, this difficult problem has been analyzed in [24] (summarized in [25, 34]) with the following conclusion:

> Harmonics may occur at all frequencies satisfying $f = Lf_{\text{LCM}} \pm nf_1$, where $L = 0, 1, 2, \cdots$, and $n = 0, 1, 2, \cdots$, . f_1 is the frequency of the fundamental voltage component and f_{LCM} is the least common multiple for the carrier frequencies $\{f_j\}$ in the pool.

To illustrate, consider the result in Fig. 5.14 obtained for $J = 3$, $f_j = \{2, 3, 4\}$ kHz, and $f_1 = 40$ Hz. For these values, $f_{\text{LCM}} = 12$ kHz, which perfectly agrees with the side bands around 12 kHz spaced 40 Hz apart. Also, the harmonics around 24 kHz seen in Figs. 5.11–5.13 comply with the theory of [24]. For the case with $J = 5$ and $f_j = \{2, 2.5, 3, 3.5, 4\}$ kHz, the least common multiple is $f_{\text{LCM}} = 420$ kHz. This explains why no harmonics appear in Figs. 5.8–5.10.

The power carried by the harmonics at $f = Lf_{\text{LCM}} \pm nf_1$ is analyzed in [34]. It turns out that the power can be analytically calculated for all harmonics, including the low frequencies ($L = 0$) and the harmonics around multiples of f_{LCM}. This analysis is quite involved, but a series of measurements reported in [34] fully verifies this theory.

At this point it may be recalled that the main objective of replacing normal PWM with random PWM is to attenuate the power carried by harmonics as much as possible. Hence, it may be argued that the analysis of harmonics in [34] is superfluous once the mechanism governing the existence of harmonics is known. Although this statement carries some truth, a unified spectral theory of the RCF dc/ac scheme must, nevertheless, pay attention to harmonics also.

Main conclusions

The main conclusion of the spectral analysis of the RCF scheme is that the developed expressions predict the continuous power spectral density spectrum very well. The disagreements associated with the harmonics are considered to be tolerable, because practical applications of the RCF-PWM should always seek to avoid generation of harmonics, since this was the purpose of using random PWM in the first place.

Also, since the criteria for the existence of harmonics are quite simple, it is straightforward to select the pool of carrier frequencies so that no harmonics are generated at all, except for the low-order components related to the modulation method.

5.5 Spectral analysis of the line-to-line voltage

Having proved that the developed mathematical model is capable of predicting the spectrum for the switching function that controls one leg of a three-phase VSC, the task of calculating the spectrum for the line-to-line voltage u_{ab} is examined in this section. u_{ab} is the voltage fed to the load, i.e. for analysis of phenomena related to the load, the driving voltages equal the set of line-to-line voltages.

A preliminary discussion of a closely related topic has been given in Chapter 4 in connection with the output voltage generated by a full-bridge dc/dc converter, and in the current section, it is shown how to extend the analysis to three-phase converters.

It turns out that the analysis of the spectrum for u_{ab} may be attacked in at least three different ways — this is elaborated in the first two subsections below, which include a review of previous work besides an outline of a new procedure to find the density spectrum in question. The remaining part of this section presents the necessary algebraic expressions and in the end, measurement results are compared to the spectra obtained by the developed theory for a series of examples.

5.5.1 Preliminaries and review of previous work

First of all, a precise definition of the waveform to be analyzed is needed. The signal of interest is the line-to-line voltage and by referring to Fig. 5.4 (page 123), it is seen that the voltage u_{ab} between output terminals a and b is

$$u_{ab} = (q_a - q_b)U_{dc} \triangleq q_{ab}U_{dc} \tag{5.39}$$

at any time instant for an ideal converter. To avoid many U_{dc} factors in the following equations, the normalized voltage defined by q_{ab} in (5.39) is preferred to u_{ab}. This may be done without any loss of generality.

Comments on previous work

In the literature, the problem of finding the spectrum for q_{ab} using dc/ac random PWM schemes has been attacked by two groups of authors: Kirlin et al. [35, 36] and Stanković et al. [4, 5], respectively. In all these references, it is assumed that the switching functions for the three legs are mutually displaced in time by one third of the fundamental period, i.e. $q_b(t) = q_a(t - \frac{1}{3}T_1)$, where T_1 is the period of the fundamental voltage. Using that idea, the spectrum $S_{ab}(f)$ for q_{ab} may be found using a fundamental theorem of linear time-invariant systems, which relates the output $S_{ab}(f)$ to the input $S_a(f)$ by the system transfer function $H(f)$ [37, 38]

$$S_{ab}(f) = S_a(f)|H(f)|^2, \tag{5.40}$$

where $|H(f)|^2$ is the power transfer function of the system. Specifically, by Fourier transformation of $q_{ab}(t) = q_a(t) - q_b(t) = q_a(t) - q_a(t - \frac{1}{3}T_1)$, the frequency-domain transfer function from q_a to q_{ab} becomes

$$H(f) = 1 - e^{-j\frac{2}{3}\pi f T_1}. \tag{5.41}$$

Inserting this result into (5.40) yields

$$S_{ab}(f) = S_a(f)\left|1 - e^{-j\frac{2}{3}\pi f T_1}\right|^2 = 2S_a(f)\left(1 - \cos\left(\tfrac{2}{3}\pi f T_1\right)\right). \tag{5.42}$$

Hence, the spectrum $S_{ab}(f)$ for q_{ab} may be calculated quite easily, once $S_a(f)$ has been obtained. This is the method used in the cited references.

To gain further insight into the consequences of the $q_b(t) = q_a(t - \frac{1}{3}T_1)$ assumption, the following comments apply, where the fundamental frequency defined by $f_1 = 1/T_1$ has been introduced:

1. The spectrum does not contain $3nf_1$ components (n: any integer)

This follows directly from (5.42), because for $f = 3nf_1$ the $(1 - \cos(\frac{2}{3}\pi f T_1))$ term equals zero. This behavior is well known for dc/ac PWM techniques using a constant carrier frequency, where zero-sequence components in the switching function cancel each other in the line-to-line voltage.

2. Constraints on the carrier frequency

The requirement $q_b(t) = q_a(t - \frac{1}{3}T_1)$ imposes constraints on the allowable randomization of the carrier frequency among the three legs. Two sub-cases exist:

A. Synchronized control of the converter legs

If it is required that all legs of the converter must be synchronized, the duration of all carrier periods must be identical in order to fulfill $q_b(t) = q_a(t - \frac{1}{3}T_1)$. Hence, the randomness of the modulator is ruined, because of the constant carrier frequency operation.

B. Asynchronous control of the converter legs

If q_b must be a time-delayed copy of q_a and the carrier frequency for leg a is randomized, then the instantaneous carrier frequencies for leg a and leg b must be different. Currently, such asynchronous operation does not have any practical relevance.

A discussion of related topics may be found in section 2.4.2 starting on page 32.

It is apparent from the above comments that the assumption $q_b(t) = q_a(t - \frac{1}{3}T_1)$ is hardly ever met in practical applications of the RCF technique, because it is required that the instantaneous carrier frequency must be different from one leg to another leg. Stated in other words, the generalization from classic PWM to random PWM may be in order for the periodic (and hence, deterministic) part of the switching functions, but it is impossible to include the random part of the modulator within the assumption of the mutual phase displacement.

At this point, it may be asked what happens if (5.42) is used to approximate $S_{ab}(f)$ for the RCF scheme used in practice (synchronized, but randomly varying carrier frequencies). Obviously, if the error is small, the assumption on which (5.42) is derived, becomes insignificant. To clarify this question, the plots shown in Fig. 5.15 may be considered. Here, the measured spectrum for $\hat{S}_{ab}^p(f)$ is compared to the approximation (5.42) using RCF-PWM, space-vector modulation, and a fundamental frequency $f_1 = 40$ Hz. It is evident from the plots in Fig. 5.15(a, c) that the envelope curve for the predicted spectrum does not match the real spectrum at all. The more detailed view in Fig. 5.15(b) clearly shows the oscillatory course for the predicted spectrum caused by the cosinusoidal term in (5.42), which forces the spectrum to $-\infty$ dB for $f = 3nf_1$.

Similar oscillations may be observed in [35], which analyzes a random pulse-position scheme for dc/ac converters. In fact, this paper is the only reference among those cited earlier that actually shows numerical results. Later, the drawbacks of the analysis in [35] were realized by the same authors, and in the follow-up paper [39], a spectral analysis of the line-to-line voltage was reported that did not cause the same errors.

In total, the spectrum predicted by (5.42) does not resemble the actual spectrum for u_{ab} at all. This makes the approximation in (5.42) useless.

(a)

(b)

(c)

(d)
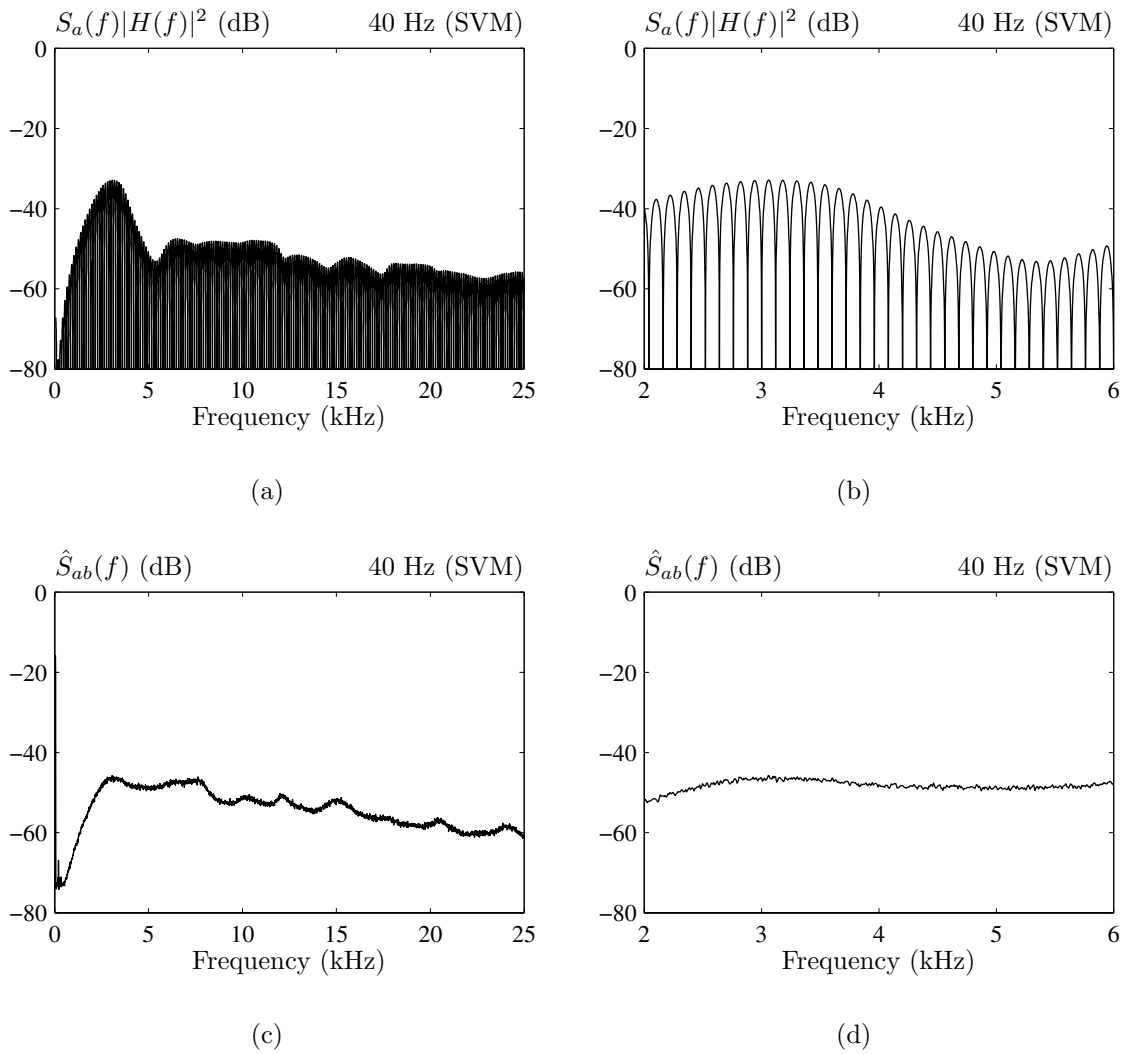
Figure 5.15 Spectra for the line-to-line voltage using space-vector modulation, pool size $J = 5$, and a fundamental frequency equal to 40 Hz. (a, b) Calculated density using the approximation (5.42) and (c, d) real (measured) spectrum.

An exact method based on cross power spectral densities

For the practical cases studied here, the carrier periods of all three legs are synchronized and dithered by the outcome of the same random experiment as earlier shown in Fig. 5.4 on page 123 and in Fig. 5.16(a) on the next page. This interdependence between the legs is unavoidable and it must be taken properly into account. Now, q_{ab} is the difference of two random variables: the switching functions q_a and q_b, which control leg a and b, respectively. It was pointed in section 4.2.1 that the proper formulation for the spectrum $S_{ab}(f)$ of the normalized output u_{ab}/U_{dc} voltage then is

$$S_{ab}(f) = S_a(f) + S_b(f) - C_{ab}(f) - C_{ba}(f), \tag{5.43}$$

where $S_a(f)$ and $S_b(f)$ are the spectrum for q_a and q_b, respectively. $C_{ab}(f)$ and $C_{ba}(f)$ are the cross power spectral densities as introduced on page 75 in connection with the full-bridge dc/dc converter.

	$d_a > d_b$	$d_a < d_b$
s	$+1$	-1
α_δ	$\frac{1}{2}(d_a - d_b)$	$\frac{1}{2}(d_b - d_a)$
α_Δ	$\frac{1}{2}(d_a + d_b)$	$\frac{1}{2}(d_a + d_b)$
α	$\frac{1}{2}(1 - d_a)$	$\frac{1}{2}(1 - d_b)$

(a)   (b)

Figure 5.16 (a) Sample waveforms for the switching functions and the normalized line-to-line voltage. (b) Auxiliary variables used for the representation of a double sampling pulse.

Equation (5.43) is valid for all kinds of randomized modulators. For example, the result in (5.42) is a special case of (5.43). The major problem associated with applying (5.43) directly is to get the required expressions for the cross spectra. Judging from the extent of the analyses needed to get closed-form expressions for the auto spectra $S_a(f)$ or $S_b(f)$, derivation of analytical expressions for the cross terms $C_{ab}(f)$ and $C_{ba}(f)$ is at best very complicated or at worst impossible. Hence, a method that preserves the accuracy of the exact analysis (5.43), but that does not require explicit knowledge of cross densities, will be of practical importance.

A supplementary discussion may be found in section 4.5.1.

5.5.2 Outline of the developed method

To overcome the problems outlined above, a novel method based on modifications of the theory for the spectrum of q_a has been developed. This new approach, which was successfully used already in Chapter 4, is mathematically speaking equally correct as the method involving cross spectral densities, but only slightly more complicated than the error-prone method given by (5.42).

The new idea is explained by the example in Fig. 5.16(a), which shows time-domain waveforms for q_a, q_b, and q_{ab}. As already explained in Chapter 4, the idea is to generalize the concept of pulse trains. Until now the interpretation of a "pulse train" has been a stream of rectangular pulses with certain deterministic as well as stochastic properties. Also, there has been only one occurrence of a rectangular pulse in each carrier period. The sampling pulse u is now redefined as the composite waveform formed by two identical rectangular pulses u_1 and u_2 as shown in Fig. 5.16(a). Hence,

$$u(t) \triangleq u_1(t) + u_2(t) = u_1(t) + u_1(t - \alpha_\Delta T), \tag{5.44}$$

where

$$u_1(t) = \begin{cases} s, & 0 \le t \le \alpha_\delta T, \\ 0, & \text{otherwise.} \end{cases} \tag{5.45}$$

The new sampling pulse is described by the parameters indicated in Fig. 5.16(a): s is the signed magnitude of the double pulse, α determines the pulse position in the carrier period, α_δ is the width of both u_1 and u_2, and finally α_Δ is the amount by which u_2 lags u_1.

In summary, the suggested procedure for analytical calculation of the spectrum for q_{ab} consists of the following steps:

1. **Redefinition of the sampling pulse**
   Formally, the sampling pulse is redefined from being a single pulse to being a double pulse[7] within each carrier period.

2. **Assignment of values to auxiliary parameters**
   From the precalculated duty ratios d_a and d_b, the parameters α, α_δ, α_Δ, and s are found as tabulated in Fig. 5.16(b). Note that the values depend on the mutual scale of the duty ratios d_a and d_b.

3. **Evaluation of the expressions for the partial spectra**
   Based on the chosen probability density function for T, the algebra needed to evaluate the expressions for the partial spectra listed in section 5.3.3 is performed.

4. **Summation of all partial spectra**
   The total spectrum is found by summing the contributions from all the partial spectra.

Compared to the method based on knowledge of the cross spectral densities, the direct approach is considerably less complicated. Also, comparing the work load needed to analyze the line-to-line voltage spectrum to the extent of the work needed to calculate the spectrum for the switching function, the overhead is moderate.

Finally, it should be mentioned that the idea of redefining the sampling pulse into something "non-rectangular" has been used in [4, 5]. In these references, a sampling pulse shaped like a trapezoid is used to calculate the input current spectrum in a buck converter with random pulse-position modulation.

5.5.3   Equations for partial spectra

Since q_{ab} has been parameterized, the formulas on page 121 is evaluated by finding expressions for the various expectations in (5.24)–(5.26).

The Fourier transformation of the dual sampling pulse defined by (5.44) and (5.45) may be expanded into:

$$
\begin{aligned}
U(f; \delta_m) = \mathcal{F}(u(t; \delta_m)) &= \mathcal{F}(u_1(t))\left(1 + e^{-j\omega\alpha_{\Delta,m}T}\right) \\
&= \frac{s_m}{j\omega}\left(1 - e^{-j\omega\alpha_{\delta,m}T}\right)\left(1 + e^{-j\omega\alpha_{\Delta,m}T}\right).
\end{aligned}
\tag{5.46}
$$

Note, index m has been appended to the subscripts to show that the parameters are functions of the carrier period counter, m.

---

[7]The replacement of the normally used rectangular pulse with a double pulse is, of course, not the only possible replacement. See further in section 5.6 and in Chapter 6.

The diagonal terms (m = m̃)

The expectations needed to evaluate the diagonal terms in (5.24) are listed below. Using (5.46) to find $|U(\cdot)|^2$ and inserting this results into (5.29), it may be shown that

$$E\Big\{|U(f;\delta_m)|^2\Big\} = \sum_{j=1}^{J} p_j \frac{2}{\omega^2}\Big(2 + 2\cos(\omega\alpha_{\Delta,m}T_j) - 2\cos(\omega\alpha_{\delta,m}T_j)$$

$$- \cos\big(\omega(\alpha_{\Delta,m} - \alpha_{\delta,m})T_j\big) - \cos\big(\omega(\alpha_{\Delta,m} + \alpha_{\delta,m})T_j\big)\Big), \quad (5.47)$$

Likewise, it may be shown that

$$E\Big\{U(f;\delta_m)e^{j\omega(1-\alpha_m)T}\Big\} = \sum_{j=1}^{J} p_j \frac{s_m}{j\omega}\big(1 - e^{-j\omega\alpha_{\delta,m}T_j}\big)\big(1 + e^{-j\omega\alpha_{\Delta,m}T_j}\big)e^{j\omega(1-\alpha_m)T_j},$$

$$(5.48)$$

$$E\Big\{U^\star(f;\delta_{\tilde m})e^{j\omega\alpha_{\tilde m}T}\Big\} = \sum_{j=1}^{J} p_j \frac{s_{\tilde m}}{j\omega}\big(e^{j\omega\alpha_{\delta,\tilde m}T_j} - 1\big)\big(1 + e^{j\omega\alpha_{\Delta,\tilde m}T_j}\big)e^{j\omega\alpha_{\tilde m}T_j}, \quad (5.49)$$

$$E\big\{e^{j\omega T}\big\} = \sum_{j=1}^{J} p_j\, e^{j\omega T_j}. \quad (5.50)$$

The off-diagonal terms (m ≠ m̃)

The off-diagonal partial spectra are found by using (5.48)–(5.50) together with:

$$E\Big\{U(f;\delta_m)e^{-j\omega\alpha_m T}\Big\} = \sum_{j=1}^{J} p_j \frac{s_m}{j\omega}\big(1 - e^{-j\omega\alpha_{\delta,m}T_j}\big)\big(1 + e^{-j\omega\alpha_{\Delta,m}T_j}\big)e^{-j\omega\alpha_m T_j}$$

$$(5.51)$$

$$E\Big\{U^\star(f;\delta_{\tilde m})e^{-j\omega(1-\alpha_{\tilde m})T}\Big\} = \sum_{j=1}^{J} p_j \frac{s_{\tilde m}}{j\omega}\big(e^{j\omega\alpha_{\delta,\tilde m}T_j} - 1\big)\big(1 + e^{j\omega\alpha_{\Delta,\tilde m}T_j}\big)e^{-j\omega(1-\alpha_{\tilde m})T_j}.$$

$$(5.52)$$

Equations (5.51) and (5.52) may then be inserted into (5.25) and (5.26) for $m < \tilde m$ and $m > \tilde m$, respectively.

5.5.4 Comparison of calculated and measured spectra

The used laboratory set-up and the settings of the modulator are the same as those used in section 5.4.3 for the examples related to the switching function. However, to limit the number of plots, only results for the $J = 5$ case are included, i.e. the carrier frequency is selected randomly in the set $f_j = \{2.0, 2.5, 3.0, 3.5, 4.0\}$ kHz.

Also, the notation used to separate different spectra is same as used in section 5.4.3 except for the replacement of indices, i.e. the measured spectrum for the voltage difference between two output terminals of the converter becomes $\hat{S}_{ab}^p(f)$, etc.
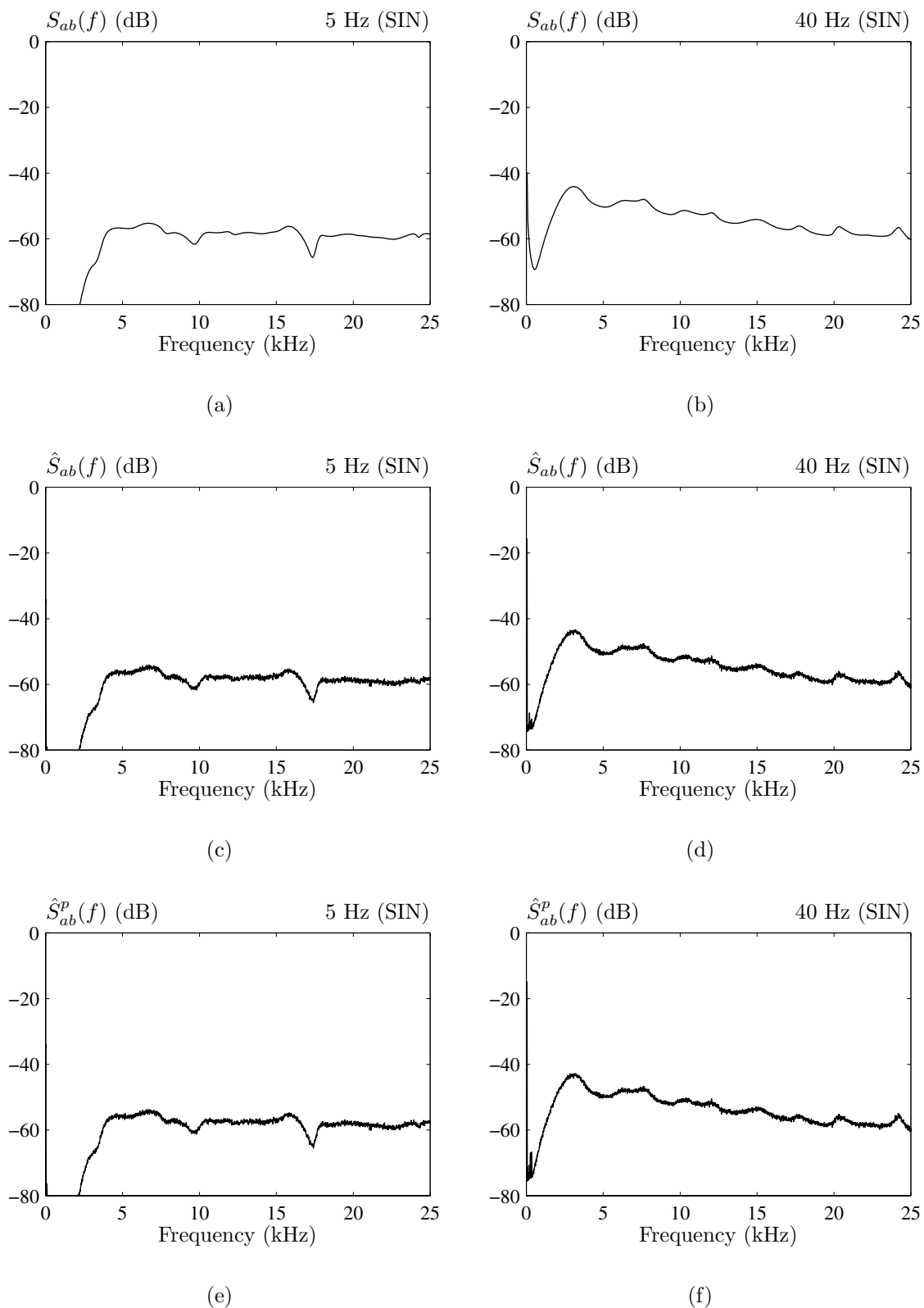
Figure 5.17 Spectra for the line-to-line voltage using sinusoidal modulation, pool size $J = 5$, and fundamental frequency 5 Hz (left column) and 40 Hz (right column). (a, b) Calculated density spectra, (c, d) measured spectrum (logic level), and (e, f) measured spectrum (power level).
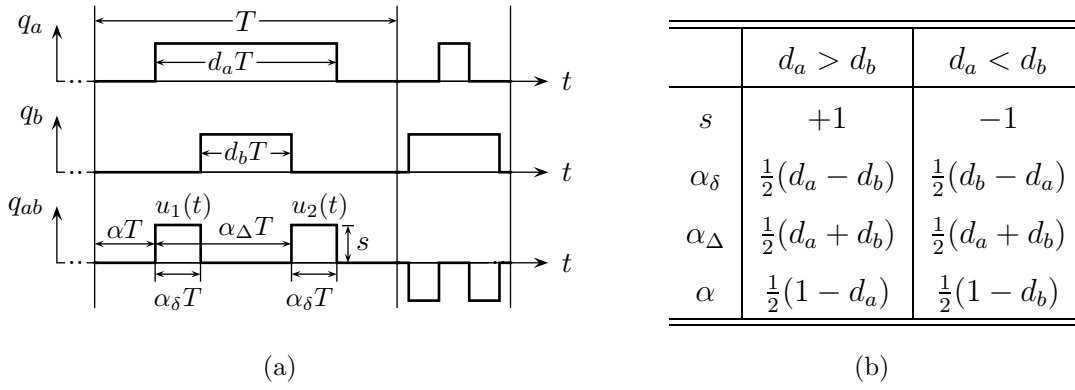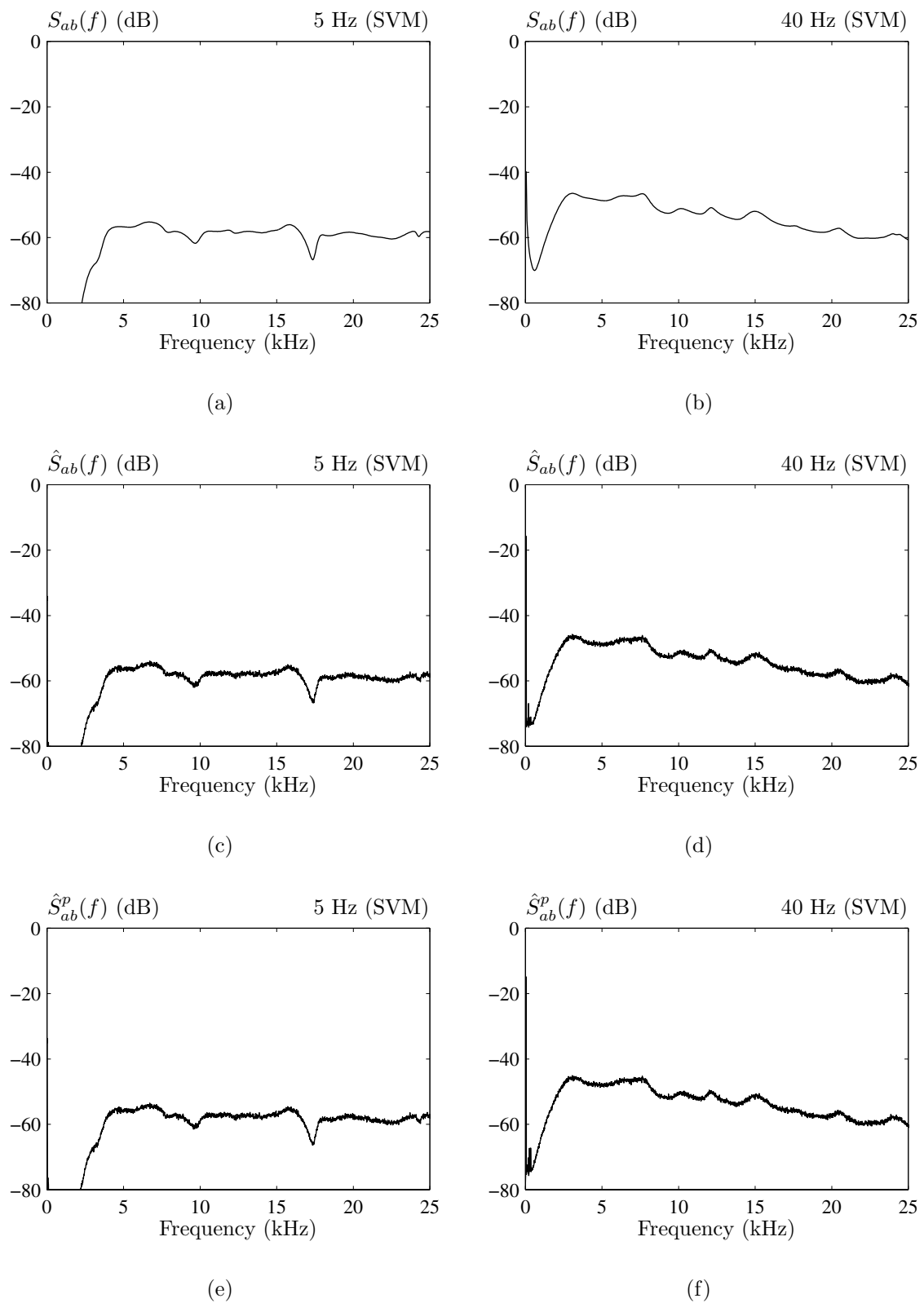
Figure 5.18 Spectra for the line-to-line voltage using space-vector modulation, pool size $J = 5$, and fundamental frequency 5 Hz (left column) and 40 Hz (right column). (a, b) Calculated density spectra, (c, d) measured spectrum (logic level), and (e, f) measured spectrum (power level).
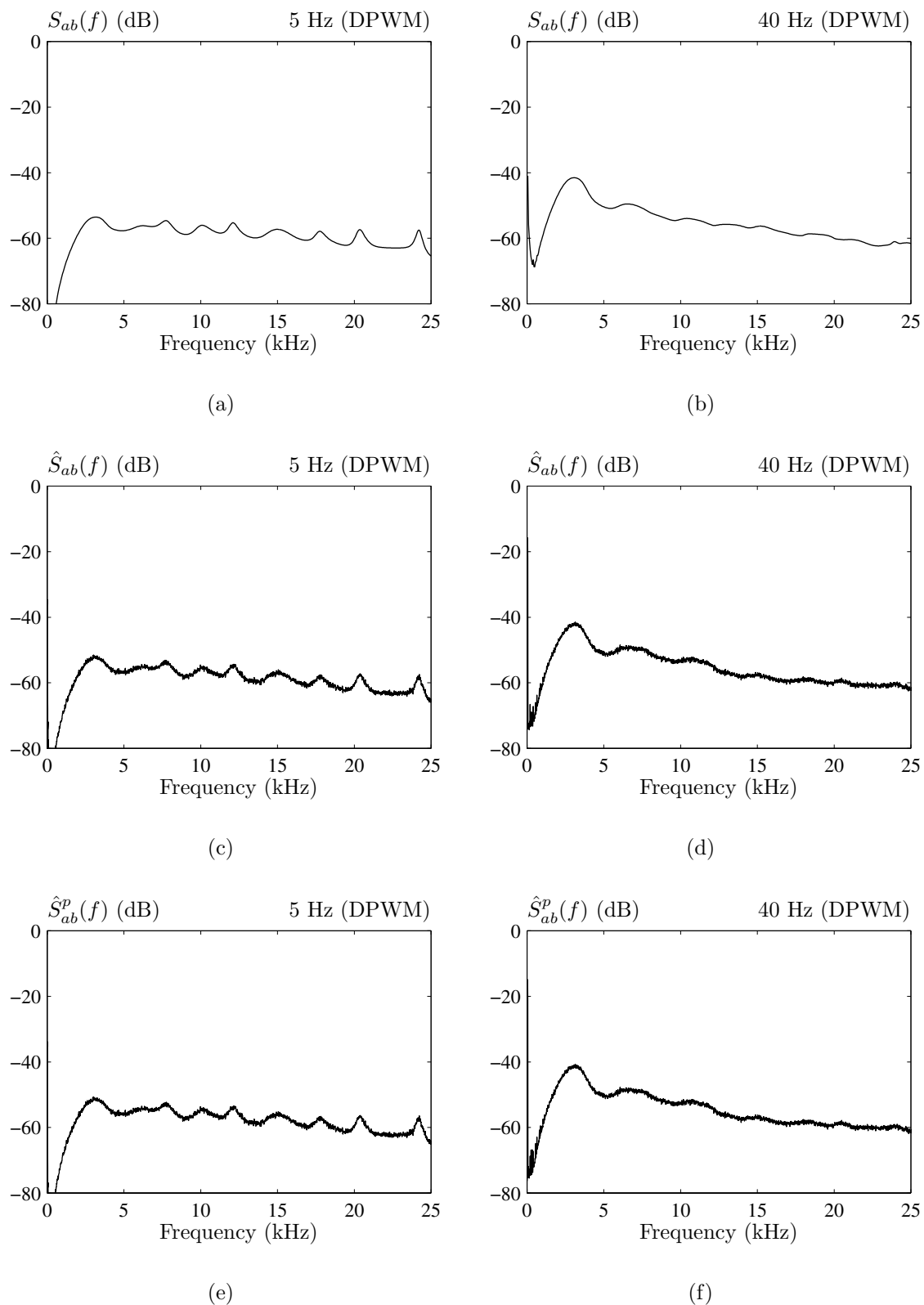
Figure 5.19 Spectra for the line-to-line voltage using discontinuous modulation, pool size $J = 5$, and fundamental frequency 5 Hz (left column) and 40 Hz (right column). (a, b) Calculated density spectra, (c, d) measured spectrum (logic level), and (e, f) measured spectrum (power level).

Examples using pool size of five carrier frequencies

Starting on page 144, Figs. 5.17–5.19 show the obtained results for the three different modulators and operating points listed in Table 5.2 (page 127).

These plots show that the agreement between the theoretically predicted and the measured power spectrum density is very good irrespective of the type of modulator; the spectral theory is capable of tracking the measured density accurately despite the quite peculiar shape of $\hat{S}_{ab}^{p}(f)$ with many local maxima and minima. It may safely be concluded that the theory developed for the spectrum of the line-to-line voltage is fully correct.

The comments given earlier in section 5.4.5 do also apply for the line-to-line case, although one distinct difference exists: the low-order harmonic components caused by the non-sinusoidal reference waveforms have disappeared.

5.6 Spectral analysis of the phase-to-neutral voltage

The discussion in section 5.5 of the problem of calculating the spectrum for the line-to-line voltage is equally valid for the topic of this section: how can the spectrum for the phase-to-neutral voltage of a three-phase load be analytically calculated? Again, the principle of the generalized sampling pulse may be used to find the spectrum at hand instead of resorting to a tedious analysis involving cross power spectral densities.

In the first subsection below, it is shown how the sampling pulse may be redefined to calculate the spectrum for the phase-to-neutral voltage. This is followed by a list of equations necessary to calculate the partial spectra, and finally the analysis is verified by comparisons to laboratory measurements.

5.6.1 Parametric representation of the sampling pulse

The waveform to be analyzed is the phase-to-neutral voltage of a symmetrical three-phase load like commonly used ac motors. If such a load is supplied from a VSC, it may be shown that the phase-to-neutral voltage u_{an} is [40]

$$u_{an} = \tfrac{1}{3}\left(2q_a - (q_b + q_c)\right)U_{dc} \triangleq q_{an}U_{dc} \tag{5.53}$$

under balanced operating conditions. The normalized voltage q_{an} is used exclusively below in order to avoid the U_{dc} multiplier. Equation (5.53) shows that q_{an} depends on all three switching functions q_a, q_b, and q_c. The corresponding duty ratios d_a, d_b, and d_c can be precalculated and since the pulses are center-aligned within each carrier period, the waveform for q_{an} can be found as well. Depending on the magnitudes of the duty ratios, one of the waveforms shown in Fig. 5.20(a) results.

Following the same route as in the previous section, the sampling pulse may now be regarded as a concatenation of four rectangular pulses as shown in 5.20(b); the used parameters are listed in the accompanying table in Fig. 5.20(c). Note that the auxiliary duty ratios $d_{\min} < d_{\mid} < d_{\max}$ are the same as the leg duty ratios, but sorted in ascending order. For example, if $d_b < d_a < d_c$ in some carrier period, then $d_{\min} = d_b$,

(a)
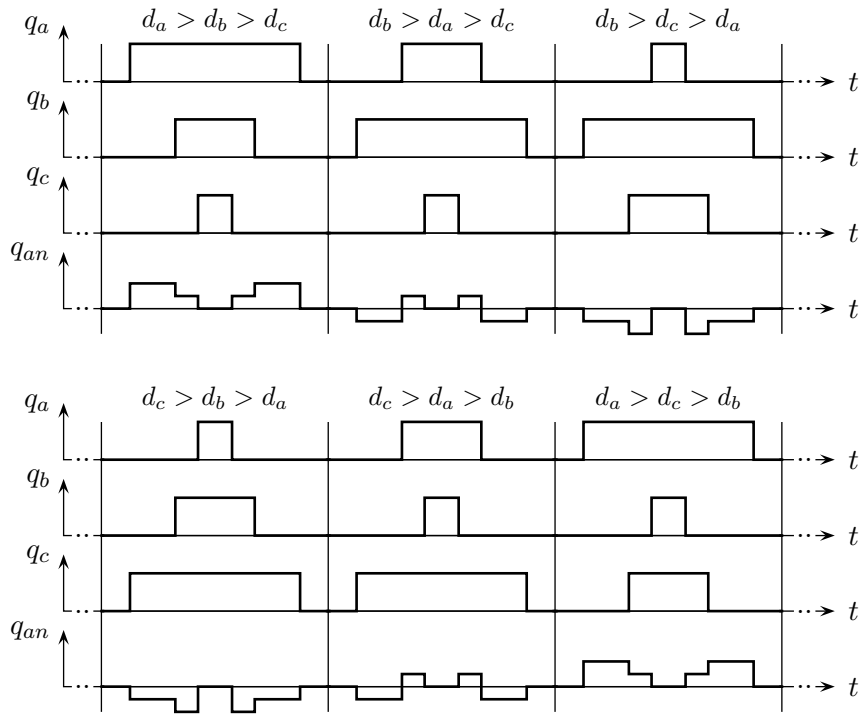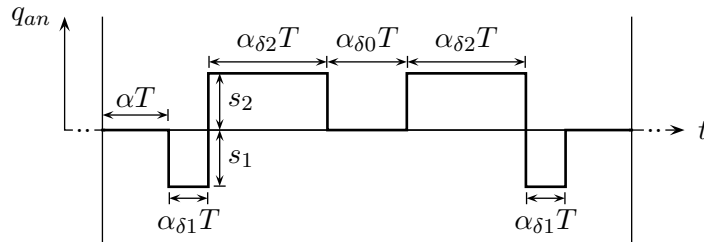
(b)

$$\alpha = \tfrac{1}{2}(1 - d_{\max}), \quad \alpha_{\delta1} = \tfrac{1}{2}(d_{\max} - d_{\mathrm{mid}}), \quad s_1 = \begin{cases} 2, & d_a = d_{\max}, \\ -1, & \text{otherwise,} \end{cases}$$

$$\alpha_{\delta0} = d_{\min}, \qquad\quad \alpha_{\delta2} = \tfrac{1}{2}(d_{\mathrm{mid}} - d_{\min}), \quad s_2 = \begin{cases} -2, & d_a = d_{\min}, \\ 1, & \text{otherwise.} \end{cases}$$

(c)

Figure 5.20 Representation of the sampling pulse $q_{an} = \frac{1}{3}\left(2q_a - (q_b + q_c)\right)$ for the phase-to-neutral voltage. (a) Possible waveforms for all combinations of the order of the leg duty ratios, (b) definition of auxiliary parameters, and (c) their values using the sorted duty ratios $d_{\min} < d_{\mathrm{mid}} < d_{\max}$.

$d_{\mathrm{mid}} = d_a$, and $d_{\mathrm{max}} = d_c$. The sampling pulse may be represented in the time domain as

$$u(t) = u_1(t) + u_2(t - \alpha_{\delta 1}T) + u_2(t - \alpha_\Delta T) + u_1(t - \alpha_\Delta T - \alpha_{\delta 2}T), \qquad (5.54)$$

where $\alpha_\Delta \triangleq \alpha_{\delta 1} + \alpha_{\delta 2} + \alpha_{\delta 0}$ is introduced. Also, it follows from Fig. 5.20(b) that

$$u_1(t) = \begin{cases} s_1, & 0 \le t \le \alpha_{\delta 1}T, \\ 0, & \text{otherwise,} \end{cases} \qquad u_2(t) = \begin{cases} s_2, & 0 \le t \le \alpha_{\delta 2}T, \\ 0, & \text{otherwise.} \end{cases} \qquad (5.55)$$

5.6.2 Evaluation of partial contribution to the total spectrum

The Fourier transformation of the sampling pulse defined by (5.54) and (5.55) becomes

$$U(f; \delta_m) = U_1(f) \left(1 + e^{-j\omega(\alpha_\Delta + \alpha_{\delta 2})T} \right) + U_2(f) \left(e^{-j\omega\alpha_{\delta 1}T} + e^{-j\omega\alpha_\Delta T} \right), \qquad (5.56)$$

where the Fourier transformations $U_1(f)$ and $U_2(f)$ are

$$U_1(f) = \frac{s_1}{j\omega} \left(1 - e^{-j\omega\alpha_{\delta 1}T} \right), \qquad (5.57)$$

$$U_2(f) = \frac{s_2}{j\omega} \left(1 - e^{-j\omega\alpha_{\delta 2}T} \right). \qquad (5.58)$$

The diagonal terms ($m = \tilde{m}$)

Using (5.56), it is possible to find $|U(\cdot)|^2$ and inserting into (5.29), some trigonometric re-arrangements lead to

$$
E\left\{ |U(f; \delta_m)|^2 \right\} =
$$
$$
\sum_{j=1}^{J} p_j \frac{16}{\omega^2} \left[s_{1,m}^2 \sin^2\left(\tfrac{1}{2}\omega T_j \alpha_{\delta 1,m} \right) \cos^2\left(\tfrac{1}{2}\omega T_j (\alpha_{\delta 0,m} + \alpha_{\delta 1,m} + 2\alpha_{\delta 2,m}) \right) \right.
$$
$$
+ s_{2,m}^2 \sin^2\left(\tfrac{1}{2}\omega T_j \alpha_{\delta 2,m} \right) \cos^2\left(\tfrac{1}{2}\omega T_j (\alpha_{\delta 0,m} + \alpha_{\delta 2,m}) \right)
$$
$$
+ s_{1,m} s_{2,m} \sin\left(\tfrac{1}{2}\omega T_j \alpha_{\delta 1,m} T_j \right) \sin\left(\tfrac{1}{2}\omega T_j \alpha_{\delta 2,m} \right)
$$
$$
\left. \cos\left(\tfrac{1}{2}\omega T_j (\alpha_{\delta 0,m} + \alpha_{\delta 2,m}) \right) \cos\left(\tfrac{1}{2}\omega T_j (\alpha_{\delta 0,m} + \alpha_{\delta 1,m} + 2\alpha_{\delta 2,m}) \right) \right],
$$
$$
(5.59)
$$

where, as before, m has been appended to the subscripts. The remaining expectations needed to get the diagonal terms in (5.24) are found by (5.56). To save space let

$$
U(f; \delta_m; T_j) \triangleq U_1(f) \left(1 + e^{-j\omega(\alpha_{\Delta,m} + \alpha_{\delta 2,m})T_j} \right)
$$
$$
+ U_2(f) \left(e^{-j\omega\alpha_{\delta 1,m}T_j} + e^{-j\omega\alpha_{\Delta,m}T_j} \right), \qquad (5.60)
$$

i.e. $U(f; \delta_m; T_j)$ is the Fourier transformation of the composite sampling pulse evaluated for the m'th carrier period with $T = T_j$.

Using this notation, the expectations may be written in a compact form as

$$E\left\{U(f;\delta_m)e^{j\omega(1-\alpha_m)T}\right\} = \sum_{j=1}^{J} p_j\, U(f;\delta_m;T_j)e^{j\omega(1-\alpha_m)T_j}, \tag{5.61}$$

$$E\left\{U^\star(f;\delta_{\tilde{m}})e^{j\omega\alpha_{\tilde{m}}T}\right\} = \sum_{j=1}^{J} p_j\, U^\star(f;\delta_{\tilde{m}};T_j)e^{j\omega\alpha_{\tilde{m}}T_j}, \tag{5.62}$$

$$E\left\{e^{j\omega T}\right\} = \sum_{j=1}^{J} p_j\, e^{j\omega T_j}. \tag{5.63}$$

The off-diagonal terms ($m \neq \tilde{m}$)

In a similar manner, the partial off-diagonal spectra are found by using (5.61)–(5.63) together with:

$$E\left\{U(f;\delta_m)e^{-j\omega\alpha_m T}\right\} = \sum_{j=1}^{J} p_j\, U(f;\delta_m;T_j)e^{-j\omega\alpha_m T_j} \tag{5.64}$$

$$E\left\{U^\star(f;\delta_{\tilde{m}})e^{-j\omega(1-\alpha_{\tilde{m}})T}\right\} = \sum_{j=1}^{J} p_j\, U^\star(f;\delta_{\tilde{m}};T_j)e^{-j\omega(1-\alpha_{\tilde{m}})T_j}, \tag{5.65}$$

To get the spectrum $\hat{S}_{an}(f)$, (5.59)–(5.65) may then be inserted into the list of general equations (page 121).

5.6.3   Comparison of calculated and measured spectra

Examples using pool size of five carrier frequencies

The examples have been calculated and measured for the same modulator settings as used in section 5.4.3 for the switching function and in section 5.5.4 for the line-to-line voltage. The spectrum $\hat{S}_{an}^p(f)$ is measured by sensing the voltage between terminal a and the star point of the wye-connected induction motor supplied from the converter.

It is apparent from the selected results shown in Fig. 5.21 on the facing page for the $J = 5$ case that the agreement is very good between the measured $\hat{S}_{an}^p(f)$ and the calculated $\hat{S}_{an}(f)$ spectrum. However, it may be noted by comparing e.g. the results in Fig. 5.21(a, b) with Fig. 5.17(a, e) for the line-to-line voltage that these spectra are identical, except for an offset on approximately 5 dB. In essence, there is no difference in the frequency-domain distribution of the power for the line-to-line voltage and the phase-to-neutral voltage for a symmetrical load.

This observation may be proved more rigorously by using the formal definition of the power spectrum given in (3.13) and (3.14) in Chapter 3 on the $q_{an} = \frac{1}{3}(2q_a - (q_b + q_c))$ expression. Hence, it may be shown that

$$9S_{an}(f) = 4S_a(f) + S_b(f) + S_c(f)$$
$$- 2\big(C_{ab}(f) + C_{ba}(f)\big) - 2\big(C_{ac}(f) + C_{ca}(f)\big) + \big(C_{bc}(f) + C_{cb}(f)\big), \tag{5.66}$$
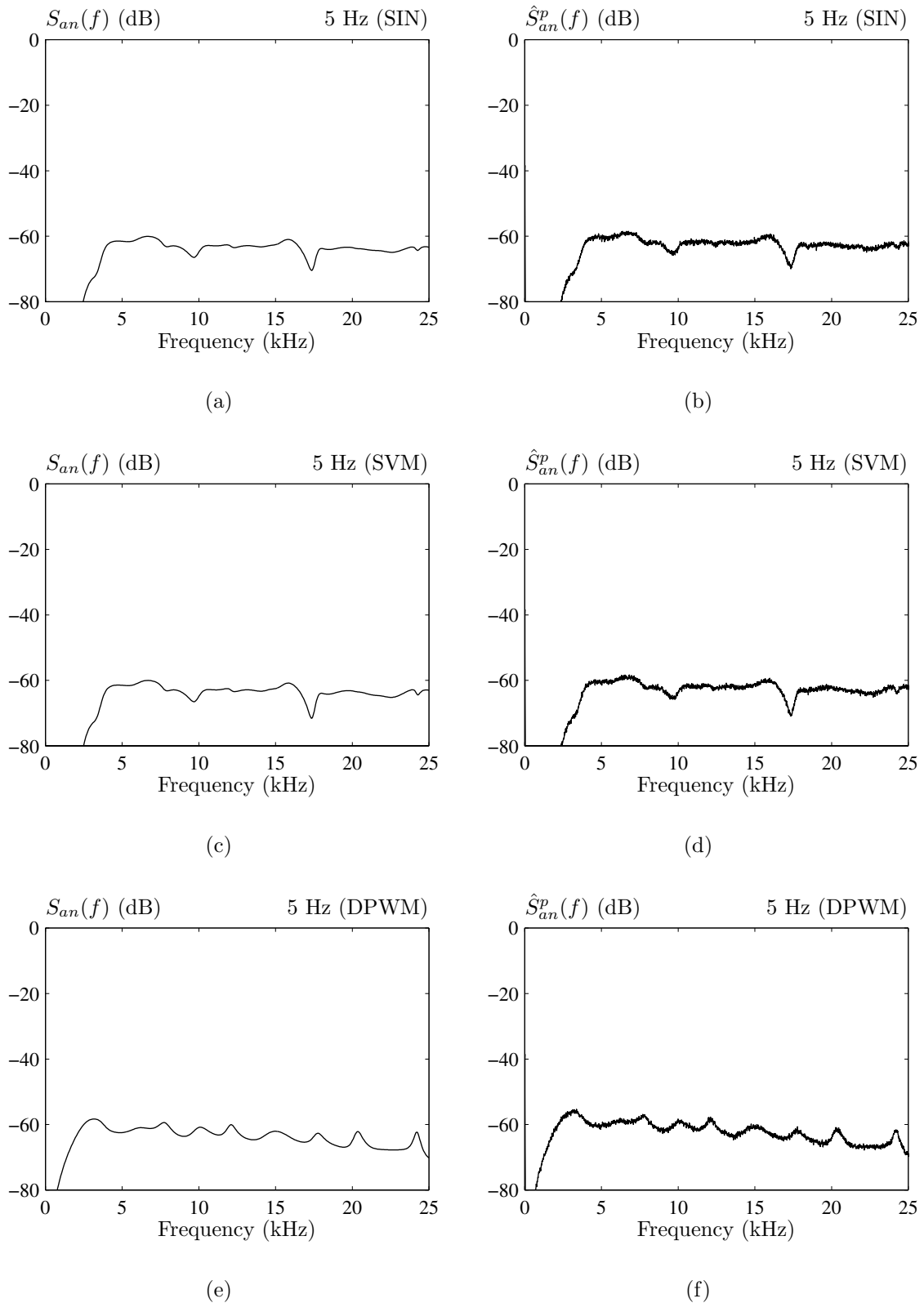
Figure 5.21 Spectra for the phase-to-neutral voltage for different modulators using pool size $J = 5$ and fundamental frequency 5 Hz. (left column) Calculated density spectra and (right column) measured spectrum (power level).

where $S_a(f)$, $S_b(f)$, and $S_c(f)$ are the auto spectra for q_a, q_b, and q_b, respectively. Also, $C_{ab}(f)$ denotes the cross spectra between q_a and q_b, etc.

Now, since all legs are controlled in similar manners, it must be expected that they all have identical spectral characteristics. Hence, for the auto spectra, we have the physically intuitive fact that $S_a(f) = S_b(f) = S_c(f)$. For the cross spectra, it must also hold that $C_{ab}(f) + C_{ba}(f) = C_{ac}(f) + C_{ca}(f) = C_{bc}(f) + C_{cb}(f)$. Using these facts, (5.66) simplifies to

$$9S_{an}(f) = 6S_a(f) - 3\big(C_{ab}(f) + C_{ba}(f)\big), \tag{5.67}$$

which should be compared to (5.43), when $S_b(f) = S_a(f)$ is used once more:

$$S_{ab}(f) = 2S_a(f) - \big(C_{ab}(f) + C_{ba}(f)\big). \tag{5.68}$$

From these two equations, it follows that $S_{ab}(f) = 3S_{an}(f)$, which corresponds to a 4.77 dB difference between $S_{ab}(f)$ and $S_{an}(f)$. This agrees perfectly with the obtained results. It should be noted that this result holds for arbitrary random PWM methods, i.e. also for the methods studied in Chapter 6.

In retrospect, the detailed spectral analysis in the previous subsection becomes superfluous, because of $S_{ab}(f) = 3S_{an}(f)$ relationship, but at least the versatility of the generalized sampling pulse has been demonstrated once more.

5.7   Summary

Spectral analysis of the RCF-PWM technique for three-phase converters has been the main theme for this chapter. Before the actual spectral analysis was commenced, a discussion of the overall implications of using either a continuous or a discrete probability density functions (pdf) for the randomized carrier frequency was given. As elaborated in section 5.2.2, the main conclusion is that the discrete type of pdf is preferable to the continuous pdf for three distinct reasons:

1. It complies very well with the spectral shaping problem,
2. The spectral analysis is significantly less complicated, and
3. The implementation in micro processors is more simple.

Although the discussion offspring from RCF-PWM, these statements are also valid for other random PWM techniques like those studied in the next chapter which randomizes the positions or the widths of the on-state part of the switching functions.

Based on the main result of Chapter 3, a set of general equations for the power spectrum for the RCF scheme was then derived. The spectral analysis is not exact in the sense that an approximation was used to render the required mathematical manipulations possible at all. As a consequence, the spectral theory is incapable of predicting the existence of pure harmonic components, nor can their strength (volt^2) be calculated. However, it has been demonstrated that by proper selection of the pool of carrier frequencies, the generation of high-frequency harmonics can be completely suppressed, which makes this weakness of little practical concern[8].

---

[8]A spectral analysis of the dc/ac RCF-PWM scheme which is capable of predicting the existence of discrete components and their strengths may be found in [25, 34]. Those references do also include formulas for the density spectrum based on the work reported in this thesis.

For RCF-PWM the spectrum is dominated by the density part (volt^2/Hz), which is distributed over the whole frequency axis. The presented analysis includes formulas that allow this density spectrum to be calculated. Despite that the analysis is not exact in a strict mathematical sense, a series of comparisons with measurements has shown that the spectral analysis is very accurate — provided that pure power components (harmonics) do not exist. Since harmonics are usually absent, the used approximations are unimportant from an accuracy point of view.

Apart from the spectrum of the switching functions controlling each leg of a three-phase VSC, the spectra for composite waveforms, such as the line-to-line voltage and the phase-to-neutral voltage, were also analyzed. It was demonstrated that certain time-domain and frequency-domain properties of deterministic PWM waveforms cannot be generalized to include random PWM waveforms, although such claims have been promoted in the literature. Instead, a simple, but still fully correct, procedure was suggested that allows the density spectra of the mentioned voltages to be accurately calculated.

In total, the following contributions are believed to be of major significance compared to results available in the scientific literature:

- The set of formulas summarized in section 5.3.3 for the density spectrum for PWM waveforms arising in dc/ac converters operating with a randomly changing carrier frequency is considered novel. In particular, the approximation used to include the deterministic variations in the phase duty ratios is considered unique.

- In contrary to similar analyses found in the literature, the developed theory does not attach any strings to how the duty ratios vary as a function of time; arbitrary modulation principles may be used, including, but not limited to, the common space-vector pulse patterns and the class of discontinuous PWM techniques.

- None of the formulas for the spectra of the switching function, the line-to-line voltage, and the phase-to-neutral voltage may be found elsewhere. Also, the detail, which is of great practical concern, of using center-aligned pulses within each carrier period is taken properly into account.

To support all theoretical analyses, it must be emphasized that extensive comparisons with laboratory measurements on an operating VSC have been reported also. The measured spectra fully verify the correctness of the presented spectral analysis of the RCF-PWM scheme for three-phase applications.

In conclusion, it may be stated that a powerful tool has been derived for spectral analysis of the RCF technique — a problem which, to the knowledge of the author, has not been solved elsewhere, despite the fact that RCF probably is the most efficient way to convert power carrier by discrete frequency components into the continuous density spectrum without jeopardizing the macroscopic behavior of the converter-load cascade.

Bibliography

[1] T. Tanaka, T. Ninomiya, and K. Harada, "Random-Switching Control in DC-to-DC Converters," *Proc. of the 20th IEEE Power Electronics Specialists Conference*, vol. 1, pp. 500–507, 1989.

[2] J. T. Boys and P. G. Handley, "Spread Spectrum Switching: Low Noise Modulation Technique for PWM Inverter Drives," *IEE Proc. Part B*, vol. 139, no. 3, pp. 252–260, May 1992.

[3] T. G. Habetler and D. M. Divan, "Acoustic Noise Reduction in Sinusoidal PWM Drives Using a Randomly Modulated Carrier," *IEEE Trans. on Power Electronics*, vol. 6, no. 3, pp. 356–363, July 1991.

[4] A. M. Stanković, *Random Pulse Modulation with Applications to Power Electronic Converters*, Ph.D. thesis, Massachusetts Institute of Technology, Feb. 1993.

[5] A. M. Stanković, G. C. Verghese, and D. J. Perreault, "Analysis and Synthesis of Randomized Modulation Schemes for Power Converters," *IEEE Trans. on Power Electronics*, vol. 10, no. 6, pp. 680–693, Nov. 1995.

[6] A. M. Trzynadlowski, R. L. Kirlin, and S. Legowski, "Space Vector PWM Technique with Minimum Switching Losses and a Variable Pulse Rate," *Proc. of the 19th IEEE International Conference on Industrial Electronics, Control, and Instrumentation*, vol. 2, pp. 689–694, 1993.

[7] C. M. Liaw and Y. M. Lin, "Random Slope PWM Inverter using Existing System Background Noise: Analysis, Design and Implementation," *IEE Proceedings — Electric Power Applications*, vol. 147, no. 1, pp. 45–54, Jan. 2000.

[8] F. Blaabjerg and J. K. Pedersen, "Digital Implemented Random Modulation Strategies for AC and Switched Reluctance Drives," *Proc. of the 19th IEEE International Conference on Industrial Electronics, Control, and Instrumentation*, vol. 2, pp. 676–682, 1993.

[9] A. M. Stanković, G. C. Verghese, and D. J. Perreault, "Randomized Modulation Schemes for Power Converters Governed by Markov Chains," *Proc. of the 4th IEEE Conference on Control Applications*, pp. 372–377, 1995.

[10] A. M. Stanković, G. C. Verghese, and D. J. Perreault, "Randomized Modulation of Power Converters via Markov Chains," *IEEE Trans. on Control Systems Technology*, vol. 5, no. 1, pp. 61–73, Jan. 1997.

[11] J. K. Pedersen and F. Blaabjerg, "Digital Quasi-Random Modulated SFAVM PWM in an AC-Drive System," *IEEE Trans. on Industrial Electronics*, vol. 41, no. 5, pp. 518–525, Oct. 1994.

[12] P. G. Handley, M. Johnson, and J. T. Boys, "Elimination of Tonal Acoustic Noise in Chopper-Controlled DC Drives," *Applied Acoustics*, vol. 32, pp. 107–119, 1991.

[13] T. Tanaka, H. Kameda, and T. Ninomiya, "Noise Analysis of DC-to-DC Converter with Random Switching Control," *Proc. of the IEEE International Telecommunications Energy Conference*, pp. 283–290, Nov. 1991.

[14] S. Legowski and A. M. Trzynadlowski, "Hypersonic MOSFET-based Power Inverter With Random Pulse Width Modulation," *Conference Record of the 24th IEEE Industry Applications Society Annual Meeting*, vol. 1, pp. 901–903, 1989.

[15] J. M. Retif, B. Allard, X. Jorda, and A. Perez, "Use of ASIC's in PWM Techniques for Power Converters," *Proc. of the 19th IEEE International Conference on Industrial Electronics, Control, and Instrumentation*, vol. 2, pp. 683–688, 1993.

[16] H. Hosei and K. Tanaka, Nippon Steel Corp., "Switching Regulator," US Patent No. 5.640.315, Filed March 17, 1995.

[17] F. Mihalič, T. Bezjak, and M. Milanovič, "Random Modulated Boost Converter with Improved Harmonic Spectrum," *Proc. of the IEEE International Symposium on Industrial Electronics*, vol. 2, pp. 268–273, 1997.

[18] W. H. Press, S. A. Teukolsky, W. T. Vetterling, and B. P. Flannery, *Numerical Recipes in C — The Art of Scientific Computing*, Cambridge University Press, second edition, 1992.

[19] J. K. Pedersen and F. Blaabjerg, "Implementation and Test of a Digital Quasi-Random Modulated SFAVM PWM in a High Performance Drive System," *Proc. of the 18th IEEE International Conference on Industrial Electronics, Control, and Instrumentation*, vol. 1, pp. 265–270, 1992.

[20] S. Y. R. Hui and S. Sathiakumar, "Optimisation of Microprocessor-based Random PWM Schemes for Power Inverters with Low Switching Frequencies," *Proc. of the 11th Annual Applied Power Electronics Conference*, vol. 1, pp. 214–218, 1996.

[21] G. A. Covic and J. T. Boys, "Noise Quieting with Random PWM AC Drives," *IEE Proc. Electric Power Applications*, vol. 145, no. 1, pp. 1–10, Jan. 1998.

[22] D. E. Knuth, *The Art of Computer Programming. Volume 2. Seminumerical Algorithms*, Addison Wesley, Reading, Massachusetts, third edition, 1998.

[23] M. M. Bech, F. Blaabjerg, J. K. Pedersen, and A. M. Trzynadlowski, "Comparative Investigation of Random PWM Techniques with Variable Switching Frequency and Pulse Position for Inverter-Fed Induction Motors," *Proc. of 7th European Conference on Power Electronics and Applications*, vol. 1, pp. 343–349, 1997.

[24] R. L. Kirlin and R. M. Dizaji, "New Analysis of Harmonics for Random Segment Width PWM DC-AC Conversion," private correspondence, Jan. 1998.

[25] R. L. Kirlin, M. M. Bech, and A. M. Trzynadlowski, "Power Spectral Density Analysis of Randomly Switched Pulse Width Modulation for DC/AC Converters," *Proc. of 10th IEEE Workshop on Statistical Signal and Array Processing*, pp. 373–377, Aug. 2000.

[26] P. E. Gill, W. M. Murray, and M. H. Wright, *Practical Optimization*, Academic Press, San Diego, California, 1981.

[27] J. T. Boys, "Theoretical Spectra for Narrow-Band Random PWM Waveforms," *IEE Proc. Part B*, vol. 140, no. 6, pp. 393–400, Nov. 1993.

[28] R. L. Kirlin and A. M. Trzynadlowski, "Spectral Design of Randomized Pulse Width Modulation in DC to AC Converters," *Proc. of the 7th IEEE Signal Pro-*

cessing Workshop on Statistical Signal and Array Processing, pp. 387–391, June 1994.

[29] R. L. Kirlin, S. Legowski, and A. M. Trzynadlowski, "An Optimal Approach to Random Pulse Width Modulation in Power Inverters," *Proc. of the 26th IEEE Power Electronics Specialists Conference*, vol. 1, pp. 313–318, 1995.

[30] F. Blaabjerg, J. K. Pedersen, L. Oestergaard, R. L. Kirlin, A. M. Trzynadlowski, and S. Legowski, "Optimized and Non-Optimized Random Modulation Techniques for VSI Drives," *Proc. of 6th European Conference on Power Electronics and Applications*, vol. 1, pp. 19–26, 1995.

[31] R. L. Kirlin, J. Wang, and R. M. Dizaji, "Study on Spectral Analysis and Design for DC/DC Conversion Using Random Switching Rate PWM," *Proc. of 10th IEEE Workshop on Statistical Signal and Array Processing*, pp. 378–382, Aug. 2000.

[32] R. L. Kirlin, A. M. Trzynadlowski, M. M. Bech, F. Blaabjerg, and J. K. Pedersen, "Analysis of Spectral Effects of Random PWM Strategies for Voltage Source Inverters," *Proc. of 7th European Conference on Power Electronics and Applications*, vol. 1, pp. 146–151, 1997.

[33] F. Blaabjerg, J. K. Pedersen, and P. Thoegersen, "Improved Modulation Techniques for PWM-VSI Drives," *IEEE Trans. on Industrial Electronics*, vol. 44, no. 1, pp. 87–95, Feb. 1997.

[34] R. L. Kirlin, M. M. Bech, and A. M. Trzynadlowski, "Power and Power Spectral Density Analysis of Random Switching PWM DC/AC Converters," Submitted to IEEE Trans. on Industrial Electronics, 2000.

[35] R. L. Kirlin, S. Legowski, A. M. Trzynadlowski, Y. Cui, and S. Kwok, "Power Spectra of a Three-Phase Inverter with Random Pulse Width Modulation Modes," *Proc. of the 3rd IEEE Workshop on Computers in Power Electronics*, pp. 265–267, Aug. 1992.

[36] R. L. Kirlin and A. M. Trzynadlowski, "A Unified Approach to Analysis and Design of Random Pulsewidth Modulation in Voltage Source Inverters," *IEEE Trans. on Circuits and Systems — I: Fundamental Theory and Applications*, vol. 44, no. 8, pp. 763–766, Aug. 1997.

[37] G. R. Cooper and C. D. McGillem, *Probabilistic Methods of Signal and Systems Analysis*, Harcourt Brace Jovanovich College Publishers, Orlando, Florida, second edition, 1986.

[38] K. S. Shanmugan and A. M. Breipohl, *Random Signals. Detection, Estimation and Data Analysis*, John Wiley & Sons, New York, 1988.

[39] R. L. Kirlin, S. Kwok, S. Legowski, and A. M. Trzynadlowski, "Power Spectra of a PWM Inverter with Randomized Pulse Position," *IEEE Trans. on Power Electronics*, vol. 9, no. 5, pp. 463–472, Sept. 1994.

[40] F. Jenni and D. Wüerst, *Steuerverfahren für Selbstgeführte Stromrichter*, B. G. Teubner, Stuttgart, 1995.

Chapter 6

Analysis of fixed carrier frequency random dc/ac PWM schemes

6.1 Introduction

The random PWM methods examined in this chapter are all applicable to multi-phase converters, although the main emphasis is put on the three-phase voltage-source converter (VSC) operating as a dc/ac inverter. In contrast to the scheme investigated in Chapter 5, the schemes treated in the present chapter all operate at a fixed carrier frequency; the randomization relies on dithering of pulse positions or pulse widths, but the carrier frequency is kept constant. Methods having these characteristics are categorized as fixed carrier frequency random PWM (FCF-RPWM) schemes. Several of such schemes are analyzed in details in this chapter.

The constant carrier frequency operation is advantageous in pulse-width modulated converter systems that incorporate digital controllers. In such systems, the sampling frequency of the controller is often synchronized to the carrier frequency of the power stage. This implies that all the random PWM schemes studied in this chapter open the opportunity to randomize the output voltage by simple modifications to the pulse-width modulator in such a way that the operation of any existing closed-loop controllers is not disrupted. This is a significant advantage of the FCF-RPWM schemes compared to random carrier frequency method studied in Chapter 5[1].

The overall objective of this chapter is to analyze various FCF-RPWM schemes of practical relevance. Like in Chapter 5, a detailed spectral analysis of the output voltage is presented for a number of selected FCF-RPWM schemes and, furthermore, the theories are compared to measurements. A second objective of equal importance is to demonstrate that some FCF-RPWM schemes affect the current supplied to the connected load in a subtle manner, which — nevertheless — has important consequences for the practical usefulness of these FCF-RPWM schemes. Among others things, it turns out that some of the FCF-RPWM schemes distort the per carrier period average load current, even if a proper volt-second balance is maintained. Apart from affecting the current quality negatively, this unfavorable characteristic deteriorates the performance in applications that rely on accurate current feedback.

---

[1]Part III starting on page 223 contains much more information on the problems of unifying random carrier frequency PWM with digital controllers. Also, methods to overcome these problems are suggested and verified by laboratory experiments in Part III.

Chapter outline

The chapter is organized in the following way: First, fundamental constraints for FCF-RPWM techniques are formulated and a review of FCF-RPWM methods available in the literature is given. Then, it is shown how the known techniques may be generalized in order to invent new FCF-RPWM schemes. Guidelines, which useful FCF-RPWM methods should adhere to, are then presented, and it is shown that the current waveforms produced by some FCF-RPWM methods complicate the use of standard techniques for current detection. Following this analysis, a novel current sampling strategy is presented, which solves the problems regarding correct detection of average currents.

In the remaining part of this chapter, focus is put on spectral analysis. A general set of formula for the voltage power spectrum generated by FCF-RPWM methods is derived. These formulas are used to derive theoretical expressions for the power spectrum for three selected FCF-RPWM methods. Finally, the correctness of the spectral analyses is verified by comparing analytical results to laboratory measurements.

6.2   Preliminaries

To support the subsequent analysis, the basic characteristics of the studied FCF-RPWM techniques are presented. Also, a brief review of FCF-RPWM techniques available in the past literature is provided and a discussion of alternatives to those known techniques is given.

A fact, which has been largely overlooked in the literature, is that not all FCF-RPWM methods are well-suited for practical applications and, therefore, at set of requirements is presented in order to ease the evaluation of a particular FCF-RPWM scheme. These guidelines are used in section 6.3 starting on page 167.

6.2.1   Constraints for fixed carrier frequency random PWM

The fundamental requirements for random PWM schemes belonging to the FCF-RPWM class studied in this chapter are that the randomization is made such that

1. the frequency used to update the modulator is constant and

2. the average voltage for each leg equals the reference voltage for that leg in all PWM carrier periods.

Note that the first requirement does not necessarily imply that the actual commutation frequency for the power devices in the converter is constant. The second requirement implies that the volt-second balance is maintained.

To facilitate the presentation, Fig. 6.1 shows two different realizations of an arbitrary FCF-RPWM scheme. The version shown in Fig. 6.1(a) assumes that three duty ratio have been calculated in some way (for example by the generalized PWM introduced in section 2.3.2) in order to impress a certain voltage on the load. The task of the FCF-RPWM unit is then to convert the values of d_a, d_b, and d_c, which arrive at constant rate, to the time-continuous switching functions q_a, q_b, and q_c needed to drive the power stage. The details of this mapping from duty ratios to switching functions depend on the FCF-RPWM technique in question.

(a)   (b)
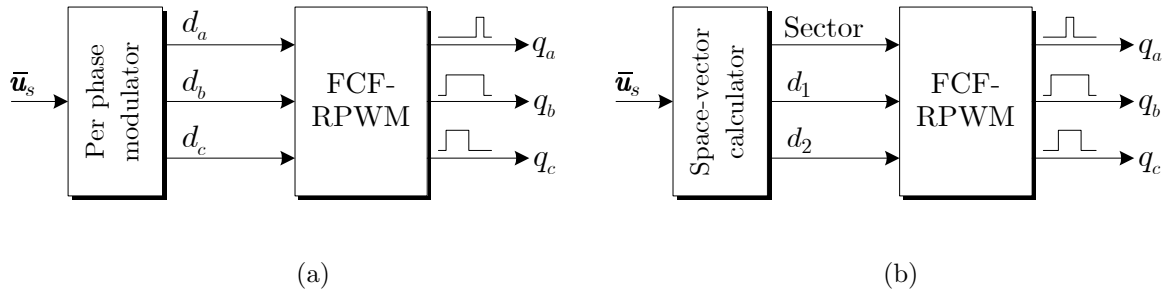
Figure 6.1 Two different kinds of input signals to a fixed carrier frequency random PWM unit, which outputs switching functions q_a, q_b, and q_c. The inputs are (a) duty ratios d_a, d_b, and d_c (the per-phase approach) or (b) duty ratios d_1 and d_2 for the two active vectors besides the sector to which the reference voltage vector belongs (the space-vector approach).

In Fig. 6.1(b), an alternative implementation is shown which is well suited for applications where the information for the wanted voltage is the output of a space-vector-based voltage calculator. Hence, in this case, it is assumed that the (normalized) duration d_1 and d_2 of the active vectors are known apart from the sector to which the reference voltage belongs. Both representations in Fig. 6.1 are used below.

6.2.2 Review of fixed carrier frequency random PWM methods

As elaborated in section 6.2.3, the requirements set forth above may be met in many different ways, but the literature dealing with FCF-RPWM has focused on the three variants introduced below. An detailed analysis may be found in section 6.3.

Random lead-lag modulation

The random lead-lag (RLL) pulse-position modulation technique is the oldest FCF-RPWM; it appeared for the first time in 1992 in a paper by Legowski et al. [1]. Later investigations of this scheme followed in [2–6]. The RLL method was used in Chapter 4 for dc/dc converters and Fig. 6.2(a) sketches how the principle applies equally well to three-phase converters. RLL modulation is normally used in conjunction with the per-phase approach shown in Fig. 6.1(a).

The RLL meets both requirements in section 6.2.1, because the average voltage produced by each leg depends only on the net duty ratio, and not on the pulse position.

Random zero-vector distribution

In the papers [7, 8], which originate from the patent [9] filed in 1996, Blasko suggested a hybrid pulse-width modulator (HPWM) based on space-vector modulation (SVM). The work reported in these references does not focus directly on random PWM, but rather the main objective is to show how the ripple in the load current depends on the zero-sequence voltage u_0 common to all three legs. In each half of the carrier, the value of u_0 is determined by the division of the total available time for zero vectors among vectors $\boldsymbol{v}_{000}$ and $\boldsymbol{v}_{111}$. In HPWM, these ratios x_1 and x_2 may attain any value in the

(a)

(b)

(c)
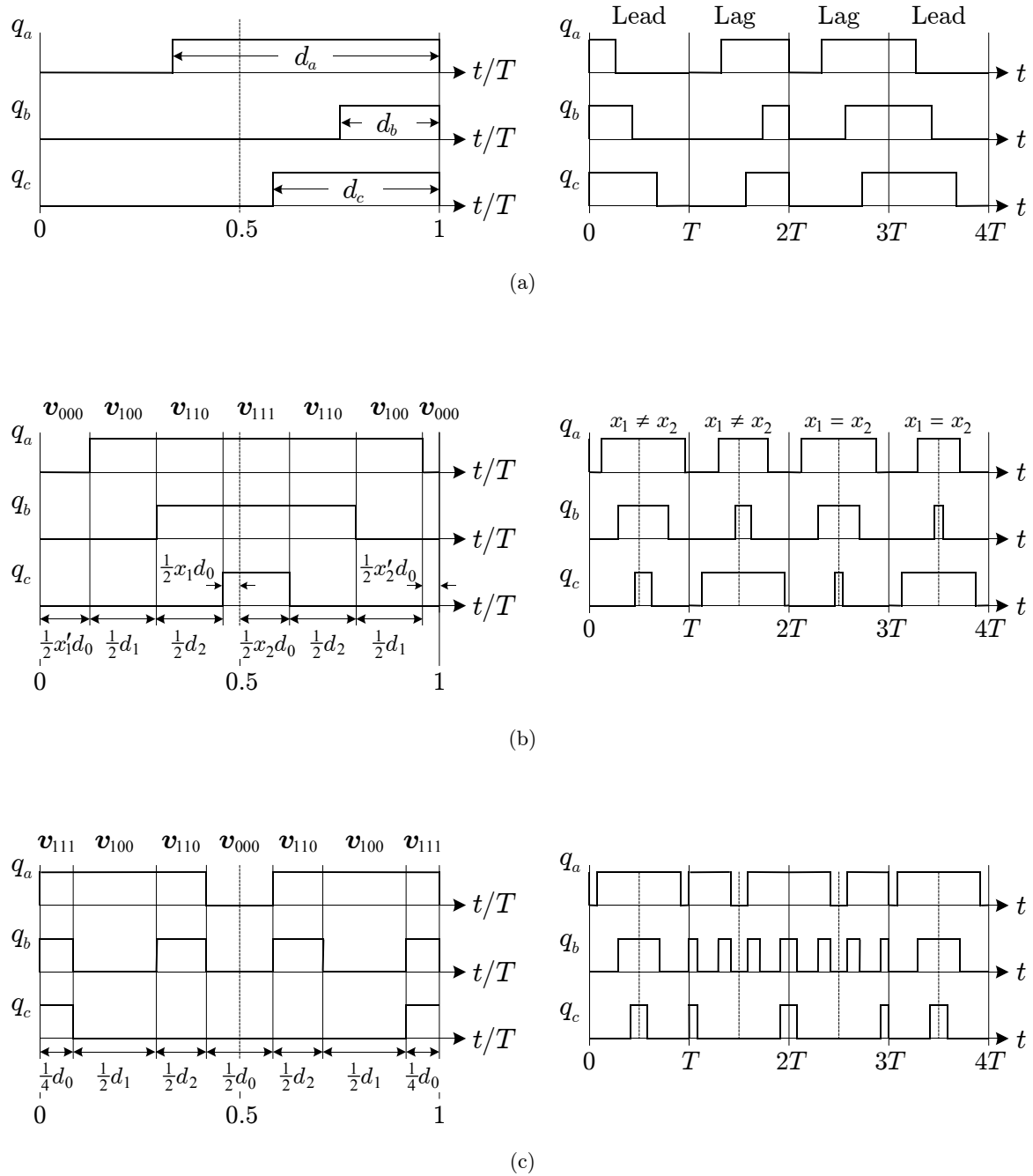
Figure 6.2 Overview of fixed carrier frequency random PWM schemes known from the literature. (a) Random lead-lag (RLL) modulation, (b) random zero-vector distribution (RZV), where $x_1' = (1 - x_1)$, $x_2' = (1 - x_2)$, $d_0 = 1 - (d_1 + d_2)$, and (c) random sequence selection (RSS).

$[0; 1]$ range in contrast to the original SVM where vectors $\boldsymbol{v}_{000}$ and $\boldsymbol{v}_{111}$ are applied for the same amount of time, i.e. $x_1 = x_2 = 0.5$ for SVM.

Now, by random selections of x_1 and x_2 in each half cycle of the full PWM period, randomization of the switching functions results as illustrated in Fig. 6.2(b). As an alternative to selecting x_1 and x_2 independently of each other, $x_1 = x_2$ may be used, i.e. the same division among vectors $\boldsymbol{v}_{000}$ and $\boldsymbol{v}_{111}$ is used in both halves of the PWM period. Sample switching functions are shown in the right-hand side of Fig. 6.2(b).

This scheme, which integrates very well with space-vector modulators, is designated random zero-vector distribution (RZV) in this thesis. Ideas very similar to those of Blasko may also be found in the independent patent [10] filed in 1995.

Random sequence selection

The last FCF-RPWM method found in the literature is due to Lai [11] in 1997. Almost identical ideas are used subsequently in [12–15] also. Again, modifications to the well-known SVM technique are made, and in this case a randomization of the sequence of switching states is used, hence the acronym RSS — random sequence selection. Denoting the two active vectors spanning the sector to which the reference voltage belongs by S_1 and S_2, the usual switching sequence is $S_0 \rightarrow S_1 \rightarrow S_2 \rightarrow S_7 \rightarrow S_2 \rightarrow S_1 \rightarrow S_0$, where S_0 and S_7 are the zero-state vectors. Now, [15] proposes a method that gives either 6, 10, or 11 commutations in each carrier period depending on the outcome of a random experiment. This unusual large number of commutations is achieved by swapping the order of applications of states; for example, the sequence $S_7 \rightarrow S_1 \rightarrow S_2 \rightarrow S_0 \rightarrow S_2 \rightarrow S_1 \rightarrow S_7$ (ten commutations) is one of the sequences suggested in [15]. Fig. 6.2(c) illustrates this particular choice.

Compared to the other FCF-RPWM schemes, a salient feature of the method advocated in [11–15] is that the number of commutations within each carrier period may exceed six.

6.2.3 Alternative fixed carrier frequency PWM schemes

Besides the three methods presented above, no other FCF-RPWM schemes for three-phase applications have been found in the literature. This is somewhat surprising given the large number of publications listed in Appendix B focusing on random PWM. Hence, in this subsection some alternative FCF-RPWM schemes are briefly described in order to show that the three known methods by no means constitute an exhaustive list of FCF-RPWM techniques.

Fundamental principles of existing FCF-RPWM schemes

Before continuing, it may be recalled that the average voltage produced by a converter leg depends on the duty ratio, i.e. the ratio of the on-time to the total duration of the PWM period, but not on the pulse position. Both the RLL and the RSS schemes are directly based on this property. Note that the switching functions produced by the RSS scheme may generate more than one on-state pulse in each PWM period, see Fig. 6.2(c), but still the volt-second balance is maintained, because the net duty ratio is kept at its reference value.

In contrary to RLL and RSS, the RZV technique (indirectly) randomizes the duty ratios of each leg by the addition of a random zero-sequence voltage, u_0. This is perfectly legitimate in three-wire, three-phase systems where the zero-sequence impedance is infinite. It may be noted that the work of [7–9] is very similar to the generalized pulse-width modulator discussed in Chapter 2.

Degrees of freedom in FCF-RPWM

At this point, it is clear that different routes may be followed to randomize a fixed carrier frequency pulse-width modulator for three-phase systems. From a theoretical point of view, the volt-second constraint may be met in different ways, including:

1. **Random pulse position**
   The pulse is shifted back and forth inasmuch as the average voltage remains unaffected. The only constraint is that a pulse must not extend beyond the boundaries of the carrier period in question.

2. **Addition of a random zero-sequence component**
   In systems without a neutral connection, the fundamental current is independent of the zero-sequence voltage u_0. Certainly, u_0 may be nondeterministic.

3. **Random sequence selection**
   This class stems from the RSS method, but further generalizations are possible: any reference duty ratio may be generated by one on-state pulse (the normal case), but the same net duty ratio may also be generated by the combined effect of two (or even more) on-state pulses (which may be randomly positioned) in a carrier period.

Also, these principles may be cascaded. For example, a random zero-sequence voltage may be added while, simultaneously, the pulse position of the resulting pulse is randomly selected.

On top on those principles relating to the actual method of randomization, attention must also be paid to how a particular scheme is implemented, i.e. how the probability density functions (pdf) are assigned. As elaborated in Chapter 5 many possibilities exist: some kind of memory can be built into the pdf (e.g. a Markov chain) or it may be a completely memory-less modulator, i.e. the present randomization is independent of the past. Also, the pdf can be either a discrete, continuous, or a mixed function of the independent variable (the outcome of the source of random numbers). Finally, some variants of FCF-RPWM may allow the randomization to be done individually on each leg as stated in Chapter 2.

Example of alternative FCF-RPWM schemes

The three methods (RLL, RZV, and RSS) presented in section 6.2.2 are all special cases of the general classification of FCF-RPWM given above. Inventing new FCF-RPWM schemes is not very difficult, but as elaborated below, simplicity and compatibility with existing hardware and software must be considered. Therefore, only two new FCF-RPWM methods are suggested here:

(a)

(b)
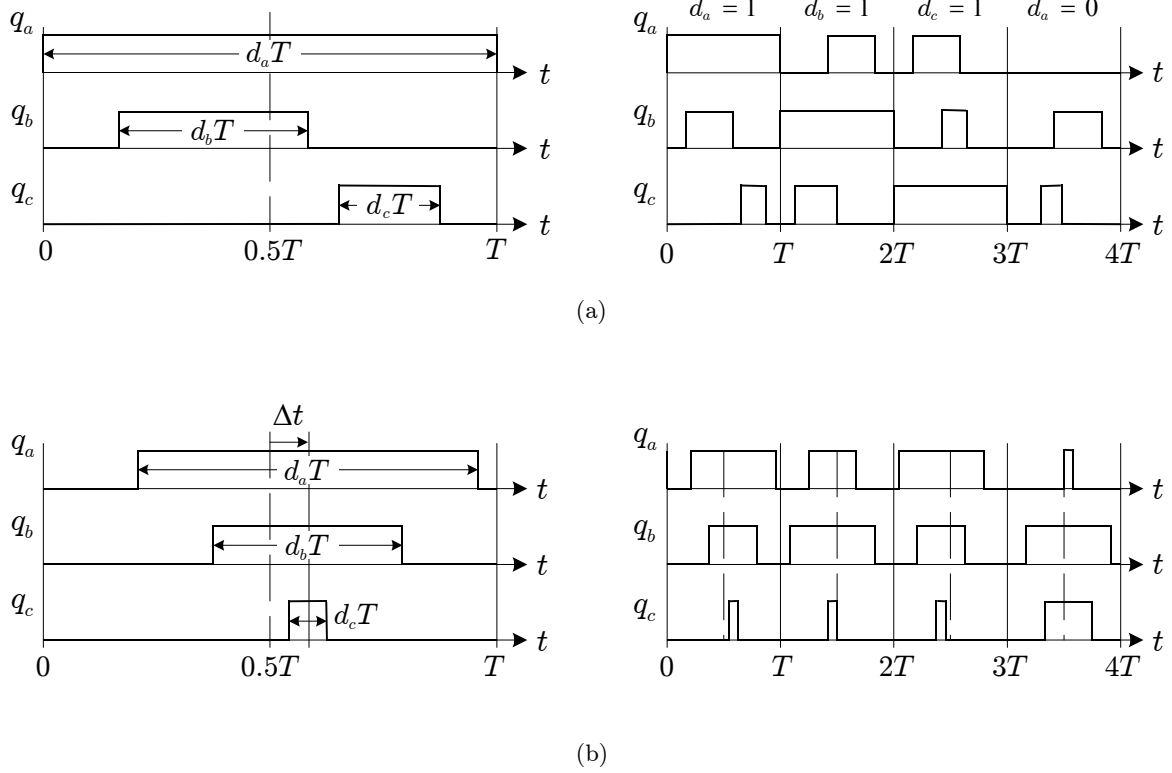
Figure 6.3 Two new fixed carrier frequency random PWM schemes. (a) Random pulse-position modulator for discontinuous PWM (RPP-DPWM) and (b) random center displacement (RCD) modulation.

Random pulse-position modulator for discontinuous PWM (RPP-DPWM)
This method is tailored towards discontinuous PWM where one leg always is clamped during the whole PWM period. As illustrated in Fig. 6.3(a), the pulse positions on the remaining two legs are randomized independently. Note that no zero-sequence voltage can be added. The only viable way to randomize a DPWM without introducing extra commutations is to modify the pulse positions in the two non-clamped legs.

Random center displacement (RCD)
Here, the three switching functions are kept mutually center-aligned, but the common pulse center is displaced by the amount Δt from the middle $\frac{1}{2}T$ of the period, see Fig. 6.3(b). To prevent overlap between consecutive PWM periods, it is required that $|\Delta t| \leq \frac{1}{2}(1 - d_{\max})T$, where $d_{\max} = \max\{d_a, d_b, d_c\}$. RCD is compatible with the per-phase modulator shown in Fig. 6.1(a).

The reasons for proposing an FCF-RPWM method for discontinuous PWM (DPWM) are twofold: First of all, DPWM has gained significant attention lately because, as stated already in Chapter 2, DPWM methods are attractive in the high modulation index range ($m > 0.6$ roughly), where the same current distortion can be achieved with reduced switching losses compared to standard PWM. Second, none of the existing FCF-RPWM methods are effective with respect to acoustic noise reduction in the high modulation index range, because here the duration of zero vectors is very short leaving

little room for randomization. An investigation of the potentials for the new RPP-DPWM sketched in Fig. 6.3(a) is left for future research, i.e. RPP-DPWM is not explored any further in this thesis.

The switching patterns generated by the RCD scheme resemble those of the RZV method, but only to some extent — it is not possible by clever selections of x_1 and x_2 to make the two schemes identical. Furthermore, RCD operates directly on the phase duty ratios, whereas RZV is a modified space-vector modulator. Finally, RCD does also partly resemble random carrier frequency (RCF) PWM, because the distance between two pulse centers in two neighboring PWM periods varies randomly like in RCF-PWM.

6.2.4 Constraints related to practical applicability

As demonstrated a great deal of ingenuity may be exercised in search for new FCF-RPWM schemes that (under ideal conditions) assure a correct volt-second balance on the macroscopic time scale. However, other issues related to the practical applicability do also need careful attention before a particular FCF-RPWM is of interest for non-academic purposes. The following issues are briefly discussed below:

- Acoustic noise

- Switching losses

- Implementation and real-time computations

- Controllability of the fundamental current

- Compliance with standard current detection methods

Acoustic noise

First of all, it must be recalled that if a certain FCF-RPWM scheme should be attractive for real applications, at least some alleviation of the acoustic noise[2] problem should be provided. This issue closely relates to the voltage spectrum.

Switching losses

In virtually all converters, the tolerable switching loss imposes an upper bound for the average commutation frequency of the power devices. In SVM, the number of commutations is $N = 6$ and for discontinuous PWM N equals 4, which makes it possible to reduce the switching losses by up to 50 percent [16].

Therefore, as a guideline it must be required that the average number of commutation in each PWM period does not exceed 6. Otherwise, additional switching losses are generated which cannot be accepted in most applications. Furthermore, the impact of blanking time on the average voltage gets more pronounced, if the power devices are turned on and off more than once in each carrier period.

---

[2]Alternatively, if random PWM is used to combat electro-magnetic interference, then a good FCF-RPWM should have a positive impact on e.g. the shielding/filtering needed to make a certain apparatus comply with relevant standards.

Implementation and real-time computations

The implementation is, of course, very specific to the chosen hardware and the available software development tools, but often switching functions are generated by special peripheral units dedicated to PWM generation. As an example, by means of the Siemens SAB 80C167 microcontroller[3], it is relatively easy to generate either symmetrical double-edge modulated or single-edge modulated PWM waveforms. Hence, implementations of SVM, RZV (for $x_1 = x_2$), and RLL are all straightforward. On the other hand, both the RCD and the RZV ($x_1 \neq x_2$) techniques and especially the RSS scheme all require considerably more computations in software to update the capture-compare unit in the 80C167 microcontroller, which must be used to generate these "non-standard" switching functions.

In brief, the more simple switching functions, the better. This suggests that FCF-RPWM schemes generating symmetrical switching functions are preferable, at least with respect to generation of PWM waveforms in hardware and to the computational burden in software. System level benefits like acoustic annoyance reduction may, however, outweigh the potential disadvantages associated with generating "non-standard" switching functions.

Controllability of the fundamental current

Complete predictability of the current is sacrificed in random PWM due to the non-deterministic behavior of the voltage fed to the load. Intuitively, this property is expected for the ripple component of the current since the ripple current depends heavily on the modulator, which has random properties on the microscopic time scale. However, since the average voltage is fully deterministic even in randomized modulators, it may also be expected that the random component of the pulse-width modulated voltage does not disturb the fundamental operation of the converter-load cascade. It turns out that this is not unconditionally true, i.e. in some cases the fundamental current component does actually depend on the modulator, even when the rule of volt-second balance is fulfilled.

A detailed analysis of this interaction between the modulator, the converter, and the load may be found in section 6.3 below. Without anticipating the conclusions of section 6.3, it may be stated that especially those FCF-RPWM methods that generate asymmetrical switching functions are problematic. In total, the risk of deteriorating the fundamental current component by injecting random properties into a modulator should not be overlooked.

Compliance with standard current detection methods

In those applications where the currents are fed back to a controller for control purposed, it is essential that an accurate measurement of the average current in each PWM period is available. This has been demonstrated in e.g. [17, 18], which analyze the consequences for the performance of a field-oriented ac drive when the current measurements are subjected to offset and scaling errors. Ref. [18] shows that such

---

[3]Refer to Appendix A for more information on this particular microcontroller, which is part of the unit controlling the power converters used in all experiments reported in this thesis.

(common) measurement errors impose low-order (first and second order) harmonics of the fundamental frequency in the developed torque. Such harmonics may induce speed fluctuations (particular during low-speed operation) besides accelerating fatigue of mechanical parts attached to the shaft [18].

Methods to acquire current feedback signals in ac drives have been treated in many publications including [19–22] and it must be required that good FCF-RPWM techniques are compatible with commonly used detection methods. To facilitate the discussion, it may be recalled that three main methods exist for the detection of average phase currents in standard voltage-source converters:

Asynchronous sampling of the instantaneous dc-link current
> The phase currents are reconstructed from samples of the dc-link current, i.e. only one current sensor is used. Since the original idea of [20] many refinements have been made. For example, it is shown in [21] how the correct values for the average phase currents can be calculated from only four samples of the dc-link current within each PWM period.

Synchronous sampling of the instantaneous phase currents
> All phase currents are sampled once simultaneously in each PWM period and furthermore, by letting this sampling instant coincide with the zero-crossing point of the ripple current, the per PWM period average current may be measured directly [19, 22]. Normally, this implies that the currents must be sampled in the center of the PWM period.

Sampling of locally averaged phase currents
> On each phase, the instantaneous current is integrated over the whole carrier period [19, 22]. In this way, the real average current in the carrier period is measured. The three integrators may be implemented in either analog hardware or by digital methods (hard- or software), if fast analog-to-digital converters are used.

No attempts are made to give a detailed discussion of the advantages and the disadvantages of the outlined methods with respect to measuring accuracy and operating area, circuit complexity, compliance with fault detection, noise immunity, and costs. However, as a rough performance indicator, it may be stated that the detection methods listed above are sorted in ascending order with respect to measuring accuracy, noise immunity, hardware complexity, and costs.

Rather, focus is put on the compliance of FCF-RPWM methods with the detection methods. The principle based on local averaging of the phase currents is compatible with all FCF-RPWM methods, because the averaging built into the detector itself will output the correct average value irrespective of the actual current waveforms.

The more commonly used method based on sampling the phase currents cannot in general, however, be guaranteed to work properly for arbitrary FCF-RPWM methods. The same holds for the method based on sampling the dc-link current. By using those two methods in their conventional forms, it is impossible to extract the average current in a PWM period directly from samples, unless the switching patterns preserve the symmetry known from e.g. the space-vector modulator of [23].

Concluding comments on applicability of FCF-RPWM

Having presented a lot of criteria that an FCF-RPWM technique must meet before it can be considered as a useful alternative to established deterministic PWM methods, an evaluation of the three existing schemes would be appropriate at this point. However, in order to facilitate this evaluation more information is needed, especially regarding the criteria relating to current quality and compliance with current sampling techniques. The analysis leading to this information is presented in the next section; refer to section 6.3.7 for a summary of the applicability of the RLL, RZV, and RSS schemes besides the new RCD method.

6.3 Impact of randomization on current waveforms

Current waveforms in converter-fed systems are investigated in this section in order to clarify which influence various FCF-RPWM techniques have on the controllability of the average current in a PWM period. A second objective is to analyze whether or not certain FCF-RPWM techniques comply with the current detection technique based on sampling the phase currents in the center of the carrier period. Once this information is available, a factual evaluation can be established of the random PWM schemes belonging to the FCF-RPWM class with respect to fundamental current quality and average current detectability.

In the first subsection below, the basis for the analysis is presented. This includes a method to separate voltages and currents into average and ripple components. Next, a series of current and voltage waveforms for the RLL, RZV, and RSS schemes is discussed. Afterwards, the impact of the modulation strategy on the average current is thoroughly investigated. To summarize the results obtained, an overview of the practical applicability of the analyzed FCF-RPWM methods is finally given using the criteria formulated in section 6.2.4.

6.3.1 Analysis of current waveforms

To facilitate the upcoming analysis, a number of concepts are defined in this subsection, including the current ripple space vector. Similar techniques have been applied in numerous publications, notably in [16, 23, 24] and many companion papers, although the main source of inspiration is the work of [7, 8].

The analysis assumes that the following complex-valued differential equation describes the relationship between the instantaneous converter voltage space vector $\boldsymbol{u}_s$ and the resulting current $\boldsymbol{i}_s$ flowing into the load:

$$\boldsymbol{u}_s = \boldsymbol{e} + L\frac{d\boldsymbol{i}_s}{dt} + r\boldsymbol{i}_s, \tag{6.1}$$

where $\boldsymbol{e}$ is the electromotive force (emf) of the load; L and r are the equivalent series inductance and resistance of the load, respectively. For the purpose of ripple-current analysis, this simple space-vector equation is sufficient to model e.g. mains-connected rectifiers and many three-phase ac machines like induction and synchronous motors[4].

---

[4]For induction machines L equals the transient inductance, r is the stator resistance, and $\boldsymbol{e}$ is the induced voltage due the rotor flux vector [25].

Provided that the duration T of the carrier is short compared to the time constant L/r, the impact of r may be ignored in (6.1). Then, the current trajectory may be obtained by adding the initial load current $\boldsymbol{i}_s(0)$ existing to $t = 0$ to the integral of the net voltage applied to L, i.e.

$$\boldsymbol{i}_s = \frac{1}{L} \int_0^t \left(\boldsymbol{u}_s - \boldsymbol{e}\right) d\tau + \boldsymbol{i}_s(0), \quad t \geq 0. \tag{6.2}$$

τ is a dummy variable of integration.

Separation into average and ripple components

During the PWM period T the voltages on the right-hand side of (6.2) may be divided into two parts:

1. average voltage components that remain constant during the whole interval T,

2. ripple voltage components that vary with time when t increases from the initial value 0 to the final value T.

The former part is responsible for the average behavior of the converter-load system on the macroscopic time scale. The ripple components relate to the switching operation on the microscopic (sub-carrier) time scale.

It is usually assumed that the back-emf $\boldsymbol{e}$ does not contain any ripple components, i.e. $\boldsymbol{e}$ is considered to be unaffected by the pulse-width synthesis of $\boldsymbol{u}_s$. The division of $\boldsymbol{u}_s$ into average $\bar{\boldsymbol{u}}_s$ and ripple $\tilde{\boldsymbol{u}}_s$ components is defined by

$$\boldsymbol{u}_s \triangleq \bar{\boldsymbol{u}}_s + \tilde{\boldsymbol{u}}_s, \tag{6.3}$$

where $\bar{\boldsymbol{u}}_s$ is constant in $t \in [0; T]$ and it is given by

$$\bar{\boldsymbol{u}}_s = \langle \boldsymbol{u}_s \rangle_T = \frac{1}{T} \int_0^T \boldsymbol{u}_s(\tau) \, d\tau. \tag{6.4}$$

The syntax $\langle \cdot \rangle_T$ is used to denote time averaging across the $[0; T]$ interval.

The effect of applying the average voltage $\bar{\boldsymbol{u}}_s$ to the load is a linear change of the average load current during the cycle of carrier. In order to distinguish the per-carrier period average current $\bar{\boldsymbol{i}}_s$ defined by

$$\bar{\boldsymbol{i}}_s \triangleq \langle \boldsymbol{i}_s \rangle_T = \frac{1}{T} \int_0^T \boldsymbol{i}_s(\tau) \, d\tau \tag{6.5}$$

from the instantaneous current caused by $\bar{\boldsymbol{u}}_s$, the notation $\underline{\boldsymbol{i}}_s$ is used for the latter:

$$\underline{\boldsymbol{i}}_s = \frac{1}{L} \left(\bar{\boldsymbol{u}}_s - \boldsymbol{e}\right) t + \boldsymbol{i}_s(0), \quad \text{for} \quad 0 \leq t \leq T. \tag{6.6}$$

Note that this current is a fictitious current introduced mainly for analytical purposes; in general, $\underline{\boldsymbol{i}}_s$ cannot be measured directly, although important exceptions utilized in section 6.3.6 exist.

To complete the division of (6.2) into average and ripple components, the ripple current $\tilde{\boldsymbol{i}}_s$ is defined by

$$\tilde{\boldsymbol{i}}_s = \frac{1}{L} \int_0^t \tilde{\boldsymbol{u}}_s(\tau)\, d\tau. \tag{6.7}$$

The instantaneous value of the total current $\boldsymbol{i}_s$ may now be found by adding $\underline{\boldsymbol{i}}_s$ and $\tilde{\boldsymbol{i}}_s$ given by (6.6) and (6.7), respectively.

Averages of ripple components

The ripple components of the voltage and current waveforms are given by $\tilde{\boldsymbol{u}}_s = \boldsymbol{u}_s - \bar{\boldsymbol{u}}_s$ and $\tilde{\boldsymbol{i}}_s = \boldsymbol{i}_s - \bar{\boldsymbol{i}}_s$. Here, it is important to emphasize that the per PWM period average of the ripple voltage $\tilde{\boldsymbol{u}}_s$ always equals zero, no matter what modulator is used:

$$\langle \tilde{\boldsymbol{u}}_s \rangle_T = \frac{1}{T} \int_0^T \tilde{\boldsymbol{u}}_s(\tau)\, d\tau = \boldsymbol{0}. \tag{6.8}$$

This result is a direct consequence of the definition (6.4) of the average voltage vector. Now, since $\langle \tilde{\boldsymbol{u}}_s \rangle_T = \boldsymbol{0}$, it follows from (6.7) that

$$\tilde{\boldsymbol{i}}_s(0) = \tilde{\boldsymbol{i}}_s(T) = \boldsymbol{0}. \tag{6.9}$$

This shows that the modulation process does not alter the final value of $\boldsymbol{i}_s$ at $t = T$, i.e. if samples of the $\boldsymbol{i}_s(t)$ waveform are taken at the end of each PWM period, correct values of the auxiliary current vector $\underline{\boldsymbol{i}}_s$ given in (6.6) can be obtained at this particular time instant. Furthermore, this is true irrespective of the modulation method used (which may be a randomized version of classic modulator); the only requirement is that the per-cycle average value of the ripple voltage equals zero, which — by definition — is fulfilled for all PWM schemes (random or not).

Definitions of average values of the ripple currents within the half-periods $[0; \frac{1}{2}T]$ and $[\frac{1}{2}T; T]$ become useful later. These averages are denoted by $\tilde{\boldsymbol{i}}_{s1}$ and $\tilde{\boldsymbol{i}}_{s2}$, where

$$\tilde{\boldsymbol{i}}_{s1} \triangleq \langle \tilde{\boldsymbol{i}}_s \rangle_{T/2} = \frac{2}{T} \int_0^{\frac{1}{2}T} \tilde{\boldsymbol{i}}_s(\tau)\, d\tau \tag{6.10}$$

and

$$\tilde{\boldsymbol{i}}_{s2} \triangleq \frac{2}{T} \int_{\frac{1}{2}T}^T \tilde{\boldsymbol{i}}_s(\tau)\, d\tau. \tag{6.11}$$

Also, the average current ripple $\tilde{\boldsymbol{i}}_{s12}$ defined over the whole carrier period becomes useful:

$$\tilde{\boldsymbol{i}}_{s12} \triangleq \langle \tilde{\boldsymbol{i}}_s \rangle_T = \tfrac{1}{2}(\tilde{\boldsymbol{i}}_{s1} + \tilde{\boldsymbol{i}}_{s2}). \tag{6.12}$$

Ideally, these currents should all equal the zero-current vector, $\boldsymbol{0}$. Finally, since $\boldsymbol{i}_s = \underline{\boldsymbol{i}}_s + \tilde{\boldsymbol{i}}_s$ it may be noted that

$$\bar{\boldsymbol{i}}_s = \langle \boldsymbol{i}_s \rangle_T = \langle \underline{\boldsymbol{i}}_s + \tilde{\boldsymbol{i}}_s \rangle_T = \langle \underline{\boldsymbol{i}}_s \rangle_T + \tilde{\boldsymbol{i}}_{s12}, \tag{6.13}$$

which is used in later subsections.

Example: Waveforms for classic space-vector modulation

It is instructive to study the trajectory of $\tilde{\boldsymbol{u}}_s$ and $\tilde{\boldsymbol{i}}_s$ for a well-known modulation technique before extending the analysis to FCF-RPWM. Using SVM as an example, sample waveforms are shown in Fig. 6.4 based on the framework presented above. Recall that phase a ripple components relate to the space vectors by $\tilde{i}_a = \mathcal{R}(\tilde{\boldsymbol{i}}_s)$ and $\tilde{u}_a = \mathcal{R}(\tilde{\boldsymbol{u}}_s)$ as defined in (2.5) on page 23. The average voltage vector $\bar{\boldsymbol{u}}_s$ is determined by the duty ratios of the active vectors: $d_1 = 0.2$ for $\boldsymbol{v}_{100}$ and $d_2 = 0.5$ for $\boldsymbol{v}_{110}$.

As shown in Fig. 6.4(a), the zero vectors are distributed uniformly as dictated by the SVM technique, i.e. $t_1 - t_0 = t_4 - t_3 = t_5 - t_4 = t_8 - t_7$. A number of additional observations can be made, including:

1. The path of the instantaneous value of $\tilde{\boldsymbol{i}}_s$ is constrained to move in directions parallel to one of the voltage vectors $-\bar{\boldsymbol{u}}_s$, $(\boldsymbol{v}_{110} - \bar{\boldsymbol{u}}_s)$, or $(\boldsymbol{v}_{110} - \bar{\boldsymbol{u}}_s)$, see Fig. 6.4(b).

2. $\tilde{\boldsymbol{i}}_s$ follows two rotational-symmetric triangular trajectories having one common side in the direction of reference voltage $\bar{\boldsymbol{u}}_s$. The two other sides are pair-wise parallel to the $(\boldsymbol{v}_{100} - \bar{\boldsymbol{u}}_s)$ and the $(\boldsymbol{v}_{110} - \bar{\boldsymbol{u}}_s)$ vectors.

3. The first triangle is spanned by $t_0 \to t_1 \to \cdots \to t_4$. At $t_4 = \frac{1}{2}T$, $\tilde{\boldsymbol{i}}_s$ has completed the first triangle; also, it may be seen that $\tilde{\boldsymbol{i}}_s(\frac{1}{2}T) = \mathbf{0}$. For $t_4 \to t_5 \to \cdots \to t_8$ the second triangle is traversed ending in the origin again for $t_8 = T$. Hence, the value of $\boldsymbol{i}_s(t)$ equals $\underline{\boldsymbol{i}}_s(t)$ for $t = \{0, \frac{1}{2}T, T\}$.

4. Fig. 6.4 illustrates that the average value of phase a ripple voltage and current both evaluate to zero across the carrier period. Furthermore, for the average ripple currents defined by (6.10) and (6.11), we have $\tilde{\boldsymbol{i}}_{s2} = -\tilde{\boldsymbol{i}}_{s1}$.

An important consequence of the last observation is that there is no contribution to the average current $\bar{\boldsymbol{i}}_s = \langle \boldsymbol{i}_s \rangle_T$ from the ripple current component $\tilde{\boldsymbol{i}}_s$. In other words, the results in Fig. 6.4 show that the microscopic current ripple $\tilde{\boldsymbol{i}}_s$ caused by a non-zero ripple voltage $\tilde{\boldsymbol{u}}_s$ does not have any influence on the change of the average current vector $\bar{\boldsymbol{i}}_s$.

At a first glance, this step-by-step procedure leading to this obvious conclusion seems superfluous, because, intuitively, one would expect that the net change of the average current can be determined from the mean voltage $\bar{\boldsymbol{u}}_s$, the back emf $\boldsymbol{e}$, the total inductance L, and the duration T of application of the mean voltage vector. Also, a very tempting conclusion to draw from this example is to state that the change of the average current during $[0; T]$ is independent of the ripple component $\tilde{\boldsymbol{u}}_s$ caused by the imperfect synthesis of $\bar{\boldsymbol{u}}_s$ by the pulse-width modulation process. As demonstrated shortly, however, this conclusion is not correct in all cases.

6.3.2   Waveforms for fixed carrier frequency random PWM

Based on the methodology outlined in the previous subsection, current ripple trajectories have been calculated for the RZV, RCD, and RLL fixed-frequency randomization methods. In all cases, the modulators produce exactly the same average voltage vector $\bar{\boldsymbol{u}}_s$ as in the SVM example in Fig. 6.4.
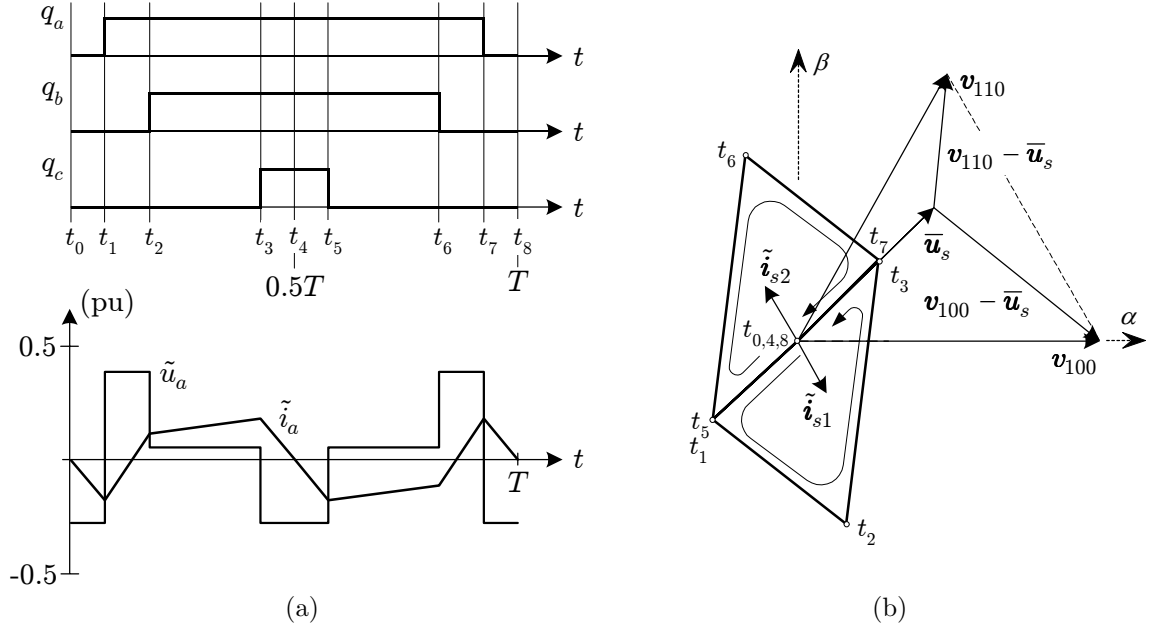
Figure 6.4 Space-vector modulation (center-aligned pulses and uniform distribution of the zero-vector times). (a) Converter switching functions q_a, q_b, and q_c (top) besides time-domain representations of phase a ripple voltage $\tilde{u}_a$ and current $\tilde{i}_a$ (bottom). (b) $\alpha\beta$ representation of the ripple current trajectory $\tilde{i}_s$ and voltage vectors during the interval $[0; T]$. The active duty ratios are $d_1 = 0.2$ for $\boldsymbol{v}_{100}$ and $d_2 = 0.5$ for $\boldsymbol{v}_{110}$.

Random zero-vector distribution

The results in Fig. 6.5 have been obtained for the random zero-vector distribution technique. In Fig. 6.5(a) the same division among $\boldsymbol{v}_{000}$ and $\boldsymbol{v}_{111}$ is used in both halves of T by letting $x_1 = x_2 = 0.2$; in Fig. 6.5(b), $x_1 = 0.2$ is used in the first half period and in $[\frac{1}{2}T; T]$, x_2 is set to 0.6.

In general, the trajectory of $\tilde{i}_s$ is still comprised by two triangles, but the path does not exhibit the same degree of symmetry as in the SVM case. The triangles slide along the direction of $\pm\bar{\boldsymbol{u}}_s$; the exact amount of the displacement depends on how the total time for zero vectors is divided among vectors $\boldsymbol{v}_{000}$ and $\boldsymbol{v}_{111}$. It may also be noted that the triangles in Fig. 6.4(b) and Fig. 6.5(a, b) all have identical shapes, but the offset from the origin of the $\alpha\beta$-plane varies. Furthermore, the figures show that at the time instants 0, $\frac{1}{2}T$, and T, the ripple current is $\tilde{i}_s(0) = \tilde{i}_s(\frac{1}{2}T) = \tilde{i}_s(T) = \mathbf{0}$ as in the SVM case, but on the microscopic time scale, the behavior differs considerably.

It is noteworthy that in the case shown in Fig. 6.5(a) the average ripple current vectors fulfill $\tilde{i}_{s2} = -\tilde{i}_{s1}$, but in Fig. 6.5(b) $\tilde{i}_{s2} \neq -\tilde{i}_{s1}$, which by way of (6.12) implies that $\tilde{i}_{s12} \neq 0$. This fact means that in the latter case, the ripple current (caused by $\tilde{\boldsymbol{u}}_s$ only) affects the value of the average current $\bar{i}_s$ defined in (6.5); the separation of the actual voltage $\boldsymbol{u}_s$ into average $\bar{\boldsymbol{u}}_s$ and ripple $\tilde{\boldsymbol{u}}_s$ components does not unconditionally imply that $\bar{i}_s$ can be determined without paying attention to $\tilde{\boldsymbol{u}}_s$. (However, the converse is true: $\bar{\boldsymbol{u}}_s$ does not contribute to $\tilde{i}_s$.) Similar analyses and conclusions have been reported in [7–9], which have spurred the author to subject other FCF-RPWM schemes to similar analyses.

(a)

(b)
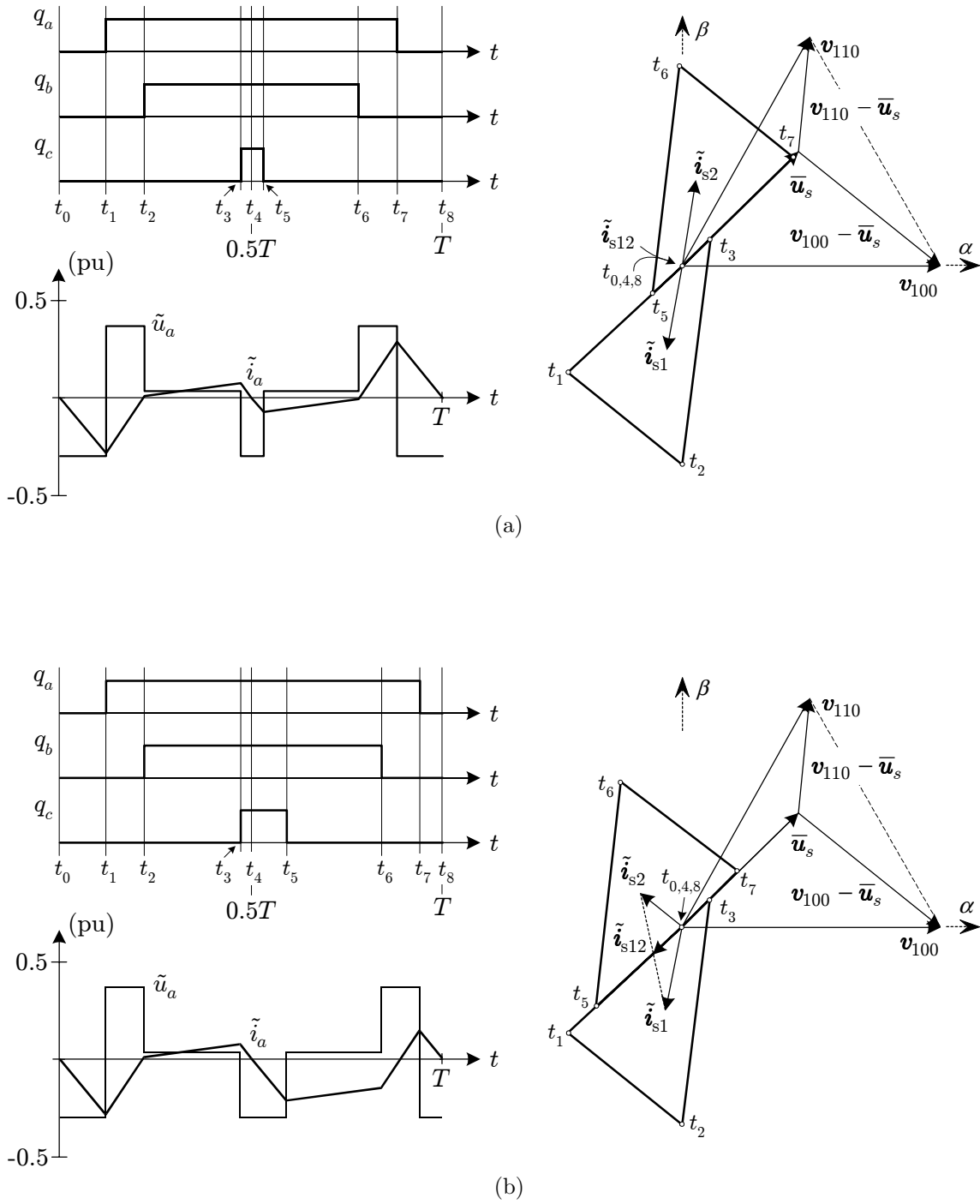
Figure 6.5 Waveforms for random zero-vector distribution (RZV) PWM using $d_1 = 0.2$ for $\boldsymbol{v}_{100}$ and $d_2 = 0.5$ for $\boldsymbol{v}_{110}$ as in Fig. 6.4. The division of the total zero-vector time among $\boldsymbol{v}_{000}$ and $\boldsymbol{v}_{111}$ is determined by (a) $x_1 = x_2 = 0.2$ and (b) $x_1 = 0.2$ and $x_2 = 0.6$. Both sub-figures show switching functions, time-domain waveforms for phase a ripple voltage $\tilde{u}_a$ and current $\tilde{i}_a$ besides the ripple current trajectory $\tilde{\boldsymbol{i}}_s$ in the $\alpha\beta$ reference frame during $0 \le t \le T$.

(a)

(b)
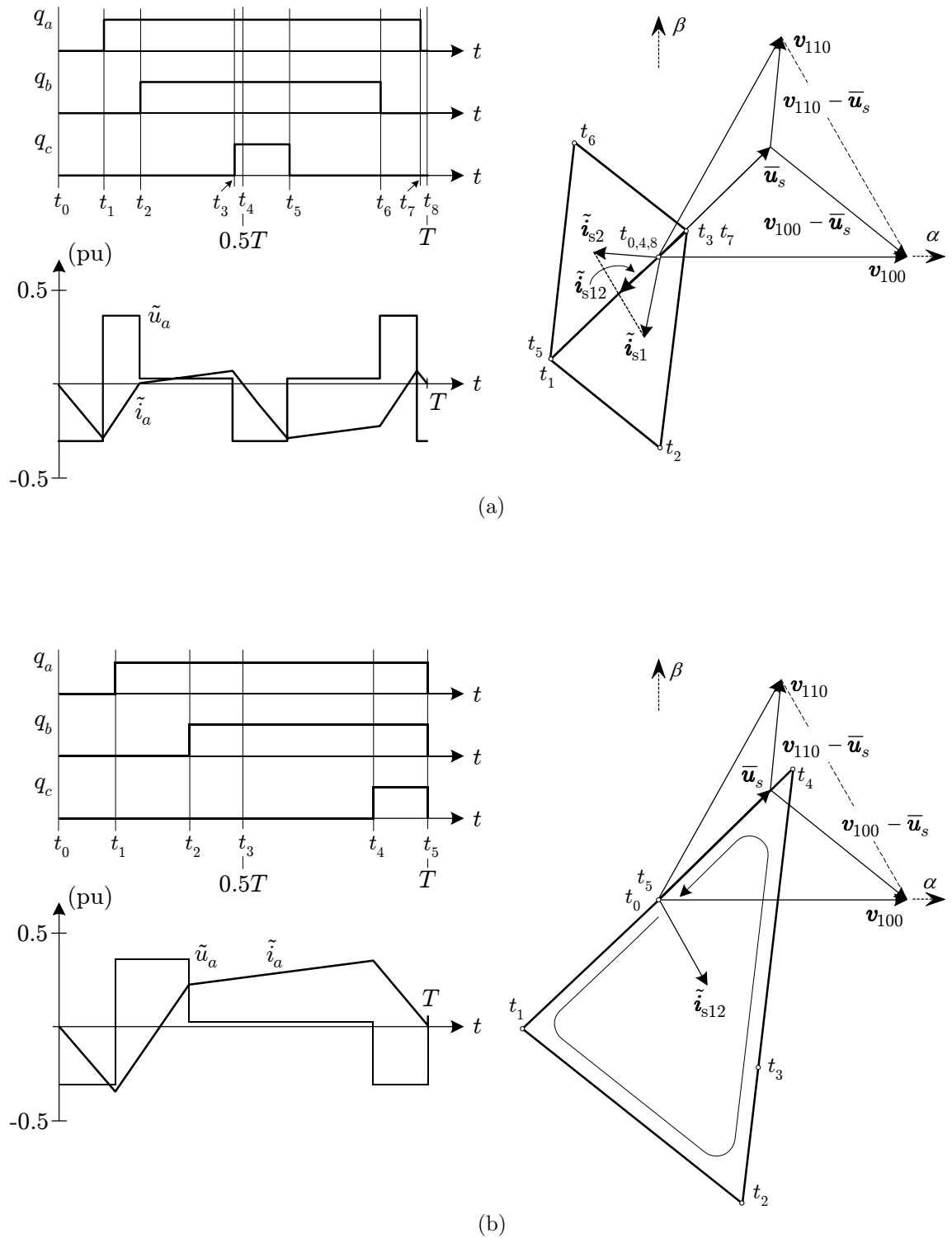
Figure 6.6 Waveforms for (a) random center displacement (RCD) using $x = 0.6$ and (b) random lead-lag (RLL) PWM. The reference voltage is determined by $d_1 = 0.2$ for $\boldsymbol{v}_{100}$ and $d_2 = 0.5$ for $\boldsymbol{v}_{110}$ as in Fig. 6.4. Both sub-figures show switching functions, time-domain waveforms for phase a ripple voltage $\tilde{u}_a$ and current $\tilde{i}_a$ besides the ripple current trajectory $\tilde{\boldsymbol{i}}_s$ in the $\alpha\beta$ reference frame during $0 \leq t \leq T$.

Random center displacement

Concerning the random center displacement method, Fig. 6.6(a) shows that the path for $\tilde{\boldsymbol{i}}_s$ is still comprised of two similar triangles as in the previous cases and also, each triangle has one side parallel to the direction for $\bar{\boldsymbol{u}}_s$. The time-domain phase a current ripple $\tilde{i}_a$ passes through zero at $t = \{0, \frac{1}{2}T, T\}$, but still the total average ripple current vector $\tilde{\boldsymbol{i}}_{s12}$ does not evaluate to zero, because $\tilde{\boldsymbol{i}}_{s2} \neq -\tilde{\boldsymbol{i}}_{s1}$ as for the RZV technique discussed above. Consequently, the value of $\bar{\boldsymbol{i}}_s$ cannot be determined directly from the mean voltage vector; the ripple voltage must be taken into account also.

Random lead-lag modulation

The lead-lag type of modulation produces the waveforms shown in Fig. 6.6(b). The characteristics are completely different from the FCF-RPWM methods commented above. Due to the poor locations of the zero-state vectors, the current ripple vector describes an area much larger than the other methods. Note also that the average ripple current $\tilde{\boldsymbol{i}}_{s12}$ does not belong to the path of $\boldsymbol{i}_s$. This (disadvantageous) property is unique to RLL. The highly asymmetrical switching functions cause a large average current ripple vector compared to the other investigated methods and again, the change of $\bar{\boldsymbol{i}}_s$ depends on both $\bar{\boldsymbol{u}}_s$ and $\tilde{\boldsymbol{u}}_s$.

6.3.3   Discussion of ripple current waveforms

It is somewhat puzzling to notice that despite that all the FCF-RPWM schemes investigated above produce the same average voltage space vector on a carrier-to-carrier basis, the change of the average current within each PWM period depends on the modulation method for those schemes that cause a non-zero value for $\tilde{\boldsymbol{i}}_{s12}$. Hence, the positioning (and the widths) of the pulses is important.

Using the random zero-vector distribution technique, the average currents supplied to the load are not distorted by the ripple voltage, provided that the values of x_1 and x_2 are the same in both half periods of the whole PWM period. Obviously, this is the expected behavior for a modulator. The other investigated random PWM techniques do not have this property — here, the ripple voltage $\tilde{\boldsymbol{u}}_s$ contributes to the average current, $\bar{\boldsymbol{i}}_s$.

One of the consequences of having $\bar{\boldsymbol{i}}_s$ dependent on $\tilde{\boldsymbol{u}}_s$ relates to the current quality in simple voltage-fed systems like motor drives, where open-loop voltage control is provided by some scalar controller. Here, the operation of the drive relies on the fact that the fundamental current component can be controlled directly by the commanded fundamental voltage component. It is well-known that blanking times, finite switching times, voltage drops across power devices, etc. may significantly deteriorate both the current quality and the stability limit in such systems. The usual remedy is to introduce some kind of compensation of the duty ratios so that the deviation between the commanded and actually produced average voltages becomes smaller than in the uncompensated case [26]. Now, the demonstrated influence of $\tilde{\boldsymbol{u}}_s$ on $\bar{\boldsymbol{i}}_s$ may be regarded as a problem of equal importance as e.g. blanking-time compensation; without a proper understanding of this phenomena, a good overall performance cannot be guaranteed.

Another case of practical concern relates to applications that include closed-loop control of the load currents. Typical examples include field-oriented control of ac machines or active three-phase mains rectifiers. The obtainable performance relies to a great extent on the quality of the feedback signals, i.e. on the current measurements. Hence, here it must be assured that true per-carrier period averages of the currents are available to the controller. In parallel to the measurement errors mentioned on page 165, any unattended deviation between actual average currents and the current supplied to the controller will have a negative impact on the performance of the system.

Final remarks

From the preceding observations and comments, a number of questions arise including:

1. Which mechanisms are responsible for that $\bar{\boldsymbol{i}}_s$ in some cases depends on $\tilde{\boldsymbol{u}}_s$, which, in turn, is caused by imperfect synthesis of the reference voltage?

2. What is the condition that $\bar{\boldsymbol{i}}_s$ is independent of the pulse-width modulation, i.e. when is the average ripple current vector $\tilde{\boldsymbol{i}}_{s12}$ equal to zero?

3. Are the correct average currents actually detected, if conventional methods are used to sample the phase currents?

4. It is possible to detect the correct average currents by modifications to the established sampling principles?

It should be emphasized that the posed questions are by no means limited to random PWM applications. Exactly the same problems may arise in systems using fully deterministic modulators.

6.3.4 Impact of the ripple voltage on the average current

In this subsection an answer is provided to the first question posed above. Also, a (partial) solution to the second problem is presented.

Expression for the average load current

An expression for the per-carrier cycle average $\bar{\boldsymbol{i}}_s$ of the load current is derived. The starting point is the definition given in (6.5) on page 168, which may be expanded by means of (6.2) into

$$\bar{\boldsymbol{i}}_s = \frac{1}{T} \int_0^T \left(\boldsymbol{i}_s(0) + \frac{1}{L} \int_0^t (\boldsymbol{u}_s - \boldsymbol{e}) \, d\tau \right) dt. \tag{6.14}$$

Next, the actual voltage $\boldsymbol{u}_s$ is rewritten in terms of $(\bar{\boldsymbol{u}}_s + \tilde{\boldsymbol{u}}_s)$ as given in (6.3). Then (6.14) becomes

$$\bar{\boldsymbol{i}}_s = \boldsymbol{i}_s(0) + \frac{1}{LT} \int_0^T \int_0^t \left((\bar{\boldsymbol{u}}_s - \boldsymbol{e}) + \tilde{\boldsymbol{u}}_s \right) d\tau \, dt. \tag{6.15}$$

Since the $(\bar{\boldsymbol{u}}_s - \boldsymbol{e})$ term is constant, a general expression for $\bar{\boldsymbol{i}}_s$ becomes

$$\bar{\boldsymbol{i}}_s = \boldsymbol{i}_s(0) + \underbrace{\frac{T}{2L}\big(\bar{\boldsymbol{u}}_s - \boldsymbol{e}\big)}_{\substack{\text{Average} \\ \text{behavior}}} + \underbrace{\frac{1}{LT} \int_0^T \int_0^t \tilde{\boldsymbol{u}}_s \, d\tau \, dt}_{\substack{\text{Caused by PWM} \\ \left(= \tilde{\boldsymbol{i}}_{s12} \text{ in (6.12)}\right)}} . \qquad (6.16)$$

The final expression for $\bar{\boldsymbol{i}}_s$ shows that this average may be regarded as a sum of three terms. The first term is due to the initial current $\boldsymbol{i}_s(0)$ and the second term shows the influence on $\bar{\boldsymbol{i}}_s$ of the average converter voltage $\bar{\boldsymbol{u}}_s$ and the load back emf $\boldsymbol{e}$. The last term is due to the ripple voltage $\tilde{\boldsymbol{u}}_s$, which is heavily correlated with the adopted method of modulation. In fact, the last term in (6.16) equals $\tilde{\boldsymbol{i}}_{s12}$ defined in (6.12). Hence, the dependency of $\bar{\boldsymbol{i}}_s$ on $\tilde{\boldsymbol{u}}_s$ has been established.

Discussion of mechanisms contributing to the average load current

For an ideal converter $\boldsymbol{u}_s$ does not contain any voltage ripple components, i.e. under idealized conditions, $\tilde{\boldsymbol{u}}_s(t) = 0$ for all values of t. This causes the double integral in (6.16) to evaluate to zero, i.e. the mean value of the real current becomes $\boldsymbol{i}_s(0) + (\bar{\boldsymbol{u}}_s - \boldsymbol{e})T/(2L)$. Clearly, it is a highly desirable property that the change of the average current only depends on the average value of the applied voltage.

In practical cases, $\tilde{\boldsymbol{u}}_s(t)$ will be non-zero for almost any value of t. This implies that the average load current depends on the pulse-width modulator, because it cannot be guaranteed that the double integral is zero. In fact, all we know from (6.8) is that $\langle \tilde{\boldsymbol{u}}_s \rangle_T = 0$, but this condition is insufficient information to conclude that the last term in (6.16) is zero also. It should be emphasized that any distortion of $\bar{\boldsymbol{i}}_s$ caused by $\tilde{\boldsymbol{u}}_s$ directly affects the fundamental component of the load current. This is a subtle, but nevertheless important phenomena to understand regarding the analysis and the practical use of pulse-width modulators.

The scenario outlined above demonstrates that a modulator must fulfill two requirements to comply with the obvious demand that the average load current should depend on $\bar{\boldsymbol{u}}_s$, $\boldsymbol{e}$, L, and T in each PWM period, but certainly not on the switching ripple voltage $\tilde{\boldsymbol{u}}_s$:

1. The average of the voltage vector defined by (6.4) should equal the reference voltage vector. "The generated volt-seconds must equal the reference volt-seconds."

2. The double integral given in (6.16) should evaluate to zero across T. A more or less idiomatic version is that "the average of the integral of the instantaneous ripple voltage vector must be zero."

Traditionally, only the first requirement is kept in mind, but the second requirement is completely overlooked during the design and the analysis of pulse-width modulated converters. In fact, no widespread acknowledgement nor understanding of the impact of $\tilde{\boldsymbol{u}}_s$ on $\bar{\boldsymbol{i}}_s$ seems to exist. In the literature, very little attention has been paid to the demonstrated dependency of $\bar{\boldsymbol{i}}_s$ on $\tilde{\boldsymbol{u}}_s$. As such, only the publications [7–9] have been found which deal with this problem to some extent.

Given the importance of having full control of the average current, it may be asked why this is so, but an exhaustive answer is hard to give. A major reason is probably the fact that the dependency of $\bar{\boldsymbol{i}}_s$ on $\tilde{\boldsymbol{u}}_s$ vanishes provided the switching functions are symmetrical about the center, $\frac{1}{2}T$. In this special case, the second requirement listed on the preceding page is fulfilled automatically, irrespective of the details of the particular modulation scheme used[5].

Symmetrical switching patterns are normally realized by means of regular (uniform) sampling PWM methods. Such methods were transferred from the communication to the power electronic community in 1975 by Bowes [27] as an alternative to the natural sampling technique (which gives asymmetrical switching waveforms) used in e.g. the classic paper [28]. Ref. [27] showed that the regular-sampled PWM techniques are superior to natural sampling techniques concerning harmonic distortion of the generated voltage. Today, variants of center-aligned PWM are widely used and, furthermore, symmetrical switching patterns are easy to generate thanks to the variety of digital controllers and dedicated PWM timers available from many vendors. In total, the symmetrical switching patterns normally adopted cause the mean current $\bar{\boldsymbol{i}}_s$ to become independent of the ripple voltage.

Before leaving the subject of symmetrical switching patterns, it should be noted that symmetry of the output voltages is hard to achieve in real converters, even if the pulse-width modulator outputs perfectly symmetrical switching functions. The reasons are the net effects of blanking time generators[6], minimum pulse-width filters (see also Appendix A), propagation delays in drivers, and the finite switching times of power devices. Hence, some degree of voltage skewing is almost inevitable; the voltages produced by the three legs in a standard converter will not be centered around $\frac{1}{2}T$ — in fact, it is very unlikely that the three pulsed voltage waveforms even have a common center at all. Then, by virtue of (6.16), $\tilde{\boldsymbol{i}}_{s12} \neq \boldsymbol{0}$, i.e. the average current $\bar{\boldsymbol{i}}_s$ has a parasitic component which is easily overlooked.

A clarification of the importance of the outlined phenomena on the average current is an interesting thread for future research, even for the center-aligned PWM methods extensively used today: Often, low-order harmonics of the fundamental current is said to be caused by blanking time and voltage drops across power devices, but one of the conclusions to be drawn from the analysis given here is that asymmetry has similar negative effects on the current quality. Volt-second balance is not a sufficient condition for having the average (macroscopic) behavior decoupled from the switching (microscopic) actions; the instantaneous ripple voltage must be taken into account.

---

[5]That symmetry of the switching functions around $\frac{1}{2}T$ is a sufficient condition to nullify $\tilde{\boldsymbol{i}}_{s12}$ defined by the double integral in (6.16) may be proved straightforwardly. First, note that $\tilde{\boldsymbol{u}}_s(T-t) = \tilde{\boldsymbol{u}}_s(t)$ for $0 \leq t \leq T$, i.e. $\tilde{\boldsymbol{u}}_s(t)$ is an even function. Then, the inner integral in (6.16) defined by $\Psi(t) \triangleq \int_0^t \tilde{\boldsymbol{u}}_s(\tau)\,d\tau$ fulfills $\Psi(T-t) = -\Psi(t)$, i.e. $\Psi(t)$ is an odd function. Also, $\Psi(\frac{1}{2}T) = \boldsymbol{0}$, because $\langle \tilde{\boldsymbol{u}}_s \rangle_T = \boldsymbol{0}$ and $\tilde{\boldsymbol{u}}_s$ is known to be even. Integrating $\Psi(t)$ over T yields the result that the total value of the double integral in (6.16) is zero. Note, however, that this does not prove that symmetry is a necessary condition to get $\bar{\boldsymbol{i}}_s$ independent of $\tilde{\boldsymbol{u}}_s$.

[6]In those cases where the insertion of blanking time is made after the actual pulse-width modulator (like shown in Fig. A.3 in Appendix A for the set-up used in this project), skewing is inevitable. A much better approach is to embed the blanking time generation into the PWM hardware (timer and comparators) itself, because this allows the symmetry to be preserved. Such a solution is provided by e.g. the motion controller ADMC401 produced by Analog Devices [29].

To summarize, (6.16) answers the first question posed on page 175. It is more difficult to give an exhaustive answer to second question, but at least it has been shown that if the switching functions are symmetrical around the middle of the PWM period, then $\tilde{\boldsymbol{i}}_{s12} = \boldsymbol{0}$. Therefore, provided the converter is ideal, $\bar{\boldsymbol{i}}_s$ is indeed independent of $\tilde{\boldsymbol{u}}_s$, which is a special case of extraordinary importance. If asymmetrical switching functions are generated by a modulator, it must be expected that $\tilde{\boldsymbol{i}}_{s12} \neq \boldsymbol{0}$ although this has not been rigorously proved[7]. As a consequence, the deliberate use of asymmetrical switching patterns in [21, 30, 31] intended for alleviation of problems with indirect phase current detection by measuring the dc-link current is likely to need revisions, because the modified switching patterns distort the current waveforms to be measured.

6.3.5   Compliance with current sampling techniques

As stated in section 6.2.4, accurate acquisition of load currents is important for feedback control purposes. In this subsection it is demonstrated that the popular method to detect the per-cycle average phase current by sampling the current in the middle of the carrier period should be used with a great deal of care, at least for some of FCF-RPWM variants.

Settings for the modulator and load parameters

For each of the methods RZV, RCD, and RLL the actual current $i_a(t)$ for phase a has been obtained by a simulation and afterwards, the per carrier period average current and the current sampled in the middle of each PWM period have been calculated. From those currents denoted by $\langle i_a \rangle_T$ and $i_a(\frac{1}{2}T)$, respectively, the difference $\langle i_a \rangle_T - i_a(\frac{1}{2}T)$ has also been calculated. A uniform probability density function has been used in all examples. For example, the x_1 factor for the RZV scheme can attain any value between zero and one.

The investigation is based on the settings shown in Table 6.1 for the deterministic part of the modulator and for the load. Furthermore, the base current defined as $I_B \triangleq U_{dc}/(8L)T$ becomes 2.7 A.

Discussion of results

Results for the two variants of the RZV technique are shown in Fig. 6.7. The graphs in the right column in Fig. 6.7 have been obtained for the special case where the same value of the random factor is used in both half periods ($x_2 = x_1$). Clearly, the randomization does not ruin the principle of obtaining the average current directly by sampling in the middle of each PWM period. Note also in Fig. 6.7(e) that $\langle i_a \rangle_T$ approximates a sine wave as expected.

---

[7]A mathematical proof for that symmetry is a necessary condition for having $\tilde{\boldsymbol{i}}_{s12} = \boldsymbol{0}$ in three-phase converters has not been found despite several attempts. However, for a single-phase converter having an inductive load connected between the output of a standard converter leg and the midpoint of the dc link, such a proof has been established. Of course, this result cannot be generalized to three-phase converters, but on the other hand, no counter examples have been found for three-phase applications.

Load inductance, L	Fundamental frequency, f_1	Carrier period, T	dc-link voltage, U_{dc}	Modulation index, m
25 mH	40 Hz	1 ms	540 V	0.64

Table 6.1 Settings used for evaluation of the compliance of different FCF-RPWM modulators with current sampling techniques. The back emf $\boldsymbol{e}$ is lagging the fundamental component of the converter voltage by 10 electrical degrees and $\boldsymbol{e}$ has the same magnitude as the fundamental of $\boldsymbol{u}_s$.

The situation is worse for the RZV technique using different values for x_1 and x_2, see further in Fig. 6.7(a–c). Now, a non-zero error between $\langle i_a \rangle_T$ and the sampled current $i_a(\frac{1}{2}T)$ exists, i.e. this particular FCF-RPWM method is not compatible with the standard current sampling technique. Furthermore, it may be noted from Fig. 6.7(b) that the $i_a(\frac{1}{2}T)$ waveform is unaffected by the randomization (compare to $i_a(\frac{1}{2}T)$ in Fig. 6.7(e)), i.e. the instantaneous current in the middle of all PWM periods is independent[8] of the randomization. However, as stated earlier, it must be emphasized that the actual average current $\langle i_a \rangle_T$ is affected; this is demonstrated by the waveform for $\langle i_a \rangle_T$ in Fig. 6.7(b), which clearly has an unwanted component.

Similar problems can be observed in Fig. 6.8 on page 181 for the RCD and the RLL techniques. The waveforms for $\langle i_a \rangle_T$ do not track a sine wave in an ideal manner, which again verifies that details of the modulator are important for the fundamental current component. Also, the larger current ripple associated with RLL can clearly be seen in Fig. 6.8(d). Note that the difference between $\langle i_a \rangle_T$ and $i_a(\frac{1}{2}T)$ is much smaller for the RCD method compared to RLL, but — more interestingly — also compared to the RZV scheme using $x_1 \neq x_2$ (Fig. 6.7(c)).

Final remarks

In summary, it may be stated that if a modulator generates asymmetric switching patterns with respect to the center of the carrier period, then it is impossible to detect the average current by a single sample at $t = \frac{1}{2}T$. Although no plots are included here, simulations have also shown that the detection method based on sampling the dc-link current in the middle of the active vectors exhibits the same limitations; the work of [21] cannot be applied to modulators producing asymmetrical switching functions.

As stipulated in earlier sections, the simulations also verify that the fundamental current is distorted[9] by the modulator in those cases where asymmetrical switching functions are used to control the converter. As a result, open-loop voltage control is problematic as already mentioned on page 174.

---

[8]The proof is as follows: Starting from $\boldsymbol{i}_s(\frac{1}{2}T) = \boldsymbol{i}_s(0) + \int_0^{T/2}(\boldsymbol{u}_s - \boldsymbol{e})\,d\tau$, it follows immediately that $\boldsymbol{i}_s(\frac{1}{2}T) = \boldsymbol{i}_s(0) + T/(2L)(\bar{\boldsymbol{u}}_s - \boldsymbol{e})$, which is independent of the randomization. Furthermore, as a consequence of (6.9) and (6.6), we also see that $\boldsymbol{i}_s(T) = \boldsymbol{i}_s(0) + T/L(\bar{\boldsymbol{u}}_s - \boldsymbol{e})$. Using this relationship, another interesting identity appears: $\boldsymbol{i}_s(\frac{1}{2}T) = \frac{1}{2}\big(\boldsymbol{i}_s(0) + \boldsymbol{i}_s(T)\big)$, which is valid for any RZV method irrespective of the values for x_1 and x_2.

[9]Note that the distortion is caused directly by the asymmetry of the switching functions. Whether this asymmetry is intentional as in e.g. the RLL technique or it is the result of effects like blanking time etc. is immaterial. See also the comment on page 177 regarding natural and regular sampling PWM.
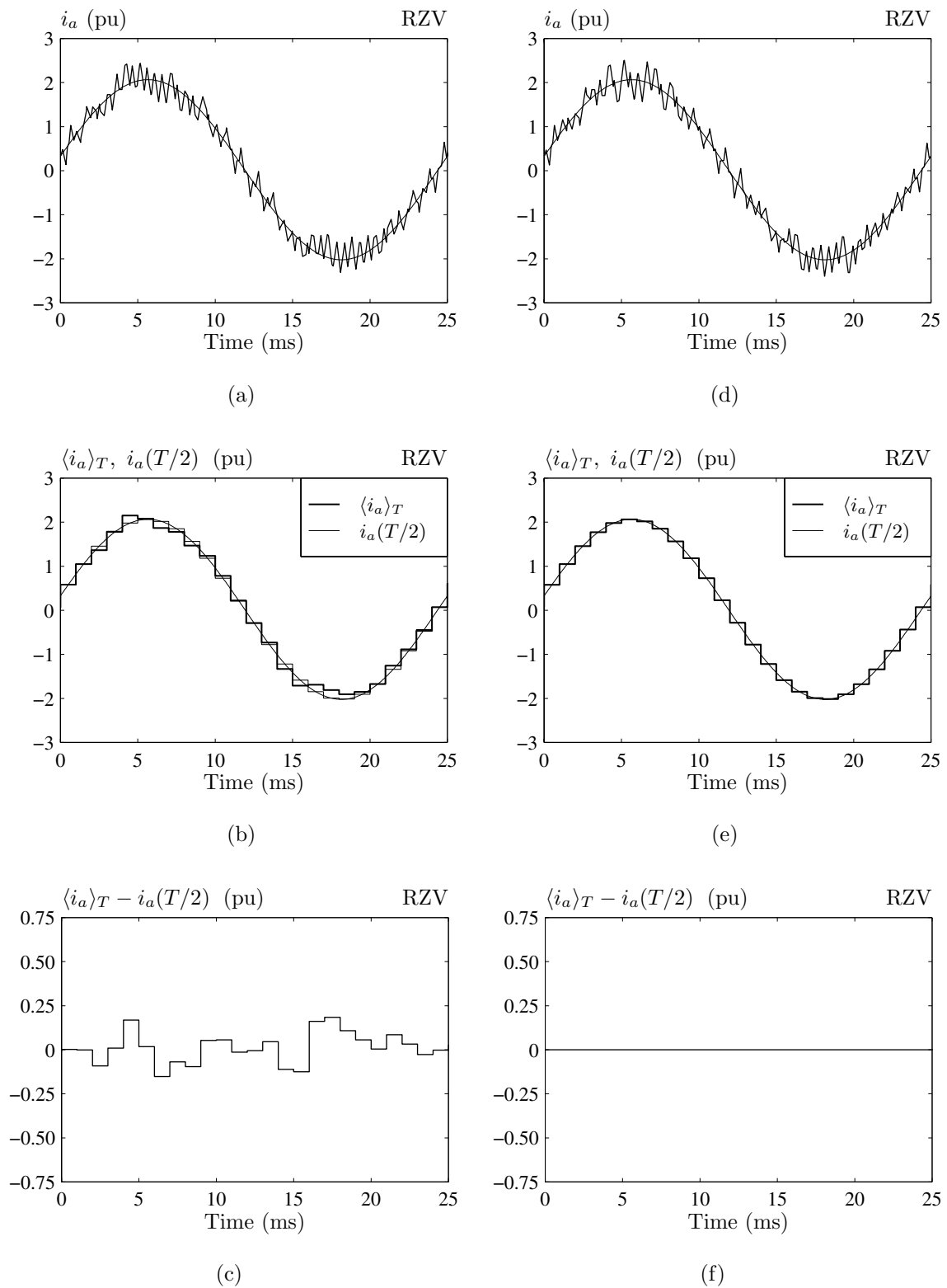
Figure 6.7 Simulation of current waveforms using the settings in Table 6.1 for the random zero-vector distribution technique. (left column): x_1 and x_2 are independent and (right column): x_1 and x_2 are equal in each half period. (a, d) actual phase a currents, (b, e) per-cycle average and current sampled in the middle of each carrier period, and (c, f) difference between average and sampled current. The sine wave is the ideal fundamental current component.
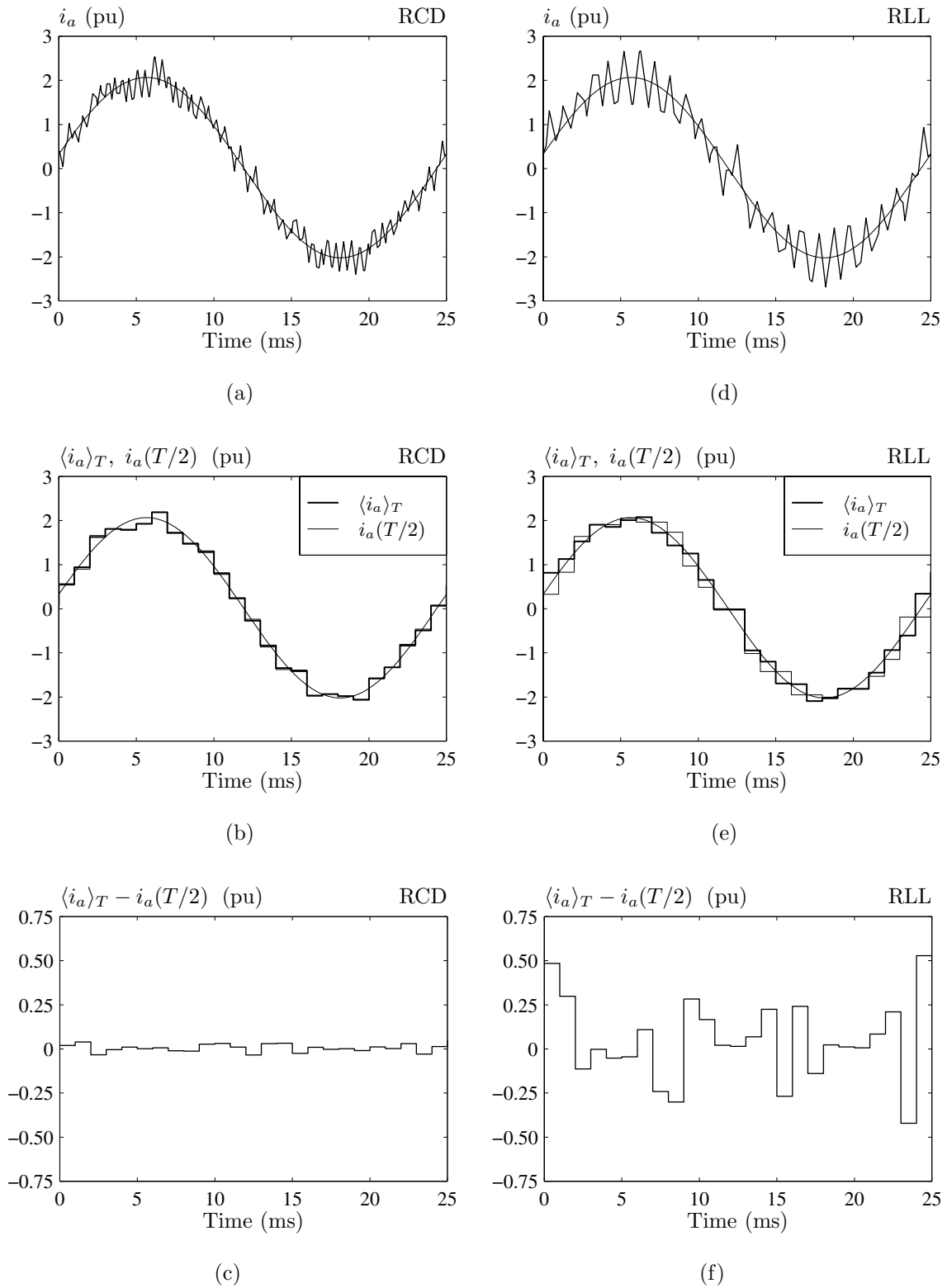
Figure 6.8 Simulation of current waveforms using the settings in Table 6.1 for (left column): random center displacement and (right column): random lead-lag modulation. (a, d) actual phase a currents, (b, e) per-cycle average and current sampled in the middle of each carrier period, and (c, f) difference between average and sampled current. The sine wave is the ideal fundamental current component.

6.3.6   New current sampling technique applicable for quasi-symmetrical switching functions

Except for the RZV technique using equal divisions of the zero vectors $\boldsymbol{v}_{000}$ and $\boldsymbol{v}_{111}$ in both halves of the carrier period, it has been demonstrated that it is impossible to detect the real averages of the phase currents by using known sampling techniques. It may be tempting to ignore those errors by letting $\langle i_a \rangle_T = i_a(\frac{1}{2}T)$, etc., but it should be recalled that errors due to an inaccurate current detector cause low-order torque distortion in AC motors as mentioned in section 6.2.4 or pulsating power components in three-phase active rectifiers.

Therefore, a new and simple current sampling technique has been developed which is capable of detecting the proper average phase current by using only two samples (per phase) of the current in each PWM period. In this way, it is not strictly necessary to use the more complex method based on detecting the integral of the current as discussed earlier in section 6.2.4.

The new sampling strategy is applicable for both the RZV scheme with $x_1 \neq x_2$ and for the RCD technique. These FCF-RPWM techniques both generate switching functions which may be called "quasi-symmetrical" meaning that the three on-state pulses have a common center, but this center needs not coincide with the midpoint of the carrier period. Before giving the details of the new sampling strategy, it may be noted that no attempts have been made to improve the current sampling technique for the RLL scheme, because this particular FCF-RPWM method is not considered as a strong candidate for practical applications at all.

Expression for the average current using RZV modulation

When a converter is controlled by an RZV modulator, the instantaneous current can be found by dividing the carrier period into seven sub intervals and then use (6.2) on each segment. Following this route, the piece-wise linear behavior of $\boldsymbol{i}_s$ may be calculated, but this cumbersome expression for $\boldsymbol{i}_s$ is omitted here for brevity.

Instead, Fig. 6.9(b) shows an example of the trajectory for $\boldsymbol{i}_s$ in the $\alpha\beta$-reference frame and Fig. 6.9(c) shows the corresponding projections of $\boldsymbol{i}_s$ on the a, b, and c axes. Notice that both the initial current $\boldsymbol{i}_s(0)$ and the back-emf $\boldsymbol{e}$ have non-zero values in those plots and that x_1 differs from x_2.

Based on the (omitted) piece-wise linear expression for $\boldsymbol{i}_s$, the per-carrier period average $\bar{\boldsymbol{i}}_s$ may be determined as

$$\bar{\boldsymbol{i}}_s = \langle \boldsymbol{i}_s \rangle_T = \boldsymbol{i}_s(0) + \frac{T}{2L}\big(\bar{\boldsymbol{u}}_s - \boldsymbol{e}\big) - \frac{T}{4L}d_0(x_2 - x_1)\bar{\boldsymbol{u}}_s, \qquad (6.17)$$

where $d_0 = 1 - (d_1 + d_2)$ is the normalized duration of the zero vectors. The quantity $T_{sh} \triangleq \frac{1}{4}d_0(x_2 - x_1)T$ is the amount by which the common pulse center is offset from the midpoint $\frac{1}{2}T$ as shown in Fig. 6.9(a). Using T_{sh}, (6.17) may be rewritten as

$$\bar{\boldsymbol{i}}_s = \boldsymbol{i}_s(0) + \frac{T}{2L}\big(\bar{\boldsymbol{u}}_s - \boldsymbol{e}\big) - \frac{T_{sh}}{L}\bar{\boldsymbol{u}}_s. \qquad (6.18)$$

This expression for $\bar{\boldsymbol{i}}_s$ should be compared to (6.16) term by term. In this way it may

(a)

(b)

(c)
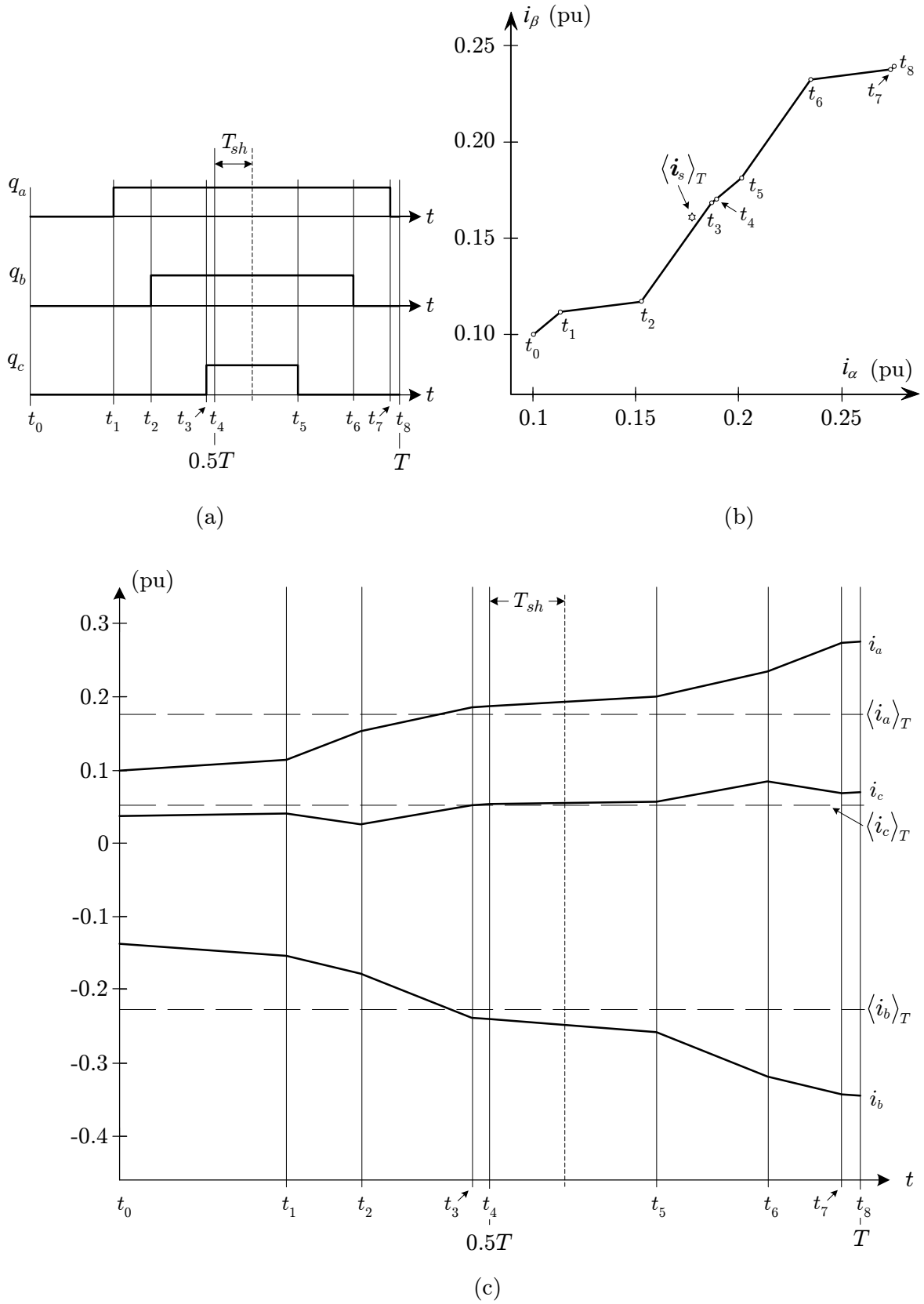
Figure 6.9 Waveforms using RZV modulation including non-zero values for the initial current and for the load back emf. $x_1 = 0.1$ and $x_2 = 0.9$ is used. (a) Switching functions, (b) trajectory for $\boldsymbol{i}_s$ in the $\alpha\beta$ plane (the hexagram locates $\langle \boldsymbol{i}_s \rangle_T$), and (c) phase current time-domain waveforms.

be seen that for RZV modulation

$$\tilde{\boldsymbol{i}}_{s12} = -\frac{T_{sh}}{L}\bar{\boldsymbol{u}}_s, \tag{6.19}$$

which can be found in [8] also. Hence (6.19) shows that the average of the ripple current $\tilde{\boldsymbol{i}}_{s12}$ depends on the mean voltage $\bar{\boldsymbol{u}}_s$ produced by the converter and on the offset T_{sh}.

The value for $\boldsymbol{i}_s(t)$ at $t = T$ is independent of the ripple voltage caused by the pulse-width modulation. This follows directly from (6.9), because this equation states that the ripple component of the current vanished equals zero for $t = T$. Hence, by using (6.6) $\boldsymbol{i}_s(T)$ becomes

$$\boldsymbol{i}_s(T) = \underline{\boldsymbol{i}}_s(T) = \boldsymbol{i}_s(0) + \frac{T}{L}\big(\bar{\boldsymbol{u}}_s - \boldsymbol{e}\big). \tag{6.20}$$

Isolating $(\bar{\boldsymbol{u}}_s - \boldsymbol{e})$ from (6.20) and inserting the result into (6.18) gives

$$\begin{aligned}
\bar{\boldsymbol{i}}_s &= \boldsymbol{i}_s(0) + \frac{1}{2}\big(\boldsymbol{i}_s(T) - \boldsymbol{i}_s(0)\big) - \frac{T_{sh}}{L}\bar{\boldsymbol{u}}_s \\
&= \frac{1}{2}\big(\boldsymbol{i}_s(0) + \boldsymbol{i}_s(T)\big) - \frac{T_{sh}}{L}\bar{\boldsymbol{u}}_s = \frac{1}{2}\big(\boldsymbol{i}_s(0) + \boldsymbol{i}_s(T)\big) + \tilde{\boldsymbol{i}}_{s12}.
\end{aligned} \tag{6.21}$$

Therefore, to get the correct value for $\bar{\boldsymbol{i}}_s$, knowledge of $\boldsymbol{i}_s(0)$, $\boldsymbol{i}_s(T)$, and $\tilde{\boldsymbol{i}}_{s12}$ is needed in the general case where x_1 and x_2 may have different values. If $\boldsymbol{i}_s(t)$ is sampled at $t = 0$ and $t = T$ only[10], an incorrect value for $\bar{\boldsymbol{i}}_s$ is obtained, i.e. the standard sampling method fails.

New current sampling technique for the RZV scheme

In order to fix the problems with determining the value for $\bar{\boldsymbol{i}}_s$ in the $x_1 \neq x_2$ case, a new sampling strategy has been developed which takes the $\tilde{\boldsymbol{i}}_{s12}$ term in (6.21) into account. Since only the total current $\boldsymbol{i}_s = \underline{\boldsymbol{i}}_s + \tilde{\boldsymbol{i}}_s$ is available for detection, it is impossible to measure the ripple component directly. (If the waveform for $\tilde{\boldsymbol{i}}_s$ was available, $\tilde{\boldsymbol{i}}_{s12}$ could be determined by sampling $\tilde{\boldsymbol{i}}_s(t)$ at $t = \frac{1}{2}T + T_{sh}$.) Instead, by noting that $\tilde{\boldsymbol{i}}_s = \boldsymbol{i}_s - \underline{\boldsymbol{i}}_s$ it is, nevertheless, possible to find $\tilde{\boldsymbol{i}}_{s12}$ by using

$$\underline{\boldsymbol{i}}_s = \boldsymbol{i}_s(0) + \frac{t}{T}\big(\boldsymbol{i}_s(T) - \boldsymbol{i}_s(0)\big), \tag{6.22}$$

which can be evaluated for any value of t in $[0; T]$ once values for $\boldsymbol{i}_s(T)$ and $\boldsymbol{i}_s(0)$ are known. Hence,

$$\underline{\boldsymbol{i}}_s(\tfrac{1}{2}T + T_{sh}) = \boldsymbol{i}_s(0) + \frac{\frac{1}{2}T + T_{sh}}{T}\big(\boldsymbol{i}_s(T) - \boldsymbol{i}_s(0)\big) \tag{6.23}$$

and therefore,

$$\begin{aligned}
\tilde{\boldsymbol{i}}_{s12} = \tilde{\boldsymbol{i}}_s(\tfrac{1}{2}T + T_{sh}) &= \boldsymbol{i}_s(\tfrac{1}{2}T + T_{sh}) - \underline{\boldsymbol{i}}_s(\tfrac{1}{2}T + T_{sh}) \\
&= \boldsymbol{i}_s(\tfrac{1}{2}T + T_{sh}) - \boldsymbol{i}_s(0) - \frac{\frac{1}{2}T + T_{sh}}{T}\big(\boldsymbol{i}_s(T) - \boldsymbol{i}_s(0)\big)
\end{aligned} \tag{6.24}$$

---

[10]Alternatively, a single sample taken at $t = \frac{1}{2}T$ may be used since $\boldsymbol{i}_s(0) + \boldsymbol{i}_s(T) = 2\boldsymbol{i}_s(\frac{1}{2}T)$, even if $x_1 \neq x_2$ in RZV. See footnote 8 on page 179.

can be calculated based on samples of three samples of the current, namely $\boldsymbol{i}_s(T)$, $\boldsymbol{i}_s(0)$, and $\boldsymbol{i}_s(\frac{1}{2}T + T_{sh})$. Inserting (6.24) into (6.21) yields

$$
\begin{aligned}
\bar{\boldsymbol{i}}_s &= \frac{1}{2}\Big(\boldsymbol{i}_s(0) + \boldsymbol{i}_s(T)\Big) + \tilde{\boldsymbol{i}}_{s12} \\
&= \frac{1}{2}\Big(\boldsymbol{i}_s(0) + \boldsymbol{i}_s(T)\Big) + \boldsymbol{i}_s(\tfrac{1}{2}T + T_{sh}) - \boldsymbol{i}_s(0) - \frac{\frac{1}{2}T + T_{sh}}{T}\Big(\boldsymbol{i}_s(T) - \boldsymbol{i}_s(0)\Big),
\end{aligned}
\tag{6.25}
$$

which can be simplified into the final result

$$
\bar{\boldsymbol{i}}_s = \langle \boldsymbol{i}_s \rangle_T = \boldsymbol{i}_s(\tfrac{1}{2}T + T_{sh}) + \frac{T_{sh}}{T}\Big(\boldsymbol{i}_s(0) - \boldsymbol{i}_s(T)\Big).
\tag{6.26}
$$

Hence, the algebra needed to calculate the true value for $\bar{\boldsymbol{i}}_s$ from three samples is not overwhelming. Also, only two samples are required in each phase in each carrier period, because the value for $\boldsymbol{i}_s(T)$ in one PWM period can be reused as the value for $\boldsymbol{i}_s(0)$ in the subsequent PWM period.

Furthermore, the calculation of $T_{sh} = \frac{1}{4}d_0(x_2 - x_1)T$ is fairly simple: T_{sh} depends on quantities whose exact values are known in the controller, i.e. T_{sh} is decoupled from the load (L and $\boldsymbol{e}$). Finally, in the special case, where $T_{sh} = 0$, it is sufficient to sample the currents at $t = \frac{1}{2}T$, which explains why the error vanishes in Fig. 6.7(f).

At this point it may be noted that it is impossible to detect the average phase currents $\langle i_a \rangle_T$, $\langle i_b \rangle_T$, and $\langle i_c \rangle_T$ by simultaneously sampling the waveforms of i_a, i_b, and i_c. This may be seen in Fig. 6.9(b), because the trajectory of $\boldsymbol{i}_s$ does not pass through the average value $\langle \boldsymbol{i}_s \rangle_T$ marked by a hexagram in this figure.

The new sampling method given by (6.26) has been tested by simulations similar to those shown earlier in Fig. 6.7. Based on those simulations, it has been verified that the proper average current can be detected by means of (6.26).

New current sampling technique for the RCD scheme

Not surprisingly, the new sampling method may also be applied to the RCD modulator. The only modification is that the offset T_{sh} in (6.26) should be replaced by the Δt value defined in Fig. 6.3(b) on page 163. Again, the correctness has been verified by simulations.

6.3.7 Applicability of FCF-RPWM schemes

To summarize the results obtained so far in this chapter, an overview of the practical applicability of the analyzed FCF-RPWM methods is presented below. This evaluation includes the three schemes known from literature (RLL, RZV, and RSS) and the new method designated as RCD.

Table 6.2 on the following page shows the ratings assigned to these methods with respect to the issues discussed in section 6.2.4. These ratings have been assigned by using information available in [1–6], [7–9], [11–15] for RLL, RZV, and RSS, respectively, complemented with investigations of the author reported in [5, 32]. Also, the preceding analysis of the impact of FCF-RPWM schemes on the current has been used to rate the individual methods. For reference, ratings for the classic space-vector modulator using a fixed-carrier frequency (FCF) have been included in Table 6.2. Also, the characteristics for the random carrier frequency (RCF) scheme investigated in Chapter 5 are listed.

Modulator	RLL	RZV $(x_1 = x_2)$	RZV $(x_1 \neq x_2)$	RSS	RCD	FCF	RCF (centered pulses)
Switching losses	+	0	0	÷	0	0	0
Implementation	+	+	0	÷	0	+	$+(0)^a$
Current quality	÷	+	0	?	0	+	+
Current sampling^b	÷	+	÷(+)	?	0(+)	+	+
Acoustics (low m)	÷	+	+	?	+	÷	+
Acoustics (high m)	÷	0	0	?	0	÷	+

^{a}Compliance with closed-loop digital controllers.
^{b}Synchronous sampling in the middle of the carrier period on all three phases is assumed.
 The score in parentheses is for the new sampling method in section 6.3.6.

Table 6.2 Ratings of practical applicability for different FCF-RPWM schemes besides fully deterministic PWM using a fixed-carrier frequency (FCF) and random carrier frequency (RCF) PWM. The used ratings are: (÷): poor/difficult, (0): fair/acceptable, (+): good, and (?): unknown (no information available).

Switching losses

The switching loss closely relates to the number of commutations N in each carrier period. The RSS method gives extra switchings compared to FCF, RZV, and RCD, which all yield six[11] commutations. RLL gives a direct opportunity to lower the average value of N to $\frac{3}{4} \cdot 6 = 4.5$ (assuming equal probabilities for the random selection of leading or lagging pulse-position modulation). Finally, a well-designed RCF modulator does not increase the switching losses compared to the benchmark (FCF using classic SVM).

Implementation

The ratings assigned to the implementation should only be considered as approximate, because the implementation of modulators heavily relates to the specific hardware. Nevertheless, the compound switching functions needed for the RSS scheme are disadvantageous compared to the other methods. All FCF-RPWM schemes integrate seamlessly with a digital control system, but as indicated in Table 6.2 the use of RCF is more tricky.

Current quality

The quality of the current relates to the problems analyzed in the preceding sections, where it was shown that the fundamental current is distorted by the modulation process when the generated switching functions are asymmetrical with respect to the midpoint

---

[11]In fact the average value for N may be smaller than six in RZV, because — depending on the chosen probability density functions for x_1 and x_2 — there may be a non-zero change that only two legs are switched in a PWM period (like in discontinuous PWM). For the RCD technique it is also possible to select probabilities so that pulses in adjacent PWM periods merge back to back, thereby eliminating commutations.

of the carrier period. The worst current waveforms are undoubtedly caused by RLL modulation; at the other extreme, FCF, RCF, and RZV using $x_1 = x_2$ all yield symmetrical switching functions, which effectively decouples the fundamental behaviour from the ripple voltage caused by pulse-width modulation.

Note that no attempts have been made to calculate traditional performance indices for the current, but rather focus has been put on the coupling between the ripple voltage and the per carrier period average current. For deterministic PWM, a performance index that quantifies the cumulative ripple current over a whole period of the fundamental is often used (see e.g. [8, 16, 33]), but an extension to random PWM is not a straightforward task due to the non-deterministic nature of the current waveforms. Such an investigation is left for future research.

Current sampling

Among the three different methods available for detection of the average load current listed on page 166, focus is put on the method based on simultaneous sampling in the middle of the carrier period. For the evaluation, it is assumed that ideal current measurements are available, i.e. the impacts of scaling and offset errors are neglected and also, the effects of time delays are assumed to be negligible[12].

Again, the RLL method is the worst performing method. For the RZV and the RCD schemes, it is impossible to sample the average phase current using the conventional sampling strategy, but the new current sampling strategy presented in section 6.3.6 may be used to get precise values for the true average currents.

Acoustic noise

Based on experimental results reported in [5, 32], scores have been assigned in Table 6.2 for the acoustic annoyance caused by an induction motor using the different modulation schemes. As pointed out on page 163, FCF-RPWM schemes are, in general, much more effective at low modulation indices m compared to high values for m. However, again RLL is underperforming the other FCF-RPWM schemes — in fact, many people find the noise caused by RLL modulation even more annoying than ordinary FCF modulation, even if m is small. Among the techniques studied here, there is no doubt that the RCF modulator is the best way to reduce acoustic noise.

6.3.8 Final comments

RLL is the oldest FCF-RPWM scheme, and it is well researched with respect to spectral analysis [3, 4]. However, a mere acknowledgement of the demonstrated problems related to the highly asymmetrical ripple currents cannot be found in the literature despite the many publications [1, 3, 4, 6, 35] dealing with RLL modulation. Apart from its simplicity, not much good can be said about RLL; practical applications of this FCF-RPWM method are difficult to imagine.

---

[12]In reality, current measurement based on sampling the current only once per carrier period is very susceptible to delays in the acquisition system [34] and to measurement noise. Also, the net effects of non-zero propagation delays in the power devices, a finite electrical time constant of the load, and limitations in current sensor bandwidth result in a phase lag [19].

The method originating from the independent patents [10] and [9] based on random division of the zero vectors has good potentials: the implementation is only slightly more complicated than standard SVM, the current quality is good (particularly for $x_1 = x_2$), and the average current can be detected based on a few samples of the load currents. Although not quite as good as a random carrier frequency modulator, the RZV is capable of reducing the acoustic annoyance over a wide range of modulation indices.

The RSS scheme has been used repeatedly by Lai in [11–15], but despite these many papers not much information is available regarding e.g. the current quality — nor has the claimed impact on the acoustic noise been documented. The references focus on the modulator without paying attention to vital defects like the excessive switching losses caused by a modulator that jumps between non-adjacent states. Such a situation is undesirable as already pointed out in 1975 by Zubek et al. in [36] and more recently in e.g. [23] also.

The last FCF-RPWM method investigated was the new technique based on displacing the common center of the three switching functions. RCD shares many characteristics with RZV; those two FCF-RPWM schemes both yield good alleviation of the acoustic noise in the low-modulation index region. Like the RZV scheme with $x_1 \neq x_2$, the main problem for RCD is the distortion of the fundamental current component and the incompatibility with existing current detection methods based on samples of either the phase currents or the dc-link current. To remedy this problem, however, the new current sampling strategy may be adopted.

6.4   Spectral analysis of fixed carrier frequency dc/ac random PWM

To calculate analytically the voltage spectra caused by FCF-RPWM, a generalized spectral analysis of three-phase converters controlled by such principles is derived. The results obtained in the current section is used in later sections to establish formulas for the spectra produced by the three different FCF-RPWM schemes of main interest: section 6.5 focuses on random lead-lag modulation, section 6.6 investigates the random zero-vector method, and in section 6.7 the random center displacement technique is analyzed.

The spectral theory is based on the general framework for spectral analysis of random PWM waveforms derived earlier in Chapter 3; reference to this chapter should also be made for a review of the existing literature dealing with spectral analysis of random PWM schemes operating with a fixed carrier frequency. However, to the knowledge of the author, the past work on this topic is limited to the RLL scheme; the two other FCF-RPWM methods, which have much better properties than the RLL modulator, have never been subjected to spectral analysis.
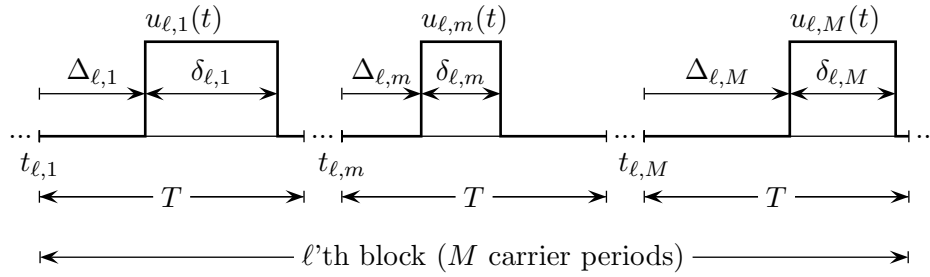
Figure 6.10 Parametric representation of a general FCF-RPWM technique showing how each block (corresponding to one cycle of the fundamental voltage) is divided into M intervals of equal width T equal to the duration of the carrier period.

6.4.1 Parametric representation of FCF-RPWM waveforms

The studied FCF-RPWM techniques may be characterized by the following properties, which are important to keep in mind for the subsequent derivations:

1. The duty ratios vary periodically with the period T_1 of the fundamental voltage.

2. All carrier periods have the same duration T.

3. The delay Δ measured from the beginning of the carrier period to the leading edge of the sampling pulse $u(t)$ is a random variable.

4. The width δ of the sampling pulse may (but not necessarily) have a random component aside from the deterministic component determined by the periodic variations of the duty ratios.

Note that Δ and δ are both random variables in the general case. For example, in RZV the pulse width δ is randomized by the zero-vector duration and, therefore, the delay Δ depends on δ. On the other hand, in RLL Δ is the only random variable, because the pulse width varies in a fully deterministic manner.

The parameters introduced above are used in Fig. 6.10 showing a parametric representation of an arbitrary switching function in FCF-RPWM. The indices appended to Δ and δ in Fig. 6.10 follow the syntax introduced in section 3.4.4 on page 63: One period of the fundamental output voltage is divided into M sampling intervals of equal duration T, which is equal to the reciprocal of the fixed PWM carrier frequency. Also, the switching function must consist of an infinity of identical blocks; the actual block number is labeled by ℓ in Fig. 6.10. Then, in total, $t_{\ell,m}$ marks the beginning of the m'th carrier period in the ℓ'th block. In this (ℓ, m)'th interval is the pulse[13] $u_{\ell,m}(t)$ of width $\delta_{\ell,m}$ delayed $\Delta_{\ell,m}$ seconds with respect to $t_{\ell,m}$.

6.4.2 Evaluation of partial contributions to the total spectrum

The spectrum $S(f)$ generated by an FCF-RPWM scheme that adheres to the constraints presented above may be regarded as a special case of the general framework

---

[13]Recall from Chapters 4 and 5 that the sampling pulse may have more complex shapes than the rectangular pulses used for the illustration in Fig. 6.10. Such modifications are also used in this chapter to calculate the spectra for the line-to-line voltage.

developed in Chapter 3 and successfully used in Chapter 5 for the random carrier frequency dc/ac technique. Hence, the starting point for the subsequent derivations is (3.40) and (3.41) on page 67, repeated here for convenience:

$$S(f) = \sum_{m=1}^{M} \sum_{\tilde{m}=1}^{M} S_{m,\tilde{m}}(f), \tag{6.27}$$

where the individual $S_{m,\tilde{m}}(f)$ entries are found by

$$S_{m,\tilde{m}}(f) = \frac{1}{M\overline{T}} E\left\{ \sum_{\ell=-\infty}^{\infty} U(f;\delta_{0,m}) U^{\star}(f;\delta_{\ell,\tilde{m}}) e^{j\omega(t_{\ell,\tilde{m}}-t_{0,m})} e^{j\omega(\Delta_{\ell,\tilde{m}}-\Delta_{0,m})} \right\}. \tag{6.28}$$

Concerning the derivations, the major difference between FCF-RPWM and RCF is that the carrier frequency is fixed in the former case. Due to that fact, it turns out that much of the algebra needed to manipulate (6.28) into useful expressions for the total spectrum becomes much less complicated than the corresponding derivations in Chapter 5.

The diagonal terms: $m = \tilde{m}$

To evaluate (6.28), the expectation of the infinite sum across ℓ must be found. As in section 5.3, the $(t_{\ell,m} - t_{0,m})$ term is rewritten as a sum of carrier periods. However, since all periods are of equal duration, the result simply becomes

$$t_{\ell,\tilde{m}} - t_{0,m} = \ell MT. \tag{6.29}$$

Using this result, (6.28) may be expanded in the same manner as shown by (5.10)–(5.12) starting on page 117 for the RCF case. The expression for the contribution $S_{m,\tilde{m}}(f)$ from $m = \tilde{m}$ to the total spectrum then becomes

$$S_{m,\tilde{m}}(f) = \frac{1}{MT} \left[E\left\{ U(f;\delta_m) U^{\star}(f;\delta_{\tilde{m}}) \right\} \right.$$
$$\left. + E\left\{ U(f;\delta_m) e^{-j\omega\Delta_m} \right\} E\left\{ U^{\star}(f;\delta_{\tilde{m}}) e^{j\omega\Delta_{\tilde{m}}} \right\} \sum_{\substack{\ell=-\infty \\ \ell \neq 0}}^{\infty} e^{j\omega MT\ell} \right]. \tag{6.30}$$

It should be noted that the summation across ℓ extends from minus to plus infinity, except for $\ell = 0$. The sum of exponentials $e^{j\omega MT\ell}$ may be rewritten using the important identity [37]

$$\sum_{\ell=-\infty}^{\infty} e^{j\omega MT\ell} = \frac{1}{MT} \sum_{\ell=-\infty}^{\infty} \delta\left(f - \frac{\ell}{MT}\right), \tag{6.31}$$

which relates a sum of complex-valued exponentials to a series of discrete frequencies separated $1/(MT)$ Hz apart. By way of (6.31) and correcting for the missing $\ell = 0$ term, (6.30) may then be rewritten as

$$S_{m,\tilde{m}}(f) = \frac{1}{MT} \left[E\left\{ |U(f;\delta_m)|^2 \right\} - \left| E\left\{ U(f;\delta_m) e^{-j\omega\Delta_m} \right\} \right|^2 \right]$$
$$+ \frac{1}{(MT)^2} \left| E\left\{ U(f;\delta_m) e^{-j\omega\Delta_m} \right\} \right|^2 \sum_{\ell=-\infty}^{\infty} \delta\left(f - \frac{\ell}{MT}\right), \tag{6.32}$$

where the fact that $m = \tilde{m}$ has been used as well. Already at this point, it may be noted that the total spectrum must have both a continuous density component (volt^2/Hz) and harmonics (volt^2) due to the occurrence of the δ-impulses in (6.32).

The diagonal terms: m < m̃

The derivation is almost identical to the $m = \tilde{m}$ case. Referring to (5.15) on page 119, it is seen that

$$t_{\ell,m} - t_{0,m} = \begin{cases} -(\ell M - (\tilde{m} - m))T, & \ell < 0, \\ (\ell M + (\tilde{m} - m))T, & \ell \geq 0, \end{cases} \tag{6.33}$$

because all instances of T are identical. Following the same steps as before, it may be shown that the partial spectrum is

$$S_{m,\tilde{m}}(f) \;=\; \frac{1}{MT} E\Big\{U(f;\delta_m)e^{-j\omega\Delta_m}\Big\} E\Big\{U^{\star}(f;\delta_{\tilde{m}})e^{j\omega\Delta_{\tilde{m}}}\Big\} e^{j\omega(\tilde{m}-m)T} \sum_{\ell=-\infty}^{\infty} e^{j\omega MT\ell},$$
$$\tag{6.34}$$

which by using the series (6.31) once more, yields

$$S_{m,\tilde{m}}(f) = \frac{1}{(MT)^2} E\Big\{U(f;\delta_m)e^{-j\omega\Delta_m}\Big\} E\Big\{U^{\star}(f;\delta_{\tilde{m}})e^{j\omega\Delta_{\tilde{m}}}\Big\}$$
$$e^{j\omega(\tilde{m}-m)T} \sum_{\ell=-\infty}^{\infty} \delta\Big(f - \frac{\ell}{MT}\Big). \tag{6.35}$$

Note the spectrum $S_{m,\tilde{m}}(f)$ for $m < \tilde{m}$ does only contribute to the harmonic part of the total spectrum. This implies that the continuous density spectrum solely depends on the diagonal terms.

The diagonal terms: m > m̃

Using a similar approach as for the $m < \tilde{m}$ case, it may be shown that

$$S_{m,\tilde{m}}(f) = \frac{1}{(MT)^2} E\Big\{U(f;\delta_{\tilde{m}})e^{-j\omega\Delta_{\tilde{m}}}\Big\} E\Big\{U^{\star}(f;\delta_m)e^{j\omega\Delta_m}\Big\}$$
$$e^{-j\omega(\tilde{m}-m)T} \sum_{\ell=-\infty}^{\infty} \delta\Big(f - \frac{\ell}{MT}\Big), \tag{6.36}$$

which is the complex conjugated of (6.35).

6.4.3 Summary of formula for the spectrum using FCF-RPWM

A compact matrix notation heavily inspired by [4] may be used to summarize the obtained results. Hence, it may readily be verified directly by (6.32), (6.35), and (6.36)

that the total spectrum $S(f)$ may be expressed as

$$S(f) = \sum_{m=1}^{M} \sum_{\tilde{m}=1}^{K} S_{m,\tilde{m}}(f) = \frac{1}{MT} \left(\left\| V(f) \right\|_1 - \left\| W(f) \right\|_2^2 \right)$$

$$+ \frac{1}{(MT)^2} I^T W(f) W^H(f) I \sum_{\ell=-\infty}^{\infty} \delta\left(f - \frac{\ell}{MT} \right). \quad (6.37)$$

The auxiliary row vectors $V(f)$ and $W(f)$ are defined by

$$V(f) = \begin{bmatrix} E\left\{ |U(f;\delta_1)|^2 \right\} \\ E\left\{ |U(f;\delta_2)|^2 \right\} \\ \vdots \\ E\left\{ |U(f;\delta_M)|^2 \right\} \end{bmatrix}, \quad W(f) = \begin{bmatrix} E\left\{ U(f;\delta_1)\, e^{-j\omega\Delta_1} \right\} \\ E\left\{ U(f;\delta_2)\, e^{-j\omega\Delta_2} \right\} e^{j\omega T} \\ \vdots \\ E\left\{ U(f;\delta_M)\, e^{-j\omega\Delta_M} \right\} e^{j\omega(M-1)T} \end{bmatrix}. \quad (6.38)$$

Here, I is a unit column vector of length M and I^T is the corresponding row vector. $W^H(f)$ is the transposed, complex conjugate of $W(f)$. Also, $\|V(f)\|_1$ is the vector 1-norm, i.e. the sum of the magnitudes of the elements in $V(f)$. Finally, $\|W(f)\|_2^2$ is the squared 2-norm, i.e. the sum of the magnitudes squared of the elements in $W(f)$.

The main constraint imposed on pulse trains for which (6.37) and (6.38) are valid is that the carrier period T is fixed, but the pulse widths and the pulse positions may have a random component apart from the deterministic component set by the duty ratio variations. It is also required that the randomization of e.g. the delay Δ is based on independent trials, i.e. Δ_m must not depend on past values like Δ_{m-1}.

6.5 Random lead-lag pulse-position modulation

Although this fundamental way of randomizing the pulse positions has been investigated in earlier publications (notably [2, 3], but also in [4, 38]), a spectral analysis is included anyhow in order to illustrate the methodology of the derivations.

Like in the two subsequent sections which provide details of the analysis of the RZV and RCD schemes, this section is organized into three parts: first, some preliminary definitions related to the randomization are given and next, derivations of equations for the spectral characteristics are given for both the switching function and for the line-to-line output voltage.

6.5.1 Preliminaries

The input to the modulator is the three duty ratios calculated by some pulse-width modulator as illustrated in Fig. 6.1(a) on page 159. Then, based on a random trial, the positioning of the on-state pulses is determined and the three switching functions are generated by using the given duty ratios. Fig. 6.11(a) illustrates the resulting

		$d_a > d_b$	$d_a < d_b$
	s	1	-1
Lead	d_{ab}	$d_a - d_b$	$d_b - d_a$
	Δ_{ab}	$d_b T$	$d_a T$
	s	1	-1
Lag	d_{ab}	$d_a - d_b$	$d_b - d_a$
	Δ_{ab}	$(1 - d_a)T$	$(1 - d_b)T$

(a) (b)
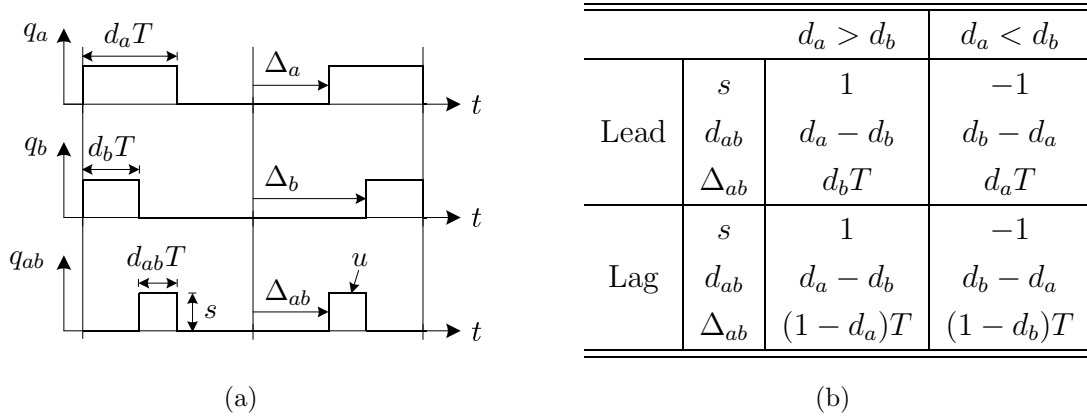
Figure 6.11 (a) Sample waveforms for the switching functions and the normalized line-to-line voltage for the RLL technique. (b) Auxiliary variables for parametric representation of sampling pulses.

waveforms and as shown in this figure, the delays in leg a and b measured from the beginning of the carrier period become

$$\Delta_a = \begin{cases} 0, & \text{for leading pulses,} \\ (1 - d_a)T, & \text{for lagging pulses.} \end{cases} \tag{6.39}$$

and

$$\Delta_b = \begin{cases} 0, & \text{for leading pulses,} \\ (1 - d_b)T, & \text{for lagging pulses.} \end{cases} \tag{6.40}$$

respectively.

In order to proceed with the evaluation of the general formulas listed on page 191, it is essential to select the probability density function $p(\Delta_a)$ for the delay. As for the dc/dc converter case studied in section 4.4.1 (page 81), the lead-lag type of modulation can be achieved by letting

$$p(\Delta_a) = r\delta(\Delta_a - 0) + (1 - r)\delta(\Delta_a - (1 - d_a)T). \tag{6.41}$$

A similar expression holds for $p(\Delta_b)$. In all schemes reported in the literature, equal weight is assigned to lead and lag ($r = 0.5$), but in principle all values in the $[0; 1]$ range may be used. The spectral characteristics will, of course, depend on the particular choice of r.

6.5.2 Spectrum for the switching function

The first step is to determine the sampling pulse and its Fourier transformation. In this case, the sampling pulse consists of a single rectangular pulse of the width $\delta_{a,m} = d_{a,m}T$, i.e. the Fourier transformation of the m'th pulse becomes

$$U(f; \delta_m) = \frac{1}{j\omega}\left(1 - e^{-j\omega d_{a,m}T}\right). \tag{6.42}$$

The $V(f)$ vector

In the m'th carrier period, the sampling pulse does only depend on the (precalculated) duty ratio $d_{a,m}$, i.e. it is a deterministic function of time. Then, the elements $V_m(f)$ for $m = 1, 2, \cdots, M$ of the vector $V(f)$ defined by (6.38) simplifies to squared magnitudes, viz.

$$V_m(f) = |U(f; \delta_{a,m})|^2 = \frac{\sin^2(\pi f d_{a,m} T)}{(\pi f)^2}. \tag{6.43}$$

The $W(f)$ vector

The expectation needed to find the elements in the $W(f)$ vector may be simplified compared to the general definition in (6.38) because the delay Δ_a is the only random variable. In total,

$$W_m(f) = U(f; \delta_{a,m}) E\left\{e^{-j\omega\Delta_{a,m}T}\right\} e^{-j\omega(m-1)T}. \tag{6.44}$$

The expectation may be found directly from (6.41), i.e.

$$E\left\{e^{-j\omega\Delta_{a,m}T}\right\} = r + (1-r)e^{-j\omega(1-d_{a,m})T}. \tag{6.45}$$

Inserting (6.45) and (6.42) into (6.44) finally yields

$$W_m(f) = \frac{1}{j\omega}\left(1 - e^{-j\omega d_{a,m}T}\right)\left(r + (1-r)e^{-j\omega(1-d_{a,m})T}\right)e^{-j\omega(m-1)T}. \tag{6.46}$$

6.5.3   Spectrum for the line-to-line voltage

In this case, the sampling pulse is defined as the difference q_{ab} between the q_a and the q_b waveforms as shown in Fig. 6.11(a). The resulting waveform does only consist of single pulse in each PWM period. Its width is independent of the random pulse position. Hence, the Fourier transformation in the m'th carrier period simply becomes

$$U(f; \delta_m) = \frac{s_m}{j\omega}\left(1 - e^{-j\omega d_{ab,m}T}\right), \tag{6.47}$$

where the value of the normalized pulse width is $d_{ab,m} = |d_{a,m} - d_{b,m}|$, which follows from Fig. 6.11(b).

Regarding the delay Δ_{ab}, its value depends on whether leading or lagging modulation is used and, furthermore, on the values of d_a and d_b. The table in Fig. 6.11(b) lists the details which may be put into the following form:

$$\Delta_{ab,\text{lead}} = \begin{cases} d_b T, & \text{if } d_a > d_b, \\ d_a T, & \text{if } d_a < d_b, \end{cases} \qquad \Delta_{ab,\text{lag}} = \begin{cases} (1 - d_a)T, & \text{if } d_a > d_b, \\ (1 - d_b)T, & \text{if } d_a < d_b. \end{cases} \tag{6.48}$$

Using these definitions for $\Delta_{ab,\text{lead}}$ and $\Delta_{ab,\text{lag}}$, the sought probability density function for the effective delay $\Delta_{ab,m}$ may be written as

$$p(\Delta_{ab,m}) = r\delta(\Delta_{ab,m} - \Delta_{ab,\text{lead},m}) + (1-r)\delta(\Delta_{ab,m} - \Delta_{ab,\text{lag},m}). \tag{6.49}$$

The $V(f)$ vector

As in section 6.5.2, the expectation may be omitted because the pulse widths are independent of the random positions, and by the use of (6.47) the m'th element in $V(f)$ becomes

$$V_m(f) = |U(f; \delta_m)|^2 = \frac{\sin^2(\pi f d_{ab,m} T)}{(\pi f)^2}. \tag{6.50}$$

The $W(f)$ vector

From (6.49), the expectation of $p(\Delta_{ab,m})$ in the m'th interval becomes

$$E\left\{e^{-j\omega\Delta_{ab,m}T}\right\} = re^{-j\omega\Delta_{ab,\text{lead},m}} + (1-r)e^{-j\omega\Delta_{ab,\text{lag},m}}. \tag{6.51}$$

Using this result together with the Fourier transformation of the sampling pulse (6.47), the total expression for the m'th element in the $W(f)$ vector becomes

$$W_m(f) = \frac{s_m}{j\omega}\left(1 - e^{-j\omega d_{ab,m}T}\right)\left(re^{-j\omega\Delta_{ab,\text{lead},m}} + (1-r)e^{-j\omega\Delta_{ab,\text{lag},m}}\right)e^{j\omega(m-1)T}. \tag{6.52}$$

6.6 The random zero-vector distribution scheme

As opposed to all other random PWM techniques treated in this thesis, this particular method of random distribution of the zero vectors changes the duty ratios calculated by some modulator before the actual switching functions controlling the converter are generated. To some extent, this difference does also propagate itself into the method to attack the spectrum analysis which will become clear when the derivations in the current section are compared to e.g. the analysis of the random center displacement scheme in section 6.7 starting on page 201. The reported spectral analysis of the RZV scheme cannot be found elsewhere to the knowledge of the author.

The details of how to calculate the spectrum for the switching function and the line-to-line voltage follow after some preliminary information needed for the derivations.

6.6.1 Preliminaries

The spectral analysis requires knowledge of the duty ratios d_a, d_b, and d_c, but those quantities are not directly available. Rather, the duration of the active vectors d_1 and d_2 is known besides the sector to which the reference belongs. It is illustrated in Fig. 6.12 how d_1, d_2, and $d_0 \triangleq 1 - (d_1 + d_2)$ may be processed. Here, d_0 is the total time (normalized with respect to T) in which either one of the two zero vectors $\boldsymbol{v}_{000}$ and $\boldsymbol{v}_{111}$ must be applied. In a certain PWM period, the division of $d_0 T$ among those vectors is governed by a single random variable x so that $x = x_1 = x_2$ in Fig. 6.2(b) on page 160, i.e. the spectral analysis is carried out for the special case of RZV where equal divisions between $\boldsymbol{v}_{000}$ and $\boldsymbol{v}_{111}$ are used in both halves of the whole PWM period[14].

---

[14]Although details of the spectral analysis are only given for the case where symmetrical switching patterns are generated, it is straightforward to extend the analysis to the $x_1 \neq x_2$ case, which yields asymmetrical switching functions.
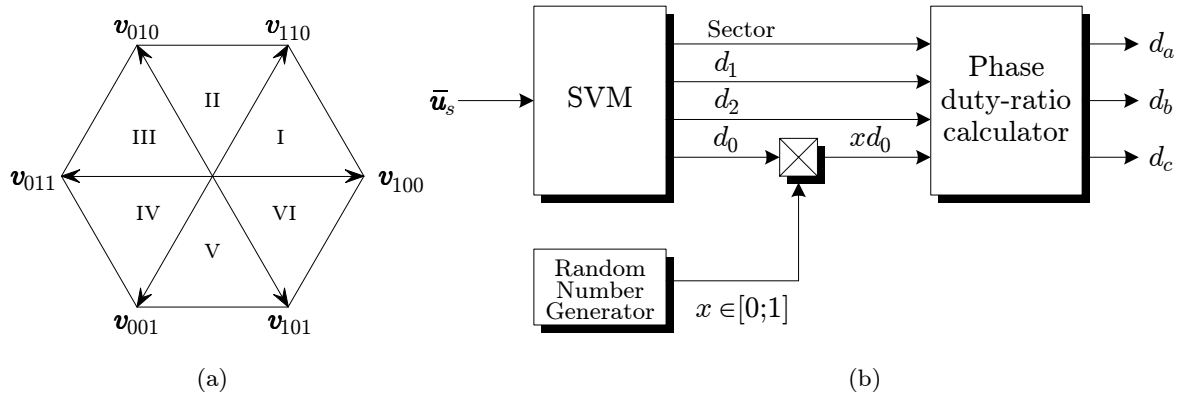
Figure 6.12 (a) Definition of sectors in the complex plane and (b) generation of phase duty ratios for the random zero-vector distribution technique.

Now, by convention, $\boldsymbol{v}_{111}$ is applied for xd_0T seconds in the center of the carrier; the remaining time $(1 - x)d_0T \triangleq x'd_0T$ is equally split between the two applications of the zero vector $\boldsymbol{v}_{000}$ at the beginning and at the end of the period T, respectively.

Fig. 6.13 on the next page shows the six possible sequences which may be determined uniquely from knowledge of the sector[15]. For example, in sector IV the vector sequence is

$$
\begin{aligned}
\boldsymbol{v}_{000}\langle\tfrac{1}{2}x'd_0T\rangle \to &\boldsymbol{v}_{001}\langle\tfrac{1}{2}d_2T\rangle \to \boldsymbol{v}_{011}\langle\tfrac{1}{2}d_1T\rangle \to \boldsymbol{v}_{111}\langle xd_0T\rangle \to \\
&\boldsymbol{v}_{011}\langle\tfrac{1}{2}d_1T\rangle \to \boldsymbol{v}_{001}\langle\tfrac{1}{2}d_2T\rangle \to \boldsymbol{v}_{000}\langle\tfrac{1}{2}x'd_0T\rangle,
\end{aligned}
\tag{6.53}
$$

where the notation introduced on page 25 has been used again.

Having the information of the sequence of applications of the voltage vectors, the duty ratios for each leg may be calculated provided the division of d_0 between the two zero vectors has been chosen. To accomplish this, the probability density function (pdf), from which x is drawn, must be known. As discussed in details in Chapter 5, the discrete type of pdf is particularly attractive in conjunction with random PWM and, therefore, it is assumed here that

$$
p(x) = \sum_{j=1}^{J} p_j\,\delta(x - x_j),
\tag{6.54}
$$

where p_j denotes the probability by which $x = x_j$ is selected. Since x is the part of the total zero-vector time spent using $\boldsymbol{v}_{111}$ in the middle of the PWM period, it is seen that $x = 0.5$ corresponds to the classic space-vector modulation. Also, $x = 0$ always eliminates switchings in one of the legs, i.e. a kind of discontinuous PWM results as briefly discussed in section 2.3.2. ($x = 1$ only eliminates switchings if $x = 1$ is selected by the random number generator in two consecutive PWM periods which, furthermore, must belong to the same sector.) However, since the value for x varies in a random

---

[15]In a certain sector, d_1 and d_2 associated with the active vectors may be calculated by (2.7) and (2.8) on page 24, respectively. Here, it must be recalled that d_1 always relates to the first active vector (sector I: $\boldsymbol{v}_{100}$, sector II: $\boldsymbol{v}_{110}$ etc.) in an anti-clockwise sense and d_2 to the second vector (I: $\boldsymbol{v}_{110}$, sector II: $\boldsymbol{v}_{010}$ etc.). In other words, the order of application of d_1 and d_2 alternates from sector to sector.
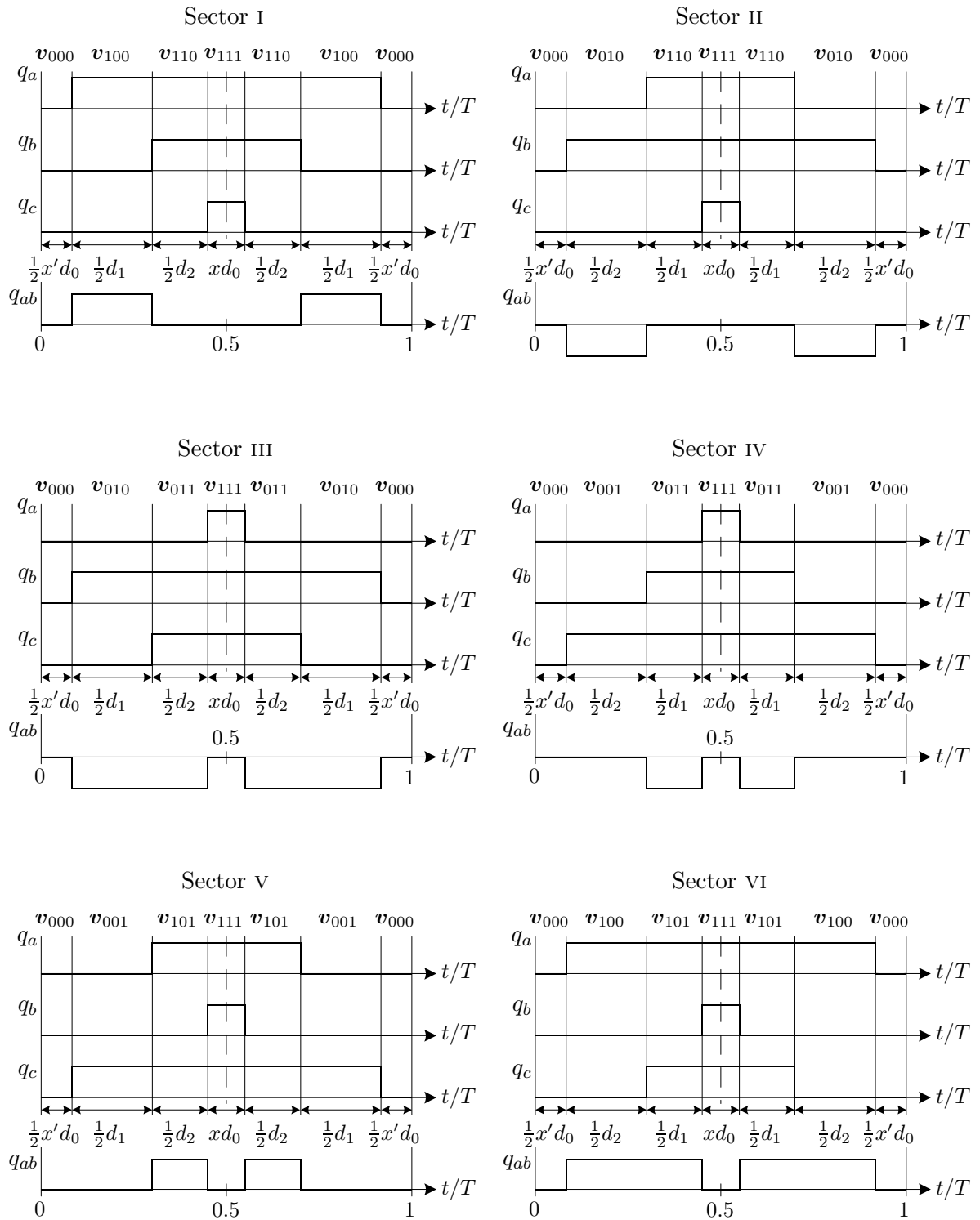
Figure 6.13 Illustration of possible vector sequences for the random zero-vector distribution technique. For each sector of the hexagon, the three switching functions and the difference $q_{ab} = q_a - q_b$ are shown. Refer to Fig. 6.12 also.

(a)
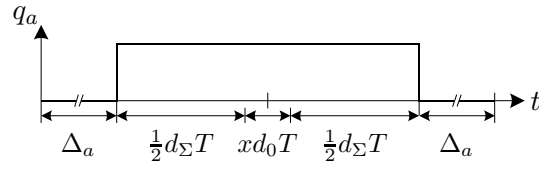
Sector	I	II	III	IV	V	VI
d_Σ	$d_1 + d_2$	d_1	0	0	d_2	$d_1 + d_2$
Δ_a	$\frac{1}{2}(1 - d_\Sigma - xd_0)T$ in all sectors					

(b)

Figure 6.14 Parameterization of the switching function for random zero-vector PWM. (a) Definition of auxiliary parameters and (b) their values depending on the sector number.

manner from one carrier period to another, the RZV scheme does not collapse to any of the well-known modulators, although they share the use of space vectors as the fundamental mechanism to achieve voltage synthesis on the macroscopic time scale.

6.6.2   Spectrum for the switching functions

To proceed with the derivations, the sampling pulse must be determined. It is apparent from Fig. 6.13 that the q_a waveform depends on the sector and on the defined duty ratios. Formally, the sampling pulse may be written as

$$u(t) = \begin{cases} 1, & 0 \le t \le (d_\Sigma + xd_0)T, \\ 0, & \text{otherwise,} \end{cases} \tag{6.55}$$

where the value to use for the d_Σ parameter may be determined from Fig. 6.14. d_Σ is a fully deterministic quantity as it depends only on the duty ratios d_1 and d_2 (besides the sector number), but the effective duty ratio $d_a = d_\Sigma + xd_0$ associated with q_a is a function of the randomization parameter, x.

  Fourier transformation of (6.55) yields

$$U(f; \delta_m) = \frac{1}{j\omega} \left(1 - e^{-j\omega(d_{\Sigma,m} + xd_{0,m})T} \right), \tag{6.56}$$

where, as usual, index m has been added to the parameters that vary in a predictable manner.

The $V(f)$ vector

The magnitude square of $U(f; \delta_m)$ is

$$|U(f; \delta_m)|^2 = \frac{\sin^2\left(\pi f(d_{\Sigma,m} + xd_{0,m})T\right)}{(\pi f)^2}. \tag{6.57}$$

Attention must be paid to the fact that $|U(f;\delta_m)|^2$ is a function of x. Hence, the expectation in (6.38) for $V(f)$ must be taken over the range of x. Then, by virtue of (6.54), the m'th element in the column vector $V(f)$ becomes

$$V_m(f) = E\big\{\, |U(f;\delta_m)|^2 \,\big\} = \frac{1}{(\pi f)^2} \sum_{j=1}^{J} p_j \sin^2\left(\pi f(d_{\Sigma,m} + x_j d_{0,m})T\right). \tag{6.58}$$

The $W(f)$ vector

For leg a, the delay Δ_a is a function of the pulse width $d_\Sigma + x d_0$. Specifically, we have $\Delta_a = \frac{1}{2}(1 - d_\Sigma - x d_0)T$ and this must be included in the expectation needed to find the elements of $W(f)$. Also, (6.56) shows that the Fourier transformation $U(f;\delta_m)$ depends on x. In total, the expression for $W_m(f)$ becomes

$$W_m(f) = E\Big\{ U(f;\delta_m)\, e^{-j\omega\Delta_{a,m}T} \Big\} e^{j\omega(m-1)T}$$

$$= \frac{1}{j\omega} \sum_{j=1}^{J} p_j \left(1 - e^{-j\omega(d_{\Sigma,m}+x_j d_{0,m})T}\right) e^{-j\omega(1-d_{\Sigma,m}-x_j d_{0,m})\frac{T}{2}}\, e^{-j\omega(m-1)T}. \tag{6.59}$$

6.6.3 Spectrum for the line-to-line voltage

The different combinations of the switching functions shown in Fig. 6.13 result in the q_{ab} waveforms as illustrated in the same figure. To encompass all outcomes, the generalized sampling pulse shown in Fig. 6.15 must be used where the parameters are listed in the accompanying table. Hence,

$$u(t) \triangleq u_1(t) + u_1(t - (\alpha_\Delta + \alpha_\delta)T), \tag{6.60}$$

where

$$u_1(t) = \begin{cases} s, & 0 \le t \le \alpha_\delta T, \\ 0, & \text{otherwise.} \end{cases} \tag{6.61}$$

Now, it must be observed from Fig. 6.15 that the amount $(\alpha_\Delta + \alpha_\delta)T$ by which the second pulse lags the first pulse has two parts: (a) a random part $(x d_0 T)$ and (b) a deterministic part, which varies from sector to sector. The latter part is characterized by the parameter d_Δ as tabulated in Fig. 6.15(b). Hence, it holds that $(\alpha_\Delta + \alpha_\delta)T = (d_\Delta + x d_0)T$ by definition.

Expressed by the introduced parameters[16] the Fourier transformation of the sampling pulse (6.60) then becomes

$$U(f;\delta_m) = \frac{s_m}{j\omega}\left(1 - e^{-j\omega\alpha_{\delta,m}T}\right)\left(1 + e^{-j\omega(x d_{0,m} + d_{\Delta,m})T}\right), \tag{6.62}$$

where index m has been added to show the dependence on the carrier period counter, m.

---

[16]Due to the excessive number of parameters, redundancy exists. However, to clarify the derivations no attempt has been made to minimize the aid of auxiliary parameters.

(a)
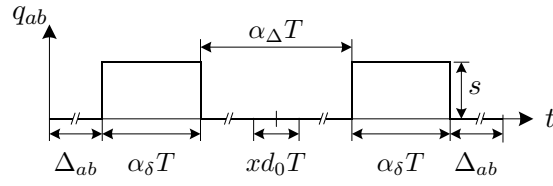
Sector	I	II	III	IV	V	VI
α_δ	$\frac{1}{2}d_1$	$\frac{1}{2}d_2$	$\frac{1}{2}(d_1 + d_2)$	$\frac{1}{2}d_1$	$\frac{1}{2}d_2$	$\frac{1}{2}(d_1 + d_2)$
α_Δ	$xd_0 + d_2$	$xd_0 + d_1$	xd_0	xd_0	xd_0	xd_0
Δ_{ab}/T	$\frac{1}{2}x'd_0$	$\frac{1}{2}x'd_0$	$\frac{1}{2}x'd_0$	$\frac{1}{2}(x'd_0 + d_2)$	$\frac{1}{2}(x'd_0 + d_1)$	$\frac{1}{2}x'd_0$
s	1	-1	-1	-1	1	1
d_Δ	$d_2 + \frac{1}{2}d_1$	$d_1 + \frac{1}{2}d_2$	$\frac{1}{2}(d_1 + d_2)$	$\frac{1}{2}d_1$	$\frac{1}{2}d_2$	$\frac{1}{2}(d_1 + d_2)$
Δ_Δ/T	0	0	0	$\frac{1}{2}d_2$	$\frac{1}{2}d_1$	0

(b)

Figure 6.15 Parameters for the difference q_{ab} for the random zero-vector PWM scheme. (a) Waveform and (b) parameters for all sectors. See also Fig. 6.13. Note $x' \triangleq 1 - x$.

The $V(f)$ vector

By straightforward manipulations of the complex exponentials in (6.62) by means of trigonometric identities, it may be obtained that

$$|U(f; \delta_m)|^2 = \left(\frac{4s_m}{\omega}\right)^2 \sin^2\left(\pi f \alpha_{\delta,m}T\right) \cos^2\left(\pi f(xd_{0,m} + d_{\Delta,m})T\right), \tag{6.63}$$

which leads directly to the m'th element in $V(f)$:

$$V_m(f) = E\left\{|U(f; \delta_m)|^2\right\} = \left(\frac{4s_m}{\omega}\right)^2 \sin^2\left(\pi f \alpha_{\delta,m}T\right) \sum_{j=1}^{J} p_j \cos^2\left(\pi f(x_j d_{0,m} + d_{\Delta,m})T\right). \tag{6.64}$$

The $W(f)$ vector

The delay Δ_{ab} from the beginning of the carrier period to the leading edge of the first rectangular pulse does also have both a deterministic and a random part; this is evident from the Δ_{ab}/T row in Fig. 6.15(b). The random contribution to the total delay is $\frac{1}{2}x'd_0T = \frac{1}{2}(1 - x)d_0T$ and the Δ_Δ parameter listed in the table is the normalized deterministic delay so that $\Delta_{ab} = (\frac{1}{2}(1 - x)d_0 + \Delta_\Delta)T$.

From the Fourier transformed sampling pulse (6.62) and those parameters, $W_m(f)$ defined as the m'th row in (6.38) becomes

$$
\begin{aligned}
W_m(f) &= E\Big\{U(f;\delta_m)\,e^{-j\omega\Delta_m T}\Big\}e^{j\omega(m-1)T} \\
&= \frac{s_m}{j\omega}\big(1 - e^{-j\omega\alpha_{\delta,m}T}\big)\sum_{j=1}^{J} p_j\big(1 + e^{-j\omega(x_j d_{0,m}+d_{\Delta,m})T}\big)e^{-j\omega(\frac{1}{2}x_j' d_{0,m}+\Delta_{\Delta,m})T}\,e^{-j\omega(m-1)T}
\end{aligned}
$$

$$(6.65)$$

where $x_j' \triangleq 1 - x_j$ has been inserted to compact the equation.

6.7 The random center displacement scheme

The method of random displacement of the common pulse center has never been subjected to spectral analysis before and hence, the objective of this section is to present the derivations required to calculate the resulting spectra. Again, the starting point is the theory summarized in section 6.4.3 and also the idea of generalizing the sampling pulse is used once more to get analytic expressions for the line-to-line voltage.

6.7.1 Preliminaries

Let the perturbation of the center from the $\frac{1}{2}T$ point be denoted by Δt as indicated in Fig. 6.16. As the pulses must not extend across the boundaries of the carrier period, it is required that $|\Delta t| \le \frac{1}{2}(1 - d_{\max})T$, where $d_{\max} = \max\{d_a, d_b, d_c\}$ is the largest of the three reference duty ratios. Fig. 6.16 shows examples for $d_{\max} = d_a$ and $d_{\max} \ne d_a$. At this point, it should be recalled that the RCD scheme does not alter the duty ratios d_a, d_b, and d_c commanded by some modulator; only the exact placement of the on-state pulses is modified compared to the usual symmetry around $\frac{1}{2}T$.

Now, to randomize the displacement by the available random number x in the $[0;1]$ range, Δt is set as

$$\Delta t = \tfrac{1}{2}(1 - d_{\max})(2x - 1)T. \tag{6.66}$$

Here, $x = 0.5$ corresponds to the usual center-alignment within T; $x = 0$ maps into placing the leading edge of the switching function with the largest duty ratio right at the beginning of the carrier period. The two pulses on the two remaining legs are offset by the same amount with respect to $\frac{1}{2}T$ thereby keeping all pulses mutually center aligned as in classic modulators.

To complete the analysis, probabilities must be assigned to x and as for the RZV scheme, a discrete type of distribution is used. Hence,

$$p(x) = \sum_{j=1}^{J} p_j\,\delta(x - x_j), \tag{6.67}$$

where, as before, p_j denotes the probability by which $x = x_j$ is selected.

The spectral theory requires knowledge of the delay Δ_a with respect to $t = 0$, i.e. the displacement from $t = \frac{1}{2}T$ defined by (6.66) must be mapped into an equivalent

(a)

	s	α_δ	α_Δ
$d_a > d_b$	1	$\frac{1}{2}(d_a - d_b)$	$\frac{1}{2}(d_a + d_b)$
$d_a < d_b$	-1	$\frac{1}{2}(d_b - d_a)$	$\frac{1}{2}(d_a + d_b)$

(b)
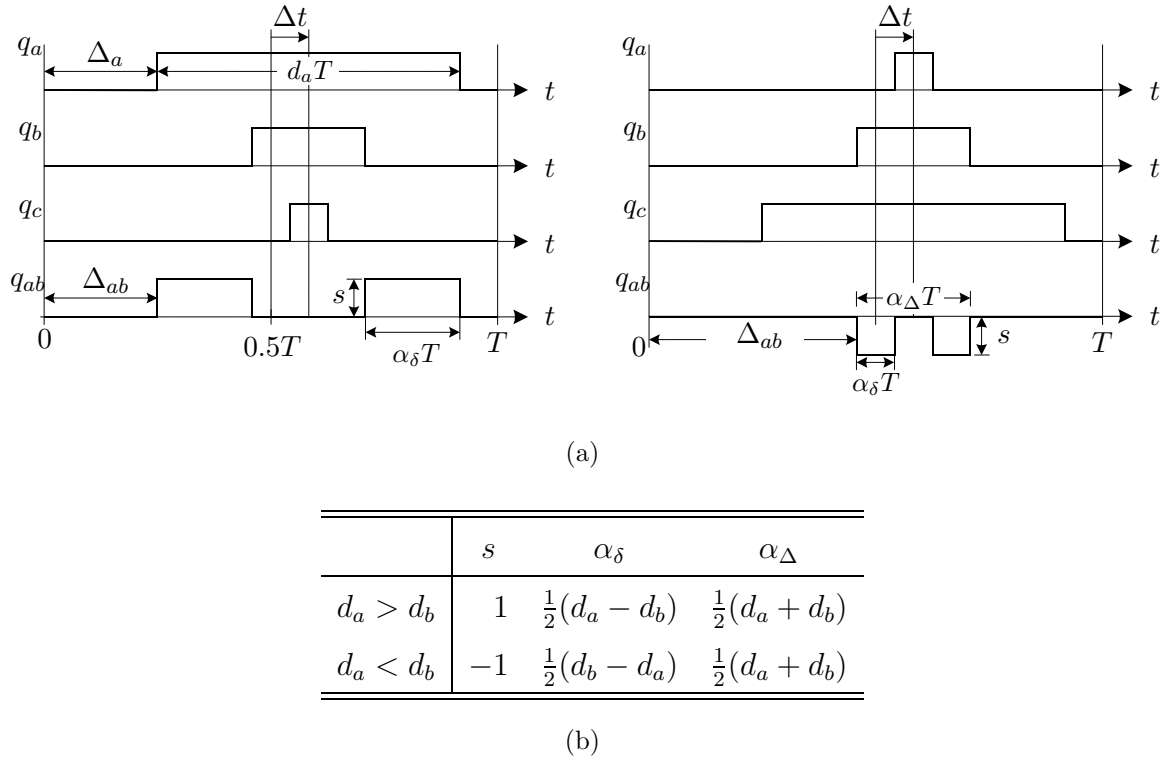
Figure 6.16 Definitions for random center displacement PWM. (a) Illustration of time-domain waveforms for the switching functions and (b) auxiliary parameters and their values expressed by the known duty ratios.

delay measured from $t = 0$. From Fig. 6.16 it may be perceived that Δ_a becomes

$$\Delta_a = \tfrac{1}{2}(1 - d_a)T + \Delta t = \tfrac{1}{2}(1 - d_a)T + \tfrac{1}{2}(1 - d_{\max})(2x - 1)T$$
$$= \left(\tfrac{1}{2}(d_{\max} - d_a) + (1 - d_{\max})x\right)T. \tag{6.68}$$

Similar expressions for the delays on the other legs follow immediately by replacing index a with b or c.

6.7.2   Spectrum for the switching functions

To proceed, the contributions to Δ_a are rewritten in terms of two auxiliary parameters defined by $\alpha_d \triangleq \tfrac{1}{2}(d_{\max} - d_a)$ and $\alpha_r = 1 - d_{\max}$, respectively. Then (6.68) may be put into the following form:

$$\Delta_a = (\alpha_d + \alpha_r x)T, \tag{6.69}$$

which clearly separates the deterministic and the random parts of the total delay from each other.

The width of the sampling pulse is not affected by the randomization and therefore, the Fourier transformation of the sampling pulse is simply

$$U(f; \delta_m) = \frac{1}{j\omega}\left(1 - e^{-j\omega d_{a,m}T}\right). \tag{6.70}$$

The $V(f)$ vector

The magnitude squared of $U(f; \delta_m)$ is equal to $V_m(f)$, i.e.

$$V_m(f) = |U(f; \delta_m)|^2 = \frac{\sin^2(\pi f d_{a,m} T)}{(\pi f)^2}. \tag{6.71}$$

The $W(f)$ vector

Equation (6.69) shows that the delay depends on x, but the Fourier transformation of the sampling pulse does not. Hence, $W_m(f)$ simplifies to averaging across the possible values of Δ_a defined by the corresponding x_j elements in (6.67). In total this yields

$$\begin{aligned}
W_m(f) &= E\left\{ U(f; \delta_m) \, e^{-j\omega\Delta_{a,m}T} \right\} e^{j\omega(m-1)T} \\
&= \frac{1}{j\omega} \left(1 - e^{-j\omega d_{a,m}T} \right) \sum_{j=1}^{J} p_j \, e^{-j\omega(\alpha_{d,m} + \alpha_{r,m} x_j)T} e^{-j\omega(m-1)T}.
\end{aligned} \tag{6.72}$$

6.7.3 Spectrum for the line-to-line voltage

The analysis of the line-to-line voltage is straightforwardly derived. The generalized sampling pulse consists of two pulses like for e.g. the RZV technique. Fig. 6.16 illustrates the waveforms together with the needed parameters (α_Δ and α_δ). Using these parameters, the sampling pulse becomes

$$u(t) \triangleq u_1(t) + u_1(t - \alpha_\Delta T), \tag{6.73}$$

where

$$u_1(t) = \begin{cases} s, & 0 \le t \le \alpha_\delta T, \\ 0, & \text{otherwise.} \end{cases} \tag{6.74}$$

In the m'th PWM period, the Fourier transformation is

$$U(f; \delta_m) = \frac{s_m}{j\omega} \left(1 - e^{-j\omega\alpha_{\delta,m}T} \right) \left(1 + e^{-j\omega\alpha_{\Delta,m}T} \right), \tag{6.75}$$

where the parameters may be determined from the values of the reference duty ratios by using the appropriate row in the table in Fig. 6.16(b).

The $V(f)$ vector

The m'th element in $V(f)$ can be found directly from (6.75) without any averaging, i.e.

$$V_m(f) = E\left\{ |U(f; \delta_m)|^2 \right\} = \left(\frac{4s_m}{\omega} \right)^2 \sin^2(\pi f \alpha_{\delta,m} T) \cos^2(\pi f \alpha_{\Delta,m} T), \tag{6.76}$$

because all parameters in (6.75) are deterministic functions of the duty ratios.

The $W(f)$ vector

The resulting delay Δ_{ab} measured from $t = 0$ depends on the value of Δt and on the magnitudes of the duty ratios d_a, d_b, and d_c. For example, if $d_{\max} = d_a$, then $\Delta_{ab} = \frac{1}{2}(1 - d_a)T + \Delta t$, but if $d_c > d_b > d_a$, then $\Delta_{ab} = \frac{1}{2}(1 - d_b)T + \Delta t$. To unify the notation for all possible combinations, an additional parameter $d_{ab,\max} = \max\{d_a, d_b\}$ is introduced and then Δ_{ab} becomes

$$
\begin{aligned}
\Delta_{ab} &= \tfrac{1}{2}(1 - d_{ab,\max})T + \Delta t = \tfrac{1}{2}(1 - d_{ab,\max})T + \tfrac{1}{2}(1 - d_{\max})(2x - 1)T \\
&= \big(\tfrac{1}{2}(d_{\max} - d_{ab,\max}) + (1 - d_{\max})x\big)T \\
&\triangleq (\alpha_{d,ab} + \alpha_{r,ab}x)T.
\end{aligned}
\tag{6.77}
$$

The division of Δ_{ab} into a deterministic and a random part is determined by $\alpha_{d,ab}$ and $\alpha_{r,ab}$ as defined in (6.77).

From (6.38), (6.75), and (6.77) the final result for $W_m(f)$ then follows:

$$
\begin{aligned}
W_m(f) &= E\Big\{U(f;\delta_m)\, e^{-j\omega\Delta_m T}\Big\}e^{j\omega(m-1)T} \\
&= \frac{s_m}{j\omega}\Big(1 - e^{-j\omega\alpha_{\delta,m}T}\Big)\Big(1 + e^{-j\omega\alpha_{\Delta,m}T}\Big)\sum_{j=1}^{J} p_j\, e^{-j\omega(\alpha_{d,ab,m}+\alpha_{r,ab,m}x_j)T}e^{-j\omega(m-1)T}.
\end{aligned}
\tag{6.78}
$$

6.8 Verification of the spectral theory

The spectral analysis in the sections 6.4–6.7 of the RZV, RCD, and RLL techniques must be compared to measurements before any decisive conclusions can be drawn regarding the correctness of the developed spectral theory. Hence, the objective of this section is to document by means of comparisons between analytically calculated and experimentally measured spectra that a very good agreement exists between theory and practice.

6.8.1 Experimental set-up

The set-up used in the experiments is identical to the system used in Chapter 5 also for evaluation of the random carrier frequency PWM technique. For convenience, the set-up consisting of a three-phase VSC supplying a two-pole 1.5 kW induction motor is repeated shown in Fig. 6.17 on the facing page. Further information regarding the set-up may be found on page 125 in Chapter 5 and in Appendix A.

Modulator and dynamic signal analyzer settings

The evaluation of the spectral theory uses the settings listed in Table 6.3(a) for the deterministic part of the modulator. To limit the number of plots, only the space-vector modulation method is used to generate reference duty ratios. As in Chapter 5, this is done in an open-loop manner by a simple scalar V/Hz controller. Two values (5 Hz and 40 Hz) are used for the fundamental frequency f_1 to evaluate the theory at different
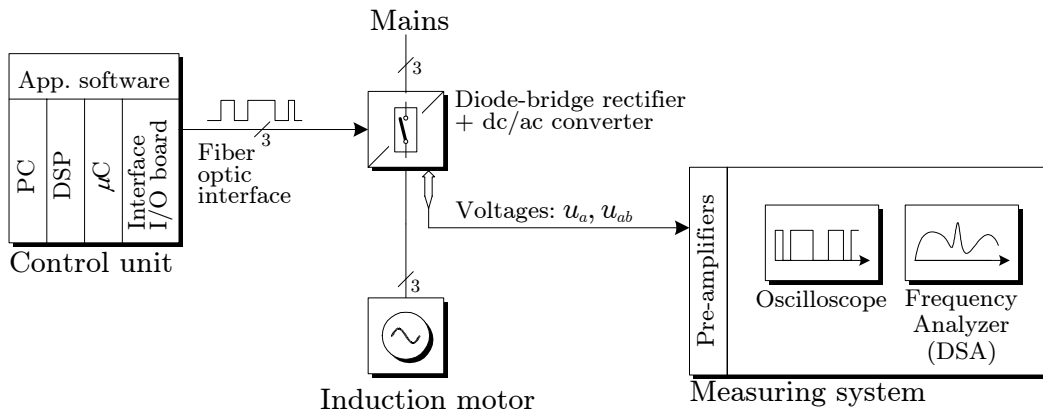
Figure 6.17 Set-up used to perform measurements of spectra for fixed carrier frequency random PWM schemes for three-phase converters. See Appendix A for more information.

Type of modulator	Fundamental frequency	Carrier frequency
SVM (space-vector)	Low: $f_1 = 5$ Hz High: $f_1 = 40$ Hz	3 kHz[a]

[a] Due to the resolution of the used PWM timers in the microcontroller (see Appendix A) generating the switching functions, actual values (accurate to two positions) are $1/(834 \cdot 400 \text{ ns}) = 2997.60$ Hz using RZV and RCD modulation and $1/(6667 \cdot 50 \text{ ns}) = 2999.85$ Hz for RLL modulation. Although the deviations from 3 kHz appear negligible, the accurate values must be used in the spectral analysis when a very precise prediction of the harmonic part of the spectra is needed.

(a)

RZV and RCD					RLL
Parameters in (6.54) and (6.67):					Parameter in (6.41) and (6.49):
x_j	0.1	0.3	0.5	0.7	0.9	$r = 0.5$, i.e. $p(\text{lag}) = p(\text{lead}) = 0.5$
p_j	0.2	0.2	0.2	0.2	0.2	

(b)

Resolution	Sampling freq.	Window type	Record length
8 Hz	65.536 kHz	Hanning	8192

(c)

Table 6.3 Used settings for examination of spectral analyses of FCF-RPWM schemes. (a) Parameters controlling the deterministic part of the modulators, (b) assignment of probabilities for the random part of the modulators, and (c) settings for the dynamic signal analyzer used to acquire measured spectra.

operating points. The modulator is updated with a constant frequency of 3 kHz, i.e. a new set of duty ratios is impressed on the converter every 333.3 μs.

The randomization of the examined FCF-RPWM schemes is governed by the probability density functions (pdf) whose values are listed in Table 6.3(b). Five different values for x_j, which each has a probability of 0.2, are used for the discrete pdf incorporated in the RZV and the RCD modulators. For the RLL technique, identical probabilities are assigned to lead and lag. Note that the chosen pdf's are by no means unique; the theory and the experiments could have been made using any other valid density functions for the random variables.

Settings for the dynamic signal analyzer (DSA)

Since the spectra produced by FCF-RPWM techniques have both density (volt^2/Hz) as well as harmonic (volt^2) components, is it important to know the settings of the DSA in order to include the effects of windowing etc. into the calculations. The problem of comparing such mixed spectra to estimated spectra was discussed in details in section 3.3 starting on page 50; to use the procedure outlined on page 58ff, the information given in Table 6.3(c) for the DSA is needed.

Notation

Spectra are calculated and measured for both the switching function q_a and for the difference $q_{ab} \triangleq q_a - q_b = u_{ab}/U_{dc}$, which apart from the U_{dc} scaling factor corresponds to the line-to-line voltage u_{ab} between two output terminals in the VSC. The following notation is used for the different spectra:

$S_a(f)$, The theoretically expected spectrum for the switching function q_a and for the
$S_{ab}(f)$ difference $q_{ab} \triangleq q_a - q_b$, respectively. $S_a(f)$ has both density and harmonic components. The same holds for $S_{ab}(f)$.

$\tilde{S}_a(f)$, The equivalent density spectra obtained by emulating the characteristics of the
$\tilde{S}_{ab}(f)$ DSA, i.e. the power carried by the harmonic part of the underlying spectrum is incorporated into the density spectrum.

$\hat{S}_a^p(f)$ The measured density spectrum for the voltage between output terminal a and the negative dc-link rail of the converter. This input to the DSA corresponds to the switching function q_a after the amplification by U_{dc}.

$\hat{S}_{ab}^p(f)$ The measured density spectrum for the line-to-line voltage at the output terminals of the converter. $\hat{S}_{ab}^p(f)$ is comparable to the spectrum $\tilde{S}_{ab}^p(f)$ for q_{ab}.

All results are given in (dB) where 0 dB $\sim$ 1 volt^2/Hz for the density parts of the spectra and 0 dB $\sim$ 1 volt^2 for the harmonics in $S_a(f)$ and $S_{ab}(f)$.

6.8.2 Comparison of calculated and measured spectra

The 0–25 kHz frequency range

The obtained spectra in the 0–25 kHz frequency range are shown in Figs. 6.18–6.23 on pages 208–213. In each of those figures the theoretically expected spectra $S_a(f)$

and $S_{ab}(f)$ are shown in the top row. The middle row contains the equivalent density spectra $\tilde{S}_a(f)$ and $\tilde{S}_{ab}(f)$, which may be compared to the measured spectra $\hat{S}_a(f)$ and $\hat{S}_{ab}(f)$ in the bottom row.

It is apparent that all three FCF-RPWM schemes generate substantial harmonics, especially at $f_1 = 40$ Hz, see Figs. 6.19(a, b), 6.21(a, b), and 6.23(a, b). The frequencies, at which the harmonics peak up, are given by $Lf_s \pm nf_1$, where L and n are integers, $f_s = 3$ kHz, and f_1 is the fundamental frequency. Note also that the side lobes become wider as L increases. In total, the harmonic spectra have many similarities to the spectra produced by deterministic pulse-width modulators.

The shape of the analytically calculated density spectra heavily depends on the FCF-RPWM method and on the value for f_1. As a general trend, it may be stated that the total power carried by the non-harmonic portion of $S_a(f)$ and $S_{ab}(f)$ becomes smaller when the fundamental frequency increases. This is expected since the randomization is much more efficient at low values for the modulation index (which is proportional to f_1 in all tests). This incapability of completely suppressing harmonics is a major disadvantage of FCF-RPWM compared to the random carrier frequency PWM studied in Chapter 5.

It should be noted that the pdf's governing the randomization in the FCF-RPWM schemes have impact on the amplitude of the harmonics around multiples of the carrier frequency. Hence, a very interesting topic for future research is to exploit the potentials of reducing harmonics by more intelligent selections of probabilities. Due to the mathematical complexity of this spectral shaping problem, numerical optimization is almost obligatory. Fortunately, as discussed in some details in section 5.2 starting on page 108, the discrete type of pdf used in all spectral analyses in this chapter is well suited together with numerical optimization routines.

Returning to the calculated spectra $S_a(f)$ and $S_{ab}(f)$, they cannot be compared directly to the measured spectra for q_a and q_{ab}. The proper procedure is to compare the modified spectra $\tilde{S}_a(f)$ and $\tilde{S}_{ab}(f)$ to the estimated spectra, $\hat{S}_a(f)$ and $\hat{S}_{ab}(f)$. Two by two comparisons of the plots shown in Figs. 6.18–6.23 reveal that a very good agreement exists in all cases between predicted spectra and spectra measured on an operating converter.

In total, it may be stated that the developed spectral theory accurately predicts both the density part and the harmonic components over the whole frequency range for all investigated FCF-RPWM methods and operating points. Note that such a decisive conclusion can only be drawn, because the characteristics of the DSA are included; it makes sense to compare e.g. $\tilde{S}_a(f)$ to $\hat{S}_a(f)$, but it is impossible to compare the true spectrum denoted by $S_a(f)$ to $\hat{S}_a(f)$.

Details around 3 kHz

To further demonstrate the excellent agreement between results obtained by the developed spectra theories and the measurements, additional plots have been included in Figs. 6.24–6.26 on pages 214–216. These figures show details of the side lobe around 3 kHz.

The two plots in the top row of Figs. 6.24–6.26 (sub-figures (a) and (b)) are based on the same data as used in Figs. 6.19, 6.21, and 6.23, i.e. the former plots are just zoomed versions of the latter. The difference between the calculated and the measured
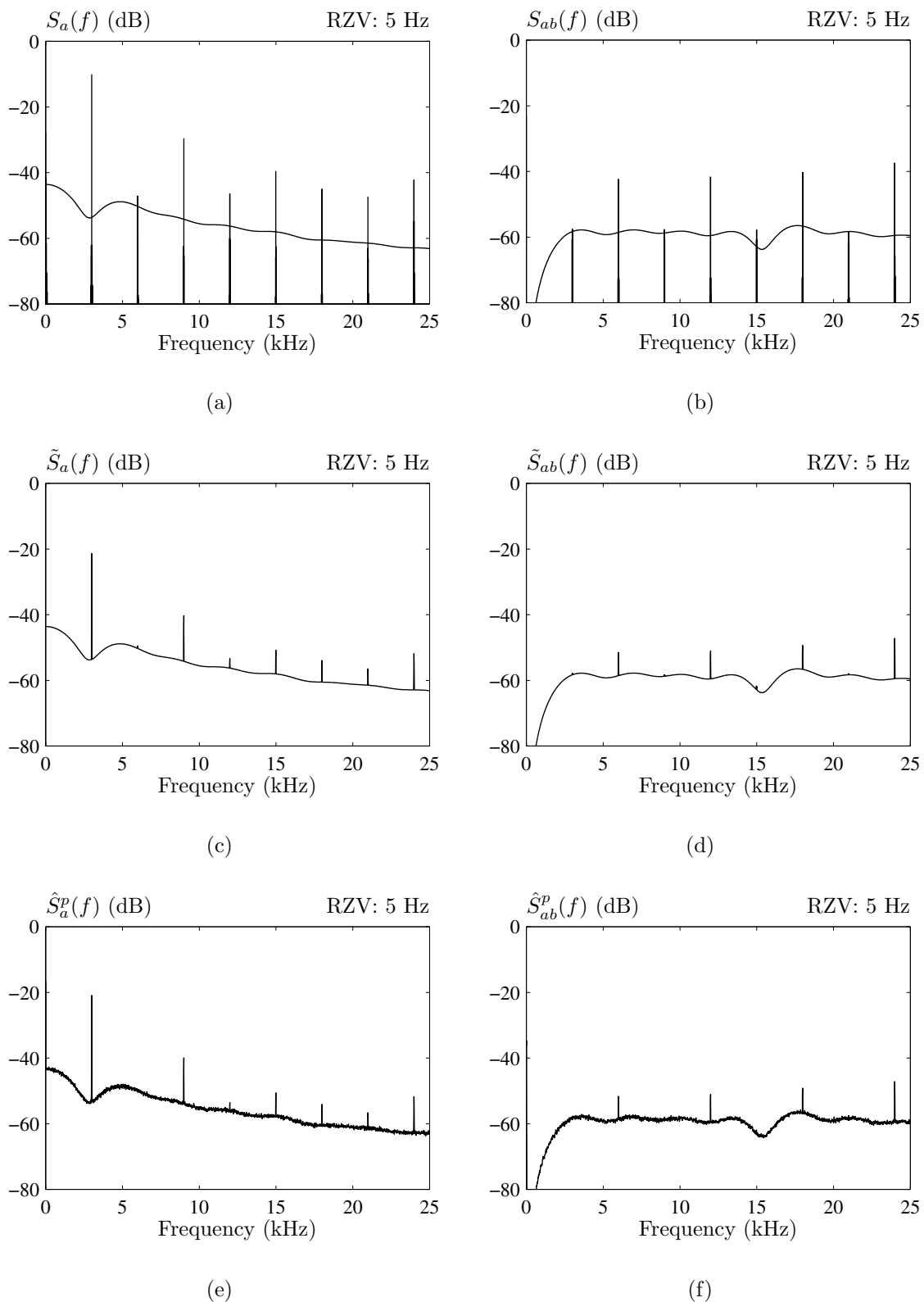
Figure 6.18 Spectra for random zero-vector (RZV) modulation using the settings for 5 Hz operation in Table 6.3 (page 205). Spectra for both the switching function (left column) and the line-to-line voltage (right column) are shown. (a, b) Calculated density and harmonic spectrum, (c, d) calculated density spectrum including power due to harmonics, and (e, f) measured density spectrum.
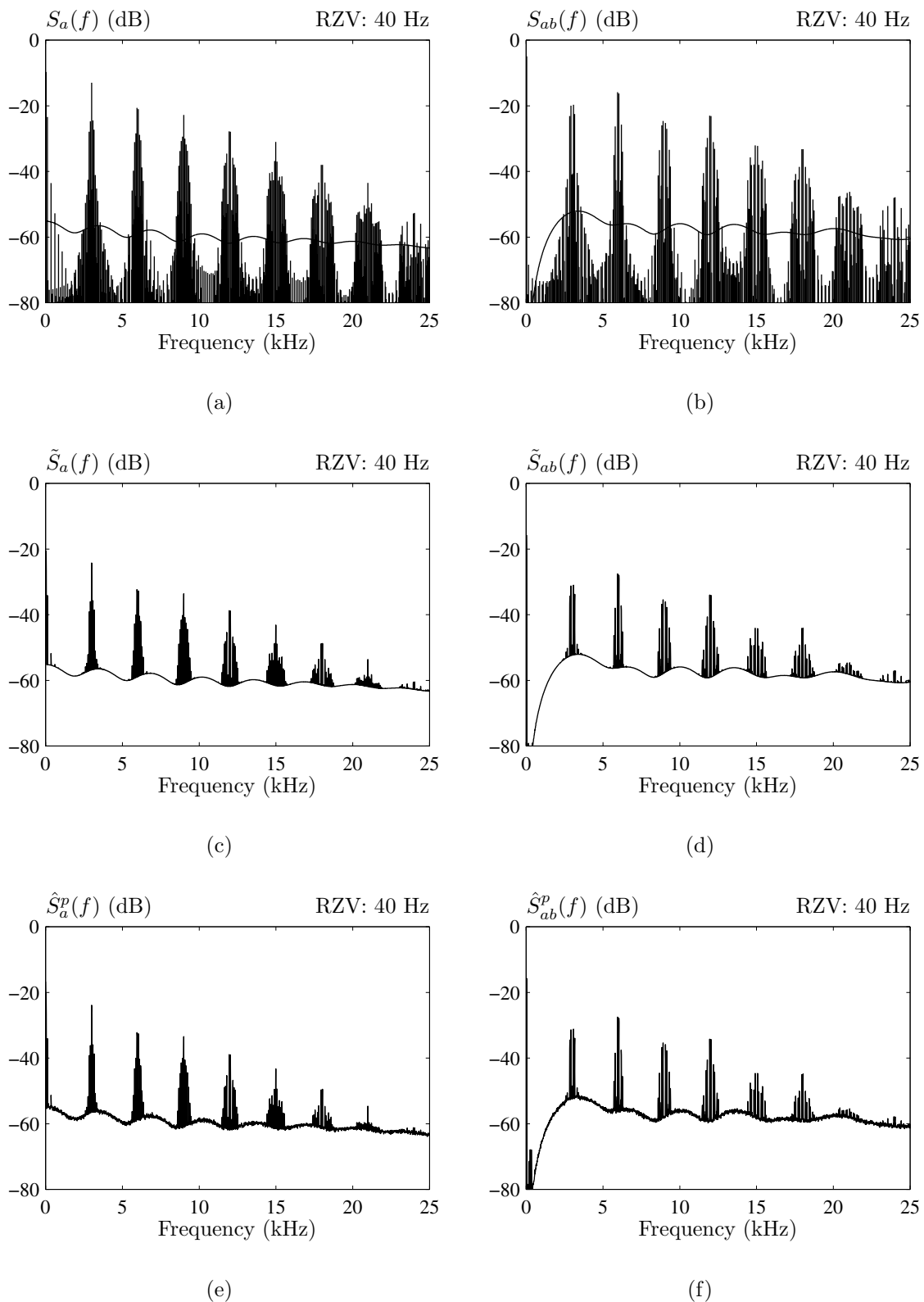
Figure 6.19 Spectra for random zero-vector (RZV) modulation using the settings for 40 Hz operation in Table 6.3 (page 205). Spectra for both the switching function (left column) and the line-to-line voltage (right column) are shown. (a, b) Calculated density and harmonic spectrum, (c, d) calculated density spectrum including power due to harmonics, and (e, f) measured density spectrum.
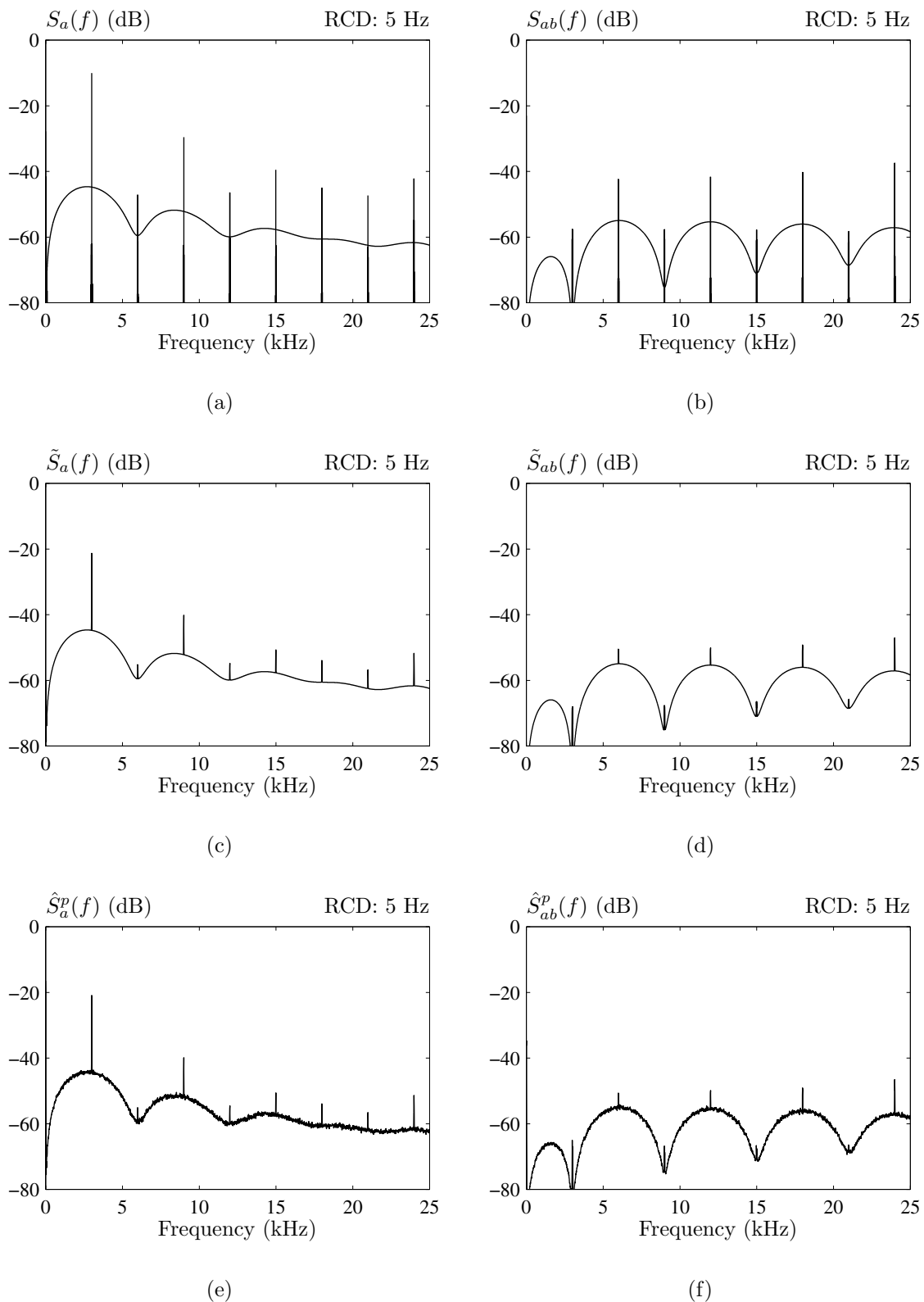
Figure 6.20 Spectra for random center displacement (RCD) modulation using the settings for 5 Hz operation in Table 6.3 (page 205). Spectra for both the switching function (left column) and the line-to-line voltage (right column) are shown. (a, b) Calculated density and harmonic spectrum, (c, d) calculated density spectrum including power due to harmonics, and (e, f) measured density spectrum.
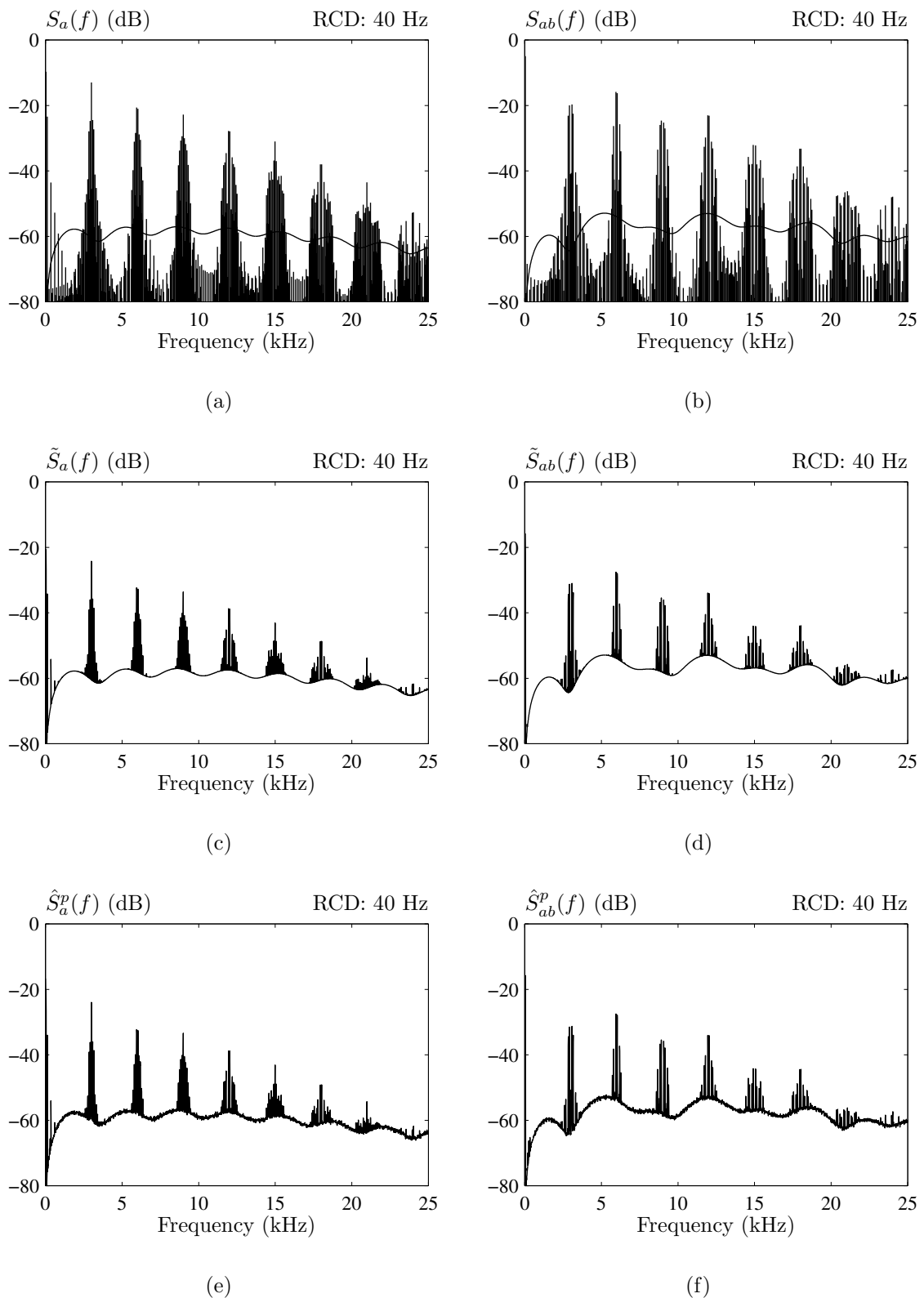
Figure 6.21 Spectra for random center displacement (RCD) modulation using the settings for 40 Hz operation in Table 6.3 (page 205). Spectra for both the switching function (left column) and the line-to-line voltage (right column) are shown. (a, b) Calculated density and harmonic spectrum, (c, d) calculated density spectrum including power due to harmonics, and (e, f) measured density spectrum.

(a)

(b)

(c)

(d)

(e)

(f)
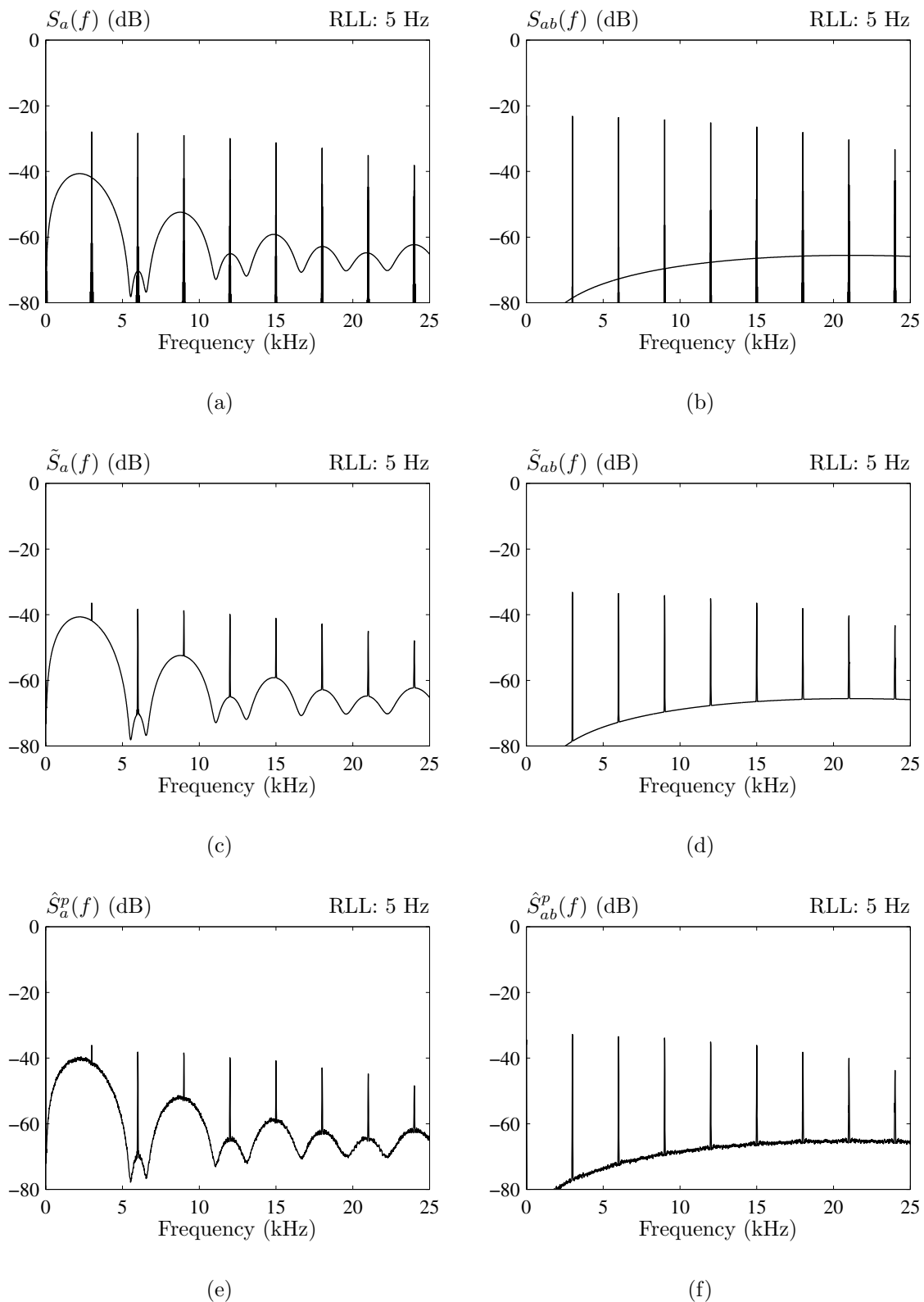
Figure 6.22 Spectra for random lead-lag (RLL) modulation using the settings for 5 Hz operation in Table 6.3 (page 205). Spectra for both the switching function (left column) and the line-to-line voltage (right column) are shown. (a, b) Calculated density and harmonic spectrum, (c, d) calculated density spectrum including power due to harmonics, and (e, f) measured density spectrum.
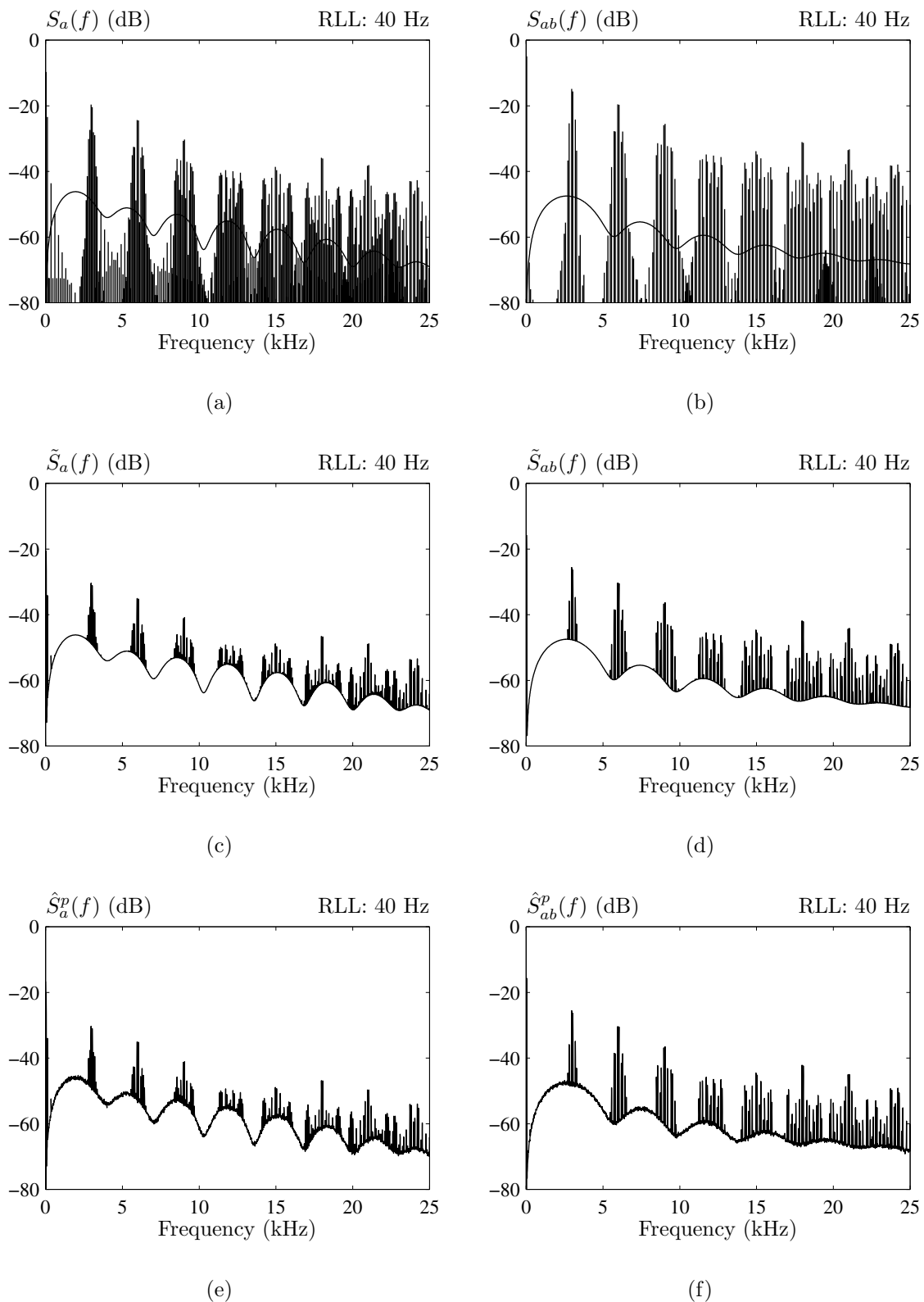
Figure 6.23 Spectra for random lead-lag (RLL) modulation using the settings for 40 Hz operation in Table 6.3 (page 205). Spectra for both the switching function (left column) and the line-to-line voltage (right column) are shown. (a, b) Calculated density and harmonic spectrum, (c, d) calculated density spectrum including power due to harmonics, and (e, f) measured density spectrum.
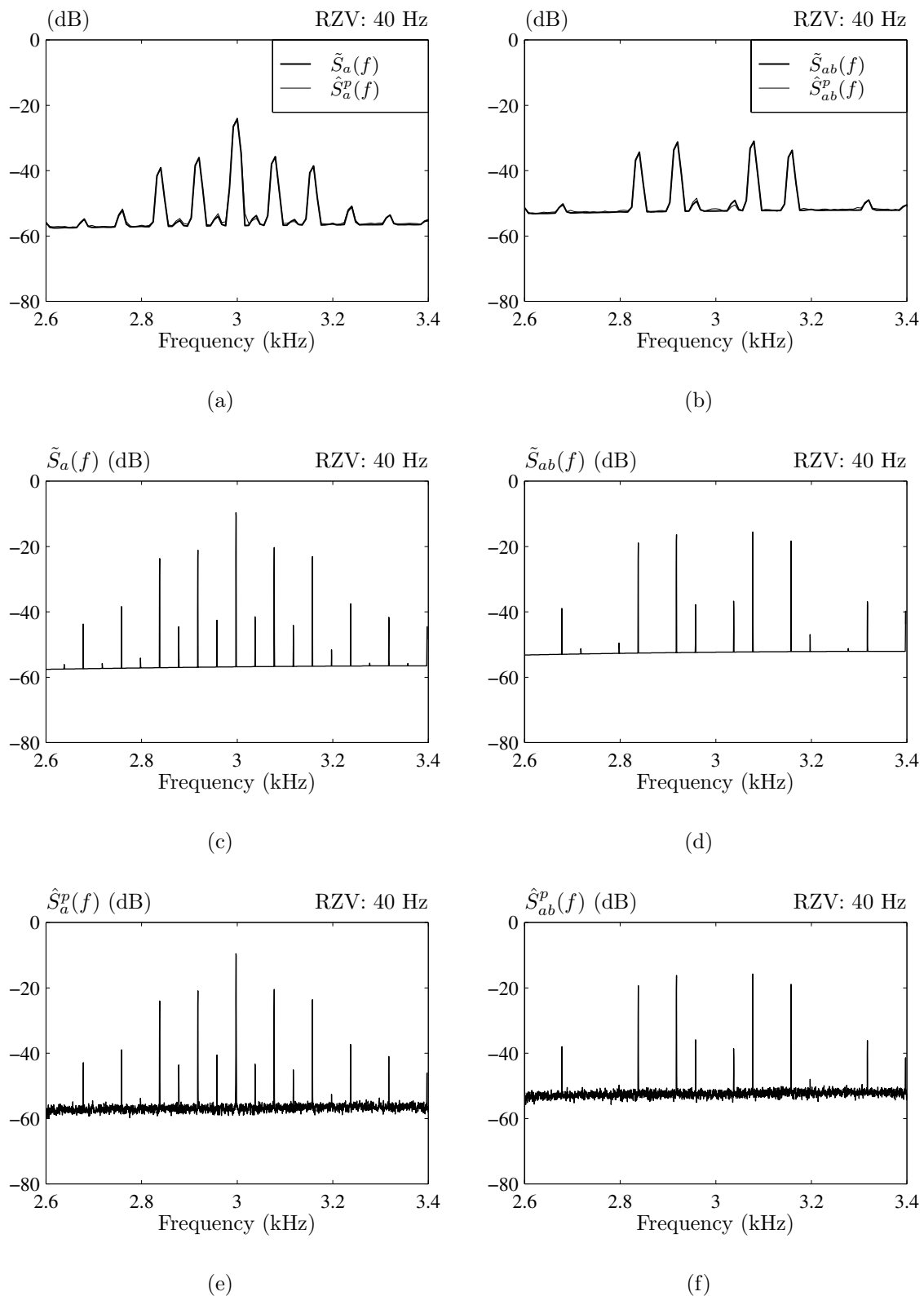
Figure 6.24 Detailed spectra around 3 kHz for random zero-vector (RZV) modulation using the settings for 40 Hz operation in Table 6.3 (page 205). Spectra for both the switching function (left column) and the line-to-line voltage (right column) are shown. (a, b) Calculated and measured spectra using 8 Hz resolution, (c, d) calculated spectra using 0.25 Hz resolution, and (e, f) measured spectra using 0.25 Hz resolution.
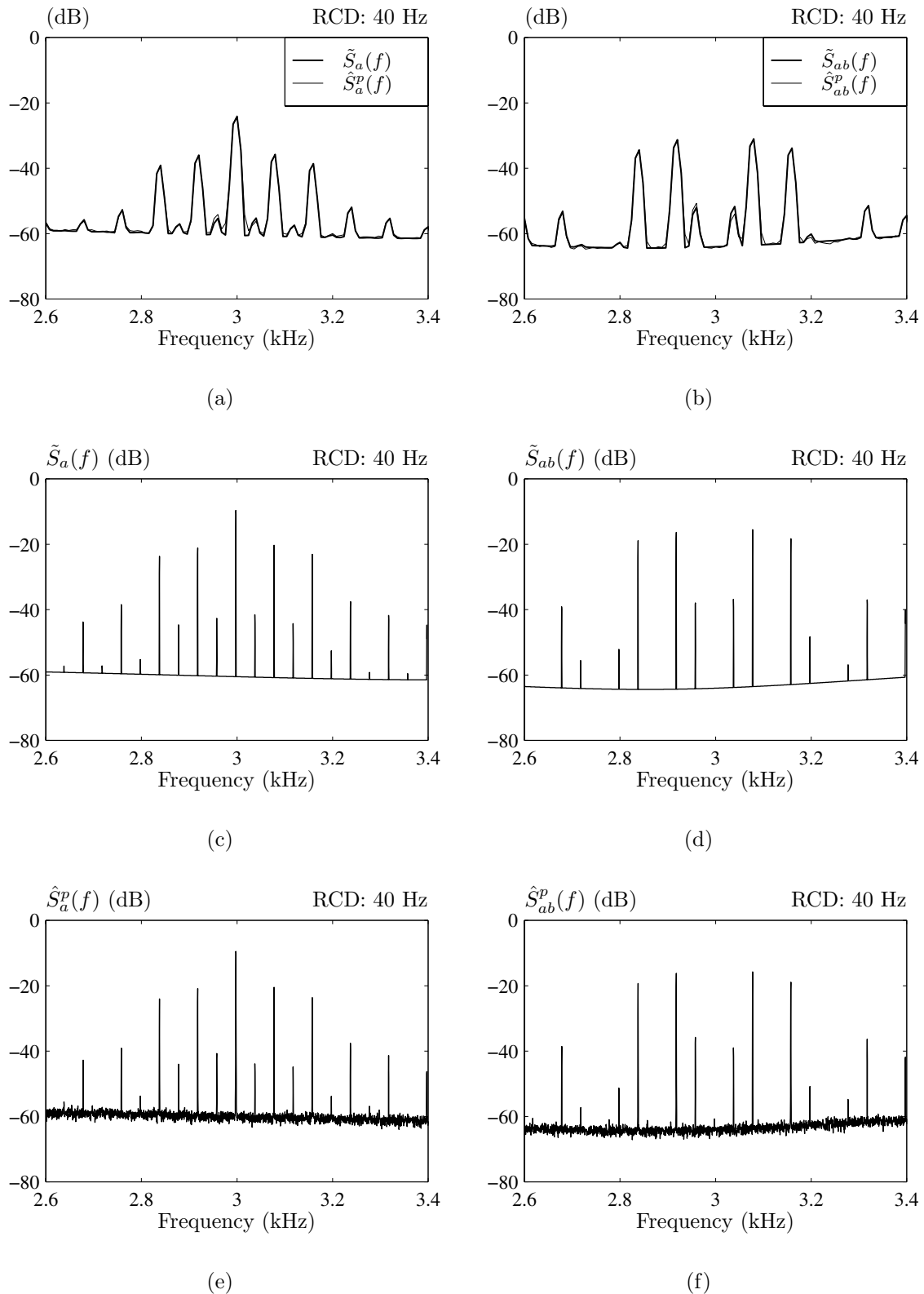
Figure 6.25 Detailed spectra around 3 kHz for random center displacement (RCD) modulation using the settings for 40 Hz operation in Table 6.3 (page 205). Spectra for both the switching function (left column) and the line-to-line voltage (right column) are shown. (a, b) Calculated and measured spectra using 8 Hz resolution, (c, d) calculated spectra using 0.25 Hz resolution, and (e, f) measured spectra using 0.25 Hz resolution.

(a)

(b)

(c)

(d)

(e)

(f)
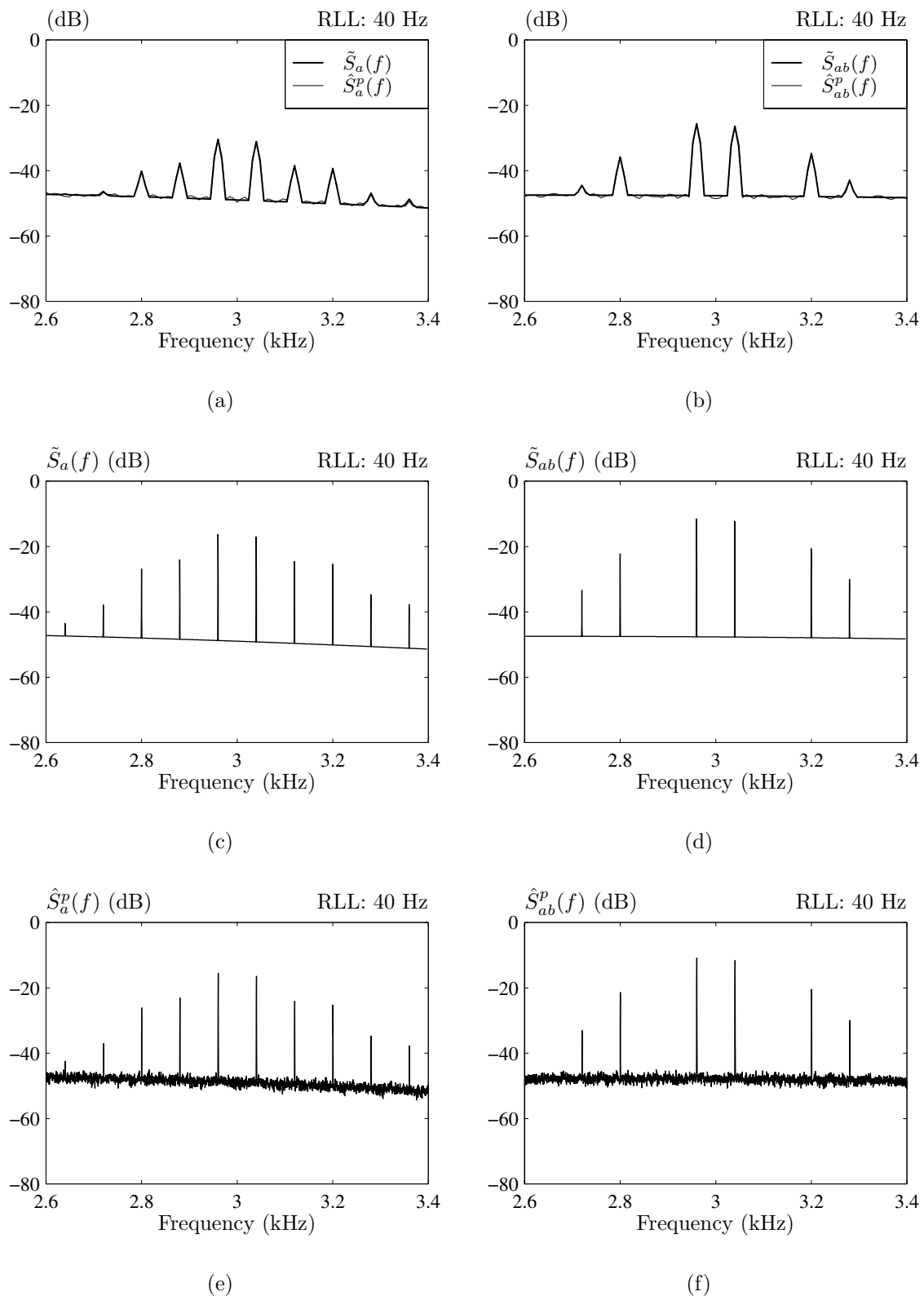
Figure 6.26 Detailed spectra around 3 kHz for random lead-lag (RLL) modulation using the settings for 40 Hz operation in Table 6.3 (page 205). Spectra for both the switching function (left column) and the line-to-line voltage (right column) are shown. (a, b) Calculated and measured spectra using 8 Hz resolution, (c, d) calculated spectra using 0.25 Hz resolution, and (e, f) measured spectra using 0.25 Hz resolution.

spectra is hardly discernible in Figs. 6.24–6.26(a, b). The spectral analysis appears very accurate even at this smaller frequency scale.

At this point, it should be recalled from Chapter 3 that measurable spectra like $\hat{S}_a(f)$ differ from the true spectrum $S_a(f)$, especially in the vicinity of harmonics when an insufficient noise bandwidth f_{nbw} for the DSA is used. As listed in Table 6.3(c), the DSA is set to use a Hanning window and it has a frequency resolution of 8 Hz. This implies that the noise bandwidth equals $f_{nbw} = 1.5 \cdot 8$ Hz $= 12$ Hz (see page 55 also), which is only about 3.3 times smaller than the frequency separation between two adjacent harmonics spaced 40 Hz apart from each other. Hence, the curves shown in e.g. Fig. 6.24(a, b) for the power spectral density should not be trusted unconditionally because of the significant spectral leakage. Despite the inaccuracy the plots can, nevertheless, still be used to benchmark the spectral theory, because the errors that the DSA makes are included in the calculations of $\tilde{S}_a(f)$ and $\tilde{S}_{ab}(f)$.

To illustrate the impact of changing the DSA settings on the estimated spectra $\hat{S}_a(f)$ and $\hat{S}_{ab}(f)$, a few additional measurements were made using a 0.25 Hz resolution. Now, $f_{nbw} = 0.375$ Hz, which gives a f_1/f_{nbw} ratio larger than 100. The results in Figs. 6.24–6.26(e, f) may be compared to the spectra for $\tilde{S}_a(f)$ and $\tilde{S}_{ab}(f)$ recalculated by using the modified settings of the DSA, see Figs. 6.24–6.26(c, d).

By comparing, for example, Fig. 6.24(a) to Fig. 6.24(c, e) several observations may be made: the noise floor remains at -58 dB, the peaks (of density) caused by the harmonics becomes much more narrow and their magnitude becomes smaller, and harmonic components not visible in Fig. 6.24(a) suddenly show up in Fig. 6.24(c, e). All this happens without changing any parameters in the RZV modulator used in this particular case; the observed differences are all caused by the much smaller value for f_{nbw}.

Again, it should be noted that the developed spectral analyses for all three investigated FCF-RPWM schemes perfectly match the measurements, irrespective of the modified DSA settings.

6.9   Summary

Random PWM methods operating with a fixed carrier frequency have been investigated in this chapter. These methods — abbreviated as FCF-RPWM— are applicable for voltage control of two-level hard-switched converters, which are commonly used in three-phase systems, such as ac motor drives, active mains rectifiers, etc.

In the first part of this chapter, a review of FCF-RPWM methods found in the literature was presented. Those methods include the random lead-lag (RLL), random zero-vector distribution (RZV), and a method denoted as random sequence selection (RSS). Next, the degrees of freedom in FCF-RPWM were identified and two novel FCF-RPWM schemes, that meet the defined constraints, were suggested.

To aid the evaluation of the practical applicability of FCF-RPWM schemes, a number of requirements were formulated and discussed. One of the requirements relates to the controllability of the fundamental component of the current. Stated otherwise, it seems natural to require that the change of the average current in a PWM period is independent of the ripple voltage caused by the pulse-width modulation, i.e. it is highly desirable that FCF-RPWM schemes are designed such that the fundamental current is

unaffected by the randomization on the microscopic time scale. For control purposes, another key constraint relates to the detection of the average phase current in each carrier period. Hence, a good FCF-RPWM should also be compatible with the commonly used method of detecting the average phase currents by sampling simultaneously all phase currents in the center of the carrier period.

To investigate whether the different FCF-RPWM schemes comply with those constraints or not, a theoretical analysis of current waveforms was given in the next part of this chapter. After having performed such an analysis for two of the existing schemes (RLL and RZV) and for the new RCD (random center displacement) method, several interesting conclusions were drawn, which cannot — to the knowledge of the author — be found elsewhere in the literature. The new contributions in this area include:

- The change of the average load current is not unconditionally independent of the modulation (more precisely, the ripple voltage), even if a proper volt-second balance is maintained.

- The coupling between the ripple voltage and the average load current was mathematically formulated and based on this analysis, precise requirements were stated that for pulse-width modulators so that the average load current is de-coupled from the ripple voltage caused by imperfect voltage synthesis.

- It was shown that pulse-width modulators generating switching functions that are symmetrical around the midpoint of the carrier period automatically fulfill the derived requirements.

- The RLL modulator does not comply with the formulated rules. Severe distortion of the fundamental current results when RLL modulation is used to control a converter due to the poor utilization of zero vectors and the highly asymmetrical switching functions.

- The RCD scheme does also introduce coupling between the modulator and the average load current, but to a lower degree than RLL modulation.

- Two variants of the RZV modulator exist. One variant gives the desirable symmetrical switching patterns, but the variant giving asymmetrical switching patterns exhibits the same problems as do RCD and RLL.

- As a consequence, even open-loop voltage control requires special attention in FCF-RPWM to ensure that the quality of the fundamental current is acceptable; the fundamental current is distorted by the switching process, if the modulator generates asymmetrical switching patterns.

- The analysis of the impact of the modulator on the load current is not tailored towards FCF-RPWM modulation only; exactly the same problems exist in fully deterministic modulators, if asymmetrical switching functions are generated. In fact, the problems may be more pronounced in deterministic PWM compared to random PWM, because here the accumulation of local errors is not neutralized to the same extent as in random PWM.

Afterwards, it was investigated whether or not it is possible to measure the true average phase current in FCF-RPWM controlled converters by sampling the phase current in the middle of the carrier period. Several new results have been achieved, including:

- It was shown that only the variant of RZV that yields symmetrical switching patterns complies with the standard sampling approach, i.e. it is impossible to detect the average current by this sampling method when RLL, RCD, or the second variant of RZV is used. This is a serious drawback in closed-loop applications that rely on accurate current feedback.

- To remedy this problem, a novel current detection method was presented, which is only slightly more complicated than the normal sampling principle. This method requires two samples of the phase current in each PWM period; the true average current can then be determined by evaluating a simple expression. The parameters in this expression are completely independent of any load parameters. This current detection method can be used for both the RZV and the RCD schemes.

In the last part of this chapter focus was put on spectral analysis of three FCF-RPWM schemes. First, a general formula for the spectrum produced by a FCF-RPWM modulator was derived based on the unified spectral analysis in Chapter 3. This formula shows that FCF-RPWM techniques cause a mixed spectra, i.e. both harmonics and distributed power (density) exist. The derived formula may be regarded as a generalization of the work in [4], but those generalizations are, nevertheless, required in order to perform spectral analysis of the RZV technique.

Next, the RLL, RZV, and RCD schemes were subjected to spectral analysis. For each scheme, theoretical expressions were derived for the spectrum of the switching function controlling one leg of a converter and also, expressions were derived for the spectrum of the line-to-line voltage. All these results are believed to be completely novel, except for the analysis of the RLL technique for which similar analyses may be found in [3, 4].

To verify the spectral theory, laboratory experiments were performed in order to gather comparative experimental data. Comparisons of calculated spectra to the spectra estimated in the laboratory on a functioning system showed that an excellent agreement exists for all examined modulators and operating conditions. Hence, it may safely be concluded that a very accurate spectral analysis has been established for FCF-RPWM techniques.

Bibliography

[1] S. Legowski, J. Bei, and A. M. Trzynadlowski, "Analysis and Implementation of a Grey-Noise PWM Technique Based on Voltage Space Vectors," *Proc. of the 7th IEEE Applied Power Electronics Conference and Exposition*, pp. 586–593, 1992.

[2] R. L. Kirlin, S. Legowski, A. M. Trzynadlowski, Y. Cui, and S. Kwok, "Power Spectra of a Three-Phase Inverter with Random Pulse Width Modulation Modes," *Proc. of the 3rd IEEE Workshop on Computers in Power Electronics*, pp. 265–267, Aug. 1992.

[3] R. L. Kirlin, S. Kwok, S. Legowski, and A. M. Trzynadlowski, "Power Spectra of a PWM Inverter with Randomized Pulse Position," *IEEE Trans. on Power Electronics*, vol. 9, no. 5, pp. 463–472, Sept. 1994.

[4] A. M. Stanković, *Random Pulse Modulation with Applications to Power Electronic Converters*, Ph.D. thesis, Massachusetts Institute of Technology, Feb. 1993.

[5] M. M. Bech, F. Blaabjerg, J. K. Pedersen, and A. M. Trzynadlowski, "Comparative Investigation of Random PWM Techniques with Variable Switching Frequency and Pulse Position for Inverter-Fed Induction Motors," *Proc. of 7th European Conference on Power Electronics and Applications*, vol. 1, pp. 343–349, 1997.

[6] B.-R. Lin and H.-H. Lu, "Three-Phase AC/DC/AC Converter with Random Pulse Position," *Proc. of 8th European Conference on Power Electronics and Applications*, Sept. 1999.

[7] V. Blasko, "Analysis of a Hybrid PWM Based on Modified Space-Vector and Triangle-Comparison Methods," *Conference Record of the 31st IEEE Industry Applications Society Annual Meeting*, vol. 2, pp. 947–955, 1996.

[8] V. Blasko, "Analysis of a Hybrid PWM Based on Modified Space-Vector and Triangle-Comparison Methods," *IEEE Trans. on Industry Applications*, vol. 33, no. 3, pp. 756–764, May/June 1997.

[9] V. Blasko, Rockwell Automation, "Hybrid Pulse Width Modulation Method and Apparatus," US. Patent No. 5.706.186, Filed Sept. 23, 1996.

[10] L. Garces and V. T. N'Guyen Phuoc, Schneider Electric SA, "Inverter Control Device," US Patent No. 5.552.980, Filed March 1, 1995.

[11] Y. S. Lai, "Random Switching Techniques for Inverter Control," *Electronics Letters*, vol. 33, no. 9, pp. 747–749, Apr. 1997.

[12] Y. S. Lai, H. C. Huang, Y. S. Kuan, and C. M. Young, "A New Random Inverter Control Technique for Motor Drives," *Proc. of the 13th IEEE Applied Power Electronics Conference and Exposition*, vol. 1, pp. 101–107, Feb. 1998.

[13] Y. S. Lai and S. C. Chang, "DSP-based Implementation of New Random Switching Technique of an Inverter Control for Sensorless Vector-Controlled Induction Motor Drives," *IEE Proceedings – Electric Power Applications*, vol. 146, no. 2, pp. 163–172, Mar. 1999.

[14] Y. S. Lai, "New Random Inverter Control Technique for Common Mode Voltage Mitigation of Motor Drives," *IEE Proceedings – Electric Power Applications*, vol. 146, no. 3, pp. 289–296, May 1999.

[15] Y. S. Lai, "Sensorless Vector-Controlled IM Drives using Random Switching Technique," *Proc. of 8th European Conference on Power Electronics and Applications*, Sept. 1999.

[16] J. W. Kolar, H. Ertl, and F. C. Zach, "Minimizing the Current Harmonics RMS Value of Three-Phase PWM Converter Systems by Optimal and Suboptimal Transition between Continuous and Discontinuous Modulation," *Proc. of the 22nd IEEE Power Electronics Specialists Conference*, vol. 1, pp. 372–381, 1991.

[17] D. Antić, J. B. Klaassens, and W. Deleroi, "Side Effects in Low-Speed AC Drives," *Proc. of the 25th IEEE Power Electronics Specialists Conference*, vol. 2, pp. 998–1002, 1994.

[18] D.-W. Chung and S.-K. Sul, "Analysis and Compensation of Current Measurement Error in Vector-Controlled AC Motor Drives," *IEEE Trans. on Industry Applications*, vol. 34, no. 2, pp. 340–345, Marts/April 1998.

[19] T. Sukegawa, K. Kamiyama, T. Matsui, and T. Okuyama, "A High Accuracy Current Component Detection Method for Fully Digital, Vector-controlled PWM VSI-fed AC Drives," *Proc. of the 19th IEEE Power Electronics Specialists Conference*, vol. 2, pp. 877–884, 1988.

[20] T.C. Green and B. W. Williams, "Derivation of Motor Line-Current Waveforms from the DC-Link Current of an Inverter," *IEE Proceedings Part B*, vol. 136, no. 4, pp. 196–204, July 1989.

[21] F. Blaabjerg, J. K. Pedersen, U. Jaeger, and P. Thoegersen, "Single Current Sensor Technique in the DC-Link of Three-phase PWM-VS Inverters. A Review and a Novel Solution," *IEEE Trans. on Industry Applications*, vol. 33, no. 5, pp. 1241–1253, Sept./Oct. 1997.

[22] V. Blasko, V. Kaura and W. Niewiadomski, "Sampling of Discontinuous Voltage and Current Signals in Electrical Drives: A System Approach," *Conference Record of the 32nd IEEE Industry Applications Society Annual Meeting*, vol. 1, pp. 682–689, 1997.

[23] H. W. Van der Broeck, H. C. Skudelny, and G. V. Stanke, "Analysis and Realization of a Pulsewidth Modulator Based on Voltage Space Vectors," *IEEE Trans. on Industry Applications*, vol. 24, no. 1, pp. 142–150, Jan./Feb. 1988.

[24] J. Holtz, "Pulse Width Modulation for Electronic Power Conversion," in *Power Electronics and Variable Frequency Drives. Technology and Applications*, B. K. Bose, Ed., New York, 1997, pp. 138–208, IEEE Press.

[25] D. W. Novotny and T. A. Lipo, *Vector Control and Dynamics of AC Drives*, Monographs in Electrical and Electronic Engineering. Oxford University Press, Oxford, 1996.

[26] F. Blaabjerg, J. K. Pedersen, and P. Thoegersen, "Improved Modulation Techniques for PWM-VSI Drives," *IEEE Trans. on Industrial Electronics*, vol. 44, no. 1, pp. 87–95, Feb. 1997.

[27] S. R. Bowes, "New Sinusoidal Pulsewidth-Modulated Invertor," *Proc. IEE*, vol. 122, no. 11, pp. 1279–1285, Nov. 1975.

[28] A. Schönung and H. Stemmler, "Geregelter Drehstrom-Umkehrantrieb mit ges-teuertem Umrichter nach dem Unterschwingungsverfahren," *Brown Boveri Mitteilungen*, vol. 51, no. 8/9, pp. 555–577, Aug./Sept. 1964.

[29] Analog Devices, *ADMC401: Single-Chip, DSP-Based High Performance Motor Controller (Rev. A)*, Analog Devices, Norwood, Massachusetts, 1999.

[30] F. Blaabjerg and J. K. Pedersen, "An Ideal PWM-VSI Inverter using only one Current Sensor in the DC-link," *Proc. of the IEEE International Conference on Power Electronics and Variable Speed Drives*, vol. 1, pp. 458–464, 1994.

[31] F. Blaabjerg and J. K. Pedersen, "A New Low-Cost, Fully Fault Protected PWM-VSI Inverter with True Phase-Current Information," *IEEE Trans. on Power Electronics*, vol. 12, no. 1, pp. 187–197, Jan. 1997.

[32] M. M. Bech, F. Blaabjerg, and J. K. Pedersen, "Random Modulation Techniques with Fixed Switching Frequency for Three-Phase Power Converters," *Proc. of the 30th IEEE Power Electronics Specialists Conference*, vol. 1, pp. 544–551, June 1999.

[33] A. M. Hava, R. J. Kerkman, and T. A. Lipo, "Simple Analytical and Graphical Methods for Carrier-Based PWM-VS Drives," *IEEE Trans. on Power Electronics*, vol. 14, no. 1, pp. 49–61, Jan. 1999.

[34] Y. C. Son, S. H. Song, and S. K. Sul, "Analysis and compensation of current sampling error in AC drive with discontinuous PWM," *Proc. of the 14th IEEE Applied Power Electronics Conference and Exposition*, vol. 2, pp. 795–799, 1999.

[35] A. M. Trzynadlowski, F. Blaabjerg, J. K. Pedersen, R. L. Kirlin, and S. Legowski, "Random Pulse Width Modulation Techniques for Converter Fed Drive Systems — A Review," *IEEE Trans. on Industry Applications*, vol. 30, no. 5, pp. 1166–1175, Sep./Oct. 1994.

[36] J. Zubek, A. Abbondanti, and C. J. Norby, "Pulsewidth Modulated Inverter Motor Drives with Improved Modulation," *IEEE Trans. on Industry Applications*, vol. IA-11, pp. 695–703, Nov./Dec. 1975.

[37] D. Middleton, *An Introduction to Statistical Communication Theory*, McGraw-Hill Book Company, New York–Toronto–London, 1960.

[38] A. M. Stanković, G. C. Verghese, and D. J. Perreault, "Analysis and Synthesis of Randomized Modulation Schemes for Power Converters," *IEEE Trans. on Power Electronics*, vol. 10, no. 6, pp. 680–693, Nov. 1995.

Part III

Random PWM in closed-loop applications

Chapter 7

Aspects of random PWM in closed-loop applications

7.1 Introduction

To encircle the needs for the results presented in this chapter it may initially be recalled that in almost all high-performance applications of switching converters one or more feed-back loops are synchronized to the pulse-width modulator itself. A key example is the current-control loop used in many different power electronic topologies ranging from single-switch converters (e.g. flyback dc/dc converters) and upwards. Focusing on the three-phase voltage-source converter (VSC), [1] lists a number of important applications, including ac motor control, rectifiers, uninterruptible power supplies, and active filters. To ensure a fast regulation of the ac currents in this kind of applications, fast-responding modulation techniques must be employed in order to track the voltage commanded by the current controller.

On this background, it is interesting to investigate if the random PWM methods advocated in this thesis are consistent with the requirement of closed-loop operation due to the superior performance obtainable in this mode. Without anticipating the conclusions drawn in the next chapter, it may already here be stated that it is indeed possible to unify random PWM and feed-back control implemented in a digital control system. Before this conclusion can be reached, an analysis of the problems pertinent to using random PWM in conjunction with discrete-time feed-back control loops is required. Therefore, the objective of this chapter is two-fold: to identify the problems and to present a method to overcome the problems of using random PWM techniques together with established feed-back control techniques in power electronic converters.

It should be observed that the ideas and techniques developed in this chapter are by no means limited to the particular applications listed above, let alone to random PWM only: in particular, this chapter contains a general treatment of the problems relating to non-uniform sampling rates in digital control systems, although the analysis is clearly motivated by random PWM applications. Chapter 8 starting on page 247 presents an example of how the results derived in the current chapter may be used to build a complete field-oriented drive based on a random carrier frequency pulse-width modulator.

Chapter outline

A discussion of the challenges of unifying a random PWM with discrete-time systems is given in section 7.2. In the following sections, closer investigations of the identified problems relating to design of digital controllers are presented and a viable design route is given. A summary and an outline of the key results conclude this chapter.

7.2 Preliminaries

The starting point for the discussion of random PWM in closed-loop applications is a brief review of previous publications dealing with the topic. Partly based on this review, a set of requirements is then formulated, which should be addressed before a successful unification of random PWM and discrete-time controllers[1] can be proclaimed.

Next, the correlation between sampling and PWM carrier frequencies is reviewed since it turns out that the major difficulty of using random PWM in feed-back systems closely relates to the constraints imposed on feasible selections of sampling rates. This information is then used to highlight the merits and demerits of different random PWM techniques in closed-loop applications.

7.2.1 Related previous work

The most important contribution in this area is due to Jacobina et al. who in 1997 described a current-regulated induction motor drive based on a VSC operating with a random carrier frequency [2]. Here, the updating of a linear PI current controller is synchronized to the random carrier periods which implies that the sampling rate of the controller is non-uniform. The coefficients of the governing difference equation are recalculated in every sampling period in order to approximate the response of the digital implementation to the response of the underlying analogue PI-controller, independently of the instantaneous sampling rate. In short, the analysis and the experiments in [2], which appears in [3] also, demonstrate that random carrier frequency PWM is compatible with standard principles for feed-back control — at least for simple first-order compensators, such as PI controllers.

In [4–6], Lin and Lu report three identical implementations of a rotor field-oriented induction motor drive using random lead-lag (RLL) pulse position modulation. The authors claim that it is possible to reduce the acoustic noise while still maintaining good control of the drive. However, practical applications of this approach are difficult to forecast due to serious defects totally ignored in [4–6]: RLL generates asymmetrical switching functions and, as shown in Chapter 6, these deteriorate the current quality (substantial ripple current besides adding distortion to the fundamental current) and furthermore, it is impossible to sample the correct value of the per carrier period average. Secondly, RLL is very poor-performing regarding reduction of annoyance due to acoustic noise [7, 8].

---

[1]The term "controller" is used in this chapter as a common label for conceptually different functional units such as actual controllers, but also for filters, estimators, and observers, i.e. elements having the property in common that they can be regarded as transfer functions.

Pulse-width modulation using a random carrier frequency is used by Lin in [9]. The modulator is implemented in analogue hardware and the controllers operate in DSP software, presumably with a fixed sampling rate. No comments are given about the timing problems related to the interface between those two subsystems; nor is comparisons with fixed-frequency PWM provided in [9]. A very similar approach to randomize a field-oriented drive is used in [10], which includes many informative measurements of noise, current, and voltage spectra. Unfortunately, [10] does not report details about the inner control loops, such as the dynamic performance of the current controller.

Sensor-less vector-control of an induction motor is reported by Lai in [11–13] where a random PWM method operating with a constant updating rate is used. Instead, the sequence in which the switching states are applied within a carrier period is subjected to randomization; in Chapter 6, this technique was designated by the acronym RSS. The converter is forced to jump between non-adjacent states, which increases the switching losses considerably, but Lai does not comment on this problem. As pointed out in Chapter 6, the impact of RSS on acoustic noise is not documented by Lai despite seven papers on this particular random PWM technique (see Appendix B).

7.2.2 Key issues for closed-loop applications of random PWM

Based on results of Part II, the investigations by the author reported in [7, 8], and on the papers reviewed in the previous subsection, the following key issues for the successful use of random PWM in closed-loop applications[2] with strict performance requirements may be identified:

Overall system performance
> This includes speed and torque dynamics, current quality, and switching losses besides the main reason of introducing random PWM in the first place: the acoustic noise problem should be alleviated under all operating conditions.

Acquisitions of feed-back signals
> In particular, error-free acquisitions of the currents fed back to the controller are crucial for a satisfactory closed-loop operation. No compensator can attenuate the impact of erroneous feed-back signals without giving excessive delays.

Design and implementation of controllers
> Discrete-time systems operating with a fixed sampling rate is well understood and widely used, but for random PWM applications, attention should be paid to that the carrier frequency may be non-constant. This affects both design and implementation of digital controllers synchronized to the PWM unit.

The first issue listed above should be self-explanatory: the randomized drive should have better subjective acoustic noise properties than a standard drive and, meanwhile, all tangible characteristics, such as torque response, speed regulation, switching losses and current quality, should remain unaffected by the randomization to the largest extent possible.

---

[2]Without any significant loss of generality, this presentation focuses on three-phase VSC-fed motor drive systems that include (current) controllers implemented in sampled-data systems, such as a DSP or a microcontroller.

Based on results of Chapter 6 again, the second requirement generally restricts the pool of candidate random PWM methods for closed-loop applications to those techniques that preserve symmetry of the generated switching patterns around the midpoint of the carrier period (at least if the detection of per-carrier period average currents is based on sampling the instantaneous current in the middle of the carrier).

The remaining part of this chapter focuses on problems related to the third topic listed above, but to facilitate the discussion it may simply be noted that the use of random carrier frequency PWM requires careful attention, if performance deterioration should be avoided. This problem was acknowledged and investigated in [2, 3] but overlooked in both [9] and [10]. It turns out that the work of [2, 3] fits nicely into the more general framework developed in sections 7.3 and 7.4.

7.2.3   Sampling rate considerations

The obtainable closed-loop bandwidth of a digital control system depends on the sampling frequency f_s. Also in high-performance applications that rely on PWM, the sampling instants of the inner-most controllers are synchronized to the PWM unit for reasons related to both performance and acquisition of currents.

Typically, the sampling rate for the current controller is equal to the carrier frequency f_c for the converter. Here, the current controller outputs a new reference voltage vector for the modulator once per PWM carrier period. Using double-sided PWM, it is also possible to update the modulator twice per carrier period ($f_s/f_c = 2$) without changing the number of commutations, i.e. without additional losses. The price paid is a twofold reduction of the time available for evaluating the controller algorithms compared to the $f_s/f_c = 1$ case. Advantage of this approach to double the maximal obtainable bandwidth can be taken if the maximum commutation frequency is low (which implies that the time available for computations is high), or if a particular application has very high performance specifications (and a fast computational unit) which cannot be met with symmetrical PWM. In either case, a synchronization of the controller to the PWM carrier implies that the control system must be able to operate with a non-uniform sampling rate when random carrier frequency (RCF) PWM is used.

7.2.4   Final remarks

At this point it may be argued that the use of fixed carrier frequency random PWM (FCF-RPWM) techniques like those discussed in Chapter 6 would eliminate the need for using non-uniform sampling rates. Unfortunately, all known FCF-RPWM techniques are less efficient with respect to acoustic noise reduction than the RCF technique in the high modulation index range. This has been demonstrated experimentally in [7, 8] by measurements of noise spectra. (In retrospect, the same conclusion can be drawn from the observed voltage spectral in Chapters 5 and Chapter 6 for RCF and FCF-RPWM, respectively.) Furthermore, as summarized in section 6.3.7 starting on page 185, the use of FCF-RPWM techniques may induce problems with respect to current distortion and sampling of currents needed for feed-back control, but, on the other hand, the RCF technique using center-aligned on-state pulses does not distort the fundamental current, and compliance with current sampling techniques is guaranteed as well.

In summary, a well-performing closed-loop application of random PWM must be able to operate with randomly changing sampling rates, simply because the RCF-PWM technique is the best way to reduce acoustic noise from, say, electric motor drives.

7.3 Feasibility of design procedures for digital control systems

The normally used procedures for design of digital control systems are reviewed below and their compatibility with the special requirements imposed by random PWM operation is discussed. It turns out that the methods based on translation of a continuous-time transfer functions into an equivalent discrete-time representation are the only feasible design procedures. Details of such procedures are discussed below as well.

7.3.1 Review of approaches to digital design

For the design of digital control systems, different routes may lead from the given system model and performance specifications to the final computer algorithm. Based on classic textbooks [14–16], the methods may be divided into two top-level categories:

Indirect digital design
> The procedure is initially to ignore the fact that the controller must be implemented in a sampled-data system, i.e. the design is performed in the continuous-time domain (or, equivalently, in the Laplace domain). When a controller has been designed (i.e. its transfer function has been determined), the controller is translated into an equivalent discrete-time controller using one of the methods listed in the next subsection.

Direct design in discrete-time
> Initially, the system model and the performance specifications are transformed to the discrete-time z-domain. Then, using standard rules for design of digital controllers, a discrete transfer function is found from which the sought difference equation may be obtained immediately.

Now, the cardinal point is to recall that according to section 7.2.3, the controller must be capable of operating with a non-uniform sampling rate. This implies that the direct design procedure based on the $\mathcal{Z}$-transformation is unsuitable for the application at hand: One of the fundamental assumptions, on which the whole framework of the $\mathcal{Z}$-transformation is based, is that the sampling interval is constant; it is required that the sampling instants are equally spaced in time[3].

Keeping this fact in mind, the direct design method is incompatible with the problem at hand, because it cannot be assumed that the sampling rate is constant.

---

[3]Theoretically speaking, it is not entirely true that the $\mathcal{Z}$-transformation is applicable to strictly uniformly spaced sequences only. It has been demonstrated in [17] that by using a method known as switch-decomposition, it is possible to analyze non-uniformly sampled filters, provided that the sampling intervals are so-called periodic non-uniform. This means that the sampling process must repeat itself after T_Σ seconds such that $T_\Sigma = \sum T_k$, where $\{T_k\}$ is a known, finite sequence of sampling intervals. Unfortunately, this approach requires a deterministic knowledge of the distribution of the sampling instants, which is not the case here.

7.3.2　Digital design by emulation of continuous-time transfer functions

The potentials of the indirect design procedure are discussed in greater details below. Before continuing the discussion, the problem to be solved may be formulated in more precise terms:

> Given a continuous transfer function $H(s)$, which represents the input-output behavior of a controller, an algorithm for an equivalent discrete-time representation of $H(s)$ that can operate at a non-uniform sampling rate is to be developed. It should be possible to implement the algorithm in a DSP without excessive computational overhead.

Initially, this resembles a standard discipline treated in virtually every textbook on digital control (see e.g. [14–16]): digital design by emulation of a continuous-time system given its transfer function $H(s)$. The following conceptually different approaches exist for the translation of the design:

Numerical integration
> The idea is that a transfer function is basically the same as a differential equation, i.e. established methods for numerical integration of a set of coupled differential equations may be adopted to the controller problem. Although an overwhelming number of integration methods exist, only a few of them are applicable for discrete-time systems. These classic methods include the forward and backward Euler methods, and the Tustin (bilinear or trapezoidal) integration rules.

Zero-pole mapping
> Since the poles of a transfer function $H(s)$ are related to the poles of the discrete transfer function $H(z)$ by the mapping $z = e^{sT}$, the idea is to use this relation to find the zeros of $H(z)$ given the zeros of $H(s)$. Although this method appears to be simple, the successful use of this approach should adhere to a set of so-called "heuristic rules" [16] instead of simply using the mapping $z = e^{sT}$ uncritically for each pole and zero in $H(s)$.

Hold equivalents (analytical integration)
> The techniques classified as hold equivalents reply on $\mathcal{Z}$-transformation of the transfer function augmented in some way depending on the applied method (typically, zero- or first-order holds are used). For the same sampling rate, these methods usually give better approximations to the continuous-time transfer function than the two approaches discussed above, provided that the selected hold equivalent fits the input signal. In a sense, hold equivalents may also be regarded as an analytical integration method, see further in subsection 7.3.3.

As stated earlier, the use of the $\mathcal{Z}$-transformation is infeasible but in order to highlight the problems further, it should be remembered that a discrete-time transfer function in the z-domain may be interpreted as a difference equation in which the next value of the output is calculated as a weighted sum of past input and output samples. Now, the following comments apply: It may be argued that is it possible to re-calculate the coefficients in the difference equation depending on the instantaneous sampling rate,
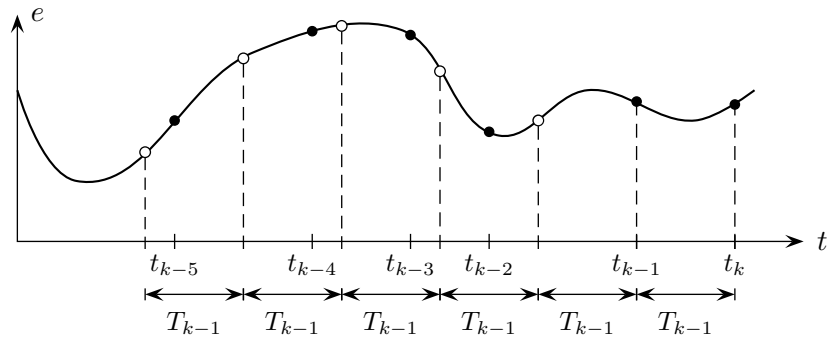
Figure 7.1 Non-uniform sampling of a continuous signal. The discretization prerequisites samples spaced T_{k-1} seconds apart (indicated by dashed lines), but the points marked by the non-solid circles ($\circ$) are not available. These values must be determined by interpolation from the known points ($\bullet$).

and thereby solve the non-uniform sampling rate problem. However, there is (at least) one major problem with this approach, which may be illustrated by means of Fig. 7.1. This figure shows an irregularly sampled waveform $e(t)$, which may represent the input to a controller or a filter. At time $t = t_k$ information about the history of $e(t)$ is available only at the sampling instants $t = \{\cdots, t_{k-2}, t_{k-1}, t_k\}$. Now it may be seen that even though the coefficients of the delay terms in the underlying difference equation are recalculated in accordance with the instantaneous sampling interval $T_{k-1} \triangleq t_k - t_{k-1}$, the values of the delay terms are faulty; the theory requires that all past samples are spaced T_{k-1} seconds apart, but this requirement is only fulfilled for the most recent sample taken at t_{k-1} due to the non-uniform sampling rate. Apart from the use of time-consuming interpolation schemes, which limit the applicability of this approach for real-time systems, this problem does not seem to have any viable solutions.

At this point it may noted that non-uniform sampling does not fit very well into the usual framework of digital control. However, the concept of non-uniform sampling is by no means an "undiscovered" discipline in engineering[4], although literature dealing with non-uniform sampling rates in control systems is difficult to find.

7.3.3 Analytic integration of state space equations

Having shown that all methods involving the $\mathcal{Z}$-transformation are incompatible with the non-uniform sampling rate requirement, the methods based on integration are investigated further. To facilitate the discussion, state-space descriptions are used below instead of transfer functions; the duality between these two different descriptions

---

[4]In other applications of discrete-time signal processing it is difficult or even impossible to obtain regular-spaced samples of the signals, which leaves no choice but to use the data obtained by this non-uniform sampling. This happens in e.g. astronomy and biological systems where non-controllable phenomena like the weather or diseases, respectively, have significant impact on when "good" samples can be obtained [18, 19].

Heavily based on [20], which gives a combined tutorial and review of more than 400 publications, it is concluded that the use of non-uniform sampling in these applications is tailored towards non-casual system analysis, i.e. it is required that all observations are available for data processing. Typical examples of this kind of analysis are (a) power spectral analysis of irregularly sampled signals, (b) reconstructions of time-domain signals from its non-uniform samples, and (c) optimal filtering.

of a dynamic system is given in the next section — here, it is sufficient to assume that the system to be discretized is available in state-space form.

Apart from the papers [2, 3] coming from the power electronic community, only one reference [18] has been found that deals theoretically with non-uniformly sampled systems in a way that is (partly) compatible with the problem at hand.

The approach of [18] is based on a state-space description of a dynamic system, i.e. it is assumed that the filter or the controller to be discretized is available in the general form

$$
\begin{aligned}
\mathrm{p}\,x &= Ax + Be \\
u &= Cx + De,
\end{aligned}
\tag{7.1}
$$

where e, u, and x are vectors representing the controller input, output, and internal states, respectively. The dimensions of the matrices A, B, C, and D depend on the system order. It is assumed that the system is linear and time-invariant, i.e. these four matrices are constants.

Given an initial state $x(t_0)$ at time t_0, the state value $x(t)$ at an arbitrary time $t > t_0$ may be calculated by integration of (7.1) using the analytic method described in [16] and other books as well:

$$
x(t) = e^{A(t-t_0)}x(t_0) + \int_{t_0}^{t} e^{A(t-\tau)}Be(\tau)\,d\tau,
\tag{7.2}
$$

where τ is a dummy integration variable. It should also be noted that the argument to the exponential function $e^{(\cdot)}$ is a matrix[5].

This result makes it possible to find an equivalent discrete-time state space form using a uniform sampling rate [16], but it is also possible to use (7.2) to find solutions for the non-uniform sampling case. Hence, it is assumed that samples of $e(t)$ are available only at the time instants $t = \{t_1, \cdots, t_{k-1}, t_k, t_{k+1}, \cdots\}$, which may be irregularly spaced. Furthermore, if the state at time $t = t_k$ is called $x(t_k)$, then the state $x(t_{k+1})$ at time $t = t_{k+1}$ becomes

$$
x(t_{k+1}) = e^{A(t_{k+1}-t_k)}x(t_k) + \int_{t_k}^{t_{k+1}} e^{A(t_{k+1}-\tau)}Be(\tau)\,d\tau.
\tag{7.3}
$$

In order to simplify further, it may be assumed that $e(t)$ is constant during the interval $t_k \leq t < t_{k+1}$ (a zero-order hold) such that $e(t) = e(t_k)$ in this interval. Then (7.3) may be reduced to

$$
x(t_{k+1}) = \Phi_k x(t_k) + \Gamma_k e(t_k).
\tag{7.4}
$$

Here, the Φ_k and Γ_k matrices are given by

$$
\Phi_k = e^{A(t_{k+1}-t_k)} \qquad \text{and} \qquad \Gamma_k = \int_{t_k}^{t_{k+1}} e^{A(t_{k+1}-\tau)}\,d\tau\,B.
\tag{7.5}
$$

---

[5]Evaluation of matrix exponentials is based on Taylor series expansion of the exponential function, see [16] and also [21]. The computation burden associated herewith is significant — at least from a real-time application's point of view.

These expressions may be modified slightly by defining the k'th sampling interval as $T_k \triangleq t_{k+1} - t_k$. Using this definition, Φ_k and Γ_k in (7.5) may be rewritten as

$$\Phi_k = e^{AT_k} \qquad \text{and} \qquad \Gamma_k = \int_0^{T_k} e^{A\zeta}\, d\zeta\, B, \qquad (7.6)$$

where $\zeta = t_{k-1} - \tau$ is another variable of integration.

For classic digital systems operating a constant sampling rate, the Φ_k and Γ_k matrices are both time invariant since all $\{T_k\}$ are equal. In this case the result reduces to the usual state-space formulation found in [16] and many other textbooks. In fact, the method of hold equivalents (see page 230) may be derived using this framework by using different approximations of $e(t)$ in (7.3).

In the general case where the sampling rate is changing from one sampling instant to the next, the following properties of the discretization (7.4) and (7.6) should be observed:

- The discrete-time state space formulation is time varying, because Φ_k and Γ_k are both functions of time.

- The discretization gives results identical to the underlying continuous-time solution to the problem at all sampling points, provided the ZOH assumption is fulfilled. Delays in the control system may also be incorporated into the model.

- The need for computations of Φ_k and Γ_k defined in terms of exponentials and integrals of matrices makes real-time calculations of $x(t_{k+1})$ impossible, because these operations are quite time consuming.

- If the limited-pool random PWM technique is used, the set of carrier periods intervals $\{T_k\}$ can attain a few values only. In this case, it is possible to calculate the corresponding Φ_k and Γ_k matrices off-line and use the pre-calculated values in the real-time updating routine. This greatly reduces the needed on-line computations.

In summary, the potential of this method to translate a continuous-time transfer function into a digital equivalent is very good, provided that all possible values of T_k are known in advance. Under these conditions this method is comparable in accuracy to the hold equivalents, which, in turn, are generally considered to be the most accurate "design by emulation" methods [16].

On the other hand, it can be concluded that if the possible set of values, that T_k can attain, is either unknown or large, the method based on analytical solution of the state-space equation is useless for real-time implementation.

7.3.4 Numerical integration of state equations

Based on the comments above, it is decided to analyze the numerical integration methods as well. Among the three variants mentioned on page 230, it is generally recommended not to use the forward Euler method because it has a number of deficiencies. One serious problem using the forward Euler method is that an unstable discrete-time realization may result even if the transfer function to be mimicked is
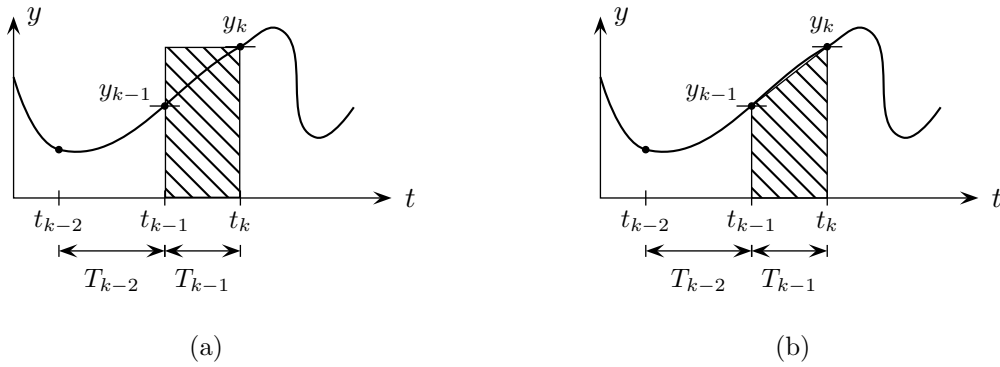
Figure 7.2 (a) Backward Euler and (b) Tustin approximation of the integral of the signal $y(t)$ using sampled values only.

stable [16]. However, the forward Euler method has the nice feature that non-linear equations can be handled in one step, i.e. an on-line iterative search for the next value may be avoided — this feature has been used for the implementation of a simple rotor-flux estimator (see page 256 in the next chapter), which is both non-linear and coupled.

The subsequent analysis is again based on a state-space description of the filter or the controller, i.e.

$$
\begin{aligned}
\mathrm{p}\,x &= Ax + Be \\
u &= Cx + De,
\end{aligned}
\tag{7.7}
$$

as in (7.1). Note that a particular transfer function $H(s) = U(s)/E(s)$ does not map into a unique state-space model; this fact is used in the next subsection.

For the backward Euler rule, the value $f(t)$ of the integration of some arbitrary signal $y(t)$ from time t_{k-1} to t_k is approximated by the backward-looking rectangle as shown in Fig. 7.2(a):

$$
f_k = f_{k-1} + (t_k - t_{k-1})y_k = f_{k-1} + T_{k-1}y_k,
\tag{7.8}
$$

where T_{k-1} is the duration between two sampling points.

Using Tustin's rule, the integral is approximated by a trapezoid as illustrated in Fig. 7.2(b). This leads to

$$
f_k = f_{k-1} + \tfrac{1}{2}T_{k-1}(y_{k-1} + y_k).
\tag{7.9}
$$

Note that for a conventional discrete-time controller $T_{k-1} = T_k = T$, but this is not the case here.

Returning now to the state-space model (7.7), the integration can be approximated using either (7.8) or (7.9). Substituting $y \leftarrow Ax + Be$ and $f \leftarrow x$ in these two equations yields

$$\text{Backward Euler:} \begin{cases} x_k = (I - T_{k-1}A)^{-1}x_{k-1} + (I - T_{k-1}A)^{-1}T_{k-1}Be_k \\ u_k = Cx_k + De_k, \end{cases} \quad (7.10)$$

$$\text{Tustin's rule:} \begin{cases} x_k = (I - \frac{1}{2}T_{k-1}A)^{-1}(I + \frac{1}{2}T_{k-1}A)x_{k-1} \\ \qquad\quad + \frac{1}{2}(I - \frac{1}{2}T_{k-1}A)^{-1}T_{k-1}B(e_{k-1} + e_k) \\ u_k = Cx_k + De_k. \end{cases} \quad (7.11)$$

The two methods have the same form, and in order to make the appearance of the expressions more readable, the equations describing the dynamics are rewritten as $x_k = A_k^{-1}x_k + B_k e_k$, where the definitions of the two auxiliary matrices A_k and B_k follow directly from (7.10) and (7.11). A number of remarks apply here:

- In order to update x_k, a matrix inversion of A_k is required. Inversion is generally considered to be a time-consuming operation because the number of multiplications goes up as n^3, where n is the dimension of the matrix to be inverted [19].

- If A_k can be manipulated into a diagonal matrix with entries $A_{11}, \cdots, A_{nn}$, the inversion task simplifies significantly, viz.

$$\begin{bmatrix} A_{11} & & \\ & \ddots & \\ & & A_{nn} \end{bmatrix}^{-1} = \begin{bmatrix} A_{11}^{-1} & & \\ & \ddots & \\ & & A_{nn}^{-1} \end{bmatrix}. \quad (7.12)$$

  For the application at hand, it will be shown later that the diagonal elements are either scalars or 2×2-matrices, which both are simple to invert.

- A diagonal A_k effectively de-couples the individual states, which implies that calculation of the matrix product $A_k^{-1}x_{k-1}$ simply involves $2n$ multiplications.

- If T_k only can attain a (relatively small) finite number of values, the A_k^{-1} matrix and the B_k vector can be pre-computed and stored for later real-time use. In this case, the on-line updating of A_k and its inverse A_k^{-1} is avoided completely. Even under these conditions, advantage of the diagonalization should be taken in order to limit the needed real-time computations further.

Based on these remarks, it seems to be a very desirable property that the system matrix A in (7.7) is a diagonal matrix since this would result in much simpler calculations compared to the case where A has non-zero off-diagonal elements.

7.4 Derivation of a controller algorithm based on numerical integration

The problem considered in this section relates to the practical implementation of controllers in case of a non-uniform sampling rate. The starting point is an input-output

description given as a transfer function $H(s)$ between the input $E(s)$ and the output $U(s)$ in the following form:

$$H(s) = \frac{U(s)}{E(S)} = \frac{b_n s^n + b_{n-1} s^{n-1} + \cdots + b_1 s + b_0}{s^n + a_{n-1} s^{n-1} + \cdots + a_1 s + a_0}, \tag{7.13}$$

where the filter coefficients $a_0, ..., a_{n-1}$ and $b_0, ..., b_n$ represent the numerator and denominator polynomials, respectively. n is the order of system; usually $\deg U(s) < \deg E(s)$, i.e. some of the b coefficients are zero.

For classic low-pass filters such as Butterworth, Bessel, and type I Chebyshev filters, the numerator evaluates to $U(s) = b_0 = 1$, since these filters are all-pole filters [22]. Zeros occur, however, if these filters are transformed into high- or band-pass filters. Also, other classic filter structures (for example, type II Chebyshev and elliptic (Cauer) filters) contain both poles and zeros, even in their low-pass prototype forms.

Below, it is shown how a low-complexity algorithm that mimics $H(s)$ can be devised in the general case where $H(s)$ contains both poles and zeros. An example of how to apply the developed procedure is then presented and, finally, a summary of the suggested design methodology is given.

7.4.1   Transformation to an equivalent state-space description

An input-output description as (7.13) can be transformed into an infinity of equivalent state-space formulations [15, 23]. It is, however, very easy to obtain the so-called controllable canonical form [23], which is also known as Kalman's first form [24], since the elements[6] of the state-space matrices A, B, C, and D relate directly to the coefficients of $H(s)$:

$$\text{p}\begin{bmatrix} x_1 \\ x_2 \\ \vdots \\ x_{n-1} \\ x_n \end{bmatrix} = \begin{bmatrix} 0 & 1 & 0 & \cdots & 0 \\ 0 & 0 & 1 & \cdots & 0 \\ \vdots & & & & \vdots \\ 0 & 0 & 0 & \cdots & 1 \\ -a_0 & -a_1 & -a_2 & \cdots & -a_{n-1} \end{bmatrix} \begin{bmatrix} x_1 \\ x_2 \\ \vdots \\ x_{n-1} \\ x_n \end{bmatrix} + \begin{bmatrix} 0 \\ 0 \\ 0 \\ 0 \\ 1 \end{bmatrix} e \tag{7.14}$$

$$u = \begin{bmatrix} b_0 - a_0 b_n \mid b_1 - a_1 b_n \mid \cdots \mid b_{n-1} - a_{n-1} b_n \end{bmatrix} \begin{bmatrix} x_1 \\ x_2 \\ \vdots \\ x_{n-1} \\ x_n \end{bmatrix} + b_n e. \tag{7.15}$$

It should be noted that the system matrix A is non-diagonal, which complicates the inversion and the implementation as remarked on the page before.

---

[6]For readability reasons, vertical bars are used in (7.15) to separate adjacent elements in a row vector from each other. This notation is used in other equations in this chapter as well.

7.4.2 Diagonalization

By a linear transformation of the state vector x it is possible to diagonalize A by means of the theory of similar transformation known from the mathematics of linear algebra [25]. Hence, by introducing a new state vector z related to the original state vector x by the transformation $x = Vz$, where V is a non-singular square matrix to be determined shortly, the following equivalent (in terms of input-output characteristics) state-space description follows:

$$
\begin{cases} \mathrm{p}(Vz) = A(Vz) + Be \\ \quad u = C(Vz) + De \end{cases}
\Rightarrow
\begin{cases} \mathrm{p}\, z = (V^{-1}AV)z + (V^{-1}B)e \\ \quad u = (CV)z + De. \end{cases}
\tag{7.16}
$$

By defining new matrices by $\hat{A} = V^{-1}AV$, $\hat{B} = V^{-1}B$, $\hat{C} = CV$, and $\hat{D} = D$, the description in terms of z-states may be rewritten as

$$
\begin{cases} \mathrm{p}\, z = \hat{A}z + \hat{B}e \\ \quad u = \hat{C}z + \hat{D}e. \end{cases}
\tag{7.17}
$$

It may be noted that the new system matrix $\hat{A}$ strongly depends upon the selection of V. Now, if the original A-matrix of size $n \times n$ possesses n distinct characteristic values (eigenvalues) $\lambda_1, \lambda_2, \cdots, \lambda_n$, it is diagonalizable by the similarity transformation $\hat{A} = V^{-1}AV$ [25]. Furthermore, the columns vectors of V equal the n distinct eigenvectors of A corresponding to the eigenvectors of A.

An elegant method that avoids the explicit calculation of the eigenvectors of A may be found in [23]. Here, it is shown that if the matrix A is in the controllable canonical form defined by (7.14), then the transformation V may be obtained directly from the eigenvalues:

$$
V = \begin{bmatrix}
1 & 1 & \cdots & 1 \\
\lambda_1 & \lambda_2 & \cdots & \lambda_n \\
\lambda_1^2 & \lambda_2^2 & \cdots & \lambda_n^2 \\
\vdots & \vdots & \cdots & \vdots \\
\lambda_1^{n-1} & \lambda_2^{n-1} & \cdots & \lambda_n^{n-1}
\end{bmatrix}.
\tag{7.18}
$$

Now $V^{-1}AV$ maps into the diagonal matrix

$$
\hat{A} = V^{-1}AV = \begin{bmatrix}
\lambda_1 & & & \\
& \lambda_2 & & \\
& & \ddots & \\
& & & \lambda_n
\end{bmatrix} \triangleq \mathrm{diag}(\lambda_1, \lambda_2, \cdots, \lambda_n)
\tag{7.19}
$$

as required.

If A does not have a complete set of linearity independent characteristic vectors, A cannot be diagonalized, but it can be transformed into a Jordan canonical form [23], which is a diagonal matrix augmented with a few non-diagonal elements. This situation occurs if $H(s)$ has multiple poles, but for the filters and controllers treated here, multiple poles do not occur. Hence, transformation into the Jordan canonical form is not considered any further.

7.4.3   Elimination of complex-valued states

For most filters, the set of characteristic values $\{\lambda_1, \cdots, \lambda_n\}$ contains pairs of complex conjugates because the denominator of the transfer function (7.13) consists partly of second-order segments, each having a damping $\zeta < 1$. In these cases the diagonal state-space realization has the following two disadvantages:

- The transition of the filter based on complex-valued states into compilable DSP code cannot be accomplished without resorting to cumbersome data structures and algorithms that handle addition, subtraction, multiplication, and division of complex numbers.

- The realization has redundant states, i.e. there is more states than strictly necessary to represent the transfer function (7.13): if the system has c numbers of complex-valued eigenvalues, then the state vector z may be rewritten into $n + c$ real-valued states by splitting the c complex-valued states into their real and imaginary components. It is, however, possible to represent an n'th order transfer function by an n'th order state-space model, which shows that we have c superfluous states.

These problems may be solved by the following procedure which introduces a few modifications to the matrices $\hat{A}$, $\hat{B}$, $\hat{C}$, and $\hat{D}$ above:

1. The state-space vector z is sorted so that the first c elements of z is half of the original complex-valued states split into their real and imaginary components. The remaining $n - c$ elements correspond to the real-valued eigenvalues of $\hat{A}$:

$$z \triangleq \Big[\underbrace{z_{1r} \mid z_{1i} \mid \cdots \mid z_{cr} \mid z_{ci}}_{\text{for complex } \lambda\text{'s}} \mid \underbrace{z_{c+1} \mid \cdots \mid z_n}_{\text{for real } \lambda\text{'s}} \Big]^T. \qquad (7.20)$$

2. By splitting the matrices $\hat{A}$ and $\hat{B}$ into their real and imaginary components, the augmented version of $\text{p}\, z = \hat{A}z + Be$ now becomes:

$$\text{p} \begin{bmatrix} z_{1r} \\ z_{1i} \\ \vdots \\ z_{cr} \\ z_{ci} \\ z_{c+1} \\ \vdots \\ z_n \end{bmatrix} = \begin{bmatrix} \mathcal{R}(\lambda_1) & -\mathcal{I}(\lambda_1) \\ \mathcal{I}(\lambda_1) & \mathcal{R}(\lambda_1) \\ & & \ddots \\ & & & \mathcal{R}(\lambda_c) & -\mathcal{I}(\lambda_c) \\ & & & \mathcal{I}(\lambda_c) & \mathcal{R}(\lambda_c) \\ & & & & & \lambda_{c+1} \\ & & & & & & \ddots \\ & & & & & & & \lambda_n \end{bmatrix} \begin{bmatrix} z_{1r} \\ z_{1i} \\ \vdots \\ z_{cr} \\ z_{ci} \\ z_{c+1} \\ \vdots \\ z_n \end{bmatrix}$$

$$+ \Big[\mathcal{R}(\hat{B}_1) \mid \mathcal{I}(\hat{B}_1) \mid \cdots \mid \mathcal{R}(\hat{B}_c) \mid \mathcal{I}(\hat{B}_c) \mid \hat{B}_{c+1} \mid \cdots \mid \hat{B}_n \Big]^T e. \quad (7.21)$$

3. By remembering that the output y is a real-valued number, the output equation $y = \hat{C}z + \hat{D}e$ must be changed into this form:

$$y = \left[2\mathcal{R}(\hat{C}_1) \mid -2\mathcal{I}(\hat{C}_1) \mid \cdots \mid 2\mathcal{R}(\hat{C}_c) \mid -2\mathcal{I}(\hat{C}_c) \mid C_{c+1} \mid \cdots \mid C_n \right]$$

$$\left[z_{1r} \mid z_{1i} \mid \cdots \mid z_{cr} \mid z_{ci} \mid z_{c+1} \mid \cdots \mid z_n \right]^T + \hat{D}e. \quad (7.22)$$

In summary, it should be noted that the complex-conjugated eigenvalues appear in 2×2 blocks on the diagonal of $\hat{A}$ and the real eigenvalues appear directly on the main diagonal.

7.4.4 Butterworth filter example

To validate that it is possible to implement a digital filter using the described technique, a Butterworth filter is discretized, and the step response is simulated. Butterworth filters are inherently all-poles filters, and, furthermore, the N poles $\{p_0, ..., p_{N-1}\}$ are located in the left half-plane on a circle of radius ω_c (the -3 dB cutoff frequency) [22]:

$$B(s) = \frac{\omega_c^N}{\prod_{k=0}^{N-1}(s - p_k)}, \quad \text{where} \quad p_k = \omega_c e^{j\pi/2} e^{j(2k+1)\pi/(2N)}. \quad (7.23)$$

For N even, all poles p_k are complex-valued, and for N odd, one pole occurs at the negative real axis; the rest of the poles fall in complex-conjugated pairs. Specifically, for $N = 3$ the filter (7.23) expands into

$$B_3(s) = \frac{b_0}{s^3 + a_2 s^2 + a_1 s + a_0}, \quad (7.24)$$

where the coefficients of the numerator and the denominator are $b_0 = 1$ and $a_2 = a_1 = 2, a_0 = 1$, respectively for $\omega_c = 1$ rad/s. The canonical state-space matrices then become

$$A = \begin{bmatrix} 0 & 1 & 0 \\ 0 & 0 & 1 \\ -2 & -2 & -1 \end{bmatrix}, \quad B = \begin{bmatrix} 0 \\ 0 \\ 1 \end{bmatrix}, \quad C = \begin{bmatrix} 1 & 0 & 0 \end{bmatrix}, \quad \text{and} \quad D = 0. \quad (7.25)$$

The characteristic values of A may be computed by either $\det(I - \lambda A) = 0$ or directly from (7.23). In either case

$$\lambda_1 = -\tfrac{1}{2} + j\tfrac{\sqrt{3}}{2}, \quad \lambda_2 = -\tfrac{1}{2} - j\tfrac{\sqrt{3}}{2}, \quad \text{and} \quad \lambda_3 = -1, \quad (7.26)$$

which by way of (7.18) results in the following transformation matrix V

$$V = \begin{bmatrix} 1 & 1 & 1 \\ -\tfrac{1}{2} + j\tfrac{\sqrt{3}}{2} & -\tfrac{1}{2} - j\tfrac{\sqrt{3}}{2} & -1 \\ -\tfrac{1}{2} - j\tfrac{\sqrt{3}}{2} & -\tfrac{1}{2} + j\tfrac{\sqrt{3}}{2} & 1 \end{bmatrix}. \quad (7.27)$$

The new matrices defined in (7.16) is then calculated from (7.25) by using (7.27) leading to the following diagonal state-space realization of (7.24):

$$\hat{A} = \begin{bmatrix} -\frac{1}{2} + j\frac{\sqrt{3}}{2} & & \\ & -\frac{1}{2} - j\frac{\sqrt{3}}{2} & \\ & & -1 \end{bmatrix}, \quad \hat{B} = \begin{bmatrix} -\frac{1}{2} - j\frac{\sqrt{3}}{6} \\ -\frac{1}{2} + j\frac{\sqrt{3}}{6} \\ 1 \end{bmatrix}, \tag{7.28}$$

$$\hat{C} = \begin{bmatrix} 1 & 1 & 1 \end{bmatrix}, \quad \text{and} \quad \hat{D} = 0. \tag{7.29}$$

In order to eliminate the complex states associated with the λ_1 and λ_2 eigenvalues, the state vector is modified according to (7.20). Dropping the z_2 state and dividing z_1 into its real and imaginary part, the new state vector then becomes $z = [z_{1r} \ z_{1i} \ z_3]^T$. By virtue of (7.21) and (7.22), the following augmented diagonal state-space formulation is then finally determined:

$$\hat{A} = \begin{bmatrix} \begin{bmatrix} -\frac{1}{2} & -\frac{\sqrt{3}}{2} \\ \frac{\sqrt{3}}{2} & -\frac{1}{2} \end{bmatrix} & \\ & -1 \end{bmatrix}, \quad \hat{B} = \begin{bmatrix} -\frac{1}{2} \\ -\frac{\sqrt{3}}{6} \\ 1 \end{bmatrix}, \tag{7.30}$$

$$\hat{C} = \begin{bmatrix} 2 & 0 & 1 \end{bmatrix}, \quad \text{and} \quad \hat{D} = 0. \tag{7.31}$$

This system of equations may now be integrated using either the backward Euler method, the Tustin's rule, or any other numerical integration scheme, provided that the input signal $e(t)$ is known. Also, a probability density function $p(T)$ for the sampling time T must be selected. According to the guidelines of [15], the product of the sampling time and the closed-loop bandwidth should fulfill $\omega_c T \approx 0.15 - 0.5$ rad. Using this rule of thumb, a reasonable nominal value of the sampling time is 0.2 s since $\omega_c = 1$ rad/s in this example.

Based on this information, the following MATLAB simulations have been performed in order to demonstrate the power of the presented procedure for the implementation of non-uniformly sampled digital filters and controllers:

- As a benchmark, the ideal step response of the continuous-time filter has been calculated.

- The step response of the designed discrete-time filter has been calculated for both the backward Euler method and the Tustin's rule where the sampling interval is randomly chosen among $T \in \{0.05, 0.1, 0.25, 1.0\}$ s. Note that values of T both greater than and smaller than the nominal value 0.2 s are used. $p(T)$ is set so that the filter (on the average) spend the same time using all these values, i.e. the ratio $p(0.05 \text{ s})/p(0.25 \text{ s}) = 0.25/0.05 = 5$, etc.

- For reference, the following simulation was also performed for both approximation techniques: In the filter algorithm, the sampling time is set to the average value, i.e. the variations in the true T are ignored even though the samples of $e(t)$ arrive at a non-uniform rate. Intuitively, one would expect this simplified approach to be reasonable, but the question is: how well does it work?
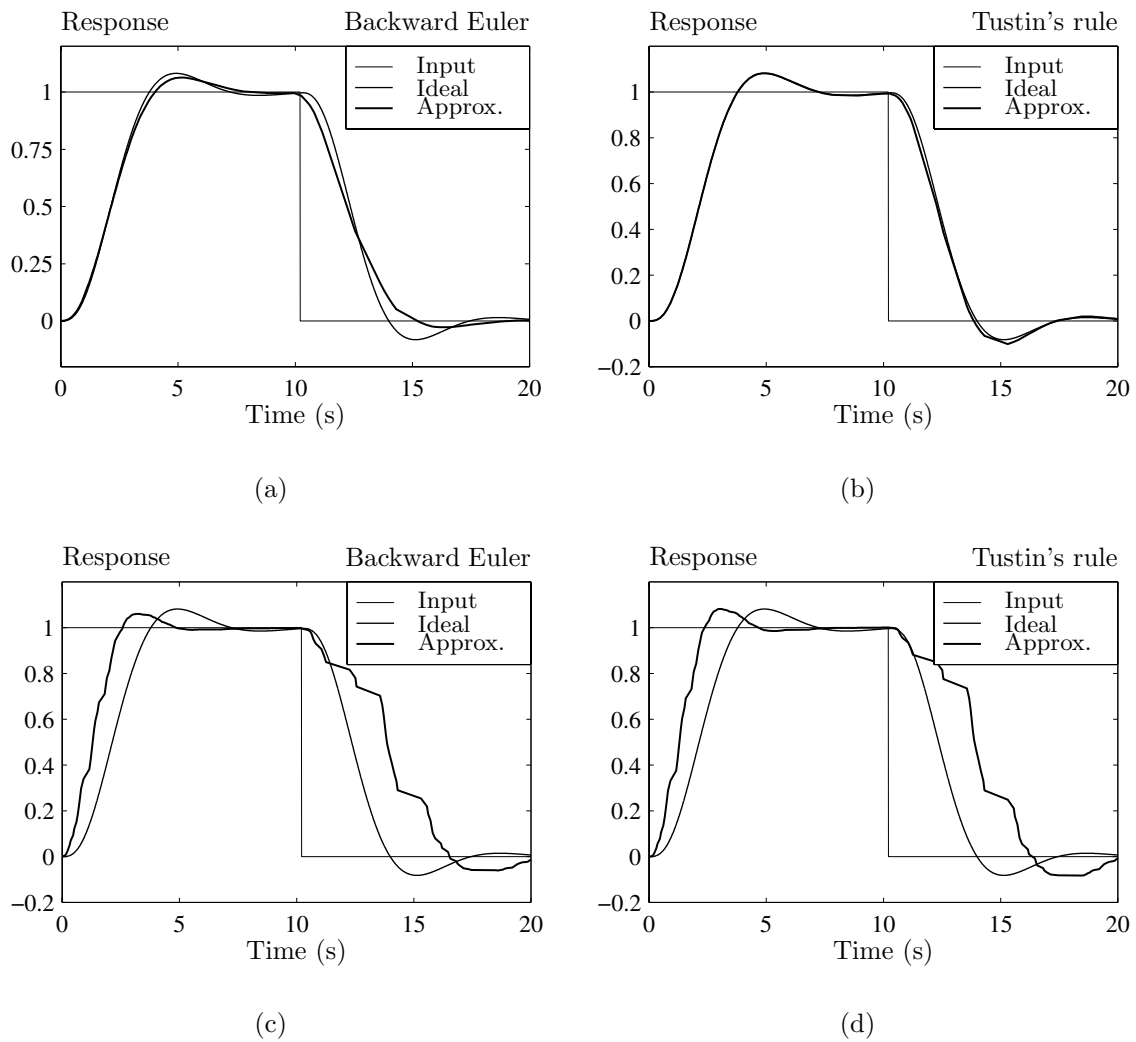
Figure 7.3 Simulated responses of a third-order, low-pass Butterworth filter with $\omega_c = 1$ rad/s. The sampling time is randomly selected among $T \in \{0.05, 0.1, 0.25, 1.0\}$ s (the same sequence is used in all plots). (a, b) The filter adapts to the instantaneous value of T according to the theory. (c, d) The average sampling time is used in the filter (no attempts are made to compensate for the non-uniform sampling rate).

The obtained results are shown in Fig. 7.3. It is seen in Fig. 7.3(a, b) that the discretized versions, which takes the non-uniform sampling interval into account, give good approximations to the ideal step response. No severe distortion is introduced despite of the random selection of the sampling interval. Also, as expected, Tustin's rule gives better results than the backward Euler method.

If the variations in T are ignored, the responses shown in Fig. 7.3(c, d) result. Considerable distortion can now be observed. In these cases it should be noted that the obtained responses depend strongly on the "local" average of T: if this value is close to the nominal mean used in filter algorithm, the filter behaves relatively well, but if the local average of T differs significantly, large errors occur. There is, however, no reason to ignore the variations in T, because the computation overhead associated with the variable sampling rate is small.

7.4.5   Algorithm overview

To summarize the ideas developed for the discrete-time approximation of an arbitrary continuous-time filter $H(s)$, the steps outlined below may be followed:

Off-line calculations

1. Write up H(s) in the form of (7.13) and determine the coefficients $a_0, \cdots, a_{n-1}$ and $b_0, \cdots, b_n$.

2. Set up the matrices A, B, C, and D according to (7.14) and (7.15).

3. Find the characteristic values of A, and determine the transformation matrix V defined by (7.18). Then, calculate $\hat{A} = V^{-1}AV$, $\hat{B} = V^{-1}B$, $\hat{C} = CV$, and let $\hat{D} = D$.

4. If A has one or more pairs of complex-conjugated eigenvalues, augment the $\hat{A}$, $\hat{B}$, $\hat{C}$, and $\hat{D}$ matrices found in step 3 according to the procedure given by (7.21) and (7.22).

5. If the probability density function for the sampling interval $p(T)$ has a (small) finite pool size, calculate the possible values of the matrices $\hat{A}(T_{k-1})^{-1}$ and $\hat{B}(T_{k-1})$ defined on page 235 for all possible values of T.

On-line calculations (Using the backward Euler method as example)

1. Update the state vector: $z_k = (I - T_{k-1}\hat{A})^{-1}(z_{k-1} + \hat{B}T_{k-1}e_k)$ (if no precalculated information exists). Otherwise, use the off-line calculated values of $\hat{A}(T_{k-1})^{-1}$ and $\hat{B}(T_{k-1})$: $z_k = \hat{A}(T_{k-1})^{-1}z_{k-1} + \hat{B}(T_{k-1})e_k$.

2. Update the output equation: $u_k = \hat{C}z_k + \hat{D}e_k$.

As earlier explained, all on-line matrix computations are more simple than they appear at first due to the decoupling obtained by the diagonalization of $\hat{A}$.

7.5   Summary

In this chapter an analysis of the problems of using random PWM in discrete-time feed-back control systems has been presented. It was shown that the main difficulty of replacing normally used fixed carrier frequency PWM with random PWM is that the control system may have to operate with a continuously changing sampling rate, i.e. the sampling frequency varies between two consecutive sampling instants. This non-uniform sampling rate renders the use of the $\mathcal{Z}$-transformation impossible, and hence, the design of discrete controllers directly in the z-domain becomes impossible, too. Also, it is impossible to realize the controller in terms of a simple fixed-coefficient difference equation when the order of the controller exceeds one.

To overcome these problems, it was suggested that the controller in question is designed in the continuous s-domain and, subsequently, translated into an equivalent

discrete-time representation that can be numerically integrated in a way that is compatible with the non-uniform sampling rate requirement. By using state-space methods, single-step numerical integration methods, like Backward Euler, may be applied. Then, the obtainable performance using a non-uniform sampling rate is almost equal to the performance for a controller operating with a constant sampling rate. Also, the amount of real-time computations needed to update the controllers is kept at a minimum by taking advantage of (off-line) matrix diagonalization techniques.

The main contributions of this chapter are believed to be:

- A discussion and an identification of the problems relating to design and implementation of sampled-data systems that must be able to operate with a non-uniform sampling rate in real time.

- Derivation of a unifying methodology for design and time-efficient implementation of linear controllers and similar structures for such randomly sampled systems by means of numerical integration of state-space equations. The values of the possible sampling rates may be either known or unknown at the design stage.

Finally, note that the procedure suggested in this chapter to solve the problem of implementing digital filters/controllers sampled at a non-uniform rate is by no means limited to random PWM applications; other applications in engineering may exist, although the scarce literature on real-time use of non-uniform sampling does not add much support to the existence of such special applications.

Bibliography

[1] M. P. Kaźmierkowski and L. Malesani, "Guest Editorial. Special Section on PWM Converter Current Control," *IEEE Trans. on Industrial Electronics*, vol. 45, no. 5, pp. 689–690, Oct. 1998.

[2] C. B. Jacobina, A. M. N. Lima, E. R. C. da Silva, and R. L. de A. Ribeiro, "Current Control for a Random PWM Voltage Source Inverter," *Proc. of the 28th IEEE Power Electronics Specialists Conference*, vol. 2, pp. 1440–1446, 1997.

[3] C. B. Jacobina, A. M. N. Lima, E. R. C. da Silva, and A. M. Trzynadlowski, "Current Control for Induction Motor Drives using Random PWM," *IEEE Trans. on Industrial Electronics*, vol. 45, no. 5, pp. 704–712, Oct. 1998.

[4] B.-R. Lin and H.-H. Lu, "Three-Phase AC/DC/AC Converter with Random Pulse Position," *Proc. of 8th European Conference on Power Electronics and Applications*, Sept. 1999.

[5] B.-R. Lin and H.-H. Lu, "Implementation of Nondeterministic PWM for Inverter Drives," *Proc. of the IEEE International Symposium on Industrial Electronics*, vol. 2, pp. 813–818, 1999.

[6] B.-R. Lin and H.-H. Lu, "Single-Phase Three-Level Rectifier and Random PWM Inverter Drives," *IEEE Trans. on Aerospace and Electronic Systems*, vol. 35, no. 4, pp. 1334–1343, Oct. 1999.

 [7] M. M. Bech, F. Blaabjerg, J. K. Pedersen, and A. M. Trzynadlowski, "Comparative Investigation of Random PWM Techniques with Variable Switching Frequency and Pulse Position for Inverter-Fed Induction Motors," *Proc. of 7th European Conference on Power Electronics and Applications*, vol. 1, pp. 343–349, 1997.

 [8] M. M. Bech, F. Blaabjerg, and J. K. Pedersen, "Random Modulation Techniques with Fixed Switching Frequency for Three-Phase Power Converters," *Proc. of the 30th IEEE Power Electronics Specialists Conference*, vol. 1, pp. 544–551, June 1999.

 [9] B.-R. Lin, "High Power Factor AC/DC/AC Converter with Random PWM," *IEEE Trans. on Aerospace and Electronic Systems*, vol. 35, no. 3, pp. 935–943, July 1999.

[10] C. M. Liaw and Y. M. Lin, "Random Slope PWM Inverter using Existing System Background Noise: Analysis, Design and Implementation," *IEE Proceedings — Electric Power Applications*, vol. 147, no. 1, pp. 45–54, Jan. 2000.

[11] Y. S. Lai, "Sensorless Vector-Controlled IM Drives using Random Switching Technique," *Proc. of 8th European Conference on Power Electronics and Applications*, Sept. 1999.

[12] Y. S. Lai, "Sensorless Speed Vector-Controlled Induction Motor Drives using New Random Technique for Inverter Control," *IEEE Trans. on Energy Conversion*, vol. 14, no. 4, pp. 1147–1155, Dec. 1999.

[13] Y. S. Lai and S. C. Chang, "DSP-based Implementation of New Random Switching Technique of an Inverter Control for Sensorless Vector-Controlled Induction Motor Drives," *IEE Proceedings – Electric Power Applications*, vol. 146, no. 2, pp. 163–172, Mar. 1999.

[14] K. Ogata, *Discrete-time Control Systems*, Prentice Hall, Englewood Cliffs, New Jersey, 1987.

[15] K. J. Åström and B. Wittenmark, *Computer-controlled Systems. Theory and Design*, Prentice Hall, Englewood Cliffs, New Jersey, 1990.

[16] G. F. Franklin, J. D. Powell, and M. L. Workman, *Digital Control of Dynamic Systems*, Addison Wesley, Reading, Massachusetts, second edition, 1990.

[17] H. W. Thomas and P. Lutte, "Z-Transform Analysis of Nonuniformly Sampled Digital Filters," *Proc. of the IEE*, vol. 119, no. 11, pp. 1559–1567, Nov. 1972.

[18] G. D. Kontopidis, D. E. Limbert, and F. H. Glanz, "A Study of Nonuniformly Sampled Systems," *Proc. of the International Conference on Cybernetics and Society*, pp. 863–869, 1979.

[19] W. H. Press, S. A. Teukolsky, W. T. Vetterling, and B. P. Flannery, *Numerical Recipes in C — The Art of Scientific Computing*, Cambridge University Press, second edition, 1992.

[20] F. A. Marvasti, *A Unified Approach to Zero-Crossings and Nonuniform Sampling of Single and Multidimensional Signals and Systems*, Nonuniform, Oak Park, Illinois, 1987.

[21] The MathWorks, *Control System Toolbox User's Guide, Version 4.1*, The Math-Works Inc., Jan. 1998.

[22] J. G. Proakis and D. G. Manolakis, *Digital Signal Processing. Principles, Algorithms, and Applications*, Prentice Hall, Upper Saddle River, New Jersey, third edition, 1996.

[23] K. Ogata, *Modern Control Engineering*, Prentice Hall, Englewood Cliffs, New Jersey, second edition, 1990.

[24] B. P. Lathi, *Signals, Systems, and Control*, Harper & Row, New York, 1974.

[25] A. L. Rabenstein, *Elementary Differential Equations with Linear Algebra*, Harcourt Brace Jovanovich, Orlando, Florida, 1982.

Chapter 8

Field-oriented control using random PWM — a case study

8.1 Introduction

As explained in Chapter 1, the majority of all publications dealing with random PWM for three-phase applications assume open-loop control strategies, i.e. the performance in terms of steady-state accuracy and dynamic response times is limited and certainly not comparable to the performance obtainable with either field-oriented control (FOC) or direct torque control (DTC). The few publications that actually investigate random PWM in conjunction with feed-back control loops were reviewed in the previous chapter, but in the opinion of the author it has not yet been convincingly demonstrated that random PWM can be unified with closed-loop control technique, such as FOC for ac drives, despite the appealing characteristics of such a combination: accurate control and, simultaneously, less acoustic annoyance due to the spread-spectrum switching.

The problems related to using random PWM together with digital control systems were discussed in section 7.2. In brief, two issues are important here: error-free acquisition of phase currents besides design and implementation of digital controllers that can operate with a randomly varying sampling rate. For that reason, the purpose of this chapter is to show that it is possible to unify random carrier frequency (RCF) pulse-width modulation with a vector controller for induction motor drives using the methods of Chapter 7 without any loss of performance compared to deterministic PWM.

Chapter outline

In section 8.2, a brief review of the principles for field-oriented control of induction machines is presented. The various functional units needed to implement a simple field-oriented drive are designed in section 8.3 where the issue of flux estimation is treated also. In accordance with the procedure given in Chapter 7 for design of digital systems that must operate with non-uniform sampling rate, the analyses are carried out in the continuous-time domain. Details of the discretization are treated in section 8.4.

Measurements performed on a laboratory set-up are reported next. Experimental results are presented for both dynamic and steady-state tests for the designed system using RCF and comparisons with a conventional deterministic modulator are provided also. Finally, the main results are summarized in the last section of this chapter.

8.2   Principles of rotor field-oriented control

In this section, the classic dynamic model of the induction motor is briefly reviewed, mainly in order to fix the nomenclature used subsequently. Also, the key principles and properties of rotor field-orientation control are outlined.

8.2.1   Induction machine model in an arbitrary reference frame

Based on complex-valued space vectors as defined in Chapter 2, a dynamic model of the induction machine may be derived as presented in [1, 2], among many others. Hence, under the usual assumptions of linear magnetics, negligible iron losses, etc., the following set of differential equations describes the cage induction machine in an arbitrary coordinate system having the instantaneous angular position θ with respect to the stationary α-axis:

$$\boldsymbol{u}_s = r_s \boldsymbol{i}_s + \mathrm{p}\,\boldsymbol{\psi}_s + j\omega\boldsymbol{\psi}_s \tag{8.1}$$

$$\boldsymbol{0} = r_r \boldsymbol{i}_r + \mathrm{p}\,\boldsymbol{\psi}_r + j(\omega - \omega_r)\boldsymbol{\psi}_r \tag{8.2}$$

$$J\,\mathrm{p}\,\omega_m = T_{em} - T_{load} - b\omega_m \tag{8.3}$$

$$\omega = \mathrm{p}\,\theta, \quad \omega_r = P\omega_m, \tag{8.4}$$

where the currents and flux linkages are related by

$$\boldsymbol{\psi}_s = L_s \boldsymbol{i}_s + L_m \boldsymbol{i}_r \tag{8.5}$$

$$\boldsymbol{\psi}_r = L_m \boldsymbol{i}_s + L_r \boldsymbol{i}_r. \tag{8.6}$$

The developed electro-magnetic torque may be calculated in different ways, for example:

$$T_{em} = \tfrac{3}{2}P\mathcal{I}(\boldsymbol{\psi}_s^\star \boldsymbol{i}_s) = \tfrac{3}{2}P\frac{L_m}{L_r}\mathcal{I}(\boldsymbol{\psi}_r^\star \boldsymbol{i}_s), \tag{8.7}$$

where $\star$ is the complex conjugate operator. In (8.1)–(8.7) the following notation is used: The stator inductance is $L_s = \ell_s + L_m$, i.e. the sum of the leakage ℓ_s and the magnetizing L_m inductance. A similar definition holds for the rotor inductance. Voltages, currents, and flux space vectors are set using boldface types, i.e. $\boldsymbol{u}$, $\boldsymbol{i}$, and $\boldsymbol{\psi}$. The subscripts s and r refer to stator and rotor quantities, respectively. The mechanical, ω_m, and electrical, ω_r, angular velocities are related by the pole pair number P as $\omega_r = P\omega_m$. J and b are the total inertia of the shaft and the friction coefficient, respectively.

Fig. 8.1(a) shows an equivalent circuit of the induction machine. Note that all space vectors are expressed in a dq coordinate system rotated by the instantaneous amount θ with respect to the stationary α-axis. As seen from Fig. 8.1(b), the mapping between a stationary $\boldsymbol{y}^s \triangleq y_\alpha + jy_\beta$ and a rotating $\boldsymbol{y} \triangleq y_d + jy_q$ representation of space vectors is given by

$$\boldsymbol{y} = \boldsymbol{y}^s e^{-j\theta} \tag{8.8}$$

where the superscript s is denotes vectors in $\alpha\beta$ coordinates.

It may also be noted that the angle θ may be chosen arbitrarily, but with respect to design of controllers, it is an advantage to select the instantaneous angular speed
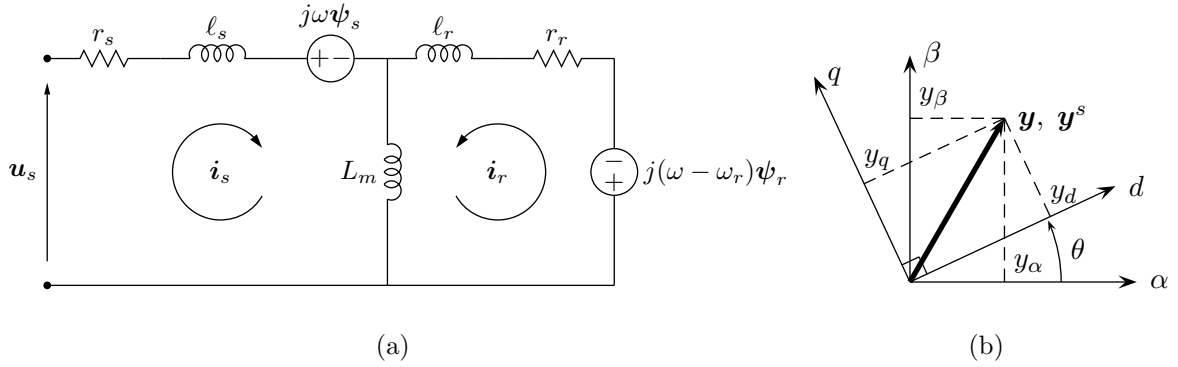
Figure 8.1 (a) Space-vector based model of an induction machine in a reference frame rotating with the instantaneous angular frequency ω and (b) representation of a space vector in either stationary $(\alpha\beta)$ or rotating (dq) coordinates.

$\omega = p\,\theta$ of the rotating frame such that all space vectors are stationary[1] in that reference frame under steady-state conditions. This requirement may be met by using the synchronous reference frame, i.e. a coordinate system rotating in synchronism with (and normally aligned to) one of the space vectors, typically the rotor flux linkage $\boldsymbol{\psi}_r^s$ or the stator flux linkage $\boldsymbol{\psi}_s^s$.

8.2.2 Decoupling through rotor-field orientation

In synchronous coordinates, all space vectors are constants (though a complex-valued constant) in steady state irrespective of the chosen reference space vector. In the scientific literature, analyses of the characteristics for different orientations have been established with respect to ease of implementation, flux estimation, parameter sensitively, etc., but here, only the fundamentals of rotor-flux orientation are reviewed.

To put it mathematically, rotor-field orientation implies that the transformation angle θ is selected as

$$\theta \triangleq \theta_{rf} = p\,\omega_{rf} = \measuredangle\boldsymbol{\psi}_r^s = \arctan\left(\frac{\psi_{r\beta}}{\psi_{r\alpha}}\right). \tag{8.9}$$

In synchronous coordinates this implies that for rotor-field orientation, the rotor-flux space vector is simply $\boldsymbol{\psi}_r = \psi_{rd}$ because the d-axis is aligned with θ_{rf} so that $\psi_{rq} = 0$, because the q-axis is perpendicular to d.

Using (8.6) to express the rotor current $\boldsymbol{i}_r$ in terms of the stator current and the rotor-flux vectors, and inserting that expression into the rotor equation (8.2) yields

$$p\,\boldsymbol{\psi}_r + j(\omega - \omega_r)\boldsymbol{\psi}_r + \frac{r_r}{L_r}\boldsymbol{\psi}_r = \frac{r_r L_m}{L_r}\boldsymbol{i}_s, \tag{8.10}$$

---

[1]Tracking of constants, by means of some feed-back control structure, is simpler to design and build than a controller which must track a sinusoidal reference. In fact, in the latter case, an oscillator is needed rather than a controller, and since an oscillator is only marginally stable, digital realization is more difficult compared to an implementation of a control structure with poles located well off the imaginary axis.

which for $\omega = \omega_{rf}$ may be split into real and imaginary parts resulting in:

$$\mathrm{p}\,\psi_{rd} + \frac{r_r}{L_r}\psi_{rd} = \frac{r_r L_m}{L_r}i_{sd} \tag{8.11}$$

$$(\omega_{rf} - \omega_r)\psi_{rd} = \frac{r_r L_m}{L_r}i_{sq}. \tag{8.12}$$

The developed electro-magnetic torque is found using (8.7)

$$T_{em} = \tfrac{3}{2}P\frac{L_m}{L_r}\mathcal{I}\Big(\psi_{rd}(i_{sd} + ji_{sq})\Big) = \tfrac{3}{2}P\frac{L_m}{L_r}\psi_{rd}\,i_{sq}. \tag{8.13}$$

Based on (8.11)-(8.13) the properties of the rotor field-oriented control philosophy may then be summarized as:

- Considering i_{sd} as the input and ψ_{rd} as the output, (8.11) shows that to perturbations in i_{sd} the rotor-flux behaves as a first-order lag element with the time constant $\tau_r = L_r/r_r$, which is a fairly large quantity.

- This indicates that it is feasible to keep ψ_{rd} constant, which by (8.13) implies that the developed torque is a function of i_{sq} only. Furthermore, neglecting saturation effects, the relationship between T_{em} and i_{sq} is purely linear, which from a control point of view, is highly desirable.

- By utilizing a feed-back loop to control the stator current space vector, decoupled control of flux and torque is possible. This is very much similar to the control of a separately excited dc motor.

- The obtainable rise time of the torque is essentially determined by the bandwidth of the current controller. Rise times in the order of a few milliseconds or even less are obtainable.

- Compared to the mechanical rotor speed ω_m and the rotor-flux ψ_{rd}, the stator current i_{sd} may be changed much faster. By virtue of (8.12) this means that decoupled control of the flux and the torque components of the stator current is equivalent to controlling the instantaneous slip $(\omega_{rf} - \omega_r)$ of the motor.

8.3　Design of rotor-field oriented drive

A design of a rotor-field oriented controller for an induction motor drive is presented in this section. The design is idealized in the sense that all analyses are made in the continuous-time domain and, furthermore, actuator saturation and time delays are disregarded. These problems related to the digital implementation in a DSP based on random carrier and sampling frequencies are treated in section 8.4 starting on page 258. Note that this indirect design procedure is compatible with the methodology outlined in Chapter 7.
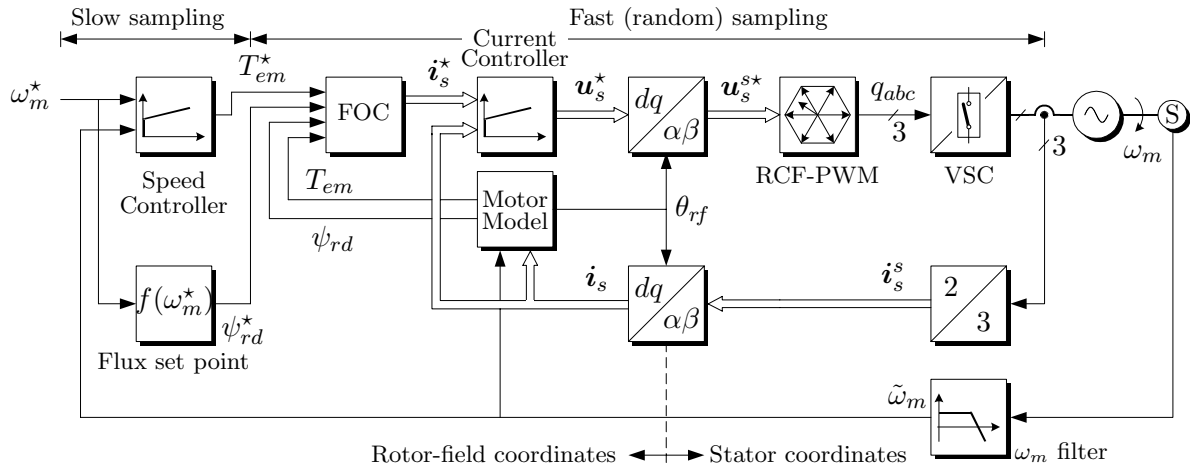
Figure 8.2 Speed-controlled induction motor based on a direct rotor-field oriented controller. The PWM carrier and the sampling frequencies are equal, but randomly varied. Double-lined connections represent signals that are space vectors. Although not shown in the figure, the dc-link voltage is also measured.

8.3.1 System overview

In Fig. 8.2 above the diagram of the used system may clarify the interactions between the different functional units. The control system is based on a standard cascaded structure extended with some transformation blocks and a motor model that estimates unmeasurable signals required for proper operation of the system. As it may be noted, no attempts are made to implement advanced facilities such as on-line adaption of motor parameters, compensation for main-flux saturation, speed sensor-less operation and, therefore, it must be expected that the performance obtainable with the used system leaves plenty of room for enhancements. However, such issues are not considered because the main objective is to demonstrate that random carrier frequency PWM can be made compatible with commonly used feed-back control techniques in ac drives without any loss of performance compared to deterministic modulation.

In brief, the core components of the system are:

Current controller

The innermost loop contains a synchronous-frame linear current controller which generates the reference voltage $\boldsymbol{u}_s^\star$. This is transformed back to $\alpha\beta$ coordinates before $\boldsymbol{u}_s^{s\star}$ is fed to the RCF modulator. The current controller should give zero steady-state error besides a quick dynamic response.

Motor model

The motor model is also a part of the loop. Given measured currents and shaft speed, the model estimates the position θ_{rf} and the amplitude ψ_{rd} of the rotor-flux besides the torque T_{em}.

Flux and torque control by FOC

This includes a torque controller and a flux controller which determine the reference current (in rotor-flux coordinates) to be impressed on the stator winding of the motor. This unit is also updated in each PWM period.

Speed controller and flux set point

> Those outer loops generate references for the torque and for flux magnitude based on reference speed and the measured speed. The sampling rate for those units is constant.

The control system consists of two subsystems that operate asynchronously to each other. The outer loop is sampled at a constant rate of 500 Hz independently of the inner loops (the motor model, the FOC, and the current controller), which run synchronously to the PWM generator. The instantaneous sampling/carrier frequency is calculated by a random number generator based on the chosen statistics for the carrier frequency.

8.3.2   Current controller

In the literature, different types of current controllers for three-phase applications have been suggested and analyzed. The techniques span from free-running analogue hysteresis controllers to more sophisticated schemes, such as linear controllers, neural networks, fuzzy logic, state feed-back, predictive, dead-beat controllers, etc. — an overview may be found in e.g. [3–5]. Here, the popular compromise between complexity and performance, namely a synchronous-frame linear controller, is used. It is possible to obtain zero steady-state error as the controller operates on dc signals.

In [6, 7] a set of simple tuning rules is presented for this type of controller based on the internal model control (IMC) method described in details in [8]. It turns out that apart from the motor parameters, only the desired closed-loop bandwidth denoted as α must be specified for the design of the controller. Guidelines to select α are also presented in [6, 7] taking inverter saturation and the carrier/sampling frequency into account as well.

Below, the design of the IMC-based synchronous-frame current controller is presented based on a simple design model.

The design model

Fig. 8.2 shows that the current controller is implemented in synchronous coordinates aligned with the rotor-flux axis meaning that the input reference current $\boldsymbol{i}_s^\star$ and the commanded voltage $\boldsymbol{u}_s^\star$ are both expressed in the rotor-flux oriented reference frame. Using the induction motor model given by (8.1)–(8.6), the following complex-valued differential equation may be derived:

$$L_\sigma \, \mathrm{p} \, \boldsymbol{i}_s + \big(r_{rs} + j\omega L_\sigma\big)\boldsymbol{i}_s = \underbrace{\boldsymbol{u}_s + \boldsymbol{\psi}_r \frac{L_m}{L_r}\left(\frac{r_r}{L_r} - j\omega_r\right)}_{=\,\boldsymbol{u}_s + \boldsymbol{u}_\psi \,\triangleq\, \boldsymbol{u}_s'}, \qquad (8.14)$$

where the total leakage inductance is $L_\sigma = L_s - L_m^2/L_r$ and the total resistance is $r_{rs} = r_s + (L_m/L_r)^2 r_r$. Including the term $\boldsymbol{u}_\psi$ in the modified stator voltage vector $\boldsymbol{u}_s'$, the transfer function becomes

$$G(s) = \frac{\boldsymbol{i}_s(s)}{\boldsymbol{u}_s'(s)} = \frac{1}{sL_\sigma + (r_{rs} + j\omega L_\sigma)}. \qquad (8.15)$$

(a)   (b)
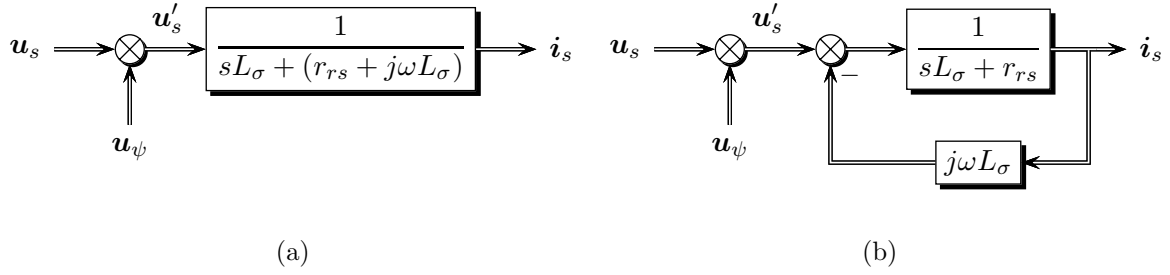
Figure 8.3 Induction machine transfer function in synchronous coordinates from impressed stator voltage to resulting stator current. (a) Directly as by (8.15) and (b) equivalent block diagram with the cross-coupling term in an outer loop.

Two equivalent block diagrams illustrating (8.15) are shown in Fig. 8.3. It appears that the system is a first-order system with the time constant L_σ/r_{rs} augmented with a $j\omega L_\sigma$ negative feed-back loop which represents the cross-coupling between the d and q axes. However, the system is in fact a second-order system; the complex-valued signals and the complex-valued transfer function (8.15) mask this fact.

Therefore, in some cases it may be more appropriate to use the equivalent transfer function matrix, which explicitly shows the multiple-input multiple-output nature of the system. This matrix may be derived from (8.14) by decomposing the system into its orthogonal dq components. Neglecting the $\boldsymbol{u}_\psi$, which may be regarded as a slowly varying disturbance, the result is

$$\begin{bmatrix} sL_\sigma + r_{rs} & -\omega L_\sigma \\ \omega L_\sigma & sL_\sigma + r_{rs} \end{bmatrix} \begin{bmatrix} i_d \\ i_q \end{bmatrix} = \begin{bmatrix} u_d \\ u_q \end{bmatrix}, \tag{8.16}$$

i.e. the transfer matrix $G(s)$ becomes

$$G(s) = \begin{bmatrix} sL_\sigma + r_{rs} & -\omega L_\sigma \\ \omega L_\sigma & sL_\sigma + r_{rs} \end{bmatrix}^{-1} = \frac{1}{(sL_\sigma + r_{rs})^2 + (\omega L_\sigma)^2} \begin{bmatrix} sL_\sigma + r_{rs} & \omega L_\sigma \\ -\omega L_\sigma & sL_\sigma + r_{rs} \end{bmatrix}. \tag{8.17}$$

This equation shows that for $\omega \neq 0$ the system is indeed a second-order system with cross couplings between the axes: a change in e.g. u_d causes a change in both the d and q currents. Furthermore, the denominator of (8.17) shows that in the synchronous reference frame the motor has a complex-conjugated pole-pair at $s = -r_{rs}/L_\sigma \pm j\omega$.

The IMC method

The internal model control structure is depicted in Fig. 8.4(a). The basic idea is to feed back the error between the outputs produced by the plant (transfer matrix $G_0(s)$) and by the model $G(s)$. If the model is perfect, i.e. $G(s) = G_0(s)$, no feed-back signal exists. Stated otherwise, the purpose of the controller $C(s)$ is to reduce the impact of plant uncertainty.

By simple block-diagram algebra it is possible to transform the IMC structure into the more familiar series controller $C_s(s)$ as shown in Fig. 8.4(b), where

$$C_s(s) = \left[I - C(s)G(s)\right]^{-1} C(s). \tag{8.18}$$
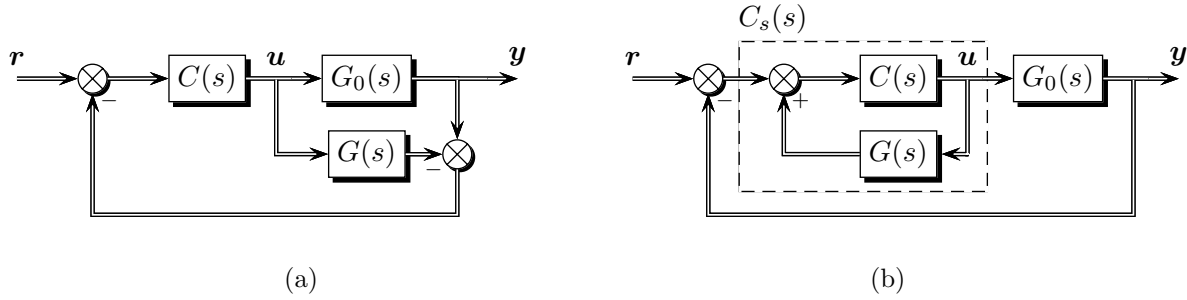
Figure 8.4 (a) Internal model control structure. (b) Equivalent series controller.

Here, I is the identity matrix.

A more detailed discussion of the properties and tuning of IMC may be found in [7], where it is demonstrated that a suitable selection of the controller is to let[2]

$$C(s) = G^{-1}(s)L(s), \tag{8.19}$$

where $L(s)$ is the low-pass filter

$$L(s) = \frac{\alpha}{s + \alpha}I. \tag{8.20}$$

Essentially, the controller is the inverse of the plant model, but de-tuned by the filter $L(s)$. Inserting the controller (8.19) into (8.18), the equivalent series controller becomes

$$C_s(s) = \left[I - G^{-1}(s)L(s)G(s)\right]^{-1}G^{-1}(s)L(s)$$

$$= \left[I - G^{-1}(s)\frac{\alpha}{s + \alpha}IG(s)\right]^{-1}G^{-1}(s)\frac{\alpha}{s + \alpha}I, \tag{8.21}$$

which may be simplified to

$$C_s(s) = \frac{\alpha}{s}G^{-1}(s). \tag{8.22}$$

The closed-loop transfer matrix $F(s)$ of the cascade of $C_s(s)$ and $G(s)$ then becomes

$$F(s) = \frac{C_s(s)G(s)}{1 + C_s(s)G(s)} = \frac{\alpha}{s + \alpha}I. \tag{8.23}$$

Under the assumption that $G(s) = G_0(s)$ this shows that for the closed-loop response the mutual couplings are removed and that the system behaves as independent first-order systems, each having a time constant given by $1/\alpha$.

---

[2]The selection of $C(s)$ in (8.19) requires that the plant model $G(s)$ does not have any zeroes in the right half-plane since this would cause $G^{-1}(s)$ to be unstable. Also, if the true plant has a delay, i.e. if $G_0(s)$ is non-rational, this term should also be excluded from the model $G(s)$. Hence, in the design stage of the current controller, the delay in the inverter and the delay introduced by the pulse width modulator and the control system itself are both ignored. The impact of this simplification is studied in section 8.4.1 starting on page 258.
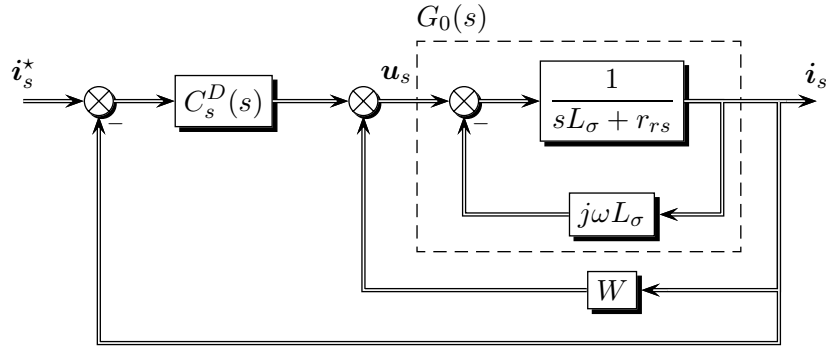
Figure 8.5 Diagonal IMC with cross-coupling terms moved outside the controller.

Design of current controller based on IMC

In the series controller form $C_s(s)$ defined by (8.22), the current controller may now be found using the transfer matrix (8.17) for the induction machine in field coordinates:

$$C_s(s) = \frac{\alpha}{s} G^{-1}(s) = \frac{\alpha}{s} \begin{bmatrix} sL_\sigma + r_{rs} & -\omega L_\sigma \\ \omega L_\sigma & sL_\sigma + r_{rs} \end{bmatrix}. \tag{8.24}$$

As shown in [6], (8.24) resembles a standard PI controller without decoupling terms, viz.

$$C_{\mathrm{PI}}(s) = \begin{bmatrix} K\left(1 + \dfrac{1}{sT_i}\right) & 0 \\ 0 & K\left(1 + \dfrac{1}{sT_i}\right) \end{bmatrix} \tag{8.25}$$

with the gain $K = \alpha L_\sigma$ and the integration time $T_i = L_\sigma/r_{rs}$. However, for systems of orders higher than two the resemblance between IMC structures and PI controllers is lost [7].

A variant of (8.24) is suggested in [7] which moves the anti-diagonal elements ($\pm\omega L_\sigma$) outside the controller. This is done to avoid oscillations in case of an imperfect model, i.e. if the motor parameters used for the design differ from the actual values. (The problem gets worse if the poles at $s = -r_{rs}/L_\sigma \pm j\omega$ are only lightly damped; this is especially true for permanent magnet machines without rotor damper windings, but the problem may also exist for the induction machine at higher speed levels [7].) Hence, by adding a decoupling loop as shown in Fig. 8.5 a modified system denoted as diagonal-IMC (DIMC) appears, where the controller $C_s^D(s)$ is given by

$$C_s^D(s) = \frac{\alpha}{s} \begin{bmatrix} sL_\sigma + r_{rs} & 0 \\ 0 & sL_\sigma + r_{rs} \end{bmatrix}, \tag{8.26}$$

and the decoupling term W in the outer loop in Fig. 8.5 corresponds to the transfer matrix

$$W = \begin{bmatrix} 0 & \omega L_\sigma \\ -\omega L_\sigma & 0 \end{bmatrix}. \tag{8.27}$$

8.3.3   Rotor-flux and torque estimation

For all practical purposes, the rotor flux cannot be sensed, i.e. its spatial position and amplitude must be estimated from measured quantities and known motor parameters. A deviation between the calculated and real rotor flux deteriorates the performance: An angle error implies that the decoupling becomes imperfect, which leads to an oscillatory torque response. An amplitude error will result in flux and torque scaling errors.

Hence, the flux estimation issue is an important problem, and a large number of publications have dealt with this problem. Advanced methods based on observer theory have been developed to make the estimated flux less sensitive to parameter uncertainty, measurement noise, etc. This kind of flux estimators include a feed-back correcting term based on the error between e.g. the measured and simulated current.

Here, however, a very simple estimator is used — the so-called current model implemented in synchronous coordinates, see [9]. This method is as an open-loop simulation of the motor without the corrections found in the advanced methods. Measurements of the rotor speed $\omega_r = P\omega_m$ and stator current vector $\boldsymbol{i}_s^s$ are required, but the stator voltage vector is not needed. Although the current model is recommended for use in the low-speed region only [9], it is used up to nominal speed for simplicity reasons. The rotor current $\boldsymbol{i}_r$ is eliminated from (8.6) and inserted into (8.2) which leads to:

$$\mathbf{0} = \frac{1}{\tau_r}\left(\boldsymbol{\psi}_r - L_m\boldsymbol{i}_s\right) + \mathrm{p}\,\boldsymbol{\psi}_r + j\left(\mathrm{p}\,\theta_{rf} - w_r\right)\boldsymbol{\psi}_r, \tag{8.28}$$

where the rotor time-constant is $\tau_r = L_r/r_r$. Now, in the rotor-flux oriented control, the q-component of the rotor flux vanishes, i.e. $\boldsymbol{\psi}_r = \psi_{rd}$. Using this fact and separating (8.28) into the real and imaginary components yield

$$\mathrm{p}\,\psi_{rd} = \frac{L_m}{\tau_r}i_{sd} - \frac{1}{\tau_r}\psi_{rd} \tag{8.29}$$

$$\mathrm{p}\,\theta_{rf} = \frac{L_m}{\tau_r}\frac{i_{sq}}{\psi_{rd}} + \omega_r. \tag{8.30}$$

A block diagram is shown in Fig. 8.6. Note that the rotor-flux angle is the integral of the sum of the estimated angular slip frequency and the measured rotor speed.

Finally, the developed electro-magnetic torque may be calculated in rotor-flux coordinates as well without using the stator voltage. From (8.13) it follows that

$$T_{em} = \tfrac{3}{2}\,P\frac{L_m}{L_r}\psi_{rd}\,i_{sq}. \tag{8.31}$$

This is only an estimate of the true developed torque: incorrect orientation as well as parameter variations influence the accuracy of the calculated torque.

8.3.4   Torque and flux controllers

The d and q components of the reference current vector $\boldsymbol{i}_s^\star$ determine the rotor-flux magnitude and the torque, respectively. Those currents denoted by $i_{sd}^\star$ and $i_{sq}^\star$ are calculated in the FOC block in Fig. 8.2 on page 251 by means of the following expressions:

$$i_{sd}^\star = \frac{\psi_{rd}^\star}{L_m} + \frac{1}{T_\psi\,\mathrm{p}}\left(\psi_{rd}^\star - \psi_{rd}\right) \tag{8.32}$$
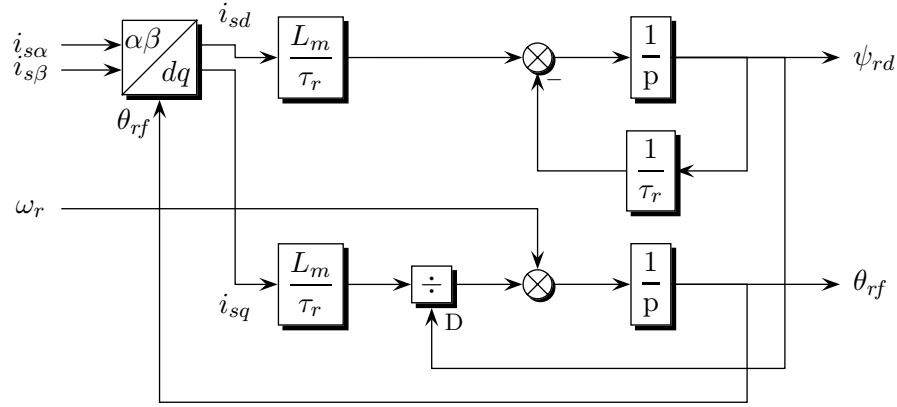
Figure 8.6 The rotor-flux estimator based on the $(\boldsymbol{i}_s, \omega_r)$-model in synchronous coordinates.

and

$$i^{\star}_{sq} = \frac{2L_r}{3PL_m}\frac{T^{\star}_{em}}{\psi^{\star}_{rd}} + \frac{1}{T_T\,\mathrm{p}}\Big(T^{\star}_{em} - T_{em}\Big). \tag{8.33}$$

Both reference currents are determined by combining a feed-forward term (which is calculated solely from reference values and motor parameters) with a feed-back term that drives the steady-state error to zero by means of a slow-acting integrator. The feed-forward terms follow directly from (8.29) and (8.31); the gain of the feedback terms can be controlled through selection of T_ψ and T_T.

8.3.5 Speed controller

Essentially, the speed controller generates the torque command $T^{\star}_{em}$ to the torque controller presented above. For the design, it is assumed that the bandwidth of the speed controller is much lower than the bandwidth of the inner loops (torque and current), i.e. it is assumed that the commanded value $T^{\star}_{em}$ is equal to the actual value T_{em}. In total, the model shown in Fig. 8.7 on the next page is used for the design.

Controller structure

The IMC tuning method used for the design of the current controller may, in principle, also be used for the speed controller. However, due to the low order of the design model the speed controller is implemented directly as a modified version of a PID-controller [10], where the q-axis reference current $i^{\star}_{sq}$ is determined by

$$T^{\star}_{em} = \underbrace{K\Big(a\omega^{\star}_m - \omega_m\Big)}_{\text{P-term}} + \underbrace{\frac{K}{T_i\,\mathrm{p}}\Big(\omega^{\star}_m - \omega_m\Big)}_{\text{I-term}} + \underbrace{\frac{T_d K N\,\mathrm{p}}{T_d K\,\mathrm{p} + N}\Big(\omega^{\star}_m - c\omega_m\Big)}_{\text{D-term}}. \tag{8.34}$$

Here, the main parameters are the gain K, the integration time T_i and derivative time T_d. It should be noted that only a fraction $a \leq 1$ (typically $a \approx 0.3$) of the reference acts on the P-term. Also, the derivative term has been modified according to the
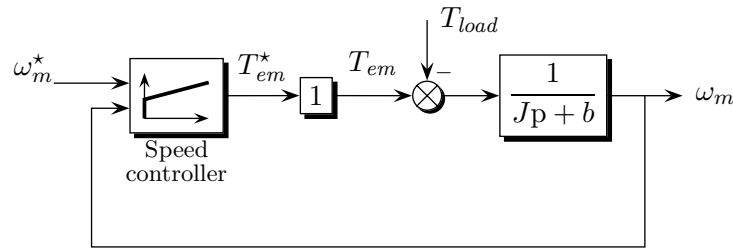
Figure 8.7 Model used for design of the speed controller.

recommendation of [10] compared to the ideal differentiation found in most textbooks: due to measurement noise only a fraction c of the measured speed ω_m is subjected to differentiation[3]. The gain of the D-term is limited to N by low-pass filtering.

Tuning

The speed controller was tuned by first performing a step-response experiment and then, an empirical set of tuning rules was used to find suitable values for K, T_i, and T_d.. More precisely, the method of Chien, Hrones, and Reswick in [10] was used, which is a modified version of the more well-known Ziegler-Nichols step-response method. Generally, the former method provides a closed-loop response that is much more well-damped than the Ziegler-Nichols tuning rule which often leads to an oscillatory response.

8.4   Field-oriented controller implementation

This section summarizes a number of issues that must be considered before a successful implementation of the total system in the laboratory set-up can be achieved. Below, the results of the design based on continuous-time models presented in section 8.3 are combined with the discretization procedure described in Chapter 7.

First, the discretization of the current controller is presented and details about how to avoid integrator wind-up due to the limited voltage capability of the inverter are given. Since the current controller has been designed without taking any time delays into account, a few simulation results are also presented in order to investigate the effects of an actual non-zero propagation delay. Finally, the discretization of the rotor-flux estimator is described.

8.4.1   Implementation of the current controller

The designed DIMC current controller is given by $C_s^D(s)$ in (8.26) on page 255 and the decoupling matrix W in (8.27). The starting point for the implementation is to identify

---

[3]In [10] the factor c is on the reference D-term, but for the particular system used here, experiments have shown that measurement noise on ω_m leads to unnecessary changes in $T_{em}^\star$. On the other hand, the reference $\omega_m^\star$ is not subjected to any noise, which makes differentiation much more safe on this term.

an equivalent state-space model for the controller. From (8.26) and the standard state-space model (7.7) on page 234, the following is obtained:

$$\mathrm{p}\,x = 0x \; + \; \alpha \overbrace{\begin{bmatrix} r_{rs} & 0 \\ 0 & r_{rs} \end{bmatrix}}^{B} e \tag{8.35}$$

$$u = Ix \; + \; \alpha \underbrace{\begin{bmatrix} L_\sigma & 0 \\ 0 & L_\sigma \end{bmatrix}}_{D} e + \underbrace{\begin{bmatrix} 0 & \omega L_\sigma \\ -\omega L_\sigma & 0 \end{bmatrix}}_{W} i, \tag{8.36}$$

where the output voltage is $u = [u_{sd} \ u_{sq}]^T$, the input current error is $e = [\Delta i_{sd} \ \Delta i_{sq}]^T$, and the current vector for decoupling is $i = [i_{sd} \ i_{sq}]^T$.

By comparing (8.35) to (7.7), it should be noted that the system matrix A vanishes and that C becomes the identity matrix — this greatly simplifies the discretization.

Discretization of the current controller

For the Backward Euler method (7.10) and the Tustin approximation (7.11) in Chapter 7, the updating of the current controller from sample $(k-1)$ to sample k then becomes

$$\text{Backward Euler:} \quad \begin{cases} x_k = x_{k-1} + T_{k-1} B e_k \\ u_k = x_k + D e_k + W i_k, \end{cases} \tag{8.37}$$

$$\text{Tustin:} \quad \begin{cases} x_k = x_{k-1} + \frac{1}{2} T_{k-1} B (e_{k-1} + e_k) \\ u_k = x_k + D e_k + W i_k, \end{cases} \tag{8.38}$$

where the B, D, and W matrices are defined in (8.35) and (8.36). Also, T_{k-1} is the elapsed time between the current and the previous sampling instants.

Anti-integrator wind-up

The voltage vector reference calculated above may exceed the voltage capability of the converter, i.e. the actuator may saturate. Since the controller includes an integrator, overshoots and a sluggish response may occur, if no precautions are taken against it. Hence, to avoid integrator wind-up, a method known as back-calculation [10] is used; this principle has been used by [7] with good results.

The idea may be grasped by the following stepwise procedure:

1. **Calculate the ideal output voltage**
   Ignoring all saturation effects the ideal commanded voltage is calculated by

$$\text{Backward Euler: } u_k = x_{k-1} + (T_{k-1}B + D)e_k + W i_k \tag{8.39}$$

$$\text{Tustin's rule: } u_k = x_{k-1} + (\tfrac{1}{2}T_{k-1}B + D)e_k + \tfrac{1}{2}T_{k-1}B e_{k-1} + W i_k, \tag{8.40}$$

2. Calculate the limited control signal

The commanded voltage is limited by applying a saturation function. The limited voltage is labeled $\overline{u}_k$ and calculated by first finding the amplitude of the commanded voltage, $|u_k| = \sqrt{u_{sd}^2 + u_{sq}^2}$. Then

$$\overline{u}_k = \begin{cases} u_k = [u_{sd}\ u_{sq}]^T, & \text{if}\quad |u_k| < |\boldsymbol{u}_s^s(\gamma)|_{\max}, \\[2mm] \dfrac{|\boldsymbol{u}_s^s(\gamma)|_{\max}}{|u_k|}\,[u_{sd}\ u_{sq}]^T, & \text{otherwise}, \end{cases} \tag{8.41}$$

which gives no phase error between $\overline{u}_k$ and u_k — this and other approaches, such as a minimum amplitude error technique, for limiting the voltage are analyzed in [11]. In (8.41), the maximum voltage $|\boldsymbol{u}_s^s(\gamma)|_{\max}$ is found by (2.12) on page 25. This requires knowledge of the PWM reference angle γ in stationary coordinates, i.e. $\gamma = \theta_{rf} + \arctan(u_{sq}/u_{sd})$, if the full hexagon should be utilized[4].

3. Find the equivalent error

Using the limited voltage $\overline{u}_k$, the equivalent error $\overline{e}_k$ is found as

$$\text{Backward Euler: } \overline{e}_k = \ (T_{k-1}B + D)^{-1}(\overline{u}_k - x_{k-1} - Wi_k) \tag{8.42}$$
$$\text{Tustin's rule: } \overline{e}_k = (\tfrac{1}{2}T_{k-1}B + D)^{-1}(\overline{u}_k - x_{k-1} - \tfrac{1}{2}T_{k-1}Be_{k-1} - Wi_k). \tag{8.43}$$

When this error is applied to the controller, the voltage found by (8.41) is produced. This explains why this method to avoid wind-up is called back-calculation.

4. Update the state variables

The internal state vector x_k is updated according to the error $\overline{e}_k$:

$$\text{Backward Euler: } x_k = x_{k-1} + T_{k-1}B\,\overline{e}_k \tag{8.44}$$
$$\text{Tustin's rule: } x_k = x_{k-1} + \tfrac{1}{2}T_{k-1}B(e_{k-1} + \overline{e}_k). \tag{8.45}$$

Simulation of current-control loop

To investigate the feasibility of the designed discrete-time current controller based on a randomized sampling frequency, a few simulation results are presented. The major concern is how the one PWM period time delay impacts on the performance, because this delay was ignored during the design in section 8.3.2.

The simulations were conducted in MATLAB using the data for the 1.5 kW, 2 pole induction machine listed in Table A.1 (page 298). The simulations are performed at both a low and a high fundamental frequency: 5 Hz and 40 Hz, respectively. The sampling/carrier frequency is fixed at 4 kHz. Different values of the current controller bandwidth α are used: 0.06, 0.08, and 0.1 times the carrier frequency. Provided that the decoupling obtained through IMC structure is perfect, these α-values should yield nominal rise times of 1.5, 1.1, and 0.9 ms, respectively. Since the sampling time is 0.25 ms, the number of updates of the controller during the current rise time is in the order of 3–6 samples.

---

[4]To save processor time, the dependence of $|\boldsymbol{u}_s^s(\gamma)|_{\max}$ on γ could be ignored by letting $|\boldsymbol{u}_s^s(\gamma)|_{\max} = u_{dc}/\sqrt{3}$ for all values of γ (in this case pulse dropping will never occur at the expense of not utilizing the full voltage range of the inverter). Alternatively, one could use $|\boldsymbol{u}_s^s(\gamma)|_{\max} = \tfrac{2}{3}u_{dc}$. However, in this case the wind-up problem is not compensated correctly.

(a)

(b)

(c)

(d)

(e)

(f)
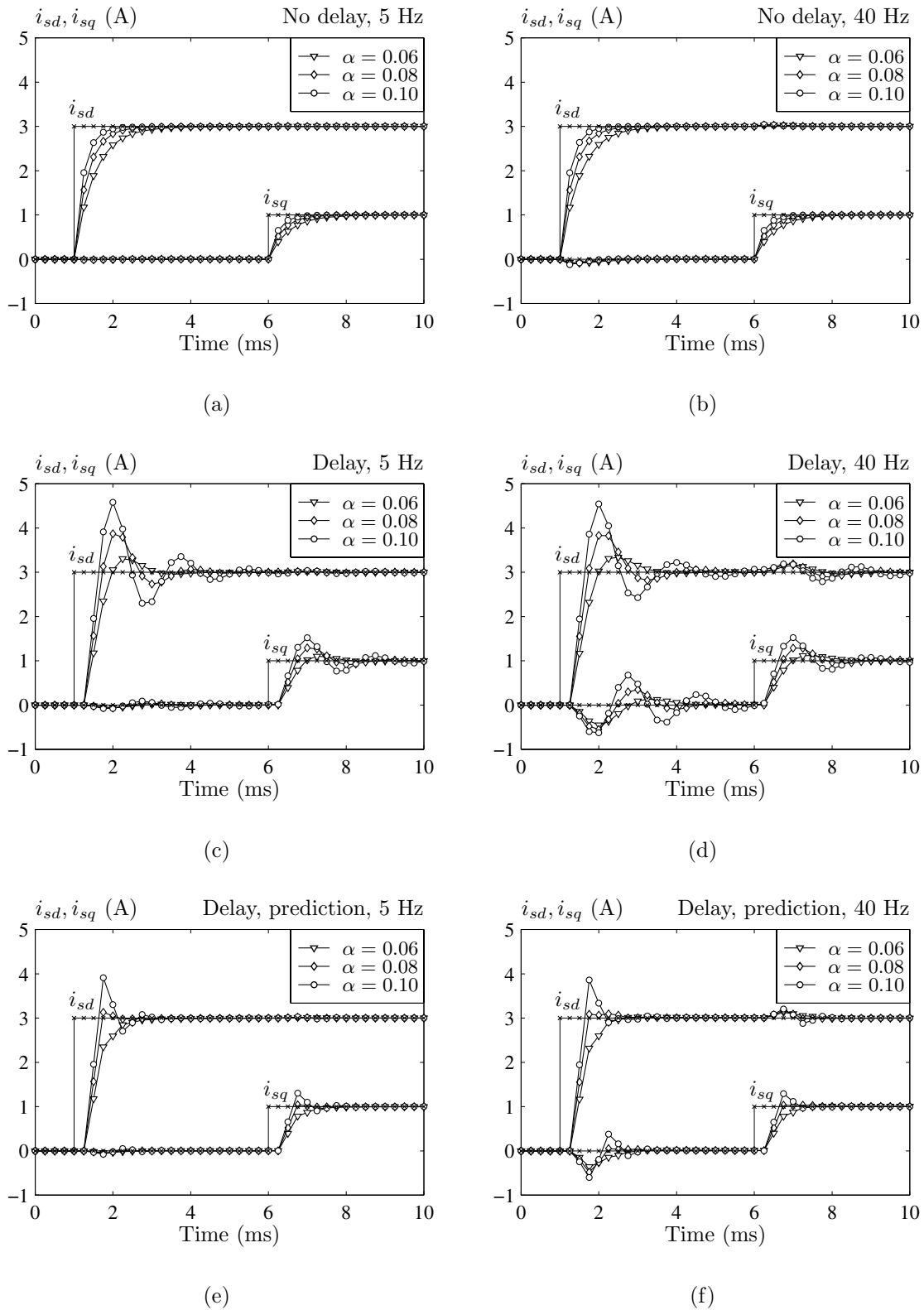
Figure 8.8 Simulation of current-control loop with a sampling frequency of 4 kHz. At $t = 1$ ms the d-axis reference is changed to 3 A. The q-axis reference is stepped at $t = 6$ ms. Left column: 5 Hz fundamental frequency. Right column: 40 Hz fundamental frequency. (a, b) No delay (the design case), (c, d) the one-sample delay is included, and (e, f) the one-sample delay is included and the simple current predictor is used.

Fig. 8.8 shows the results of a step change in the d-axis (at $t = 1$ ms) and in the q-axis reference current at $t = 6$ ms. Due to the off-line nature of the calculations, it is possible to avoid the one-sample delay, which makes it possible to judge the impact of the delay without the influence of other phenomena. If the one-sample delay is ignored (the design case), Fig. 8.8(a, b) shows that the performance is very good: no coupling exists, and, furthermore, the overshoot is zero. The graphs in Fig. 8.8(c, d) show the impact of the one-sample delay. The delay reduces the phase margin of the system. In particular for the high-bandwidth case ($\alpha = 0.1$), large oscillations occur due to phase lag introduced by the delay. The overshoot is approximately 55%, which is unacceptable. At best, the $\alpha = 0.08$ selection gives a satisfactory performance in this case.

At this point, it may be noted that if a better performance (in terms of rise time versus overshoot and sampling rate) is required, then the controller should be redesigned so that the one-sample delay is incorporated into the controller design. For classic controllers, where the sampling rate is constant, this increases the system model order by one in the z-domain. However, as explained in Chapter 7 this route cannot be followed here.

A simple compensation method has been devised, which avoids redesigning the controller. Instead of parsing the sampled currents directly to the controller, dq-currents *predicted* one sampling period ahead of time are used in the control algorithms. Specifically, by using the forward Euler method, the predicted current vector $\hat{i}_{sd}(t_{k+1})$ at t_{k+1} becomes

$$\hat{i}_{sd}(t_{k+1}) \triangleq i_{sd}(t_k) + \frac{t_{k+1} - t_k}{t_k - t_{k-1}} \left(i_{sd}(t_k) - i_{sd}(t_{k-1}) \right), \qquad (8.46)$$

where the sampling instants t_{k-1}, t_k, and t_{k+1} are all known at $t = t_k$ (t_{k+1} is precalculated based on the chosen probability density function for the carrier frequency). By index substitution the same goes for the q-axis currents. The predictor (8.46) is a very simple open-loop estimator without any feed-back correcting terms or limiters.

Using this current predictor, the simulation results shown in Fig. 8.8(e, f) show that the overshoot and the duration of the oscillations are reduced considerably compared to the results in Fig. 8.8(c, d). Similar conclusions may be drawn from the experimental tests reported in the next section of this chapter. Even better results could probably be obtained by basing the predictor on the motor-model equation (8.14), but this approach adds complexity to the controller. Such a methodology has, however, been applied successfully in [12] to stabilize an otherwise unstable high-bandwidth deadbeat current controller for a permanent magnet synchronous machine.

In summary, that impact of the delay in the combined control-inverter system should be either taken into account during the design or compensated afterwards, if $\alpha > 0.08$ is required. Below this value, the influence of delay is less significant and if simplicity is of importance, compensation may be omitted.

8.4.2   Implementation of the rotor-flux estimator

The synchronous-frame rotor-flux estimator was derived in section 8.3.3 leading to the block diagram in Fig. 8.6 on page 257. The discretization of this continuous-time estimator is not a trivial task due to the non-linear structure of the system previously

defined by (8.29) and (8.30), repeated here for convenience:

$$p\,\psi_{rd} = \frac{L_m}{\tau_r}i_{sd} - \frac{1}{\tau_r}\psi_{rd} \tag{8.47}$$

$$p\,\theta_{rf} = \frac{L_m}{\tau_r}\frac{i_{sq}}{\psi_{rd}} + \omega_r = \omega_{rf}, \tag{8.48}$$

where the currents are transformed from stationary $\alpha\beta$ to rotating dq coordinates by (8.8)

$$i_{sd} = i_{s\alpha}\cos\theta_{rf} + i_{s\beta}\sin\theta_{rf} \tag{8.49}$$

$$i_{sq} = -i_{s\alpha}\sin\theta_{rf} + i_{s\beta}\cos\theta_{rf}. \tag{8.50}$$

The inputs to the estimator are the measured stator currents $i_{s\alpha}$ and $i_{s\beta}$ besides the measured (electric) shaft speed ω_r. The principal outputs are the estimated amplitude ψ_{rd} and the angular position θ_{rf} of the rotor-flux space vector. Note that in a sense the transformed stator currents i_{sd} and i_{sq} may be regarded as intermediate internal states, which just happens to be useful for other purposes (mainly current control in this case).

Due to both the ψ_{rd} term in the denominator of (8.48) and the trigonometric functions in the current transformations, the system is nonlinear. Hence, the system cannot be put into the standard state-space form. In fact the rotor-flux estimator, including the current transformations involving θ_{rf}, constitutes a set of differential-algebraic equations (DAE)[5] due to the mixture of differential equations with algebraic equations (which cannot be eliminated due to the complex nonlinear dependency among the variables).

Therefore, approximations must be made to complete the discretization and the subsequent implementation. However, it is astonishing to notice that the otherwise extensive literature dealing with field-oriented control hardly ever addresses these fundamental problems relating to the real-world implementation of rotor-flux observers (or similar structures). Usually, an ad hoc "solution" is chosen without paying too much attention to the limitations of the discretization.

Discretization of rotor flux estimator

A simple time-inexpensive algorithm for the rotor-flux estimator problem is presented below taking the current transformation problem into account as well. A more thorough analysis of the problems pertinent to the discretization is left for future research. The following steps outline the algorithm:

1. **Prediction of the rotor-flux angle**
   Using the forward Euler rule between t_{k-1} and t_k (the present time) calculate the predicted value $\hat{\theta}_{rf}(t_k)$ by

$$\hat{\theta}_{rf}(t_k) = \theta(t_{k-1}) + \omega_{rf}(t_{k-1})(t_k - t_{k-1}) \triangleq \theta(t_{k-1}) + \omega_{rf}T_{k-1}. \tag{8.51}$$

---

[5]The understanding of DAE's and algorithms for time-efficient numerical solutions of DAE's are of outmost importance in simulators like SABER, which has been used in this research to test many ideas. A good introduction to numerical algorithms for solution of DAE may be found in [13]. Unfortunately, these specialized algorithms are both iterative and non-casual, which makes them unsuitable for real-time evaluation.

2. $\alpha\beta$ to dq transformation

The sampled currents are transformed into the dq frame by inserting the predicted position $\hat{\theta}_{rf}(t_k)$ into (8.49) and (8.50).

3. Update the rotor-flux magnitude

The value of ψ_{rd} may be found using the backward Euler rule,

$$\psi_{rd}(t_k) = \left(1 + \frac{T_{k-1}}{\tau_r}\right)^{-1} \left(\psi_{rd}(t_{k-1}) + \frac{T_{k-1}}{\tau_r} L_m i_{sq}(t_k)\right), \qquad (8.52)$$

i.e. there is no reason to use the forward Euler for the update of the rotor-flux magnitude.

4. Update the rotor-flux angular position

The backward Euler method is used again to update (8.48):

$$\theta_{rf}(t_k) = \theta_{rf}(t_{k-1}) + T_{k-1}\left(\frac{L_m}{\tau_r}\frac{i_{sd}(t_k)}{\psi_{rd}(t_k)} + \omega_r(t_k)\right), \qquad (8.53)$$

where the required value of $\psi_{rd}(t_k)$ is found above in (8.52).

5. Accept results?

The question is now whether to accept or to reject the results. As a simple measure, the difference between the predicted field angle $\hat{\theta}_{rf}(t_k)$ from (8.51) and the field angle obtained by (8.53) is calculated. If the error exceeds some chosen threshold, this indicates that the predicted position of the field is inaccurate; then, the algorithm in step 2 may be re-evaluated, but now using $\theta_{rf}(t_k)$ as the initial estimate of $\hat{\theta}_{rf}$. Other more advanced schemes for modifying the selection of $\hat{\theta}_{rf}$ could also be used.

The values calculated in the first evaluation of step $1 \rightarrow 4$ are used directly without further corrections in the laboratory implementation. Hence, a high degree of accuracy is sacrificed, but at least the calculation burden is kept constant.

8.4.3   Final comments on the implementation

The system shown in Fig. 8.2 on page 251 is realized in the laboratory. Specifically, all control algorithms are implemented in a floating point DSP; further information about the laboratory set-up may be found in Appendix A. The implementation closely follows the presented theory taking the following remarks into account also:

The speed controller

The discrete implementation has been obtained by a straightforward discretization of (8.34) on page 257. To avoid integrator wind-up, a method advocated by [10] has been used: an extra tracking loop is added around the integrator which resets the integrator to an appropriate value, when the commanded torque exceeds the maximum torque.

Flux set point

>   The flux amplitude must be reduced when the speed exceeds the rated speed due to the limited voltage capability of the converter. For simplicity reasons, however, field-weakening operation[6] is not considered here, i.e. the reference flux $\psi_{rd}^\star$ is fixed in all experiments at its nominal value.

Flux and torque controller

>   The continuous-time versions of those two first-order controllers given in section 8.3.4 were discretized by the Backward Euler method. The outputs $i_{sd}^\star$ and $i_{sq}^\star$ were limited to prevent overloading conditions.

After the system was set into operation, initial tests showed that the measured shaft speed ω_m was somewhat distorted by measurement noise. In order to lower the influence of the noise on the flux estimation, a third-order Butterworth low-pass filter with a 100 Hz cutoff frequency was added as indicated in Fig. 8.2 on page 251. The implementation of the filter, which is updated in each PWM carrier period on an irregular time basis, closely follows the guidelines summarized in section 7.4.5.

8.5   Laboratory measurements

This section presents various measurements performed on the developed system. Results of both dynamic and steady-state tests are reported. For reasons of comparison, the tests are performed for both random carrier frequency PWM and for fixed carrier frequency PWM. The used modulator settings are:

Random carrier frequency (RCF) PWM

>   The carrier/sampling frequency is selected at random in the 4–6 kHz range in each PWM period. A uniform probability density function is used.

Fixed carrier frequency (FCF) PWM

>   The carrier frequency is fixed at 5 kHz; the sampling frequency is also 5 kHz.

Note that the average carrier frequency is almost the same in these two cases: for the RCF technique the value is not exactly 5 kHz, but rather $(f_{\max} - f_{\min})/(\ln f_{\max} - \ln f_{\max}) = 4.93$ kHz — see [16] for details. Also, the classic space-vector modulation with equal duration of the two zero vectors in each PWM period is used for both FCF and RCF. All phase currents are sampled simultaneously.

8.5.1   Dynamic performance

The current controller is tested under the conditions specified below. Also, the overall system is tested by speed ramping tests with and without a load connected to the shaft. All data used to produce the plots shown in this subsection have been recorded by the DSP, i.e. no inter-sample information is available.

---

[6]As discussed in [14, 15], operation in the field-weakening region requires specialized overmodulation PWM techniques. This fact may make a direct replacement of a deterministic modulator with a randomized modulator difficult, if possible at all. (Ultimately, in six-step operation no randomization is possible at all.)
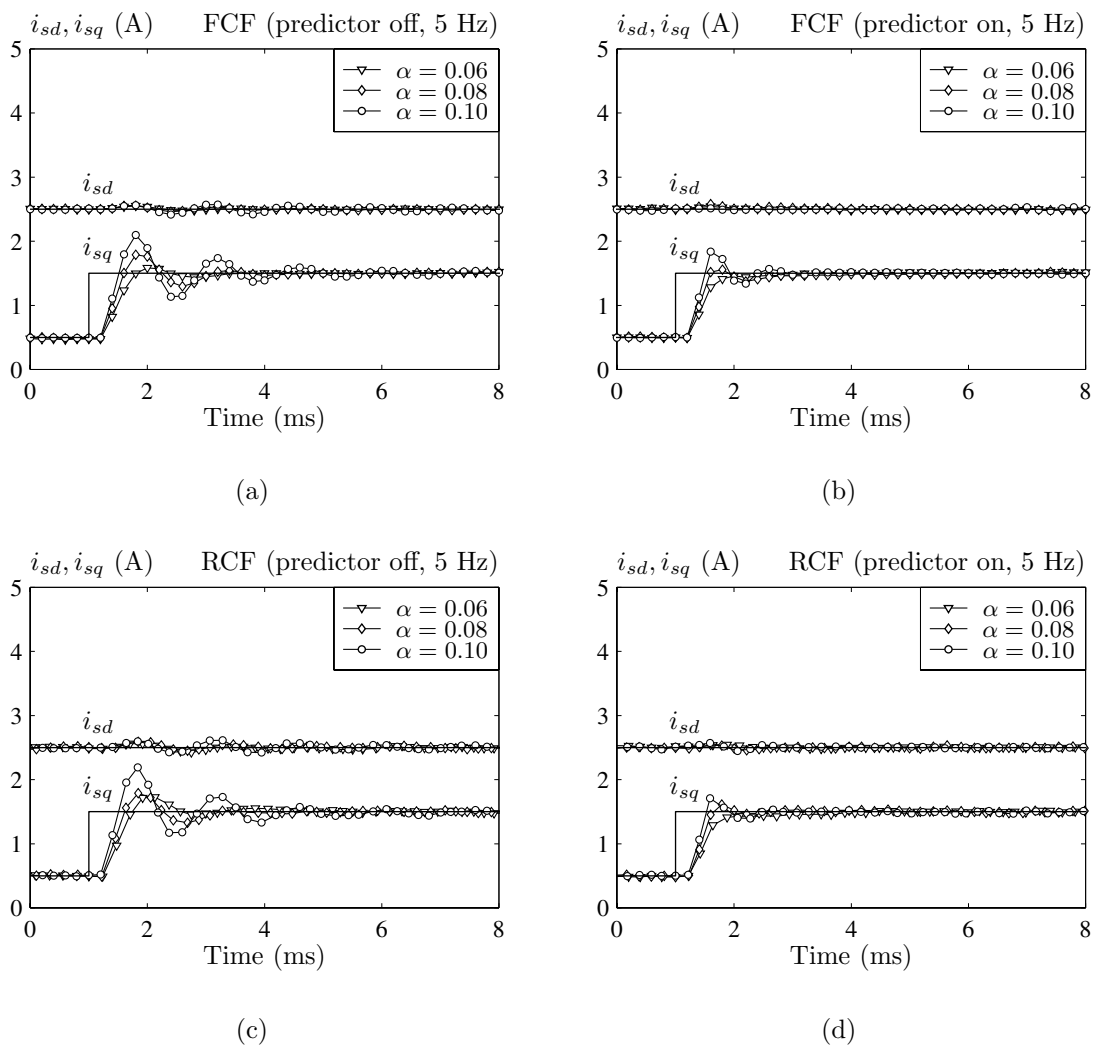
Figure 8.9 Measurements of current-control loop performance at low speed (5 Hz fundamental frequency) for three values of the bandwidth α (normalized with respect to 5 kHz). At $t = 1$ ms, the q-axis reference is stepped from 0.5 A to 1.5 A. The d-axis reference is fixed at 2.5 A. (a, b) FCF without and with current predictor. (c, d) RCF without and with current predictor.

Current controller

Apart from testing RCF versus FCF, the tests are also conducted for different values of the current controller bandwidth parameter α. The normalized values $\alpha = \{0.06, 0.08, 0.1\}$ are used. For a 5 kHz base value, this corresponds to bandwidths of 300 Hz, 400 Hz, and 500 Hz, respectively. The impact of the simple current predictor defined by (8.46) is also examined by repeating the experiments with and without the predictor enabled. In these tests, the speed, flux, and torque controllers are all disabled, but the rotor-flux angle estimated by the motor model is used in the $\alpha\beta/dq$ transformation blocks. Hence, the drive operates in an open-loop torque mode.

Results for low (5 Hz) and high speed (40 Hz) operation are given in Figs. 8.9 and 8.10, respectively. The plots show that the current controller works as expected

(a)

(b)

(c)

(d)
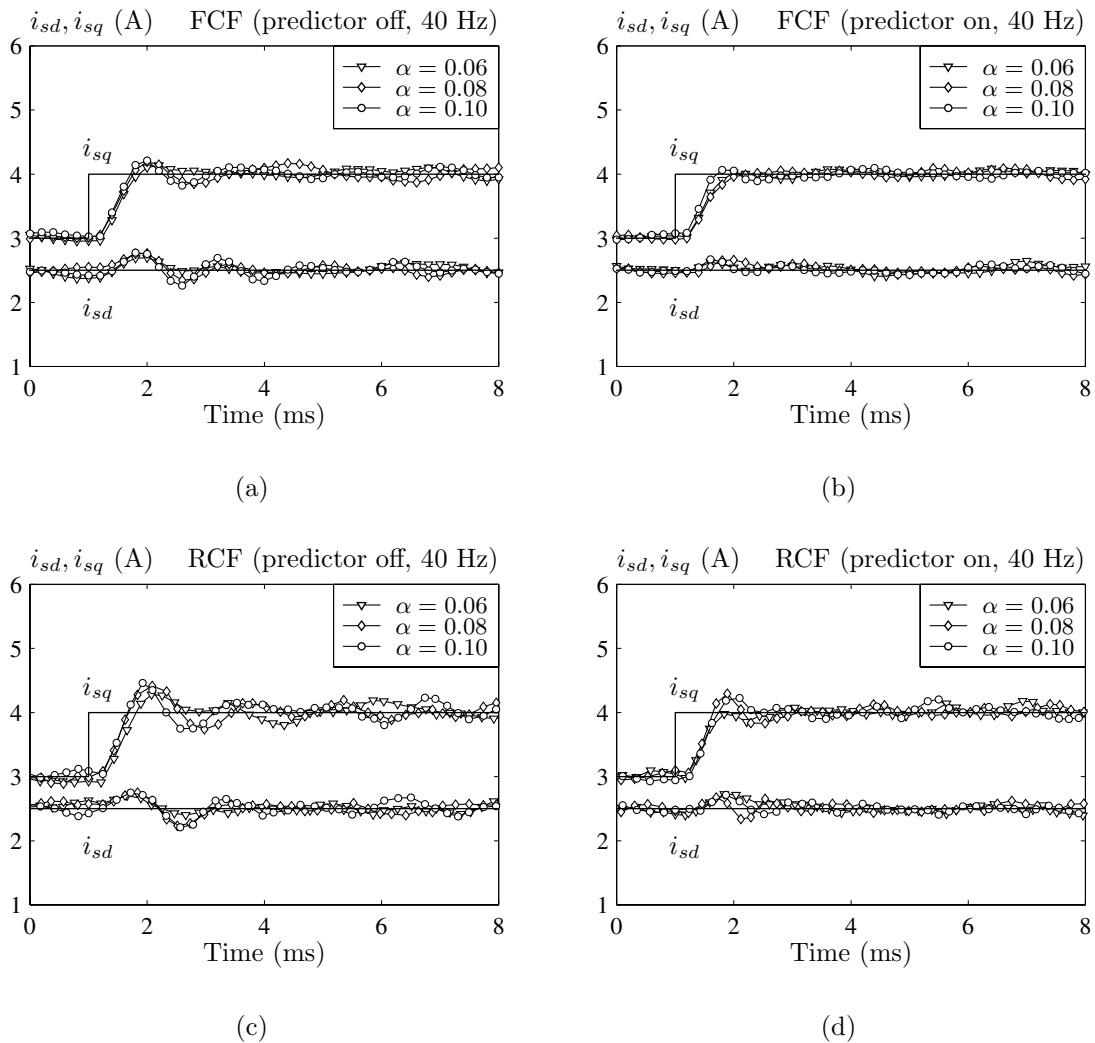
Figure 8.10 Measurements of current-control loop performance at high speed (40 Hz fundamental frequency) for three values of the bandwidth α (normalized with respect to 5 kHz). At $t = 1$ ms, the q-axis reference is stepped from 3 A to 4 A. The q-axis reference is fixed at 2.5 A. (a, b) FCF without and with current predictor. (c, d) RCF without and with current predictor.

with respect to zero steady-state error, but the net time delay in the system affects the dynamic response compared to the ideal first-order behavior given by (8.23) on page 254. However, by using the simple current predictor (8.46), Fig. 8.9(b, d) shows that the influence of the delay may be reduced significantly. These observations comply well with the conclusions drawn from the simulations shown in Fig. 8.8 on page 261.

The results obtained by the randomized PWM technique do not differ much from the responses recorded for the fixed PWM frequency operation. Hence, it may be concluded that RCF does not deteriorate the performance of the current controller, even though the instantaneous sampling rate is varying in an unpredictable manner from one sampling instant to the next.

(a)

(b)

(c)

(d)
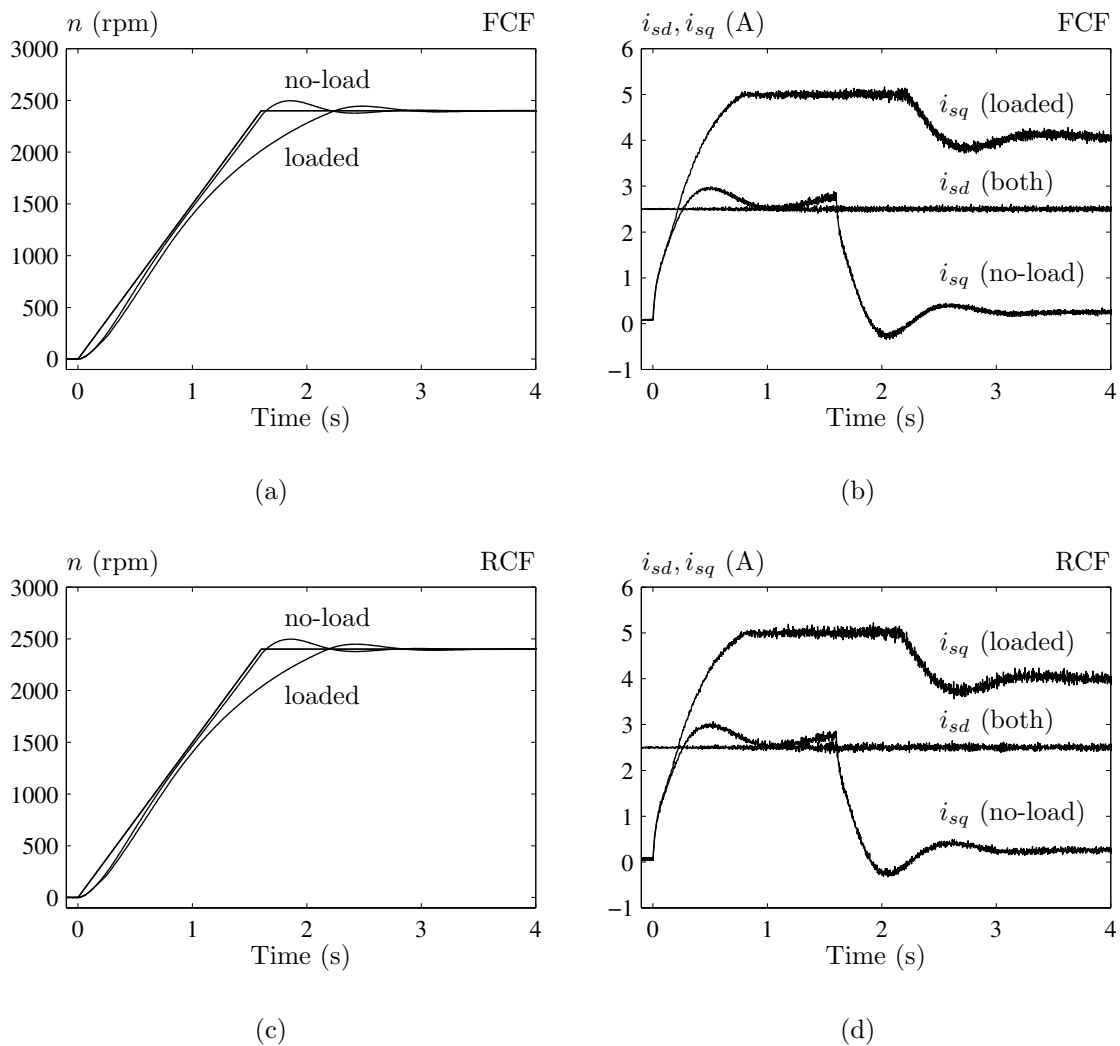
Figure 8.11 Speed ramping tests from standstill (but pre-magnetized) to 2400 rpm. The load torque is quadratic; at 2400 rpm the induction motor is loaded about 90 % of the rated load. Plots of reference and actual shaft speed as well as dq stator current components are shown. (a, b) FCF and (c, d) RCF modulation.

Speed ramping tests

The speed ramping tests are performed for the same modulator settings as used for the tests of the current controller. The bandwidth parameter α is set to 0.08 pu, i.e. 400 Hz in all experiments. Two kinds of loads are applied to the shaft. In the first case, the motor is loaded only by the inertia (and friction) of the dc-generator used in the load test: here, the dc-generator feeds power into a resistor bank, which implies that the static shaft torque increases roughly in proportion to the shaft speed squared.

The results shown in Fig. 8.11 were recorded. It may be seen in Fig. 8.11(b, d) that when the induction motor is loaded, the applied torque-component of the current i_{sq}, saturates at 5 A which is the current limit programmed into the control system. After $t = 2.2$ s, the anti integrator wind-up assures that i_{sq} decreases below the 5 A limit again; the final transition to 2400 rpm happens almost without shaft speed oscillations.

The obtained results illustrate that there is virtually no difference between the performance for fixed and random PWM frequency operation on this time scale.

8.5.2 Steady-state performance

The steady-state characteristics are visualized in both time domain or in the frequency domain. This includes recordings of current waveforms and measurements of spectra for the inverter output voltage, the phase currents, and the emitted acoustic noise.

Current trajectories

A digital storage oscilloscope (Tektronix 510A, see Table A.3(a) on page 299 for key specifications) was used to acquire simultaneous samples of two phase currents, i_a and i_b. A sample rate of 250 kSample/sec was used, i.e. the true phase currents are measured including the ripple components caused by the inverter switchings in the 4–6 kHz interval. The $\alpha\beta$-components of the stator currents have been calculated to show polar plots of $i_{s\beta}$ versus $i_{s\alpha}$.

Sample results are shown in Fig. 8.12 for different values of the current reference, the bandwidth α, and the fundamental frequency. In these experiments the outer control loops are disabled to assure that the references $i_{sd}^\star$ and $i_{sq}^\star$ are constants throughout the experiments. Comparing the $\alpha = 0.02$ pu case in Fig. 8.12(a) to the $\alpha = 0.1$ pu case in Fig. 8.12(c), it may be noted that the current controller gets better to attenuate the non-linearities caused by the inverter imperfections for higher α-values. This is, especially, clear around the zero crossings of the current.

In this context, however, the most important conclusion to draw from Fig. 8.12 is that the same closed-loop performance is obtained with random carrier frequency PWM as with classic fixed frequency PWM.

Voltage, current, and acoustic noise spectra

Finally, the frequency-domain performance of the developed field-oriented drive was measured. The operation conditions for the tests are as follows: the speed reference is set at 2400 rpm and the induction motor is loaded with the nominal torque. The current controller bandwidth is set at 400 Hz (0.08 pu).

Using the PULSE dynamic signal analyzer system described in Appendix A, spectra were measured for the inverter output line-to-line voltage, the phase current, and the total emitted acoustic noise. Note that the measured noise includes the noise caused by the dc generator used to load the induction machine. The test results are shown in Fig. 8.13 on page 271 for an equivalent noise bandwidth equal to 12 Hz. Also, the ordinate axis uses the PWR units introduced in section 3.3, i.e. the strength of all harmonic spectral components is correctly scaled, but the density part of the RCF spectra has an offset.

The fixed PWM frequency operation results in the well-known harmonics around Nf_c (N any positive integer), but the RCF modulation attenuates the carrier frequency harmonics by transferring their power into the continuous density spectrum. Fig. 8.13 also shows many harmonics peaking up below 1 kHz. These peaks are probably caused by small perturbations around a stationary operating point due to the
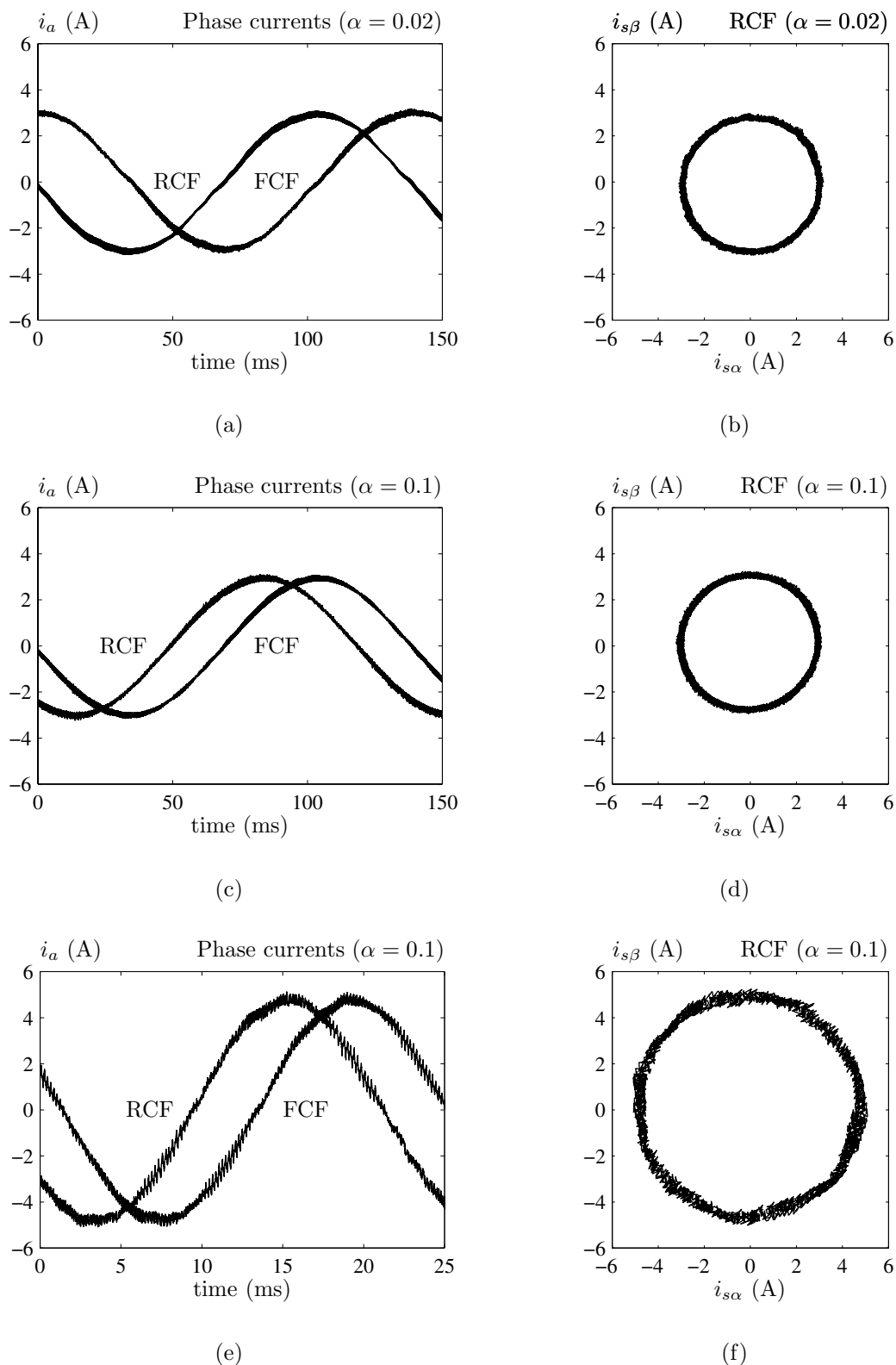
Figure 8.12 Measurement of time-domain phase current i_a (left column) and $i_{s\beta}$ versus $i_{s\alpha}$ (right column) in polar plot. The magnetizing current reference is fixed at $i_{sd}^\star = 2.5$ A. The q-axis reference and the bandwidth α are varied: (a, b) $i_{sq}^\star = 1.5$ A and $\alpha = 0.02$ pu; the fundamental frequency is 7 Hz, (c, d) $i_{sq}^\star = 1.5$ A and $\alpha = 0.1$ pu; the fundamental frequency is 7 Hz, (e, f) $i_{sq}^\star = 4.0$ A and $\alpha = 0.1$ pu; the fundamental frequency is 40 Hz.
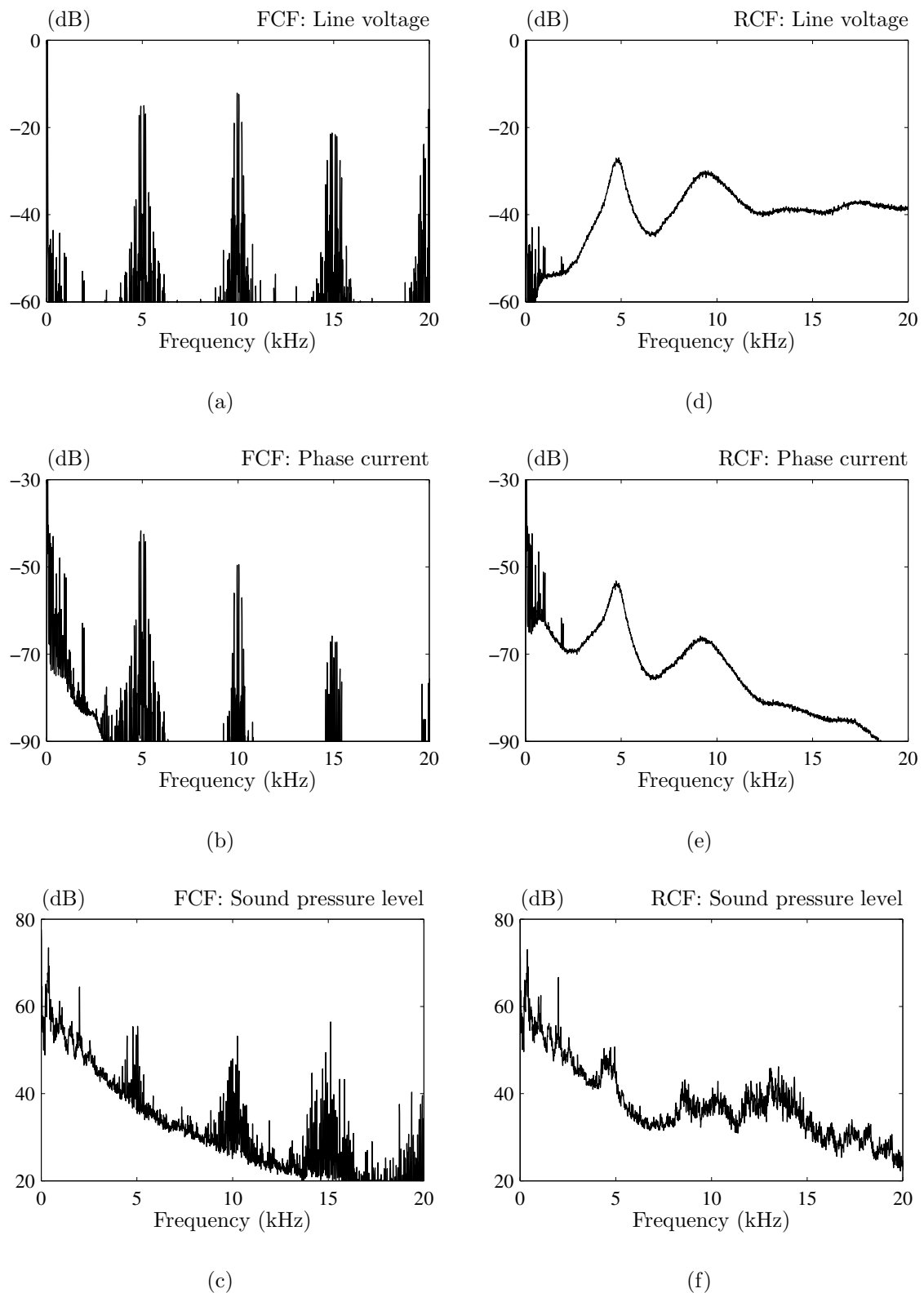
Figure 8.13 Measurement of power spectra for the field-oriented drive loaded with nominal torque at 2400 rpm using (a–c) FCF and (d–f) RCF modulation. All spectra are given in normalized PWR units (amplitudes squared). 0 dB corresponds to $(300 \text{ V})^2$, $(3 \text{ A})^2$, and $(20 \ \mu\text{Pa})^2$ for the line voltages, phase currents, and the sound pressure levels, respectively.

combined influence of measurement noise, inaccurate rotor-flux estimation, converter non-linearities, etc. Furthermore, the individual current harmonics below 1 kHz all carry an amount of power, which is more than 40 dB below the power carried by the fundamental current component. If this 40 dB power ratio is converted into a linear scale, it corresponds to an amplitude ratio of 1:100 or less.

Concerning the sound pressure level measurements, peaks occur around 0.4 kHz and 2 kHz under both RCF and FCF operation. Without an elaborative investigation, it is difficult to identify the cause of these large spectral components — one possibility is that they originate from an interaction between space harmonic fields due to stator and rotor slots, see [17]. More important for this investigation is, however, that the carrier frequency harmonics are totally eliminated by combining RCF operation with a field-oriented control strategy.

8.6   Summary

In this chapter a rotor field-oriented induction motor drive has been designed, implemented, and experimentally tested. The digital control system itself consists of standard functional units, i.e. no attempts have been made to implement advanced features, such as speed sensor-less operation, etc. Rather, the objective has been to demonstrate that random PWM (in particular, random carrier frequency PWM) is compatible with sampled control structures like those part of an FOC drive, even for operation with non-uniform sampling rates.

All innermost loops (current controller, rotor-flux estimator, and flux- and torque controllers) are updated on a non-equidistant time basis determined by the instantaneous carrier frequency for the modulator, which is selected at random within a predetermined range. An outer speed controller running with constant sampling rate is also part of the system. In accordance with the guidelines in Chapter 7, the entire system is designed in the continuous time domain before it is translated into a discrete-time equivalent.

Tests show that the dynamics of the current controller during RCF operation are hardly discernible from the results obtained with a fixed carrier/sampling frequency. Other experiments have also shown that the tracking capability of the speed controller is immune to the randomization of the inner loops. With respect to steady-state operation, it has been demonstrated that the fundamental current component is unaffected by the randomization; the difference between RCF and FCF modulation is constrained to the ripple component of the current.

Measurements of frequency-domain properties during field-oriented control in steady state show that RCF eliminates almost all carrier frequency harmonics existing with FCF modulation. This has a significant impact on the voltage and the current spectra and, hence, also on the emitted noise, which attains a more broad-band characteristic.

In total, it is concluded that RCF-PWM, which is the best performing random PWM technique with respect to acoustic noise reduction, is compatible with normal discrete-time feed-back control techniques used in direct field-oriented ac drives. Using this approach, FOC can be combined with random PWM to yield a drive that has good control properties and, simultaneously, the whistling acoustic noise known from fixed carrier frequency modulation is significantly reduced.

Comparing the work reported in this chapter to previous publications on random PWM in closed-loop applications (notably [18–21] — see section 7.2 in the previous chapter for a review), the following improvements are regarded as significant:

- A fully operating FOC drive capable of running with a variable sampling rate synchronized to a randomly varying PWM carrier frequency has been realized in such a way that the dynamic characteristics are almost equal to those obtainable with FCF modulation. In contrast to [18–20], which use a similar random modulator, all details pertinent to the design and the digital implementation are included.

- In contrary to the poor-performing random lead-lag (RLL) modulator used in [21], full advantage of the RCF-PWM technique is taken. First of all, symmetrical switching functions are generated, which eases current detection and avoids distortion of the fundamental current component. Secondly, RCF is superior to RLL with respect to acoustic annoyance reduction.

As mentioned already in Chapter 1, the recent analysis [17] shows that DTC and a simple V/Hz-regulated drive based on RCF-PWM have similar steady-state characteristics regarding voltage, current, and acoustic noise spectra. The results reported in this chapter extend the similarity between DTC and RCF combined with FOC to also include the dynamic performance of these two — conceptually very different — methods to control an ac machine for high-performance applications.

Bibliography

[1] M. P. Kaźmierkowski and H. Tunia, *Automatic Control of Converter-Fed Drives*, Studies in Electrical and Electronic Engineering 45. Elsevier, Amsterdam–London–New York–Tokyo, 1994.

[2] W. Leonhard, *Control of Electrical Drives*, Springer-Verlag, Berlin–Heidelberg–New York, second edition, 1996.

[3] M. P. Kaźmierkowski and M. A. Dzieniakowski, "Review of Current Regulation Techniques for Three-Phase PWM Inverters," *Proc. of the 20th IEEE International Conference on Industrial Electronics, Control, and Instrumentation*, vol. 1, pp. 567–575, 1994.

[4] J. Holtz, "Pulse Width Modulation for Electronic Power Conversion," in *Power Electronics and Variable Frequency Drives. Technology and Applications*, B. K. Bose, Ed., New York, 1997, pp. 138–208, IEEE Press.

[5] R. D. Lorenz, T. A. Lipo, and D. W. Novotny, "Motion Control with Induction Motors," in *Power Electronics and Variable Frequency Drives. Technology and Applications*, B. K. Bose, Ed., New York, 1997, pp. 209–276, IEEE Press.

[6] L. Harnefors and H.-P. Nee, "Model-Based Current Control of AC Machines Using the Internal Model Control Method," *IEEE Trans. on Industry Applications*, vol. 34, no. 1, pp. 133–141, Jan. 1998.

[7] L. Harnefors, *On Analysis, Control and Estimation of Variable-Speed Drives*, Ph.D. thesis, Royal Institute of Technology, Stockholm, Sweden, 1997.

[8] M. Morari and E. Zafiriou, *Robust Process Control*, Prentice Hall, Englewood Cliffs, New Jersey, 1989.

[9] P. L. Jansen and R. D. Lorenz, "A Physically Insightful Approach to the Design and Accuracy Assessment of Flux Observers for Field Oriented Induction Machine Drives," *IEEE Trans. on Industry Applications*, vol. 30, no. 1, pp. 101–110, Jan./Feb. 1994.

[10] K. J. Åström and T. Hägglund, *PID Controllers: Theory, Design, and Tuning*, Instrument Society of America, Research Triangle Park, North Carolina, second edition, 1995.

[11] A. M. Hava, *Carrier Based PWM-VSI Drives in the Overmodulation Region*, Ph.D. thesis, University of Wisconsin–Madison, 1998.

[12] L. Springob and J. Holtz, "High-Bandwidth Current Control for Torque-Ripple Compensation in PM Synchronous Machines," *IEEE Trans. on Industrial Electronics*, vol. 45, no. 5, pp. 713–721, Oct. 1998.

[13] J. Vlach and K. Singhal, *Computer Methods for Circuit Analysis and Design*, Van Nostrand Reinhold, New York, second edition, 1994.

[14] J. Holtz, W. Lotzkat, and A. M. Khambadkone, "On Continuous Control of PWM Inverters in the Overmodulation Range Including the Six-Step Mode," *IEEE Trans. on Power Electronics*, vol. 8, no. 4, pp. 546–553, Oct. 1993.

[15] A. M. Hava, R. J. Kerkman, and T. A. Lipo, "Carrier-Based PWM-VSI Overmodulation Strategies: Analysis, Comparison, and Design," *IEEE Trans. on Power Electronics*, vol. 13, no. 4, pp. 674–689, July 1998.

[16] M. M. Bech, F. Blaabjerg, J. K. Pedersen, and A. M. Trzynadlowski, "Comparative Investigation of Random PWM Techniques with Variable Switching Frequency and Pulse Position for Inverter-Fed Induction Motors," *Proc. of 7th European Conference on Power Electronics and Applications*, vol. 1, pp. 343–349, 1997.

[17] L. Xu, Z. Q. Zhu, D. Stone, and D. Howe, "Acoustic Noise Radiated by Space Vector PWM, Random PWM and Direct Torque Controlled Induction Motor Drives," *Proc. of the International Conference on Electric Machines*, vol. 3, pp. 1746–1751, 1998.

[18] C. B. Jacobina, A. M. N. Lima, E. R. C. da Silva, and R. L. de A. Ribeiro, "Current Control for a Random PWM Voltage Source Inverter," *Proc. of the 28th IEEE Power Electronics Specialists Conference*, vol. 2, pp. 1440–1446, 1997.

[19] C. M. Liaw and Y. M. Lin, "Random Slope PWM Inverter using Existing System Background Noise: Analysis, Design and Implementation," *IEE Proceedings — Electric Power Applications*, vol. 147, no. 1, pp. 45–54, Jan. 2000.

[20] B.-R. Lin, "High Power Factor AC/DC/AC Converter with Random PWM," *IEEE Trans. on Aerospace and Electronic Systems*, vol. 35, no. 3, pp. 935–943, July 1999.

[21] B.-R. Lin and H.-H. Lu, "Three-Phase AC/DC/AC Converter with Random Pulse Position," *Proc. of 8th European Conference on Power Electronics and Applications*, Sept. 1999.

Part IV

Conclusion

Chapter 9

Conclusion

In the last decade random pulse-width modulation for power electronic converters has been promoted in the literature as an alternative to deterministic PWM, which is widely used today in industrial products. In some applications random PWM may alleviate the whistling acoustic noise problems often encountered when magnetic components, such as ac motors, are subjected to a periodical excitation due to a deterministic pulse-width modulator. Alternatively, random PWM may reduce the filtering/shielding needed to ensure that a certain apparatus complies with electro-magnetic emission standards.

To gain a better understanding of the properties of randomized pulse-width modulators, a number of aspects of random PWM has been analyzed in this thesis. The investigations range from spectral analysis of various randomized modulators for both dc/dc converters and three-phase converters to analysis of applications that include a random PWM unit which is part of a discrete-time control system synchronized to a randomly changing PWM carrier frequency.

9.1   Summary of the thesis

To establish a basis for the analysis of random PWM a review of the principles for pulse-width modulation was initially given, including the fundamental concepts of switching functions and duty ratios. Also, since a major part of this thesis is dedicated to analysis of random PWM techniques for use in three-phase converters, the ideas of space vectors and the well-known principles for voltage synthesis by both space-vector modulation and different zero-sequence injection were reviewed.

Afterwards, the principles for random PWM were described and it was explained that two fundamental approaches exist: the duration of the carrier period may be randomized or the pulse position within a (fixed) carrier period may be selected at random. Modulation techniques belonging to the former class are denoted as random carrier frequency (RCF) PWM whereas variants of the latter method are classified by the acronym RPP, random pulse position PWM.

By extending these two basic principles for randomization, which both assure that the correct average voltage is produced, it was shown how other random PWM schemes may be constructed. It has been argued, however, that only a few of the resulting random PWM techniques can be considered as realistic candidates for practical applications. Therefore, the main emphasis in this thesis is put on random carrier frequency PWM and different variants of random pulse position modulation.

As stated in Chapter 1 the first topic of this thesis relates to spectral analysis of the output voltage waveforms generated by randomly modulation three-phase and dc/dc converters. To investigate such issues, a general spectral analysis theory has been developed allowing an analytic prediction of the power spectral density (the distribution of the power versus frequency) for random PWM waveforms. This general theory is not tailored towards a specific randomization scheme, but rather the theory is valid for a generalized class of modulators where variables, such as the carrier frequency, the pulse width, and the pulse position within each carrier period, are subjected to random variations (but with known statistical properties determined by proper probability density functions). Also, the general spectral analysis theory takes periodical variations in the duty ratio properly into account — this is mandatory in order to analyze random PWM for dc/ac converters where the voltage reference follows a sinusoidal which is typically "distorted" with harmonics to realize the classic space-vector modulation or other non-sinusoidal reference waveforms.

Based on this general spectral theory closed-form expressions for the power spectral density have subsequently been derived for a variety of random PWM schemes for both dc/dc and dc/ac applications. Due to the complexity of the mathematics involved in the analyses, a high priority has been given to experimental verifications of the derived theoretical results. However, it has been demonstrated that a direct comparison of calculated spectra with measured spectra requires careful attention due to the operating principles of digital signal analyzers (DSA). In particular, the random PWM techniques that produce a spectrum having both a density part (volt^2/Hz) and a harmonic part (volt^2) do easily lead to misinterpretation, because the DSA is incapable of measuring these parts separately; only the total power around some frequency of interest may be estimated by the DSA. This complicates a direct comparison and, therefore, a simple, but yet very powerful, methodology has been developed that ensures a mathematical correct comparison of calculated and measured spectra, even when the spectrum has both density and harmonics. Basically, the idea is to emulate the non-ideal characteristics of the DSA by convoluting the calculated spectra with the power transfer characteristics of DSA before the comparison is made.

The validity of both the general spectral analysis and the methodology for comparison of calculated and measured spectra was first examined for two different random PWM schemes applicable for a full-bridge dc/dc converter. After having completed a spectral analysis for both an RCF-PWM and a random lead-lag pulse-position modulation scheme, measurements on an operating dc/dc converter laboratory set-up were recorded. Comparisons showed an excellent agreement between the theoretically expected and the actually measured spectra. These obtained results unambiguously document the correctness of the spectral analysis for those two particular random PWM techniques for full-bridge dc/dc converters.

Next, random PWM techniques for three-phase dc/ac converters were studied. A discussion of the consequences of using a discrete or a continuous probability density function (pdf) for e.g. the instantaneous carrier frequency in the RCF scheme was initially given. It was argued that the use of a limited pool of carrier frequencies is preferable because this selection significantly simplifies the theoretical spectral analysis, the spectral shaping problem, and also the practical implementation becomes less complicated when a discrete pdf is used compared to a continuous pdf.

Four different random PWM techniques for three-phase dc/ac converters were subjected to spectral analysis. The first technique is the RCF method using center-aligned on-state pulses within each period of the carrier; the remaining three techniques all use a fixed carrier frequency (FCF) while either the pulse positions or the pulse widths are randomized (these kinds of methods are labeled FCF-RPWM). When averaged across one period of the carrier, all studied random PWM techniques guarantee a correct voltage-second balance between the voltage reference and the actual voltage produced by the randomly modulated converter.

The spectra for both the switching function controlling one leg of the converter and the line-to-line output voltage have been calculated analytically. Extensive comparisons with measurements on an operating laboratory system have been made. In all cases, very good agreements have been obtained which fully verifies the correctness of the derived closed-form expressions for the power spectra produced with four different random PWM schemes for three-phase dc/ac (or ac/dc) converters.

Focusing mainly on three-phase converters, another part of the research concerned the practical applicability of random PWM. In particular, fundamentals of the impact of the modulation process on the quality of the load current have been analyzed besides issues relating to the interactions between a randomized PWM unit and the overlying control system generating the reference voltage to the modulator.

To support this evaluation, a number of requirements were formulated and discussed. One of the requirements relates to the controllability of the fundamental component of the current. Stated otherwise, it seems logical to require that the change of the average current in a PWM period is independent of the ripple voltage caused by the pulse-width modulation process (which may be governed partly by a random process). For control purposes, another key constraint relates to the detection of the average phase current in each carrier period. Typically, this is accomplished by simultaneously sampling all phase currents in the center of the PWM carrier period.

An analysis of the current waveforms in one period of the carrier was completed. This revealed that the PWM switching process itself may affect the change of the average load current during one carrier period, even if the correct average voltage vector is generated. Most variants of the FCF-RPWM techniques share this unattractive property which leads to low-frequency distortion of the load current in voltage-controlled converters. Furthermore, for the same random PWM schemes it has been shown that detection of the average phase currents is impossible by means of the standard approach using samples taken only at the center of the carrier period. It was also shown that the cause of the described problems is the fact that some random PWM schemes generate switching functions which are asymmetric with respect to the center of the carrier period. To remedy this problem a new current sampling strategy was presented which allows the precise average phase current to be detected for two of the studied variants of FCF-RPWM. This sampling strategy is only slightly more complicated than the standard sampling strategy: it does not involve any load parameters and only two samples of the current in each phase are required in each carrier period.

Next, problems relating to the design and the implementation of closed-loop control systems for randomly modulated converters were studied in order to investigate the feasibility of using random PWM for high-performance applications (field-oriented control of ac drives, active mains rectifiers, etc.). Usually, such control systems are

implemented in a sampled-data system, i.e. information about the state of the system is available at discrete time instants only. Typically, the sampling frequency for the inner-most control loops equals the PWM carrier frequency in order to get the best possible utilization of the converter with respect to switching losses versus the obtainable closed-loop bandwidth.

It was demonstrated that two major challenges exist for a successful use of random PWM in such applications. First, it follows from the discussion above that for the FCF-RPWM schemes producing asymmetrical switching functions, attention must be paid to the fact that accurate values for the current feedbacks are available to get correct current control, flux estimation, etc. Fortunately, since all FCF-RPWM schemes operate with a constant carrier frequency, the requirement of synchronization between the controller and the modulator does not complicate the use of FCF-RPWM compared to deterministic PWM. However, for the RCF scheme, which is much better with respect to acoustic noise reduction than all known FCF-RPWM schemes, the synchronization requirement implies that the (digital) control system must be capable of operating with a randomly changing sampling frequency.

Therefore, starting from a brief review of normally used design procedures for digital control systems, it was argued that it is impossible to use classic discrete-time design procedures in the z-domain for the problem at hand, because the sampling rate is non-constant when RCF is used. A viable design route for a non-uniformly sampled controller was then suggested: First, a suitable continuous-time controller is designed using one of many well-known Laplace-domain techniques. Then, this transfer function is approximated by using a first-order numerical integration method in order to get a discrete-time state-space equivalent which may be evaluated at a non-uniform sampling rate. Details were given of how to obtain a relatively low-complexity algorithm which is suitable for real-time evaluation in, for example, a DSP. The suggested procedure allows continuous-time transfer functions of arbitrary order to be emulated by a discrete-time equivalent.

Using this two-step procedure for design and implementation of non-uniformly sampling digital controllers, a complete rotor field-oriented induction motor drive based on RCF modulation was designed, implemented in a laboratory set-up, and tested. Measurements show that tangible performance characteristics ranging from the rise time of the innermost current control loop to the tracking capability of the outer speed control loop are almost inseparable from each other whether fixed carrier frequency PWM or random carrier frequency PWM is used. This verifies the usefulness of the suggested methodology to unify random PWM with closed-loop applications in order to get a system with good dynamic properties, and meanwhile the acoustic annoyance problem may be reduced thanks to the random carrier frequency operation.

9.2   Conclusions and new contributions

By the results presented in this thesis it is believed that all objectives of the research project have been fulfilled. To solve the two problems stated in Chapter 1 many new aspects of random pulse-width modulation have been thoroughly investigated. This has led to the main conclusions and recommendations summarized below where the key novel scientific contributions are identified also.

Problem #1: Spectral analysis of random PWM

- A general mathematical framework for spectral analysis of random pulse-width modulated signals has been presented. Starting from this general theory, it is possible to derive expressions for the spectral characteristics of a variety of modulators where the carrier frequency, the pulse width, or the pulse position within each carrier period may be subjected to randomization. This spectral theory has proved to be very powerful.

- The derivations leading to the general spectral theory are based on related work found in the literature. It is believed, however, that important details regarding the exact course of the switching functions have been included in a unique way. In particular, the method to include deterministic variations of the duty ratio for dc/ac (ac/dc) converters controlled by an RCF strategy significantly simplifies the needed algebra compared to earlier investigations. This new approach is of great practical importance, because arbitrary modulators (sinusoidal, space-vector, discontinuous PWM, etc.) may all be analyzed in a consistent manner.

- A method has been presented that allows the spectrum for the difference of, say, two (correlated) switching functions to be calculated. In this way the spectrum of e.g. the line-to-line voltage or the line-to-neutral voltage may be calculated. The suggested approach is exact in a mathematical sense, but, nevertheless, it does not involve the use of cross power spectral densities which are often difficult to calculate analytically for correlated functions. The method is considered — and has proved to be — a very strong and a unique tool for analysis of composite waveforms found in, for example, random PWM converters.

- The general spectral theory was successfully applied on different random PWM schemes which may be of practical interest due to their simplicity and close resemblance with well-known deterministic PWM strategies. Two schemes for full-bridge dc/dc converters were analyzed; four random PWM methods for three-phase dc/ac converters were studied. In all cases, closed-form expressions were derived for the spectrum of the switching function and for the spectrum of the line-to-line voltage, once statistics for the relevant random variables were known.

- Excluding some of the results for the random lead-lag (RLL) scheme, all spectral expressions are believed to be new and unprecedented in the literature. In particular, the successful analysis of the density spectrum of the RCF scheme for dc/ac applications is considered unique and of great practical use because RCF modulation is probably the best way to combat tonal acoustic noise and to avoid harmonic spectral peaks in general.

- With respect to experimental verifications, it is concluded that a comparison between theoretically calculated spectra and spectra measured in the laboratory requires that the operating characteristics of the used DSA are taken properly into account. In this connection a useful methodology has been presented (and extensively used) which allows a scientifically correct comparison of calculated and measured spectra. Surprisingly, such fundamental issues have not been recognized in the existing random PWM literature.

- To verify the derived spectral expressions, extensive laboratory measurements have been made. Taking the imperfections of the DSA properly into account, it is concluded that all spectral analyses are fully correct; despite the complexity of the mathematics, excellent agreements exist between calculated spectra and spectra existing in a fully operating converter system. These thorough experimental verifications of the theoretical analyses are considered unique.

Problem #2: Random PWM in closed-loop (high-performance) applications

- The use of random PWM in high-performance applications requires careful attention. For the asymmetrical variants of the FCF-RPWM modulators it must be assured that the current fed back to control system correctly represents the per PWM carrier period average. Acknowledgement of this fundamental problem is believed new.

- It is concluded that the major difficulty in using symmetrical RCF-PWM for high-performance applications, where the inner-most digital control loops must be synchronized to the PWM unit, is that the controller is updated on a non-equidistant time basis; the sampling frequency varies randomly.

- For RCF modulation this renders design of linear controllers, filters, and similar structures of orders greater than 1 directly in z-domain impossible due to the non-uniform sampling rate requirement. An implementation of such structures in form of a fixed-coefficient difference equations is impossible. A clarification of such fundamental problems regarding the use of a random carrier frequency PWM unit as part of a digital control system has not been found elsewhere.

- For RCF-based systems, it is concluded that the only viable way to design and to implement e.g. a current controller is to do the design in the continuous s-domain and then approximate the found s-domain transfer function by a numerical algorithm.

- A systematic procedure for such a discretization was presented that allows linear continuous-time structures to be emulated by a discrete-time algorithm that may be updated at a non-uniform (including a random) rate. This procedure, which also attempts to minimize the necessary real-time computations, makes use of well-known state-space control theory, but since applications of non-uniform sampling rates in real-time systems are largely undiscovered in the literature, it is still believed that the suggested procedure has some originality.

- The FOC drive designed to demonstrate the practical usefulness of the suggested method to unify RCF with a high-performance application is considered original.

- Based on experiments with the FOC drive, it is concluded that the obtainable performance is equal to the performance obtainable with deterministic PWM, both during dynamics and during steady-state operation. The emitted acoustic noise is, however, much less annoying with RCF modulation. It is believed that the unification of RCF-PWM and FOC gives an ac drive with characteristics very similar to those obtainable with the direct torque control philosophy.

Miscellaneous conclusions and recommendations

- Based on the analysis of the current waveforms, it is concluded that the PWM process (more precisely, the ripple voltage caused by the switchings) may influence the change of the average load current, even when the reference voltage is correctly synthesized in terms of the per PWM period average. The use of (possibly randomized) symmetrical switching functions is highly recommended to ensure complete decoupling between the ripple voltage coming from the modulation process and the change of the average load current. This recommendation is valid for both random PWM and for deterministic PWM.

- The problem of detecting the correct average current on a per PWM carrier period basis for modulators giving asymmetrical switching functions has not been recognized elsewhere. The modified current sampling strategy, which allows a precise detection of the average load currents for modulators generating quasi-symmetrical switching functions, is also believed to be unseen in the existing literature.

- Regarding the overall practical applicability of random PWM for three-phase systems it is concluded that the highly asymmetrical RLL scheme is the most poor-performing method, whereas the fully symmetrical RCF scheme using center-aligned switching functions is the best one. The latter may, however, be more complicated to use in high-performance systems due to the non-uniform sampling rate requirement. For some applications, quasi-symmetrical FCF-RPWM schemes may be an acceptable compromise between RLL and RCF modulation.

- It is recommended that random PWM schemes giving asymmetrical switching are not used in open-loop voltage mode, unless a non-zero level of low-frequency distortion around the fundamental current component is acceptable. Even closed-loop current control is problematic with asymmetrical modulators due to the difficulty with the current detection. Exposition of such fundamental problems with the use random PWM is believed to be novel.

- Regarding the choice of probability density functions (pdf) for the random variables (carrier frequency, pulse position, etc.) a discrete pdf is preferable to a continuous pdf. The former simplifies the theoretical spectral analysis, it complies much better with the spectral shaping problem, the practical implementation becomes simpler, and the smoothness of the spectrum remains unaffected. Some applications, however, such as converters using purely analogue control circuitry, may be better served with a continuous pdf.

- The replacement of a deterministic modulator with a randomized modulator is not a trivial task — in fact, it may be impossible at all; care should always be exercised to ensure that a certain randomized modulator complies with the operating principles of the power converter it is intended for. Random PWM is — in the opinion of the author — better suited for "simple" converter topologies, like those studied in this thesis which all consist of parallel-connected half-bridges, than for e.g. dc/dc converters. In the latter a proper intrinsic operation is usually closely connected to the modulator. This complicates the use of random PWM.

9.3   Future work

Several topics worthwhile a more in-depth study have not been pursued in this thesis. For example, the derivation of a unified spectral theory for random PWM schemes has been a major topic, but apart from the actual verifications, more practical use of the spectral theory still remains. Other interesting topics for future research include:

- Use the developed spectral analysis to establish an objective comparison of voltage spectra generated by different random PWM techniques. For example, the total power in a certain frequency range may be quantified.

- The spectral shaping problem mentioned in Chapters 1 and 5 may be explored using the spectral analysis as a part of a numerical optimization process. The objective may be to minimize the total power carried around a known system resonance frequency by letting the optimizer determine the optimal probability for e.g. each carrier frequency in a given pool of frequencies for the RCF technique.

- Derive a transfer function between the spectrum of the voltage and the spectrum of the emitted noise in e.g. an ac drive in order to gain a better insight into which voltage spectrum is optimal with respect to acoustic noise reduction.

- Quantify precisely the extent of the low-frequency current distortion caused by the use of asymmetrical switching functions, which may be generated either deliberately as in some random PWM schemes or unintentionally due to e.g. imperfect blanking-time compensation, PWM timer quantization, gate drivers, etc.

- The performance deterioration caused by the erroneous current detection for those PWM techniques that generate asymmetrical switching functions could also be further investigated.

- Study which impact a wide-band excitation has on different systems having resonances within the frequency range of the (random) excitation. Some claim that resonances are not excited to any significant extent — in fact, systems may even benefit from a non-periodic excitation[1]. Other investigations indicate, however, that a wide-band excitation is disadvantageous, because even though the excitation is non-repetitive, harmful resonances may still be built up[2].

- Use random PWM for estimation of parameters in e.g. ac motor models. This may be useful for auto-tuning of controllers in frequency converters.

- Study the merits and demerits of the novel random PWM technique denoted as RPP-DPWM in Chapter 6 which is a randomized version of discontinuous modulators for three-phase applications.

---

[1]For instance, for ac drives ABB states that the DTC technology results in "No harmful mechanical resonances. Lower stresses in gear boxes, fans, pumps." This quotation is taken from page 19 in "Technical Guide No. 1 — Direct Torque Control," (42 pp.) published by ABB Drives in 1999.

[2]Investigations by Morten Simonsen and Jens Engen Sørensen in their Master's project in the spring 2000 have shown that the resonance frequency in an LCL line filter for a three-phase active mains rectifier is easily triggered when a wide-band excitation (RCF modulation in this case) is used.

Part V

Appendices

Appendix A

Laboratory facilities

A.1 Introduction

To support the spectral analysis presented in this thesis a large number of measurements on laboratory set-ups have been made. The objective of this appendix is to present an overview of the laboratory facilities used in the experiments underlying the results reported in the main parts of this thesis.

Apart from supporting the spectral analysis, measurements on the set-ups described below have also been used to acquire time-domain waveforms of signals of interest, such as the phase currents supplied to a load from a randomly pulse-width modulated converter.

Appendix outline

The appendix is divided into five sections. The first section presents an overview of the hardware used in the experiments. The next three sections each gives a more elaborative description of different parts of the set-up. Finally, a section listing several tables with key specifications for the used instrumentation concludes the appendix.

A.2 Laboratory system overview

To facilitate the presentation, the overview shown in Fig. A.1 on the following page may be used. As shown, the laboratory system may conveniently be divided into three functional units:

Control unit
> This part of the system includes all the auxiliary functions needed to generate switching functions for the power converter. All computations are performed by a PC-hosted digital signal processor (DSP) that interfaces to a micro controller. The micro controller generates the actual switching functions, which are the input signals to the gate drivers. To accomplish this task, the control system does also include miscellaneous interfacing hardware between the power converters and the control unit.
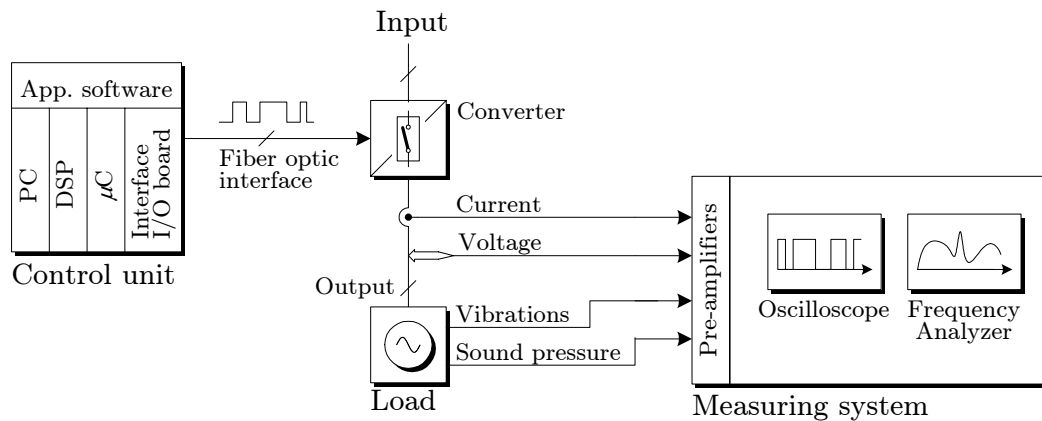
Figure A.1 Overview of laboratory facilities showing the power electronic converter, the control unit, and the measuring system.

Power circuits

The power stage includes the main power electronic converter and the load connected to the converter. Depending on the experiment, either a full-bridge dc/dc converter or a three-phase voltage source converter is used. Both converters have built-in protective circuits, which ensure automatic shut down, if a fault occurs (short-circuit/overload currents, etc.). Apart from the mains supply, the only external signals needed to operate the converters are the switching functions provided by the control unit.

The measuring system

To record the characteristics of the power converter, state-of-the-art measurement equipment is used. The primary instruments are a four-channel digital storage oscilloscope for time-domain measurements and an advanced dynamic signal analyzer for frequency-domain measurements. The measuring system also includes transducers and pre-amplifiers for accurate acquisition of voltage, current, and acoustic noise

More details regarding the laboratory facilities are given in the subsequent sections.

A.3   The control unit

The control unit maintains two important tasks: (a) it handles all computations pertinent to the pulse-width modulator besides the overall control of the converter and (b) it provides an interface between the software and the optic fibers used to convey information to the converter. The block diagram in Fig. A.2 outlines the control unit.

Originally, this system was designed and built by graduate students[1] in 1996 at the Institute of Energy Technology as a part of their Master's project. However, in order to adapt the system to the particular needs in the present project, a number of hardware modifications have been made to the original system. Also, of course, almost nothing of the original software has been reused, but, nevertheless, the original source code has been a great source of inspiration.

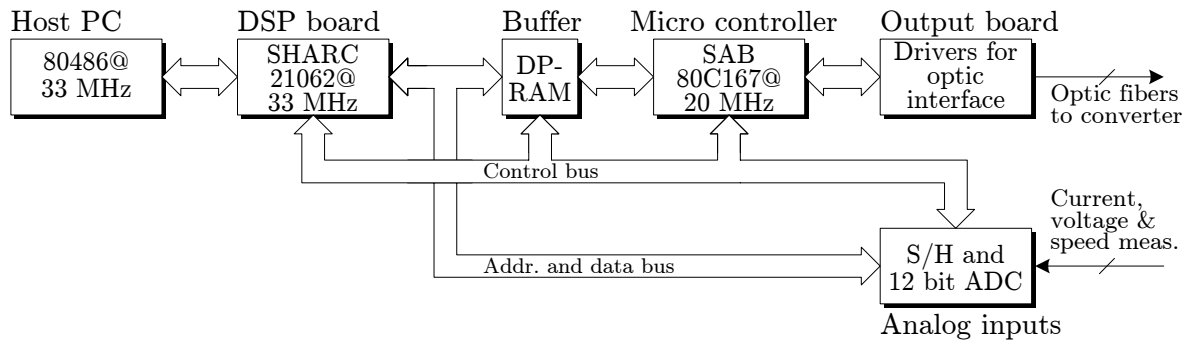[1]Uffe B. Jensen, Tonny I. Mortensen, and Morten P. Rasmussen.

Figure A.2 Block diagram of the control unit.

A.3.1 Overall description of the control unit

Referring to Fig. A.2, the PC hosts the EZ-LAB Development System evaluation board. This board has been designed by BittWare Research Systems and it is equipped with an Analog Devices 21062 DSP and a number of peripheral functions. This 32/40 bit floating-point DSP is based on the Super Harvard Architecture (SHARC).

The DSP has four internal buses that assure a very fast access to the the on-chip memory used for both data and programme storage. Also, all instructions are executed in a single clock cycle of duration $1/(40$ MHz$) = 25$ ns. The DSP does also have a number of I/O peripherals, including external data and address buses.

In addition to hosting the DSP board, the PC is used as a terminal where the user may select the modulation method, change reference values, collect data, etc. All algorithms for the control of the converter are implemented in the DSP.

Since the DSP lacks dedicated PWM timers, a Siemens 16-bit fixed-point micro controller SAB 80C167 is used. Since the two systems are not synchronized to the same clock, the DSP and the micro controller communicate through a dual-ported (DP) RAM interface. A number of control lines are used to facilitate the communication. In particular, interrupt request lines are important to assure proper timing of events.

The output from the micro controller is the commanded switching functions needed to control the converter in form of a TTL-compliant digital signal. However, in order to provide electrical isolation between the control unit and the power converters, a fiber optic interface is used to transmit the gate signal to the converter. The needed drivers, and the optic transmitters themselves, are physically located on the output board shown in Fig. A.2.

Since the field-oriented control system studied in Part III relies on feed-back control, an eight-channel analog-to-digital (A/D) interface board is used to measure the phase currents, the dc-link voltage, and the shaft speed. These signals are sensed based on Hall effect LEM modules (LA 50-P), an isolation amplifier (Hewlett-Packard HCPL-7800), and a 2500-line encoder (Scancon 2R-series), respectively. The resolution of the A/D converter (Analog Devices AD7891) is 12 bit, and the conversion time is 2.5 μs per channel. All channels are sampled and held simultaneously by two four-channel Analog Devices AD684 sample-and-hold amplifiers. The result of each conversion can be read directly by the DSP into its on-chip memory.

Detailed descriptions and specifications for the components may be found in the hardware manuals provided by the manufactures. In particular, the DSP evaluation

board is described in [1] and all details regarding the SHARC 21062 DSP may be found in [2]. Details of the micro controller are documented in [3].

A.3.2 Aspects of the implementation of modulators

No thorough descriptions of neither the hardware nor the software are provided, but rather some of the key elements related to the implementation of random modulation methods are highlighted below. The somewhat scattered list of topics treated in this subsection includes (a) the PWM timers, (b) the problem of generating random number, and (c) the software development.

PWM timers

The Siemens SAB 80C167 micro controller includes peripheral units dedicated to generation of PWM patterns. The so-called PWM module makes it possible to obtain a 50 ns resolution on the pulse widths. In this mode of operation, the output pulse is either symmetric and center-aligned within the PWM period or alternatively, the output pulse may be leading- or lagging-edge modulated. The PWM module is well suited for the random carrier frequency PWM technique (Chapter 5) and the random zero-vector distribution scheme (Chapter 6) that both generate switching functions that are symmetric around the center of the carrier. Also, the random lead-lag PWM method has been successfully implemented using the PWM module in the micro controller.

For the PWM schemes that rely on dithering of the pulse position, the Capture/Compare unit is used. This unit allows the leading and lagging edges of the pulse to be modulated independently of each other at the expense of a poorer resolution, i.e. 400 ns. This approach to implement the random center displacement method is investigated in Chapter 6.

Random number generator

As explained on page 32 in Chapter 2, a source of random numbers with a known distribution is required in all random modulation schemes. As intrinsically random systems only exist in physical processes[2], it is evident that an ideal noise source cannot be programmed in software, no matter how complicated an algorithm is constructed.

Fortunately, thoroughly tested software-based random number generators (RNG) suited for the purpose at hand can be found in the scientific literature. The literature on RNG's is vast and very mathematically oriented, but among others [6] provides an introduction to RNG's on an accessible level; source code is also provided in this book. A much more in-depth treatment may be found in the book [7] by the renowned Donald E. Knuth. This is the standard reference on RNG's, frequently cited in [6] also.

The RNG implemented in the DSP for real-time use is the `ran1.c` algorithm in [6]. This generator outputs uniformly distributed random numbers in the range $x \in [0; 1]$. The sequence length is $m \approx 20 \cdot 10^8$ before the sequence repeats over again. Less complicated algorithms requiring less computations for each new x may also be found in [6, 7].

---

[2]For example, the literature focusing on random PWM includes examples of how a random variable may be generated by means of analog electronics. Ref. [4] relies on thermal noise in a reverse-biased zener diode and [5] uses a similar approach, but here the noise is caused by a small-signal transistor.

These so-called "quick and dirty" linear congruential generators have been popular in the existing literature on random PWM (see [8–10] among others), because they can be implemented in fixed-point micro controllers using only a very few multiplications and additions. However, due to the power of the floating-point DSP used in the present project, these simpler algorithms with inferior statistical characteristics have not been used since the computation burden is of minor concern. Also, [6] recommends the use of `ran1.c`, because this algorithm passes all statistical tests that are used to judge the goodness of general-purpose RNG's.

Software development

During the development of the software running in the DSP and in the micro controller, emphasis has been put on the functionality rather than on the appearance. In other words, no fancy graphic user interface has been made when a simple text-based menu is sufficient, but rather, care has been exercised during the coding of hardware-near routines. As an example of the latter, it may be mentioned that when using floating-point arithmetic, it is very unlikely that the carrier period and the pulse width calculated by some (random) modulator conform to the resolution of the PWM timers in the micro controller. If precautions are not taken, an accumulation of errors in the generated volt-second results, which is undesirable.

Also, the algorithms discussed in Part III for closed-loop control using a non-uniform sampling rate will deteriorate if the actual sampling periods differs from the values used in the algorithm. Therefore, the DSP includes a routine which ensures that the impressed PWM period is rounded to the nearest value which the PWM timers can reproduce; the same happens for the pulse width. To prevent the built-up of local deviations, the rounding error caused in one PWM period is added to the reference value in the next.

Finally, it may be mentioned that all programming of the DSP and the micro controller was made in the "C" programming language. Even the most hardware-specific interfaces have been coded without the direct use of assembler routines. This is possible because the C-compilers included with the used development systems provide many C macro extensions dedicated to efficient use of the hardware.

A.4 Power circuits

As mentioned in section A.2, two different set-ups are used to test random PWM schemes for dc/dc and dc/ac full-bridge converters, respectively. An overall description of these two systems are provided below focusing on the parts of the systems that are important in the context of this project.

A.4.1 Set-up for test of three-phase dc/ac PWM techniques

Apart from the control unit, this set-up includes an induction motor supplied from a frequency converter. The induction motor is loaded by a dc generator feeding power into a bank of resistors.
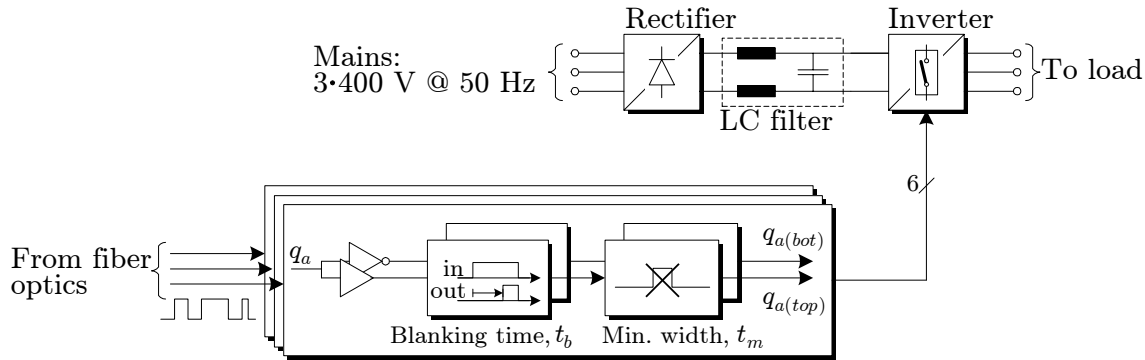
Figure A.3 Block diagram of the VLT 3004 converter showing the signal paths of main interest.

Power electronic converter

A modified DANFOSS VLT 3004 frequency converter is used for the tests. This converter is rated at an input voltage of $3 \cdot 400$ V @ 50 Hz, and it is capable of supplying 5.6 A/phase at the output terminals. Other characteristics may be found in the user manual [11].

A block diagram of the parts of interest of the converter is shown in Fig. A.3. A diode-bridge rectifier and an LC filter convert the mains voltage into an uncontrolled dc-link voltage. The dc/ac inversion is maintained by a standard three-phase voltage-source converter as presented in Chapter 2.

The original control board in the VLT 3004 was removed in order to get almost direct access to the IGBT's in three converter legs. In this way, the converter state may be controlled from the control unit through the fiber-optic interface. As shown in Fig. A.3 it should be noted, however, that the switching functions are split into two signals: one for the upper transistor and another for the lower transistor in each leg. These signals propagate through a blanking-time circuit and a minimum pulse-width circuit before they are transferred to actual gate drivers. The value of the blanking time is $t_d = 2$ μs and the minimum pulse width is programmed to eliminate all pulses shorter than $t_m = 0.875$ μs (this causes a delay of t_m). Clearly, these circuits distort the ideal switching functions commanded by the control unit, but still these circuits are needed to ensure a proper operation of the converter.

In addition to the power circuitry and the gate drives including their electrical isolated power supplies, the original protective functions in the VLT 3004 are also intact. This includes protection against short-circuit currents, over-load currents, and thermal protection of the power module. The dc-link voltage is also monitored, and the converter automatically trips, if the dc voltage leaves certain fixed limits.

Load system

The frequency converter is loaded by an 1.5 kW induction motor with the data listed in Table A.1 on page 298. To the shaft of this motor, a dc generator is attached making it possible to dissipate power in a bank of power resistors.

A.4.2 Set-up for test of dc/dc random PWM techniques

In this set-up, the control unit is connected to a dc power supply, which is loaded by a dc motor. The power supply is operating at a single-phase input (230 V @ 50 Hz) and it is capable of delivering 10 A to a load at the full output voltage.

Power electronic converter

The dc power supply used for the testing of modulators suited for full-bridge dc/dc converters has been designed and built by Per Sandholt[3] and the author. From a functional point of view, this converter behaves almost identical to the (modified) DANFOSS VLT 3004, except that the dc converter does only have two output terminals. The interface to the control unit is the same as for the VLT 3004, and the dc converter does also provide protection against short circuits, etc. making the converter easy to use in the kind of tests of interest here. In this converter, the blanking time is 2.2 μs, whereas it does not contain a minimum pulse-width filter.

Load system

The load connected to the power supply is comprised of two dc machines connected to the same shaft. These dc machines are rated at 170 V/4.8 A; the rated speed is 3000 rpm. Again, the machine operating as a generator is loaded by a variable resistance capable of dissipating the required power.

A.5 Measurement system

This section presents an overview of the instrumentation used to record all measurement results reported in this thesis. Key specifications for instruments, pre-amplifiers, and transducers are given. The physical signals of interest are

- the pulse-width modulated voltage generated by the power converter,
- the current supplied to the load, and
- the acoustic noise emitted from the test object.

For these signals, the frequency-domain properties are of outmost importance as much of theory presented in the main parts of the thesis is devoted to frequency-domain models of the voltage generated by random PWM converters. Also, accurate acquisition of time-domain waveforms is important, both during the final tests, but also during the preceding design and debugging of the system.

A.5.1 Main measuring instrumentation

The most important instruments in the measuring system are a dynamic signal analyzer and a digital storage oscilloscope used for frequency-domain and time-domain measurements, respectively. Further details follow below.

---

[3]Currently, Per Sandholt is an Assistant Professor at the Institute of Energy Technology.

Multi-channel dynamic signal analyzer

This instrument is a Brüel & Kjær (B&K) 3560 Multi-Analyzer System, also known as PULSE. The PULSE system incorporates an acquisition front-end that houses a number of slots available for input, output, communication, and signal processing modules. The acquisition front-end is connected to a special DSP board hosted in a PC. All processing of the signals sampled by input modules mounted in the acquisition front-end is performed in this special DSP board.

Due to the modular design, no unique hardware configuration exists; the PULSE system available to this project consists of the following main parts:

Acquisition front-end
The front-end is a B&K 2825 mainframe unit. The front-end houses four input modules and an interface module to the PC-hosted DSP board.

Input modules
Among the input modules available, one B&K 3022 four-channel general-purpose input module, one B&K 3028 four-channel microphone input module, and two single-channel 0–102.4 kHz modules are installed in the front-end. The key specifications for these modules are listed in Table A.2 (page 298).

PC-hosted DSP board and application software
The DSP board performs all calculations regarding the signal processing of the sampled data. The DSP board provides many different analyses, including e.g. power spectral density calculations, octave analysis, cross spectra, coherence functions. The PC is used as a virtual instrument and as a graphical user terminal showing the result of all analyses.

The PULSE system is tailored towards the analysis of acoustic noise and vibrations, but the system may also be used as a general-purpose signal analyzer for signals in the dc to 102.4 kHz range. A screen shot of the PULSE system is shown in Fig. A.4. Additional information about the features of the PULSE system may be found in [12].

Digital storage oscilloscope

The oscilloscope is a TEKTRONIX 510A, which is a general-purpose instrument for design, debugging, and analysis of electronic systems. The specifications are listed in Table A.3(a) on page 299.

A.5.2   Transducers

As mentioned on page 295, the measuring system is capable of acquiring the following signals: the output voltage and current from the power converter besides the acoustic noise emitted by the converter-fed load, typically an electric motor. These signals are sensed using the transducers and pre-amplifiers specified below.
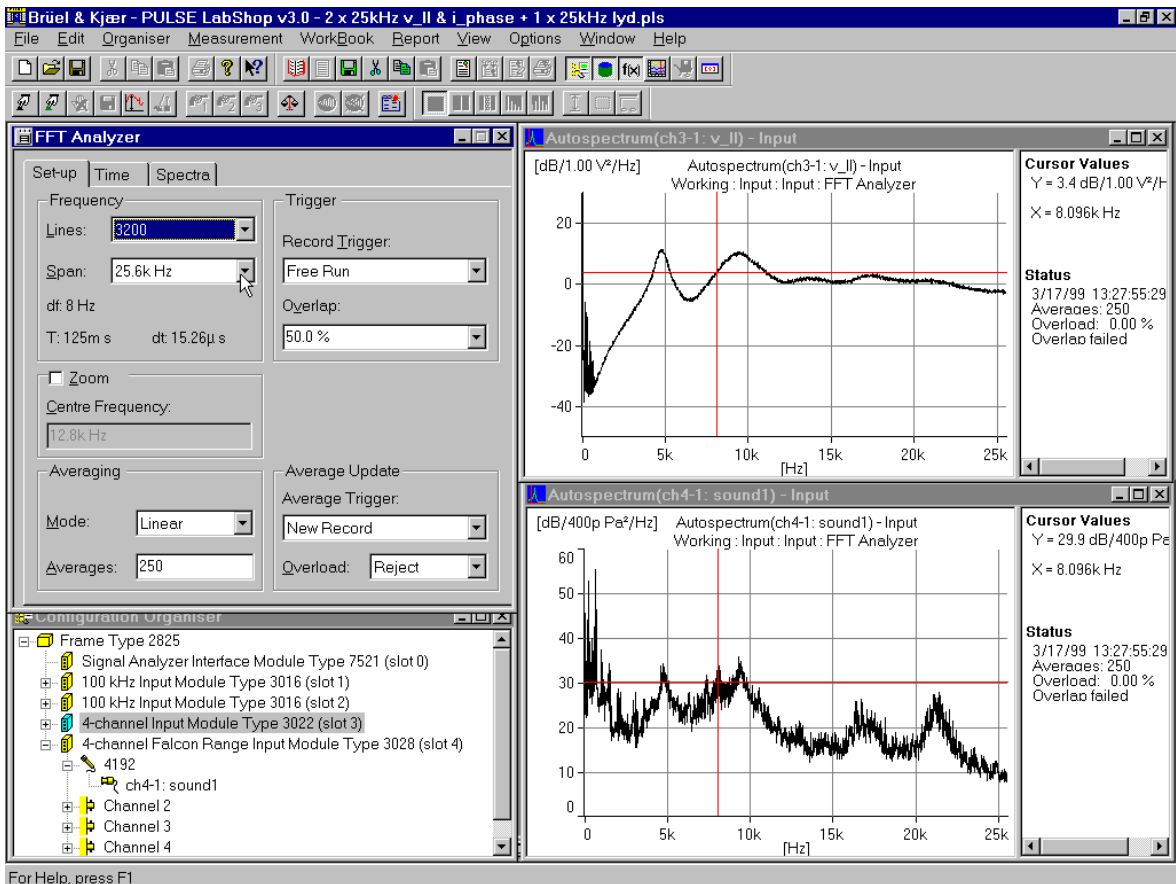
Figure A.4 Screen shot taken from the PULSE LABSHOP software. On the left, some of the properties for the FFT Analyzer may be seen; below an overview of the configuration of the acquisition front-end appears. On the right, sample spectra of the line-to-line voltage and the emitted acoustic noise are shown.

Voltage and current measurements

Equipment from TEKTRONIX is used for the sensing of both voltages and currents. The P5205 high-voltage differential probe and the AM503S current measuring system are used; specifications are listed at the end of this appendix in Table A.3(b) and Table A.3(c), respectively. The output from these instruments can be directly connected to either the TEKTRONIX oscilloscope or the PULSE analyzer.

Acoustic noise measurements

Here, Brüel & Kjær equipment, which integrates seamlessly with the PULSE system described earlier, is used. The microphones are of the pressure-field type suitable for measurements in reflective acoustic environments like a reverberation chamber (such a chamber is used here). Specifically, a B&K 4192 microphone connected to the PULSE system through a B&K 2669 pre-amplifier is used. The specifications are given in Table A.4 on page 299.

A.6   Specifications for equipment and instruments

P (kW)	U (V)	I (A)	$\cos\varphi$	n (rpm)
1.5	380	3.75	0.75	2900

(a)

r_s (Ω)	r_r (Ω)	ℓ_s (mH)	ℓ_r (mH)	L_m (mH)
5.6	3.2	13	13	452

(b)

Table A.1 1.5 kW induction motor data: (a) nameplate data and (b) motor parameters. r_s and r_r are the stator and rotor resistance, respectively. ℓ_s and ℓ_r are the leakage inductances, and L_m is the magnetizing inductance.

	B&K 3022 4-ch. input	B&K 3016 1-ch. input	B&K 3028 4-ch. microphone input
Freq. range	0–25.6 kHz	0–102.4 kHz	0–25.6 kHz
Input voltage[a]	4 mV to 30 V	1 mV to 80 V	4 mV to 30 V
Dynamic range	>80 dB for max. input >10 mV		
Sampling rate	max. 132 kHz	max. 262.5 kHz	max. 132 kHz
A/D converter	16 bit	14 bit	16 bit
Attenuation	>80 dB of those frequencies which can cause aliasing		
CMMR[b]	0–1 kHz: 70 dB 1–25.6 kHz: 50 dB	0–1 kHz: 60 dB 1–25.6 kHz: 50 dB >25.6 kHz: 40 dB	0–25.6 kHz: >40 dB

[a]The peak input voltage range can be set in 28 steps in the interval listed.
[b]Common mode rejection ratio (CMMR): typical values are listed.

Table A.2 Key specifications for the input modules for the PULSE system.

No Ch.	Bandwidth (MHz)	Max. sample rate (MSample/sec)	Vert. resolution (bit)	Record length (Points)
4	500	500	8	50K per channel

(a)

Bandwidth (MHz)	Max. diff. input dc+ac (V)	Max. input to gnd (V)	Attenuation	CMMR (dB)
100	1300	1000	50X/500X	>80 @ 60 Hz >50 @ 100 kHz

(b)

Bandwidth	Max. cont. current	Max. peak current
dc–50 MHz	20 A	50 A

(c)

Table A.3 Specifications for TEKTRONIX (a) 510A oscilloscope, (b) P5205 high-voltage differential probe, and (c) AM503S current measuring system.

Sensitivity	Frequency range	Dynamic range	Frequency response
12.5 mV/Pa	3.15 Hz–20 kHz	20–162 dB	5 Hz–7 kHz: ±1 dB 3.15 Hz–20 kHz: ±2 dB

Table A.4 Specifications for Brüel & Kjær 4192 microphone.

Bibliography

[1] BittWare Research Systems, *EZ-LAB Development System Manual. Hardware Rev. 3*, Analog Devices, Norwood, Massachusetts, April 1996 edition.

[2] Analog Devices, *ADSP-2106x SHARC User's Manual*, Analog Devices, Norwood, Massachusetts, second edition, May 1997.

[3] Siemens, *C167 Derivatives User's Manual. Edition 03.96, Version 2*, Siemens AG, Munich, Germany, 1996.

[4] H. Hosei and K. Tanaka, Nippon Steel Corp., "Switching Regulator," US Patent No. 5.640.315, Filed March 17, 1995.

[5] K. K. Tse, H.-S. Chung, S. Y. R. Hui, and H. C. So, "Analysis and Spectral Characteristics of a Spread-Spectrum Techniques for Conducted EMI Suppression," *IEEE Trans. on Power Electronics*, vol. 15, no. 2, pp. 399–410, Mar. 2000.

[6] W. H. Press, S. A. Teukolsky, W. T. Vetterling, and B. P. Flannery, *Numerical Recipes in C — The Art of Scientific Computing*, Cambridge University Press, second edition, 1992.

[7] D. E. Knuth, *The Art of Computer Programming. Volume 2. Seminumerical Algorithms*, Addison Wesley, Reading, Massachusetts, third edition, 1998.

[8] S. Bolognani, R. Conton, and M. Zigliotto, "Experimental Analysis of the EMI Reduction in PWM Inverters Using Random Space Vector Modulation," *Proc. of the IEEE International Symposium on Industrial Electronics*, vol. 1, pp. 482–487, June 1996.

[9] S. Y. R. Hui, S. Sathiakumar, and K. K. Sung, "Novel Random PWM Schemes with Weighted Switching Decision," *IEEE Trans. on Power Electronics*, vol. 12, no. 6, pp. 945–952, Nov. 1997.

[10] J. K. Pedersen and F. Blaabjerg, "Implementation and Test of a Digital Quasi-Random Modulated SFAVM PWM in a High Performance Drive System," *Proc. of the 18th IEEE International Conference on Industrial Electronics, Control, and Instrumentation*, vol. 1, pp. 265–270, 1992.

[11] Danfoss Drives, *VLT 3000 series User's Manual*, Danfoss, Nordborg, Denmark, 1995.

[12] Brüel and Kjær, *Multi-Analyzer System Type 3560. User Manual*, Brüel and Kjær Sound and Vibration Measurement A/S, Nærum, Denmark, 1996.

Appendix B

References on random PWM

The references included in this Appendix do all relate to random pulse-width modulation techniques for power electronic converters. The list is believed to include the majority of all publications dealing with this subject published in the period 1970 to August 2000.

Bibliography

[1] V. G. Agelidis and D. Vincenti, "Non-Deterministic AM-PWM Strategy for Three-Phase VSI," *Proc. of the 20th IEEE International Conference on Industrial Electronics, Control, and Instrumentation*, vol. 1, pp. 73–78, 1994.

[2] V. G. Agelidis and D. Vincenti, "Optimum Non-Deterministic Pulse-Width Modulation for Three-Phase Inverters," *Proc. of the 19th IEEE International Conference on Industrial Electronics, Control, and Instrumentation*, vol. 2, pp. 1234–1239, 1993.

[3] M. Alaküla, L. Sjöberg, and P. Johansson, "Random Modulation of Line Commutated Power Converters," *Proc. of 7th European Conference on Power Electronics and Applications*, vol. 1, pp. 278–280, 1997.

[4] K. A. Almarri and J. C. Balda, "The Effect of PDFs on the Line-to-Line Voltage and Noise Generated by PWM Inverters," *Texas Instruments DSPS FEST'99*, Aug. 1999.

[5] K. A. Almarri, J. C. Balda, and K. Carr, "Optimized Selection of the Random PWM Switching Frequencies in a Limited Pool," *Proc. of the 15th IEEE Applied Power Electronics Conference and Exposition*, vol. 1, pp. 569–576, Feb. 2000.

[6] K. A. Almarri, J. C. Balda, and K. Carr, "An Improved RPWM Method Based a Novel Multi-Level Linear Congruential Random-Number Generator," *Proc. of the 31st IEEE Power Electronics Specialists Conference*, vol. 1, pp. 218–223, June 2000.

[7] M. Andrews and J. T. Boys, "Improvements in Estimating the Spectra of Random PWM Waveforms," *Electronics Letters*, vol. 29, no. 21, pp. 1822–1823, Oct. 1993.

[8] M. M. Bech, F. Blaabjerg, and J. K. Pedersen, "Random Modulation Techniques with Fixed Switching Frequency for Three-Phase Power Converters," *Proc. of the 30th IEEE Power Electronics Specialists Conference*, vol. 1, pp. 544–551, June 1999.

[9] M. M. Bech, F. Blaabjerg, and J. K. Pedersen, "Field-Oriented Control of an Induction Motor using Random Pulse Width Modulation," *Proc. of the 15th IEEE Applied Power Electronics Conference and Exposition*, vol. 2, pp. 924–931, Feb. 2000.

[10] M. M. Bech, F. Blaabjerg, J. K. Pedersen, and A. M. Trzynadlowski, "Comparative Investigation of Random PWM Techniques with Variable Switching Frequency and Pulse Position for Inverter-Fed Induction Motors," *Proc. of 7th European Conference on Power Electronics and Applications*, vol. 1, pp. 343–349, 1997.

[11] M. M. Bech, F. Blaabjerg, J. K. Pedersen, and A. M. Trzynadlowski, "A Methodology for True Comparison of Analytical and Measured Frequency Domain Spectra in Random PWM Converters," *Proc. of the 29th IEEE Power Electronics Specialists Conference*, vol. 1, pp. 36–43, May 1998.

[12] M. M. Bech, F. Blaabjerg, and A. M. Trzynadlowski, "Experimental Evaluation of Modern Random PWM Techniques for Induction Motor Drives," *Conference Record of the 1997 IEEE International Electric Machines and Drives Conference*, pp. TB3–10.1–TB3–10.3, May 1997.

[13] M. M. Bech, J. K. Pedersen, and F. Blaabjerg, "Random Modulation Techniques in Power Conversion — an Update," *Proc. of the International Power Electronics and Motion Control Conference*, vol. 3, pp. 357–365, 1996.

[14] M. M. Bech, J. K. Pedersen, F. Blaabjerg, and A. M. Trzynadlowski, "A Methodology for True Comparison of Analytical and Measured Frequency Domain Spectra in Random PWM Converters," *IEEE Trans. on Power Electronics*, vol. 14, no. 3, pp. 578–586, May 1999.

[15] T. Biskup, B. Grzesik, and J. Teluk, "Random Modulation — A Comparison of Realizations," *Proc. of the International Power Electronics and Motion Control Conference*, pp. 5.13–5.18, 1998.

[16] F. Blaabjerg and J. K. Pedersen, "Digital Implemented Random Modulation Strategies for AC and Switched Reluctance Drives," *Proc. of the 19th IEEE International Conference on Industrial Electronics, Control, and Instrumentation*, vol. 2, pp. 676–682, 1993.

[17] F. Blaabjerg, J. K. Pedersen, L. Oestergaard, R. L. Kirlin, A. M. Trzynadlowski, and S. Legowski, "Optimized and Non-Optimized Random Modulation Techniques for VSI Drives," *Proc. of 6th European Conference on Power Electronics and Applications*, vol. 1, pp. 19–26, 1995.

[18] F. Blaabjerg, J. K. Pedersen, L. Oestergaard, R. L. Kirlin, A. M. Trzynadlowski, and S. Legowski, "Optimized and Non-Optimized Random Modulation Techniques for VSI Drives," *EPE Journal*, vol. 6, no. 2, pp. 46–53, 1996.

[19] F. Blaabjerg, J. K. Pedersen, E. Ritchie, and P. Nielsen, "Determination of Mechanical Resonances in Induction Motors by Random Modulation and Acoustic Measurement," *Proc. of 5th European Conference on Power Electronics and Applications*, vol. 4, pp. 319–324, 1993.

[20] F. Blaabjerg, J. K. Pedersen, E. Ritchie, and P. Nielsen, "Determination of Mechanical Resonances in Induction Motors by Random Modulation and Acoustic Measurement," *IEEE Trans. on Industry Applications*, vol. 31, no. 4, pp. 823–829, July/August 1995.

[21] V. Blasko, "Analysis of a Hybrid PWM Based on Modified Space-Vector and Triangle-Comparison Methods," *Conference Record of the 31st IEEE Industry Applications Society Annual Meeting*, vol. 2, pp. 947–955, 1996.

[22] V. Blasko, "Analysis of a Hybrid PWM Based on Modified Space-Vector and Triangle-Comparison Methods," *IEEE Trans. on Industry Applications*, vol. 33, no. 3, pp. 756–764, May/June 1997.

[23] V. Blasko, M. M. Bech, F. Blaabjerg, and J. K. Pedersen, "A New Hybrid Random Pulse Width Modulator for Industrial Drives," *Proc. of the 15th IEEE Applied Power Electronics Conference and Exposition*, vol. 2, pp. 932–938, Feb. 2000.

[24] S. Bolognani, R. Conton, and M. Zigliotto, "Experimental Analysis of the EMI Reduction in PWM Inverters Using Random Space Vector Modulation," *Proc. of the IEEE International Symposium on Industrial Electronics*, vol. 1, pp. 482–487, June 1996.

[25] A. Bonnet, T. Alukaiday, and P.C.K. Luk, "A High Performance Space Vector Motor Drive Controller," *IEE Colloquium on DSP Chips in Real Time Measurement and Control (Digest No: 1997/301)*, pp. 4/1–4/4, 1997.

[26] J. M. Bourgeois, "PWM Technique for Acoustic Noise Reduction in Power Applications," *Proc. of the 8th IEEE Applied Power Electronics Conference and Exposition*, vol. 1, pp. 141–145, 1993.

[27] J. T. Boys, "Theoretical Spectra for Narrow-Band Random PWM Waveforms," *IEE Proc. Part B*, vol. 140, no. 6, pp. 393–400, Nov. 1993.

[28] J. T. Boys and M. Andrews, "Random PWM Inverter Drive Systems: Theory and Practice," *Proc. of the 19th IEEE International Conference on Industrial Electronics, Control, and Instrumentation*, vol. 2, pp. 695–700, 1993.

[29] J. T. Boys and P. G. Handley, "Spread Spectrum Switching: Low Noise Modulation Technique for PWM Inverter Drives," *IEE Proc. Part B*, vol. 139, no. 3, pp. 252–260, May 1992.

[30] D. E. Cameron, J. H. Lang, and S. D. Umans, "The Origin and Reduction og Acoustic Noise in Doubly Salient Variable-Reluctance Motors," *IEEE Trans. on Industry Applications*, vol. 28, no. 6, pp. 1250–1255, Nov./Dec. 1992.

[31] P. J. Chrzan, A. Haras, and D. Roye, "Random and Programmed Modulation Schemes for Power Converters - Microcontroller Implementation," *Proc. of the International Power Electronics and Motion Control Conference*, pp. 93–98, 1994.

[32] P. W. Clarke, "Self-Commutated Thyristor DC-to-DC Converter," *IEEE Trans. on Magnetics*, vol. 6, no. 1, pp. 10–15, Mar. 1970.

[33] G. A. Covic and J. T. Boys, "Noise Quieting with Random PWM AC Drives," *IEE Proc. Electric Power Applications*, vol. 145, no. 1, pp. 1–10, Jan. 1998.

[34] J. Doval, A. Nogueiras, L. Eguzeábal, A. Lago, and C. M. Peeñalver, "Improving Pulse Width Modulation in order to get a Silent AC Motor," *Proc. of the IEEE International Symposium on Industrial Electronics*, vol. 2, pp. 274–278, 1997.

[35] J. Doval, A. Nogueiras, L. Eguzábal and C. M. Peñalver, "Random Modulation in Inverters Feeding Induction Motors," *Proc. of the 28th IEEE Power Electronics Specialists Conference*, vol. 1, pp. 601–605, 1997.

[36] I. Ekdahl, L. Sjöberg, H. Weibull, and J. Valis, "Annoyance from Inverter-Fed Induction Motors," *Proc. of Internoise — People versus Noise*, Leuven, Belgium, 1993.

[37] T. G. Habetler and D. M. Divan, "Acoustic Noise Reduction in Sinusoidal PWM Drives Using a Randomly Modulated Carrier," *Proc. of the 20th IEEE Power Electronics Specialists Conference*, vol. 2, pp. 665–671, 1989.

[38] T. G. Habetler and D. M. Divan, "Acoustic Noise Reduction in Sinusoidal PWM Drives Using a Randomly Modulated Carrier," *IEEE Trans. on Power Electronics*, vol. 6, no. 3, pp. 356–363, July 1991.

[39] D. C. Hamill, J. H. B. Deane, and P. J. Aston, "Some Applications of Chaos in Power Converters," *Proc. of the IEE Colloquium on Update on New Power Electronic Techniques*, pp. 5/1–5/5, May 1997.

[40] P. G. Handley, M. Johnson, and J. T. Boys, "Elimination of Tonal Acoustic Noise in Chopper-Controlled DC Drives," *Applied Acoustics*, vol. 32, pp. 107–119, 1991.

[41] J. Holtz, "Pulsewidth Modulation — A Survey," *IEEE Trans. on Industrial Electronics*, vol. 39, no. 5, pp. 410–420, Dec. 1992.

[42] J. Holtz, "Pulsewidth Modulation for Electronic Power Conversion," *Proc. of the IEEE*, vol. 82, no. 8, pp. 1194–1214, Aug. 1994.

[43] J. Holtz and B. Beyer, "Optimal Pulsewidth Modulation for AC Servos and Low-Cost Industrial Drives," *Conference Record of the 27th IEEE Industry Applications Society Annual Meeting*, vol. 1, pp. 1010–1017, 1992.

[44] J. Holtz and L. Springob, "Reduced Harmonics PWM Controlled Line-Side Converter for Electric Drives," *Conference Record of the 25th IEEE Industry Applications Society Annual Meeting*, vol. 2, pp. 959–964, 1990.

[45] S. Y. R. Hui, I. Oppermann, F. Pasalic, and S. Sathiakumar, "Microprocessor based Mathematical and Logical Random PWM Methods for Power Inverters," *Proc. of 6th European Conference on Power Electronics and Applications*, vol. 1, pp. 707–712, 1995.

[46] S. Y. R. Hui, I. Oppermann, F. Pasalic, and S. Sathiakumar, "Microprocessor-based Random PWM Schemes for DC-AC Power Conversion," *Proc. of the 26th IEEE Power Electronics Specialists Conference*, vol. 1, pp. 307–312, 1995.

[47] S. Y. R. Hui, I. Oppermann, and S. Sathiakumar, "Microprocessor-Based Random PWM Schemes for DC-AC Power Conversion," *IEEE Trans. on Power Electronics*, vol. 12, no. 2, pp. 253–260, Mar. 1997.

[48] S. Y. R. Hui and S. Sathiakumar, "Optimisation of Microprocessor-based Random PWM Schemes for Power Inverters with Low Switching Frequencies," *Proc. of the 11th Annual Applied Power Electronics Conference*, vol. 1, pp. 214–218, 1996.

[49] S. Y. R. Hui, S. Sathiakumar and Y. Shrivastava, "Progressive Change of Chaotic PWM Patterns in DC-AC Random PWM Schemes using Weighted Switching Decision," *Proc. of the 28th IEEE Power Electronics Specialists Conference*, vol. 2, pp. 1454–1461, 1997.

[50] S. Y. R. Hui, S. Sathiakumar, and K. K. Sung, "Novel Random PWM Schemes with Weighted Switching Decision," *Proc. of the 6th International Conference on Power Electronics and Variable Speed Drives*, pp. 348–353, 1996, IEE Conf. Publication No. 429.

[51] S. Y. R. Hui, S. Sathiakumar, and K. K. Sung, "Novel Random PWM Schemes with Weighted Switching Decision," *IEEE Trans. on Power Electronics*, vol. 12, no. 6, pp. 945–952, Nov. 1997.

[52] S. Y. R. Hui, Y. Shrivastava, S. Sathiakumar, K. K. Tse, and S. H. Chung, "A Comparison of Nondeterministic and Deterministic Switching Methods for dc-dc Power Supplies," *IEEE Trans. on Power Electronics*, vol. 13, no. 6, pp. 1046–1055, Nov. 1998.

[53] B. Huo and A. M. Trzynadlowski, "Random Pulse Width PWM Modulator for Inverter-fed Induction Motor Based on the TMS320F240 DSP Controller," *Texas Instruments DSPS FEST'99*, Aug. 1999.

[54] C. B. Jacobina, A. M. N. Lima, E. R. C. da Silva, and R. L. de A. Ribeiro, "Current Control for a Random PWM Voltage Source Inverter," *Proc. of the 28th IEEE Power Electronics Specialists Conference*, vol. 2, pp. 1440–1446, 1997.

[55] C. B. Jacobina, A. M. N. Lima, E. R. C. da Silva, and A. M. Trzynadlowski, "Current Control for Induction Motor Drives using Random PWM," *IEEE Trans. on Industrial Electronics*, vol. 45, no. 5, pp. 704–712, Oct. 1998.

[56] B. Kaku, I. Miyashita, and S. Sone, "Novel Random PWM Method Based on Normally Distributed Random Data," *Proc. of 7th European Conference on Power Electronics and Applications*, vol. 1, pp. 152–157, 1997.

[57] M. P. Kaźmierkowski and F. Blaabjerg, "Impact of Emerging Technologies on PWM Control of Power Electronic Converters," *IEEE Industrial Electronics Society Newsletter*, vol. 42, no. 4, pp. 9–13, Dec. 1995.

[58] R. L. Kirlin, "Continuous Spectrum for Random Segment Width PWM DC-AC Conversion," private correspondence, Jan. 1998.

[59] R. L. Kirlin, M. M. Bech, and A. M. Trzynadlowski, "Power Spectral Density Analysis of Randomly Switched Pulse Width Modulation for DC/AC Converters," *Proc. of 10th IEEE Workshop on Statistical Signal and Array Processing*, pp. 373–377, Aug. 2000.

[60] R. L. Kirlin, M. M. Bech, and A. M. Trzynadlowski, "Power and Power Spectral Density Analysis of Random Switching PWM DC/AC Converters," Submitted to IEEE Trans. on Industrial Electronics, 2000.

[61] R. L. Kirlin and R. M. Dizaji, "New Analysis of Harmonics for Random Segment Width PWM DC-AC Conversion," private correspondence, Jan. 1998.

[62] R. L. Kirlin, S. Kwok, S. Legowski, and A. M. Trzynadlowski, "Power Spectra of a PWM Inverter with Randomized Pulse Position," *IEEE Trans. on Power Electronics*, vol. 9, no. 5, pp. 463–472, Sept. 1994.

[63] R. L. Kirlin, S. Legowski, and A. M. Trzynadlowski, "An Optimal Approach to Random Pulse Width Modulation in Power Inverters," *Proc. of the 26th IEEE Power Electronics Specialists Conference*, vol. 1, pp. 313–318, 1995.

[64] R. L. Kirlin, S. Legowski, A. M. Trzynadlowski, Y. Cui, and S. Kwok, "Power Spectra of a Three-Phase Inverter with Random Pulse Width Modulation Modes," *Proc. of the 3rd IEEE Workshop on Computers in Power Electronics*, pp. 265–267, Aug. 1992.

[65] R. L. Kirlin, H. Lou, and A. M. Trzynadlowski, "A Unified Design and Analysis Approach to Randomized Pulse Width Modulation in DC to AC Inverters," *Proc. of the 7th IEEE Digital Signal Processing Workshop*, 1996.

[66] R. L. Kirlin and A. M. Trzynadlowski, "Spectral Design of Randomized Pulse Width Modulation in DC to AC Converters," *Proc. of the 7th IEEE Signal Processing Workshop on Statistical Signal and Array Processing*, pp. 387–391, June 1994.

[67] R. L. Kirlin and A. M. Trzynadlowski, "A Unified Approach to Analysis and Design of Random Pulsewidth Modulation in Voltage Source Inverters," *IEEE*

Trans. on Circuits and Systems — I: Fundamental Theory and Applications, vol. 44, no. 8, pp. 763–766, Aug. 1997.

[68] R. L. Kirlin, A. M. Trzynadlowski, M. M. Bech, F. Blaabjerg, and J. K. Pedersen, "Analysis of Spectral Effects of Random PWM Strategies for Voltage Source Inverters," *Proc. of 7th European Conference on Power Electronics and Applications*, vol. 1, pp. 146–151, 1997.

[69] R. L. Kirlin, J. Wang, and R. M. Dizaji, "Study on Spectral Analysis and Design for DC/DC Conversion Using Random Switching Rate PWM," *Proc. of 10th IEEE Workshop on Statistical Signal and Array Processing*, pp. 378–382, Aug. 2000.

[70] H. Kragh, F. Blaabjerg, and J. K. Pedersen, "Reduce of the Acoustic Noise Effect from PWM-VSI Inverter Controlled AC-Drives by Music and Random Modulation," *Proc. of the IEEE Power Conversion Conference*, vol. 1, pp. 85–92, 1993.

[71] M. Kuisma, P. Silventoinen, T. Järveläinen and T. Vesterinen, "Effects of Nonperiodic and Chaotic Switching on the Conducted EMI Emissions of Switch Mode Power Supplies," *Proc. of the IEEE Nordic Workshop on Power and Industrial Electronics*, pp. 185–190, 2000.

[72] Y. S. Lai, "Random Switching Techniques for Inverter Control," *Electronics Letters*, vol. 33, no. 9, pp. 747–749, Apr. 1997.

[73] Y. S. Lai, "New Random Inverter Control Technique for Common Mode Voltage Mitigation of Motor Drives," *IEE Proceedings – Electric Power Applications*, vol. 146, no. 3, pp. 289–296, May 1999.

[74] Y. S. Lai, "Sensorless Vector-Controlled IM Drives using Random Switching Technique," *Proc. of 8th European Conference on Power Electronics and Applications*, Sept. 1999.

[75] Y. S. Lai, "New Random Technique of Inverter Control for Common Mode Voltage Reduction of Inverter-Fed Induction Motor Drives," *IEEE Trans. on Energy Conversion*, vol. 14, no. 4, pp. 1139–1146, Dec. 1999.

[76] Y. S. Lai, "Sensorless Speed Vector-Controlled Induction Motor Drives using New Random Technique for Inverter Control," *IEEE Trans. on Energy Conversion*, vol. 14, no. 4, pp. 1147–1155, Dec. 1999.

[77] Y. S. Lai and S. C. Chang, "DSP-based Implementation of New Random Switching Technique of an Inverter Control for Sensorless Vector-Controlled Induction Motor Drives," *IEE Proceedings – Electric Power Applications*, vol. 146, no. 2, pp. 163–172, Mar. 1999.

[78] Y. S. Lai, H. C. Huang, Y. S. Kuan, and C. M. Young, "A New Random Inverter Control Technique for Motor Drives," *Proc. of the 13th IEEE Applied Power Electronics Conference and Exposition*, vol. 1, pp. 101–107, Feb. 1998.

[79] L. Laskai, P. Enjeti, and I. J. Pitel, "White-Noise Modulation of High-Frequency High-Intensity Discharge Lamp Ballasts," *Conference Record of the 29th IEEE Industry Applications Society Annual Meeting*, vol. 3, pp. 1953–1961, 1994.

[80] L. Laskai, P. Enjeti, and I. J. Pitel, "White-Noise Modulation of High-Frequency High-Intensity Discharge Lamp Ballasts," *IEEE Trans. on Industry Applications*, vol. 34, no. 3, pp. 597–605, May/June 1998.

[81] C. K. Lee, S. Y. R. Hui, and H. Chung, "A Randomized Voltage Vector Switching Scheme for 3-Level Power Inverters," *Proc. of the 31st IEEE Power Electronics Specialists Conference*, pp. 27–32, June 2000.

[82] S. Legowski, J. Bei, and A. M. Trzynadlowski, "Analysis and Implementation of a Grey-Noise PWM Technique Based on Voltage Space Vectors," *Proc. of the 7th IEEE Applied Power Electronics Conference and Exposition*, pp. 586–593, 1992.

[83] S. Legowski and A. M. Trzynadlowski, "Hypersonic MOSFET-based Power Inverter With Random Pulse Width Modulation," *Conference Record of the 24th IEEE Industry Applications Society Annual Meeting*, vol. 1, pp. 901–903, 1989.

[84] S. Legowski and A. M. Trzynadlowski, "Power-MOSFET, Hypersonic Inverter with High-Quality Output Current," *Proc. of the 5th IEEE Applied Power Electronics Conference and Exposition*, pp. 3–7, 1990.

[85] S. Legowski and A. M. Trzynadlowski, "Advanced Random Pulse Width Technique for Voltage-Controlled Inverter Drive Systems," *Proc. of the 6th IEEE Applied Power Electronics Conference and Exposition*, pp. 100–106, 1991.

[86] T.-J. Liang, J.-F. Chen, and J.-L. Shyu, "Novel Multi-Random PWM Technique for Inverter Design," *Proc. of the IEEE 1999 International Conference on Power Electronics and Drive Systems*, vol. 2, pp. 942–946, 1999.

[87] C. M. Liaw and Y. M. Lin, "Random Slope PWM Inverter using Existing System Background Noise: Analysis, Design and Implementation," *IEE Proceedings — Electric Power Applications*, vol. 147, no. 1, pp. 45–54, Jan. 2000.

[88] B.-R. Lin, "High Power Factor AC/DC/AC Converter with Random PWM," *IEEE Trans. on Aerospace and Electronic Systems*, vol. 35, no. 3, pp. 935–943, July 1999.

[89] B.-R. Lin and H.-H. Lu, "Three-Phase AC/DC/AC Converter with Random Pulse Position," *Proc. of 8th European Conference on Power Electronics and Applications*, Sept. 1999.

[90] B.-R. Lin and H.-H. Lu, "Implementation of Nondeterministic PWM for Inverter Drives," *Proc. of the IEEE International Symposium on Industrial Electronics*, vol. 2, pp. 813–818, 1999.

[91] B.-R. Lin and H.-H. Lu, "Single-Phase Three-Level Rectifier and Random PWM Inverter Drives," *IEEE Trans. on Aerospace and Electronic Systems*, vol. 35, no. 4, pp. 1334–1343, Oct. 1999.

[92] W. McMurray, "Power Electronics in the 1990s," *Proc. of the 16th IEEE International Conference on Industrial Electronics, Control, and Instrumentation*, vol. 1, pp. 839–843, 1990.

[93] F. Mihalič, T. Bezjak, and M. Milanovìc, "Random Modulated Boost Converter with Improved Harmonic Spectrum," *Proc. of the IEEE International Symposium on Industrial Electronics*, vol. 2, pp. 268–273, 1997.

[94] F. Mihalič, T. Bezjak, and M. Milanovìc, "Improved Harmonics Spectrum and Reduced EMI in Boost Converter by Using the Random Modulation," *Proc. of 7th European Conference on Power Electronics and Applications*, vol. 2, pp. 366–371, 1997.

[95] F. Mihalič and M. Milanovìc, "Power Spectrum Estimation of the Input Current in Random Modulated Boost Converter," *Proc. of the 24th IEEE International Conference on Industrial Electronics, Control, and Instrumentation*, vol. 3, pp. 1382–1387, 1998.

[96] F. Mihalič and M. Milanovìc, "Wide-Band Analysis of the Random Modulated Boost Rectifier," *Proc. of the 31st IEEE Power Electronics Specialists Conference*, vol. 2, pp. 946–951, 2000.

[97] J. K. Pedersen and F. Blaabjerg, "Implementation and Test of a Digital Quasi-Random Modulated SFAVM PWM in a High Performance Drive System," *Proc. of the 18th IEEE International Conference on Industrial Electronics, Control, and Instrumentation*, vol. 1, pp. 265–270, 1992.

[98] J. K. Pedersen and F. Blaabjerg, "Digital Quasi-Random Modulated SFAVM PWM in an AC-Drive System," *IEEE Trans. on Industrial Electronics*, vol. 41, no. 5, pp. 518–525, Oct. 1994.

[99] J. K. Pedersen, F. Blaabjerg, and P. S. Frederiksen, "Reduction of Acoustical Noise Emission in AC-Machines by Intelligent Distributed Random Modulation," *Proc. of 5th European Conference on Power Electronics and Applications*, vol. 4, pp. 369–375, 1993.

[100] J. M. Retif and B. Allard, "A PWM ASIC using Stochastic Coding," *Proc. of the 23rd IEEE Power Electronics Specialists Conference*, vol. 1, pp. 587–594, 1992.

[101] J. M. Retif, B. Allard, X. Jorda, and A. Perez, "Use of ASIC's in PWM Techniques for Power Converters," *Proc. of the 19th IEEE International Conference on Industrial Electronics, Control, and Instrumentation*, vol. 2, pp. 683–688, 1993.

[102] Y. Shrivastava and S. Y. R. Hui, "Analysis of Random PWM Switching Methods for Three-Level Power Inverters," *IEEE Trans. on Power Electronics*, vol. 14, no. 6, pp. 1156–1163, Nov. 1999.

[103] Y. Shrivastava, S. Y. R. Hui, and S. Sathiakumar, "Noise Analysis of DC-AC Random PWM Schemes," *IEEE Trans. on Power Electronics*, vol. 14, no. 4, pp. 761–770, July 1999.

[104] Y. Shrivastava, S. Y. R. Hui, S. Sathiakumar, and K. K. Tse, "Effects of Continuous Noise in Randomised Switching DC-DC Converters," *Electronic Letters*, vol. 33, no. 11, pp. 919–921, May 1997.

[105] Y. Shrivastava, S. Sathiakumar and S. Y. R. Hui, "Random Discrete PWM Method for DC-DC Power Converters," *Electronics Letters*, vol. 32, no. 23, pp. 2105–2106, Nov. 1996.

[106] Y. Shrivastava, S. Sathiakumar and S. Y. R. Hui, "Improved Spectral Performance of Random PWM Schemes with Altered Chaotic Behavior," *Proc. of the 28th IEEE Power Electronics Specialists Conference*, vol. 2, pp. 1447–1453, 1997.

[107] Y. Shrivastava, S. Sathiakumar, and S. Y. R. Hui, "Improved Spectral Performance of Random PWM Schemes with Weighted Switching Decision," *IEEE Trans. on Power Electronics*, vol. 13, no. 6, pp. 1038–1045, Nov. 1998.

[108] A. M. Stanković, *Random Pulse Modulation with Applications to Power Electronic Converters*, Ph.D. thesis, Massachusetts Institute of Technology, Feb. 1993.

[109] A. M. Stanković, G. C. Verghese, and R. O. Hinds, "Monte-Carlo Verification of Power Spectrum Formulas for Random Modulation Schemes," *Proc. of the 3rd IEEE Workshop on Computers in Power Electronics*, pp. 187–194, Aug. 1992.

[110] A. M. Stanković, G. C. Verghese, and D. J. Perreault, "Analysis and Synthesis of Random Modulation Schemes for Power Converters," *Proc. of the 24th IEEE Power Electronics Specialists Conference*, pp. 1068–1074, 1993.

[111] A. M. Stanković, G. C. Verghese, and D. J. Perreault, "Randomized Modulation Schemes for Power Converters Governed by Markov Chains," *Proc. of the 4th IEEE Conference on Control Applications*, pp. 372–377, 1995.

[112] A. M. Stanković, G. C. Verghese, and D. J. Perreault, "Analysis and Synthesis of Randomized Modulation Schemes for Power Converters," *IEEE Trans. on Power Electronics*, vol. 10, no. 6, pp. 680–693, Nov. 1995.

[113] A. M. Stanković, G. C. Verghese, and D. J. Perreault, "Randomized Modulation of Power Converters via Markov Chains," *IEEE Trans. on Control Systems Technology*, vol. 5, no. 1, pp. 61–73, Jan. 1997.

[114] D. A. Stone and B. Chambers, "Effect of Spread-Spectrum Modulation of Switched Mode Power Converter PWM Carrier Frequencies on Conducted EMI," *Electronic Letters*, vol. 31, no. 10, pp. 769–770, May 1995.

[115] D. Stone and B. Chambers, "The Effect of Carrier Frequency Modulation of PWM Waveforms on Conducted EMC Problems in Switched Mode Power Supplies," *EPE Journal*, vol. 5, no. 3/4, pp. 32–37, Jan. 1996.

[116] D. A. Stone, B. Chambers, and D. Howe, "Random Carrier Frequency Modulation of PWM Waveforms to ease EMC Problems in Switched Mode Power Supplies," *Proc. of the IEEE 1995 International Conference on Power Electronics and Drive Systems*, vol. 1, pp. 16–21, 1995.

[117] D. A. Stone, B. Chambers, and D. Howe, "Easing EMC Problems in Switched Mode Power Converters by Random Modulation of the PWM Carrier Frequency," *Proc. of the 11th IEEE Applied Power Electronics Conference and Exposition*, vol. 1, pp. 327–332, 1996.

[118] K. K. Sung, S. Sathiakumar, S.Y.R. Hui, and Y. Shrivastava, "Randomness and Random PWM," *Proc. of the International Power Electronics and Motion Control Conference*, pp. 2.212–2.217, 1998.

[119] K. K. Sung, S. Sathiakumar, S.Y.R. Hui, and Y. Shrivastava, "Randomness and Random PWM," *Proc. of 8th European Conference on Power Electronics and Applications*, 1999.

[120] T. Tanaka, H. Hamasaki, and H. Yoshida, "Random-Switching Control in DC-to-DC Converters: an Implementation using M-sequence," *Proc. of 19th International Telecommunications Energy Conference*, pp. 431–437, 1997.

[121] T. Tanaka, H. Kameda, and T. Ninomiya, "Noise Analysis of DC-to-DC Converter with Random Switching Control," *Proc. of the IEEE International Telecommunications Energy Conference*, pp. 283–290, Nov. 1991.

[122] T. Tanaka and T. Ninomiya, "Random-Switching Control for DC-to-DC Converter: Analysis of Noise Spectrum," *Proc. of the 23rd IEEE Power Electronics Specialists Conference*, vol. 1, pp. 579–586, 1992.

[123] T. Tanaka, T. Ninomiya, and K. Harada, "Random-Switching Control in DC-to-DC Converters," *Proc. of the 20th IEEE Power Electronics Specialists Conference*, vol. 1, pp. 500–507, 1989.

[124] A. M. Trzynadlowski, "An Overview of Modern PWM Techniques for Three-Phase, Voltage-Controlled, Voltage-Source Inverters," *Proc. of the IEEE International Symposium on Industrial Electronics*, vol. 1, pp. 25–39, June 1996.

[125] A. M. Trzynadlowski, M. M. Bech, F. Blaabjerg, J. K. Pedersen, R. L. Kirlin, and M. Zigliotto, "Optimization of Switching Frequencies in the Limited-Pool Random Space Vector PWM Technique for Inverter-Fed Drives," *Proc. of the 14th IEEE Applied Power Electronics Conference and Exposition*, vol. 2, pp. 1013–1018, 1999.

[126] A. M. Trzynadlowski, F. Blaabjerg, J. K. Pedersen, R. L. Kirlin, and S. Legowski, "Random Pulse Width Modulation Techniques for Converter Fed Drive Systems — A Review," *Conference Record of the 28th IEEE Industry Applications Society Annual Meeting*, vol. 2, pp. 1136–1143, 1993.

[127] A. M. Trzynadlowski, F. Blaabjerg, J. K. Pedersen, R. L. Kirlin, and S. Legowski, "Random Pulse Width Modulation Techniques for Converter Fed Drive Systems — A Review," *IEEE Trans. on Industry Applications*, vol. 30, no. 5, pp. 1166–1175, Sep./Oct. 1994.

[128] A. M. Trzynadlowski, S. Ji, and S. Legowski, "Random Pulse Width Modulation of Delta Inverter for Automotive Applications," *Conference Record of the 26th IEEE Industry Applications Society Annual Meeting*, vol. 1, pp. 826–833, 1991.

[129] A. M. Trzynadlowski, R. L. Kirlin, and S. Legowski, "Space Vector PWM Technique with Minimum Switching Losses and a Variable Pulse Rate," *Proc. of the 19th IEEE International Conference on Industrial Electronics, Control, and Instrumentation*, vol. 2, pp. 689–694, 1993.

[130] A. M. Trzynadlowski, R. L. Kirlin, and S. Legowski, "Space Vector PWM Technique with Minimum Switching Losses and a Variable Pulse Rate," *IEEE Trans. on Industrial Electronics*, vol. 44, no. 2, pp. 173–181, Apr. 1997.

[131] A. M. Trzynadlowski, S. Legowski, and R. L. Kirlin, "Random Pulse Width Modulation Technique for Voltage-controlled Power Inverters," *Conference Record of the 22nd IEEE Industry Applications Society Annual Meeting*, vol. 1, pp. 863–868, 1987.

[132] A. M. Trzynadlowski, S. Legowski, and R. L. Kirlin, "Random Pulse Width Modulation Technique for Voltage-controlled Power Inverters," *International Journal of Electronics*, vol. 68, no. 6, pp. 1027–1037, 1990.

[133] K. K. Tse, S.-H. Chung, S. Y. R. Hui, and H. C. So, "Spectral Characteristics of Random Carrier Frequency Switching in Off-line Switched Mode Power Supply," *Proc. of the 14th IEEE Applied Power Electronics Conference and Exposition*, vol. 1, pp. 139–145, 1999.

[134] K. K. Tse, H.-S. Chung, S. Y. R. Hui, and H. C. So, "Analysis and Spectral Characteristics of a Spread-Spectrum Techniques for Conducted EMI Suppression," *IEEE Trans. on Power Electronics*, vol. 15, no. 2, pp. 399–410, Mar. 2000.

[135] K. K. Tse, S.-H. Chung, S. Y. R. Hui, and H. C. So, "A Comparative Investigation on the Use of Random Modulation Schemes for DC/DC Converters," *IEEE Trans. on Industrial Electronics*, vol. 47, no. 2, pp. 253–263, Apr. 2000.

[136] K. K. Tse, W. M. Ng, S.-H. Chung, and S. Y. R. Hui, "Evaluation of A Chaotic Switching Scheme for Power Converters," *Proc. of the 31st IEEE Power Electronics Specialists Conference*, vol. 1, pp. 412–417, June 2000.

[137] A. Wang and S. R. Sanders, "Random and Programmed Pulse-Width Modulation Techniques for DC-DC Converter," *IEEE International Symposium on Systems Engineering*, pp. 589–592, 1990.

[138] A. C. Wang and S. R. Sanders, "Programmed Pulsewidth Modulated Waveforms for Electromagnetic Interference Mitigation in DC-DC Converters," *IEEE Trans. on Power Electronics*, vol. 8, no. 4, pp. 596–605, Oct. 1993.

[139] L. Xu, Z. Q. Zhu, and D. Howe, "Effect of Zero Space Vector and PWM Carrier on Acoustic Noise from Induction Motor Drives," *Proc. of the 32nd Universities Power Engineering Conference*, vol. 1, pp. 209–212, 1997.

[140] L. Xu, Z. Q. Zhu, D. Stone, and D. Howe, "Acoustic Noise Radiated by Space Vector PWM, Random PWM and Direct Torque Controlled Induction Motor Drives," *Proc. of the International Conference on Electric Machines*, vol. 3, pp. 1746–1751, 1998.

[141] Z. Q. Zhu, L. Xu, and D. Howe, "Influence of Mounting a Coupling on the Natural Frequencies and Acoustic Noise Radiated by a PWM Controlled Induction Machine," *Proc. of the Ninth International Conference on Electric Machines and Drives*, pp. 164–168, 1999, IEE Conf. Publication No. 468.

[142] M. Zigliotto and A. M. Trzynadlowski, "Effective Random Space Vector Modulation for EMI Reduction in Low-Cost PWM Inverters," *Proc. of the IEEE International Conference on Power Electronics and Variable Speed Drives*, pp. 163–168, 1998, IEE Conf. Publication No. 456.

[143] Kone Osakeyhtiö, "Förfarande och anordning för minskning av bullerolägenheterna vid en med chopperprincip matad elmotor (*Method and Apparatus for Reduction of Noise from Chopper-Fed Electrical Machines*)," Finnish Patent Application No. 861.891, Filed May 6, 1986.

[144] P. W. Clarke, Bell Telephone Laboratories, "Switching Regulator with Random Noise Generator," US Patent No. 3.579.091, Filed May 18, 1969.

[145] L. Garces and V. T. N'Guyen Phuoc, Schneider Electric SA, "Inverter Control Device," US Patent No. 5.552.980, Filed March 1, 1995.

[146] H. Hosei and K. Tanaka, Nippon Steel Corp., "Switching Regulator," US Patent No. 5.640.315, Filed March 17, 1995.

[147] V. Blasko, Rockwell Automation, "Hybrid Pulse Width Modulation Method and Apparatus," US. Patent No. 5.706.186, Filed Sept. 23, 1996.

[148] Y. Kawashima and K. Tokuoka, Toyo Electric, "PWM Inverter," Japanese Patent No. 1.136.572, Filed Nov. 20, 1987.

[149] T. Koga and H. Hayashi, Toyo Electric, "Modulation System for PWM Inverter," Japanese Patent No. 6.014.557, Filed June 23, 1992.